I-2

GEOLOGICA ULTRAIECTINA

Mededelingen van
het Mineralogisch-Geologisch Instituut der Rijksuniversiteit
te Utrecht

No. 8

TECTONICS OF THE CHRYSTALLINE BASEMENT OF THE DOLOMITES IN NORTH ITALY

F. P. AGTERBERG

GEOLOGICA ULTRAIECTINA

No. 1 Boer, J. C. den, 1957: Etude géologique et paléomagnétique des Montagnes du Coiron, Ardèche, France *f* 7.50

No. 2 Landewijk, J. E. J. M. van, 1957: Nomograms for geological problems (with portfolio of plates) . . . . . *f* 10.—

No. 3 Palm, Q. A., 1958: Les roches cristallines des Cévennes médianes à hauteur de Largentière, Ardèche, France *f* 12.50

No. 4 Dietzel, G. F. L., 1960: Geology and permian paleomagnetism of the Merano Region, province of Bolzano, N. Italy . . . . . *f* 5.—

No. 5 Hilten, D. van, 1960: Geology and permian paleomagnetism of the Val-di-Non Area, W. Dolomites, N. Italy *f* 7.50

No. 6 Kloosterman, 1960: le Volcanisme de la Region D'Agde (Herault France) . . . . . *f* 10.—

No. 7 Loon, W. E. van, 1960: Petrographische und geochemische Untersuchungen im Gebiet zwischen Remüs (Unterengadin) und Nauders (Tirol) . . . . . *f* 9.—

No. 8 Agterberg, F. P., 1961: Tectonics of the crystalline Basement of the Dolomites in North Italy . . . . . *f*

The Netherlands Organization for the Advancement of Pure Research (Z.W.O.) has granted financial aid to publish this thesis.

„Geologica Ultraiectina" is een ongeregelde serie, hoofdzakelijk bestemd voor het opnemen van dissertaties afkomstig uit het Mineralogisch-Geologisch Instituut der Rijksuniversiteit te Utrecht.
„Geologica Ultraiectina" is een voortzetting der „Geologisch Geografische Mededeling: Geologische Reeks", welker uitgave in 1947 gestopt is.
„Geologica Ultraiectina" wordt toegezonden aan alle instellingen die ruilverkeer onderhouden met het Utrechtse instituut. Losse nummers zijn — voor zover de voorraad strekt — verkrijgbaar bij de administratie van het instituut, Oude Gracht 320, Utrecht.

„Geologica Ultraiectina" is an odd series with the main purpose of publishing D. Sc. theses from the „Mineralogisch-Geologisch Instituut" of the Utrecht State University.
„Geologica Ultraiectina" is a continuation of the „Geologisch-Geografische Mededelingen: Geologische Reeks", which came to an end in 1947.
„Geologica Ultraiectina" is sent to all departments which exchange publications with the Utrecht institute. Separate copies — when available — may be obtained from the administrator of the institute, Oude Gracht 320, Utrecht.

„Geologica Ultraiectina" est une série irrégulière de mémoires qui vise essentiellement à publier des thèses de doctorat en Sciences présentées au „Mineralogisch-Geologisch Instituut" de L'Université d'Etat d'Utrecht.
„Geologica Ultraiectina" continue la série des „Geologisch-Geografische Mededelingen: Geologische Reeks", achevée en 1947.
Tout laboratoire faisant des échanges de publications avec l'institut d'Utrecht recevra „Geologica Ultraiectina". Les exemplaires disponibles sont déposés chez L'administrateur de l'institut, Oude Gracht 320, Utrecht.

„Geologica Ultraiectina" erscheint in unregelmässigen Abständen und enthält hauptsächlich Doktorarbeiten des Mineralogisch-Geologischen Institutes der Universität Utrecht.
„Geologica Ultraiectina" ist die Fortsetzung der „Geologische Geografische Mededelingen: Geologische Reeks" welche Ausgabe 1947 eingestellt wurde.
„Geologica Ultraiectina" wird allen Instituten zugesandt, welche mit dem Institut in Utrecht im Tauschverkehr stehen. Einzelnummern sind — soweit vorrätig — bei der Institutsverwaltung, Utrecht, Oude Gracht 320, kaüflich zu erhalten.

GEOLOGICA ULTRAIECTINA

Mededelingen van
het Mineralogisch-Geologisch Instituut der Rijksuniversiteit
te Utrecht

No. 8

TECTONICS OF THE CHRYSTALLINE BASEMENT OF THE DOLOMITES IN NORTH ITALY

F. P. AGTERBERG

1961

DRUKKERIJ EN UITGEVERSMAATSCHAPPIJ V/H KEMINK EN ZOON N.V. - UTRECHT

PROMOTOR: PROF. DR. IR. W. VAN BEMMELEN

This memoir contains a doctoral thesis defended before the Senate of the State University at Utrecht on June 12th, 1961.

Ce mémoire a fait l'objet d'une thèse de doctorat en Sciences à l'Université d'Etat d'Utrecht le 12 juin 1961.

Diese Schrift ist eine Doktorarbeit, verteidigt vor dem Senat der Reichsuniversität Utrecht am 12. Juni 1961.

CONTENTS

SUMMARY

PART I

The crystalline basement of the Dolomites consists of mainly mesozonal quartz phyllites (quartzites, graphitic phyllites), and green phyllites. Among the latter both types "ortho" and "para" are present.

In most rocks of the Bressanone region, albite is a primary mineral. This indicates either albitization, or the presence of many metamorphic altered tuff intercalations.

The planation of the mica's (S_1) parallels the sedimentary stratification. In many places, the S_1-planes are folded with development of a secondary schistosity (S_2) parallel to the axial planes of minor folds. The S_1 probably originated by regional metamorphic crystallization without shearing movements. The S_2 indicate shearing movements and are closely related to kinematics.

Two types of minor folds occur. Subsymmetrical minor folds originated by compression and overturned minor folds may indicate mass transport increasing in the higher levels. Regional overturn is given by the overturn of the larger folds; some single minor folds may show overturn in the opposite direction.

PART II

Tectonic elements generally build up populations with a distinct mean and the individual values scattered around it. Samples may be drawn from a population with a frequency distribution resembling the population frequency distribution. These frequency distributions in an ideal case are two-dimensional normal. Pearson's χ^2 test and contour analysis demonstrate isotropic two-dimensional normal distribution for an example of 35 minor folds at Monguelfo, Pusteria.

About 500 samples of *S*-planes and minor folds have been studied. Pole diagrams indicate the general presence of two symmetry planes at right angles. An accurate approximate mean can be calculated readily, as the mean azimuth approximates the azimuth of the mean, and the mean dip the mean's dip. Excepted is the case of minor folds strongly dispersed in the mean *S*-plane. In that case, the deviation may be eliminated utilizing the theorem that the mean minor fold lies in the mean *S*-plane.

A distinct mean *S*-plane and mean minor fold have been determined in all places. The variation from place to place is gradual and shown by the constructed mean azimuth lines and the iso-lines of mean dip on the structure maps.

PART III

The present geometry of the crystalline rocks originated by Alpine deformation of a Hercynian pattern. The latter consists of an isoclinally folded series of strata in the NNE (Pusteria and S. Stefano regions) and an unfolded subhorizontal series in the SSW (southern Bressanone, Cima d'Asta, Strigno, and Gosaldo regions) and originated during a first Hercynian phase of major folding due to N-S compression. This phase was followed by a Hercynian phase of minor folding with formation of N-S directed minor folds in the unfolded series, analogous vertical minor folds in the western isoclinally folded series, and subhorizontal minor folds in the eastern isoclinally folded series. Intermediate regions show gradual transitions.

The Alpine deformation of the Hercynian folded rocks may be determined by comparison with the Alpine tectonics of the adjacent Permotriassic sediments.

The Bolzano quartz porphyry plate, the Dolomites block, and the Austrian gneisses North of the Pusteria Line acted as rigid bodies with respect to the more plastic crystalline basement.

It has been proved that

a) The S. Stefano Crystalline forms the core of an anticlinal structure which is about 6 km wide and has an amplitude of more than 3 kms. The pre-Alpine isoclinally folded *S*-planes made the Alpine shearing movements possible.

b) The Pusteria Crystalline has been strongly compressed between the Austrian gneisses to the North and the Dolomites to the South. The present width of 2½ km of the crystalline belt at S. Candido originated from another also isoclinally

folded belt, at least 7½ km wide, in which Alpine shearing movements took place.

c) The crystalline rocks of the Cima d'Asta and Gosaldo regions show a thickening, respectively from 1 to 5 km and from ½ to 4½ km. These increases in thickness are probably due to a plastic deformation of the crystalline rocks, which were adjusted to the borders of the adjacent rigid sedimentary masses during the intrusion of the Cima d'Asta granite. The thickening probably was accompanied by cristallization with material supply.

d) The crystalline rocks of the Strigno region overly Tertiary rocks; their position and internal Alpine deformations indicate a southward overthrust along the subhorizontal *S*-planes.

The crystalline areas surrounding the Dolomites moved diapyrically upward with respect to the adjacent sedimentary masses:

a) The S. Stefano and Pusteria crystalline rocks moved upward by squeezing out.

b) The Bressanone and Cima d'Asta crystalline masses were dragged upward by Alpine granite batholiths.

c) The deviating Alpine strike of the Gosaldo Crystalline also indicates an upward movement independent of the surrounding rigid sedimentary masses.

The Dolomites region is bordered by the Pusteria Line in the North and the Sugana Line in the South. Both represent toppled over normal faults as indicated by the southward overturn and the downward decreasing intensity of deformation. Both are locally accompanied by antithetic normal faults causing tectonic graben structures South of the main faults:

a) The small western Drauzone (Pusteria Line) was rotated from its originally subvertical into a 50° - 70° North dipping position.

b) The Strigno graben (Sugana Line) was filled up by Tortonian conglomerates and nappes sliding downwards from the North (M. Lefre and Civeron nappes). The position of the Sugana faultplane in this region is subhorizontal in the higher and subvertical in the lower levels.

These Alpine tectonics are Miocene in age and coherent to the uplift of the Tauern-Engadin axis with respect to the Venetian and Po plains.

PART IV

Earlier Alpine tectonics have been studied in the M. Spico region. The Austrian Nappe consisting of gneisses was thrusted over the Tauern Inlier consisting of Pennine nappes with a mantle of Mesozoic "schistes lustrés". In the M. Spico region the originally subhorizontal overthrust plane was folded in Miocene time during the formation of the Tauern dome to the North and the Rieserferner dome in the South.

The Rieserferner tonalite intrusion was accompanied by the formation of the Rieserferner augen-gneiss (with K^* supply) locally containing migmatites. The latter consist of the original augen-gneiss and many irregular dykes of leucocratic tonalite. The composition of some dykes and some large augen (diameter of 10 cm) resemble each other.

In many places, the schistosity of the augen-gneiss continues into the dykes; in that case, the material of the latter is called "dyke gneiss". The schistosity is regional and deformed by the Rieserferner intrusion, and older than the dykes. The schistosity of the dyke gneiss is caused by parallel muscovite and biotite crystals which probably are enclosed relict minerals. This supports the concept that the migmatites originated by metasomatism.

The steeply dipping series of M. Spico gneisses originated by vertical doming with secondary sideward movements with synchronous elongation by tension of the folded rock proper and its adjacent prolongations, whereas large-scale regional shortening was absent.

The structure of the Alpine root zone indicates an intermediate compression phase between the earlier Alpine formation of the Pennine and Austrian nappes, and the Late Alpine doming of the Tauern and Rieserferner masses with secondary southward movements. The Dolomites block moved northward with respect to the Bergamasc Alps causing the sinistral wrench flexure of the Austrian gneisses actually indicated by the Giudicaria Line. The Pusteria Line probably formed the eastward prolongation of the Insubric Line and afterwards was displaced toward the North. During this intermediate phase the "Schlinge" with subvertical axes originated by sideward squeezing out in front of the Dolomites block.

SAMENVATTING

Dit proefschrift is gebaseerd op vier zomers veldwerk van de schrijver (1957-1960), terwijl tevens een aantal candidaten van het Mineralogisch-Geologisch Instituut der Rijksuniversiteit te Utrecht gegevens verzameld heeft.

De structuur van de mesozonale micaschisten, die de kristallijne ondergrond van de Noord Italiaanse Dolomieten vormen, wordt vergeleken met de structuur van de aangrenzende Permotriassische sedimenten. Op deze wijze kan de Alpiene vervorming van het Hercynisch geplooide kristallijn bepaald worden.

Het blijkt dat de kristallijne gebieden rondom de Dolomieten gedurende de Laat Alpiene orogenese diapyr omhoogbewogen werden: a) Het S. Stefano en Pusteria kristallijn werd plastisch uitgeknepen tussen aangrenzende vaste massa's. b) Het Bressanone en Cima d'Asta kristallijn werd door Alpiene granietbatholithen opwaarts gesleurd, waarbij regionale uitwiggingen en verdikkingen ontstonden.

De Pusteria Lijn en de Sugana Lijn, die het Dolomietengebied begrenzen, corresponderen met secundair omgeklapte afschuivingen ontstaan tengevolge van de Neogene opheffing van de Tauern en de gelijktijdige daling in de Povlakte.

RIASSUNTO

Questa dissertazione è fondata su ricerche nel terreno che l'autore ha effettuato durante quattro estati 1957-1960 con l'ausilio di diversi laureandi del "Mineralogisch-Geologisch Instituut" dell' università di Utrecht, Olanda, che hanno fatto misurazioni.

La struttura delle micascisti mesozonali che costituiscono il basamento cristallino delle Dolomiti italiane è comparata colla struttura tettonica delle formazioni limitrofe del Permiano e del Trias. È determinata in questa maniera la deformazione Alpina del sustrato cristallino con le sue pieghe erciniche.

Ne segue che i terreni cristallini intorno alle Dolomiti sono risultati: (a) il cristallino di S. Stefano e della Pusteria da spremimento plastico in alto fra masse consistenti limitrofe e (b) il cristallino di Bressanone e della Cima d'Asta da innalzamento di complessi intrusivi Alpini con simultanea formazione di addensamenti e assottigliamenti regionali.

Le Linee di Pusteria e di Sugana che limitano la regione delle Dolomiti corrispondono a faglie normali rivolte posteriormente e provenienti dalla levata dei Tauri e dallo sprofondamento della zolla adriatico-padano.

„Quos interim Natura cum suis coniecturis magnifice riet. Nam nihil apud illos esse comperti, vel illud satis magnum est argumentum, quod singulis de rebus inexplicabilis inter ipsos est digladiatio."

ERASMUS, STULTITIAE LAUS

„Maar Moeder Natuur lacht wat om hen met al hun theorieën. Want dat ze nimmer tot enig positief resultaat komen, blijkt wel hieruit, dat zelfs over de onbelangrijkste punten onoplosbare meningsverschillen tussen hen bestaan."

ERASMUS, DE LOF DER ZOTHEID
Paris, Amsterdam

INTRODUCTION

The present thesis deals with a number of crystalline regions around the Dolomites in North Italy. The geographic position is shown on sheet I, which is depicted in fig. 105. The Dolomites proper consist mainly of Permotriassic, overlying a transgression plane, which cuts off the studied crystalline rocks. The tectonics of this crystalline basement have been scarcely studied hitherto, in contradistinction with the overlying sediments, the Alpine tectonics of which are rather well-known. The complexity of the geometry of the crystalline basement, which may have caused this apparent lack of interest, is due to several factors. In the first place, a general stratigraphy of these uniform and for the greater part mesozonal micaschists has not been established. Therefore, it is necessary to base the tectonic interpretation almost entirely on the schistosity and the generally present minor folds. The age of these tectonical elements is generally pre-Permian. It can be proved that originally subhorizontal schistosity-planes have been folded twice during the Hercynian orogenesis. In the second place, this Hercynian folded basement was deformed intensively during the Alpine orogenesis. A clear distinction between Hercynian and Alpine orogenesis is possible only by studying the pure Alpine tectonics of the adjacent Permotriassic sediments. For this reason, and because the existing geologic maps appeared to be inadequate, certain parts of these sediments have been mapped again.

The fundamental tectonical values are scattered around the mean of the group to which they belong. Only the mean of a number of single values is a basis for regional tectonics. The means vary from place to place. Many measurements had to be made to determine the geometry of the means. A methodology had to be developed for calculating the means and for constructing the structure maps.

This thesis consists of four parts.

The first part (I) contains a description of the rocks and those deformation types which can be directly studied.

The second part (II) consists of a general methodology, which has been applied to the various areas. The deformation types, which individually cannot be analyzed, have been collectively integrated in the methodology. The result is a geometric pattern from which the kinematics can be derived. This will be discussed in the part on regional tectonics (III).

First, the tectonics South of the Pusteria Line will be discussed. The position of the Dolomites and their basement in the general framework of the Alps is the subject of part IV.

The interpretation of the tectonics of the crystalline basement of the Dolomites is based on our own investigations. For this reason, practically no references will be found in parts II and III. For petrographic and stratigraphic information, use has been made of existing data, and our contribution to these subjects is not considered important.

The fourth part can be partly considered as a synthesis based on the investigations of others. It starts, however, with our own investigations of some gneisses of the Austrian Nappe in the M. Spico area, overlying the Pennine structures of the Tauern Inlier. These subjects do not belong to the tectonics of the crystalline basement of the Dolomites, but served for adapting the tectonics of the latter to those of the Eastern Alps in general.

Fieldwork was carried out during four summers (1957-1960), and topographic maps on a scale of 1 : 25,000 (Tavolette della carta italiana) were used. Survey data of students of the "Mineralogisch-Geologisch Instituut" of Utrecht have been used for this thesis. Their measurements have been summarized in the appendices. These observations on easily measurable tectonical elements by the various observers have been collected in diagrams of the same type. The interpretation of these diagrams and the conclusions drawn form a reliable basis for the ideas presented in this thesis.

PART I

Petrografy and deformation types of the region South of the Pusteria Line.

CHAPTER 1

PETROGRAPHY OF THE CRYSTALLINE BASEMENT OF THE NORTH ITALIAN DOLOMITES

It is emphasized that the petrography of the rocks was studied only in so far as this was of importance for the tectonic studies. No exact determinations of the plagioclases and potassium feldspars have been made, no chemical analyses are given, and the mineral composition is not measured in percentages. Approximately 200 slides have been studied, amongst which about 90 are dealing with the petrography of the M. Spico region (chapter 20).

The microscopic studies served as a basis for the structural analysis and further for the determination of the mineral composition.

However, this thesis is mainly based on fieldwork. No detailed measurements were made on the axes of quartz and mica for obtaining structural information as field observations are sufficient for this purpose.

All tectonic elements, on which conclusions are founded, can be studied in outcrops. However, in several cases a schistosity, measured in the outcrop, appears to be a secondary schistosity under the microscope and a microscopic check appeared to be necessary. This secondary schistosity (S_2) occurs next to an older one (S_1). Separation of these two can be carried out statistically when two distinct contoured groups can be observed in the pole diagram. In case these two groups cannot be distinguished, occasional measuring of S_1 instead of S_2 introduces an error in the mean S_1 which is smaller than the accuracy of the applied statistical method (see chapter 8).

The relation between crystallization and deformation has been determined in thin sections, but not in a quantitative manner. In such cases, the microscope may also show rock-properties not visible in the hand specimen. These observations on the texture are given in the chapters 2 and 3.

The author has studied the crystalline of the S. Stefano and Pusteria regions in greatest detail. Furthermore, some slides were studied of the Bressanone region, which at its western side borders on the Sarnthaler Alps studied by Skall (1959). The Bressanone region was studied by Sander (1925) and the surroundings of Funès by Ladurner (1936).

The petrography of the quartz phyllites in the Cima d'Asta region has been discussed by d'Amico (1957). The same author also studied the Gosaldo region (personal information), and, therefore, the present author only studied the texture of some slides of these regions and not the specific petrographic problems, such as "granitization" (d'Amico, 1957).

§ 1A *Nomenclature.*

The rock names as used on the geologic maps represent the readily recognizable rock types. E.g. the quartz phyllites may contain biotite schists or even quartzfeldspar gneisses; among the green phyllites, also chlorite schists ("ortho" and "para") and amphibolites may be present. These specifications may be found in the chapters on petrography (chapters 1 and 20).

Following German and Italian literature, the term quartz phyllite is used for the most frequent types of South-Alpine crystalline rocks, respectively called "Quarzphyllite" (German) and "filladi quarziferi" (Italian).

The quartz phyllite has a marked schistose texture. It generally consists mainly of fine to medium grained quartz and sericite-muscovite.

The age of these quartz phyllites cannot be established with certainty.

A *Rastrites* has been described from the graphitic variety in the vicinity of Funès, Bressanone

region, proving this part of the series to be Silurian (Dal Piaz, 1942). It is known that the quartz phyllites have been deformed at least twice during Hercynian orogenesis prior to being abraded and covered by Permian conglomerates. The Hercynian age of these kinematics will be discussed in part III.

When the quartz phyllite is green-coloured, it is called green phyllite on map sheets I, III, and VIII. Under the microscope, the green mineral has been determined in most cases as a chlorite and in cases as epidote or green hornblende. The occasionally very high content of albite and chlorite of some green phyllites may have been formed by the lowgrade regional metamorphism of some igneous rocks with originally a basaltic or dacitic composition. Both types, "ortho" and "para" green phyllites, may be expected to be present.

In the surroundings of Lappago-Lutago (M. Spico region, sheet VIII) calcareous rocks occur, which alternate with quartz phyllites and green phyllites. To be consistent, these rocks have been called calcareous phyllites as they have the same texture and grade of metamorphism as the intercalated quartz phyllites. For this reason, the name schist has not been used on the map sheets. The calcareous phyllites, however, have been called "Kalkschiefer" and "Calcescisti" respectively in the German and Italian literature.

§ 1B *Quartz phyllites.*

As mentioned before, a quartz phyllite is a fine or medium-fine grained schistose rock consisting of quartz and muscovite-sericite with albite, biotite, and accessory minerals. Examples of thin sections of the quartz phyllites are given in photographs 20, 21, and 22.

Between the quartz phyllites, conformable

TABLE I

Mineral content of 21 thin sections of quartz phyllites of the crystalline basement of the Dolomites. x = > 5% and * = < 5%; the 5% value has been estimated visually by comparison with Terry's (1955) examples.

Sample Nr.	Co-ordinates of the grid		quartz	muscovite and sericite	plagioclase	biotite	garnet	opaque minerals	chlorite	epidote	calcite
Pusteria region											
1	792-827	quartz phyllites	×	×	*	×		*			
2	794-827		×	×	*	×		*	×		
3	823-825		×	×	*			*			
4	823-825		×	×		*		*			
5	836-828		×	×				×			
6	838-828		×	×				×			
7	818-820		×	×		×		×			
8	850-831		×	×				×			
9	788-843		×	×				*			
10	856-831		×	×				*			
11	783-819		×	×		×	*	*	*		
Bressanone region											
12	088-811	quartz phyllites (Verrucano)	×	×		×		*			
13	973-793		×	×	×		×	*	×		
14	011-767		×	×	×	×		*	×	×	
15	019-687		×	×		×		*	×		
16	048-782		×	×	×	*	*	*	×	×	×
17	111-806		×	×	×	×		×	×	*	
18			×	×	×			*	*		
S. Stefano region											
19	108-648	quartzitic phyllites	×	×		*		×			
20	154-586		×	×		*		×		*	
21	101-607	quartzite	×								

quartz veins are generally present. In the Bressanone region coarse biotite and garnet may be distinguished in the field.

Table I gives the mineral content of 11 quartz phyllites from the Pusteria region and 7 from the Bressanone region.

Studying the slides, the only quantitative estimate has been made at 5 % of the slide area. The comparison charts for visual estimation of percentage composition by Terry (1955) have been used.

The 11 thin sections of the Pusteria region are from samples in the vicinity of Monguelfo and from the Eggerberg. Their true location is indicated by the co-ordinates of the grid.

Only in three slides, some small grains of albite are present. Biotite appears to be a primary mineral in four slides, and opaque minerals in four other slides.

In one case, chlorite occurs. This sample (nr. 2 of table I) shows a greenish lustre, and this rock may be closely related to our green phyllites.

The quartz phyllites of the Bressanone region frequently show macroscopic differences with the quartz phyllites of the Pusteria region, as the three minerals albite, biotite, and garnet often occur in the form of coarse grains (> 2 mm). Six slides were studied of the quartz phyllites and one of a quartz phyllite pebble from the Permian Verrucano conglomerate (S. 18 of table I). Probably both types "ortho" and "para" are present.

The most important difference between the Bressanone region and the Pusteria region is that albite generally is a primary mineral in the former.

The presence of biotite and garnet proves that part of the quartz phyllites belongs to the "micaschistes inférieurs" of the scheme published by Jung and Rock (1952). In general, the quartz phyllites represent their "micaschistes supérieurs et inférieurs".

In the Bressanone region albite occurs, the presence of which continues westward in the Sarntaler Alps (Skall, 1959 and Dietzel, 1960). Assuming that the original clayey sediments from which the quartz phyllites in both regions are derived were the same, the Bressanone region may be considered as subjected to albitization.

As indicated by fig.'s 25 and e.g. 21-22 of App. I, the formation of some albite, and of many conformable quartz veins took place prior to the deformation by minor folds. The regional metamorphic formation of garnet and micas was probably simultaneous with the formation of quartz veins and albitization. The latter processes possibly point to a quartz and albite supply from lower levels. This hypothesis, however, does not exclude the possibility of the greater part of the Bressanone Crystalline to consist of altered volcanic tuffs or other igneous rocks.

The sample of the Verrucano conglomerate (S. 18) shows the same mineral content as the other samples. However, the slides 14, 16, and 17 at least possibly belong to altered igneous rocks. They have the characteristic properties of the green phyllites, described in the following paragraph, excepting the colour which at most may be called greenish.

In some instances, the quartz phyllite alternates with a harder schistose rock which almost entirely consists of quartz. These rocks have been indicated in the S. Stefano region with the name quartzitic phyllites and quartzites.

In table I the mineral content is given of three thin sections of these quartzitic phyllites and quartzites. They differ from quartz phyllites by their greater content of quartz, which may be determined in the field.

The name conglomeratic quartzite is used for small pebbles with a diameter of more thans 2 mm in a quartzitic matrix.

In the Pusteria region, in a few places (sheet III) a conglomeratic quartzite occurs with reddish quartz pebbles in a quartzitic matrix. The average diameter is 2 cm (figure 23 of App. I).

In the Bressanone, Cima d'Asta, and Gosaldo regions, quartz phyllites only were mapped. Contact-metamorphic hornfelses are not indicated, nor the augen-containing variaties in the Cima d'Asta region which have been discussed comprehensively by d'Amico (1957). This subject will be treated in dealing with the augen-gneisses of the M. Spico region (chapter 20).

For all other crystalline rocks, as the amphibolite of Gufidaun (sheet III), reference is made to the literature (principally Sander, 1925; Dal Piaz, 1934).

§ 1C *Green phyllites.*

As green phyllites have been mapped the green

varieties of the quartz phyllites in the Pusteria, S. Stefano, and M. Spico regions.

The green colour appears to be caused by the three green minerals chloride, epidote, and green hornblende.

The green phyllites have been mapped by Cornelius Furlani (1912) and Dal Piaz (1934) as "Grünschiefer" and "Scisti verdi e tufi diabasici" respectively in the Pusteria region and as "Grünschiefer" or "Grüne oder violette Thonschiefer und Diabastuffe" by Geyer (1902) in the S. Stefano region. On the later map of Gortani (Carta geologica, nr. 13), the "Grünschiefer" zones of Geyer have not been distinguished in the S. Stefano region. Microscopic examples of green phyllites are shown in photographs 18 and 19.

TABLE II

Mineral content of 22 thin sections of green phyllites. x = > 5% and * = < 5%.

Sample Nr.	Co-ordinates of the grid	quartz	muscovite and sericite	plagioclase	biotite	opaque minerals	chlorite	epidote	calcite	tremolite	clinozoisite (zoisite?)
Pusteria region											
1	792-827	x	x	x		x	x				
2	894-820	x	x	x		*	x	x			
3	900-822	x	x	x	x	x	x				
4	900-822	x	x	x		*	x				
5	952-806	x	x	x	*	*	x				
6	941-797	x	x	x	x	*	x				
7	972-805	x	x	x			x		*		
8	972-805	x	x				x		x		
9	794-791	x	x	x	x	*		x		x	x
10	775-796	x	x	x	*	*	x				
11	820-788	x	x	x		*	x				
12	240-863	x	x	x	*	*	x	*			
13	759-829	x	x	x	*	*	x				
14	723-863	x	x	x	*	*		x			
2 S. Stefano region											
15	098-652	x	x	x	*	*	x	*			
16	095-657	x	x		*	*	*				
17	119-590	x	x	x		*	x				
18	109-617	x	x	x	*	*	*		x		
19	128-646	x	x	x	*						
20	130-647	x	x	x	x		*				
21	161-623	x	x	x		*	x				
22	111-663	*	x	x		*	x		x		

PUSTERIA REGION.

In the first place, the green phyllites of the Pusteria region will be discussed. The mineral content of 14 samples is given in table II. The difference with the quartz phyllites is the occurrence of the green chlorite or, in two cases, epidote without chlorite, and the presence of plagioclase as a primary mineral; the latter is an accessory mineral in the quartz phyllites of the Pusteria region.

The plagioclase (albite-oligoclase) occurs as coarse crystals up to more than 2 mm in diameter, suggesting that these rocks are altered igneous rocks. The occurrence of epidote, calcite, tremolite, and (clino)zoisite can be explained by assuming that the present plagioclase has been derived from a plagioclase with a higher Ca-content. The ore content of the chlorite suggests it to be an alteration product of pyroxene, amphibole, or biotite (Palm, 1957, p. 25).

Remarkable are the many quartz grains, suggesting that the original rock had a dacitic composition. However, it is possible that the greater part of the quartz was supplied by hydrothermal solutions. In many cases (photograph 20), quartz appears to be the latest crystallized mineral, and the original rock might have been of basaltic composition.

From the preceding observations it follows that the term diabase tuffs used in literature is questionable, as the diabasic nature of this rock has not been proved.

The original rocks are probably tuffs, because they appear to have been deposited in large areas parallel with the stratification in the quartz phyllites. This is supported by the observation that the contact plane between green phyllite and quartz phyllite is parallel to the schistosity-planes, and the schistosity-planes are parallel to the frequently alternating quartzitic phyllites and quartz phyllites.

In view of the quartz content, it is possible that the original igneous rocks were for instance ignimbrites or tuffs of a more acid, i.e. dacitic, composition.

The green phyllites have been observed in zones, e.g. the zone South of the Pusteria Line extending from Naso to Prato alla Drava, shown on the geologic map (sheet III).

Another zone was discovered North of the southern boundary with the Grödener sandstones and conglomerates, between the Rio Furcia and S. Candido. The number of outcrops, however, is too scarse to determine the complex structure of the boundary plane between the quartz phyllites and the green phyllites. Green phyllites have been observed in many places outside the two mentioned zones. For this reason, no boundaries have been drawn and only the outcrops of green phyllites have been marked with the letter G on the maps.

S. STEFANO REGION.

The composition of the green phyllites from the S. Stefano region is the same as from the Pusteria region.

Geyer (1902) mapped two zones in the region covered by our map, but green phyllites occur in many other outcrops, which are marked with G. The zones of Geyer are rather hypothetical and we restricted ourselves to this simple indication of the green outcrops.

Geyer (1902) established a stratigraphy of the quartz phyllites according to which the upper part of the quartz phyllites contains green phyllites. Above these series follow slates which in some cases also contain green phyllites. Cornelius-Furlani (1912) called this latter complex "Carnian Rocks".

This stratigraphy, in which quartz phyllites and slates with green phyllites are younger than the quartz phyllites proper, cannot be proved. However, this interpretation corresponds with the division into younger and older rocks, which was established by the present author on the basis of tectonics (chapter 12).

CHAPTER 2

SCHISTOSITY OF THE CRYSTALLINE ROCKS

In the region under discussion, the crystalline rocks show a definite schistosity (*S*) and generally these schistose rocks are folded.

The term schistosity is used to describe all megascopically conspicuous parallel fabrics of non-sedimentary origin causing a definite fissility to the rocks in which they occur (Schieferdecker, 1959, note under 5411).

In some cases, two schistosities can be distinguished, an older one, called the first schistosity, and a younger one being parallel to the axial planes of the minor folds present.

The term first schistosity (S_1) is used when a second schistosity (S_2) does exist also. If one schistosity only is visible, it is called the schistosity or *S*.

When S_2 is present on the limbs of the microfolds, the mica may parallel this S_2. It is possible that these microfolds are discernible only under the microscope; in that case, a so-called *S* actually appears to be a S_2.

In thin sections, the schistosity appears to be caused by parallelism of the muscovite and other tabular minerals. On the other hand, some mineralogical banding is generally present. This banding may be a remainder of original sedimentary banding or it may be caused by metamorphic diffusion. These two possibilities cannot be clearly distinguished in all cases (see photograph 22).

It is assumed that e.g. the boundary plane in

photograph 22 between quartz phyllite and muscovite-containing quartzite has a sedimentary origin. In many outcrops, such alternations of quartzitic phyllites or quartzites with quartz phyllites can be observed. Other examples of stratification may be encountered at the boundaries of graphitic quartz phyllites and green phyllites. Photograph 9 shows the boundary plane between a green phyllite (above) and a graphitic quartz phyllite (below). Stratification evidently is parallel to S_1 here. The S_2, which is also present, has a later origin and is left out of consideration.

These observations lead to the following generalization: Commonly, the schistosity or the first schistosity parallels the sedimentary stratification.

In chapter 12, we will see that exceptions may be expected to this rule in the cores of macrofolds, as a crestal bend of these probably present folds has never been observed. As the folds have a deformed schistosity, they are younger and, therefore, the crestal schistosity-planes intersecting the bedding may be classified as a special type of S_2.

It is supposed that the schistosity is of metamorphic origin or that in the epizone of Grubermann and Niggli (1924) the muscovite-sericite crystallized with their tabular planes subhorizontally, which is parallel to the bedding-planes.

The schistosity of the crystalline basement of the Dolomites in general is a regional metamorphic schistosity, without large lateral displacements along the schistosity-planes. In the Bressanone region North of the Dolomites, and in the Cima d'Asta and Gosaldo regions South of the Dolomites, the schistosity is still subhorizontal. The present dips are parallel to the dips of the overlying Permotriassic.

It may be concluded that the Permotriassic in these regions was deposited on a crystalline basement with subhorizontal bedding and subhorizontal schistosity. Prior to the Permian, this basement had only been deformed by an E-W directed shortening which in the southern region was accompanied by an upward increasing mass transport to the West. This will be discussed in the following chapter. The second schistosity, which merely represents a fissility parallel to the axial planes of some minor folds, has been left out of consideration.

In the Pusteria and S. Stefano regions, the schistosity as well as the bedding generally show

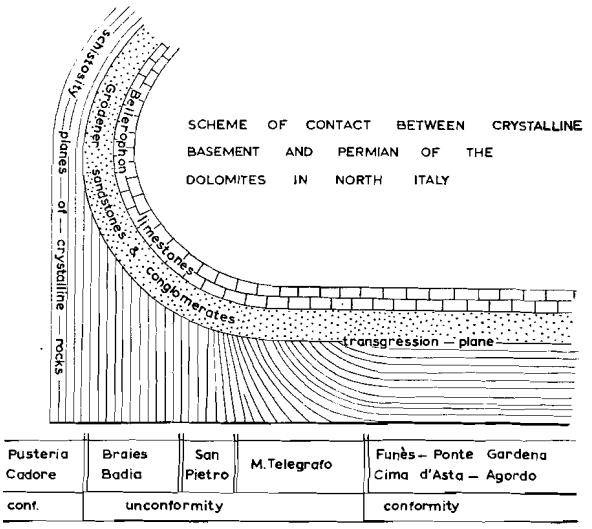

Fig. 1

Scheme of the position of the Permian transgression plane in relation to the underlying schistose rocks. The pseudo-conformity in Pusteria and Cadore originated by Alpine shearing movements along the subvertical pre-Permian schistosity-planes.

steep dips, which have been cut off by the Permian transgression plane. Fig. 1 represents the different attitudes of the latter in relation with the position of the schistosity-planes of the basement.

In the part on tectonics, we will see that the schistose rocks of these regions firstly were folded in major folds causing the steep dips, and secondly were deformed by minor folds which gradually pass into the minor folds of the Bressanone and Cima d'Asta regions. These two phases of deformation are the only ones that can be distinguished. There is no reason to suppose that the subhorizontal schistosity represents another phase indicating lateral displacement along the *S*-planes.

Such a subhorizontal schistosity was called a "load-schistosity" by Daly (1933) who considered the load of the overlying rocks to have caused a flattening in the subhorizontal underlying rocks. As all tabular crystals are about parallel and indications for rotation are not present, it is supposed that the crystals have grown in a subhorizontal plane.

In this connection a separate observation made in the Tauern gneisses of the M. Spico region should be mentioned.

The schistosity of the Tauern gneisses in the M. Spico region is generally subvertical. After the deformations which caused the schistosity and its subvertical attitude, crystallization must have

taken place. This post-kinematic crystallization is the so-called "Tauern Kristallisation". A chief post-kinematic mineral here is biotite, and the new biotites have grown partly parallel to the older schistosity and partly at right angles to it in a subhorizontal plane. This new subhorizontal schistosity obscured the subvertical *S*. The biotites, which developed parallel to *S*, only accentuated this older structure ("Passive Gefügeregelung" after Sander, 1950).

The subhorizontal biotites may be compared with the subhorizontal crystals crystallizing during regional metamorphism. Here also, lateral movements have not taken place as they should be visible as a deformation of the older, mostly still visible, schistosity.

Riecke's principle of orientated crystallization under directed stress (1912) possibly is the best explanation for this sort of schistosity where notable movements within the rock cannot be expected. Is is assumed that the rocks have been subjected to a subvertical principal stress, simply caused by the load of the overlying rocks.

Schistosity is known from other regions. In many cases, the stress field had a subhorizontal principal stress thus causing a subvertical schistosity, in places accompanied by bending of the competent beds in folds. It is generally supposed that the axial planes of folds are at right angles to the direction of principal stress; on account of the parallelism of *S* with these foldplanes, the rule was established that schistosity originates at right angles to the principal stress (Goguel, 1945, de Sitter, 1956, Collette, 1958).

This relation between folding and schistosity confirms the supposition that our subhorizontal *S* has been formed by a subvertical principal stress, as the microscopic texture of our subhorizontal *S* is exactly the same as for instance the subvertical *S* described by Hoeppener (1956) in the Rheinische Schiefergebirge.

However, in the case of schistosity folding, cleavage planes are often shear planes as demonstrated by de Sitter (1956).

No distinction is made between the different sorts of cleavage and schistosity. All these fissilities have been called schistosity.

It is generally supposed that the axial planes of folds have been formed at right angles to the principal stress. We concur with this assumption in the case of symmetrical folds. For asymmetrical folds, the rule is probably not generally applicable.

In a region folded during an orogenesis, two of the principal stresses of the stress field have to be subparallel to the existing topographic surface, this being a free surface. The topographic surface may be regionally considered subhorizontal when the region is compressed from both sides; the principal stress therefore is also subhorizontal. However, highly asymmetrical folds may develop during such compression and axial planes will show a considerable degree of overturn.

Our own example is taken from the Cima d'Asta — Gosaldo region which was folded with folds overturned to the West during Hercynian orogenesis. The photographs 7 and 12 show the overturn of the greater folds of the region. Fig.'s 35-40 of App. I and photographs 8-9 show similar minor folds.

In the latter case the degree of overturn in some instances is such that the axial planes are subparallel to the folded first schistosity.

It is evident that this general overturn cannot be explained by assuming local deviations of the stress field. If the axial planes had developed at right angles to the principal stress, the direction of the latter should dip steeply to the West in the studied region, from Borgo in the West to Agordo in the East. This is an impossibility as the principal stress actually must have been subhorizontal. The overturn will be explained by assuming an upwards increasing mass transport toward the West.

All mentioned schistosities have as a common feature the parallelism of the tabular minerals which are not finely folded.

All minor folding had its origin in a certain well-recognizable phase of Hercynian orogenesis (chapter 18).

The *S* was locally folded; parallel to the axial planes and by preference on the limbs of the small folds, another fissility developed (S_2). This S_2 is clearly illustrated in fig. 2 and e.g. photograph 20.

In fig.'s 3-4 is shown that S_2 is related and restricted to fine folding. This suggests that its origin is restricted to a compressed area with the possibility of upward escape. It may be assumed that the stress in all places of fig. 3 was the same during

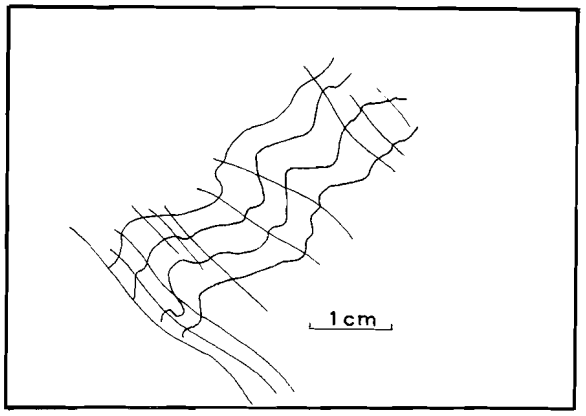

Fig. 2
Example of S_2. Drawn after photograph of boulder.

compression. The cause of S_2-formation in certain places was not a greater stress but a greater possibility of sagging.

In consequence of the lack of a distinct mineralogical banding, the shearing character of the S_2 planes cannot be demonstrated distinctly in most cases. A favourable exception is shown in photograph 23, where a muscovite layer was moved along the S_2-planes, thus proving their shearing character.

It can be concluded that shearing movements took place along the S_2. The compressed and finely folded layers between the schistosity-planes correspond with the "microlithons" of de Sitter (1957).

Hoeppener (1956) also studied examples of S_2. He found that in the Rheinische Schiefergebirge the angle between S_1 and S_2 is about 32° average

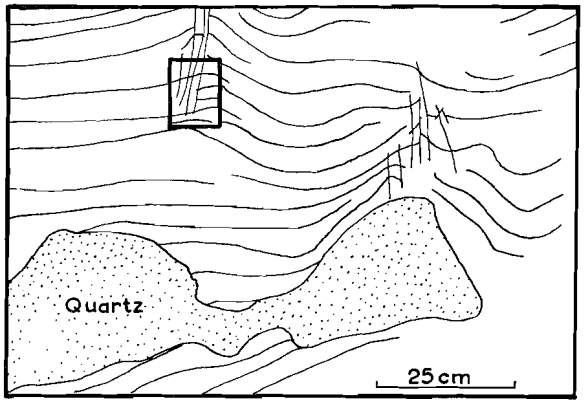

Fig. 3
S_2- formation in anticlinal axial planes. Drawn after photograph of boulder. Fig. 4 is depicted.

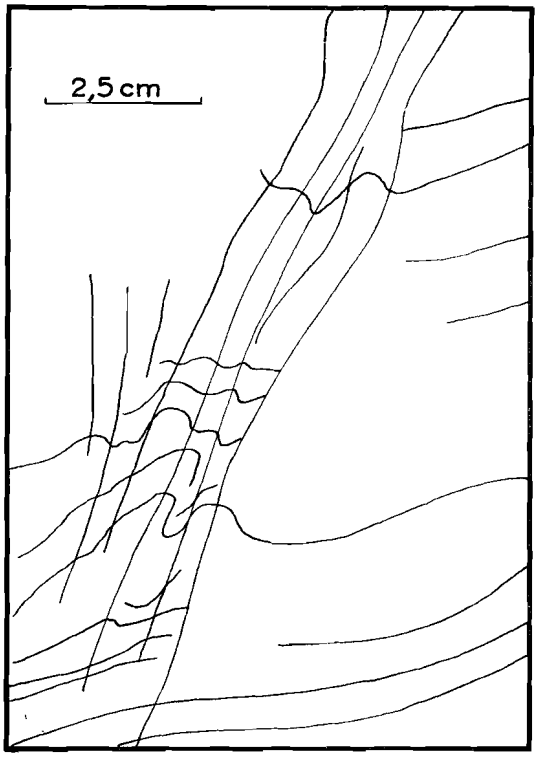

Fig. 4
Detail of fig. 3.

and does not exceed 65°. In our examples of S_2, all angles between S_1 and S_2 are present. The regularity as observed by Hoeppener therefore is not present in the regions studied. In Pusteria, the angle generally is about 90°. In the Cima d'Asta and Gosaldo region, it is mostly small. The S_2 here is parallel to overturned folds. The enveloping contour, which normally represents the unfolded S_1, forms all sorts of angles with the S_2 in the mentioned regions. Measuring the unfolded S_1 by drawing the enveloping contour does not permit to distinguish distinct schistosity groups, which are characterized by a general mean value.

On the other hand, the S_2 has a rather constant attitude. As will be demonstrated, this S_2 may be used as an approximation of the S_1 (chapter 17). This is an advantage as in some places the S_2 character is not visible macroscopically and in such cases the visible schistosity has been called S. Under the microscope, however, it appears to be S_2. It appears that the S and S_2 groups cannot be recognized by statistical methods. This means that the angle between the unfolded S and S_2 is too small as compared to the accuracy obtained by the applied methods.

In conclusion, it may be stated that two sorts of schistosity are present: S_1 and S_2. The S_2 represents shear planes.

In the chapters 10 and 12 we will see that the S' of the Pusteria- and S. Stefano regions have been partially used as shear planes during a later phase of Alpine orogenesis. In both cases, a subvertical isoclinal series of strata was compressed which caused squeezing out of material in subvertical direction. These shear phenomena have been summarized statistically.

It is possible that these later shear movements were accompanied by mylonitization. The quartz phyllite of Pusteria e.g. is partially a phyllonite.

CHAPTER 3

FOLDS OF THE CRYSTALLINE ROCKS

All folds are younger than S. Minor folds are folds, the amplitude of which does not exceed a few meters. Generally, their width is about 1 dm. The amplitude of major folds varies from 100 meters to several kilometers.

Microfolds are only visible under the microscope. Macroscopically, they sometimes resemble ribs. Some photographs of ribs in the outcrop were given by Agterberg (1959). In the present paper, see photograph 4. In thin sections, textures as shown in photograph 20 have been observed. Ribs are a sort of symmetrical microfolds. Asymmetrical microfolds do not resemble ribs in the field.

The shape of the minor folds can be demonstrated by illustrations. Three sorts are used, photographs, sketches after photographs, and sketches of actual outcrops. The latter have been collected in appendix I. These drawings are more or less schematic as topographic irregularities have been eliminated. They all represent cross sections which are about at right angles to the axis of the fold. Every sketch has its own explanation in appendix I, to avoid lengthy explanations in the text. A short summary follows.

The type of minor fold most frequently present is a regular subsymmetrical folding of S. A fold is called symmetrical when its axial plane is at right angles to the enveloping contour which constitutes the surface comprising the crestal lines, and generally representing the original unfolded plane.

When some overturn occurs, the fold is called asymmetrical. These folds are divided into inclined folds and overturned folds. Asymmetrical folds in some cases indicate a regional mass transport whereby the overlying mass has moved in the direction of overturn. An extrapolation from local mass transport of the observed fold to a mass transport of regional dimensions should be made carefully.

Inclined folds probably generally have originated by the same shortening as the adjacent symmetrical folds. When folds originate on the limb of larger folds with axial planes parallel to that of the larger fold, they are inclined without any mass transport.

It is possible (fig. 15 of appendix I) that asymmetrical folds lie on both sides of a vertical plane of symmetry, thus together representing a symmetrical mushroom-shaped fold. The deformation is a shortening without upwards increasing mass transport into a certain direction. It seems that these mushroom-shaped folds by preference occur in quartzitic beds which were deformed more plastically than the quartz phyllites between which they occur. It is assumed that the distance between the limbs of a mushroom fold may be considerable. When in the same bed overturn in opposite directions equally occurs, one may say that the folding shows orthorhombic symmetry. It is caused by a regular compression, without upwards increasing mass transport.

It is concluded that distinct regional mass transport has taken place in the Cima d'Asta, Gosaldo, and M. Spico regions. In the Cima d'Asta and Gosaldo regions, overturned folds are widely distributed. The folds may show a width of several meters, as shown in photographs 7 and 12. All these folds are overturned to the West. In the M. Spico region, the larger folds also show an overturn in the same direction, in this case to the North (e.g. fig. 69 of App. I).

It is assumed that overturned folds with a width of about 10 m represent systematic movements of the overlying mass in the direction of overturn.

Minor folds with an overturn in the opposite direction have been rarely observed in the Cima d'Asta and Gosaldo regions to the East and in the M. Spico region to the South (fig. 65 of App. I). So a single minor fold is no criterion for mass transport. If, however, a considerable number of minor folds are overturned into a certain direction, it may be concluded that a mass transport has taken place in the same direction, because, if all these overturned minor folds belong to mushroom-shaped folds, overturns in both directions would be equally present.

In the case of some minor folds, it seems possible to conclude a direction into which mass transport must have taken place. When the overlying or underlying mass is not folded as in figures 35, 66, 68, and 73 of appendix I, it is certain that a lateral displacement has occurred along the plane between folded and unfolded layers. In such cases, the direction of overturn of these dragfolds also indicates the direction of the mass transport. No exceptions to this rule were observed.

In some cases, the same rock has been folded more than once parallel to the same axis. Interesting examples are given in fig.'s 42 and 43 of appendix I. The S_1 was folded into minor folds with a S_2 parallel to their axial planes. Fig. 43 of App. I shows that this S_2 was also folded. It is remarkable that a mineralogical banding is present parallel to S_2.

Thin layers of a feldspar-mica rock alternate with quartz rock. Microscopically, the feldspar-mica rock consists of albite, muscovite, biotite, and quartz. The quartz rock consists of quartz and some mica.

With d'Amico (1957) it may be assumed that the feldspar crystals belong to the intrusion of the Cima d'Asta tonalite. They are post-kinematic as also shown in figure 47 of App. I. It is assumed that the mineralogical banding originated after the folding which caused S_2 which resembles the flexure zone type of deformation (§ 4 C). It is noted that the feldspar crystals are limited to the flexure zones, whereas the quartz (quartzification?) is found in the quartz phyllite, which was not deformed during the folding process. Possibly the feldspars preferred a somewhat cataclastic rock.

§ 3A *Rôle of the quartz in veins and lenses.*

Quartzveins and quartzlenses acted as competent bodies during folding. Most of the quartzveins were already present when folding commenced. In some places, however, the folds are intersected by quartzveins. The competent quartzveins were folded parallelly (fig.'s 22 and 40 of App. I) whereas the overlying and underlying incompetent quartz phyllite produced schistosity folding. Sander's rule for the width of compression folds ("Regel der Stauchfaltengrösse", 1928) appears to be correct and is shown in fig.'s 22 and 40 of App. I. The thicker quartzveins result in larger folds then the thinner schistosity-beds of the quartz phyllite.

The phenomenon of protection against folding by quartzlenses is demonstrated in fig. 21 of App. I. In the neighbourhood of the lens, the quartz phyllite is not folded.

All these phenomena prove the pre-kinematic character of the greater part of the quartz in veins and lenses. Sander (1925) already observed in the Bressanone region pre-kinematic albite under the microscope. In one case, it appeared possible to prove the pre-kinematic nature of the albite in the outcrop. Fig. 25 of App. I is a sketch of a schistosityplane in which locally albite crystals are present. The folds in the vicinity of these crystals are ribs with a smaller amplitude than the minor folds which developed elsewhere in the *S*-plane. It may be assumed that the large competent albite crystals prevented the development of the minor folds and permitted the development of ribs only.

CHAPTER 4

OTHER DEFORMATION TYPES OF THE CRYSTALLINE ROCKS

The other deformation types of the Crystalline are joints, minor faults and flexure zones.

These features are of minor significance for regional tectonics. They demonstrate the existence of deformations which are negligible in comparison to the deformations indicated by the geometry of the mean *S* and mean minor folds.

§ 4A *Joints.*

Joints are generally present in the crystalline rocks. They appear as cracks with a rather flat surface without indications of movement. For this reason, joints do not participate in the process of kinematics although they are spectacular and are supposed to represent certain stress fields. The time of origin and the character of such stress fields cannot be determined in the crystalline basement of the Dolomites.

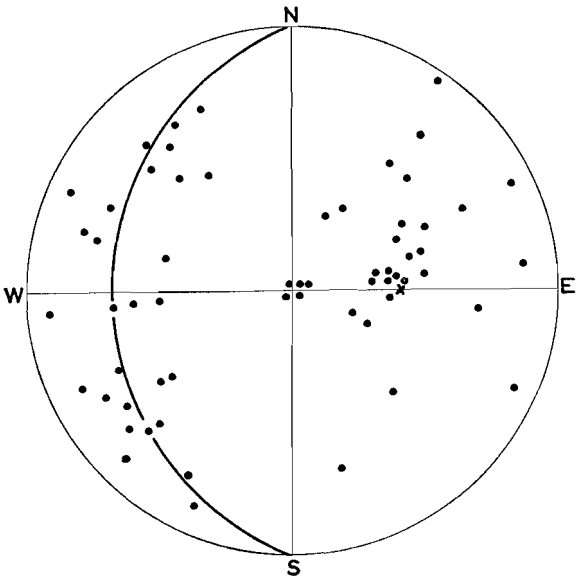

Fig. 5

Pole diagram (Schmidt net, lower hemisphere) of 61 joints in the vicinity of Monguelfo, Pusteria region. For further explanation see text.

Fig. 5 shows 61 poles of joints measured in the neighbourhood of Monguelfo. The minor folds dip about 55° East in this region, whereas the schistosity is subvertical, striking E-W. The relation of the joints to the geometry of m.f. and *S* is evident. Two families occur. One consists of joints which are at right angles to the minor folds (Sander's 010-joints). The other consists of joints parallel to the m.f. (Sander's h0l-joints). The latter family which is distributed around the great circle at right angles to mean m.f. shows a minimum at the place where its joints would be parallel to *S*. Probably, the fissility called *S* also acted the part of joints belonging to the latter family.

The relation between joints and minor folds suggests that the origin of the joints is synchronous with or later than that of the minor folds.

§ 4B *Minor faults.*

Although during the process of minor folding the crystalline rocks were plastical, which prevented faults to originate, still minor faults do occur, which are apparently younger. The net slip generally cannot be determined in the uniform crystalline rocks. Its direction, however, is indicated by the accompanying drag.

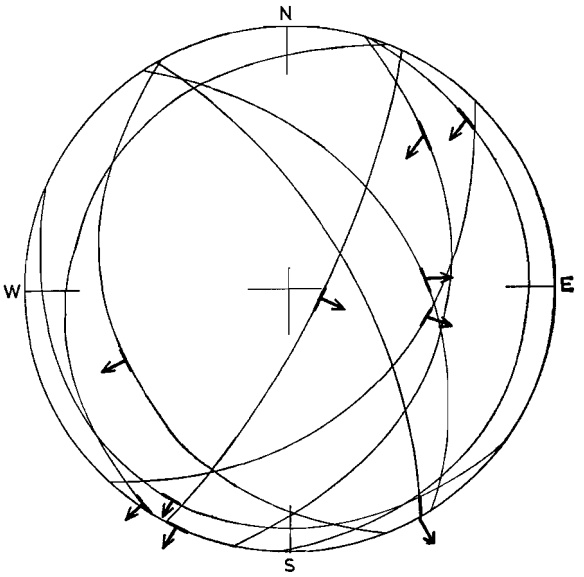

Fig. 6

Diagram (Schmidt net, lower hemisphere) of 10 minor faults from the surroundings of Monguelfo. Arrows indicate the direction of movement of the upper block.

Figure 6 represents ten minor faults from the surroundings of Monguelfo and the western Eggerberg. On the fault planes the direction of net slip has been indicated by an arrow which also gives the direction of movement of the upper block. Two families of minor faults appear to be present. The most important family consists of subhorizontal planes with overthrusting toward the South. Another family consists of eastward dipping normal faults. The last family is probably local, as it has not been observed in other places.

The overthrusting to the South was mapped in the whole Pusteria region, in the Crystalline of the Defereggen Mountains (fig. 83 of App. I), in the Monte Spico region (fig. 84 of App. I), and in the Upper Silurian Limestones of Prato alla Drava (fig. 48 of App. I). These overthrusts also occur in the Permotriassic of the S. Stefano region

(§ 6A).

It is on the basis of these and other results (chapter 12) that all these small overthrusts are assumed to belong so the Alpine orogenesis. They may be considered as an accompanying feature of the general tendency of overthrusting towards the South during the latest phase of Alpine orogenesis.

The complete net slip of all these overthrusts is small and their significance should not be overestimated. Their regional deformation is small in comparison with the other Alpine deformations, which mainly took place along the still existing pre-Alpine *S*-planes.

The frequently present mylonites (phyllonites) probably originated during the Alpine deformations; the *S*-planes, along which movements occurred, may be classified as faults. Their fault nature, however, cannot be determined in the field.

Next to the mentioned minor faults in the surroundings of Monguelfo, other minor faults are present elsewhere. These other minor faults generally have not been measured, as their importance seems to be subordinate to other deformations.

As another example the tectonic fault graben of M. Croce (North of the S. Stefano region) is mentioned as being accompanied by minor grabens (fig. 52 of App. I).

§ 4C *Flexure Zones.*

In all regions flexure zones are present. They consist of two flat flexure planes at a few centimeters distance, between which the rock has been rotated (photograph 13; fig.'s 49, 53, 55, and 56 of App. I). The angle of rotation generally is about 50°. The blocks on both sides of a flexure zone have moved with respect to each other.

Our observations are in agreement with Hoeppener's conclusions on the flexure zones in the Rheinische Schiefergebirge (Hoeppener, 1956).

Flexure zones may occur in two mutually intersecting systems. In this case, they may be considered as an orthorhombic shortening of the schistose rock. The direction of maximal shortening forms equal obtuse angles with the flexure zones seen in a cross section.

The two above mentioned systems of flexure zones have rarely been observed. Where they are present, the angle between the direction of maximal shortening and the schistosity is small (type I, fig. 53 and 56 of App. I).

A single system of flexure zones generally occurs. It is a common deformation type in parts of the Cima d'Asta region and the Gosaldo region.

It was stated that if the angle between the flexure zones and the direction of maximal shortening passes a certain value, the transporting agency of one of the systems is taken over by the schistosity itself. For the rest, a flexure zone parallel to the schistosity cannot originate, as the *S* of the flexure zone cannot be rotated. This concept on lateral compression is depicted in fig. 7.

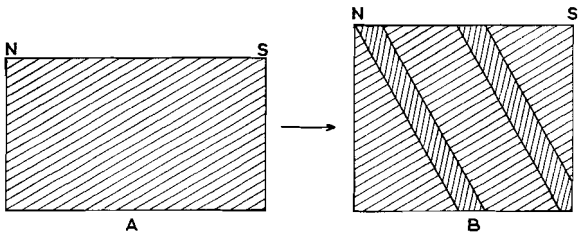

Fig. 7
For explanation see text.

It has been supposed that the geometry of fig. 7B consisting of 30° N dipping *S*-planes and 60° South dipping flexure zones with an internal rotation of 50° has originated from fig. 7A. The areas of both rectangles must be the same. The diagonal of A, which represents the *S*-plane, must be the diagonal of B in its deformed shape.

The shortening in this hypothetical model appears to be 15 %. Photograph 13 shows an outcrop with exceptionally many flexure zones. A comparison with fig. 7 learns that the shortening actually is smaller than given in our present model.

In both cases of one and two systems of flexure zones, lateral compression has been assumed, but it is possible that an original rectangle is deformed into a parallelogram when one system has stronger developed than the other.

Fig. 8 is the pole diagram of 27 systems of flexure zones, measured in different outcrops along the Rivo Conseria West of the Cima d'Asta Complex. Together they form a group wich is about at right angles to the axes of minor folds, and, consequently, at right angles to the schistosity. 23 flexure zones belong to sample region 167 of App. II, the mean *S* and m.f. of this region have been plotted in figure 8. Since 4 flexure zones only

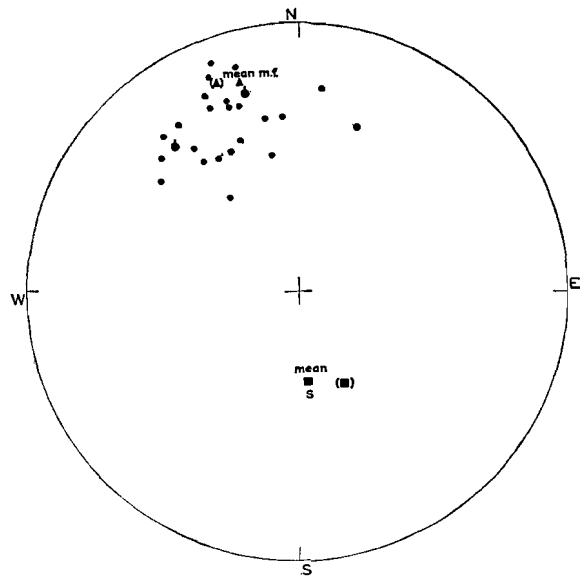

Fig. 8

Pole diagram (Schmidt net, lower hemisphere) of 27 flexure zones along the Rivo Conseria, Cima d'Asta region. Cross strokes indicate two equal poles. Rectangle and triangle represent mean s. and mean m.f. of meas. sample 167; ditto in parentheses, mean s. and maen m.f. of meas. sample 168.

belong to sample region 168, the means of this last sample have been placed in parentheses.

Dealing with joints, is was noted that the plane at right angles to the minor folds probably is a plane of weakness, as in most outcrops the cohesion disappeared along these planes, thus causing a joint system.

The fact that the flexure zones are mostly at right angles to the axes of the m.f. may be caused by weakness along these planes. The photograph 13 gives an example of this situation.

The above conclusions enable us to interpret the southward dipping flexure zones of the Cima d'Asta and Gosaldo regions not as an upthrust towards the North but as a lateral compression of the Crystalline. The time of origin of this compression was probably later than the tilting of the originally subhorizontal *S*-planes in their present northward dipping position. This tilting will be proved to be Alpine (chapter 15), and the flexure zones are also Alpine.

In the other regions, the flexure zones are not so widely distributed. They can be explained as local deformations without regional importance.

An exception is formed by the flexure zones North of S. Candido (Pusteria region), which show an eastward dipping system within the subhorizontal *S*-planes (fig. 49 of App. I). An E-W directed compression is assumed to be present here. Perhaps, the overthrusting movement on the subhorizontal *S* was stronger than the upthrusting movement along the flexure zones. Here, also some minor folds occur with axes that are at right angles to the axes of the common Hercynian minor folds and which have westward dipping axial planes (App. I fig. 50).

This concept implies that one of the latest phases of deformation in the Crystalline North of S. Candido would be an E-W directed compression with an overturn to the East. A sideward escape of the quartz phyllites may be assumed; they have been laterally compressed in the narrow Pusteria Zone during the last phase of Alpine orogenesis. As we will see, the quartz phyllites have been deformed at that time beween the rigid masses of the Austrian Crystalline in the North and the Dolomites in the South. The abrupt widening of the narrow Pusteria Zone toward the Carnian Alps in the vicinity of the S. Candido might have been responsible for this remarkable movement along the E-W line which is at right angles to the general Alpine direction of movement.

The Alpine compression of the Pusteria Zone will be discussed extensively in other chapters. However, no reference will be made to the flexure zones, which are not very frequent and restricted to subhorizontal *S*. The latter are exceptionally scarce in the strongly folded Pusteria region. Their total effect of deformation is negligible as compared to the other deformations.

It was stated before that where the time of origin of the minor faults and of the flexure zones could be established, it appeared to be Alpine. They differ from the earlier deformation types, *in casu* the *S* and the Hercynian m.f. It is considered probable, that the difference is due to the different P,T conditions at which the processes took place.

During Alpine orogenesis, the studied Crystalline was located in the zone of fracture, whereas during Hercynian orogenesis it belonged to the underlying zone of flowage.

However, Alpine folds shown in fig.'s 50, 54, 57 of App. I may also be distinguished. In all these cases, the foldaxes are at right angles to the deformed common Hercynian minor folds, and

TABLE III

Time-stratigraphic table with positions of the legends of the sheets II, III, and V—VI. The numbered series' of these legends are given in the tables IV, V, and VI.

Absolute Age, according to Time-stratigraphic Table of B.P.M. (1958) (in millions of years)	GENERAL CLASSIFICATION			Position of legends: SHEET II	SHEET III	SHEET V & VI
	Quaternary			locally omitted		
2	Tertiary		Pliocene			
16			Miocene			13
						12
30			Oligocene			11
42			Eocene			
			Paleocene			
70	Cretaceons		Upper Cr.			10
			Lower Cr.			9
110	Jurassic		Malm	14	6	8
			Dogger			
			Liassic	13		7
145	Triassic	Upper	Rhaetic	12		6
			Norian	11		
			Carnian	10		
				9		
		Middle	Ladinian	8 / 7		5
			Anisian	7	5	
		L.	Werfenian	6	4	4
190	Permian		Upper Permian	5 / 4	3	3
			Lower Permian	3 / 2 / 2	2	2
	Crystalline basement			1	1	1

the direction of axes corresponds with the direction of Alpine orogenesis. The folds of figs. 54 and 57 of App. I occur in the Cima d'Asta region in the surroundings of the Alpine Sugana Line, which they parallel. Both show cataclastic deformation of the folded rock as a characteristic feature. It demonstrates that these folds belong to the zone of fracture.

CHAPTER 5

STRATIGRAPHY OF THE PERMOTRIASSIC AND YOUNGER SEDIMENTS

The Crystalline is the basement of the Permotriassic and younger sediments.

A clear distinction of Hercynian and Alpine tectonics of the crystalline basement is based on a comparison with the overlying sediments. For this reason, the definitely Alpine tectonics of these sediments will be discussed.

Tectonics of sedimentary rocks are based on stratigraphy, which is well-established in the Dolomites.

The present chapter is restricted to the stratigraphic classification as used on the legends of the various geologic maps, and a summary of the stratigraphy follows.

§ 5A *Classification.*

Some new data are added and a new interpretation is given on the tectonics of five sedimentary areas which are:

1. The surroundings of S. Stefano and Auronzo (Sheet II)
2. The northern boundary of the Permotriassic of the Dolomites between Rio Furcia and Rio di Braies (Sheet II)
3. The western Drauzone (Sheet III)
4. The surroundings of the Brocon Pass (Sheet V)
5. The surroundings of Strigno (Sheet VI).

The stratigraphy of these regions is given in the tables III, IV, V, and VI. Thus, a reasonable geologic map can be compiled, which also gives an adequate picture of the tectonical pattern.

The author has combined certain series of the existing geologic maps, on which a further classification is given.

TABLE IV

LEGEND OF SHEET II

For the greater part according to G. Geyer's map (1902).

14 Jurassic siliceous limestones
13 Red Liassic limestones
12 Rhaetic limestones and marls
11 Hauptdolomit (Norian)
10 Raibler strata of S. Stefano
9 Wengen - and S. Cassiana strata
8 Buchenstein strata with Pietraverde
7 Dolomites of Mendola-Schlern with limestone base and locally a marly intercalation (Anisian - Ladinian)
6 Werfenian strata
5 Upper Permian Dolomites and Bellerophon limestones
4 Permian gypsiferous marls and gypsum
3 Quartz porphyries
2 Grödener sandstones and conglomerates
1 (Crystalline basement)

Additional remarks, taken from Geyer (1902) and Carta Geologica 13

10 also called *Cardita* strata, in this place, consisting of limestones with *Tropites subbullatus*
9 dark tuffs, marls, and limestones
8 siliceous limestones (in some places, fragmentary plant remains), marls, green porphyritic tuffs, and pietra verde = ophiolite
6 greenish-reddish marls and shales (in some cases, sandstones, oolites and limestones)
2 partially oolitic limestones and limestone breccias ("Uggowitzer Breccie") present in the conglomerates.

TABLE V

LEGEND OF SHEET III

6 Mesozoic of the Western Drauzone
5 Anisian strata
4 Werfenian strata
3 Bellerophon limestones and Upper Permian dolomites
2 Grödener sandstones and conglomerates
1 (Crystalline basement)

Additional remarks

6 occurs in separate blocks (chapter 13) of Hauptdolomit, and Rhaetic limestones and marls
At Prato alla Drava also Red Liassic limestones and light-coloured limestones of Upper Jurassic and Lower Cretaceous (?) (Cornelius-Furlani, 1912)
5 Mendola dolomite on limestones base (Merla, 1930), marls (in some places, sandstones, shales and oolites, and limestones)
3 Upper Permian dolomites contain gypsum

TABLE VI

LEGEND OF SHEETS V AND VI, BASED ON S. VENZO'S MAP (1940)

13 Upper Miocene
12 Middle and Lower Miocene
11 Oligocene and Eocene
10 Upper Cretaceous (Scaglia)
9 Lower Cretaceous (Biancone)
8 Upper and Middle Jurassic
7 Lower Jurassic
6 Upper Triassic
5 Ladinian strata
4 Werfenian strata
3 Bellerophon Limestones
2 Grödener sandstone and conglomerates, tuffs
1 (Crystalline Basement)

Additional remarks according to S. Venzo's map (1940)

13 = "Pontian", calcareous conglomerates
12 limestones, marls, in some places lignite containing sandstones and calcareous conglomerates
11 limestones, marls, and limestones
10 red limestones
9 light siliceous limestones
8 light-coloured limestones and oolites
6 Hauptdolomit (Norian) and layered dolomites (probably Rhaetic after Venzo, 1940)
5 Schlern dolomite
4 marls
3 sometimes oolitic

§ 5B *Summary of the Stratigraphy.*

The total thickness of the sedimentary series of the Dolomites is several kilometers. De Sitter (1948) mentions 3½ km at Cortina d'Ampezzo and 5 km in the Pale di S. Martino.

The sedimentary series transgresses over the crystalline basement with clastic sediments. These have been called the Grödener sandstones and conglomerates after Geyer (1902) and van Bemmelen (1957).

The quartz porphyries of Bolzano are found on a basal conglomerate of mainly quartz phyllite components in the western part of the region. At Bolzano, their thickness is more than 1 km. They form an extensive plate-shaped deposit wedging out towards the margins. In the S. Stefano region, they still appear as lenses on the geologic map.

The rate of geosynclinal subsidence was not the same in all places during the deposition of the Grödener. In the Pusteria region its thickness is about 200 m in the West. The thickness increases at S. Candido, where Dal Piaz (1934) mentions about 630 m. To the SE, the thickness decreases to ± 250 m at Padola (section I). At S. Stefano, however, the thickness is 2 km (Sheet II), decreasing to ± 100 m in the eastern part of Sheet II.

The composition of the thicker part differs from that of the thinner part. In general, the thicker part consists of conglomerates + sandstones + shales + quartz porphyries + limestones and limestone breccias, whereas the thinner part consists of sandstones + shales. It is assumed that during the Lower Permian some troughs were formed locally by greater subsidence of the basis and by filling up with coarsely clastic sediments. The shape of these troughs cannot be determined by lack of data. To the West, at S. Stefano, where the Grödener reaches its maximal thickness, it is covered by a relatively thick series of gypsum-containing marls and some gypsum beds. This proves that the trough continued to exist during the Upper Permian, although the great thickness of the gypsum series is probably partially influenced by tectonic causes (chapter 11).

The Bellerophon limestones and Werfenian strata are rather uniformly distributed over the Dolomites.

The great facies heteropy in the Dolomites region begins in the Middle Triassic. The Ladinian consists of reefdolomites which are interfingered with tuffs, porphyries and shales (see stratigraphic tables).

Ogilvie-Gordon (1929) explained the interfingering heteropy at Cortina d'Ampezzo as horst and graben-like structures.

The reefdolomites which form flat and raised areas, and the volcanics which are found in the basins are separated by faults, from which the Ladinian volcanics originated. The basins were filled with volcanics, and reefs could form on top of the volcanics.

A facies heteropy was actually observed in the S. Stefano region. Intraformational faults, formed in Ladinia time, can be expected but have not been observed. However, the paleogeographic pattern of the S. Stefano region indicates a platform and basin structure to have existed during the Middle and Upper Triassic. Fig. 9 shows the location of the Middle and Upper Triassic in the S. Stefano region according to the Italian geologic maps. The above mentioned heteropies are not visible as the Middle Triassic is shaded on the

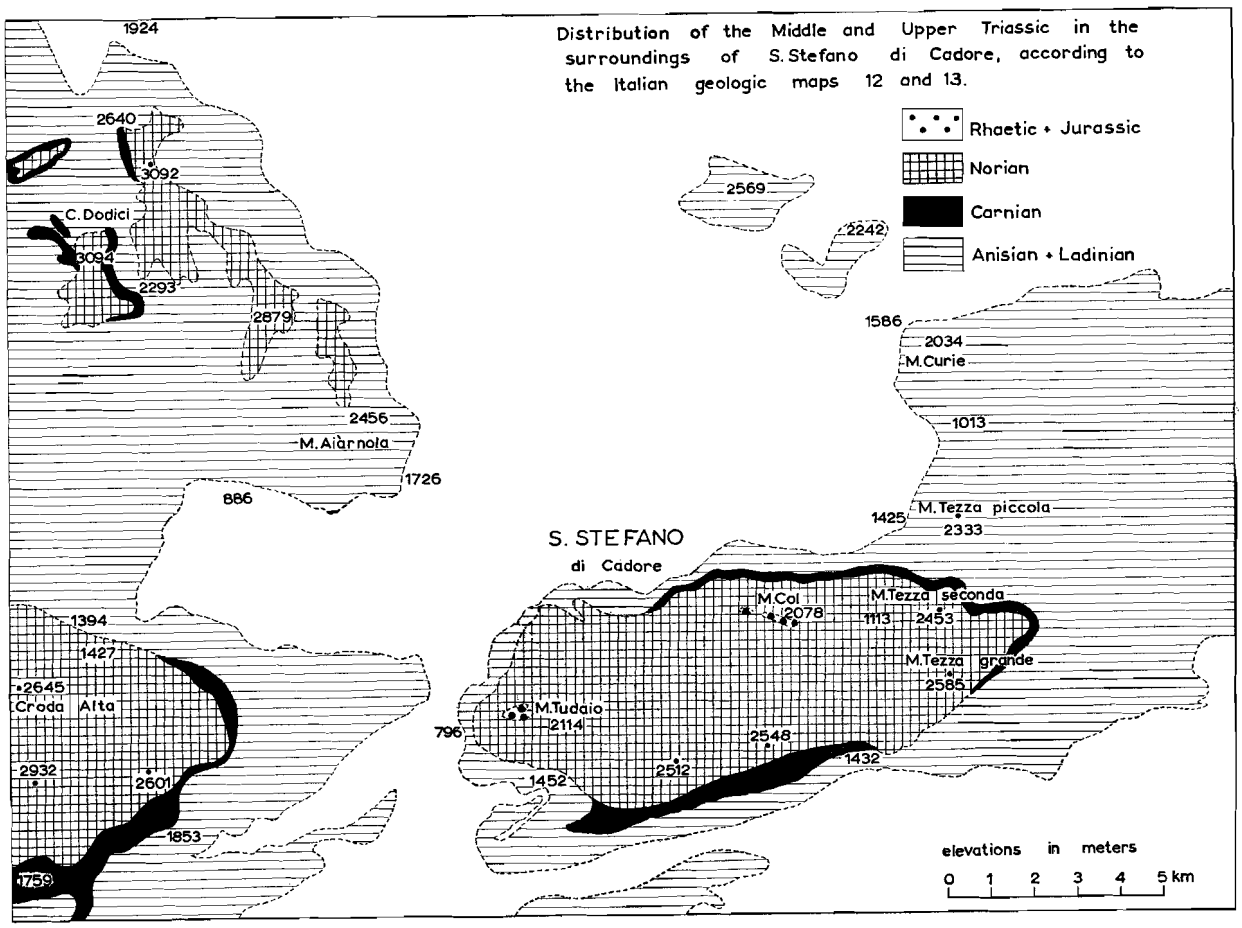

Fig. 9

Remarks: 1) Some (hatched) Schlerndolomite is assumed to be Carnian on the Italian geologic map 12. 2) The hatched zone West of the M. Tudaio is called Norian on sheet II according to Geyer (1902). The position of strata supports Geyers's concept.

maps. A remarkable wedging out of the Middle Triassic appears to be present.

The M. Aiarnola (2456 m), the M. Curie (2034 m), and the M. Tezza piccola (2333 m) consist of Middle Triassic (for the greater part Mendola-Schlern dolomite). On the other hand, the M. Tudaio (2114 m) and the M. Tezza grande (2585 m) consist of Upper Triassic (Hauptdolomit).

The dip of the reefdolomites is slight in the generally basin-shaped occurrences.

It seems permitted to compose two schematic stratigraphic columns from these two groups of mountain summits, which are principally different.

It is assumed that the Middle Triassic of the first group reaches a thickness of 1½ km, as already a thickness of more than 1 km could be observed in the field. The same thickness may be accepted for the Upper Triassic of the second group (see elevations of fig. 9).

Both groups rest on the Lower Triassic. For the northern group, this is the normal picture found in the Dolomites. In the southern group, however, the Middle Triassic appears to have wedged out almost entirely.

Following Geyer (1902), it is supposed that West of the M. Tudaio the Norian Hauptdolomit rests on the Werfenian (Sheet II, fig. 9). The contact is probably a fault plane, but the autochthonic nature of the Dolomite masses in general and of those South of the M. Tudaio mass in particular contradict an overthrust of many kilometers which might explain a tectonic wedging out in post-triassic time (see also chapter 19). The southern group of mountain summits is surrounded by a zone of Lower Triassic, covering a few hundred meters of the stratigraphic column.

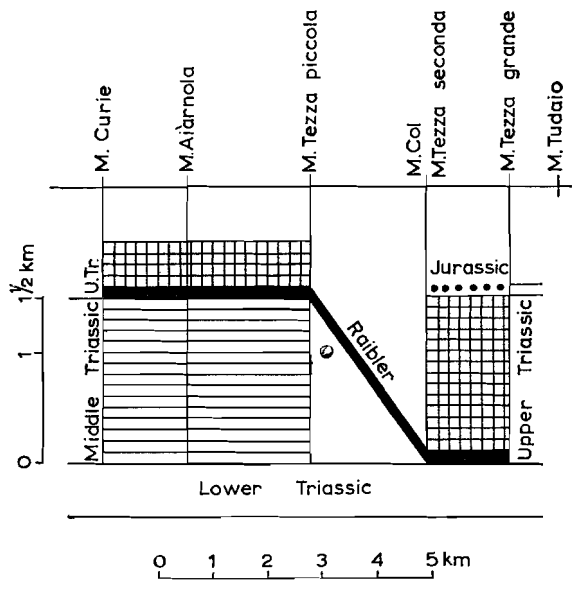

Fig. 10

Idealized N-S section across the S. Stefano region, showing the wedging out of the Middle Triassic. The mountain summits have been projected at right angles to the N-S line.

Fig. 10 shows an idealized section in which both groups are represented schematically. It seems probable that the Middle Triassic wedges out from 1½ km at an E-W line over the M. Tezza piccola to almost zero at an E-W line over the M. Col - M. Tezza seconda.

Two explanations are possible. In the first place, it is possible that the proposed stratigraphy is incorrect; in the second place, it may be assumed that the M. Tudaio mass represented a platform during the Middle Triassic upon which practically no sedimentation took place.

The first seems the least probable, as the lower part of the Upper Triassic consists of the characteristic fossiliferous Raibler strata (Carnian). This Raibler occurs in the surroundings of the Cima Dodici, containing the Carnian index fossil *Myophoria kefersteini* MÜNSTER (Carta geol. Ital. 12) as well as in the surroundings of the M. Col, etc., with the Carnian index fossil *Tropites subbullatus* HAUER (Geyer, 1902). Both fossils are depicted by Kayser-Brinckmann (1954, p. 171).

The Raibler strata with *Tropites subbullatus* form the base of the M. Tudaio dolomite mass which, consequently, cannot be older than Carnian-Norian. Moreover, the M. Tudaio dolomite was also covered by Rhaetic and Liassic deposits (Sheet II).

During the whole Middle Triassic, the M. Tudaio area probably existed as a platform. Fig.'s 9 and 10 prove that the Middle Triassic diminishes rapidly in thickness near the northern boundary of this platform. An E-W fault may be assumed, the intraformational nature of which probably causes the lack of field evidence indicating its existence.

The thickness of the Middle Triassic on the platform increases toward the West, although fig. 9 shows that it is still abnormally thin in the vicinity of the Croda Alta.

In conclusion, it may be stated that the variations of thicknesses during the Triassic suggest a horst and graben structure of the South Alpine geocyncline on a larger scale than the horst and graben structure as it was proposed by Ogilvie-Gordon on the basis of the existing facies heteropy during the Ladinian.

Jurassic, Cretaceous, and Tertiary strata were only found in the Cima d'Asta region (Sheet V) and the Strigno region (Sheet VI). Sedimentation seems to have been rather continuous until the Miocene, apart from a stratigraphic hiatus between the Scaglia (Upper Cretaceous) and the Upper Eocene (Venzo, 1940).

This continuous sedimentation in the Southern Limestone Alps is in contrast to the presence of several unconformities in the Northern Limestone Alps (e.g. those before the Cenomanian and Gosau transgressions) indicating large-scale orogenesis prior to the Tertiary.

In the Strigno region the first unconformity indicating orogenesis does not occur before the Middle-Late Miocene (Tortonian). On Sheet VI, the M. Lefre nappe rests upon Tortonian sediments which in the southern part consist of conglomerates with calcareous and dolomitic components. A similar conglomerate occurs NW of the M. Lefre, in between the Werfenian and the Norian strata (Sheet VI and Section V). If this conglomerate is Tortonian in age, too, it may be assumed that it has been deposited unconformably on the Werfenian beds, prior to being overthrusted by the M. Lefre nappe (chapter 16).

This interpretation is given in section V. Two other occurrences of Tortonian sediments are located in the NE corner of Sheet VI, next to Jurassic. The contacts, however, are not exposed, and it is not known whether they are faults or transgres-

sion planes. The Tortonian occurrences South of the M. Lefre and West of the M. Civeron may rest on Werfenian limestones and marls and that of Tomaselli on Grödener. The other exposed Miocene (Strigno, Carzano, Telve) is older.

Our explanation of the contacts being transgression planes seems better acceptable than Venzo's explanation (1940).

Venzo does not assume such an unconformity below the Tortonian series. He supposed that the Tortonian sediments are the top of a complete stratigraphic series (Permian-Miocene), and the exposed downthrown block of four tectonic graben structures.

It is unlikely that in all these grabens the exposed part of the downthrown block, by coincidence, would consist exclusively of Tortonian beds and not of other Tertiary and Mesozoic. This would be expected in the case of a normal sequence of series, the more so as the exposed part of the blocks next to Venzo's downthrown blocks in fact consists of different series (Grödener, Werfenian strata, and Jurassic).

After this summary of the stratigraphy, we may end the first part with a short description of the deformation types which have been observed in the outcrops of the Permotriassic and younger sediments.

CHAPTER 6

DEFORMATION TYPES OF PERMOTRIASSIC AND YOUNGER SEDIMENTS

§ 6A *Folds and Faults.*

Bedding in carbonate rocks may be indicated by massive layers, which might be a tectonical accentuation of an originally sedimentary anisotropy in the massive layer itself or in adjacent strata.

The folds of the Permotriassic are more or less concentric and are related to movements along the bedding planes. Folds occur in layered rocks only. In the massive quartz porphyries of Bolzano and the massive Triassic dolomite reefs of the Dolomites, folding is negligible, whereas rather strong folding indicating mobility is present in intermediate stratified rocks.

Next to folding, faulting constitutes another type of deformation in sedimentary rocks. Faults may also occur in massive rocks. They are frequently accompanied by mylonitization zones. On the attached geologic maps only faults are shown which apparently cause stratigraphic throws.

The larger faults may be accompanied by minor faults, which may also occur independently. Fig. 91, 93, and 94 (App. I) show respectively small overthrusts, a normal fault and a wrench fault. Fig. 93 (App. I) belongs to a system of minor faults which could not be connected to larger tectonical deformation types. It represents dipping normal faults in the studied northern part of the Permotriassic of the Dolomites in Pusteria (sheet III). The eastern block is downthrown. The particular folds and faults will be discussed under the regional tectonics (part III).

It is probable that folds are formed at right angles to the direction of principal stress. Generally, the principal stress is originally parallel to subhorizontal bedding. But during refolding, new foldaxes also form a plane at right angles to the probable direction of principal stress. In this last case, the principal stress is not parallel to the beds. The possibility remains that internal or other conditions of the mobile material cause folds which are not at right angles to the direction of principal stress.

The folds are symmetric and asymmetric. The latter are predominant. Inclined and overturned folds are present. Transport of the overlying layers during folding is generally the cause of overturned folds. The axial plane is probably not at right angles to the direction of principal stress; however, the foldaxis is perpendicular to the direction of principal stress. Major asymmetric folds are frequently accompanied by upthrusts (section II). Minor asymmetric folds are not accompanied by faults.

When a certain degree of overturn of folds can be observed, it is concluded that an upwards increasing mass transport in the direction of overturn took place.

To determine whether a movement belongs to an overthrust or to an underthrust, it is required

Photograph 1
(grid co-ordinates 793-826; photograph azimuth N)
Eastward dipping minor folds in quartz phyllites of the Monguelfo syncline, Pusteria region.

Photograph 2 (206-767; N75°E)
Subvertical minor folds in quartz phyllites. North of S. Martino in Badia, Bressanone region.

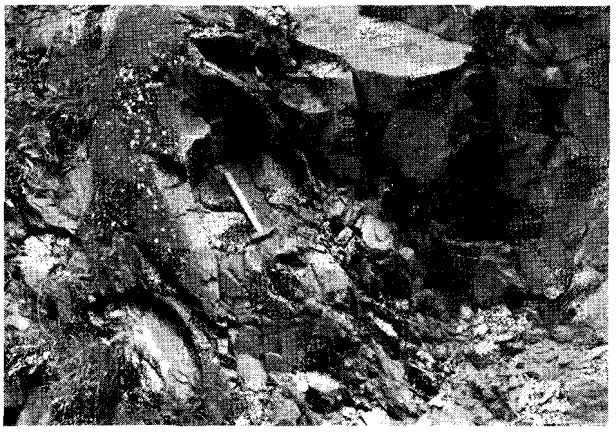

Photograph 3 (208-756; S80°E)
Minor anticline. North of S. Martino in Badia, Bressanone region.

Photograph 4 (208-758; N)
Ribs, parallel to the eastward dipping Hercynian minor folds, and crossfolds at right angles to the ribs. This type of crossfolds seldom occurs in all crystalline rocks studied, and is not given in appendix II. North of S. Martino in Badia, Bressanone region.

Photograph 5 (245-866; N60°E)
60° East dipping m.f. in stratified limestone of Brunico, Bressanone region. The parallelism with the m.f. of the Hercynian folded quartz phyllites indicates a pre-Hercynian age of the limestone.

Photograph 6 (792-826; N40°E)
Plastic folding of quartzitic phyllite of the Monguelfo syncline (p. 14 of fig. 11), Pusteria region.

Photograph 7 (090-140; N10°W)
Westward overturned larger fold of Calmandrino quartz phyllites, Cima d'Asta region.

Photograph 8 (084-137; N35°W)
Westward overturned minor folds of Calmandrino quartzite, Cima d'Asta region. The axial planes parallel a secondary schistosity.

Photograph 9 (298-244; ± SW)
Photograph by M. Freudenthal, 1959
Boundary plane between green phyllite (upper side) and graphitic phyllite (lower side). S_1 parallels sedimentary banding, and is intersected by a gently North dipping S_2 with westward overturned minor folds. NE of Gosaldo.

Photograph 10 (038-597; N15°W)
Southward overturned minor folds in Werfenian beds North of Auronzo, S. Stefano region (case 3 of table VII).

Photograph 11 (018-578; E)
Overthrust flexure with southern overturn in Werfenian beds of S. Stefano region (case 3 of table VII).

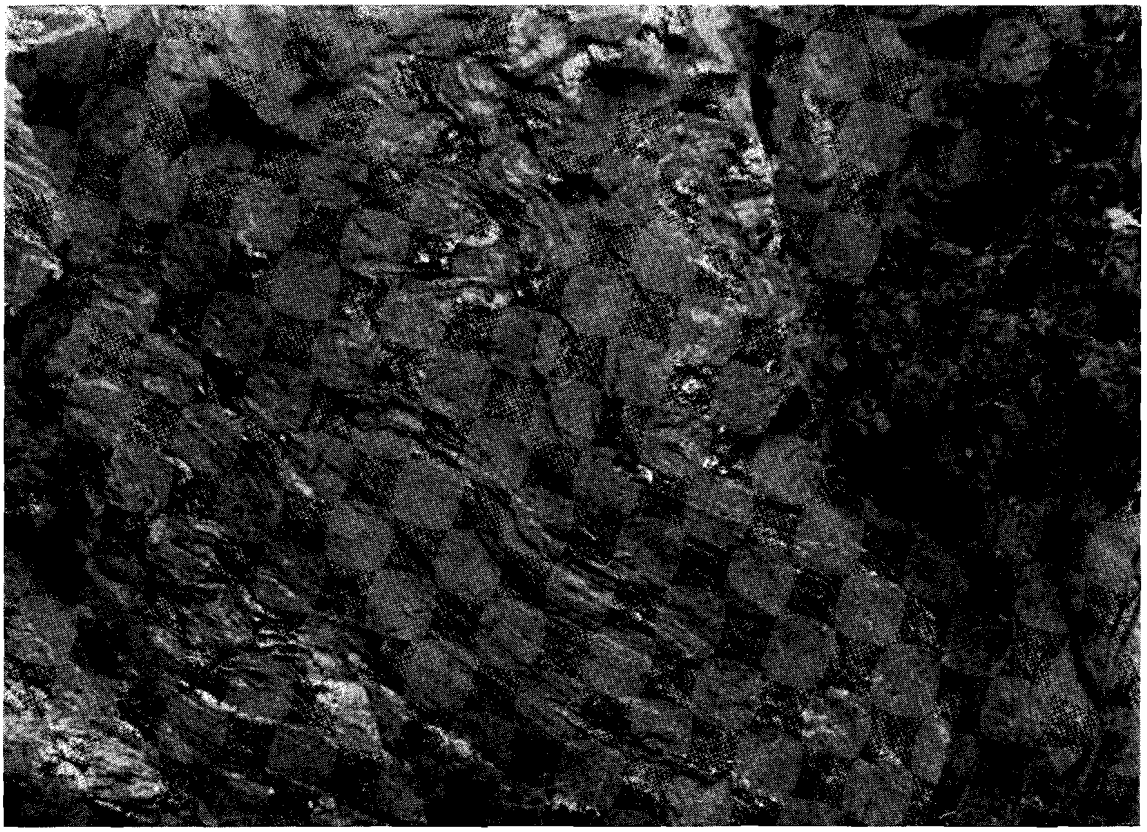

Photograph 12 (295-227; ± N)
Photograph by M. Freudenthal, 1959
Westward overturned larger fold with S_2 parallel to axial plane. ESE of Gosaldo.

Photograph 13 (294-227; N70°E)
Photograph by M. Freudenthal, 1959
Flexure zones at right angles to North dipping *S*-planes. For further explanation see text. ESE of Gosaldo.

Photograph 14 (059-561; N45°E)
Origin of a southward overturned minor fold in Werfenian beds of S. Stefano region (case 4 of table VII).

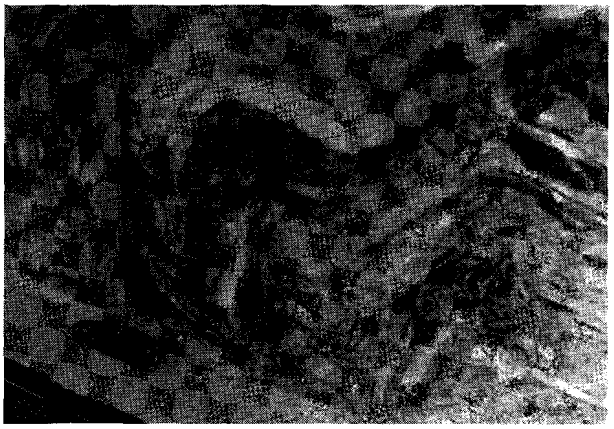

Photograph 15 (058-554; N60°E)
Subsymmetrical minor folds with steeply East dipping axes of the southern limb of the Werfenian syncline along the F. Ansiei, South of Villapiccola, S. Stefano region (case 5 of table VII).

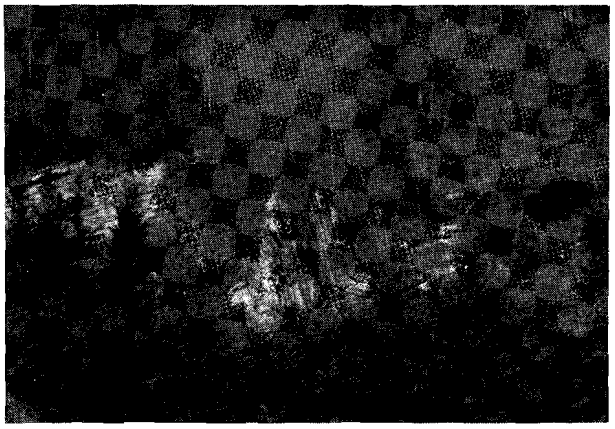

Photograph 16 (220-731; S65°W)
Northward overturned fold in Bellerophon limestones South of S. Martino in Badia, Bressanone region (case 10 of table VII).

Photograph 17
(158-287; ± E)
Northward overturned folds in Bellerophon gypsum beds North of S. Martino di Castrozza, Cima d'Asta region (case 11 of table VII).

Photograph 18 (792-827; enlargement 27½ ×)
Green phyllite from core of Monguelfo syncline, Pusteria region (p. 6 in fig. 11; s. 1 of table II). Albite porphyroblasts with opaque grains included; matrix of chlorite and albite; muscovite-chlorite aggregates indicating schistosity. The latter is intersected by some muscovite porphyroblasts.

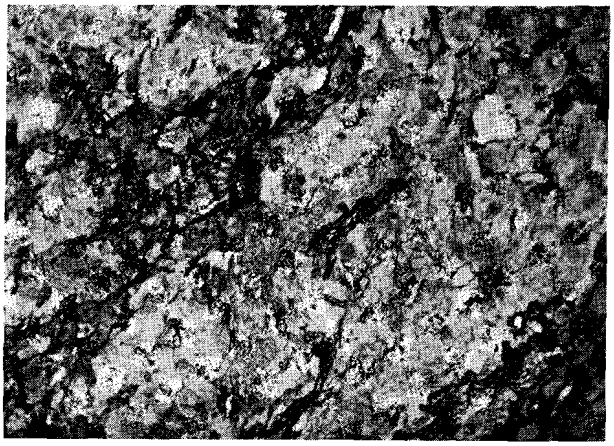

Photograph 19 (794-791; 21 ×)
Green phyllite from the vicinity of Braies, Pusteria region (s. 9 of table II). Coarse albite crystals; biotite indicating schistosity. Further some quartz, calcite, tremolite needles, and clinozoisite grains.

Photograph 20 (850-831; 14 ×)
Quartz phyllite with microfold. Planca di Sotto, Pusteria region (s. 8 of table I). S_1, indicated by muscovite; S_2, subparallel to axial plane. Some quartz augen.

Photograph 21 (973-793; 27½ ×)
Quartz phyllite with crumpled schistosity. Rio di Scalères, Bressanone region (s. 13 of table I). Poikiloblastic garnets with kelyphitic border of chlorite.

Photograph 22 (019-687; 21 ×)
Probably sedimentary boundary plane between muscovite quartzite (upper side) and quartz phyllite (lower side). South of Funès Line, Bressanone region (s. 15 of table I). The S_1 is indicated by muscovite and parallels stratification; intersected by S_2 with a more acute angle in the quartz phyllite. The latter shows a secondary mineralogical banding (local quartzification?).

Photograph 23 (287-223; 38 ×)
Graphitic phyllite of V. dei Molini, Gosaldo region. The S_1 is indicated by muscovite. Displacements of a S_1-parallel muscovite layer indicates shearing movements along the S_2-planes.

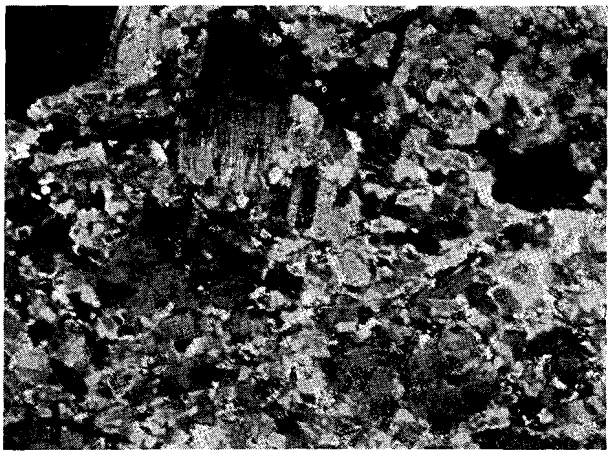

Photograph 24 (152-022; 14 ×; × nicols)
Tauern tonalite gneiss, type IIa, M. Spico region (s. 4 of fig. 91). Microcline, locally twinned or zoned plagioclase, quartz, and some biotite and muscovite.

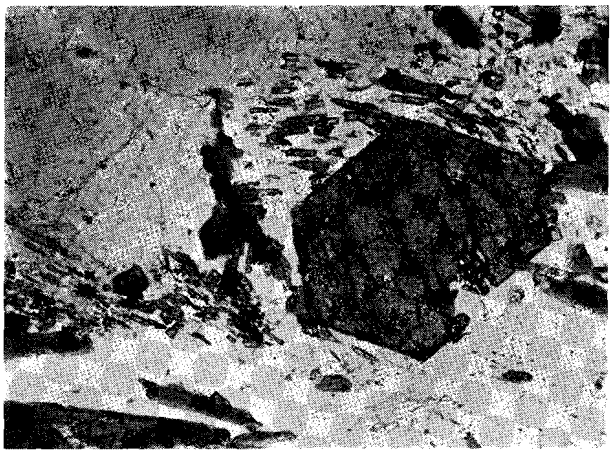

Photograph 25 (173-038; 27½ ×)
Tauern tonalite gneiss, type IIs, M. Spico region (s. 9 of fig. 91). Garnet, biotite, and sillimanite "trains".

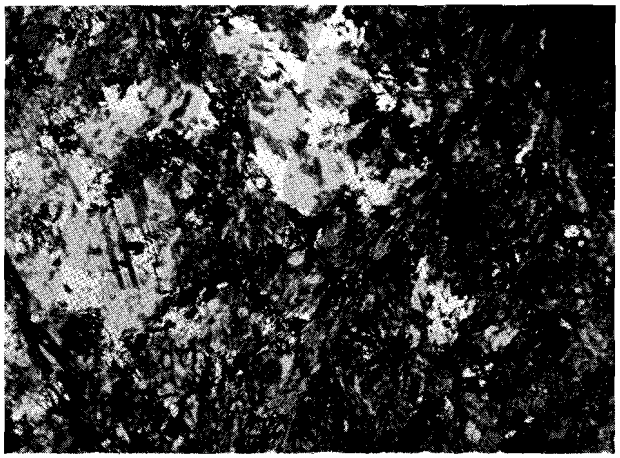

Photograph 26 (124-015; 14 ×; × nicols)
Amphibolite North of Lappago, M. Spico region. Green hornblende and zoned plagioclase augen.

Photograph 27 (244-011; 14 ×; × nicols)
Rieserferner augen-gneiss North of Campo di Tures, M. Spico region. The augen consists of a microcline, albite, and quartz aggregate. Biotite indicating schistosity.

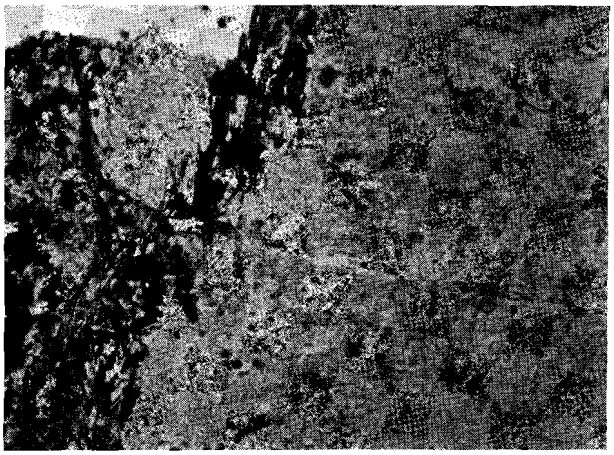

Photograph 28 (213-980; 27½ ×)
Rieserferner augen-gneiss West of Molini, M. Spico region. Border of an albite augen. The dark mineral is biotite.

Photograph 29 (230-986; 21 ×)
Dyke gneiss West of Molini, M. Spico region. (The schistosity is indicated by macroscopically parallel biotites.) Part of coarse albite crystal with inclusions of somewhat orientated muscovite, and opaque minerals. The resemblance with photograph 28 supports a metasomatic origin.

Photograph 30 (227-985; 21 ×)
Dyke gneiss from the core of an open anticline West of Molini, M. Spico region (see fig. 92). The schistosity is indicated by muscovite and elongated epidote crystals. The planations of these minerals seem to intersect each other.

Photograph 31 (227-985; 27½ ×; × nicols)
Leucocratic dyke from the same outcrop as photograph 30 (see fig. 92). Coarse quartz and albite crystals. No marked schistose structure.

to have a fixed point outside the deformed area. In some cases, it will be possible to prove the true nature of an overthrust movement indicated by the overturn (chapter 19).

For the present, we have collected all systems of overturns by asymmetric folds, up- or overthrusts and subhorizontal flexures in the regions studied. The last deformation type (photograph 11) seldom occurs but shows the mass transport clearly.

The following table is a summary of our illustrations of asymmetric folds.

TABLE VII

Asymmetric folds of 11 mapped areas.

1) *S. Stefano region:* Padola - Lago Cestella
SW - W overturn
See section I. The Permian is overturned as a whole; within the gypsum, folds with an overturn to SW - W occur.

2) *S. Stefano region:* Valle Ostera
W - NW overturn
Within the Werfenian strata, some folds occur. Dip of axial plane of four folds: 45°, 60°, 45°, and 35°.

3) *S. Stefano region:* Auronzo - M. Agudo
S - overturn
Section II. Two major anticlines with thrust faults.
Photograph 10, accompanying minor folds.
Photograph 11, overthrust flexure.

4) *S. Stefano region:* Werfenian beds along F. Piave NW of M. Tudaio (Sheet II)
S - overturn
Fig. 89 of appendix I. Some minor folds. (The minor fold of photograph 14 probably belongs to this system too.)

5) *S. Stefano region:* F. Ansiei, South of Villapiccola
Flexures with vertical axis and South-moved eastern block.
Sheet II, chapter 11.
The flexures are accompanied by symmetrical minor folds (photograph 15, and fig. 90 of appendix I).

6) *S. Stefano region:* Rio Giao
Minor flexures with vertical axis and West-moved northern block.
Fig. 's 87 and 88 of App. I.

7) *Pusteria region:* Northern boundary of Permotriassic of Dolomites between Rio Furcia and Rio di Braies
S - overturn
Sheet III. Bedding planes are locally overturned.

8) *Pusteria region:* ditto
Sheet III. Flexures with vertical axes and South-moved eastern block. The flexures are accompanied by symmetrical minor folds (chapter 13).

9) *Western Dolomites:* Funès Line, etc. (chapter 19)
S. Martino in Badia
N - overturn
Photograph 16.

10) *Cima d'Asta region:* S. Martino di Castrozza, Rolle Pass
N - overturn
Photograph 17. Major and minor folds in Grödener - Anisian strata.

11) *Cima d'Asta and Strigno region:* Sugana Line.
S - overturn
Sections III, IV, V, and VI. Overturned syncline with accompanying minor folds and faults.

The first six examples of table VII are in the S. Stefano region with its complicated tectonics.

It has been stated that mass transport is mostly indicated by overturn. But in some cases, blocks moved independently into a certain direction. This also is a mass transport with internal deformation, resulting in wrench faults and flexures with a vertical axis in the border zone of the independent block. Case 5 and 6 may be explained in this way.

§ 6B *Other Minor structures.*

Subvertical cleavage is locally present in the Scaglia marls and Biancone limestones (fig. 92 of App. I). The intermediate distance between the cleavage planes amounts to some mms and some cms respectively. The phenomenon may be caused by compression at right angles to this cleavage.

PART II

General Methodology

Methodology is a method to arrange various data and observations in an orderly fashion.

The methodology will be treated in two parts. The first and general part (the present Part II), consisting of three chapters, is a general discussion. In the second part (Part III), the methods applied will be discussed in relation to the tectonics of the studied regions.

In the preceding chapters, the crystalline and the sedimentary rocks together with their minor structures have been discussed. Conclusions on the kinematics were based on local structures as observed in the field.

The purpose of this thesis is to interpret the kinematics on a regional scale in order to visualize the process of deformation.

Kinematics are based on geometry. Firstly, the geometrical pattern of the whole region has to be composed from individual observations. It appears that tectonic features as schistosity and minor folds are more or less strongly dispersed around the mean value. The first two chapters of the part "General Methodology" are based on this statement. The third chapter deals with the variation of the mean of a population of tectonical phenomena.

The dispersion around the mean value is due to many causes, and the shape of the frequency curve in an ideal case represents a Gauss curve. From a regional point of view, this dispersion is a disturbing factor which must be eliminated. The method of pole diagrams cannot be applied to many of our diagrams, because the dispersion is too strong. At the other hand, students of paleomagnetism determine the mean direction of magnetization by calculating. This method of calculating the mean values can always be used and has the advantage of all measurements equally contributing to the mean value. It is a time consuming method. As we are dealing with about 500 mean values, a method is required, which is accurate and readily applicable.

For presenting the methods for determining mean values and dispersions an example will be discussed comprehensively. This example comprises the 35 axes of minor folds from a number of outcrops in the quartz phyllites North of Monguelfo. The choice of this example may be called aselective.

CHAPTER 7

METHODS FOR CALCULATING THE MEAN VALUE AND DISPERSIONS OF A POPULATION OF TECTONICAL ELEMENTS

These methods apply to 35 minor folds at Monguelfo, Pusteria region.

Fig. 11 gives the position of 38 outcrops of quartz phyllite. These observation points are distributed at random throughout the mapped region.

This quartz phyllite shows a schistosity and minor folds. The attitudes of these features have been measured in these 38 places (see table VIII). It is assumed that these measurements are representative for all quartz phyllites in the mapped region.

§ 7A *Populations and Samples of measurements.*

In the tectonical phenomena, populations may be distinguished. A population or family is the collection of all tectonical elements scattered around a distinct mean. A given set of measurements is interpreted as a sample taken at random from the population. The sample mean X is given by $X = \frac{\sum_{i=1}^{n} x_i}{n}$ where x_i is a single value and n

is the number of observations. The sample dispersion $S = \sqrt{\frac{\sum_{i=1}^{n} (X - x_i)^2}{n}}$.

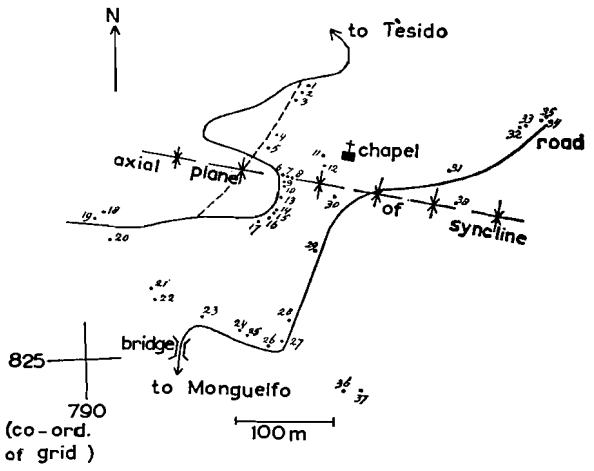

Fig. 11

Map with 38 observation points from the surroundings of Monguelfo. For explanation see text.

As the quartz phyllite may continue towards depth, the population actually consists of so many elements that the measurements sample only represents a very small part of the population. The frequency curves of the sample indicate the nature of the population.

A single or a few measurements are not conclusive for determining the dispersion of the population. The degree of representativeness may be determined accurately by statistical formulas.

The mean of the population, M, is estimated from the sample mean, X, or $M = X$. The dispersion of the population

$$\sigma = \sqrt{\frac{\sum_{i=1}^{n} (X - x_i)^2}{n-1}}.$$

We see $\sigma = S \cdot \sqrt{\frac{n-1}{n}}$, and therefore $\sigma > S$.

In general, a sample is considered representative when another sample of the same size from the same sampling region has about the same mean and the same dispersion.

In our maps the accuracy of the population mean, which is estimated from the sample mean in a certain place, is also compared for checking with the adjacent means. The mean may vary gradually within a certain region and a certain mean is intermediate between two adjacent means. A large deviation indicates the samples to be too small. In our samples, large deviations do not occur, thus indirectly proving that the samples are truly representative.

Although the studied Crystalline is rather uniform, the quartzites are better exposed than the phyllonites. More measurements can be made in harder rock (quartzites). As the dispersion in this rock may be different from that in softer rock, the combined dispersion is not representative for the population. However, the mean does not vary, unless different rocks in the same region have different means.

Different dispersions in different rocks have not been proved to exist in a statistical way. Yet the presence of some indications is suggested. In one and the same outcrop of a soft phyllite with little quartz, many strongly dispersing directions of minor folds occur, and each of which may vary its attitude within a meter. Such differences cannot be laid down statistically, which means that, if they do exist, their influence is smaller than the accuracy of the used statistical methods.

Most outcrops occur along brooks, and may be continuously exposed for several kilometers. The direction of the brooks generally intersects the direction of strike of the schistosity and all types of rocks are exposed, which avoids a topographical selection of outcrops.

§ 7B *Mutual Dependence of adjacent measurements.*

A minor fold generally has the same attitude as an adjacent minor fold. This means that a sample of a population may contain mutual dependent values, which by their number suggest an accuracy of the mean which actually does not exist. As mentioned, this accuracy is inversely proportional to the square root of the number of values.

The values of mean and dispersion of a sample, however, do not change when the values of the independent samples are combined with those of intermediate and dependent values.

It may be assumed that the dependence of one value with respect to another is negligible when the mutual distance passes a certain critical value which is determined by a certain criterion.

Dealing with the mutual dependence of concentrations of essays of adjacent ore samples, the

TABLE VIII

The *S*-planes and minor folds of 38 observation points from the surroundings of Monguelfo (see fig. 11). (Strikes and azimuths are given without the magnetic correction of —2°.)

number of observation point	co-ordinates of the grid	S - plane (33)	δ = rake of m. f. (30)		minor fold (35)			x from 91°-54°	angle with V	angle with E	angle with S	direction cosines		
				x_δ	$\gamma - \alpha$	x_γ	x_α					V	E	S
1	792—827	270°— 90°	130°	6°	90°—50°	0°	— 3°	4°	40°	50°	90°	0,766	0,643	0,000
2		270°—115°	120°	4°	126°—52°	36°	— 1°	21°	38°	60°	69°	0,788	0,500	0,359
3		270°—100°	130°	6°	101°—49°	11°	— 4°	9°	41°	50°	83°	0,755	0,643	0,122
4		270°— 90°	120°	4°	90°—60°	0°	7°	6°	30°	60°	90°	0,866	0,500	0,000
5		255°—110°	120°	4°	105°—55°	15°	2°	9°	35°	56°	82°	0,819	0,559	0,139
6		310°— 90°	120°	4°	90°—60°	0°	7°	6°	30°	60°	90°	0,866	0,500	0,000
7		280°— 90°	100°	24°	90°—80°	0°	27°	26°	10°	80°	90°	0,984	0,174	0,000
8		240°—120°	120°	4°	101°—49°	11°	— 4°	9°	41°	50°	83°	0,754	0,643	0,122
9		280°— 90°	120°	4°	90°—60°	0°	7°	6°	30°	60°	90°	0,866	0,500	0,000
10		285°— 85°	125°	1°	98°—55°	8°	2°	5°	35°	56°	85°	0,818	0,559	0,087
11		240°—115°	130°	6°	96°—52°	6°	— 1°	4°	38°	52°	86°	0,787	0,616	0,070
12		270°—100°	135°	11°	100°—44°	10°	— 9°	12°	46°	45°	83°	0,664	0,707	0,122
13	792—826	280°— 70°	130°	6°	78°—46°	—12°	— 7°	11°	44°	48°	99°	0,678	0,669	—0,157
14					90°—60°	0°	7°	6°	30°	60°	90°	0,866	0,500	0,000
15					80°—55°	10°	2°	6°	35°	56°	96°	0,819	0,559	—0,104
16		280°— 70°	90°	34°	10°—70°	—80°	17°	37°	20°	86°	110°	0,940	0,070	—0,342
17		280°— 85°	150°	26°	97°—30°	7°	—23°	24°	60°	30°	84°	0,500	0,866	0,104
18	790—827	285°— 70°	124°	4°	74°—54°	—16°	1°	10°	36°	55°	100°	0,808	0,574	—0,174
19		270°— 80°	110°	14°	64°—68°	—26°	15°	18°	22°	70°	100°	0,927	0,342	—0,174
20	790—826	315°— 68°	110°	14°	88°—61°	— 2°	8°	7°	29°	61°	92°	0,874	0,485	—0,035
21		300°— 85°	125°	1°	112°—55°	22°	2°	12°	35°	58°	78°	0,819	0,530	0,215
22		275°— 90°	130°	6°	95°—50°	5°	— 3°	5°	40°	50°	86°	0,767	0,643	0,070
23	791—826	270°—100°	120°	4°	106°—58°	16°	5°	10°	32°	60°	83°	0,848	0,500	0,122
24		280°— 90°	120°	4°	100°—60°	10°	7°	8°	30°	60°	85°	0,866	0,500	0,087
25		300°— 60°												
26	791—825	270°— 70°	140°	16°	74°—37°	—16°	—16°	20°	53°	40°	103°	0,602	0,767	—0,225
27		285°— 80°	150°	26°	102°—30°	12°	—23°	25°	60°	32°	79°	0,500	0,848	0,190
28		280°— 65°												
29	792—826	280°— 90°	120°	4°	90°—60°	0°	7°	6°	30°	60°	90°	0,866	0,500	0,000
30		280°— 90°	125°	1°	100°—55°	10°	2°	6°	35°	56°	85°	0,819	0,559	0,087
31	793—826	270°— 90°	130°	6°	90°—50°	0°	— 3°	4°	40°	50°	90°	0,767	0,643	0,000
32	794—827	270°— 90°												
33					90°—45°	0°	— 8°	9°	45°	45°	90°	0,707	0,707	0,000
34		265°— 90°	125°	1°	85°—55°	— 5°	2°	3°	35°	56°	93°	0,819	0,559	—0,052
35					100°—40°	10°	—13°	15°	50°	42°	82°	0,643	0,742	0,139
36	792—825	280°— 65°	125°	1°	68°—50°	—22°	— 3°	14°	40°	54°	104°	0,767	0,588	—0,242
37		270°— 70°	130°	6°	67°—45°	—23°	— 8°	18°	45°	50°	106°	0,707	0,643	—0,276
38					120°—45°	30°	— 8°	21°	45°	53°	69°	0,707	0,602	0,358
MEAN	792—826	277°— 88°	124°		90°—53°							0,781	0,570	0,017
RESULTANT VECTOR					91°—54°				36°	54°	89°	0,808	0,590	0,018

author has called this critical distance the independent cell distance (Agterberg, 1961). Each value lies in the middle of a cell and influences all other values within this cell, whereas all values outside the cell are independent of the central value. The dependence may vary in different degrees in different directions, and therefore the independent cell may have a rather irregular shape. The author proposed two methods for checking the mutual dependence. He pointed out that it is possible to combine adjacent values to new values for comparing the new frequency curve with the old one. When there is no difference, it may be concluded that the distance between adjacent samples is smaller than the independent cell distance. Only, when by combining adjacent values, another fre-

quency curve appears with a dispersion equal to a certain theoretical value, the values are mutual independent.

The other method is based on the theory of relation coefficients. The relation coefficient, r, is defined as

$$r = \frac{1/n \sum_{i=1}^{n} (x_i \cdot y_i)}{S(x) \cdot S(y)}$$

with x_i and y_i being the deviations from the mean of two different series of values. When x_i is independent of y_i, $r = 0$; When x_i is equal or proportional to y_i, $r = 1$. This last case suggests total dependence. A certain value may be called x_i, and its adjacent value y_i, in consequence $y_i = x_{i+1}$. When each value is independent of its adjacent values, the relation coefficient $r = 0$.

In dealing with the mutual relation of adjacent zinc essays of an ore deposit at Pulacayo (Bolivia), it was proved that r decreases gradually with increasing distance between x_i and x_{i+1} (Agterberg, 1961). Such an exact analysis is not possible in the present case, because the measuring distance is not constant, as can be seen in fig. 11. The relation coefficient method only serves to show dependence or independence in a qualitative manner.

Table IX shows the method of calculating r for the azimuths and the dips of the 35 minor folds of table VIII. The above formula, somewhat simplified, is

$$r = \frac{\frac{1}{n-1} \Sigma_i (x_i \cdot x_{i+1})}{\sigma^2}$$

where σ equals the calculated dispersion of the population as shown in table XIV.

It appears that for the azimuths, γ, $r_\gamma = 0.04$, and for the dips, α, $r_\alpha = 0.03$.

Consequently, the mean measuring distance is probably greater than the mean independent cell distance, as no considerable mutual dependence between adjacent measurements appears to be present.

The independent cell distance amounts to approx. 10 m in the present case. This distance of approx. 10 m should be considered only as an illustration as the independent cell probably has no constant dimensions and varies with the composition of the rock. The mutual independence of about the same values in a continuously exposed outcrop can be demonstrated when between these values one other strongly deviating value occurs, which is definitely independent of the adjacent values. When the interjacent value is the same as the adjacent values, dependence of the three values is assumed. This is probable but not certain, as within the sample of the population, the deviations from the mean of adjacent values may almost equal each other.

TABLE IX

Method for calculating r_γ and r_α

$$r_\gamma = \frac{\sum_{i=1}^{35} \left(x_{\gamma_i} \cdot x_{\gamma_{i+1}} \right)}{(n-1) \cdot \sigma_\gamma^2} = \frac{480}{34 \times 19{\cdot}6^2} = 0.04 \text{ and}$$

$$r_\alpha = \frac{\sum_{i=1}^{35} \left(x_{\alpha_i} \cdot x_{\alpha_{i+1}} \right)}{(n-1) \cdot \sigma_\alpha^2} = \frac{110}{34 \times 10.2^2} = 0.03$$

x_γ and x_{α_i} are given in table VIII, and σ_γ and σ_α in table XV.

i – i + 1	$x_{\gamma_i} \cdot x_{\gamma_{i+1}}$	$x_{\alpha_i} \cdot x_{\alpha_{i+1}}$
1— 2	0	3
2— 3	396	4
3— 4	0	— 28
4— 5	0	14
5— 6	0	14
6— 7	0	189
7— 8	0	—108
8— 9	0	— 28
9—10	0	14
10—11	48	— 2
11—12	60	9
12—13	—120	63
13—14	0	— 49
14—15	0	14
15—16	800	34
16—17	—560	—391
17—18	—112	— 23
18—19	416	15
19—20	52	120
20—21	— 44	16
21—22	110	— 6
22—23	80	— 15
23—24	160	35
24—25	—160	—112
25—26	—192	368
26—27	0	—181
27—28	0	14
28—29	0	— 6
29—30	0	24
30—31	0	— 16
31—32	— 50	— 26
32—33	—220	39
33—34	506	24
34—35	—690	64
35— 1	0	24
$\sum_{i=1}^{35}$	480	110

It is not known how the dependence decreases from the centre of an independent cell towards its

periphery, but it is not supposed to be linear.

The deviation from the mean is caused by numerous small causes. This is indicated by the fact that the frequency distribution in an ideal case is a two-dimensional normal one (see further on in this chapter).

For the cause of symmetry, it may be expected that the influence of a certain value on its adjacent values is active in all directions. The value is a property of a certain constant volume.

The number of affected values at a distance, r, from the centre value will be proportional to r^2, and increases rapidly when r becomes larger. Consequently, and apart form the variation of the numerous causes, there are no geometric arguments for a gradually decreasing linear influence.

It is known, however, that a certain mutual dependence, if present, does not change the values of the population mean and dispersion. It only simulates an accuracy greater than actually present. In practice, the accuracy of the mean is not determined by means of frequency curves, but by the more or less regular shape of constructed mean azimuth and mean dip lines as will be shown in chapter 9.

It is emphasized that these calculations are permitted only, when the mean does not vary in the studied region. Such a variation is negligible in the small region of fig. 11, but may be greater in larger sample regions with a considerable variation of the mean. This problem will be discussed in another chapter (Ch. 9).

§ 7C *Dispersion of* S *around the axes of folding.*

Diagram 17 of appendix III is a pole diagram (Schmidt net) of the 35 minor folds (m.f.) and the 33 *S*-planes of table VIII.

The position of the mean *S*-plane is 277° - 88° (resp. strike and dip; strike is direction of dip less 90°). The mean axis of the minor folds is 90° - 53° (resp. azimuth and dip), calculated in table VIII according to a method to be explained afterwards. The mean *S*-plane is roughly vertical, and has an E-W strike, whereas the mean axis of minor folds is situated within the mean *S*-plane, dipping 53° East.

For convenience sake a rectangular co-ordinate system x, y, z is introduced. y is parallel to the mean minor fold, x at right angles to this fold and within the mean *S*-plane. Consequently z is the normal of the mean *S* (see fig. 12).

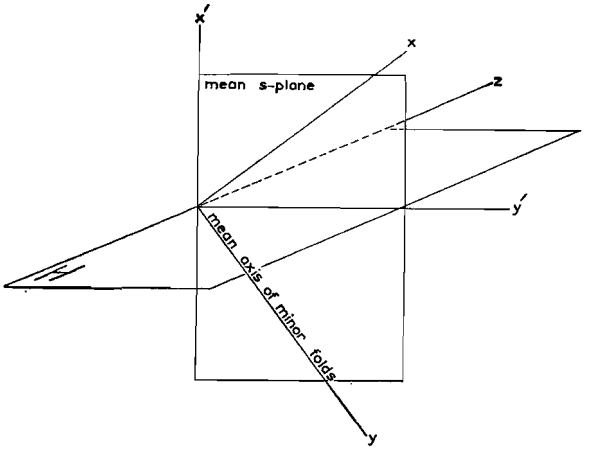

Fig. 12

x, y, and z represent a rectangular co-ordinate system. z makes right angles with the mean *S*, and y is parallel to the mean m.f. For further explanation see text.

In chapter 12, it will be pointed out that prior to folding *S* was subhorizontal. The subhorizontal *S* was isoclinally folded with respect to a subhorizontal axis and afterwards refolded about the steeply East dipping axes of minor folds. The first phase of folding did not result in minor folds. It seems reasonable to assume that the mean axis of minor folds lies within the mean *S*-plane, as all single axes of minor folds lie within a *S*-plane, folded by these minor folds. This rule cannot be applied in all cases. The *S*-planes are strongly folded in some places, so that no exact measurements of *S* can be made, but only the attitude of the minor folds can be measured. On the other hand, the most exact measurements of *S* may be made in places, where no minor folds are found. It can now be explained why in many sampling regions the position of the mean minor fold does not coincide with the mean *S*-plane, as is apparent from our structure maps.

The example of the 35 minor folds has been schematically represented in fig. 12. All single measurements are scattered around their mean. It can readily be seen, that *S* may be scattered around x and y, but scarcely around z, as z is at right angles to the mean *S*-plane and this plane retains the same position when it is rotated around z. The position of the individual *S*-planes may vary a little around this mean value and a

negligible amount of dispersion may exist around z.

The minor folds are dispersed around z and x and scarcely around y. The shape of the frequency curves, representing the dispersion of the individual values around their mean, resembles a Gauss curve around both axes z and x.

The dispersion of *S* around x equals the dispersion of m.f. around x, and the values form the same frequency curve.

The dispersion of *S* around y does not influence the positions of the single m.f. The shape of the frequency curve may be different from that of the Gauss curve. Firstly, the dispersion of *S* around y will be discussed.

In the observation points 6, 7, 8, 30, and 38 of fig. 11 and table VIII, green phyllite occurs, a sample (s. 1) of which at point 6 is described in table II (see also photograph 18). This green phyllite is distinguished from the ordinary quartz phyllite by its green colour, its massive appearance, and the local presence of pyrite crystals of about one centimeter.

The outcrops are located on an E-W striking line. As it is considered probable that the contact between green phyllite and quartz phyllite is a bedding plane, which is parallel to *S* (chapter 2), it may be assumed that this narrow E-W striking zone of green phyllite is the core of a syncline or anticline. The *S*-planes North of this core dip toward the South, whereas the *S*-planes on the southside dip toward the North. Consequently, a syncline probably exists. The *S*-planes of the points 1-5, 11, 12, and 31-34 (all North of the core) are plotted in fig. 13; the *S*-planes of the points 9, 10, 13-29, 36, and 37 (all South of the core), in fig. 14. On the northern limb, the strike of $S \leqslant 88°$ and on the southern limb $\geqslant 268°$. This suggests an axial plunge toward the East.

The mean *S* of the northern limb is calculated as 83° - 81°, and the mean *S* of the southern limb as 280° - 78°. The intersecting line of these planes is 90° - 40° (see fig. 15). This line can be compared with Sander's β (Sander, 1950). Normally it represents the axis of a syncline. On the other hand, it appears that the mean m.f. equals 89° - 54°. Although these values do not correspond too well, it might be expected that the axes of the minor folds are parallel to the axes of the major

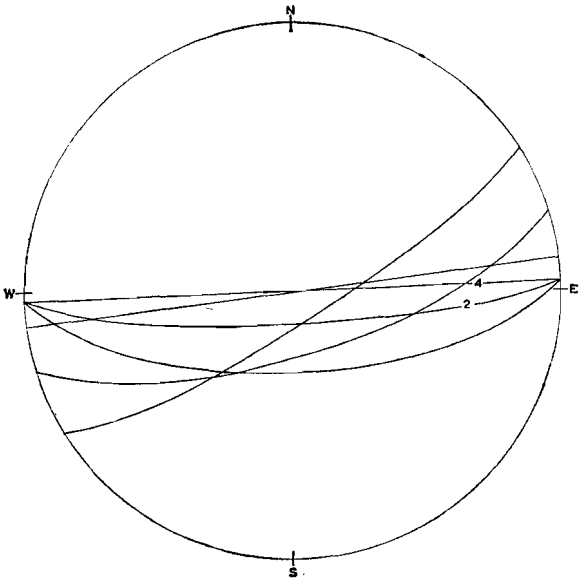

Fig. 13

The 10 *S*-planes of the northern limb of the syncline of Monguelfo (Schmidt net, lower hemisphere).

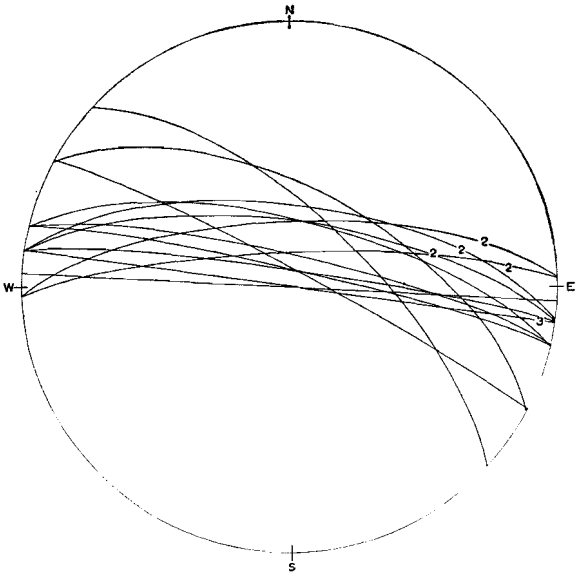

Fig. 14

The 19 *S*-planes of the southern limb of the syncline of Monguelfo (Schmidt net, lower hemisphere).

folds. This assumption, however, is geometrically not possible, as is proved in chapter 12.

If the positions of the *S*-planes were determined exclusively by folding about the subhorizontal axes of the major folds, y would be subhorizontal. The actual position of y is explained as follows.

The minor folding also produced folds on a larger scale. The measured *S*-planes lie as well on

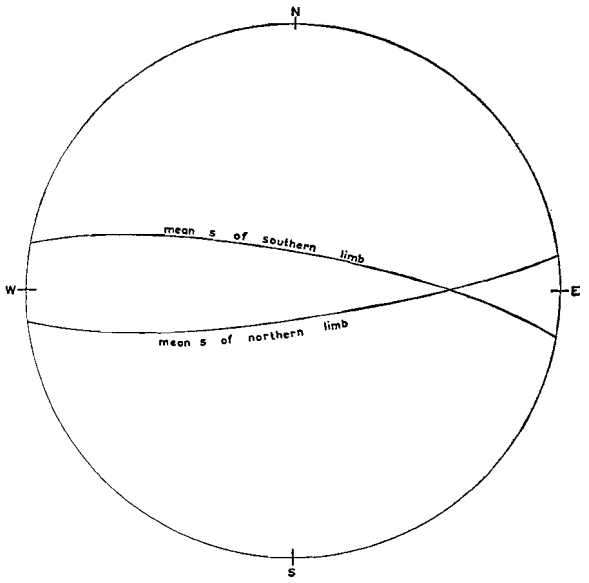

Fig. 15

Construction of the intersecting line between the mean *S* of northern and southern limbs of the syncline of Monguelfo (Schmidt net, lower hemisphere). For further explanation see text.

the limbs of the major syncline as well as on the limbs of slight folds belonging to the minor folding phase. It has been attempted to measure *S*-planes which were not affected by the minor folding phase. However, this influence cannot be avoided entirely. The question may be posed whether the *S*-poles are scattered in the x , z-plane or in the vertical N-S striking plane which is at right angles to the subhorizontal E-W striking axis of major folding (y').

This question is answered by the construction of the intersecting line of both mean limbs of the syncline, which line has a position of 90° - 40° (see fig. 15). The dip lies between 54° (dip of y) and 0° (dip of y'). This question can be solved also by a more exact method.

Fig. 16 is a pole diagram of *S*, in which the x, z-plane, located between the x , z- and x', z-planes, ted. The position will be calculated of the x'', z-plane, located between the x, z- and x', z-planes, and in which *S* is scattered around an y''-axis. All poles of *S* are supposed to lie in westward dipping planes with strike z. The hades of these planes are given in table X *). When the *S*-poles are subparallel to z, the resulting hade is not accurate. All the *S*-poles, forming an angle with z

*) The hade is the dip's complement.

TABLE X

Hades of N-S striking planes, containing the numbered S-poles (see table VIII).

$$\text{Mean hade} = \frac{718^\circ}{22} = 33^\circ$$

— indicates *S*-pole, which forms an angle with z smaller than 9½°, and has been omitted.

1	—
2	3°
3	8°
4	—
5	37°
6	90°
7	—
8	42°
9	—
10	71°
11	48°
12	8°
13	24°
14	
15	
16	24°
17	62°
18	34°
19	— 7°
20	60°
21	80°
22	—
23	8°
24	—
25	40°
26	— 3°
27	54°
28	19°
29	—
30	—
31	—
32	—
33	
34	—
35	
36	19°
37	— 3°
38	
$\sum_{i=1}^{22}$	718°

smaller than 9½°, have been omitted. The 9½° cones around z are shown in fig. 16.

The mean hade of the planes is 33°. This corresponds with the dip of the y''-axis. The angle between x , z and x'', z ($x , z \wedge x'', z$) = 21°, and ($x', z \wedge x'', z$) = 33°. It is assumed that the hade of the x'', z, which has been introduced, is a measure for determining the influence by which *S* was affected by minor folding. These *S*-planes were originally dispersed around y'. Later folding around y, however, caused the actual dispersion around y'', which has an intermediate position between y' and y.

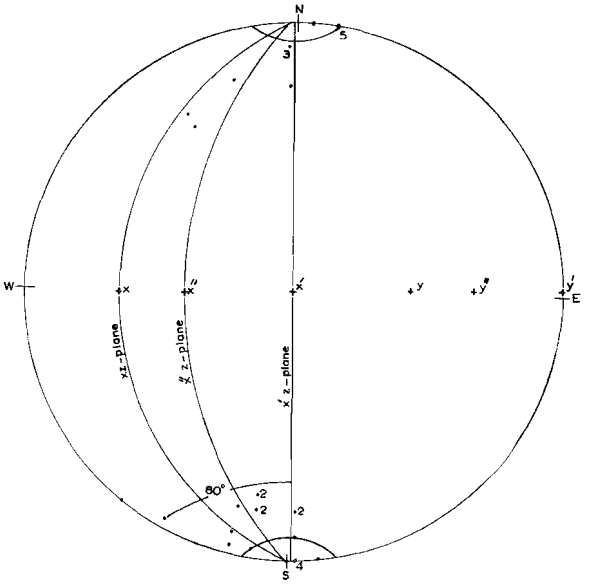

Fig. 16

Pole diagram (Schmidt net, lower hemisphere) of the 33 *S*-planes of Monguelfo. For further explanation see text.

If this disturbing influence had not been present, y″ would equal y′. If the influence of the minor folding would largely exceed the influence of the major folding, y″ would equal y.

From the preceding considerations it follows that the theory of two phases of folding, based on other regional data, appears to be in better agreement with the data obtained in a small sampling region than the hypothesis of minor folds being parallel to major folds.

The above analysis gives another result. A mean *S* was calculated of 275° - 88°. The geometrical meaning of this mean *S* is obvious. It is a first approximation of the axial plane of a syncline. It is better to apply the mean between the mean *S* of both limbs. The southern limb contributes too much to the above value, as most observation points are located on this limb. The mean between 263° - 99° (northern limb) and 280° - 78° (southern limb) is given by the bisecting line of the poles, and is 273° - 91°, which indeed is somewhat different from 275° - 88°.

This difference is due to the fact that the mean of the schistosity-planes varies about the y-axis or more precisely about the y″-axis in the sample region. The frequency curve, with a particular shape by reflecting folding around an axis, scarsely influences the frequency curves of the minor folds around x and z.

It is emphasized that merely calculating of the mean from the measurements is not correct. The shape of the frequency curves must be checked by pole diagrams and contourlines. The influence of a varying mean on the frequency curve will be discussed in chapter 9.

§ 7D *Dispersion of minor folds around x and z with application of Pearson's χ^2 test.*

The frequency distribution of the individual m.f.'s around their mean in an ideal case is two-dimensional normal. This was indicated by comparing a cross section of the observed distribution of the 35 minor folds with a Gauss curve (Agterberg, 1959). This comparison was according to a method which will be discussed here more extensively. First, Pearson's χ^2 test is applied, which generally is used in statistics to test a certain hypothesis on the shape of the frequency curve of the population.

A certain observed distribution may resemble a predictable theoretical distribution. Pearson has found a method for checking the observed data and those calculated by means of the formula which corresponds with this theoretical distribution.

In the present case, it is assumed that the population to which the 35 minor folds belong, has an isotropic two-dimensional normal distribution. If this is correct, each cross section of the sample through the mean will result in a histogram resembling a Gauss curve. As the population consists of numerous values, the sample of measurements may have numerous different shapes, the most probable of which are Gauss curves. χ^2 is a value of the probability that the sample actually is taken from an isotropic two-dimensional normal distribution with parameters M and σ which correspond with the estimations as calculated from the sample.

The single measurements are combined in a histogram. The classes are plotted on an x-axis, and the number of observations in each class on the y-axis.

Our basic hypothesis of the population having an isotropic two-dimensional normal frequency distribution, is based on the following considerations. The 35 minor folds have been plotted in a pole diagram with stereographic projection (Wulff net). In this projection a circle on the

sphere is projected as a circle in the corresponding diagram.

When the two-dimensional frequency distribution of minor folds around their mean is isotropic, the frequencies will diminish equally in all directions. The class boundaries are cone-shaped. The constructed contourlines of the diagrams are the projections of these cones, and must be circles. Indeed the shapes of the different contourlines approximate circles as is shown in fig. 18. In conclusion, it may be stated that the distribution is isotropic two-dimensional. The distribution follows the normal, which is based on the following assumptions.

In statistics, a normal distribution is frequently observed, and can be explained by the so-called "Expanded theorem of de Moivre" (Freudenthal, 1957). This learns that a distribution is normal when three conditions are fulfilled.

1. The causes from which the deviations from the mean originate, are numerous.
2. The causes are independent of one another.
3. The effect of each cause of dispersion is small as compared to the effect of all causes together.

These three general conditions are readily fulfilled in general, and can be expected to be fulfilled in our example. Consequently, an isotropic two-dimensional normal distribution may be expected and will be discussed.

A normal distribution has three parameters, the situation of M, and the values M and σ. The number of the so-called "degrees of freedom" of the sample taken from the normal distributed population equals the quantity of classes minus the number of parameters of the theoretical distribution. One degree of freedom is required at least, and four classes must consequently be formed. Further Cramer (1946) proved that each class must have more than five observations. When these two conditions are fulfilled, the test can be applied.

χ^2 is defined as $\chi^2 = \sum_{i=1}^{i=p} \frac{(f_i - F_i)^2}{F_i}$

p is the number of classes

f_i is observed and F_i is calculated frequency.

The technique of the calculation is given in diagram 17 and table XI. Around the mean of the minor folds 89° - 54°, cones with a regularly increasing top angle of 6° have been constructed. These cones are the class boundaries of f_i.

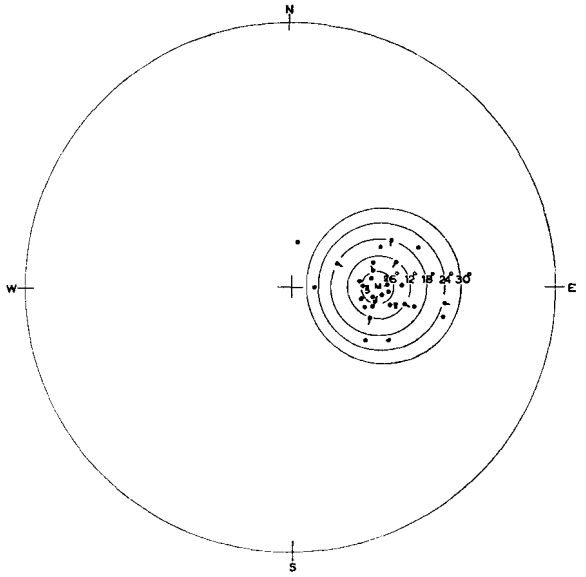

Fig. 17

Pole diagram (Wulff net, lower hemisphere) of 35 axes of minor folds at Monguelfo. The calculated mean M = 89° —54°, around M cones have been constructed with top angles of 6°, 12°, 18°, 24°, and 30° respectively. Cross strokes of boundary values point to adjacent class to which these values are considered to belong.

A few single values coincide with the class boundaries and are considered to belong to one of the adjacent classes. This is not done systematically, as the minimum class number had to be reached in class 3. This method is permitted by the following reasoning. Different values are located on the same class boundary, due to inexact measuring. When a more exact method of measuring would be possible, the values would probably be scattered around the class boundary. The class boundaries can be shifted somewhat in order to adapt the frequencies to those of table XI. The required shiftings from the originally 6° boundaries are so small that the other values of table XI are affected to a negligible degree only. The classes 4 - 7 are combined to reach a frequency larger than 5. The result is four classes with each more than 5 observations. The F_i will be calculated from the standardized cumulative normal distribution with $\sigma = 1$. It is known that $\sigma = 14°.4$ for the population.

The values x_i and y_i for the class boundaries of the standardized distribution are given in table XI.

TABLE XI

Method for calculating χ^2.

														Σ_i
class-number i :		7		6		5		4		3		2	1	
class-boundary :	42°		36°		30°		24°		18°		12°	6°	0°	
x_i	2,9169		2.5002		2.0835		1.6668		1.2501		0.8334	0.4167	0	
y_i	0,0019		0,00621		0.01876		0.04746		0,1056		0.2033	0.3372	0.5000	
2 y_i	0.00		0.01		0,04		0,09		0.21		0,41	0,67	1,00	
F'_i		0,01		0,03		0,05		0,12		0,20		0,26	0,33	1,00
F_i		0,35		1,05		1,75		4,20		7,00		9,10	11,55	35.00
					7,35									
f_i					7					6		10	12	
Δ_i					0,35					1,00		0,90	0,45	
Δ^2_i					0,1225					1,00		0,81	0,2025	
$\frac{\Delta^2_i}{F_i}$					0.017					0,143		0.089	0,018	$\chi^2 = 0.275$

The values y_i have been doubled because the classes are located on either side of the mean.

$F_i' = y_i - y_{i-1}$

and $F_i = 35.\ F_i'$, which brings out the required normal distribution pattern with $\sigma = 14°.4$.

These values resemble the f_i.

The difference amounts to $\Delta_i = |F_i - f_i|$.

For Δ_i, Δ_i^2, and $\frac{\Delta_i^2}{F_i}$, see table XI.

$$\chi^2 = \Sigma_i \frac{\Delta_i^2}{F_i} = 0.267.$$

This value must be compared to the fractiles of the χ^2 distribution (see e.g. tables of Hald, 1960).

With one degree of freedom a $\chi^2 = 0.275$ is found with 60 % confidence in this case. By applying the χ^2 test, the common confidence level is selected at 5 %. When this value is not reached, the test hypothesis should be rejected.

When the value is surpassed, the basic hypothesis is considered to be correct. Vistelius (1960) was very cautious and assumed 50 % confidence because he had no data about the mutual independence of his observations. As mentioned in our example, the independence was proved and 5 % confidence has been accepted, which corresponds to a $\chi^2 = 3.84$.

Our calculated χ^2 is actually smaller than 3.84 and even below $\chi^2 = 0.455$, which corresponds with the 50 % level of Vistelius.

Consequently, our initial assumption that the distribution is isotropic two-dimensional normal, may be considered to be correct.

§ 7E *Contour analysis of the frequency distribution of the minor folds.*

In fig. 18 eight contourlines have been plotted. These contourlines represent the density of the individual values around the mean, and can be compared to the frequency distribution. The relation between the contourlines and the frequency curve will be discussed.

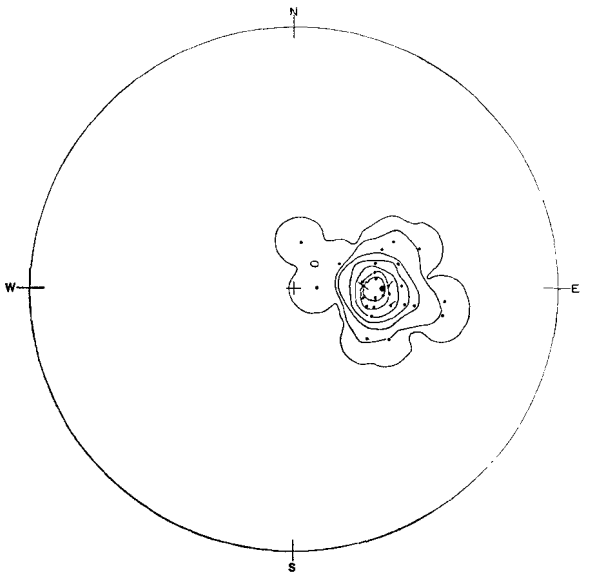

Fig. 18

Pole diagram (Wulff net, lower hemisphere) of 35 axes of minor folds at Monguelfo. Each cross stroke represents a measurement. The 3—9—17—26—34—43—57% contours have been drawn, the 63% contour is represented by a black dot.

It has been stated before that the shape of the contourlines indicates an isotropic distribution.

The irregular contourlines may be replaced by circles representing an equal area (0). The intersecting lines of the contour cones with the sphere are circles and the radii of these circles (measured on the sphere) can be derived from the formula $r_{mean} = \sqrt{\frac{0}{\pi}}$. This mean is the arc corresponding to the top angle of the cone. However, we are dealing with the projections of the circles on the sphere. These projections are also circles in stereographic projection, but of a different size. When the dispersion is small the above formula is an useful approximation.

A test-curve has been constructed (fig. 19) giving the relation between the area of the projected cone in mm² (abcis) and the top angle of the cones in degrees (ordinate). This curve can only be used when the cone axis dips 54°, as does the mean minor fold of the present example.

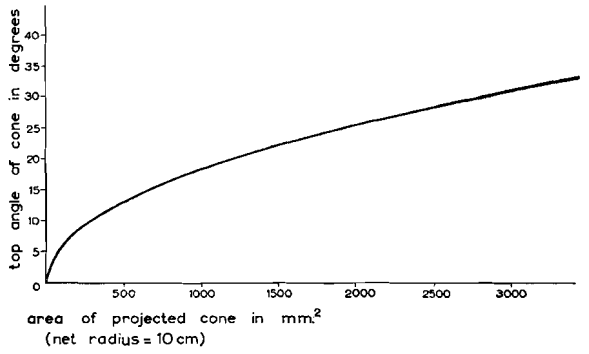

Fig. 19

Test-curve giving the relation between the area of a projected cone and the cone's top angle. The cone axis dips 54°.

This test-curve can be readily calculated from fig. 17, in which cones with known top angles are shown. Its shape resembles a parabola as could be expected from the mentioned formula.

The areas enclosed by the contourlines are determined by counting squares with an area of a mm² (see table XII).

It is obvious that these areas are proportional to the net area. A net with a net radius of 10 cm was used.

The frequency curve is formed by plotting the contour % against the top angle of its corresponding cone (fig. 20), and resembles a Gauss curve.

To continue the analysis and to calculate the σ of this frequency distribution this observed frequency curve will be compared with the theoretical Gauss curve, this time following a graphical method.

TABLE XII

Relation between contoured area and top angle of corresponding cone.

number of contourlines = points in 1 % area	% of contourlines	area of cone projection in mm²	top angle of cone
1	3	2739	30°
3	9	1168	20°
6	17	648	15°
9	26	416	12°
12	34	274	9½°
15	43	129	7°
20	57	59	4½°
22	63	0	0°

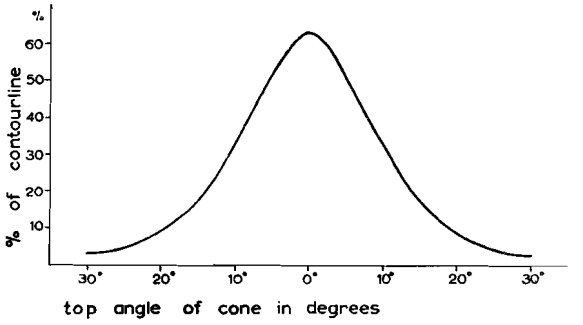

Fig. 20

Frequency curve of 35 m.f. at Monguelfo showing a contour % against the top angle of its corresponding cone.

Fig. 21 is a histogram of the distribution. The class boundaries lie between the top angles of the cones which correspond with the constructed contours. The height of each class is given by the percentage of these contours.

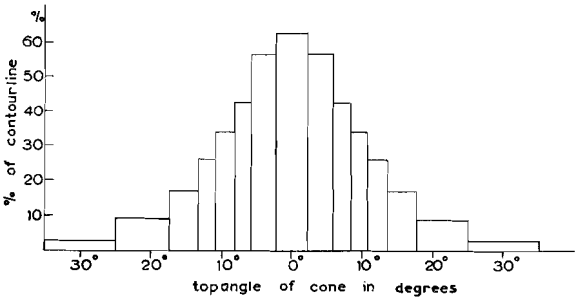

Fig. 21

Histogram of 35 m.f. at Monguelfo.
For explanation see text.

σ will be calculated by means of the cumulative frequency curve. Table XIII gives the mode of

calculation for one half of the curve. It has an area of 770¾ units. The total area must be 1541½ units for the sake of symmetry. The single values of the cumulative curve are standardized by dividing them by 1541½ units. When the curve would be normal, $\sigma = 0.159$. In the table, this value appears to correspond with a top angle of 12°. It is indeed assumed that we are dealing with a normal distribution with $\sigma = 12°$.

TABLE XIII
Method for calculating the standardized cumulative frequency curve.

	these values are for half a curve only								
top angle of cone	30°	20°	15°	12°	9½°	7°	4½°		0°
class boundaries 35°	25°	17½°	13½°	10¾°	8¼°	5¾°	2¼°		
width of class	10°	7½°	4°	2¾°	2½°	2½°	3½°		4½°
contour percentage	3%	9%	17%	26%	34%	43%	57%		63%
area of column	30	67½	68	71½	85	107½	199½		141¾
cumulative area	30	97½	165½	237	322	429½	629		770¾
ditto, standardized	0.019	0.063	0.108	0.154	0.208	0.278	0.407		0.500

To test this supposition, the cumulative curve has been plotted on probability paper on which a cumulative normal curve appears as a single straight line.

The straight line, which may be expected for a normal distribution with $\sigma = 12°$, has been drawn in fig. 22.

Our assumption appears to be correct because all points of the cumulative frequency curve practically coincide with this line.

The single points may be scattered around this line within certain limits.

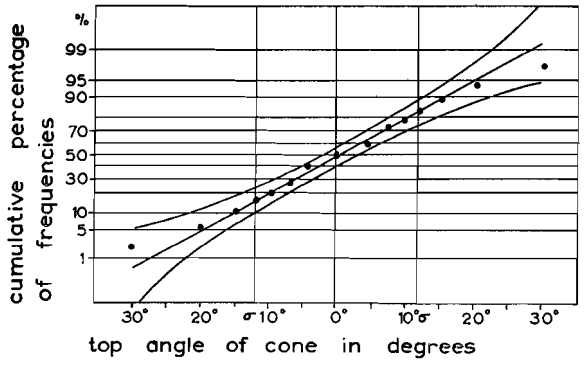

Fig. 22
The distribution of 35 m.f. at Monguelfo plotted on probability paper on which a cumulative normal curve appears as a straight line. A normal distribution with $\sigma = 12°$ is represented with its 95% confidence limits.

In fig. 22 the 95 % limits are drawn which are generally taken for confidence. When one or more values lie outside these limits, the basic hypothesis must be rejected. In our example, however, a normal distribution is observed.*)

It is remarkable that the above method results in a dispersion of 12° which differs from the value $\sigma = 14°.4$ applied before.

The dispersion will be determined by other methods. Firstly, methods for calculating the mean will be discussed.

§ 7F *Methods for calculating the Mean of a population of tectonic elements; General.*

In the preceding pages, the mutual independence of adjacent measurements at Monguelfo, composing a sample, has been proved. This sample represents the population adequately. This population possesses one mean with single values scattered around it. The frequency distribution in this ideal case is isotropically two-dimensional normal.

Before starting to calculate the properties of a population from a sample, it must be ascertained that the sample indeed represents one single population. A priori, it is possible that a sample contains values of different populations. To check this, a pole diagram of the sample should be constructed. Only when a single maximum appears, it

*) The limits are derived from Hald's (1957) fig. 6. 12. and have been calculated for a binomial distribution with n = 100, which fairly well approaches a normal distribution. This method can be criticized, as shown by Hald. But for the present case, it gives the required information.

is permitted to calculate the properties of the corresponding population. Tectonic geologists generally consider the net maxima only, and students of paleomagnetism calculate the mean according to Fisher (1953).

We found many samples with a dipersion too strong to apply the net maximum method, and the mean had to be calculated. To be consistent, a simplified method for calculating the mean has been applied to all samples.

The first procedure with a sample is to construct a pole diagram and to apply this to the interpretation of the properties of the population(s).

§ 7G *Application of the Pole diagram.*

Tectonic geologists generally use projections to represent lines, planes, and cones in the horizontal plane, such as the stereographic projection (Wulff net) and the equivalent azimuth projection of Lambert (Schmidt net).

In the stereographic projection, a cone is projected as a circle.

In the Schmidt net a cone is projected as an ellipse, but the area of this ellipse equals the area of the spherical surface cut by the cone. For this reason, the Schmidt net is also called the equal-area net. This projection generally was applied by us, using lower hemisphere.*)

All measurements in the Crystalline of the studied regions are mentioned in appendix II with their grid co-ordinates. These co-ordinates are accurate up to 50 m.

The measurements in a certain region have been combined into one sample, the pole diagram of which is given in appendix III.

Tectonic geologists generally publish these diagrams only, but these diagrams do not show the geographical positions of the single values, and the size of the sample regions is unknown. Further the single observation points can be grouped in many ways. Our method of combining samples is one of various methods possible.

In the regions studied, the mean varies rather strongly in some places. This necessitates a careful determining of the location of the mean which we calculated from the co-ordinates as given in appendix II.

Diagram 17 of App. III shows the 33 poles of *S*-planes and the 35 m.f. at Monguelfo. The single measurements are given in table VIII.

In this case, the minor folds were mostly determined by measuring the angle of rake in the *S*-plane. The angle of rake of a line in a plane is the angle between the strike of the plane and the line itself, measured in the direction of dip. The minor fold is plotted in the pole net as the intersecting point of a) the projection of the *S*-plane and b) the cone with the *S*-strike as axis and the angle of rake as top angle.

In many places, however, the minor folding is so strong that no exact *S* can be measured. In such cases, the m.f. is determined by its azimuth and dip. In the Pusteria region the number of measurements of m.f. largely exceeds the *S*. When in other regions the number of m.f. in a certain place exceeds the number of *S*, this place is strongly folded.

When all poles of a sample have been plotted in the net, contourlines can be constructed. The usual technique is applied, counting with a circle with an area of 1 % of the net area (e.g. as described by Sander, 1950). However, the generally small number of elements allowed a rapid way of counting as the most exact method.

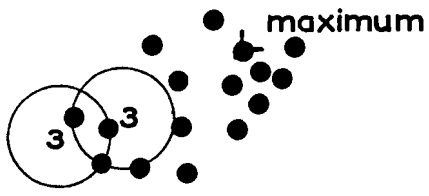

Fig. 23

Part of the margin of a hypothetic distribution. For calculation of the contour % the number 3 must be multiplied by $^1/_n$. 100%, with n being the number of plotted measurements. For further explanation see text.

Fig. 23 illustrates the following possibilities. Firstly, the 1 % counter can be moved towards the maximum and is stopped when it contains a certain number of points (being 3 in the example).

*) For indicating planes and lines the method of Trooster was followed (Trooster and Van Landewijk, 1958). The strike of a plane is not only the horizontal line in that plane, but also the direction of the horizontal line obtained by 90° anticlockwise turning of the direction of dip of the plane.
The azimuth of a line is determined by the direction of dip of the line.

This number is indicated in the centre of the 1 % area. By connecting the equal numbers by moving the counter from all possible directions, the result is the geometrical locus of points, which exactly contains the above mentioned required number of points. The contourlines have been constructed in this manner.

However, the counter can be moved also away from the maximum. Following the same procedure, another contour would be obtained which lies within the first one, but which has an equal percentage. Both lines are iso-density lines.

It is evident that the method of indicating the number obtained from a non-systematic use of the counter produces a contour with an irregular shape between the above mentioned contourlines. This irregular line is actually not an iso-density line, but it differs slightly from such a line.

The iso-density lines have been constructed within the horizontal plane. Strictly, the iso-density lines should be determined on the sphere and then be projected on the net. The result differs negligibly from the constructed contour picture, as all single measurements determining the shape of contours are projected in the right place. The 1 % circle may be replaced by 1 % ellipses which are the projections of 1 % circles on the sphere. As this method is seldom applied and the deviations from the common method are so small, it has not been used.

The sample of Monguelfo consists of 35 m.f. which have been plotted in the Schmidt net (diagram 17 of App. III) as well as in the Wulff net (figure 18). The position of the maximum can be estimated by the centre of one of the central contours. For the Schmidt net it appears to be 91° - 54° for the 23 % contour, and for the Wulff net 91° - 56° for the 51 % contour, and 90° - 53° for the 63 % contour. These small differences show the approximate character of the obtained maxima.

The maximum coincides with the mean when the population possesses two symmetry planes at right angles to each other. The present population of m.f. is isotropic and all planes through the mean m.f. are symmetry planes. In this case, the maximum coincides with the mean to be calculated also.

From the diagrams of appendix III it appears that the condition of two symmetry planes being at right angles to each other is more or less fulfilled for about all studied populations. The distribution, however, is generally not isotropic. It was stated in another paper (Agterberg, 1959) that the dispersion of m.f. within the mean *S* or around z of fig. 12 is not equal to the dispersion of m.f. and *S* around x. When the *S*-planes have not been folded by major folds, no important dispersion around x can exist, as the *S* are subhorizontal. This conclusion is supported by the pole diagrams showing that the scattering around z generally exceeds the dispersion around x.

It may be assumed that the common frequency distribution of tectonic elements is non-isotropic two-dimensional normal in an ideal case. When the normal character has been disturbed two symmetry planes at right angles are still present. For the m.f. they are x , y and y , z and for the *S*: x , z and y , z.

When the dispersion of m.f. and *S* around x is small, one might assume that this may be partially explained by measuring errors. Measuring errors are generally distributed according to a Gauss curve. It is assumed that our measuring errors also belong to equal isotropic two-dimensional distributions around the actual position of the measured tectonic element. These errors have to be added to the natural frequency distribution.

According to statistics the sum of two or more independent normal distributions of the same element results in another normal distribution with a somewhat greater dispersion.

The contribution of the measuring errors, however, can be neglected in our case as strike, azimuth, and dip can be observed up to one degree. The rounding off to 5° generally applied is justified by the variation of the tectonic elements within a single outcrop.

The value of the pole diagram lies in its easy picture of the sample. The contours are constructed from adjacent points. This means that the maximum is formed also by its adjacent points. Removed points do not contribute to the maximum. It may be possible that these removed points of the sample do not belong to the population. E.g. they may belong to slumped blocks. In this case, their contribution to the mean, which always exists when calculating the mean, introduces an error. Consequently, the maximum may be a better ap-

proximation for the population mean than the calculated mean.

Such an assumption cannot be proved. The influence of a single deviating measurement can be neglected. If it could be proved, the influence of single deviating measurements can be observed and eliminated. Rotations in opposite directions may neutralize these influences on the mean.

Many of our diagrams do not show a distinct maximum and this manner of determining the mean has not been applied for constructing our maps. The mean has been calculated, and all measurements of the sample have been considered.

§ 7H *Calculation of the Mean of a population.*

Every line may be considered as a unit vector. The angles of the single m.f. with three rectangular axes V, E, and S (Vertical, East, and South) are given in table VIII with the cosines of these angles, being the direction-cosines of the single m.f. Their means have to be divided by the square root of the sum of their squares to find the direction-cosines of the resultant vector.

This pole appears to be 91° - 54°, or with the magnetic correction: 89° - 54°, this value was used before.

This method is rather cumbersome and it was tried to find another method which can be easily applied and which is sufficiently accurate.

It appears that the mean *S* is adequately represented by the mean strike and the mean dip, and the mean m.f. by the mean azimuth and the mean dip.

In appendix II these means for all samples have been calculated. They have been plotted in the diagrams of appendix III. Upon a preliminary comparison these means appear to correspond satisfactorily with the maxima (tables XVI-XXI). Possible deviations can be ascribed to the asymmetry of the distribution.

For our present example, a mean azimuth and a mean dip of 88° and 53° were calculated, which correspond fairly well with the resultant vector of 89° - 54°.

A third method to calculate the mean is to determine the mean angle of rake within the mean *S*. These two values are respectively 124° and 275° - 88° (table VIII), corresponding to a mean of 91° - 56°.

§ 7I *Median.*

Instead of the mean values the medians of these values may be determined. All values are placed in ascending order. The middle value is called the median. In the case of the 35 m.f. at Monguelfo, the median is 88° - 54°.

When the median is taken from a symmetrical distribution, as in the case of Monguelfo, the median equals the mean. When asymmetry occurs, the median and the mean are different. The contribution of some strongly deviating measurements to a median is smaller than to a mean. When such deviating measurements occur, the median will take an intermediate position between the mean and the maximum. Table XXI serves to compare the means and the medians of the M. Spico region.

§ 7J *Graphical calculation of the Resultant Vector.*

A graphical method will be discussed as the last method for calculating the mean. This method is based on the fact that determining the mean between two lines is rapidly done in a stereographic or equal-area net.

Both lines are rotated in a great circle and the bisecting line can be determined. The resultant vector of four unit vectors can also be found in this way, by combining the two resultants of two unit vectors. When the number of unit vectors is not a whole power of two, the problem can be solved otherwise. In the case of Monguelfo, the number of 35 m.f. is resolved to the largest possible power of two plus a rest: $35 = 2^5 + 2 + 1$.

These three vectors can be calculated according to the mentioned method.

Observations 1 - 35 of table VIII result in a vector of 93° - 54°; observations 36 - 37 give 68° - 48° and 38 = 120° - 45°.

These values must be added by two additions to determine the resultant vector again.

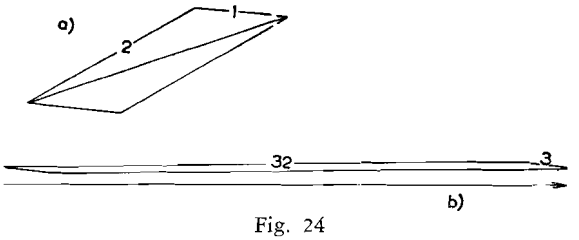

Fig. 24

Two vector diagrams for calculating the mean m.f. at Monguelfo. For explanation see text.

At first, 68° - 48° and 120° - 45° are added in their common plane 358° - 49°. The angle between the vectors is 36°. The graphical vector addition is shown in fig. 24. The 36 - 37 vector consists of two unit vectors, and its contribution to the resultant has been taken twice. It appears that the angle between the 36 - 37 vector and the resultant within 358° - 49° is 12°, which determines the resultant. Similarly, this resultant can be combined with the 1 - 35 vector; the lengths of the vectors are in the proportion of 32 and 3. The ultimate result is a vector 90° - 54° (with magnetic correction).

This chapter may be concluded with table XIV showing the mean, as determined according to different methods.

TABLE XIV

Different values of the mean axis of minor folds at Monguelfo.

DIFFERENT VALUES OF THE MEAN (with magnetic correction)	
calculated resultant vector	89° — 54°
centre 57% contour, Wulff net	91° — 56°
centre 63% contour, Wulff net	90° — 53°
centre 23% contour, Schmidt net	91° — 54°
mean azimuth and dip	88° — 53°
mean S / mean rake = 275°—88° / 124° →	91° — 56°
median of azimuth and dip	88° — 54°
graphical resultant vector	90° — 54°

§ 7K *Dispersion, σ, and Accuracy of the mean.*

The dispersion of the mean σ_m, indicating the accuracy, is $\sigma_m = \frac{\sigma}{\sqrt{n}}$

Column x of table VIII shows the deviation of the m.f. from the mean 89° - 54°. σ has been calculated according to the formula of § 7A at σ = 14°.4. This value was used in applying the χ^2 test.

From the cumulative frequency distribution, calculated from the contours, σ = 12°.0 was obtained.

Table XV shows other values of σ.

Table VIII shows the deviations of the single azimuths, γ, from the mean azimuth 90° (without magnetic correction). Consequently, σ_γ = 19.°6.

The γ's correspond with the angles between the individual m.f. and their mean, δ', within y , z (fig. 12) according to the formula: tg $x_{\delta'}$ = tg x_γ. cos 54°.

with x_γ = deviation of γ from mean γ, and
$x_{\delta'}$ = deviation of δ' from mean δ'
(54° = dip of mean).

This reduction, however, can be made by a direct method utilizing a net. It appears that $\sigma_{\delta'}$ = 12°.0.

The dispersion within y, z can also be calculated directly from the deviations of the single δ's from the mean angle of rake (Column x_δ of table VIII).

Therefore σ_δ = 12°.0.

At last σ_α = 10°.2 for the dispersion in x , y.

TABLE XV

Different values of the dispersion, σ, of the minor folds at Monguelfo.

DIFFERENT VALUES OF THE DISPERSION, σ				
Σx^2 =	7002		σ =	14.°4
Σx_γ^2 =	12995	→ δ_γ = 19.°6 →	$\sigma_{\delta'}$ =	12.°0
Σx_δ^2 =	4170		σ_δ =	12.°0
Σx_α^2 =	3526		σ_α =	10.°2
From cumulative frequency distribution from contours			σ =	12.°0

§ 7L *Fisher's formula.*

Students of paleomagnetism generally apply Fisher's formula

$$1 - \cos\theta = \frac{n - R}{R} \{ (1/p)^{1/n-1} - 1 \}$$

θ = top angle of cone of confidence
n = number of vectors
R = length of Resultant vector with
$R^2 = (\sum_i \cos\alpha_i)^2 + (\sum_i \cos\beta_i)^2 + (\sum_i \cos\gamma_i)^2$
confidence.
α_i, β_i, and γ_i are the angles between a certain vector i and the three rectangular axes of the co-ordinates system.

p = probability of the mean being located within the cone of confidence with top angle θ.

The formula can only be applied in the case of an isotropic two-dimensional normal distribution (Fisher, 1953, p. 296), as it has been derived for this distribution. For this reason, we may apply the formula to the sample of m.f. at Monguelfo.

Generally, p = 5 % is selected. In this case, and as $\frac{R}{n}$ = 0.967 and n = 35 : θ = 4° 21'.

All means of table XIV, determined according to different methods, lie within this 5 % cone of

Fisher's formula concerns a normal distribution. Whether it can be applied or not should be tested. The supposition that a distribution of paleomagnetic or tectonic values is always normal, and that Fisher's formula can be applied, is not correct.

E.g. secular variations might cause the scattering of the direction of magnetization of specimens (van Hilten, 1960). These variations act with a relatively strong effect and this is in contradiction to the conditions for normal distribution (§ 7D).

It is emphasized that the normal character of a frequency distribution has to be checked.

It is obvious that it would be too cumbersome to apply all different methods discussed in the present chapter to the ± 500 measurements samples collected.

For each sample, however, the following data are given:

1. the single measurements with their co-ordinates (App. II)
2. a pole diagram (Schmidt net) (App. III)
3. an approximation of the population mean (App. II and III).

The approximate method (nr. 3) will be discussed in the following chapter.

CHAPTER 8

ACCURACY OF THE APPROXIMATE METHOD OF CALCULATING THE POPULATION MEAN

It will be attempted to prove the following theorem: The azimuth and dip of the mean of a distribution of tectonic elements are sufficiently approximated by the mean azimuth and the mean dip of the individual elements.

The tectonic elements under discussion are the *S* and m.f. of appendix II. It was stated before that the diagrams of appendix III apparently permit the conclusion that all distributions possess two planes of symmetry at right angles to each other. The very existence of this idealized geometry is caused by the relation between the mean *S* and the mean m.f. When the co-ordinates of fig. 12 are maintained, the planes of symmetry are x , y and y , z for m.f., and x , z and y , z for *S*.

The basic theorem may be formulated as: The azimuth and dip of the mean of a distribution of tectonic elements with two planes of symmetry at right angles are sufficiently approximated by the mean azimuth and the mean dip of the single elements.

The proof consists of two parts:

A. One of the planes of symmetry is vertical.
B. None of the planes of symmetry is vertical.

§ 8A *One of the planes of symmetry of the distribution is vertical.*

This part of the theorem can be proved in two steps:

1) Vertical planes are constructed through all single lines. All these planes scatter around the vertical plane of symmetry containing the mean.

The mean strike of these vertical planes is equal to the strike of the plane of symmetry, or the mean azimuth equals the azimuth of the mean.

2) Cones are constructed with a vertical axis through all single lines. The mean of these cones equals the mean dip and is a plane at right angles to the vertical plane of symmetry. As this plane is not flat, it does not coincide with the other plane of symmetry of the distribution. The approximation is only correct when it can be considered as a flat plane within that part of the distribution containing most lines.

To prove the theorem, the deviation between mean dip and dip of the mean must be calculated for a number of models.

These models should answer two requirements. They should approximate the observed distributions, and they must be suited for a simple analysis. When both these requirements are contradictory, a model must be found that can be analyzed, and showing a deviation exceeding the deviation of the approximated distribution.

The only model for the observed distributions which can be utilized for simple analysis and which contains all possible forms and positions, is the cone-chaped linear distribution. Within the

cone all lines are regularly distributed and equal areas of its projection in the Schmidt net will contain an equal number of lines. The parameters of this distribution are its top angle and the angle between its axis and the vertical. Starting point of our considerations is a cone with a small top angle and with a steeply dipping axis. The projections of these cones in the central area of the Schmidt net can be approximated by circles.

Fig. 25 shows a cone with a top angle of 15° and an axis dipping 75° toward the South. The direction of dip does not influence the deviation which will be calculated.

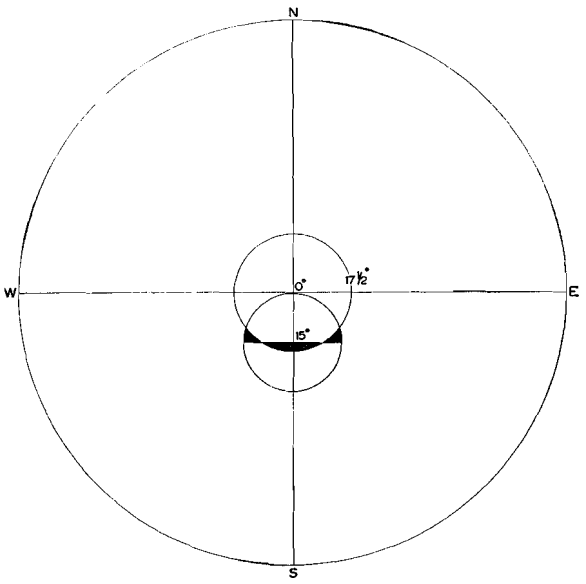

Fig. 25
(Schmidt net, lower hemisphere) For explanation see text.

The mean dip of the lines of this cone-shaped distribution are determined by dividing the circle in two parts by another circle, the centre of which coincides with the net centre. The cone has been projected as a circle. The diameter of this circle, which is perpendicular to the NS line of the net, is drawn. This line divides the distribution into two equal parts. Then, a circle is sought with its centre in the net centre, and also dividing the distribution into two equal parts. The areas enclosed by this circle, the constructed diameter, and the distribution cone above the diameter, must equal the area that is enclosed by this circle and the diameter. These areas are black in fig. 25. The resultant circle corresponds with a cone with vertical axis and a top angle of 17°. This top angle is the complement of the mean dip. The deviation between mean dip and dip of mean is 2½°. Following, it will be proved that this deviation of 2½° is the maximum deviation for all cone-shaped linear distributions with a top angle of 15°.

Firstly, however, it will be determined which distributions are approximated by the latter. All observed distributions show a maximum, meaning that the frequency increases to this maximum. The deviation of a cone-shaped linear distribution is stronger than the deviations of all these observed distributions of lines inside of the cone of the linear distribution, and which have the same vertical plane of symmetry. This last condition must be fulfilled as it implicates the similarity of the azimuth of the mean and the azimuth of the approximated mean.

The distribution of m.f. at Monguelfo can be approximated by an isotropic two-dimensional normal one. The question arises which isotropic two-dimensional normal distribution can be compared to our example, or which isotropic two-dimensional normal distribution has a 75° South dipping axis and a deviation of 2½° between this axis and its mean dip. To solve this problem, firstly, a model of the isotropic two-dimensional normal distribution is projected. This model must be simple in order to carry out the analysis. Its cross section is given in the histogram of fig. 26. The exterior class boundaries include 96 % of the area of a standardized Gauss curve, the interior ones 48 %.

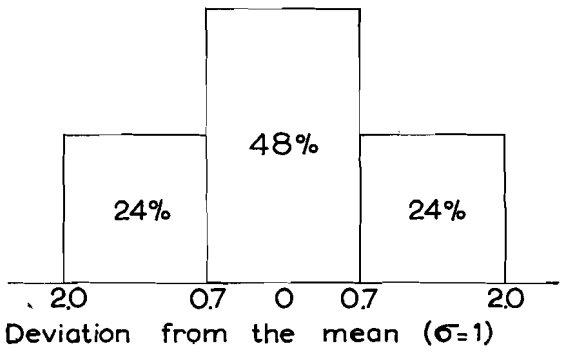

Fig. 26
Simplified histogram of a standardized normal distribution.

A linear distribution is assumed within the three classes. The corresponding two-dimensional distribution consists of two circles around the projected 75° dipping axis, with a ratio of the radii of about 1 : 3. When this ratio is maintained, the

radii may be varied untill the distribution with a deviation of 2½° between mean and calculated mean is found.

The solution is shown in fig. 27; the 17½° cone divides the resultant distribution into two equal parts.

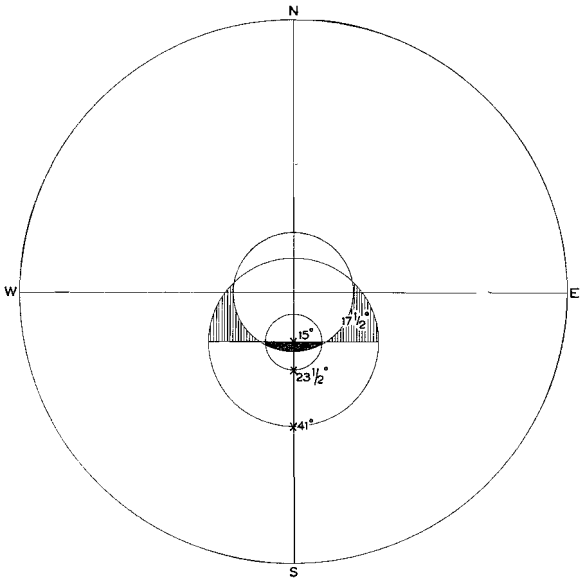

Fig. 27
(Schmidt net, lower hemisphere) For explanation see text.

The black area in fig. 27 counts eight times as much as the shaded areas, as it lies within the inner class. As the ratio of the class boundaries is 1 : 3, the ratio of the class areas is 1 : 8.

The outer class boundary, which includes 96 % of the distribution, has a top angle of about 26°. If a histogram as fig. 26 with more classes would be constructed, which better approximates the Gauss curve, and the position of their most exterior class boundary would be calculated, this cone would have a top angle of more than 26°. This statement appears to be acceptable, considering that the last example with a linear distribution within the classes is intermediate between the cone-shaped linear distribution with its single class and the actual isotropic two-dimensional Gaussian distribution with its infinite classes. It demonstrates that the models of fig. 26 and fig. 27 can be used for the distribution of m.f. at Monguelfo shown in fig. 18, when the latter would have an average dip of 75° instead of 54°, for the most exterior class boundaries of fig. 27 and fig. 18 are the same.

It may be concluded that the deviation is definitely smaller than 2½° for the isotropic two-dimensional distribution of the m.f. at Monguelfo, whatever the attitude of the mean may be.

By means of table XIII the mean dip of the m.f. at Monguelfo was calculated to be 53°. The apparent deviation of only 1° with the calculated mean corresponds with the above conclusion.

Maintaining a cone-shaped linear distribution with a top angle of 15°, it will now be proved that the deviation is maximal when the vertical is a line coinciding with the cone.

After having proved this theorem, the top angle of the cone will be changed and the maximum deviation for all possible cone-shaped linear distributions will be calculated.

The theorem will be proved in two steps:

1) The axis dips less than 75°

2) The axis dips more than 75°.

1) The axis of the cone-shaped linear distribution with a top angle of 15° dips less than 75°. In this case, the top angle of the cone dividing the distribution into two equal parts increases. This means that the same part of the conical surface will better approximate a flat plane, and the deviation between the axis and the conical surface is smaller.

Fig. 28 gives two examples of cone axes dipping 45° and 15°.

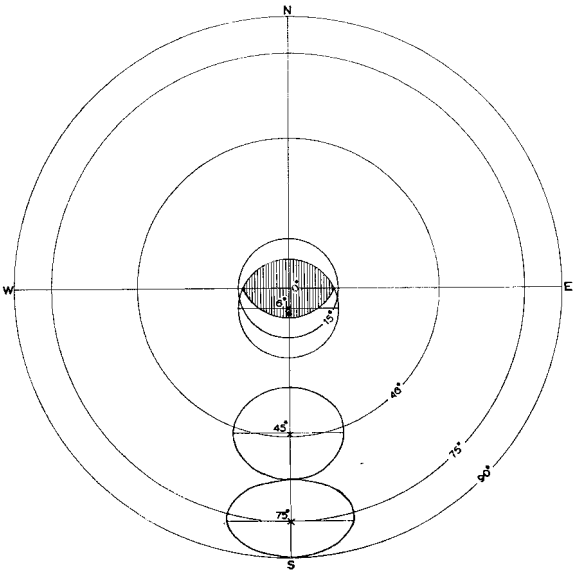

Fig. 28
(Schmidt net, lower hemisphere) For explanation see text.

The cone is projected as an ellipse in the Schmidt net. The cone axis does not coincide with the long

axis of the ellipse but dips less than the line which is represented by the intersecting point of the long axis and the NS line.

The ellipses may be divided into two equal parts as in fig. 25. The top angles of the vertical cones, which divide the example cones with axes making 45° and 75° with the vertical, amount to 46° and 75° respectively. The deviations are 1° and 0°.

2) The axis dips more thans 75°.

In this case, the vertical belongs to the distribution, as do the lines above the EW line of fig. 28 located inside of the conical surface. This EW line is a critical line for indicating the dip of the single lines. In appendix II, the lines above the EW line have been shown with the supplements of their dips.

E.g. any line dipping 80° below the EW line changes into a line dipping 100°, being the supplement of 80°, above this EW line.

If this change to the supplement would not occur, the deviation would increase to a maximum of as much as 10°.6, which equals $(\sqrt{\tfrac{1}{2} \cdot 15^2})°$. in case of a vertical distribution axis.

The deviations in the centre of the net cannot be neglected, and this would mean a failing of the theorem for distributions with a subvertical mean. In some cases, the m.f.'s are subvertical, or the *S*'s are subhorizontal, and our mode of notation is modified in order to apply our theorem in these cases. An example follows. The axis of the cone-shaped linear distribution makes an angle of 6° with the vertical in fig. 28. Dips have been indicated by their supplements in the shaded region above the EW line. One may take the image of this area at the other side of the EW line, which is shaded also. The mean dip of this shaded area is 90°, and it is parallel to the vertical. The mean of the other, not shaded, part of the distribution has been determined in the usual way, by dividing it into two equal parts by a vertical cone. In the present example, this mean has a dip of 15°.

The actual mean dip of the distribution is the resultant vector of two vectors being parallel to the vertical and to the mean dip of the not-shaded distribution. The length of these vectors is proportional to the number of lines of the distribution from which they have been determined.

In our example, the shaded and not-shaded part of the distribution equal each other, and the resultant vector is parallel to the bisecting line between both partial vectors. So, the mean dip amounts to 7½° and the deviation is 1½°.

According to this method we can calculate the deviation for all other cases in which the distribution axis dips more than 75°. For 80° dip, the deviation is about 2°. For 90° dip the deviation is 0°, which is evident.

As a result, it has been proved that the deviation is maximum when the conical surface is tangent to a vertical plane. The maximum deviation may be calculated for other cases, as follows.

Fig. 29 shows other cone-shaped linear distributions with top angles of 15°, 30° and 45° respectively. The deviation has been calculated as in the case of fig. 28. It increases gradually, as the values are 2½°, 4½° and 6½° respectively. The last deviation belongs to distributions with a dispersion exceeding almost all dispersions, mentioned in appendix III.

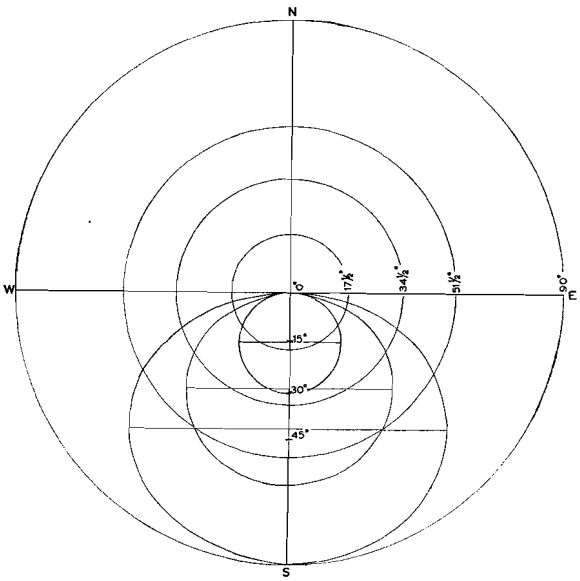

Fig. 29
(Schmidt net, lower hemisphere) For explanation see text.

In some cases, however, the dispersion of the m.f.'s within the mean *S* is very strong and a vertical plane of symmetry is present also. These particular cases, for which the present theorem has not been proved, may be approximated by models in which the dispersion of m.f. around x has been eliminated.

These models will be discussed in the following paragraphs.

This first part of the proof of the theorem learns that the deviation between mean dip and dip of the mean does not exceed a few degrees in most cases of distributions having a subvertical plane of symmetry.

This deviation can be avoided by projecting at right angles all lines of the distribution to the vertical plane of symmetry before calculating the mean of the reduced dips. In most cases, however, the deviation is so small that it may be neglected.

The criteria for this methodological deviation are determined by the natural deviation between sample mean and population mean.

The possibility has been discussed that e.g. slumped blocks may cause a discrepancy between these means (§ 7G). When the dispersion of e.g. 30 dips is strong, one of these dips belonging to a boulder may have caused a deviation of 60°. This deviation of an individual value results in a deviation of 2° for the mean value. This hypothetical case already demonstrates that the methodological deviation is negligible, as a considerable discrepancy has always to be taken into account between sample mean and population mean. These natural deviations can be estimated by comparing adjacent sample means (see chapter 9).

§ 8B *None of the planes of symmetry of the distribution is vertical.*

This case particularly refers to m.f. with a relatively strong dispersion within the mean *S*. The *S* mostly show an isotropic two-dimensional distribution in the ideal case and belong to case A).

If a distribution of m.f. is not isotropic, a vertical plane of symmetry must be present when the mean *S* is subvertical or subhorizontal.

In the case of a dipping mean *S*, a vertical plane of symmetry only exists when the mean m.f. coincides with the strike or with the direction of dip of the mean *S*.

Most samples can be approximated by one of these particular cases.

In consequence of the exceptions and as some distributions of m.f. with a vertical plane of symmetry are not covered by the models of fig. 29, the theorem will be verified with models in which the distribution lies within a single plane of all possible attitudes.

Apart from those cases in which the distribution of the m.f. covers e.g. more than 90° of rake within the mean S, the basic theorem has been proved for a distribution with a vertical plane of symmetry.

This vertical plane of symmetry has to be replaced by an arbitrary plane to represent a distribution within a single plane. In that case, the theorem proves its validity for all distributions intermediate between this last type and the isotropic type. The last type shows the strongest deviations in this series. All possible dispersion around the plane of strongest dispersion represents an approach to the isotropic case for which the

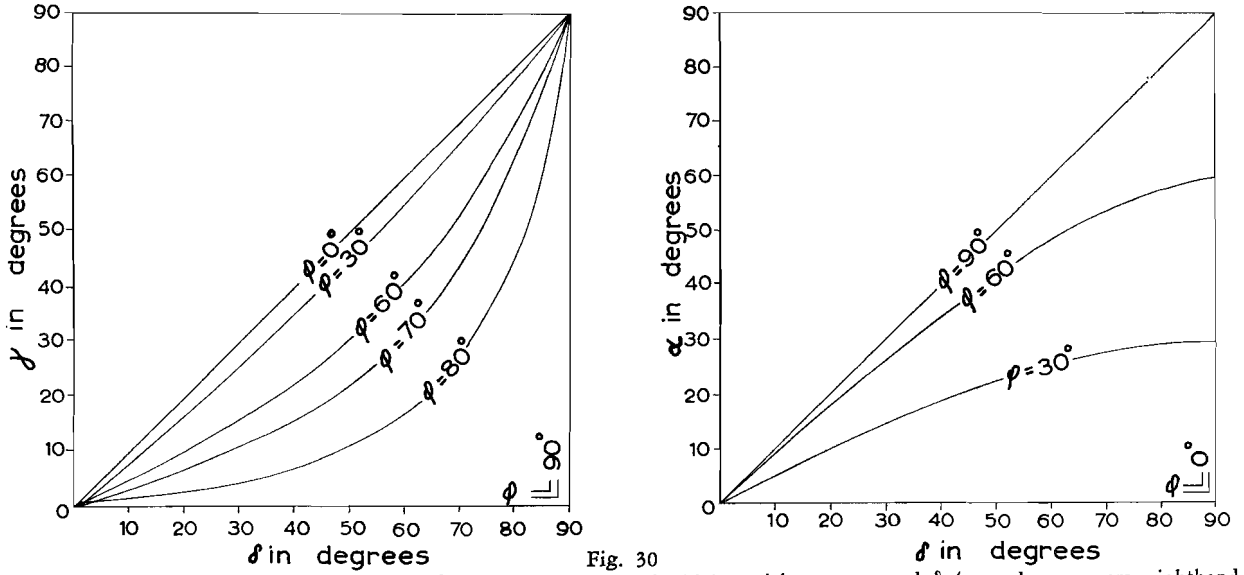

Fig. 30
Nomograms of the relations between γ and δ (first nomogram, left side), and between α and δ (second nomogram, righthand side), for different values of φ.

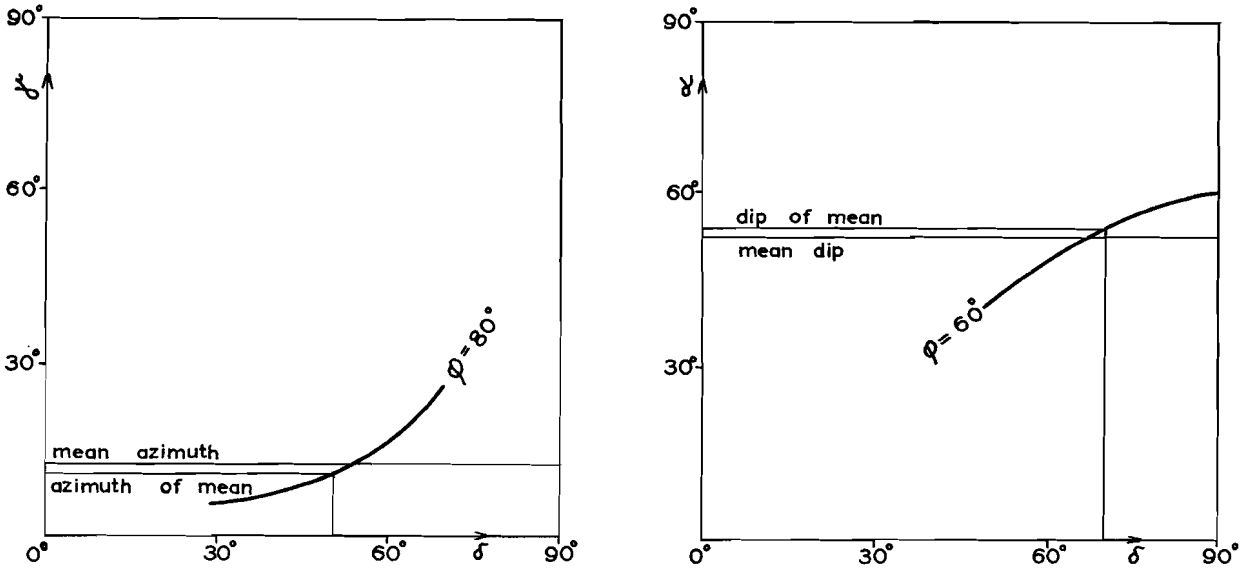

Fig. 31

Left side: example of graphical calculation of the deviation between the mean azimuth and the azimuth of the population mean. Righthand side: ditto for the the mean dip and the dip of the population mean. For further explanation see text.

deviations have been proved to be negligible in the preceding paragraph.

If it can be proved that the deviations are negligible in the present case, they must be negligible for all other distributions with a strong dispersion.

The true mean of the distribution can be determined by calculating the mean angle of rake of the lines in the plane. The question arises whether azimuth and dip of this mean deviate from the mean azimuth and dip. To answer this question two nomograms (fig. 30) have been constructed.

The first one gives γ, the azimuth, and δ, the rake, for different φ's. φ = the dip of the plane of distribution.

The formula for the relation between these angles is: $\operatorname{tg} \gamma = \cos \varphi . \operatorname{tg} \delta$.

The second nomogram gives the dip, α, and δ for different φ's. It is based on: $\operatorname{tg} \alpha = \operatorname{tg} \varphi \cdot \sin \gamma$.

By means of these nomograms the deviations can be calculated for all cases. Use had been made of the fact that the deviations of a linear distribution exceed the deviations of all symmetrical distributions with a maximum between the same boundaries.

The mean may be readily determined. It divides the projection of the distribution along the φ-line on the δ-axis in two equal parts. The mean azimuth and the mean dip must be calculated from the projection of all lines of distribution on the γ- and α-axes.

It is obvious that the mean azimuth and the azimuth of the mean coincide when the φ-line is straight. The curvature of the φ-lines in the nomograms is a measure for the deviation.

In the first diagram, the curvature increases with increasing φ. The deviation, however, does not exceed a few degrees when the dispersion is not too strong.

Fig. 31 gives an example for $\varphi = 80°$ and a linear distribution with δ between 30° and 70°. The mean azimuth has been calculated by approximating the φ-curve by constructing a polygon consisting of equal distances. The centers of these distances have been projected on the γ-axis, and represent an equal number of lines of the linear distribution. Their mean approximates the mean azimuth. The deviation is 2°.

In the same manner, a deviation of 2° has been calculated between mean dip and dip of the mean for a planimetric linear distribution with $\varphi = 60°$ and $50° < \delta < 90°$.

If the dispersion is not too strong, the theorem is applicable to case B), in which none of the planes of symmetry is vertical.

Hitherto, however, a number of cases has been left out of consideration. Concerning the cases where the m.f. are dispersed very strongly in the

mean S, new models have to be constructed. These cases cannot be replaced by cone-shaped linear distributions.

The distributions without a vertical plane of symmetry have been considered as being intermediate between a planimetric distribution and an isotropic distribution. Their deviations would be smaller than the deviations of the latter, and stronger than the deviations of the first case. This was permitted as the cone-shaped linear models indicated that the deviations of the first case are negligible.

An arbitrary distribution will be considered in which the dispersion of one plane (the mean S for m.f.) largely exceeds the dispersion in the other plane of symmetry.

Fig. 32 is an example of such a distribution, which lies between two tangent planes making equal angles with the plane of strongest dispersion and being at right angles to the plane of smallest dispersion.

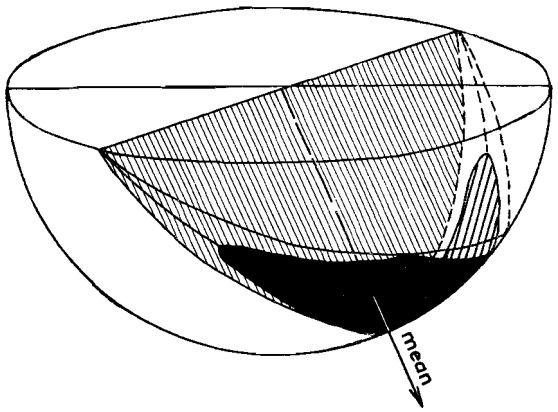

Fig. 32
Example of a distribution with two planes of symmetry. The dispersion in the dipping plane exceeds the dispersion in the vertical plane of symmetry. For further explanation see text.

The lower tangent plane has been shaded. The distribution is assumed to be linear. It is postulated that the deviations of a planimetric linear distribution in the lower tangent plane — which has the same strongest dispersion and the same azimuth of axis as the drawn distribution — exceed the deviations of the drawn distribution.

To prove this theorem is very simple, as the drawn distribution can be divided into a number of planimetric linear distributions with the same axial azimuth, but lying in an array of planes between the two tangent planes. All these planimetric linear distributions have their own deviations. These may be multiplied with the number of lines of their distribution, added, and then divided by the number of distributions to arrive at the deviation of the drawn distribution. This resultant deviation will be smaller than the deviation of all these planimetric linear distributions after their projection at right angles to the lower tangent plane, as the latter has the greatest φ.

This deviation in its turn will be smaller than the deviation of a linear distribution in a plane with the same boundaries, as it has a maximum between these boundaries.

A linear distribution of the same size in the lower tangent plane will provide us with a suitable model for calculating the deviations.

The present discussion applies to strongly dispersed m.f. within the mean S of some meas. samples of the southern Bressanone region and the Cima d'Asta region (table XVIII). The dips of the mean S are not steep in these regions. Apart from a single exception at most a 60° dip may be accepted for the lower tangent plane in all cases.

The maximum deviations in this plane will be determined as follows.

§ 8C *Deviation between the mean azimuth and the azimuth of the mean in case of m.f. strongly dispersed in a certain plane.*

By approximating the $\varphi = 60°$ line of fig. 30 by a polygon the deviation for a linear distribution within this plane can be calculated for $0° < \delta < 90°$. This deviation is 6°.

It is difficult to calculate the maximal deviation, which must be approximated. Fig. 33 gives the $\varphi = 60°$ curve, which has been approximated by two straight lines.

The first one connects ($\delta = 0$, $\gamma = 0$) with ($\delta = 57°$, $\gamma = 32°$) and the second one ($\delta = 57°$, $\gamma = 32°$) with ($\delta = 90°$, $\gamma = 90°$).

The centre point of the first part of this simple polygon has a $\gamma = 17°$. The second one has $\gamma = 62°$, and the mean azimuth of the polygon is 39½°. The deviation must be 7½°, which resembles the deviation of 6°, calculated from a polygon consisting of nine equal distances.

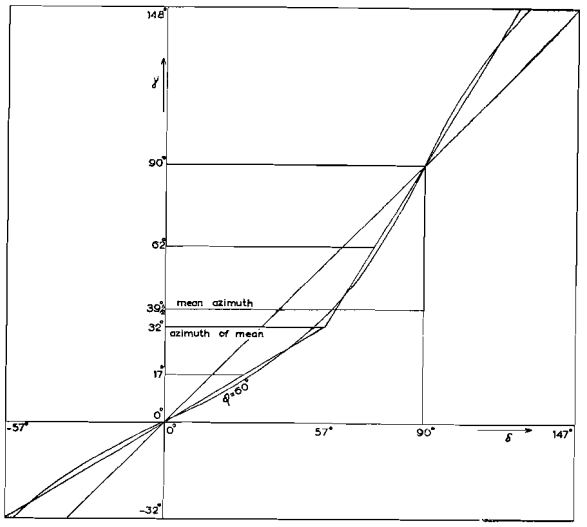

Fig. 33
For explanation see text.

The maximal deviation is twice as great as this value, and is 15°. This maximum occurs for $-57° < \delta < 147°$ (see fig. 33).

It may be remarked that a planimetric linear distribution with $-57° < \delta < 147°$ is regular, with an equal number of lines in any direction. Strictly, the deviation cannot be determined in this case, as all values of δ may be called the mean, and, consequently, one mean azimuth does not exist. However, this deviation may be considered as an extremum.

The maximum of 15° is rather strong. It has not been possible to construct models which adequately approximate the actual distributions and which result in lower maxima. The possibility of deviations between mean azimuth and azimuth of the mean as large as 15° clockwise (e.g. $-57° < \delta < 147°$) and anticlockwise (e.g. $57° < \delta < 237°$) must be considered.

For the case $0° < \delta < 180°$, no deviation exists. Other ranges for δ will have intermediate values.

For two reasons the basic theorem will be applied: 1). The deviations are positive and negative, and a great number of distributions with different δ-ranges at all places will show no deviation when they have been combined. This is opposite to the deviation between mean dip and dip of the mean which is always positive.

2) The maximum of 15° is lower than the maximal deviation between mean dip and dip of the mean (= 25°). In the latter case, the theorem may be checked in an empirical way, and a mean deviation of 8° will be calculated, which is rather small.

An empirical check is not possible in the present case on account of reason 1).

Notwithstanding, the method is maintained as the methods for calculating the deviation are analogous and the present maximum is smaller than that discussed in the following paragraph.

§ 8D *Deviation between mean dip and dip of the mean in case of m.f. strongly dispersed in a certain plane.*

The deviation between mean dip and dip of the mean for $\varphi = 60°$ amounts to 2° for $50° < \delta < 90°$, and 3° for $0° < \delta < 90°$.

When $0° < \delta < 180°$, it is 25°. This is a maximum value as is obvious from increasing δ to 180° in the case of $\varphi = 60°$ (fig. 30). The part $90° < \delta < 180°$ is the image of the drawn part $0° < \delta < 90°$, with respect to the $\delta = 90°$-ordinate. The value of 25° cannot be neglected. It may be stated that in the case of a strong dispersion of m.f. in the mean S around a vertical plane of symmetry, this method should be carefully applied. For $\varphi = 30°$ the maximal deviation is 9°. A planimetric linear distribution with $0° < \delta < 180°$ has a mean which equals all values of δ due to its regular nature. As in the analogous case of the azimuthal deviation, this deviation may be considered as an extremum.

In these particular cases, the deviation between mean dip and dip of the mean has to be calculated, as the negligible size of the deviation cannot be proved theoretically.

For this purpose, the following reasoning is used. The basic theorem can be applied to the S-distributions of the discussed special cases, but not to the m.f. The relation between the mean S and the mean m.f. is as follows. The mean m.f. must lie within the mean S. Exceptions of minor importance occur, as the m.f. and S co-ordinates do not always coincide.

Systematic deviations cannot be expected; these would occur when the deviations of the applied approximate method become too strong.

Table XVIII shows the mean S and the mean m.f. for the cases under discussion. The approxi-

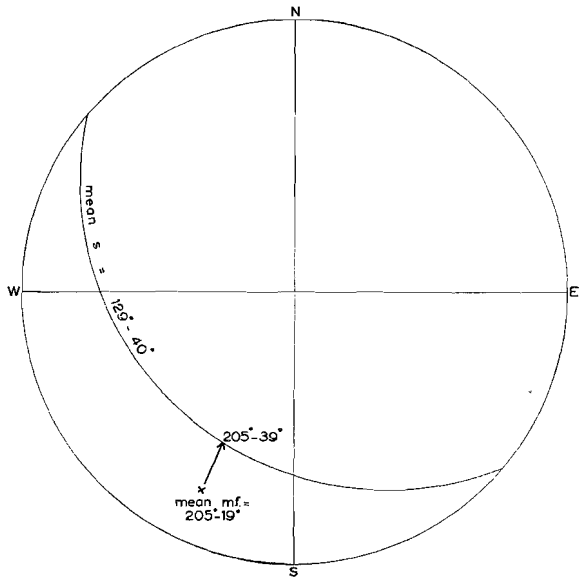

Fig. 34

Example of an approximate mean m.f. which does not lie in the approximate mean *S*. The mean dip of the m.f. must be enlarged by 20° for calculating a more accurate dip of the mean m.f. (Schmidt net, lower hemisphere). For further explanation see text.

TABLE XVI

Table for comparing the mean calculated by approximation with the contour maximum of the pole diagram. (with magnetic correction) S. Stefano region (meas. samples 1-16)

Meas. sample	calculated mean s.	contoured maximum s	calculated mean m.f.	contoured maximum m.f.
1	287°— 65°		303°— 7°	295°— 5°
2	306°— 52°	310°— 50°	112°— 15°	116°— 17°
3	296°— 48°		289°— 8°	298°— 10°
4	309°— 30°		313°— 18°	316°— 14°
5	294°— 48°	290°— 50°	110°— 14°	
6	266°— 58°		293°— 14°	
7	293°— 58°		326°— 35°	328°— 37°
8	285°— 54°		105°— 16°	104°— 17°
9	297°— 68°	298°— 55°	110°— 15°	110°— 25°
10			340°— 12°	340°— 15°
11	262°— 90°		273°— 41°	266°— 34°
12	287°— 56°	281°— 45°	87°— 16°	
13			107°— 60°	
14			292°— 21°	285°— 28°
15			309°— 17°	
16			305°— 18°	305°— 27°

TABLE XVII

See table XVI. Pusteria region (meas. samples 17-91)

Meas. sample	calculated mean m.f.	contoured maximum m.f.						
17	88°— 53°	91°— 54°	43	103°— 55°	103°— 54°	69	94°— 13°	88°— 14°
18	79°— 51°	89°— 55°	44	50°— 19°	42°— 11°	70	87°— 19°	85°— 22°
19	92°— 33°	91°— 28°	45	80°— 49°	82°— 53°	71	89°— 25°	88°— 29°
20	140°— 25°	147°— 19°	46	92°— 6°	87°— 4°	72	104°— 58°	107°— 60°
21	106°— 13°		47	83°— 11°	87°— 9°	73	101°— 53°	100°— 52°
22	92°— 37°	93°— 36°	48	91°— 7°	91°— 5°	74	94°— 26°	98°— 28°
23	67°— 21°	66°— 21°	49	115°— 23°	105°— 19°	75	78°— 14°	76°— 12°
24	227°— 8°	226°— 5°	50	284°— 14°	286°— 13°	76	83°— 20°	83°— 20°
25	53°— 15°	51°— 12°	51	269°— 6°	267°— 1°	77	104°— 38°	
26	137°— 6°	144°— 4°	52	282°— 17°	281°— 20°	78	96°— 39°	
27	108°— 8°	100°— 8°	53	280°— 18°	282°— 15°	79	89°— 43°	88°— 42°
28	49°— 24°	58°— 22°	54	298°— 15°	301°— 26°	80	84°— 41°	86°— 44°
29	102°— 11°	104°— 12°	55	321°— 6°	317°— 6°	81	100°— 40°	101°— 39°
30	103°— 21°	103°— 23°	56	60°— 12°	60°— 14°	82	99°— 47°	92°— 54°
31	39°— 24°	34°— 20°	57	112°— 1°	107°— 7°	83	114°— 26°	116°— 32°
32	47°— 38°	50°— 37°	58	115°— 6°	107°— 7°	84	106°— 39°	104°— 42°
33	71°— 30°	75°— 31°	59	316°— 13°	320°— 12°	85	94°— 24°	94°— 25°
34	47°— 34°	42°— 36°	60	291°— 12°	283°— 0°	86	97°— 34°	100°— 36°
35	47°— 25°	43°— 28°	61	99°— 4°	101°— 4°	87	82°— 47°	82°— 49°
36	41°— 19°	37°— 13°	62	107°— 12°	106°— 10°	88	103°— 37°	103°— 38°
37	107°— 16°	107°— 16°	63	91°— 23°	88°— 24°	89	109°— 50°	108°— 55°
38	101°— 6°		64	127°— 35°	125°— 36°	90	109°— 24°	120°— 28°
39	67°— 26°	70°— 26°	65	121°— 10°	122°— 10°	91	108°— 19°	108°— 20°
40	108°— 49°	108°— 50°	66	122°— 11°	124°— 11°			
41	95°— 37°	98°— 41°	67	105°— 19°	104°— 16°			
42	100°— 58°	100°— 60°	68	108°— 20°	100°— 22°			

mate mean m.f. does not necessarily lie within the mean *S*. in that case, it has been rotated about a horizontal axis at right angles to the mean azimuth. The rotation angle is called positive when the mean m.f. dips less than the mean *S*.

Fig. 34 gives an illustration of this technique. The mean $S = 129° - 40°$ and the mean m.f. $= 205° - 19°$ are plotted. The mean m.f. is rotated into the position $205° - 39°$, and lies within the mean *S*. The rotation angle or deviation $= + 20°$.

The 11 cases of table XVIII showing strongly dispersed m.f. in combination have a mean deviation of $+ 8°$.

This chapter will be concluded with an empirical check of the theorem.

In the tables XVI - XXI the approximated mean is compared to the contour maximum of the corresponding sample if contours could be constructed. These tables may be considered as a summary of the appendices II and III.

TABLE XVIII

See table XVI. Bressanone region (meas. samples 92-142) In the meas. samples 117, 118, 119, 127, 129, 132, 135, 138, 139, 140, 141, (and 161 of table XIX) the distribution of the m.f. within the mean *S* distinctly exceeds 90°; in these cases, a correction has been calculated according to § 8D

Meas. sample	calculated mean s.	contoured maximum s.	calculated mean m.f.	contoured maximum m.f.	correction of mean dip according to § 8 D
92			217°— 77°	195°— 81°	
93			194°— 73°	203°— 72°	
94			103°— 54°	106°— 54°	
95			103°— 58°	107°— 58°	
96			86°— 39°	89°— 39°	
97	116°— 47°	117°— 38°	140°— 25°	146°— 24°	
98	130°— 50°	135°— 40°	158°— 36°		
99	115°— 41°	126°— 43°	143°— 23°	148°— 19°	
100	125°— 40°	120°— 36°	161°— 25°		
101	122°— 34°	115°— 29°	153°— 19°	155°— 22°	
102	82°— 48°	78°— 45°	159°— 38°	156°— 38°	
103	93°— 96°	88°— 40°	175°— 36°		
104	18°— 41°	22°— 41°	141°— 36°	138°— 37°	
105	109°— 62°	117°— 63°	126°— 43°	128°— 48°	
106	157°— 15°	165°— 4°	173°— 4°	168°— 5°	
107	140°— 17°	145°— 15°	166°— 13°	160°— 13°	
108	118°— 55°	126°— 50°	154°— 37°	150°— 34°	
109	93°— 56°		140°— 44°	140°— 50°	
110	83°— 69°	81°— 69°	104°— 43°	102°— 43°	
111	99°— 82°	101°— 72°	113°— 52°	115°— 56°	
112	104°— 86°	86°— 78°	101°— 51°	100°— 52°	
113	105°— 75°	96°— 76°	201°— 74°	195°— 85°	
114	91°— 67°		190°— 73°	198°— 67°	
115			15°— 0°		
116			202°— 16°	203°— 20°	
117	88°— 34°	84°— 27°	187°— 23°		+3°
118	85°— 38°	85°— 35°	156°— 23°	135°— 26°	+10°
119	129°— 40°	130°— 37°	154°— 14°	169°— 25°	+ 8°
120	112°— 32°		199°— 23°		
121	102°— 35°	96°— 32°	152°— 27°		
122	84°— 41°	84°— 37°	156°— 39°	156°— 42°	
123	102°— 35°	98°— 30°	169°— 14°		
124	112°— 25°	113°— 22°	187°— 15°	187°— 18°	
125	216°— 29°	213°— 31°	356°— 8°	352°— 10°	
126	153°— 23°	168°— 22°	185°— 9°	185°— 12°	
127	349°— 5°	40°— 5°	169°— 5°		?
128	99°— 36°		186°— 31°		
129	102°— 29°	104°— 27°	170°— 18°	175°— 27°	+ 9°
130	114°— 23°	115°— 23°	166°— 20°		
131	112°— 37°	112°— 37°	177°— 27°	180°— 32°	
132	127°— 39°	131°— 38°	190°— 25°	174°— 31°	+10°
133	110°— 91°	121°— 82°	110°— 36°	129°— 57°	
134	95°— 55°	85°— 50°	151°— 40°	150°— 43°	
135	87°— 50°	88°— 37°	140°— 38°	152°— 34°	+ 5°
136	122°— 43°		142°— 17°	143°— 20°	
137	303°— 55°	310°— 60°	79°— 38°	80°— 40°	
138	101°— 24°	65°— 24°	176°— 7°	178°— 14°	+ 8°
139	138°— 40°	140°— 54°	152°— 13°		— 4°
140	305°— 25°	301°— 22°	43°— 11°		+18°
141	88°— 29°	100°— 23°	181°— 21°		+ 8°
142	80°— 78°	86°— 88°	82°— 47°	81°— 47°	
(161	236°— 28°	228°— 20°	337°— 19°		+ 9°)

TABLE XIX See table XVI. Cima d'Asta region (meas. samples 143-192)

Meas. sample	calculated mean s.		contoured maximum s.		calculated mean m.f.		contoured maximum m.f.	
143	273°	25°			296°	12°		
144	262°	33°	261°	29°	329°	23°	332°	32°
145	290°	29°	288°	25°	346°	19°		
146	248°	24°	248°	16°	348°	17°	346°	18°
147	135°	16°			159°	4°	163°	5°
148					156°	2°	150°	2°
149	287°	33°	287°	33°	334°	24°		
150	268°	36°	262°	33°	7°	24°		
151	239°	11°	180°	2°	348°	3°	346°	1°
152	286°	38°	284°	35°	334°	21°		
153	207°	25°			342°	7°		
154	272°	28°	268°	30°	344°	21°	338°	28°
155	271°	74°	268°	80°	266°	87°	270°	85°
156	247°	30°			343°	21°		
157	271°	39°	269°	39°	339°	32°	341°	35°
158	287°	39°			346°	37°	340°	43°
159	312°	31°			352°	19°	352°	18°
160	202°	32°	203°	30°	8°	7°	15°	3°
161	236°	28°	228°	20°	337°	19°		
162					348°	30°	355°	33°
163	254°	32°	254°	24°	339°	22°	339°	21°
164	250°	18°	275°	15°	328°	9°	331°	10°
165	314°	32°			6°	18°	5°	22°
166	194°	31°	182°	23°	353°	15°	350°	17°
167	265°	27°	260°	28°	344°	20°	340°	23°
168	234°	30°			338°	18°	338°	17°
169	225°	18°			340°	10°	338°	12°
170	224°	25°	225°	18°	351°	12°	350°	12°
171	174°	2°			345°	5°	345°	7°
172	260°	19°	225°	16°	351°	9°	354°	11°
173	266°	32°	263°	30°	356°	22°	358°	23°
174	327°	48°	336°	54°	16°	30°	9°	25°
175	322°	25°	316°	14°	354°	15°	352°	14°
176	264°	30°	249°	33°	10°	30°	12°	30°
177	303°	28°	302°	25°	351°	16°	353°	15°
178	358°	31°	253°	26°	5°	28°	8°	27°
179	355°	50°	348°	49°	357°	13°	353°	14°
180	244°	33°	241°	30°	7°	27°	11°	25°
181	243°	36°	259°	35°	5°	26°	13°	27°
182	314°	13°	270°	12°	355°	13°	357°	13°
183	232°	37°	236°	35°	2°	27°	3°	27°
184	237°	32°	240°	32°	1°	29°	2°	27°
185	294°	27°	292°	25°	348°	12°	347°	12°
186	319°	39°	314°	27°	354°	18°	353°	19°
187	17°	54°	15°	54°	18°	11°	20°	12°
188	342°	31°	342°	26°	353°	9°	355°	9°
189	312°	46°	317°	43°	348°	30°	350°	28°
190	322°	46°	338°	47°	352°	33°	353°	30°
191	336°	38°	339°	35°	353°	12°	356°	12°
192	267°	38°	268°	37°	351°	19°	350°	20°

TABLE XX

See table XVI. Gosaldo region (meas. samples 193-215)

Meas. sample	calculated mean s.		contoured maximum s.		calculated mean s.		contoured maximum m.f.	
193	227°	47°	227°	48°	356°	23°		
194	265°	44°	248°	39°	8°	36°	358°	7°
195	249°	43°	250°	44°	357°	34°	356°	40°
196	290°	38°			4°	19°		
197	269°	44°	270°	36°	350°	29°	357°	36°
198	260°	49°			328°	29°		
199	239°	51°	240°	49°	10°	37°	10°	36°
200	233°	48°	238°	48°	4°	33°	6°	35°
201	286°	39°	284°	36°	354°	24°		
202	269°	39°			2°	28°		
203	247°	39°	241°	36°	0°	36°	0°	38°
204	256°	32°	238°	27°				
205	237°	41°	241°	34°	335°	32°		
206	242°	36°	242°	28°	348°	16°	341°	29°
207	192°	5°			334°	11°	334°	11°
208	232°	40°	235°	44°	351°	35°	2°	36°
209	254°	30°	272°	22°	340°	15°	337°	16°
210	211°	33°	207°	24°	329°	22°		
211	226°	31°			350°	14°	355°	18°
212					343°	13°		
213	211°	40°			351°	30°		
214	245°	40°			3°	28°	4°	26°
215	78°	70°			146°	44°		

TABLE XXI

See table XVI. M. Spico region (meas. samples 216-270). The median s. and the median m.f. are given. If the number of measurements is even, no single median value is present. In that case, the median has been calculated as the mean of adjacent values. E.g., a median strike lies between 268° (2 meas.) and 263° (3 meas.), and amounts to $^1/_5$ (2 x 268° + 3 x 263°) = 265°.

Meas. sample	calculated mean s.	contoured maximum s.	median s	calculated mean m.f.	contoured maximum m.f.	median m.f.
216	88°— 89°	88°— 89°	88°— 90°	89°— 37°	86°— 37°	88°— 35°
217	91°— 84°	89°— 83°	88°— 84°	90°— 11°	90°— 11°	88°— 10°
218	104°— 44°	85°— 41°	88°— 60°	94°— 6°		93°— 5°
219	271°— 45°	263°— 52°	268°— 40°	88°— −9°	89°—−12°	88°— −5°
220	66°— 76°	66°— 78°	68°— 78°	70°— 24°	70°— 24°	68°— 25°
221	85°— 83°	85°— 83°	88°— 85°	85°— 4°	88°— 9°	85°— 6°
222	80°— 53°	85°— 56°	78°— 53°	87°— 20°	87°— 22°	88°— 21°
223	80°— 64°	77°— 60°	78°— 63°	86°— 14°	87°— 16°	88°— 15°
224	78°— 41°	74°— 43°	73°— 41°	82°— 10°	74°— 5°	78°— 5°
225	280°— 25°	283°— 23°	283°— 25°	97°— 5°	97°— 6°	98°— 3°
226	268°— 81°		268°— 85°	88°— 2°	88°— 1°	88°— 0°
227	258°— 49°		250°— 45°	89°— −5°	90°—−10°	88°— −5°
228	268°— 33°		283°— 35°	72°— 10°	75°— 15°	73°— 11°
229	87°— 91°	87°— 89°	88°— 90°	85°— 32°	85°— 31°	88°— 20°
230	266°— 85°	265°— 85°	263°— 85°	265°— −1°	266°— −1°	268°— −5°
231	272°— 73°	274°— 73°	273°— 70°	272°— 6°	271°— 2°	268°— 3°
232	90°— 69°	90°— 73°	93°— 65°	92°— 8°	91°— 8°	93°— 7°
233	87°— 46°	87°— 38°	88°— 43°	96°— 9°	87°— 9°	98°— 7°
234	86°— 93°	87°— 90°	83°— 90°	86°— 23°	88°— 21°	88°— 20°
235	281°— 8°	305°— 10°	288°— 15°	98°— 8°	103°— 8°	98°— 10°
236	276°— 69°	275°— 69°	278°— 72°	86°— 21°	87°— 21°	86°— 25°
237	264°—−13°	244°—−16°	263°—−25°	88°— 1°	89°— 2°	88°— 0°
238	94°— 51°	98°— 49°	98°— 50°	96°— 0°	94°— 4°	98°— 3°
239	92°— 43°	93°— 43°	93°— 45°	103°— 12°		101°— 10°
240	104°— 64°	101°— 64°	103°— 61°	266°— 7°	256°— 13°	263°— 7°
241	92°— 20°		93°— 33°	282°— 3°	285°— 3°	283°— 3°
242	73°— 91°	70°— 90°	73°— 90°	252°— 10°	254°— 7°	253°— 10°
243	76°— 96°	74°—100°	78°—100°	258°— 8°	261°— −1°	261°— 3°
244	77°— 81°	75°— 82°	73°— 80°	76°— 31°	75°— 30°	73°— 30°
245	66°— 80°	68°— 81°	68°— 85°	72°— 18°	75°— 23°	73°— 18°
246	77°— 82°	79°— 79°	78°— 80°	78°— 4°	79°— 7°	78°— 5°
247	281°— 24°	276°— 22°	278°— 24°	88°— 4°	89°— 2°	88°— 3°
248	65°— 77°	65°— 70°	68°— 75°	67°— 7°	69°— 1°	68°— 7°
249	66°— 88°	65°— 83°	68°— 88°	67°— −5°	68°— 0°	68°— −5°
250	61°— 78°	58°— 76°	58°— 75°	63°— 15°	61°— 13°	58°— 15°
251	64°— 81°	62°— 81°	63°— 80°	65°— 9°	63°— 10°	63°— 10°
252	80°— 90°	80°— 90°	78°— 90°	86°— 2°	80°— 2°	83°— 0°
253	82°— 89°	81°— 88°	78°— 90°	78°— −2°	78°— −1°	78°— 0°
254	89°— 89°	93°— 91°	88°— 90°	89°— 22°	89°— 23°	88°— 24°
255	254°— 78°	254°— 78°	256°— 77°	73°— −2°	73°— 0°	73°— 0°
256	66°— 85°	64°— 82°	63°— 83°	67°— 11°	66°— 14°	66°— 12°
258	79°— 66°	80°— 66°	78°— 65°	84°— 29°	84°— 28°	83°— 29°
258	277°— 22°	277°— 26°	288°— 25°	289°— 8°	295°— 12°	293°— 6°
259	231°— 93°		235°— 97°			
260	73°— 63°	79°— 67°	78°— 64°	253°— 13°	257°— 13°	253°— 10°
261	78°— 82°	72°— 80°	73°— 81°	80°— 22°	71°— 23°	73°— 20°
262	77°— 69°	76°— 64°	73°— 65°	247°— 40°	246°— 39°	248°— 40°
263	272°— 24°	268°— 21°	268°— 26°	275°— 9°	275°— 9°	277°— 10°
264	92°— 81°	92°— 81°	93°— 80°	271°— 15°	270°— 16°	268°— 15°
265	70°— 74°	64°— 72°	68°— 75°	69°— −4°	70°— −9°	68°— −5°
266	74°— 72°		73°— 75°	250°— 10°	250°— 9°	253°— 5°
267	244°— 20°	244°— 18°	239°— 20°	261°— 2°	266°— 1°	268°— 2°
268	73°— 76°	75°— 72°	73°— 74°	72°— −8°	71°—−13°	75°—−10°
269	75°— 90°	78°— 90°	73°— 90°	76°— 6°	75°— 5°	74°— 6°
270	63°— 79°	63°— 78°	63°— 80°	64°— 3°	63°— 1°	63°— 3°

CHAPTER 9

VARIATION OF THE POPULATION MEAN

In the preceding chapters the methods for calculating the mean of a supposed population have been discussed, and the approximated means may be plotted on the structure maps in their correct places. To find these correct places, the mean co-ordinates were calculated from collections of single measurements.

The position of the mean is accurate up to 50 m. The exact elevation has not been calculated. Generally, the mean elevation of a collection of single measurements can be approximated by the elevation of the point with the mean co-ordinates.

The condition to be fulfilled is that the elevations of the single measurements are scattered around a flat plane. As a sample region nearly always lies on a single mountain slope, this flat plane may be considered to be represented by the topography.

The mean elevations have been left out of consideration in constructing the mean strike lines, and similar lines. This implies that the observed three-dimensional pattern of a varying mean has been represented by a two-dimensional one, in which all means have been projected in a horizontal plane. This approximation is justified as follows. After its application an observable variation of the mean in that part of the vertical which is covered by the mean elevation cannot be proved. The absence of a relation between mean and mean elevation is considered to indicate the applied approximation to be permitted.

In the preceding chapters it has been tried to prove the existence of populations with a mean and with single scattered values. In the present chapter the relation between the comparable means will be discussed. If these means build up a regular pattern the results of the preceding chapters are verified indirectly.

The following types of lines will be used:

1. *mean strike lines* giving the variation of the mean strike of schistosity in the horizontal plane at the mean topographic level.
2. *iso-lines of mean strike* connecting points with the same mean strike.
3. *mean azimuth lines* giving the variation of the mean azimuth of minor folds.
4. *iso-lines of mean azimuth* connecting points with the same mean azimuth of minor folds.
5. *iso-lines of mean dip of minor folds* connecting points with the same mean dip of minor folds.

The structure maps (sheet IIa, III, IIIa, IV, V, VII, and VIII) show these types of lines. The regular pattern of the lines indicates the applied approximations to be justified.

These approximations can be summarized as follows:

1. The population of tectonic elements is approximated by a sample. This sample, however, may contain elements of other populations (slumped blocks; minor folds of more than one compression phase).
2. The mean of the population is calculated by an approximate method.
3. All means are projected in a horizontal plane at mean topographic level.
4. The mean strike and mean azimuth lines are constructed by assuming a linear variation between the corresponding iso-lines.
5. The iso-lines have a supposed course as given on the structure maps.
6. Iso-lines of mean dip of minor folds are drawn by assuming a linear variation between adjacent mean dips of minor folds.

§ 9A *Frequency curve of a distribution with Varying Mean.*

Firstly, it will be attempted to determine the shape of the frequency curve of a measurements sample from a region in which the mean varies.

From the structure maps it follows that the mean azimuth as well as the mean dip of minor folds may show sudden variations. Variations

have been noted of 50° per km of mean azimuth and dip of the m.f. at the Eggerberg (sheet III) and of the mean rake of the m.f. in the mean *S* along the Rio Larice (Sheet II).

A particular frequency curve of the sample results when the variation of the mean cannot be neglected in the sample region. A theoretical example will be given, starting from an isotropic two-dimensional normal distribution of the population at one point. Numerous observation points are assumed to be distributed at random in a square sample region with an area of 1 km². The mean m.f. varies linearly within the constant mean *S* with an amount of 50° per km, and along a line parallel to one of the sides of the square sample region.

It is possible to compute the non-Gaussian frequency curve in the x , y-plane (see fig. 12), whereas the Gaussian frequency curve in the y , z-plane is not changed.

The contourlines in the Schmidt net have an oblong ellipsoidal shape. Each infinitesimal rectangle at right angles to the line of maximal variation (50° per km) possesses the original isotropic two-dimensional normal distribution, shown in fig. 35 (upper part).

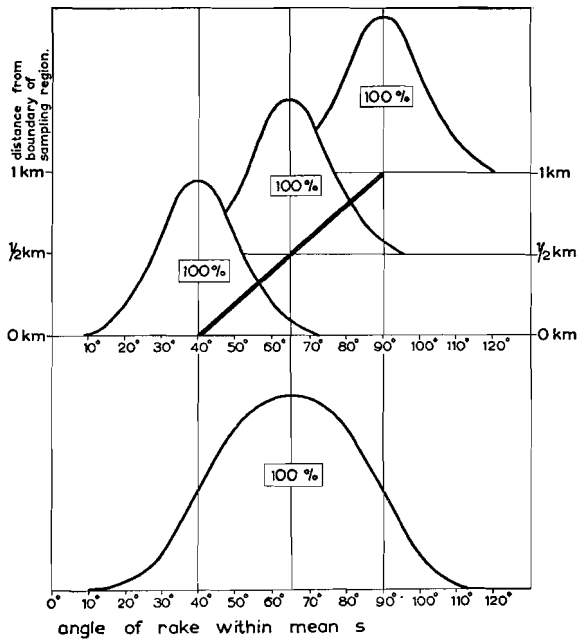

Fig. 35

Upper part: The heavy line gives the variation of the mean m.f. within the mean *S* in °rake per km. The frequency curve is a Gauss curve in all points of this line.
Lower part: Frequency curve of the entire sampling region.

The total distribution is compiled from these single isotropic two-dimensional normal distributions.

If the sample region would begin at a boundary point with mean rake = 40°, as in fig. 35, but have no other boundaries, the curve resulting from an accumulation of Gauss-curves of the infinitesimal rectangles is the cumulative Gauss curve (fig. 35, lower part). Actually, however, this is impossible as the periodicity of the rake would result in a linear distribution. This makes it clear that for our example the produced frequency curve may be approximated by two cumulative Gauss curves which are images (fig. 35, lower part).

The frequency formula at the left boundary of the sample region (upper side of fig. 35) is approximated by

$$y = c. \int_{-\infty}^{x} e^{-\frac{1}{2}\left(\frac{x - b_1}{\sigma}\right)^2} dx$$

with c being a constant and b_1 being the population mean at the boundary of the sampling square ($b_1 = 40°$ in figure 35).

The cumulative frequency curve for $-\infty° < x < 65°$ is approximated by

$$y = c. \int_{-\infty}^{x} \int_{-\infty}^{x} e^{-\frac{1}{2}\left(\frac{x - b_1}{\sigma}\right)^2} dx^2$$

(lower side of fig. 35).

The formula's for the righthand half are the same when the x = 0° line is reflected by the x = 65° line, which represents the mean of the new distribution.

If the above theoretical example would serve as a model for non-isotropic distributions, the amount of the linear variation of the mean could be calculated as follows.

1. Determine the intersecting points between the contourline enclosing almost the whole distribution and their planes of symmetry.
2. Read the angles of rake between these intersecting points within the two planes of symmetry.
3. Subtract these rake values to determine the linear variation.

The example of fig. 35, however, is theoretical. Under actual conditions the strong variations of the mean are not linear. A *condicio sine qua non*

for an exact frequency curve is a regular distribution of observation points within a rectangular sample region. This condition is generally not fulfilled. Finally, the isotropic two-dimensional normal distribution is not always a good starting point.

An example was selected from the S. Stefano region. Most observation points of the meas. samples 7 and 8 (App. II) lie along the Rio Larice. The quartz phyllites are exposed continuously along this river, and the distances between adjacent measurements are fairly constant. The observation points are regularly distributed along a straight line, about at right angles to the strike of the mean schistosity.

Sample 7 contains 23 m.f. with mean 327° - 33°, and sample 8 contains 26 m.f. with mean 105° - 16°. These m.f. have been plotted in fig. 36.

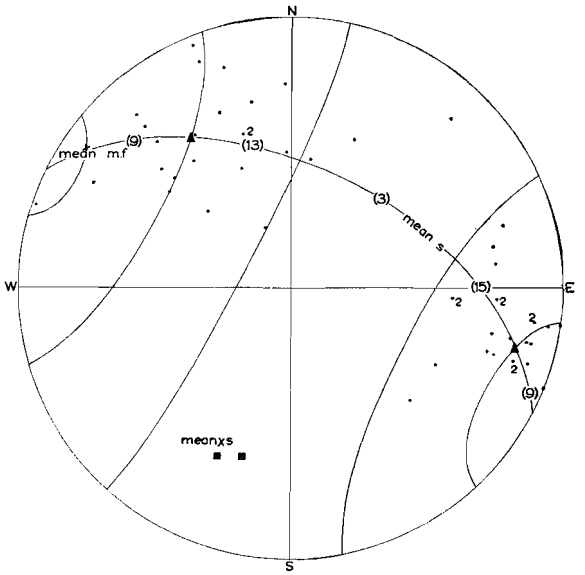

Fig. 36

Pole diagram (Schmidt net, lower hemisphere) of 49 m.f. along the Rio Larice, S. Stefano region. Triangles represent the mean m.f. 's of the meas. samples 7 and 8 (App. II), and rectangles the mean *S'* of these samples. For further explanation see text.

It has been supposed that both mean m.f.'s determine the attitude of the mean *S*, which has been drawn as a great circle in the net. Its pole nearly coincides with the mean of 7 *S* of sample 7 being 293° - 58° and the mean of 10 *S* of sample 8 being 285° - 54°.

The mean m.f. varies within the not varying mean *S*. The difference between the sample means with co-ordinates 112-620 and 116-627 respectively is 63° rake. This is a variation of 63° in position over 800 m.

This variation, however, does not continue beyond the Rio Larice as follows from structure map II^{A}. The shape of the frequency distribution of fig. 36 does not resemble fig. 35 which is not surprising. Four classes of each 31½° rake were made, and the sample means are the outer class boundaries of classes at both sides of their bisecting line, being the mean m.f. of both samples together.

The class boundaries are small circles which are the projections of cones around the strike of the mean *S*. The frequencies of the classes at the one side of the mean m.f. are 9 and 13. At the other side, we see 9 and 15. If the classes should be reduced, the middle ones would appear to be almost devoid of m.f. If follows that around the mean m.f. the frequency distribution shows a local minimum.

This particular shape may be explained as follows.

The area in the southern part of Rio Larice has a mean m.f. of about 327° - 33° (sample 7) and the northern part a mean m.f. of about 105° - 16° (sample 8). The variation between these different means is rather abrupt. It arises almost completely over a small stretch of the Rio Larice between both sample areas.

This geometrical fact, however, may be concluded from the structure map II^{A}. The analysis of single diagrams contributes little to this picture. For this reason, the structure maps will be considered as the geometrical base for kinematical considerations. The kinematics are dealt with in another part of this thesis; it is mentioned here that the strong variation of the mean m.f. along the Rio Larice cannot be explained by one single deformation of the *S*-planes, which would result in an equal mean m.f. along the Rio Larice. The strong variation of the mean m.f. indicates a later 63° rotation of blocks along the *S*-planes.

§ 9B *Construction of the Structure maps.*

From the preceding paragraph it follows that the separate samples do not produce valuable information on the variation of the mean, but they are used as a base for our structure maps. The types of lines on the structure maps have already been summarized in the beginning of this chapter.

The construction of the mean strike and mean azimuth lines requires an explanation.

A methodological approach is not always possible as in the case of unexposed formation boundaries and of iso-lines of mean dip of m.f. By using hand-drawn curves, more regular patterns are obtained as small deviations of individual basic values from these patterns can be avoided. This method is arbitrary as it is influenced by personal taste. In applying hand-drawn curves, the adjectives "schematic" and "hypothetic" are used. By giving basic values in the same figure, the accuracy of the hand-drawn lines may be verified.

The mean azimuth and mean strike lines, however, are constructed according to rather simple methods.

The construction of the mean azimuth lines is similar to the construction of the mean strike lines, and the latter will not be discussed.

Our considerations are based on Busk's construction methods for sections (Busk, 1929). The isoclines of the section must be replaced by iso-mean azimuth lines.

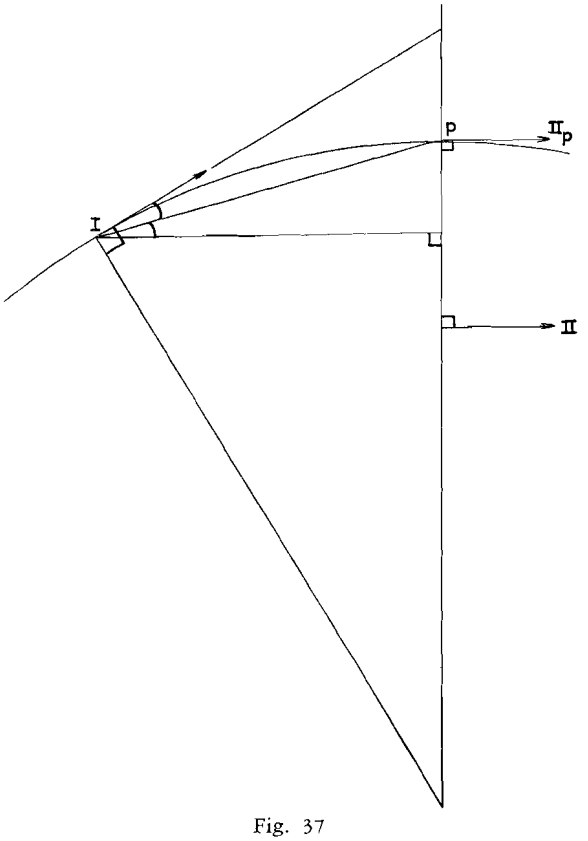

Fig. 37
Constructon of the mean azimuth line based on Busk's method. For explanation see text.

In the theoretical case of parallel folding the isoclines are at right angles to the bedding planes (de Sitter, 1941). Busk's method is based on isoclines which are supposed to be at right angles to the direction of dip in the section (= reduced dip).

Figure 37 gives the construction of a circle arc between I and II_p on the isocline of II. I and II are mean azimuths and II - II_p is the supposed iso-mean azimuth line of II.

Busk proved that the bisecting line between the directions of I and II, at point I, intersects the supposed mean azimuth line of II in P, which is a point of the arc. For this reason, it suffices to construct a point P on every new supposed iso-mean azimuth line found during construction. The connecting line of these points P is the required mean azimuth line. If the top angle α of the triangle with bisecting line I - P is not too large, this line may be replaced by the median I P' (Fig. 38). (Busk, 1929, and Molengraaff, 1941).

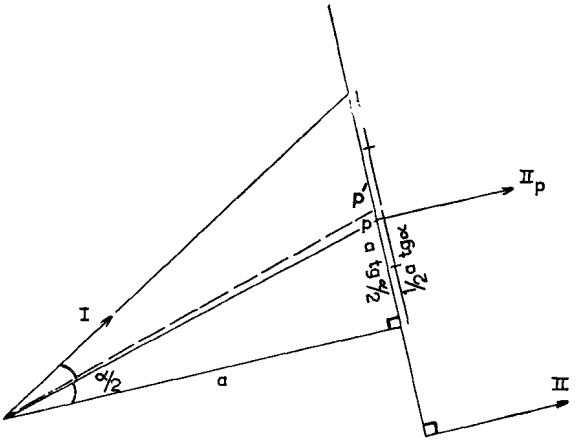

Fig. 38
Construction of P and P'. For explanation see text.

$PP' = a/2 \cdot \operatorname{tg} \alpha - a \operatorname{tg} \alpha/2$ (Fig. 38) or
$PP' = a/2 \cdot \operatorname{tg}^2 \alpha/2 \cdot \operatorname{tg} \alpha$

This formula proves the above qualitative conclusion.

If e.g. $\alpha = 20°$: $PP' = 0.0058a$. The distance a never exceeds a few kilometers, and for $\alpha \leqq 20°$ the deviation always is negligible.

In fig. 38, $\alpha = 31°$ which means that PP' is about 2½ % of a. This deviation is still small but obvious.

It may not be assumed, *a priori*, that the iso-mean azimuth lines are at right angles to the mean azimuth. Notwithstanding, Busk's method will be used for the following theoretical reasons.

Generally, the mean azimuth varies slightly in the studied regions. The mean azimuth of the adjacent points of a computed mean azimuth may be approximated by the latter. The iso-mean azimuth line is replaced by an iso-mean azimuth area around a computed mean azimuth.

The radius of this circular area is inversely proportional to α and proportional to a. The mean azimuth line is to touch the circle in point P (fig. 39) which is the point of this line closest to II. The iso-mean azimuth line of fig. 37 is replaced by a new line making an angle of $\alpha/2$ with the mean azimuth line. If α is small, the P of fig. 39 lies approximately on the arc of fig. 37 (see fig. 39) and Busk's method appears to be a good approximation when II lies in the vicinity of the arc. This is not the case in fig. 39 and frequently not in the structure maps. For this reason, auxiliary means have been constructed.

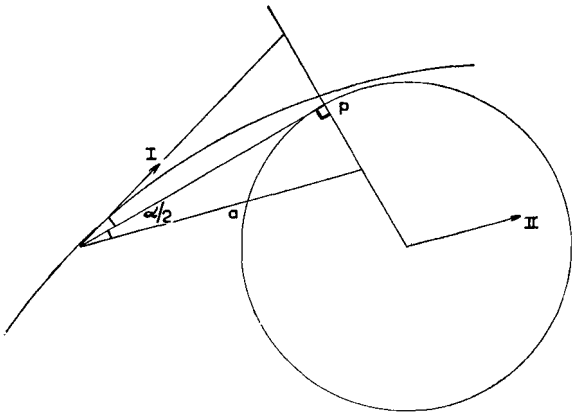

Fig. 39
For explanation see text.

An auxiliary mean between two adjacent measurements is halfway and its direction is formed by the bisecting line. Auxiliary means have been constructed for regions with a small variation of the mean which may be called linear.

It is concluded that Busk's method can be applied without preliminary information on the shape of the iso-lines, when a) the variations are small, and b) the applied measurements lie close to the constructed line. In that case, this method is based on two conditions a) linear variation between I and II_p; and b) $II_p \approx II$.

When the folding appears to be parallel and the iso-mean azimuth line is at right angles to II, Busk's method can be applied. This condition is an advantage but it is not the only condition for applying the method.

In the S. Stefano and the Pusteria regions convergences to the SE and the E have been found. A convergence of straight lines implies that the variation is maximal along the lines at right angles to the mean azimuths. In this case, the iso-mean azimuth lines coincide with the mean azimuth lines. Busk's method may still be applied when the convergence is small. Excepted is the Eggerberg structure (Pusteria region): The strongly varying mean indicates that for constructing the mean azimuth lines the particular course of the iso-mean azimuth lines has to be considered. They have approximately an E-W course parallel to the axis of the structure.

Fig. 40 gives the general method for constructing the mean azimuth lines, when P-II is not at right angles to II, and a linear variation between I and P is assumed.

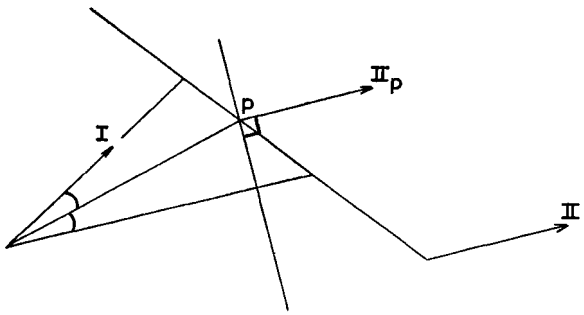

Fig. 40
For explanation see text.

It is obvious that P lies on the bisecting line between the directions I and II, as the centre of the arc of the mean azimuth circle lies on the line through P at right angles to II_p.

Such a well-defined course of the iso-mean azimuth lines is only found in regions with a strongly varying mean, as the Eggerberg area. When the variation is not so strong, the course of the iso-mean azimuth lines cannot be determined, but, in that case, the earlier described methods of Busk may be applied.

The points P have been constructed according to three methods, a) Busk's method; b) the approximate Busk's method of fig. 38; c) the last mentioned method of fig. 40 with parallel iso-mean azimuth lines. All points P are plotted on the structure maps, and it may be readily determined

which method has been used and by which mean azimuths point P is determined.

The accuracy of the applied methods for constructing the mean strike lines may be judged in the Cima d'Asta region. The contact plane between the crystalline basement and the overlying Permotriassic series is parallel to the schistosity-planes of the Crystalline. For this reason, it may be expected that the mean strike line of the latter at the contact will be parallel to the strike line of the contact plane.

The structure map of the Cima d'Asta region indeed clearly demonstrates this parallelism at the northeastern boundary of the Crystalline. Both the mean strike lines and the strike lines of the Permotriassic have turned more than 90° and their mutual parallelism is preserved.

The application of a construction method has the advantage of all means about equally contributing to the resulting mean azimuth or mean strike line.

However, these means may be scattered around a mean mean, which causes fluctuations in the mean-lines. The deviations either may be due to numerous small, mutually independent causes, and the frequency curve of all deviations would be normal, or the deviations may be due to some distinct causes as e.g. the occurrence of boulders in the measurements sample regions. There is no reason to assume systematic errors. No analysis can be given, as the applied construction methods are not accurate enough for determining these deviations. All individual means in the studied regions have been integrated. The regularity of the resulting structure maps indicates that an adequate approximation of the actually existing geometry has been obtained.

On these structure maps, the kinematic considerations of the following part are based.

PART III

Regional tectonics South of the Pusteria Line

This part links up with the geometry of the crystalline rocks as obtained from the general methodology in part II making use of the deformation types described in part I. In the first part, the tectonics of surveyable structures have been discussed. In this third part, the regional tectonics are dealt with, and all surveyable structures are integrated in order to gain some insight into the regional kinematics. The regions are treated one by one, and crystalline rocks and sediments are discussed respectively.

At the beginning of this tectonic part, it will be explained why so little attention has been paid to statics or to the study of the forces and stresses responsible for the kinematics.

The anisotropic nature of a rock may affect the direction of the principal stress. The latter may form an angle with the direction of maximal shortening, which is determined by conditions at the limits of the system being the possibility of escape from the confining frame. It is further possible that the boundary conditions determining the stress field have not such a relation to the possibilities of escape that maximal shortening is parallel to principal stress. Perhaps, the fact that the regional principal stress mostly was subhorizontal and the material could escape upwards, may have introduced the frequently supposed parallelism of principal stress and shortening. The possibility remains that, for instance, cross-folding originates at right angles to the principal stress. An example will be given.

It is assumed that a narrow belt of a plastic material is compressed between two rigid masses, and that upward movement is not possible. The rock may then be squeezed out sidewards, which is accompanied by folding. This results in a regional compression at right angles to the belt, which possibly parallels the regional principal stress. The material of the belt, however, is shortened in a direction at right angles to this regional principal stress. The material in the belt may be subjected to another principal stress. This may be possible, but it is assumed that (local) kinematics cause (local) statics in the adjacent areas. This statement permits to consider the kinematics as the last cause for local tectonics, and even as the last cause for regional tectonics. Many of the latter are definitely gravitational tectonics. The principal stress, which causes gravitational tectonics, is parallel to the vertical. In a mountain chain, the possibility of escape from the stress field by sagging is present in a sideward direction. The kinematics of these sideward movements cause new subhorizontal principal stresses, which, consequently, are of a secondary nature.

These considerations serve to illustrate the idea that kinematics are the ultimate goal of tectonic investigations.

In conclusion, the genetic events: statics → kinematics → geometric structure may be considered to consist of: statics (e.g. due to gravity) → kinematics → more local statics in adjacent areas → more local kinematics in the latter → more local statics still farther away, etc. (like a spreading wave) → geometric structures. As size and direction, and often even the mere existence of a directed principal stress are unknown, the statics are omitted from our studies and the above is written as kinematics → geometry or more in general: successive phases of kinematics lead to the geometric structures studied in geology.

CHAPTER 10

TECTONICS OF THE CRYSTALLINE ROCKS OF THE S. STEFANO REGION

The crystalline basement has been deformed several times.

The main phase of folding occurred during the Hercynian orogenesis. Our problem is to distinguish the successive phases of deformation leading to the present geometry. The schistosity is parallel to the bedding planes (Ch. 2).

In the Pusteria and S. Stefano regions, this schistosity has been rotated into a subvertical position during the Hercynian orogenesis. This statement is proved in the S. Stefano region by the position of the unconformity at the base of the Permian. E.g. Southwest of S. Stefano di Cadore, the schistosity-planes are subvertical with an E-W strike, whereas the Permian dips to the West. The schistosity is at right angles to the plane of unconformity between them. Although this plane is not exposed, the unconformity is evident.

The mountain summits in the area of crystalline rocks in some cases are covered by Permian. The M. Rosso North of the M. Croce Pass is an example (On Sheet I the most northern Permian area in the Carnian Alps). Fig. 41 shows the dips of the Permian and of the surrounding quartz phyllites.

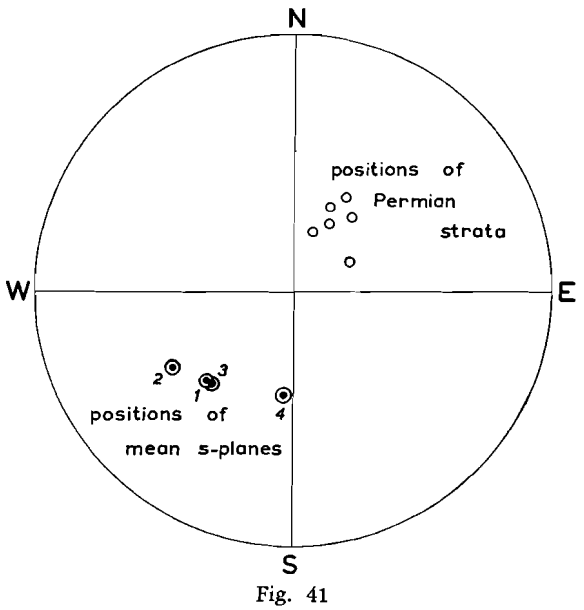

Fig. 41

Position of the M. Rosso Permian in relation to the crystalline basement. 1, 2, 3, and 4 give positions of the mean *S*-planes of the adjacent SW, NW, NE, and SE areas respectively.

The isoclinally folded schistosity-planes show minor folds. It is possible to prove that in Pusteria the phase of minor folding is later than the rotation of *S* into a subvertical position (Ch. 12). This rotation occurred about a subhorizontal axis and was an accompanying effect of the isoclinal folding.

In the S. Stefano region and in the Carnian Alps, the minor folds are subhorizontal, and a distinction into two different deformation phases cannot be made. The gradual transition, however, of the m.f. in the Carnian Alps into those of the Pusteria region suggests that the m.f. of the S. Stefano region which belongs to the Carnian Alps originated during a separate phase of deformation that would likewise be later than the primary isoclinal folding.

To ascertain the part of the Alpine deformation in the S. Stefano Crystalline, the geometry caused by the Hercynian orogenesis must be known.

It is supposed that prior to the Alpine deformations the schistosity was subvertical with WNW strike, and that the m.f. were subhorizontal with the same azimuth (see further on in this chapter).

Sheet II[a] shows that the attitude of the mean *S* is rather constant. The mean strike is between W and NW, whereas the mean dip fluctuates around a mean of about 53°.

Fig. 42 is a histogram of the dip of the *S* of the

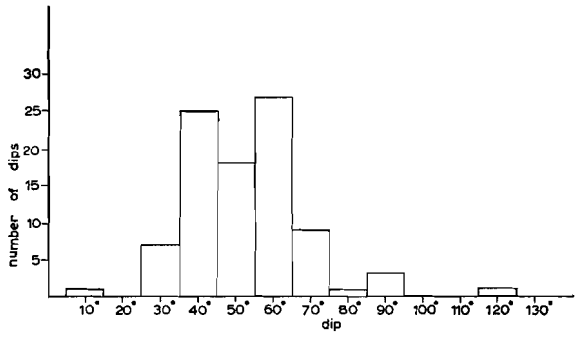

Fig. 42

Histogram of 94 *S*-dips from the S. Stefano region.

measurements samples. The *S* are isoclinal but not subvertical.

According to the following considerations it can be stated that the deviation of about 25° is caused by an Alpine rotation about an axis parallel to the strike of *S*.

The Alpine age of this rotation in the S. Stefano region is probable, as the Hercynian major folds in nearby regions are isoclinal without overturn (e.g. in Pusteria) and as an Alpine overturning to the SSW is recognizable in the Permian of S. Stefano (Section I of fig. 50).

West of S. Stefano, the mean strike is W; going to the North, the strike becomes NW. An eastward convergence of the schistosity-planes in the western part of the region appears to be present. Such a convergence of the strike in isoclinally folded *S*-planes occurs more distinctly in the Pusteria region (e.g. Eggerberg structure, Sheet III). Parallel strikes are to be expected in a series folded isoclinally about a subhorizontal axis. The convergences of the *S*-planes mentioned above can be explained by the Alpine deformations just as well as the pattern of the minor folds.

It is possible to divide the S. Stefano Crystalline into two parts by the iso-line of horizontal axes of minor folds, drawn on Sheet II[a]. To the SW of this iso-line of zero dips the mean m.f. dips to the WNW; NE of this line the mean m.f. dips to the ESE.

Fig. 43 is based on observations in the Rio Larice which crosses the iso-line of zero dips. This diagram has already been discussed in chapter 9. It has been concluded that the sudden geometrical rotation of 63° of the mean m.f. at the iso-line

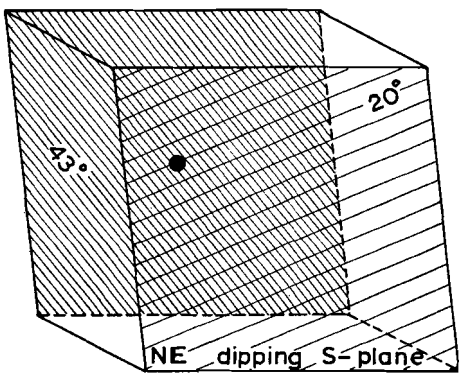

Fig. 43
Diagram of the relation between mean *S* and mean m.f. along the Rio Larice. For further explanation see text.

could not have been formed in one phase of deformation.

This would mean that two adjacent parallel *S*-planes had been compressed by stresses at a mutual angle of 63°. Such a deformation is mechanically not possible.

Fig. 43 gives the observed geometry and fig. 44 our explanation. It is assumed that the m.f. in the set of *S*-planes were originally parallel to each other. Thereafter, the blocks at both sides of the intermediate *S* have rotated 63° with respect to each other.*)

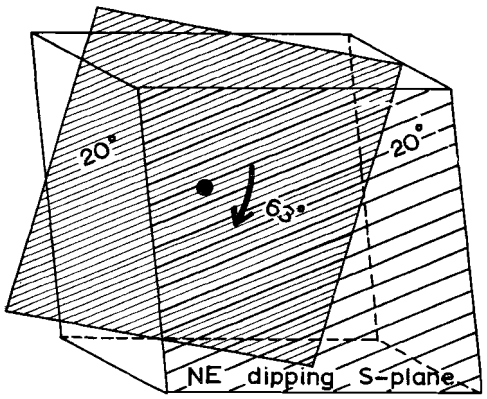

Fig. 44
For explanation see text.

Such great abrupt rotations as have been derived from fig. 43 are rare. They have been observed also at the Eggerberg structure (Pusteria region). The variation of the mean m.f. is generally more gradual. But the present example is a good illustration as it brings out that there were later rotations at one or at both sides of intermediate *S*. When the variation of the mean m.f. is more gradual, one might assume a single phase of deformation. Now, however, on the strength of this example, the possibility should be considered of smaller variations of the mean m.f. due also to later rotations around axes at right angles to the *S*-planes. Abrupt bends in the axes of exposed m.f. are demonstrated in fig. 51 of appendix I. This proves that the m.f. may also have been bent in the *S*-plane around an axis lying in these planes. This feature is also indicated by the course of the mean strike lines on the structure maps. Along these lines, the attitude of the mean m.f. varies.

*) The intermediate *S*-zone is a belt of about one hundred meters width between the eastdipping and westdipping axes of the m.f. (see Ch. 9).

The later rotations must have occurred not only along the *S*-planes, but also along planes making an angle with the mean schistosity.

The Alpine age of the above features will now be proved. For simplifying this rather complicated stereometric problem, first some imaginary experiments will serve as model for the geometric structure of the S. Stefano region.

A zone of ductile material is compressed laterally while the material can escape upwards. When the material is a clay or a shale it may be altered into a slate. In this case, the slaty cleavage that develops will obtain a subvertical position. The *S*-planes surround microlithons that are thinned between them.*) In this way a zone of shales may be shortened gradually in a horizontal direction while the surplus matter escapes vertically upwards.

Another possibility is that the mobile material already possesses a schistosity. This schistosity may have diverse attitudes.

An example will be given and discussed comprehensively. After some modifications the conclusions arrived at can be applied to the actual structures of the S. Stefano region and the Pusteria region (chapter 12).

Fig. 45 shows a belt with parallel rigid borders.

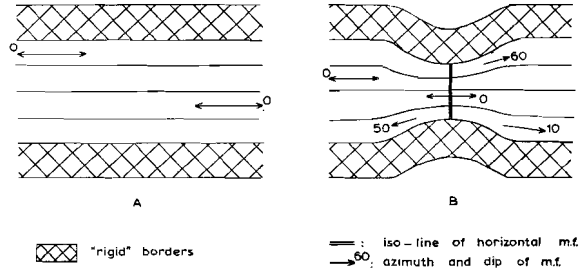

Fig. 45
Unequally compressed belt of more plastic material.

The subvertical *S*-planes are parallel to the borders. The zone is compressed unequally and the resulting upward movements are assumed to be uniform along a section across the centre (= along the iso-line of horizontal m.f. of fig. 45B).

Fig. 45A results in fig. 45B.

This discussion can be considered as the first introduction to a more general concept concerning the use of pre-existing schistosity-planes by later deformations. This topic will be discussed also in the chapters 12 and 21 in case an old schistosity-plane is present. It seems probable that the new compression will make use of this old anisotropy. But how can such successive phases of deformation be distinguished? Two conditions have to be fulfilled for such a distinction.

a) The original subparallel schistosity-planes must have a lineation.

b) The compression must result in rotations along the *S*-planes.

The mere presence of a lineation is not sufficient to prove later deformations because if the zone is compressed again in the same sense the lineation will remain parallel in all *S*-planes after this later compression, and nothing can be concluded at all. Only if there is some relative rotation the new position of the lineations can be distinguished from the original one.

The only lineations that are actually encountered in the quartz phyllites of the area under discussion are minor folds. Therefore, we will speak of m.f. in the following pages.

Presently, the geometry of fig. 45B will be discussed. The irregular shortening had two results. The strike of *S* (= azimuth of m.f.) converges from both sides of the zone to the centre where compression attains a maximum.

It should be kept in mind that fig. 45 is a map; in other words, it is a cross section of the structure along a horizontal plane. The compression may decrease or increase with depth. This cannot be deduced from the convergence of the *S*-planes. Fig. 45 gives information only on the compression at map level.

The other result of the irregular compression can be concluded from the dip of the m.f. In the centre of fig. 45, shortening was maximal and most of the plastic material was squeezed out in this centre.

In the most western part of fig. 45B, the m.f.'s are horizontal, because no compression occurred there. Where the zone has been compressed, the m.f.'s dip westwards on the West side of the centre and eastwards on the East side. In the centre itself, subhorizontal m.f. is found. The iso-line of mean dip of m.f. is at right angles to the mean strike lines (= mean azimuth lines. For definitions

*) For convenience's sake no distinction is made between cleavage and schistosity. The definition of schistosity of chapter 2 can also be applied to cleavage.

see chapter 9). Thus from the dips of the m.f., information may be obtained on the amount of material squeezed out.

The two results of the irregular compression, convergences of the strike and rotations of the m.f., are closely related. When a convergence is observed, also a rotated m.f. may be expected, but this relation is not a functional one. This means that the rotation of the m.f. cannot be calculated from the convergence of the *S*-planes, for, as stated above, the rotation of m.f. refers to the volume of the squeezed out material, whereas the convergence refers only to the compression at map level.

This qualitative relation between convergence and rotated m.f. can be observed on Sheet IIa, and Sheet VIII; it is best illustrated on Sheet III and III^a, on which the Eggerberg structure is depicted.

When the rotation and the convergence are exactly known, some more exact calculations are possible. This will be done when dealing with the Pusteria region (chapter 12).

The S. Stefano region serves to prove that the theory developed above indeed is valid for that crystalline area. The theoretical model of fig. 45, however, does not give the actual history of the S. Stefano case.

It may be applied for the principal points if a zone of schistose material has been squeezed out along the *S*-planes between rigid borders, and the originally subhorizontal m.f. was rotated into opposite directions at both sides of the iso-line of subhorizontal mean m.f. The rigid borders, however, remained parallel during deformation, and the upward movement was not uniform across the belt. The squeezing out was maximum in the middle between the borders (fig. 46) causing a convergence of the *S*-planes toward the iso-line of horizontal m.f. in sheet IIa.

This convergence of the *S* actually appears in the western part of the structure map II^a that is best known on account of the abundant outcrops.

In the eastern part, however, a convergence is not so evident. Not enough observations could be made here, and the geometry of the northeastern part of Sheet II^a, largely obtained by construction, is somewhat uncertain. The scarsity of observations allows also in that part the drawing of hypothetic mean strike lines with a distinct convergence. This would only mean introducing a preconceived idea and ostensibly support the evolved theory. The lines as drawn on the map according to some constructions and their extrapolations may not give a sufficient approximation of the real geometry of that northheastern part of the region.

The model represented in figure 45, moreover, differs from the actual situation in the S. Stefano Crystalline in that the mean *S* does not dip 90° but 53° and by the fact that the mean strike lines intersect the rigid borders with an average angle of about 25° (fig. 46).

The course of the iso-line of subhorizontal m.f. is more or less parallel to the borders of the blocks of Permotriassic rocks bordering the Crystalline to the NE and the SW. Because these Permotriassic masses have a NE and SW inclination respectively due to the Alpine deformations, this course of the iso-line in the crystalline basement parallels the Alpine direction.

The probable Alpine rotation of the *S*-planes parallel to their strike has been discussed before. This rotation must have been synchronous with the Alpine compression and it is to be expected that the dip becomes steeper downwards. The southern part of the S. Stefano Crystalline has not been rotated as demonstrated by the samples of measurements 11 and 13. The kinematics in relation to the lower layers with a subvertical *S* can be determined and thus the "absolute" direction of movement can be found. The latter appears to consist of two components:

1. A general upward movement along the *S*-planes by compression;
2. A general movement towards to the SSW, decreasing in importance towards depth. This caused the rotation of the *S*-planes.

Three arguments support the foregoing analysis of the kinematics of the Alpine deformations in the crystalline rocks of the S. Stefano region. All three are based on the structure of the Permotriassic frame.

(a) Case 1 of table VII (the overturn of the Permian strata in the SW);

(b) Case 6 of table VII (the deformations of the Bellerophon in the SE corner of the S. Stefano area); and

(c) the deformation of the Grödener sandstones in the centre of the S. Stefano Crystalline.

The cases 1 and 6 (table VII) indicate internal mass transport within these plastic strata and show that they are affected in correspondence with the kinematics of the S. Stefano Crystalline. Both cases indicate a movement of the Crystalline to the SW - SSW in relation to the more rigid borders. Another fact that appears to agree with the foregoing is the following.

The thick Grödener lense (chapter 5) West of S. Stefano seems to be folded into two synclines with an EW striking axial plane and an axis dipping steeply to the West.

This structure can be seen on Sheet II, on which strike lines of the Grödener are shown by a dashed line. This compression was synchronous with the compression of the Crystalline.

The steep West dip of the fold axes in the Permian is the same as the observed dip in the adjacent crystalline rocks.

The measurements sample 11 shows that there the mean dip of the axis of m.f. is 41°. The single dips may be as much as 80° W. This parallelism is a strong argument for our concept on the Alpine kinematics of the S. Stefano Crystalline. The fold axes of the Grödener lie in the bedding planes which were originally subhorizontal. They must have been rotated from a subhorizontal into a westward dipping position. When this rotation is eliminated by turning back the axes of the Permian folds into their subhorizontal position, the axes of the m.f. in the adjacent Crystalline also assume a subhorizontal attitude.

The subhorizontal position of the axes of the m.f. in the crystalline rocks was the premise of our analysis of the Alpine kinematics. This premise is thus substantiated by the above instance.

In summary, it can be stated that the Crystalline of S. Stefano was deformed into a SW overturned Alpine anticlinal structure. The axis of the anticlinal structure (iso-line of subhorizontal m.f.) is SE - NW and it intersects the ESE - WNW striking pre-Alpine schistosity along which the Alpine movements occurred.

§ 10A *Calculations on a simplified Model of the S. Stefano region.*

The present situation is illustrated by the schematic block diagram fig. 49. The shape of the base of the Permian represents the shape of the anticlinal structure. The maximal movement from the horizontal plane upwards was calculated in the following manner:

Fig. 46 is a simplified model of Sheet II[a]. The iso-line of horizontal m.f. is drawn parallel to the rigid borders. This axial line is located in the middle between the borders, which are at an average distance of six kilometers. The schistosity-planes intersect this line with an average angle of

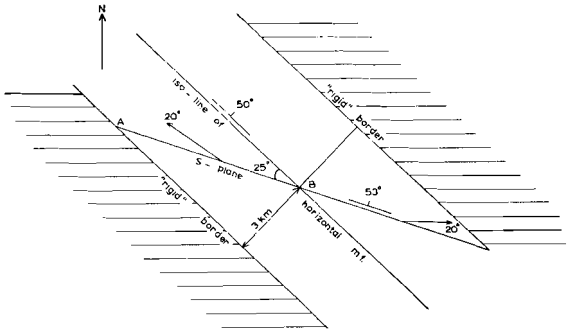

Fig. 46
Structural scheme of the S. Stefano region (Sheet IIa).

about 25°. The m.f. dip 20° NW at the SW side of the zero line and 20° E at the NW side. These values are based on actual observations. The 10 measurements samples SW of the hypothetic iso-line of subhorizontal m.f. on Sheet II[a] have an average value of 20°.

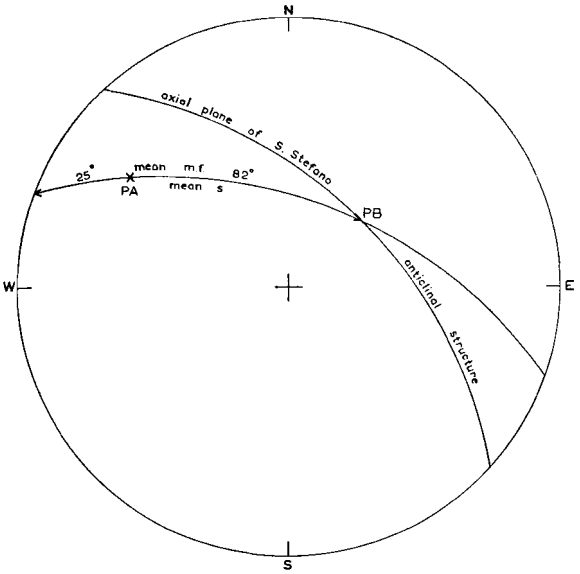

Fig. 47
Diagram (Wulff net, lower hemisphere) of mean *S* with mean m.f. (= PA) and axial plane of S. Stefano anticlinal structure. For further explanation see text.

For the sake of symmetry, about this same value has to occur at the other side of the zero line of

our model. Actually, 6 measurements samples are found here with an average m.f. of 23°, which is a fair result.

Fig. 47 shows that a 20° dipping m.f. corresponds with a m.f. in the *S* with a rake of 25° (PA in fig. 48).

It was assumed that the movement along the *S*-planes occurred in a SW direction and at right angles to the iso-line of horizontal m.f. This assumption cannot be checked directly in the quartz phyllites, but the adjacent Permian frame shows a similar deformation. As the movement also took place in the *S*-planes, the line PB in fig. 47 represents its direction. The angle between PA and PB is 82°. The triangle PAB has been drawn in fig. 48 for calculating the length of PB, which represents the maximal upward movement from the horizontal plane. This triangle can be drawn as its basis AB is known. The later follows from the simplified map (fig. 46). It appears that PB = 2.8 km, or about 3 km. The block diagram fig. 49 has been developed on the base of this value. In addition, a SW dipping topographic plane and a curved axial plane of the anticlinal structure have been assumed. The latter assumption can be made on account of our former concept that the *S*-planes have been rotated from a subvertical position. As the dip of the schistosity increases downwards, it probably also decreased upwards in the parts now removed by erosion. The mere existence of the anticlinal structure was already obvious from the attitudes of the bordering Permian strata. But the preceding considerations resulted in more exact data on the shape and dimensions of this structure and on the kinematics, which caused it to be formed.

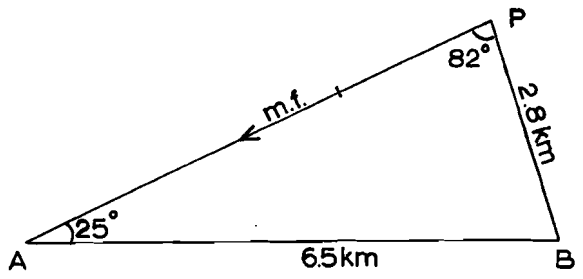

Fig. 48
△ ABP. For explanation see text.

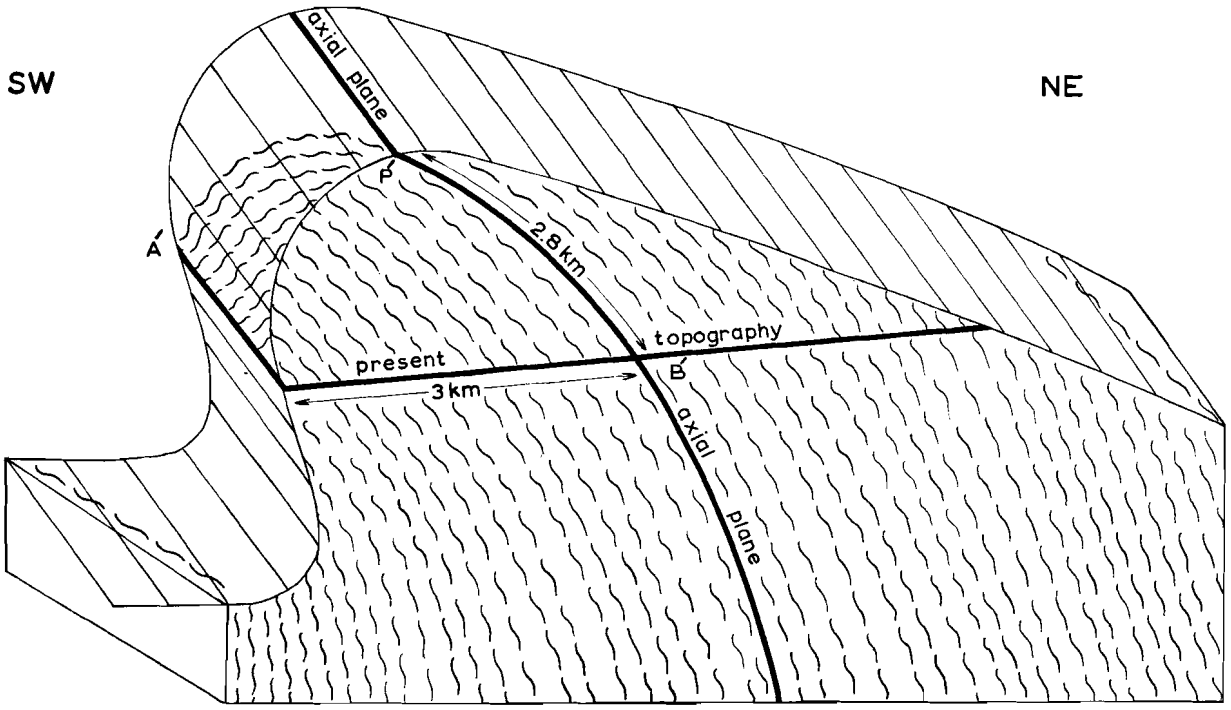

Fig. 49

Block diagram of the S. Stefano anticlinal structure determined by the Permian transgression plane overlying the crystalline basement with mean *S*-planes indicated. A', B', and P' correspond with A, B, and P of fig. 48. The front side of the block diagram is formed by a schematic cross section in scale.

CHAPTER 11

TECTONICS OF THE PERMOTRIASSIC OF THE S. STEFANO REGION

Sheet I demonstrates that the S. Stefano region may be considered as a point of junction of faults. The important faults of the Dolomites are converging towards this region. Therefore, it is not surprising to meet complicated tectonics here which are particularly characterized by sudden changes in the direction of strikes.

The tectonics of the S. Stefano region have been divided into a Hercynian part which is restricted to the crystalline basement, a sedimentary part during the geosynclinal evolution (chapter 5), and a post-sedimentary Alpine part.

The influence of the Alpine orogenesis on the crystalline basement has already been discussed in the preceding chapter in connection with the structure of this basement complex.

In the present chapter the following three subjects will be discussed:

A) The tectonic graben structures of Candide-Padola;
B) The southward overturned folds in the surroundings of Auronzo;
C) The Alpine movement of the M. Tudaio mass.

§ 11A *Tectonic Graben structures of Candide-Padola.*

In the surroundings of Candide, mostly steeply NE dipping Grödener sandstones occur amidst of the crystalline rocks. They are fairly well exposed as follows from the number of measurements on Sheet II.

The Grödener shows a remarkable bifurcation NW of Candide. Section I (fig. 50) illustrates the succession of steeply NE dipping crystalline rocks and Grödener sandstones.

Sheet I shows that this structure continues in a NW direction up to the M. Croce Pass. The SW border of the Grödener is formed by a normal fault with a net slip of about 25 m. This M. Croce structure resembles a tectonic graben, and the occurrences of Candide-Padola may also represent a tectonic graben.

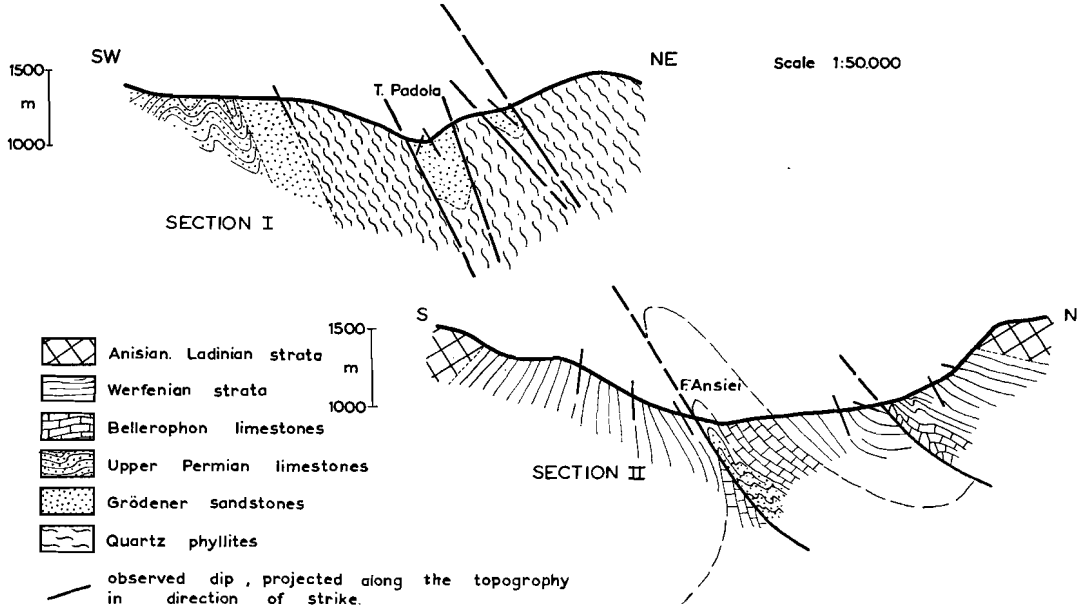

Fig. 50
Two cross sections (I and II) from the S. Stefano region. The positions are depicted on sheet II.

On the tectonic map, the borders of the Grödener are indicated as faults. Although different attitudes of strata are encountered in this Grödener, its dips mostly are parallel to these faults and also parallel to the *S*-planes of the crystalline rocks beyond the faults.

These *S*-planes have a normal position and it is supposed that they determined the position of the faults. Along these faults the Grödener subsided with considerable drag, and its strata were pulled into a position almost parallel to the faults. It may be possible that the adjacent Crystalline participated in these fault movements and that the faults are not so strictly localized as is suggested by Sheet II.

Before attempting to give a mechanical explanation, the characteristic features of the Candide-Padola structure may be summarized as follows:

1. The Grödener is bordered by faults or fault-zones which are parallel to the schistosity of the crystalline rocks;

2. The strata of the Grödener are mostly subparallel to the faults but locally may have other attitudes, for instance, along the Torrente Padola to the West of Candide, where also subhorizontal positions have been observed.

3. The structure bifurcates to the SE;

4. To the NW the structure passes into a graben structure. At the M. Croce Pass it is bordered to the SW by a normal fault, with SW dipping Grödener at both sides. The NE boundary probably is a normal fault which has been transformed into a southwestward overthrust (or upthrust).

Similar tectonic graben structures are frequently found in the Alps. In chapter 13, the western Drauzone will be discussed, in which the first two features are also present.

The tectonic graben structure of Candide-Padola may serve as a basis for a mechanical explanation.

Apart from the four features mentioned above, there is an additional feature which has been observed more clearly in the Gandella structure of the Pusteria region (western Drauzone, see fig. 73). The Gandella structure indicates that the younger sediments of the western Draugraben in some instances consist of large boulders, with totally different orientations of the strata. The Gandella graben is a chaotic mixture of boulders.

It is obvious that the younger material of the tectonic graben structures moved downwards with respect to the crystalline rocks. The latter retained their original attitude of schistosity.

The mechanism, in accordance with the above properties, is as follows: Large tension rifts, filled by wedges of the overlying sedimentary strata, originated in the crystalline basement.

This concept agrees with

1. The parallelism of the faults with the subvertical schistosity of the crystalline rocks which retained their original position;

2. The great drag of the sedimentary strata that caused their parallelism to the border faults;

3. The possibility of bifurcation;

4. The gradual passage into a graben bordered by normal faults without considerable drag;

5. The occurrence of large individual boulders with different orientations.

Cornelius Furlani (1902) already mentioned this mechanism as a possible alternative of another concept accepted by her, namely that the overlying sedimentary cover was strongly compressed thus causing synclines which were pressed into the crystalline basement. However, it is evident that this mechanical concept does not agree with the possibility of abrupt bifurcation, the gradual transition into a graben that is bordered by normal faults without considerable drag, and the occurrence of large boulders with totally different orientations.

It is assumed that these tectonic graben structures represent rifts caused by local tension in the earth crust.

In the present cases, these tension rifts were filled by material from the sedimentary cover which thereafter has been compressed. They further were rotated from their original subvertical position into a North dipping position (see fig. 68). An original subvertical position is probable as the ten-

sion probably was parallel to the subhorizontal topographic surface. Further, an originally vertical attitude of the schistosity is probable in the S. Stefano region as well as in the Pusteria region of the western Drauzone.

It may be concluded that the compression and rotation of the S. Stefano Crystalline were preceded by a phase of tension with formation of riftlike grabens which were filled by subsiding wedges and boulders of the overlying Permotriassic.

§ 11B *Southward overturned folds in the vicinity of Auronzo.*

Sheet II and Section II (fig. 50) show the structure of the Werfenian West of Auronzo. This structure can be interpreted as an anticline, overturned to the South, with a thrust fault cutting along its axial plane. Another southward upthrust occurs in the northern limb of this anticline. The anticline is situated between two more or less symmetrical synclines, in which the shortening is less.

The M. Aiarnola mass to the North is only slightly folded, the Croda Alta mass to the South somewhat more (fig. 9). The shortening of the latter increases eastwards. This syncline will be discussed more fully at the end of this chapter, in relation with the Werfenian beds so well exposed along the F. Ansiei South of Villapiccola.

The southward overturn of the Auronzo - M. Agudo region has been described as case 3 of table VII. This overturn may be due to a southward mass transport which increases in importance upon approaching the surface as well as to a north ward underthrusting mass transport which increases in importance towards depth.

It is assumed that the intensity of deformation increased upwards.

Upwards increasing deformation combined with overturning determines the absolute direction of movement with respect to the basement complex, and is in the direction of overturn.

In the surroundings of Auronzo, this assumption cannot be proved directly. In a number of analogous cases of overturning, however, it appears to be the most probable interpretation (Sugana Line, chapter 16; Pusteria Line, chapter 12).

In this case, the absolute movement occurred in a southward direction. It has already been indicated that the S. Stefano Crystalline moved to the SW. There, the deformation appeared to decrease downward as may be derived from the relatively small amount of mass squeezed out (see fig. 49). This proves the shallow depth at which the kinematic process took place.

The relation between the southward movement of the Aiarnola mass and the SW movement of the Crystalline of S. Stefano is a very interesting mechanical problem.

In fig. 51, the massive Aiarnola dolomites are intercalated between more ductile strata.

The strata East of the Aiarnola mass have been compressed with a W to SW overturn, whereas the Aiarnalo mass proper compressed the ductile strata South of it into a southward overturned anticline.

Let us suppose that both movements are synchronous. In that case, interference structures may be expected in the more plastic strata SE of the Aiarnola mass. There are two possible positions for the axial planes of the folds. These are shown in fig. 51A and B. They may converge to the SE,

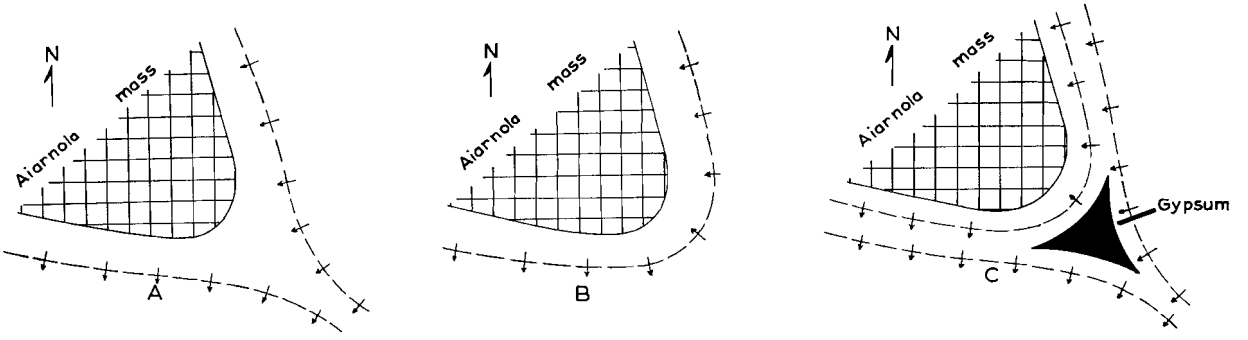

Fig. 51

Three possibilities (A, B, and C) of folding of the more plastic strata surrounding the rigid Aiarnola mass. Dashed lines indicate the axial planes of folds, and arrows the direction of overturn.

and the direction of overturn does not show abrupt changes (fig. A). On the other hand, folds may be expected to bend around the Aiarnola mass (fig. B). The same fold now shows a westward overturn East of the Aiarnola mass and a southward overturn South of it. At the bending point, the direction of overturn, changes abruptly.

Now the deductions from the imaginary experiment are compared with the observations of the actual situation at the bend. The folds in the Werfenian beds close to the Aiarnola mass show curved axial planes. They die out to the North as well as to the West, but they form an obvious link between the westward overturned fold of Section I and the southward overturned folds of Section II (fig. 50).

It can be concluded that possibility B may be applied.

The axial plane of the major anticline of the Auronzo region (section II), however, continues to the ESE without bends. West of S. Stefano, it is accompanied by some folds in the Grödener series with steeply westward dipping axes. The axial planes of these folds, which also die out rather quickly, converge to the SE. This represents possibility A as these folds form an obvious link between the westward overturned folds of Section I and the southward overturned folds of section II.

It may be concluded that both patterns of interference are actually present. This situation is represented by fig. 51C. The mass deficiency that may be expected between the two patterns at the bend has been compensated by Upper Permian gypsum. This highly plastic gypsum probably has been squeezed into the pressure shadow. On the other hand, the presence of small amounts of gypsum elsewhere in the Upper Permian of the S. Stefano region suggests that the great thickness of the gypsum is not only the result of tectonic accumulation but also of stratigraphic origin (see chapter 5).

This paragraph has given an explanation of the cases 1 and 3 of overturn mentioned in table VII. The intermediate case number 2 may be discussed also in this connection. Case 2 concerns the west- to northwestward overturn of some minor folds of the Valle Ostera (Sheet II).

The presence of the preceding interference structures renders it probable that the movements occurred synchronously and also during the compression of the crystalline basement. They belong to a phase of compression which was later than the formation of the tectonic graben structures of Candide-Padola, but which preceded the Alpine movements of the M. Tudaio mass to be discussed in the next paragraph.

§ 11C *Southward movement of the M. Tudaio mass.*

The M. Tudaio mass is bordered by normal faults on the northside and by wrenchfaults on the westside (case 5 of table VII).

Case 4 of this table indicates that the Werfenian strata underlying the M. Tudaio Mass were dragged southward.

Moreover, Sheet I shows that the more plastic sediments South of the M. Tudaio mass have been folded and thrustfaulted with a southward overturn.

These combined deformation systems suggest a youngest independent southward movement of the rigid M. Tudaio dolomite mass over and between the more plastic sediments.

At the rear, several normal tension faults are found. The most important one runs from the M. Piedo in the West to Transacqua and to the South slope of the M. Tezza Piccola in the East. This fault separates the Triassic strata of the M. Tudaio mass from the Permian strata North of it. Other normal faults are encountered in the Rio Mauria, the Rio Pinie, and the Rio Giao. The strike of the Grödener strata along both first mentioned faults is at right angles to the fault plane at the other side of which crystalline rocks occur in places. The folds of the Permian belong to the compression phase described in the preceding paragraph. The fact that the folds are cut off obliquely by the normal faults here under discussion, indicates that the latter are younger. In the next paragraph, the younger age of the wrenchfaults will be proved.

In summary, the latest tectonic phase of the S. Stefano region was an independent southward movement of a rigid unit with tension phenomena at its backside and compression at its front. At the outcrop of its floor at the western side, drag features have been observed. These structural features in combination indicate that the movement was not a reaction to a pushing effect of other masses, but suggest an independent movement. The only force that may have caused such an independent

movement of a body is the gravity which accumulated potential energy into every particle of the mass. This is the first time a force is mentioned as the cause of movements. In chapter 19, this subject will be discussed in further detail. In the present chapters, it will be mainly attempted to deduce the kinematics from the observed geometry.

The surveyability of the M. Tudaio mass with its four deformation types, however, so strongly suggests that the very weight of the mass caused a southward sliding movement, that in this instance also the force has been mentioned. It appears that almost all Alpine movements South of the Pusteria Line caused southward overturns. In consequence, it seems possible that all these movements originated by southward sliding of the superficial masses as a result of the Late Alpine doming of the Central Alps accompanied by subsidence in the Po Plain and the Venetian Plain.

§ 11D *Wrenchfaulting of the Werfenian beds along the F. Ansiei South of Villapiccola*

The Werfenian beds exposed along the F. Ansiei South of Villapiccola form a syncline extending to the West as far as the Croda Alta mass, which is less shortened (fig. 9). To the East, this syncline disappears against the M. Tudaio mass. North of the axial plane the strata dip to the South, and South of it they dip to the North. Several exceptions, however, disturb this simplified picture.

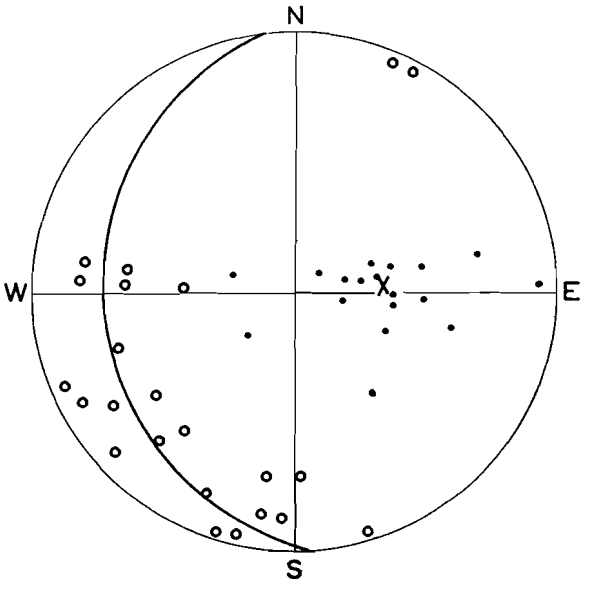

Fig. 52

Diagram (Schmidt net, lower hemisphere) of 23 bedding planes (circles) and 17 minor folds (dots) from the southern limb of the Ansiei Werfenian syncline. The axial plane of refolding (great circle) and its pole (cross) are indicated.

Diagram 52 shows 23 bedding planes of the southern limb and diagram 53, 32 of the northern limb.

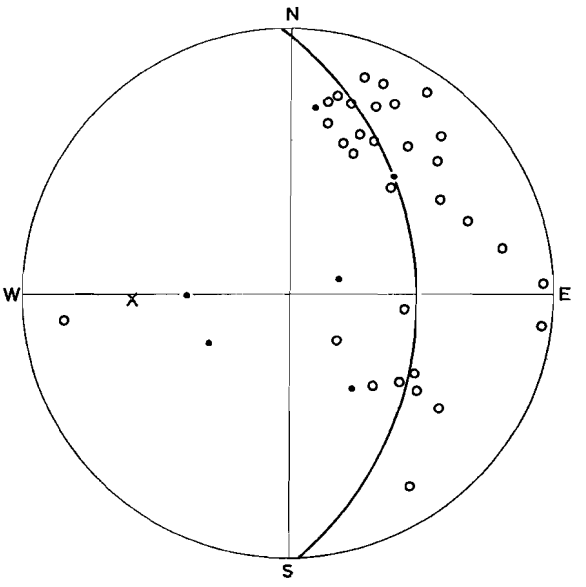

Fig. 53

See fig. 52. 32 bedding planes and 6 minor folds from the northern limb of the Werfenian syncline.

In the first diagram also 17 minor folds have been plotted. These are more or less symmetric folds. Photograph 15 and fig. 90 of App. I are examples. This synclinal structure has been strongly disturbed.

Fig. 54 shows a flexure with a steeply dipping axis. Many features of this type are responsible for the deviating strikes in the syncline.

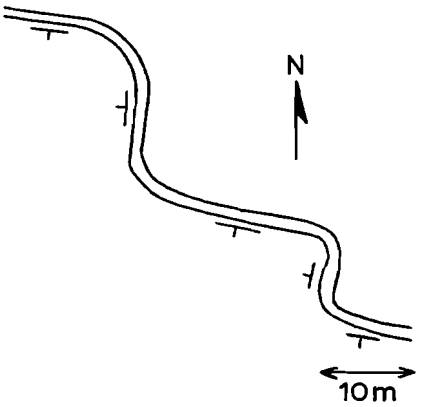

Fig. 54

Schematic dextral wrench flexures from the northern limb of the Werfenian syncline.

The measurements of the diagrams are from similar flexures of various dimensions. The axes of these flexures must be located in the bedding planes of the folded strata.

The E-W striking beds of the southern limb have been bent to NW and N strikes about the 84° - 62° axis. The pole of the great circle of the bedding planes has been plotted in the net. The mean of the minor fold axes coincides with the pole of this great circle.

The E-W striking beds of the northern limb have been bent into NW-SE and N-S strikes along the 268° - 40° axis.

The few minor folds found on this northern limb have irregular positions. The many minor folds on the southern limb, however, show that not only wrench flexures represent deformation, but that some compression occurred also.

It is interesting to determine the direction of the principal stress which caused this compression. It cannot be assumed that the principal stress lies in the refolded bedding plane, at right angles to the fold axis, but it may have an arbitrary position in the plane at right angles to the minor folds. The following considerations confirm the latter possibility. At first the theory of refolding has to be considered and afterwards this theory is applied to the present example.

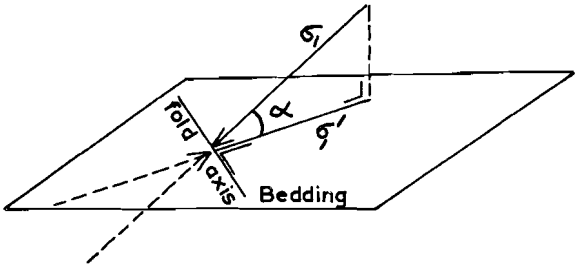

Fig. 55
For explanation see text.

Fig. 55 shows a bedding plane which is compressed as a result of a stress, σ_1, forming an acute angle (= α) with the strike of the bedding plane. A fold in de bedding plane with an axis at right angles to σ'_1, can be expected, because this is the vertical projection of σ_1, in the plane.

It has been assumed that a principal stress exists and that its course has not been distinctly influenced by the anisotropy of the rocks. This assumption must be checked first.

Fig. 56 is a model of the Werfenian syncline South of Villapiccola. Let us assume a horizontal NS principal stress forming an acute angle with

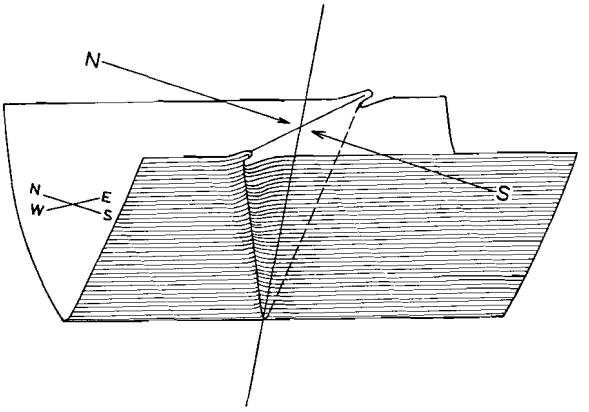

Fig. 56
Schematic diagram of the Ansiei Werfenian syncline with westward dipping m.f. in the northern limb and eastward dipping m.f. in the southern limb. The N-S directed principal stress is indicated.

the axis of the syncline. The figure shows that westward dipping folds may be expected in the northern limb and eastward dipping folds in the southern limb.

A better picture of the situation can be obtained by means of diagrams 52 and 53. It is assumed that the observed N and S strikes are disturbances. The E and W striking bedding planes represent

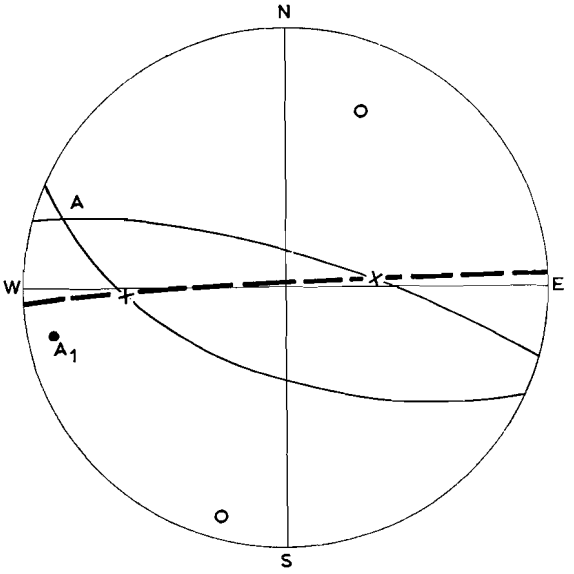

Fig. 57
Diagram (Schmidt net, lower hemisphere) with the undisturbed limbs of the Werfenian syncline (great circles) and their poles (circles) intersecting in A (= primary foldaxis). The secondary foldaxes of refolding (crosses) lie in the plane (dashed great circle) at right angles to the principal stress. A_1 is the not "externally" rotated primary foldaxis (see text).

the original syncline. The probably undisturbed poles of the northern and southern limb have been plotted in fig. 57. The intersecting line of the limbs gives the synclinal axis. It dips 12° in the direction 288°. This West dip corresponds with the westward dip of the undisturbed Croda Alta syncline, farther to the West. The azimuth of the present axis, however, makes an angle of about 30° with the Croda Alta synclinal axis (with the same azimuth of A_1, in fig. 57). This difference can be interpreted as due to a drag by the M. Tudaio mass. This dragging concerns all of the Werfenian beds in this region; it may be called an "external dragging" whereas the flexures of fig. 54 represent "internal dragging". Both types of dragging show dextral rotations.

As the undisturbed limbs of the Werfenian syncline lie in the great circles of fig.'s 52 and 53, they are at right angles to the corresponding poles of these great circles. These poles have been plotted also in fig. 57, and represent the axes of refolding. They form together an E-W striking subvertical plane. When the assumption applied in fig.'s 55 and 56 is correct, the pole of this plane gives the direction of maximal stress which caused compression features. It also gives the direction of movement of the rigid Tudaio mass causing the flexures. The first calculated subhorizontal direction of the principal stress coincides exactly with the southward movement of the M. Tudaio mass, which has already been deduced from the geological observations discussed in the preceding chapter.

This is a confirmation of the correctness of the theoretical assumptions which have been made in deducing the direction of the principal stress.

CHAPTER 12

TECTONICS OF THE CRYSTALLINE ROCKS OF THE PUSTERIA REGION

The quartz phyllites of Pusteria have been investigated as much in detail as possible. The number of outcrops is sufficient for compiling an accurate regional map of the mean azimuth and the mean dip of the minor folds. Sheets III and IIIa show that the mean axes of the minor folds vary strongly but gradually in the studied region. The mean m.f. form a regular pattern and in the present chapter the kinematics involved will be discussed.

The planes of schistosity have been strongly folded by these minor folds, and not many measurements of simple *S*-planes are available in Pusteria. It was stated before that the measured number of *S*-planes in the S. Stefano region is less than the number of m.f. The *S*-planes of the Pusteria region are not included in the tables and diagrams of the appendices, because the measurements of m.f. (about 1700) are about seven times as high as the measurements of *S*-planes (about 250).

Fig. 58 shows the dips of the 257 *S*-planes measured in the Pusteria region. This histogram shows that the mean dip of *S* is subvertical with a small deviation to the North, which is negligible.

It follows that the mean azimuth lines also indicate the mean strike of the subvertical schistosity.

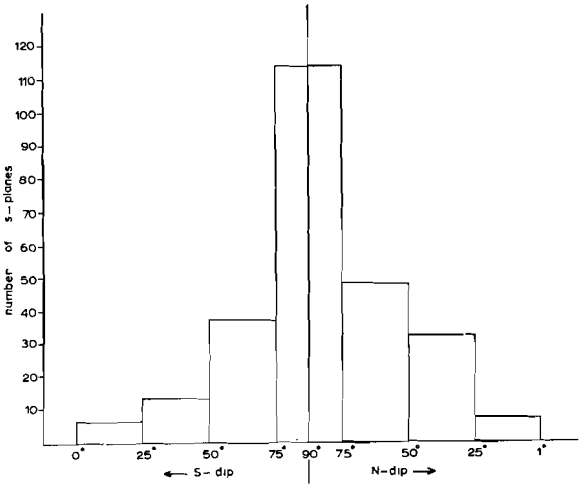

Fig. 58
Histogram of 257 *S*-dips from the Pusteria region (Sheet III).

And as the observed stratification is parallel to *S*, the mentioned lines also indicate the strike lines of the bedding planes. In the western part of the Pusteria region, the minor folds dip steeply to the East. This fact implicates that the dip of the folded *S*-planes is larger than this value, if the strike is not at right angles to the azimuth of the m.f. The E-W strike of the *S* is apparent and it may be deduced that the steeply East dipping m.f.

in the *S*-planes implicates a subvertical attitude of *S*. By this reasoning, the geometry appears to be not very complicated and can be used for some calculations.

On account of the position of the plane of unconformity of the overlying Permian, it may be assumed that the isoclinal subvertical position of *S* is of Hercynian origin. The picture of the Hercynian geometry has been obscured by later deformations. It probably was an isoclinally folded series at the end of the Hercynian as illustrated by fig. 59. This folding occurred about subhorizontal axes.

The arguments in favour of this geometric picture are the following: The N-S section between the Pusteria Line at Brunico in the North and the northern boundary of the Permotriassic of the Dolomites at S. Martino in Badia in the South shows 11½ km of exposed isoclinal subvertical *S*-planes (Sheet IV). Actually, the subvertical quartz phyllites will be thicker, because they extend beneath the Permotriassic. It is certain that some redoublings of the originally subhorizontal series must have occurred as the total thickness of the series will probably not surpass some kms.

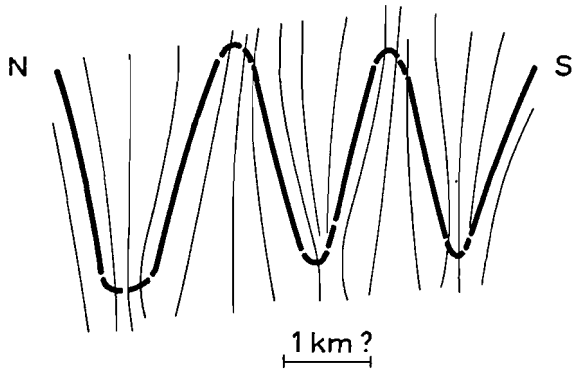

Fig. 59
Assumed relation between stratification (heavy line) and schistosity-planes in the South Alpine isoclinally folded crystalline basement.

Such redoublings may have originated by isoclinal folding. However, an anticlinal or synclinal bend with a subhorizontal axis has not been observed, and for this reason it is supposed that the folds do not possess bends.

From a theoretical point of view, bends are even improbable. It can be expected that the originally subhorizontal *S*-planes acted as a medium for the deformation again after having obtained a certain dip by rotation during folding. In the anticlinal crest, an acute angle between *S* and stratification is probable.

Fig. 92 shows minor anticlines, the structure of which is in agreement with the above theory. The original *S*-planes indeed have acted as axial plane schistosity of the new anticlines. This will be discussed again in the summary of Hercynian orogenesis (chapter 18) after the discussion of the other regions.

The syncline at Monguelfo has been treated already in some detail (chapter 7). It was concluded that the observed data of that structure can be best explained by assuming an original folding around a subhorizontal axis, followed by refolding around 55° East dipping minor folds.

A first assumption on the relation between the first mentioned major folds and the minor folds might be that their axes are parallel as is the case in the S. Stefano region. But again the unprobability of the total thickness of the quartz phyllites exceeding a few kilometers already contradicts this premise. In going from Brunico eastward, 55° East dipping axes of m.f. are found over about 14 km. If the position of the axis of the m.f. coincides with the planes of the stratification this would implicate a thickness of 14 sin 55° = about 11 km for the quartz phyllites. This already too high value has to be augmented by 20 km for the E-W section West of Brunico which shows subvertical axes of m.f., and still some more kilometers for the eastern Pusteria region where the m.f. dip less than 55°.

These considerations prove conclusively that the axes of the m.f. are not parallel to the axes of the major folds which might be present. The subhorizontal attitude of the latter follows from the fact that one and the same type of rock is found in the entire region of Bressanone, Pusteria and the Carnian Alps. It must be kept in mind, however, that this argument is based on the relative thinness of the folded quartz phyllites and not on the thickness of the unfolded quartz phyllites.

Further, the local occurrence of limestones intercalated in the quartz phyllites near Brunico provides some information on the subhorizontal axis of the syncline, of which they probably form the core. These limestones locally show an apparent stratification. As could be expected, the latter is parallel to the subvertical E-W striking *S*-planes

of the surrounding quartz phyllites. These bedding planes have been folded into minor folds. It is interesting that the axes of these minor folds are subvertical or steeply dipping eastward as do also the m.f. of the surrounding quartz phyllites. Photograph 5 is an example of these steeply dipping m.f. of the Brunico limestones. This situation demonstrates that the limestones belong stratigraphically to the crystalline basement.*)

Moreover, the parallelism of the m.f. in stratified limestone and quartz phyllite seems to demonstrate in a surveyable structure that the angle between the axes of respectively the major and the minor Hercynian folds is 60° - 90°.

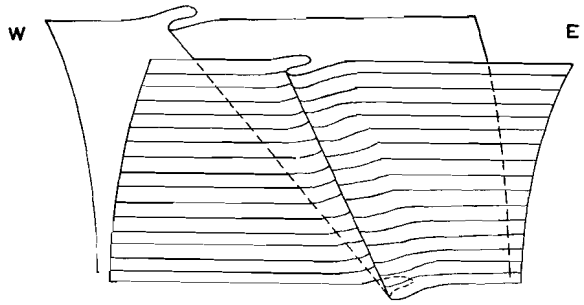

Fig. 60
Diagram of the Monguelfo syncline with steeply East dipping crossfolds (m.f.) at both limbs.

The Hercynian phase of minor folding is apparently younger than the formation of the major folds. This statement can be proved as follows. Fig. 60 shows the syncline of Monguelfo. A synclinal bend is not shown, as the younger green phyllites forming the core of this syncline do not show such a bend. On the northern as well as on the southern limb the minor folds are dipping 55° to the East.

Three possibilities can be enumerated for the relation between major folding and minor folding: The minor folds may be older, they may be synchronous, and they may be younger.

Fig. 61 is the result of the unfolded major syncline of Monguelfo. The abrupt variations of the m.f. at the axes of the major folds prove that the m.f. cannot be older or synchronous. They must have formed parallel to each other after the *S*-planes already had reached their subvertical attitude. The different positions of the *S*-planes in both limbs are too small to show differences in the positions of m.f. In the Bressanone region, evidently different positions of the *S*-planes will be found, which have been deformed by the m.f. (chapter 14). It appears that the m.f. are located in a plane which is at right angles to the direction of maximal shortening.

*) They are not intercalations of later Mesozoic rocks, as has been recently supposed by Tollman (1959) in his synthesis of the Austrian nappes.

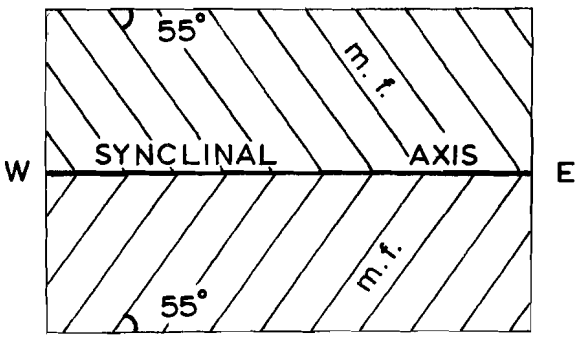

Fig. 61
The Monguelfo syncline unfolded about its synclinal axis.

The m.f. are subvertical at Chienes in the Bressanone region, and dip towards the East in the Pusteria region; they are subhorizontal in the Carnian Alps. This variation of their mean dip is demonstrated in fig. 62. The Pusteria region forms a transition between the subvertical m.f. in the area to the West and the subhorizontal m.f. to the East. This pattern of the m.f. is a Hercynian pattern, which has been affected by Alpine movements.

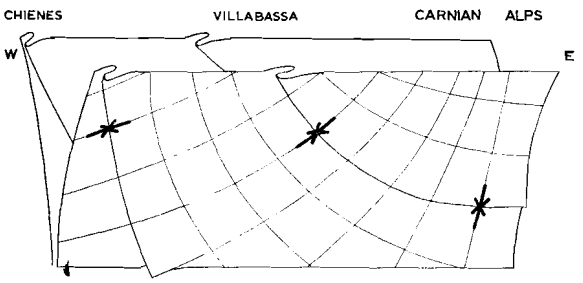

Fig. 62
Diagram of the variation of the mean m.f. in the Pusteria region. Arrows indicate principal stress of minor folding.

In the following, the complicated structure of the m.f. on Sheet III[a] will be explained by a simple approach of the rigid Crystalline of the Defereggen Mountains in the North and the rigid Dolomites in the South. At this stage of our analysis, the Alpine

influence can be deduced from the parallelism between the strike lines of the quartz phyllite and the shape of its northern and southern boundaries.

Moreover, the rapid variations of the azimuths and dips, as large as 50° per km at the Eggerberg structure, cannot have formed during a single phase of deformation. These are local disturbances of the more regional and gradual Hercynian pattern of fig. 62, just as has been stated for the S. Stefano region. Furthermore, the steep dips at the northern border of the Permotriassic of the Dolomites (between which even overturns occur) speak in favour of movements along the subvertical *S*-planes, as in the S. Stefano region.

Along this northern boundary the bedding planes of the Permian and the *S*-planes of the crystalline basement in places are subparallel. It is known that they were at right angles to each other before Alpine deformation (chapter 10).

The character of this Alpine deformation will be analyzed.

The pattern of the mean m.f. of Pusteria (Sheet III[a]) shows two characteristic properties.

1. The mean azimuth lines converge eastwards.

2. The iso-lines of the mean dips show an echelon arrangement of the oblong local minima. The strongest convergence accompanied by a local minimum is observed in the Eggerberg structure, which shows that both properties are closely related.

The other minima are also accompanied by an eastward convergence of the strike lines but the relation is less obvious.

As the border masses do not show such properties, it will be attempted to develop a concept to explain the two features as the result of a squeezing out of a plastic zone between straight borders. This links up with the considerations concerning the S. Stefano Crystalline.

On Sheet III is shown that the convergence of the mean azimuth lines is about equal to the convergence of the borders. It may be supposed that prior to compression the borders were parallel to each other and to the mean azimuth lines, because the quartz phyllite series was isoclinally folded. The compression increased gradually eastward as the mutual distance between the borders becomes smaller in this direction. This concept is illustrated by model I (fig.'s 63 and 64).

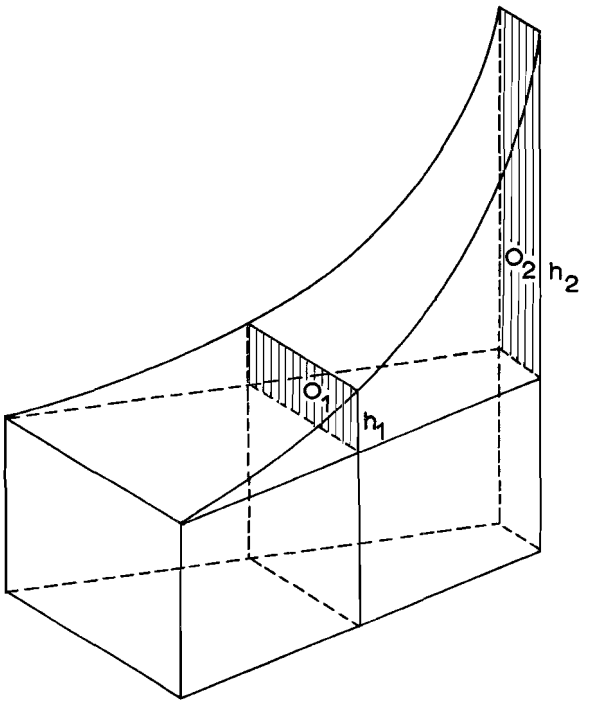

Fig. 63

Model I. The upward squeezed out material increases eastward and $0_2 = 20_1$ (see text).

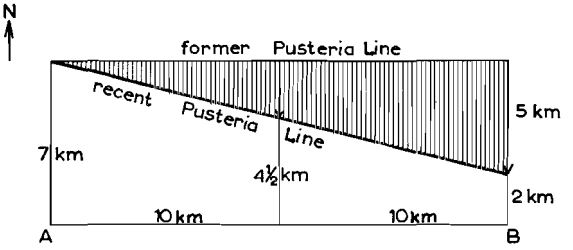

Fig. 64

Model I. It is assumed that the Pusteria Line was dextrally rotated about a hinge point above A. For further explanation see text.

The structural outlines of the Pusteria region between Sorafurcia and S. Candido are given in fig. 65.

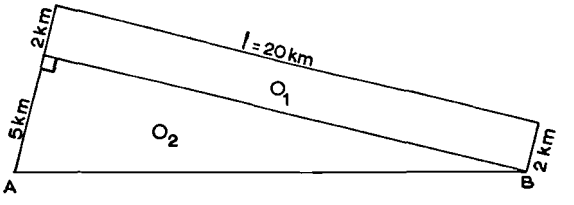

Fig. 65

Schematized dimensions of the Pusteria region. A ∾ Sorafurcia and B ∾ S. Candido.

Model I is based on the concept that at Sorafurcia the Pusteria quartz phyllite has been compressed negligibly. The Pusteria Line has been rotated dextrally along the hinge point. Actually, the hinge point lies some kilometers to the West of Sorafurcia.

It may be assumed that this hinge point is situated NW of Brunico at the easternmost end of the Bressanone granite massif.

Perhaps, the southward push exerted on the quartz phyllites, which were protected by this granite massif, may be neglected in comparison to the southward movements of the crystalline masses North of the Pusteria Line, East of Brunico.

In model I (fig. 64), which is based on fig. 65, the width of the belt of quartz phyllites is about 7 km at Sorafurcia in the West, and about 2 km at S. Candido in the East. It has already been assumed that the crystalline rocks North of the Pusteria Line moved southward, and all distances were measured at right angles to this line. This assumption will be supported by further considerations in the following but for the present analyses it may also be assumed that the southern Dolomites block moved northwards, taking the distances at right angles to this southern boundary of the Pusteria zone. This alternative only negligibly influences the following calculations.

The difference between both distances mentioned above amounts to 5 km. At S. Candido, the Pusteria Line moved 5 km or more southwards, causing the observed convergence of the strike lines of *S* and the upward rotation of the m.f. in the *S*-planes.

At Sorafurcia, no material has been squeezed out and at S. Candido the squeezed out material reaches a maximum. At the half-way point, the squeezing out is intermediate and must be half of the maximum at S. Candido.

A totally different premise is represented by model II, which also links up with fig. 65. In this case, it is supposed that the compression is equally distributed on the entire Pusteria Line, and the Crystalline of the Defereggen Mountains moved the same distance southwards at Sorafurcia and S. Candido. The characteristic properties of the Alpine deformation (a convergence of the *S*-planes and an upward rotation of the m.f.) then have to be explained by assuming an original convergence of the rigid borders. This concept will be analyzed presently.

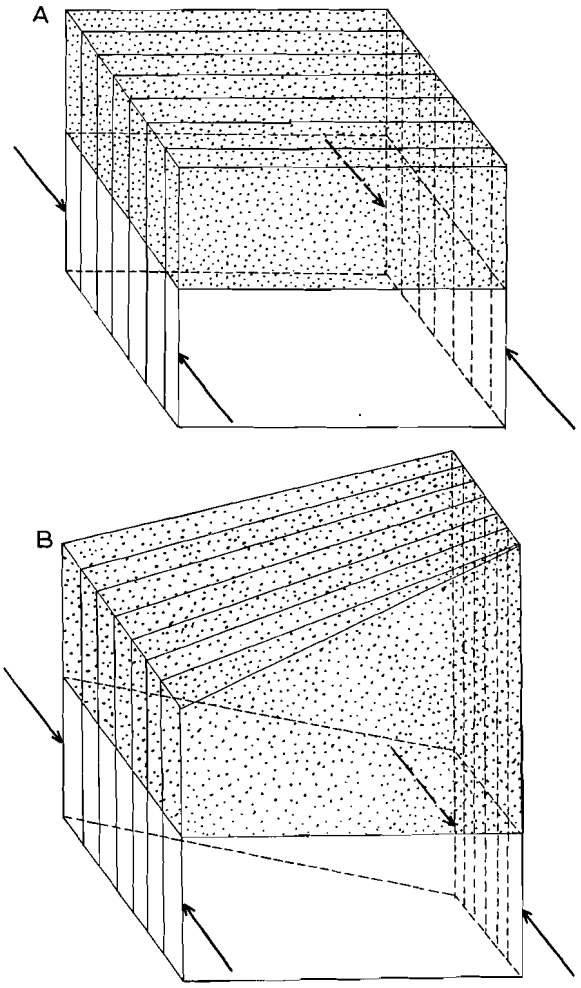

Fig. 66

Model II. The sideward compression of the plastic belt is equal in all places and the squeezed out material (dotted in A and B) too. Case A: The *S*-planes parallel the rigid borders. Case B: The *S*-planes intersect one of the rigid borders and the zone narrows toward the righthand side. The squeezed out column increases in this direction causing an upward rotation of the lineations in the *S*-planes and a convergence of the strike lines of the latter.

Fig. 66A is a block diagram of a plastic zone with a subvertical schistosity parallel to the rigid borders. It has been squeezed out equally over its entire area, and there is no maximal squeezing out in the centre. Lineations within the *S*-planes will not be rotated during such deformation.

An acute angle may have existed between plane borders of the zone before the deformation. The result of the squeezing out in this case is given in fig. 66B. As the borders have approached each

other equally, the height of the squeezed out column must have increased in the direction of convergence of the plane borders.

Pre-existing lineations within the *S*-planes must have rotated upward in the direction of convergence of the plane borders.

As the strike lines of the *S*-planes were assumed as parallel prior to deformation, they must make an acute angle with one or both of the rigid borders. After the deformation the strike lines of the *S*-planes converge in the direction of convergence of the borders.

The absence of an apparent acute angle between the mean azimuth lines and the rigid borders is the main objection against model II. But it can be demonstrated that an acute angle of only a few degrees is already in favour of model II. The constructed mean azimuth lines of sheet III are not of such an accuracy that an angle of some degrees between constructed lines and actual lines is definitely excluded. For this reason, the possibility of model II will be developed also quantitatively. Model II is also in accordance with the other characteristic properties of the Pusteria region being the gradual convergence of the plane borders to the East, an eastward convergence of the *S*-planes and an upward rotation of the m.f. in eastward direction.

Although the first model seems to correspond best with actual circumstances, model II has the advantage that an uniform southward movement on the Pusteria Line is a very simple concept supported by the conformity of the situation all along the northern boundary of the Pusteria quartz phyllites.

In the second part (methodology), it was stated that the models had to answer the following requirements. It must be possible to submit them to simple calculations and they should correspond sufficiently with actual circumstances.

Although the geometry of the Pusteria region is well known from many observations, the complexity of the different deformations is caused by an interference pattern of the kinematics, which can only be partially solved.

It may be remarked that actual conditions may be intermediate between the two extreme concepts represented by the models I and II. Each combination of both mechanisms is possible. It is not possible to draw a conclusion based on the facts on hand.

Some quantitative calculations based on these models will be given. It is possible that the magnitude of the variables used in these calculations is not correct, but these calculations may aid in attaining an insight into the magnitude of the processes involved. Furthermore, these quantitative calculations will serve for arriving at some qualitative conclusions concerning the Alpine tectonics of this region, and the meaning of the used values will not be overestimated.

The Pusteria region again shows the existence of Alpine movements along Hercynian planes of schistosity. The situation resembles that of the S. Stefano region discussed in the preceding chapters. In both regions the abnormal conformity between the *S*-planes of the Crystalline and the bedding planes of the Permian is the effect of a rotation of about 90° in the Permian strata whereas the *S*-planes of the crystalline rocks remained in their original position (fig. 1).

§ 12A *Rotation of the mean m.f.*

The iso-lines of mean dip on sheet III[a] show an echelon arrangement of local minima.

These local minima are indicated by the lowest adjacent calculated mean dips. The sample regions, from which the mean dips have been calculated, have an arbitrary geographic position, so that the real minima may be assumed to be somewhat lower.

Moving from West to East a minimum of 19° is found in the Rio Furcia,

26° SE of Rasùn - Valdàora,
10° N of Braies,
—8° at the Eggerberg,
6° at the Pusteria Line (Planca di Sotto),
—18° NW of S. Candido.

The echelon arrangement of these minima is evident (Sheet III[a]). Apparently, the Pusteria Crystalline has been squeezed out as a whole. The squeezing out was greater along three parallel EW striking lines. The southern line runs through the 19° and 10° minima. The central line runs through the 26°, —8° and —18° minima and the northern line runs just South of the Pusteria Line.

Consequently, the rotation of the m.f. was not evenly distributed over the whole width of the

plastic quartz phyllite zone. Squeezing out preferably occurred along three anticlinal structures. Rotation and squeezing out should not be confused. Every upward rotation in Pusteria indicates a relative squeezing out of mass to the East. E.g. the mass between the 19° and the 10° minima has not been squeezed out less than the mass with 26° minimum North of it. Although the 19° minimum exceeds the 26° minimum, the latter case represents a greater amount of material squeezed out.

Rotation indicates an increase of the amount of squeezed out material and not its absolute amount.

The angle of rotation may be estimated in the following manner. The northern zone of the Pusteria Crystalline between Brunico and Monguelfo seems to be not squeezed out at all. The mean dips present from West to East are 58°, 50°, 49°, 55°, 58°, 51°, and 53°, whereas the mean azimuths are subparallel; no convergence towards the East has been observed.

It is assumed that the Hercynian minor folds had an average dip of 55° East. The 19°, 26° and 10° minima are the results of Alpine rotations in this belt.

When this situation at the end of the Hercynian orogenesis is assumed to represent the starting point of the Alpine cycle of deformations, the mean angle of rotation over the whole width of the crystalline zone can be estimated and amounts to about 15°.

A priori, it is not certain that the 15° upward rotation of a 55° dipping m.f. corresponds with a 15° upward rotation of a horizontal m.f. This is only the case when $a = b$ in fig. 67, or when a describes a circle with the centre M.

If, on the other hand, only vertical movements occur, a is shortened to b, as demonstrated in fig 67.

Furthermore, a vertical upward movement, p, causing a 15° rotation of the 55° dipping a, effects a 30° rotation on the horizontal b.

In the calculations and for the sake of convenience, it is assumed that a has not been shortened to b, but this point is of minor importance for the outcome. It is not, a priori, certain, that no shortening occurred, although no field evidence for such an internal shortening has been found. It is possible that the entire quartz phyllite zone was

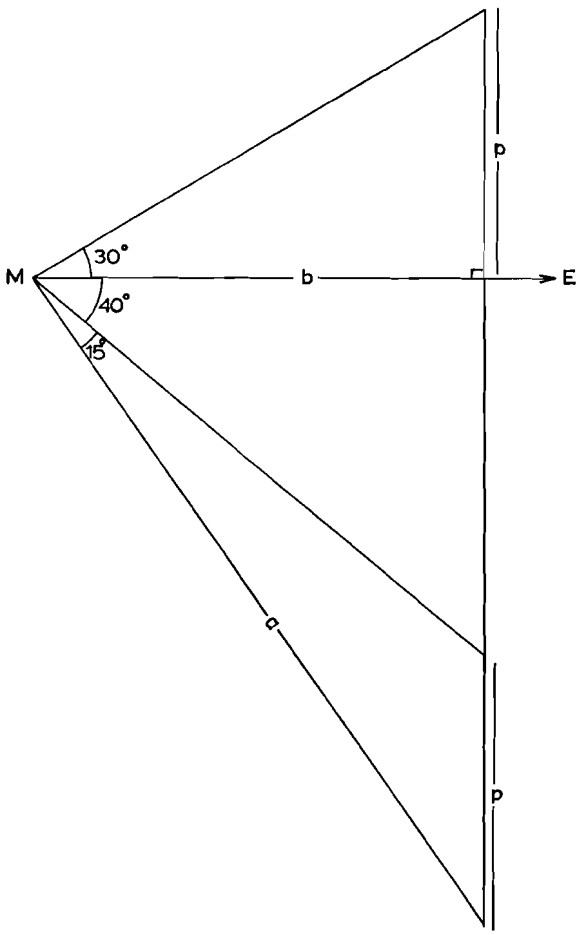

Fig. 67
The 15° and 30° upward rotations for respectively 55° East dipping and horizontal lineations originated by a relative vertical movement (= p) at the East side.

enlarged sidewards as the result of rotations of not internally deformed blocks.

When estimating the mean angle of rotation over the whole width of the crystalline zone at about 15°, this value may be used for some calculations. East of Monguelfo, the rotation cannot be determined as the observed pattern is the product of interference of Hercynian and Alpine deformations. But the rigid borders of crystalline rocks North of the Pusteria belt and the Dolomites South of it converge gradually to the East, which allows a calculation of the rotation of m.f. South of Monguelfo-Dobbiaco. The mean strike lines indicate a local enlargement of the zone with respect to this gradual narrowing. The observed dips in the Permotriassic of Sheet III demonstrate that this enlargement is due to the fact that the southern (Permotriassic) boundary of this belt could be

somewhat indented southward over this distance. Apart from this indenture, the southern boundary of the Pusteria belt runs E-W. This gradual convergence of the rigid borders has been assumed in both models. In the following part, some calculations for estimating the angle of rotation in the eastern part of the Pusteria region are given.

Both models give a rotation of about 45°. The order of magnitude of the amounts of matter squeezed upward can be determined.

§ 12B *Calculations on Model I.*

Model I is represented in figures 63 and 64. Both are approximations on which model I is based.

As the average angle of rotation has been estimated at 15°, it follows that $h_1 = 10 \text{ tg } 15° = 2.7$ km.

Then $O_1 = 4\frac{1}{2} \times 2.7 = 12.2$ km^2.

It is assumed that also below the mean topographic plane of fig. 64, the Pusteria Line rotated gradually.

Then, $O_2 = 2\,O_1 \rightarrow h_2 = 12.2$ km.

$h_2 - h_1 = 12.2 - 2.7 = 9.5$ km.

$$\text{tg } \varphi_2 = \frac{9{,}5}{10} \rightarrow \varphi_2 = 44°$$

φ_2 is the average angle of rotation of the eastern half of the Pusteria region at the upper side of the squeezed out material.

In the mean topographic plane, this angle will be smaller.

$O_2 = 24.4$ km^2 implicates that the Defereggen Crystalline in cross section has replaced this area of quartz phyllite.

Hitherto, a southward movement of the crystalline rocks has been assumed. This concept is supported by the observed southward overturn of the Permotriassic series at the southern border of the Pusteria belt (case 7 of table VII). The occurrence of minor subhorizontal faults indicating southward displacements in the quartz phyllites (§ 4 B) and the average northward dip of the Mesozoic along the Pusteria Line are additional arguments for this supposition.

As will be discussed in the following chapter, the western Drauzone along the Pusteria Line probably is a rift or tension zone resembling the tectonic graben structures in the S. Stefano region described in paragraph 11A. The original position probably must have been subvertical. The present 50 - 70° North dip of this western Drauzone has been caused by rotation.

This northward dip implicates a downwards decrease of the compression. And, as stated before, overturn into a certain direction, in combination with a downward decrease of the deformation, means an absolute movement of the material into this direction of overturn. For this reason, the Pusteria Line must have moved southward, whereas the southern boundary of the Pusteria quartz phyllites has not moved northward.

Solving the type of compression below the mean topographic surface, the following data are given. The southward movement in the topographic surface amounts to 5 km (fig. 64). The area of the replaced crystalline is $O_2 = 24$ km^2. The present dip of the original subvertical Pusteria fault amounts to 50° - 70° North.

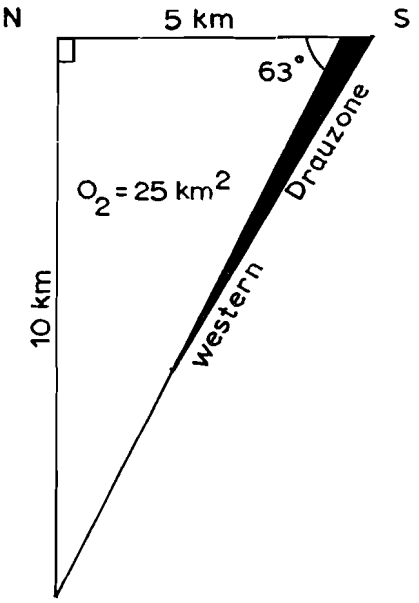

Fig. 68

Schematic section across the western Drauzone at San Candido based on model I. Three independent data are combined:

a) The southward movement at mean elevation amounts to 5 km. b) The area of replaced Austrian crystalline $O_2 = \pm 25$ km^2. c) The actual North dip of the Pusteria fault amounts to 50°—70°.

Fig. 68 gives a reasonable combination of these three data. The squeezing out is maximum at S. Candido, another schematic cross section of which is shown in fig. 69. The value for O_2 (fig. 68) is only estimated, and it may be somewhat too high. The emphasis is laid on the vertical movement by the quartz phyllites, which are at present

exposed at the topographic surface. Basing the calculations on fig. 68, this distance x can be

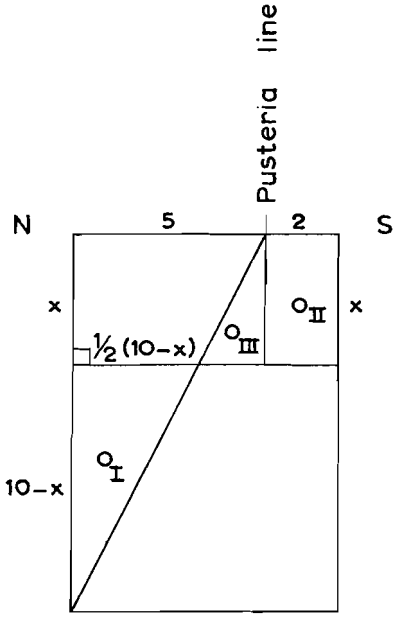

Fig. 69
Calculation of the average Alpine vertical movement (= x) of the rocks exposed at San Candido. Based on fig. 68.

solved by an equation taken from fig. 69. Here $O_I = O_{II} + O_{III}$, as $O_{II} + O_{III}$ is the material replaced by O_I .

$$O_I = \tfrac{1}{2}(10 - x) \cdot \tfrac{1}{2}(10 - x)$$
$$O_{II} = 2x$$
$$O_{III} = \{5 - \tfrac{1}{2}(10 - x)\}\ \tfrac{1}{2}x$$

It follows that:

$$\tfrac{1}{2}(10 - x) \cdot \tfrac{1}{2}(10 - x) = 2x + \tfrac{1}{2}x\ \{5 - \tfrac{1}{2}(10 - x)\}.$$

Or $x \simeq 3\tfrac{1}{2}$ km.

This value is considered reasonable. The youngest quartz phyllites occur at the northern and southern side of the quartz phyllite zone, as might be expected from our theoretical considerations and as supported by field data.

As already stated in the first part of this paper, green phyllites occur at the northern as well as the southern side of the quartz phyllite zone East of Rasùn Valdàora. At the northern side they are locally accompanied by slates. Cornelius Furlani (1912) called these rocks younger "Carnian Rocks", and also Geyer (1902) assumed the green phyllites to be younger than the monotonous quartz phyllites.

This stratigraphic concept is supported by our observations and calculations as on account of an inward increasing squeezing out the youngest sediments are to be expected at the sides of the quartz phyllite zone. Indeed, the green schists occur on both sides of the axial line of maximum upward movements.

The isoclinally folded series of quartz phyllites and green phyllites are probably thicker than (x =) 3½ km, which does not contradict the calculations.

It can be said that the Permian was deposited on quartz phyllites which became younger to the East.

East of Rasùn Valdàora, the green phyllites had originally covered the quartz phyllites. But due to the squeezing upward of the latter, the layer of green phyllites has been pierced diapyrically, and now the green phyllites are exposed on both sides of the quartz phyllites.

§ 12C *Calculations on Model II.*

Model II is based on a uniformly compressed plastic zone narrowing eastwards. This model is illustrated in fig. 70. The angle of rotation in the western part of the Pusteria region is 15°.

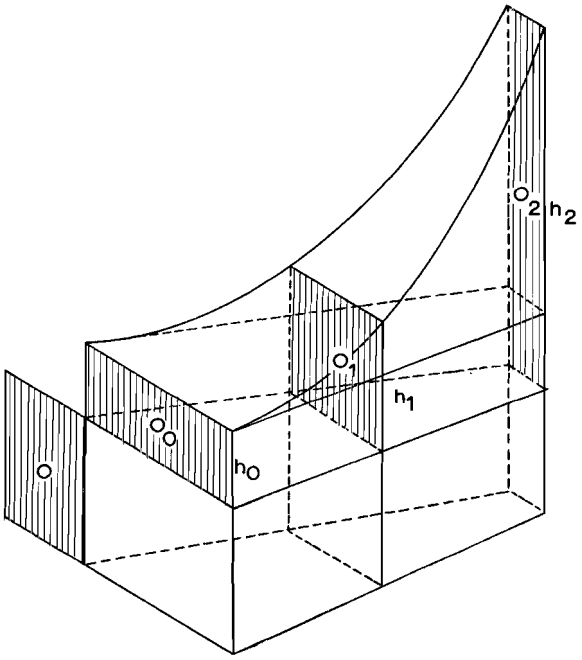

Fig. 70
Model II applied on the Pusteria region. The replaced Austrian crystalline (= 0) equals the squeezed out material in all places, and $0 = 0_0 = 0_1 = 0_2$.

Consequently, $h_1 - h_0 = 2.7$ km.

The squeezed out area 0 is the same in all places $0_0 = 0_1 = 0_2 = 0$.

Thus $0 = 7\, h_0 = 4\frac{1}{2}\,(2.7 + h_0)$ or $h_0 = 4.8$ km.

$0 = 7 \times 4.8 = 33$ km^2,

$h_1 = h_0 + 2.7 = 7.5$ km,

$h_2 = \frac{0_2}{2} = 16.5$ km.

Further $h_2 - h_1 = 9$ km $\rightarrow$ tg $\varphi_2 = {}^9/_{10}$ $\rightarrow \varphi_2 = 42°$.

It appears that the average angle of rotation in the eastern part, φ_2, almost equals its equivalent of Model I.

The replaced area, $0 = 33$ km^2, is somewhat larger than the maximum 0_2 of model I.

The section at right angles to the Pusteria Line resembles fig. 68 in all places.

The great amount of material squeezed out over its entire length renders model II less probable than model I.

Another objection is that an acute angle is required between mean azimuth lines and at least one of the rigid borders. The size of this angle has to be calculated and it should be small enough to fall within the range of the possible error in the constructed mean azimuth lines.

It will now be attempted to explain the convergence of these lines by means of model II.

The process of squeezing out between converging borders implicates a convergence of the mean azimuth lines as demonstrated in fig. 36B.

The rotation determines the amount of material squeezed out. The convergence only indicates the shortening within the mean topographic plane.

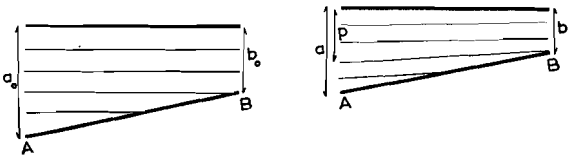

Fig. 71

Model II. The righthand map originated from the left map by equal compression and shows the convergence of the originally parallel strike lines of the vertical *S*-planes. For further explanation see text.

An attempt to calculate this amount of shortening follows. Fig. 71 represents a zone of ductile material with converging rigid borders. The indicated *S*-planes are subvertical. If the northern border moves southward over a distance x, the squeezing out is equal in all places and fig. 71 I results in the situation represented in fig. 71 II.

At the points A and B, the width of the plastic zone amounts to a_0 and b_0 in fig. 71 I, and to a and b in fig. 71 II. b at B is bordered by the same *S*-planes as p at A.

$$a_0 = a + x$$
$$b_0 = b + x$$

The relative shortening, S_A at A is defined as:

$$S_A \equiv \frac{x}{a_0}$$

Therefore, $S_B = \frac{x}{b_0}$

At A: $a = a_0 - a_0 \cdot S_A$, and also $p = b_0 - b_0 \cdot S_A$

A formula is required which expresses x in the values, p a, and b. Successively, the following equations can be set up:

$$p = b_0\,(1 - S_A)$$

$$p = (b + x)\,(1 - \frac{x}{a_0})$$

$$p = (b + x)\,(1 - \frac{x}{a + x})$$

$$p = \frac{b + x}{a + x} \cdot a \qquad x = a \cdot \frac{p - b}{a - p}$$

This formula can be applied to Pusteria.

Again all compression West of Sorafurcia has been eliminated.

A lies in Sorafurcia, and B at S. Candido.

The values a and b are well known.

Fig. 65 gives $a = 7$ km, and $b = 2$ km. p must be deduced from the mean azimuth lines. It may be assumed that the constructed course of these lines is not sufficiently accurate in approximating reality that exact calculations are allowable. For this reason, a diagram (fig. 72) has been constructed based on the formula for x and therefore giving the relation between p and x for the above mentioned values of a and b.

It can be derived from sheet III[a] that p approximately equals a. This means $x = \infty$, which is impossible and which may suggest that Model II is not possible.

On the other hand, the mean azimuth line drawn North of Sorafurcia (p. 1360 on Sheet III) is almost tangent to the Permian at S. Candido. If it is assumed that the Pusteria Line is parallel to the mean azimuth lines, and that these lines form an acute angle with the Permian of the Dolomites, the two possibilities $p = 4$ km and $p = 5$ km may not be, a priori, excluded. The acute angle would

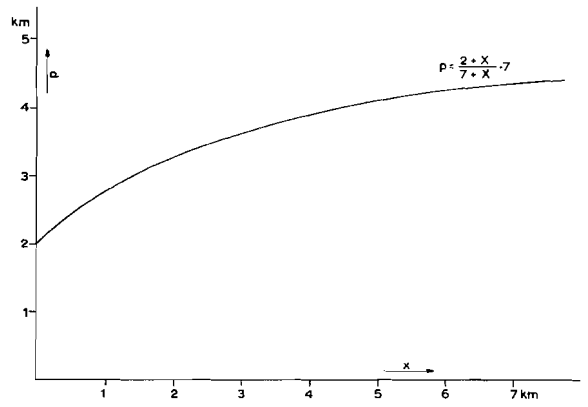

Fig. 72
Diagram of the relation between x and p, based on the formula $p = \frac{2 + x}{7 + x} \cdot 7$ (see text).

then be $\psi = 8°$ and $\psi = 6°$ respectively for these two values of p.
p = 4 km means x = 4 km and
p = 5 km means x = 11½ km. The latter value is probably too high. But when p = 4 km or somewhat greater, the value of x approaches that of the southward movement of the Pusteria Line obtained in fig. 68, based on Model I. The replaced area of quartz phyllite O = 33 km² according to Model II does not differ greatly from the value of O_2 = 24 km² obtained for fig. 63 based on Model I.

It may be concluded that indeed if $\psi = 8°$, Model II gives a reasonable explanation of the present situation. In this case fig. 68 would represent a cross section valid for the entire Pusteria Line and not only a cross section of S. Candido, as in the case of Model I.

Both models give average angles of 15° and 45° respectively for the mean angles of rotation in the western and the eastern part of the Pusteria zone. All combinations of these models will give a similar result. The amount of squeezed out material will increase eastwards and in the case of a combination the angle of ψ will decrease from the maximum value of 8° accepted in Model II.

CHAPTER 13

TECTONICS OF THE PERMOTRIASSIC OF THE PUSTERIA REGION

The tectonics of the non-crystalline rocks in the Pusteria region may be divided into the tectonics of the western Drauzone along the Pusteria Line, situated at the northern side of the quartz phyllite zone, and the tectonics of the Permotriassic between the Rio Furcia and the Rio di Braies, along the southside of the quartz phyllites.

§ 13A *Tectonics of the western Drauzone.* (North of the quartz phyllite zone)

Between the crystalline rocks of the Defereggen Mountains to the North and the Pusteria quartz phyllites to the South, some intercalations of younger rocks are present. The stratigraphy of the Mesozoic components of these intercalations has been summarized in chapter 5. The western Drauzone was comprehensively described by Cornelius Furlani (1912) and Gb. Dal Piaz (1934).

The rocks consist for the greater part of tectonic breccias. The Pusteria Line appears as a morphologic depression and the western Drauzone is not well exposed. The differences between the geologic map of Furlani (1912) and the present map, which was compiled in 1957, may be explained by rapid erosion.

The width of the western Drauzone gradually decreases towards the West. The younger rocks consist of Mesozoic rocks, Upper Silurian (?) limestones, and tonalitic intrusions. The latter are only exposed North of Monguelfo and at Planca di Sotto. The first two rock types together are filling up the western Drauzone, and the Mesozoic is generally located North of the Upper Silurian (?). At some places, however, e.g. NNE of S. Candido, the zone only consists of Mesozoic rocks, whereas at other places (e.g. Rasùn-Valdàora) only Upper Silurian (?) is present.

The thinly laminated Silurian(?) limestones pass eastward uninterruptedly into the Upper Silurian limestones of the Carnian Alps, containing *Orthoceras*, but in the Pusteria region fossils have not been found. These limestones have been folded during Hercynian orogenesis. Their stratification is subvertical, and parallel to the schistosity of the Pusteria quartz phyllites. The strike of the bedding planes is E-W. Frequently, minor folds occur,

mostly as ribs but in some cases they may have a width of some cms.

At Prato alla Drava, the following measurements have been made on these m.f.:

co-ordinates of the grid	az. — dip of m.f.
983 - 800	290° - 10°
982 - 801	100° - 0°
979 - 802	285° - 12°
975 - 804	110° - 15°
974 - 805	105° - 30°

North of Dobbiaco, at the Kühbach, (fig. 73) 260° - 10° has been found.

These dips are about equal to the dips of the m.f. in the adjacent Pusteria quartz phyllites.

The fault which probably borders the western Drauzone at its southern side apparently is a normal fault parallel to the mean schistosity with a downthrown block consisting of younger "Carnian Rocks" at its northern side (fig. 75).

The structural position of the Mesozoic rocks generally filling up the northern part of the western Drauzone North of the Silurian rocks is complex.

Strikes parallel to the Pusteria Line are predominating but many deviations have been observed.

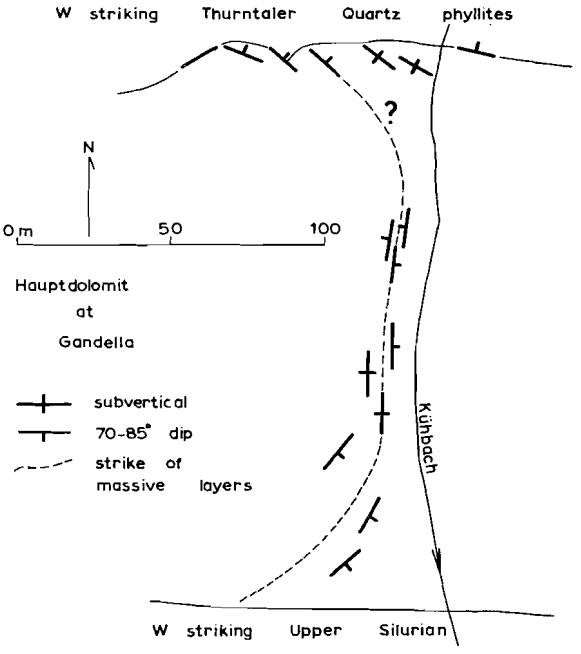

Fig. 73
Structural sketchmap of the Hauptdolomit along the Kühbach North of Dobbiaco, Pusteria region.

Fig. 73 shows the structure of the "Hauptdolomit" at Gandella (NNE of Dobbiaco). This Hauptdolomit block is subvertical with a N-S strike. West of the Kühbach, some low ridges with exposures of Hauptdolomit are present, parallel to the Pusteria Line. This Hauptdolomit probably strikes parallel to the Pusteria Line. Also East of the Gandella structure of fig. 73, E-W strikes are found along the Rio di S. Silverstro (Sheet III).

Apparently, the Hauptdolomit of the western Drauzone consists of large boulders in different positions.

As stated in chapter 11, this structural independence of separate boulders is an argument in favour of the concept that these wedges of younger rocks intercalated in the crystalline basement were

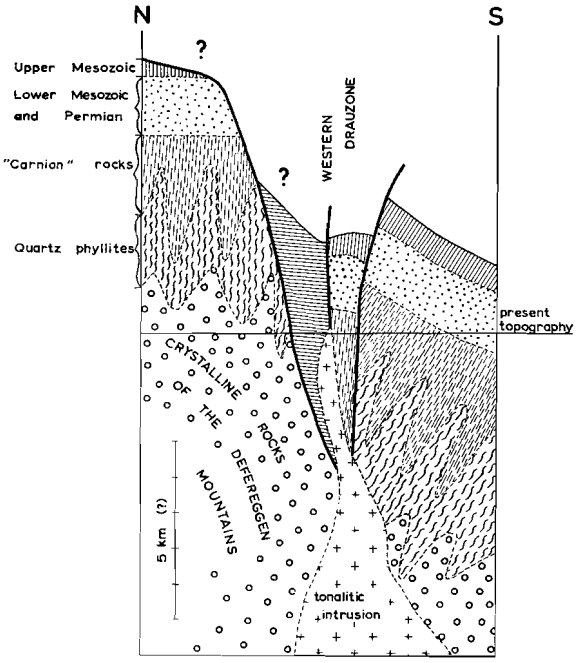

Fig. 74

SCHEMATIC SECTION ILLUSTRATING THE FORMATION OF THE PUSTERIA LINE

The Pusteria Line is considered as a downthrow fault with a tension rift along the southside of the fault plane. This rift has been filled up as a result of:

a) Subsidence of "Carnian Rocks"
b) Subsidence of Mesozoic blocks
c) Rise of magmatic matter.

Remarks: 1) The width of the western Drauzone has been exaggerated about 10 times. 2) The thickness of the folded crystalline series is unknown. 3) The later southward toppling over of the Pusteria fault plane has not been depicted. 4) Due to earlier Alpine kinematics, the position of the rocks North of the Pusteria Line had been disturbed (chapter 22) which has not been depicted either.

formed by subsidence in grabenlike rifts, which were subsequently compressed.

The Pusteria Line is a fault line and the origin of the hypothetic tension rifts probably is about synchronous with faulting.

As the younger rocks occur South of this originally subvertical fault, the southern side is probably the downthrown side of a normal fault. The nature of the Pusteria Line will be discussed in greater detail in chapter 19.

For the present, fig. 74 gives the possible mode of filling up of the tension zone by the three kinds of younger rocks mentioned above.

The tonalitic intrusions are in support of the concept that originally tension existed along the Pusteria Line. This tension enabled the igneous material to rise. The tonalites filled the western Drauzone from below, whereas the Mesozoic and Upper Silurian rocks filled the western Drauzone from above.

Dal Piaz (1942) mentioned contact metamorphism of the tonalites in the Mesozoic. This means that at least locally the downward movement of the sedimentary wedges preceded the upward movement of the magmatic material.

§ 13B *Tectonics of the Permotriassic between the Rio Furcia and the Rio di Braies.* (South of the quartz phyllite zone).

Sheet III is considerably different from the Carta Geologica delle Tre Venezie, foglia Monguelfo (= F. 7, Merla's contribution, 1930). Fig. 75 gives Merla's map.

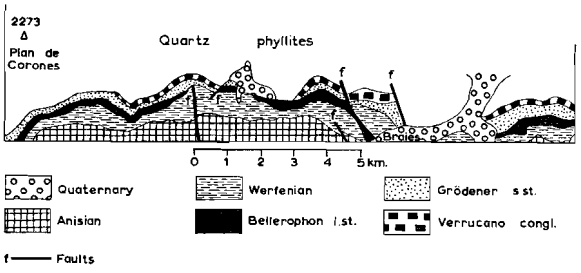

Fig. 75
Geology of the vicinity of Braies according to Merla (Carta geologica, 7, 1930).

The most important difference is the distinction between the Upper Permian Bellerophon limestones and the Werfenian beds which resemble each other in the Pusteria region, based on observations in the surroundings of Braies where the Bellerophon is well exposed.

The dip symbols on Sheet III also represent the outcrops and indicate an E-W strike, apart from the flexures with a subvertical axis, already mentioned as case 8 in table VII. The rocks at Braies called Bellerophon limestones by Merla are gypsum containing dolomites which disappear below the Quaternary (fig. 75). Indeed, they probably belong to the Upper Permian. In that case, the stratigraphically older, E-W striking marly limestones North of them are Permian and not Lower Triassic Werfenian strata as supposed by Merla.

The five faults distinguished by Merla have been reduced to a single sinistral transverse fault, the presence of which may be deduced from the displacement of about 500 m of the stratigraphic boundaries along the fault plane.

Its horizontal slip is indicated by accompanying minor faults (see § 6A).

The faults on Merla's map North of Braies have to be replaced by a set of dextral wrench flexures which are not restricted to three distinct NNW striking lines as the faults on his map.

The cases 7 and 8 of table VII summarize the two systems of deformation types which determine the structure of the Permotriassic under discussion.

Case 7 is a bending around an E-W striking axis giving the strata a subvertical or even an overturned attitude.

These subvertical or steeply dipping strata have been folded around subvertical or steep axes, resulting in the system, distinguished as case 8 in table VII.

The flexures of this system indicate that the eastern block moved southward with respect to the western block. These flexures may be compared with those of case 5 (table VII) and have been discussed in some detail in paragraph 11D. They seem to be younger than the phase of folding around E-W axes. It is highly probable that these flexures are synchronous with the indenture in the general strike of the quartz phyllites South of Monguelfo-Dobbiaco.

This indenture has been explained in chapter 12 as the result of a southward push of the quartz phyllites into the Permotriassic of the Dolomites. The parallelism of the strikes of the schistose rocks on the one side and of the Permotriassic on the

other proves the Alpine age of this indenture. From these considerations it may be concluded that the Permotriassic under discussion has dextrally rotated, not only internally (case 8, table VII) but also externally. Also on this point the present region may be compared with the Werfenian rocks along the F. Ansiei, South of Villapiccola (chapter 11).

The wrench flexures are accompanied by subsymmetrical minor folds, although not as frequent as along the F. Ansiei. The measured axes of m.f. are:

co-ordinates of the grid	az. - dip m.f.
771 - 779	135° - 60°
759 - 787	130° - 60°
759 - 787	145° - 45°
759 - 786	125° - 40°

Moreover, movements parallel to the bedding planes around similar axes are indicated by striae. E.g. the bedding planes of the Bellerophon limestones North of Braies (co-ordinates: 785 - 778) are dipping 70° - 75° in the direction 210°.

The numerous striae in the bedding planes have an angle of rake of 135° - 145°.

The observations on the minor folds in the Permotriassic of Braies are too few to allow an exact analysis as made in chapter 11 for the m.f. of the Werfenian beds along the F. Ansiei. The axes are probable parallel to the line of intersection between the generally southward dipping bedding planes and a subvertical, 125-145° striking, plane in which all axes of m.f. are situated, making right angles with the probable direction of principal stress.

CHAPTER 14

TECTONICS OF THE BRESSANONE REGION

The structure of the Bressanone quartz phyllites is less complicated than the structure of the quartz phyllites in the S. Stefano and Pusteria regions. The structure and the kinematics follow clearly from the structure map (Sheet IV).

The Bressanone quartz phyllites are bordered on their northside by the Bressanone granite and the Pusteria Line. The Bressanone granite belongs to the so-called "Periadriatic intrusions", which intruded at the end of the Alpine orogenesis. The granite of Bressanone on the westside (W. of the F. Isarco) resembles a laccolith, the boundary of which is parallel to the schistosity of the surrounding quartz phyllites; on the East side it is a batholith cutting the schistosity. To the SE of Rio di Pusteria, the contact makes right angles with the S-planes. The contact along the F. Rienza between Vandoies and Falzes, however, is parallel again to the schistosity. It may be assumed for the latter situation, that the *S*-planes which were already subvertical, have been dragged farther upwards by this intrusion, thus causing an apparent parallelism between plane of contact and schistosity. The very intense drag along the contacts of a batholith is generally confined to a zone with a width of a few hundreds of meters, and the effect decreases outwards.

Still farther away from the intrusion the mean strike of the schistosity-planes makes an angle with the contact plane.

The sample of measurements SW of Sciaves (meas. s. 140 of App. II) shows obvious drag on account of the abnormal NNE strike, which is parallel to the contact in this place. A zone of intense drag of some hundreds of meters wide has also been found along the Cima d'Asta and Rieserferner batholiths (see chapters 15 and 21). The entire crystalline basement complex of the Cima d'Asta region has been influenced by the intrusion, notwithstanding the fact that in some cases the distance from the contact amounts to many kilometers. At first sight one may believe that the southward dip of the southern and western part of the Bressanone quartz phyllites has also been effected by an Alpine rotation, which resulted from the upward movement of the Bressanone granite at that time.

By this concept, however, the situation is only partially explained. It is true that the Permian is dipping to the South, but the quartz phyllites are dipping steeper in this direction. This different amount of dip is demonstrated most obviously by the construction of cross sections through the relicts of Permian which cover the mountain summits of the Bressanone quartz phyllites in two places (Sheet IV[a]).

The connecting line between the M. Telegrafo (2504m) and the summit of 1835 m located to the South gives about the dip of the contact plane between the Crystalline and the Permotriassic cover.

This plane dips about 9°, whereas the *S*-planes are dipping 20° - 30° here (Sheet IV).

The effect of the Alpine kinematics may be eliminated by not taking into account the measurements in the marginal belts around the intrusive rocks and by rotating the Permian into its original subhorizontal position. Furthermore, the probably Alpine anticline in the SW corner of Sheet IV between Novale di Sopra and Rasciesa di Fuori, which indicates an Alpine shortening of the subhorizontal Crystalline, must be left out of consideration in analyzing the pre-Permian situation.

The remaining Hercynian geometric pattern is rather simple. Nevertheless, some important conclusions can be drawn. The *S*-planes are dipping to the S to SW in the whole Bressanone region. The amount of dip increases from South to North and in some degree from West to East.

The N-S cross section South of Brunico in the NE corner of Sheet IV shows subvertical or steeply southward dipping *S*-planes in all places. It has been demonstrated in chapter 12 that this section probably represents an isoclinally folded series.

Consequently, the Bressanone region is the transitional region between an unfolded subhorizontal Crystalline in the South (also found in the Cima d'Asta and Gosaldo regions South of the Dolomites, see chapters 15 and 17) and an isoclinally folded series in the North (continuing in the Pusteria and S. Stefano regions).

This Hercynian macrofolding occurred around an E-W axis. The SE strike of the *S*-planes NE of Bressanone may be explained as the result of the eastward increasing dip of these planes.

Steepening of the dip in the direction of strike is always accompanied by a convergence of the strike lines in this direction. Fig. 76 is a theoretical model of the Bressanone region. The convergence of the mean strike lines has been calculated with an eastward steepening of 15°. The mean dip between two mean strike lines bordering an equally thick crystalline layer has been indicated in a western and an eastern section (fig. 76).

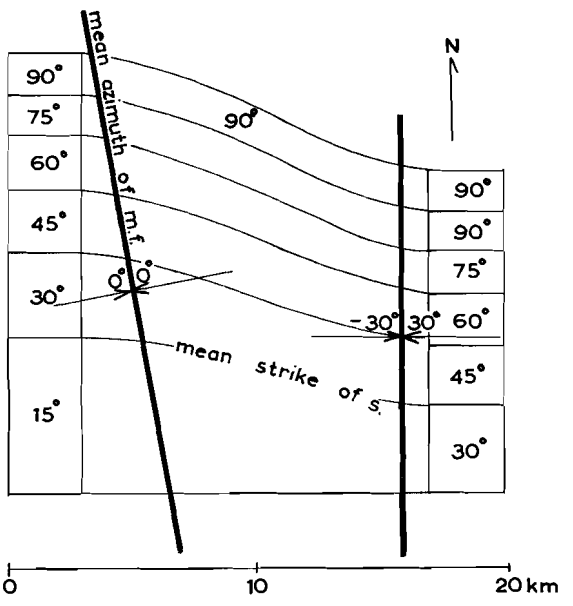

Fig. 76

Theoretical model of the Bressanone region. The SE strikes have orignated by an eastward steepening of the mean dip up to 15°. The principal stress during minor folding is indicated by arrows (in the eastern part 30° West dip and in the western part a subhorizontal position).
For further explanation see text.

It has been supposed that in the South the mean strike lines continue their E-W course towards the East.

As this model resembles actual circumstances, it may be stated that the eastern part of the Bressanone region has been compressed more strongly than its western part, while the material was pushed towards the South.

Hitherto, is was assumed that the quartz phyllites of Bressanone had a NW to NNW strike (Heritsch in Schaffer's volume, 1951, p. 262). This direction was interpreted as the original Hercynian strike and this strike served as a means of distinction between the Bressanone quartz phyllites and the Thurntaler quartz phyllites which are located North of the Pusteria Line (Sheet I). The Thurnthaler quartz phyllites are striking E-W. This assumption of a mean SSE strike for a great part of the Bressanone Crystalline was based on a few measurements by Sander (Carta geologica, 6, 1924).

Our tables and diagrams (appendices II and III) demonstrate, however, that although some SSE strikes do occur, these are exceptions from the many *S*-planes which together from a group with

a mean having a SE strike at the most. This SE strike probably is the result of an eastward increasing dip; for the Hercynian orogenesis the N-S direction of compression has to be accepted also for the Bressanone region.

The preceding discussion shows the necessity of a great number of measurements for reaching dependable conclusions. Some single values belonging to groups of strongly dispersed measurements may introduce incorrect conclusions.

Up to now, nothing has been said on the minor folds of the Bressanone region.

It has been explained in chapter 12 that the minor folds are probably younger than the macrofolds. The Hercynian minor folds grow steeper from East to West in Pusteria. At Brunico, they are dipping about 60° East. This tendency continues in the Bressanone region. In the surroundings of Chienes, subvertical minor folds are found. In this place, the direction of maximal shortening was E-W and horizontal (fig. 76).

In the Bressanone region, the macrofolding not only effected subvertical attitudes of the *S*-planes as in the Pusteria region, but varying southward dips are present.

An E-W directed compression produced minor folds the dip of which equals the southward dip of the *S*-planes folded by this compression. Sheet IV shows S-SSE dipping minor folds in all places with the exception of the NE corner. Notwithstanding the strong dispersion of the measurements, the mean azimuth lines appear to be subparallel. The mean dip of the m.f. may be somewhat smaller than the dip of the mean m.f. located within the mean *S*-plane which it approximates. The causes of such deviations were discussed at length in chapter 9. The proper deviations are given in table XVIII. The relation between major folding and minor folding is also shown in fig.'s 62 and 88.

The parallelism of the mean azimuth lines causes various angles between these lines and the mean strike lines, the strike of which varies from E to SE. This angle is ± 30° in the surroundings of Lusòn and ± 80° at the T. Eores.

The variations in the course of the mean strike lines result from the phase of major folding.

Dealing with the Pusteria quartz phyllites it was proved that the m.f. in this region are younger. It is obvious that an EW horizontal compression will cause parallel mean azimuth lines in E striking as well as in SE striking *S*-planes. The subject of refolding was discussed in chapter 11 to which may be referred.

On the other hand, the younger age of the m.f. has not been proved in the Bressanone region. Subhorizontal N-S striking m.f. may be assumed in the subhorizontal *S*-planes which were afterwards folded as shown in fig. 76. Probably, all movements occurred in vertical N-S planes and for this reason the N-S m.f. maintained their N-S azimuth during this phase of major folding.

It may also be assumed that the SW dips of the *S*-planes of the central part of Sheet IV originated by folding along a SE running axis. In this case, the m.f. indeed would have rotated about a vertical axis, but the amount of rotation would be too small to be measured. However, this case seems to be less probable than that in which the movements in the Bressanone region are restricted to vertical N-S planes. The calculations on the possible variation of the azimuth of the m.f. by later major folding parallel to another axis will be given in chapter 15.

In the NE corner of Sheet IV, the mean azimuth lines show a sharp deviation from the N-S course in the remaining Bressanone region to the W-E course in the Pusteria region. The structural meaning of this bend must not be overestimated. It has resulted from the exaggeration of the influence of the steep dips on the course of these mean azimuth lines by the projection method which has been applied. Sheet IVa, in the lower right corner of Sheet IV, gives the angle between the mean m.f. and the strikes of the mean schistosity, in other words the rake of the m.f.

In the Bressanone region the schistosity-planes are generally dipping southward, with a few exceptions of northern dips in the SW corner. For the sake of obtaining comparable rakes, they all have been measured clockwise with respect to the eastward strike of these *S*-planes, observed from above.

Furthermore, only the rakes belonging to the mean strikes varying from 80° to 130° have been used for map IV^a. By representing the mean m.f. in this way, the exceptional character of the NE corner of Sheet IV disappears, as the variation of the rake is not greater than in other places of this region.

CHAPTER 15

TECTONICS OF THE CRYSTALLINE ROCKS OF THE CIMA D'ASTA REGION

In the crystalline basement exposed at the southside of the Dolomites (Sheet V, VI, VII) the schistosity-planes and the stratification are parallel to the bedding planes of the overlying Permian sediments.

The major Hercynian folding around an E-W axis is absent. Minor folds with N-S axes are present. Most minor folds are overturned, generally to the West (chapter 3). They are accompanied by larger folds and a N-S strike of the *S*-planes has been observed in places.

The Cima d'Asta Crystalline is bordered to the NW by the NW dipping Lagorai quartz porphyries, to the E by the reef dolomites of the Pale di S. Martino, and to the SE by the Sugana Line. This crystalline basement complex can be divided into two parts. The western part consists mainly of intrusive rocks (granites, tonalites, diorites, and gabbros) with intercalated and isolated areas of quartz phyllites. This part has been called the "Cima d'Asta Complex" (fig. 78).

The eastern part consists of metamorphic rocks.

§ 15A *The Cima d'Asta Complex.*

The intrusive rocks of the Cima d'Asta Complex belong to the "Periadriatic intrusions", comparable with the Bressanone granite North of the Dolomites.

The Cima d'Asta granites have intruded the quartz phyllites during Late Alpine orogenesis. According to Mittempergher their Alpine age has been determined by radioactive methods (personal information). The more basic gabbroic rocks at the Val Lozen in the eastern part of the Cima d'Asta Complex (point 1136 m) have a direction of paleomagnetization which is about the same as the present direction (non-published data of the geophysical department of the Geological Instit. at Utrecht supplied by T. L. R. Findhammer). In this chapter will be demonstrated, that a relation exists between the mechanism of the Cima d'Asta intrustion and the Alpine boundaries of the quartz porphyries layer and the Schlern dolomites. Mittempergher (personal information), moreover, found contact-metamorphism in the Lower Permian Lagorai quartz porphyries, and the earlier concept of a Hercynian age of the intrusion, still accepted by Andreatta (1932) and d'Amico (1957) must be abandoned.

The contact-metamorphism is generally restricted to a belt some hundreds of meters wide along the contact planes of the intrusive rocks. According to d'Amico (1957), the great post-kinematic feldspar crystals (see fig.'s 45-47 of App. I) and some other minerals in the Val Lozen area may be considered as a recrystallization of the quartz phyllites with some supply of material (e.g. alkalies, see chapter 20) related to the Cima d'Asta intrusion. The intrusive bodies are diapyric batholiths. The contact planes are generally parallel to the *S*-planes, or subvertical. In the latter case, they generally intersect the *S*-planes. Upward drag of the originally subhorizontal *S*-planes has been observed in many places. South of the M. Tauro, at the southern contact plane of the Cima d'Asta granite, the *S*-planes are overturned towards the South in a zone about 150 m wide.

Subhorizontal *S*-planes occur South of this overturned zone in the Crystalline of the Strigno region (Sheet VI).

These *S*-planes are not overturned, as they are conformably overlain by the Permian (Section V, fig. 83). The overturning of the *S*-planes South of the M. Tauro must be the effect of local drag, which disappears to the East. South of the M. Castelletto the contact plane dips to the South and almost coincides with the present topography.

The subparallelism between the contact plane and the present topography is indicated by alternating contact-metamorphic quartz phyllites and

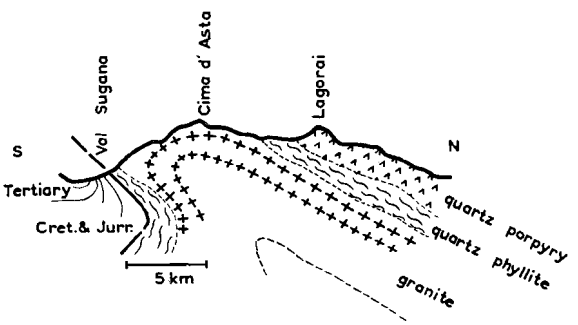

Fig. 77
Trener's concept on the Cima d'Asta granite (1957, p. 613).

granite on the southern slope of the M. Castelletto. The local overturning of the *S*-planes disappears also westward. South of the M. Cima the *S*-planes have an average dip of ± 32° NE up to the contact plane, without any overturning and drag at the contact. These observations on the southern contact of the Cima d'Asta granite refute Trener's view represented by fig. 77. Trener (1957) was of the opinion that the Cima d'Asta granite intruded as a Hercynian laccolith, and that it had been folded together with the surrounding quartz phyllites into a southward overturned anticline. However, as this intrusion most probably has an Alpine age, it is more probable that it ascended vertically, locally dragging the quartz phyllites upward into a subvertical position.

The contact zone at the North side of the Cima d'Asta Complex is not so well exposed, and the absence of overturn does not definitely prove that overturn cannot be present.

Local overturn to the South at the South side is evident, but an equivalent overturn at the North side has not been observed. The dimensions of the phenomenon of overturn at the South side are small in comparison to the dimensions of the entire Cima d'Asta Complex, and this feature will not be used as a factor in our considerations on regional tectonics.

Next to features of drag close to the contact plane, the curvatures of the mean strike lines on Sheet V represent a general doming of the quartz phyllites around the intrusive masses. This doming is most evident in the eastern part of the Cima d'Asta region to be discussed in the following paragraph.

An exception is formed by the Calmandrino

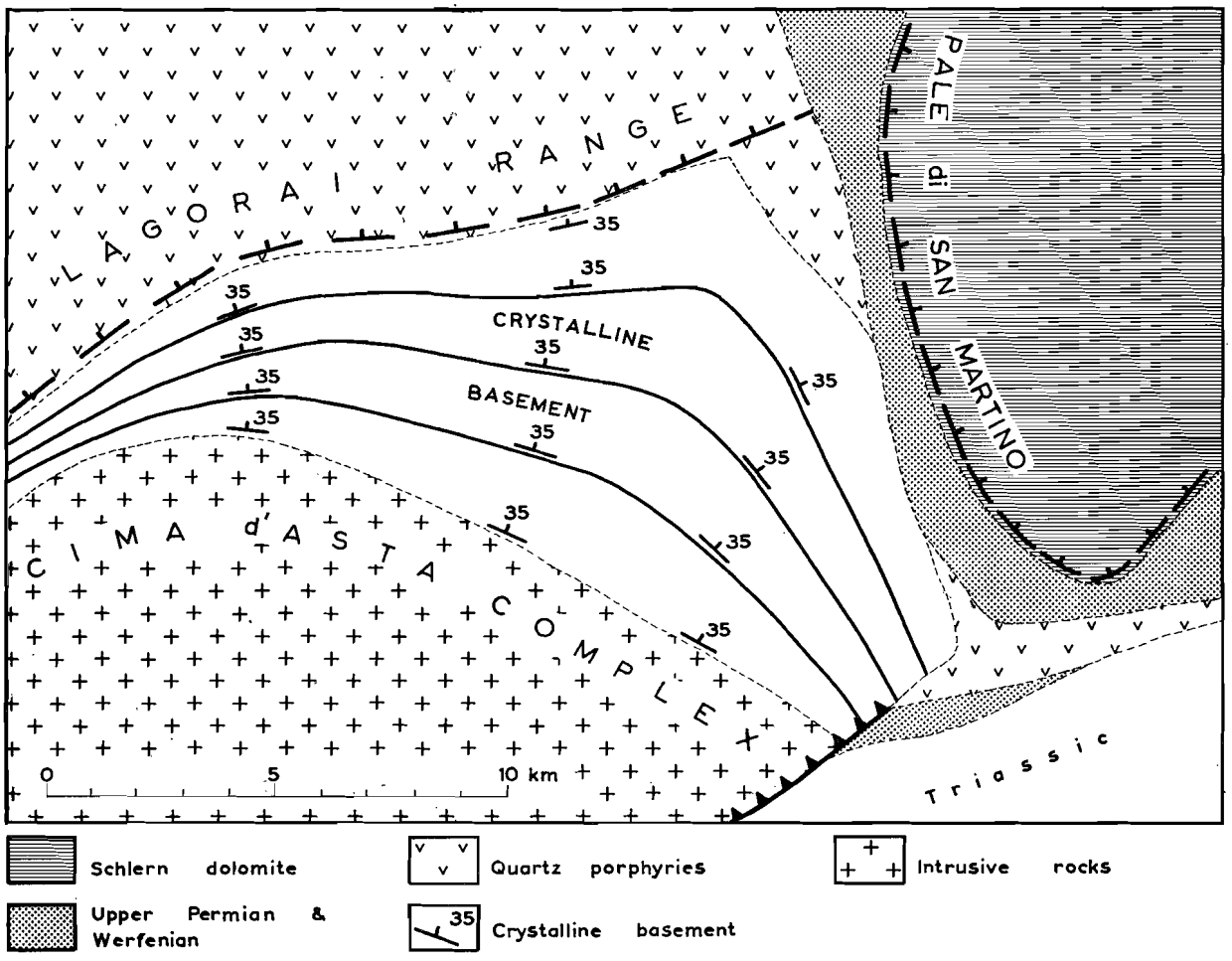

Fig. 78
Schematized structure map of the Cima d'Asta region. It is assumed that the mean dip is 35° in all places of the crystalline triangle.

area West of Canale San Bovo. The *S*-planes are dipping toward the North, that is in the direction of the Mezzogiorno diorite. They seem to make right angles with the contact plane of the latter.

The contact plane of the Cima d'Asta granite dips steeply to the East, and is well exposed SE of the M. Tolvo. The gently westward dipping *S*-planes are intersected at right angles by the steeply eastward dipping contact plane. No drag is present.

The 20° northward dip in the Calmandrino area indicates that this area is the northern limb of an anticlinal structure with an overturn to the South, the reduced middle limb of which is formed by the Sugana Line (Ch. 16).

The quartz phyllites in the surroundings of the M. Cengello belong to the roof of the granite, and contain all sorts of veins (Carta geologica, 22 by Trener, 1943). These veins and dykes have been omitted from our maps. In some places breccias have been found consisting of fragments of quartz phyllites with different attitudes of the *S*-planes.

E.g. at the M. Cengello, on about a quart of a square meter, a number of fragments with diameters of about one decimeter were observed with orientations of 270° - 40°, 215° - 55°, 205° - 58°, 305° - 55°, and 255° - 50°, respectively. This is possibly the cross section of a funnel-shaped body in which the rotations of the independent blocks were caused by escaping gases.

The mantle of quartz phyllites reacted more or less plastically during the Alpine intrusion. This will be demonstrated in the following paragraph.

§ 15 B *Tectonics of the NE part of the Cima d'Asta Region.*

Fig. 78 is a simplified structural representation of the crystalline triangle NE of the Cima d'Asta Complex and its Permotriassic framework. The strike lines of the *S*-planes in the crystalline basement are parallel with the NE border of the Cima d'Asta Complex, with the southern border of the Lagorai Range, and with the western border of the Pale di San Martino unit.

These strike lines converge from the central area of the crystalline triangle to its southeastern and southwestern cornerpoints. This convergence is not caused by a variation of the dip as was the case in the Bressanone region. As the dip is fairly consistent all over the region, this convergence must be due to a wedging out from the centre to the corner points. The 22 mean dips of *S*-planes of the crystalline triangle have a mean of 35°. This value will be used in some calculations. In the centre of the triangle, the exposed crystalline series is about 5 km thick. In the western angular point it has wedged out to about 1 km. Such wedging out is probably caused by a subsequent deformation and not a pre-Permian property of the crystalline rocks.

The mean azimuth lines of the minor folds are subparallel in the whole Cima d'Asta region. Their direction is about N-S, as in the Bressanone region.

The rotation of the *S*-planes is younger than the formation of the m.f. At first sight, it seems that rotations of subhorizontal *S*-planes with subparallel m.f. around different axes would disturb the subparallelism of the m.f. by variation of the azimuth during the rotation. When the angle of rotation is not too great, this variation of the azimuth may be neglected. In fig. 79, the variation has been calculated for an angle of rotation of 35°. The axis of rotation makes all possible angles between 0° and 90° with the originally horizontal, N-S directed m.f. After rotation, the rake of

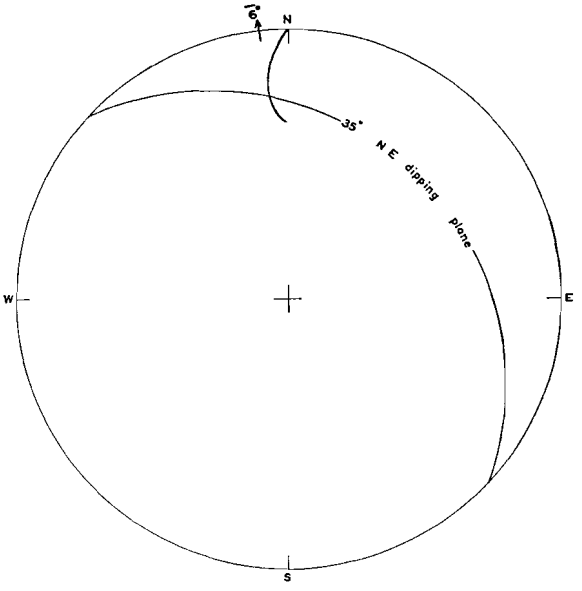

Fig. 79

Diagram (Schmidt net, lower hemisphere) of the after-rotational positions of originally horizontal, N-S directed, m.f. which lie in planes rotated 35° about axes between N and W. The maximal deviation of the after-rotational azimuth is —6° in case of a NW directed rotation axis.

the m.f. is the same. It appears that the deviation between the original N-S direction and the after-rotational direction of the m.f. reaches a maximum when the axis of rotation makes an angle of 45° with this original N-S direction.

The maximal deviation of the after-rotational azimuth from the original one is only N 6° W. For this reason, the after-rotational variations of the azimuth may be neglected in the Cima d'Asta region.

On account of the preceding analysis, the position of the m.f. is of no importance for the following considerations on the Alpine deformations of the crystalline basement complex.

Fig. 78 may be considered as a sufficiently accurate approximation of true circumstances. The following theory is based on these considerations.

The Cima d'Asta Complex ascended during the Late Alpine orogenesis. This upward movement caused the tilting of the adjacent crystalline rocks and of the overlying Lagorai quartz porphyries. The latter are about 1 km thick. This layer of quartz porphyries was tilted without internal deformation; it reacted as a rigid plate. At its eastern side the crystalline rocks are bordered by the Pale di S. Martino, which consist of reef-like Schlern dolomite, about 1½ km thick, which might have been overlain by an equally thick layer of Hauptdolomit. These reef dolomites are slightly folded. The Lagorai quartz porphyries and the Pale di S. Martino dolomites reacted as rigid bodies in comparison with the crystalline basement. It may be assumed that the actual limits of these rigid blocks are more or less represented by their present boundaries.

The supposition that the quartz porphyries wedged out South of their present boundary is supported by the absence of these rocks at the eastern boundary of the crystalline triangle. Moreover, these quartz porphyries do not occur in the Permian of the Strigno region South of the Cima d'Asta Complex. These quartz porphyries were apparently more or less confined to a volcano-tectonic basin. A sideward wedging out of the reef dolomites is observed in many parts of the Dolomites. Generally, the reef dolomites form saucer-shaped plates, which at their borders interfinger with more plastic sediments (see chapter 19).

The relative movements of the Cima d'Asta Crystalline with respect to the rigid framing masses (porphyries and reef dolomites) caused an accumulation of the more plastic crystalline rocks in the pressure shadow between these two. This accumulation is relative as the original thickness of the crystalline rocks is unknown. It is possible that the 5 km at the centre of the triangle represent the original thickness, and the strong thinning out towards the angular points is caused by squeezing out.

In the preceding discussion the apparent relation between the distribution of the thickness of the crystalline rocks and the positions of the rigid confining masses has been explained by assuming that this change of thickness was caused by the framework. It is highly improbable that the present boundaries of the rigid framework have been caused by deformations of the crystalline basement complex during or preceding the deposition of the rocks of this framework.

§ 15C *Check of the Approximation applied in fig. 78.*

As a conclusion to this chapter, the correctness of the simplification, used as a basis for the preceding considerations (fig. 78), will be checked stereometrically. This check can be effected by investigating whether an average dip of 35° of the *S*-planes in all places can correspond stereometrically with a gradual wedging out of these 35° dipping strata.

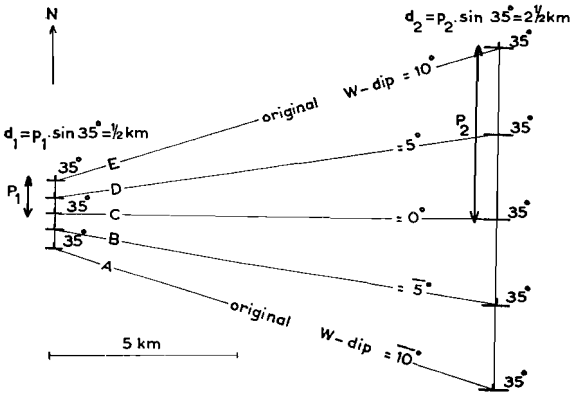

Fig. 80
For explanation see text.

Fig. 80 is an approximation of the western half of the crystalline triangle of fig. 78. The *S*-planes A, B, C, D, and E converge gradually westward. A and E respectively represent the borders with the Cima d'Asta Complex and the Lagorai Range.

The distance between C and E, $d_1 = p_1$, sin 35° = 2½ km in the West, and $d_2 = p_2$ sin 35° = 2½ km in the East. The thinning out between C and E is 2 km.

It may be assumed that the present position is the result of this thinning out and a later rotation of 35° around an E-W axis. However, such movements as assumed above have not actually occurred during the Alpine orogenesis. They serve only for describing the geometric pattern.

The rotation of 35° around the E-W axis (C in fig. 80) can be eliminated. The plane A appears to dip 10° East. The plane E dips 10° West. This westward wedging out series again may be rotated 35° around a horizontal line in C. Fig 81 shows this rotation and fig. 82 shows the new positions of the planes A, B, C, D, and E. The planes A and E dip 36° instead of the 35° assumed as a starting point. In fig. 82 the gradual convergence of the *S*-planes agrees with the drawn dips. Fig. 78, with an overal dip of 35° is, strictly seen, a stereometric impossibility, but the variations of dip, represented in fig. 82 are too small to be distinguished in the schematic fig. 78.

For this reason, a constant mean dip (of 35°) of the *S*-planes in the crystalline triangle is a satisfactory approximation which is not contradicted by the above geometric considerations.

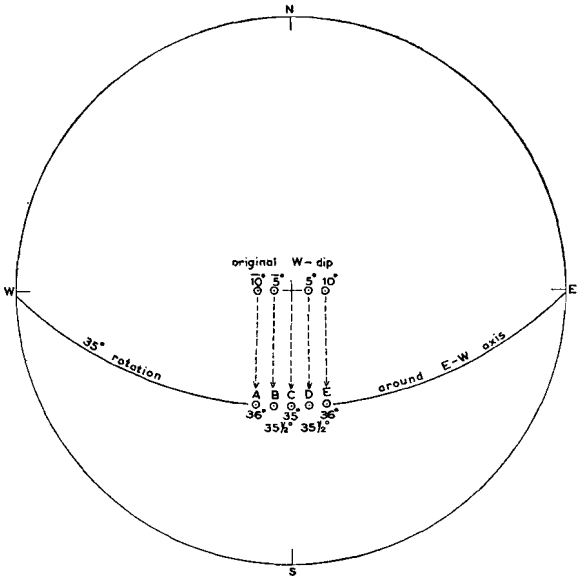

Fig. 81
(Schmidt net, lower hemisphere) For explanation see text.

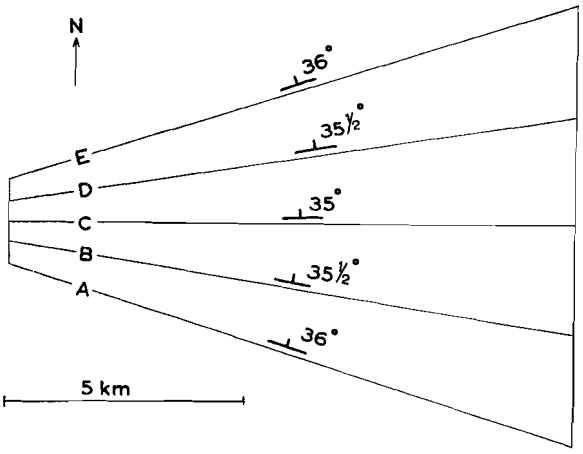

Fig. 82
For explanation see text.

CHAPTER 16

TECTONICS OF THE PERMOTRIASSIC AND YOUNGER SEDIMENTS OF THE CIMA D'ASTA AND STRIGNO REGIONS

This chapter deals with the tectonics of the Sugana Line at the Brocon Pass in the Cima d'Asta region and the tectonics of the Strigno region.

§ 16A *Tectonics of the Sugana Line in the surroundings of the Brocon Pass.*

The Sugana Line separates the crystalline complex of the Cima d'Asta region at its northern side and the younger Mesozoic at its southern side. It is the intersecting line of a fault plane and the topography and may be approximated by the straight lines 80° - 18° and 169° - 10° in the vicinity of section IV. These lines lie in the plane 266° - 74° being the approximate flat fault plane.

The sections III and IV (fig. 83) have been combined as they are at different elevations above sealevel.

Section III probably represents the underlying layers of Section IV. The 72° (NNW) reduced dip of the approximate Sugana fault plane has been used for orientation of the sections in relation to each other.

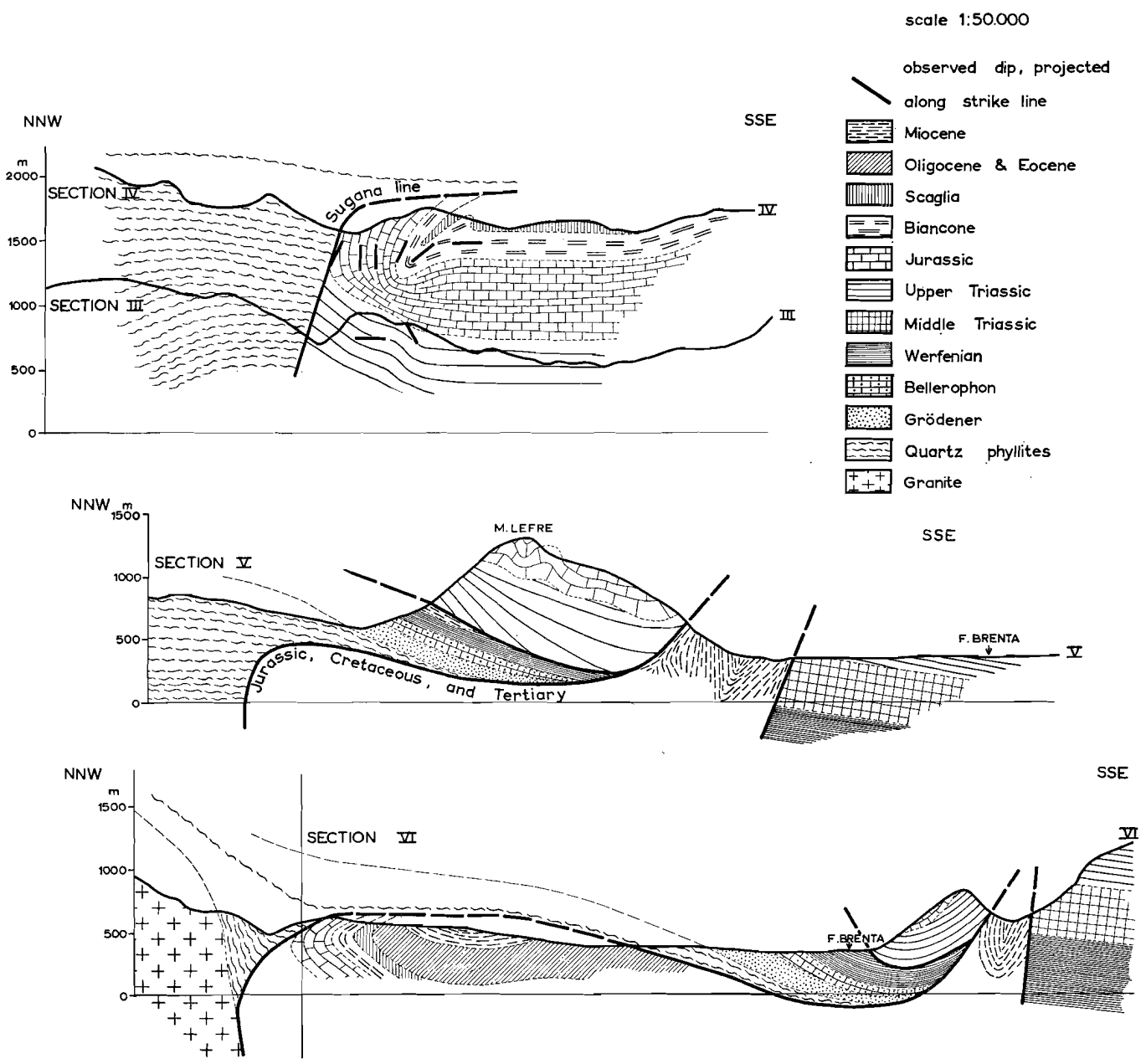

Fig. 83
Four sections across the Sugana Line. The positions are depicted on sheet V—VI.

The Hauptdolomit along the T. Vanoi is subhorizontal up to the fault plane. The overlying more plastic Jurassic and Cretaceous have been strongly folded into a southward overturned syncline.

In the vicinity of the fault plane the Jurassic is overturned. The core of the syncline is well-exposed along the road NE of the Brocon Pass, and it consists of Biancone. The axial plane dips $\pm$ 40° N.

The southward movement of the overlying strata indicates an abrupt bend of the fault plane to an almost subhorizontal position as shown by section III-IV. The syncline is probably a drag feature caused by southward overthrusting of the crystalline rocks over a subhorizontal fault plane. This situation is actually exposed along Section VI in the Strigno region.

The crystalline rocks overlying the younger sediments are phyllonites with a subhorizontal

schistosity, along which Alpine thrust movements have been observed.

In the crystalline rocks of section III-IV, Alpine folds (e.g. fig. 54 of App. I) have been observed.

The Sugana Line may be considered as the axial plane of a southward overturned anticline with a reduced middle limb, only the Mesozoic part of which exists.

Probably no overturned subhorizontal *S*-planes occur in the quartz phyllites above the subhorizontal fault plane.

The bend of the fault plane is younger than the downthrown movement of the younger sediments South of this fault.

The subvertical position of the faultplane cutting through the lower strata in sections III-IV suggests that the fault originally was a downthrow fault with a subvertical position. The downward movement of the southern block caused a topographic escarpment. The height of this step was partially reduced by a southward overthrusting of the relatively high-lying material North of it. The movements were restricted to the uppermost part of the crystalline basement complex and its sedimentary cover. The underlying layers were apparently not deformed. This allows the conclusion that the true direction of the movements was towards the South, and that it was not an underthrusting of the southern block to the North.

The most probable initial force is the gravity which provided potential energy (relief energy). The southward toppling over of the Sugana fault was the result of gravitational tectonics. Additional arguments for the gravitational character of these tectonics will be given in the following paragraph.

§ 16B *Tectonics of the Strigno Region.*

The Strigno region is a tectonic graben which is bordered by the Sugana Line in the North and a southern fault line passing along the Val Coalbia and Ospedaletto (Sheet VI).

In the surroundings of Carzano (Section VI), the Sugana Line separates the crystalline rocks at the northern side and the Jurassic rocks exposed at its southern side.

The dip of the Jurassic is to the North. The series is apparently overturned as it becomes older in northward direction. The curved shape of the Sugana Line near Carzano-Strigno almost parallel to the contourlines shows that it is the outcrop of a subhorizontal faultplane. The subhorizontal quartz phyllites above this faultplane are overlying the E-W striking younger sediments below this plane. The structure of the southward overturned syncline of T. Maso (section VI) is analogous to that of the Brocon syncline (Section IV).

Some E-W striking folds in the Crystalline, more or less phyllonitized, rocks make right angles with the N-S striking Hercynian folds. This proves an Alpine deformation of the crystalline rocks. The subhorizontal *S*-planes have been used as planes of internal differential displacements during the Alpine orogenesis, thus enabling the southward overthrusting movements. These movements are also indicated by folds of the type of fig. 57 of App. I.

At both sides of the same *S*-plane, a compressed and a non-compressed rock is present and this *S*-plane must have been a plane of internal shear. Figure 57 with a subvertical position of the schistosity is part of an exposure of an Alpine anticline along the road between Tomaselli and Samone.

The curvatures of the Sugana Line are caused by the topography cutting off a subhorizontal faultplane. They do not indicate abrupt bends of a steep faultplane. The crystalline rocks of the upper block are not overturned as they are normally overlain by Permian in Section V. This subhorizontal Permian in its turn is overlain by southward dipping Werfenian beds, which form the base of the M. Lefre Nappe consisting of Hauptdolomit and Jurassic (Section V). Between the Werfenian and the Hauptdolomit locally some Middle-Late Miocene (Tortonian) deposits are probably exposed (chapter 5).

It is assumed that the crystalline rocks, the Permian, and the Werfenian beds are wedging out below the M. Lefre and M. Civeron Nappes (Section V-VI). South of these nappes, Tortonian occurs in a southward overturned syncline. This indicates a strong compression of the area South of the nappes in contradistinction to the area SW of the M. Civeron where only gently folded Middle and Upper Miocene strata occur.

The latter form a saucer shaped syncline which is the westward continuation of the isoclinal Val Coalbia syncline. As mentioned in chapter 5 the

Tortonian is probably a syn-tectonic deposit. In this southern syncline it may overly older Tertiary (Section V-VI) but also Werfenian beds or older rocks may be present below it (Chapter 5).

Originally, the tectonic graben of Strigno probably was bordered by two steeply dipping normal faults, the Sugana fault at its northern side and the Val Coalbia-Ospedaletto fault at its southern side. The smaller net slip of the latter fault indicates that it is an antithetic fault in relation to the former and main fault. The Strigno region subsided between these two faults during the Middle Miocene, until the top of the younger Tertiary sediments reached the height of the present topographic surface.

The morphologic depression which came into existence during the formation of the tectonic graben was filled up by Tortonian conglomerates and other sediments, but, even for the greater part, by masses sliding down from the escarpment on the North side.

The crystalline rocks with their overlying sedimentary cover slid southward into this depression. After this movement, which probably was followed by deposition of Tortonian conglomerates, the M. Lefre and M. Civeron nappes in their turn slid down into the graben using the Werfenian as a lubricating layer.

The present theory is in contrast to Venzo's concepts of the tectonics of this area (Venzo, 1940) represented by fig. 84.

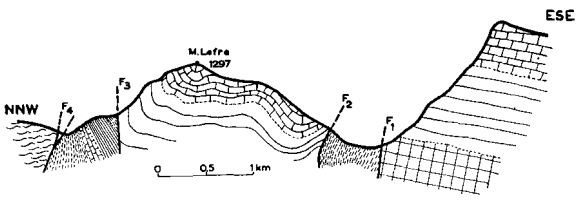

Fig. 84

Venzo's concept of the Strigno region (according to Venzo's section III, 1940). For legend see fig. 83.

According to Venzo, all faults of the Strigno region have steep faultplanes. It has to be stressed, however, that the sharp bend of the outcrops of the fault and the gentle dip of the strata along the faults indicate gently dipping or even subhorizontal faultplanes.

The bedding planes of the Grödener North and West of the M. Lefre mass are not subvertical as assumed in Venzo's section III (fig. 84). All outcrops show gentle dips to the South and even to the North (Sheet VI).

Only the Tortonian strata of the southern syncline form a larger zone with steep strata. However, at the faultplane North of Ospedaletto these strata are overturned and dipping 45° N. The fact that the M. Lefre and M. Civeron masses are surrounded by Werfenian and Tortonian sediments indicates that they are isolated basin-shaped klippes on a Werfenian and Tortonian base.

CHAPTER 17

TECTONICS OF THE GOSALDO REGION

The denudation plane between the crystalline rocks of the Gosaldo region and the overlying Permian is subparallel to the schistosity-planes of the Crystalline. The Hercynian minor folds might have caused local unconformities.

The crystalline rocks are bordered by Permian on three sides, and at their SE side by the Sugana Line (sheet VII). The strata of the Hauptdolomit at the SE side of the Sugana fault are locally dipping NW (e.g. at the V. Imperina). The Sugana fault probably dips steeply NW, just as in the Cima d'Asta region.

South of California, the Sugana fault extends into a southward overturned anticline of the crystalline rocks and a NNE striking fault. The latter disappears gradually in SSW direction.

The anticlinal structure continues westward in the overlying Permian and passes into the Sugana fault of the Cima d'Asta region. The phyllonites along the Torrente Mis indicate that the anticlinal structure is accompanied by a southern upthrust in the Gosaldo Crystalline.

The Permian Northwest of the crystalline rocks strikes NE; this direction parallels the southeastern border of the Schlern reefdolomites of the Pale di S. Martino, the base of which is Permian.

The strike of the *S*-planes below this Permian is also NE. The strike in the central part of the crystalline rocks is E-W with an average dip of 40° North.

The strata Southeast of the Sugana Line have a NE strike. It may be concluded that the crystalline rocks have a strike which differs from the regional Alpine NE strike.

Castiglioni (1939) assumed the strike of the crystalline rocks to be parallel to the strike of the adjacent Permotriassic strata and of the Sugana Line. This assumption is supported by the NE striking belt of gneisses which forms the central part of the Gosaldo Crystalline and which is bordered by quartz phyllites at its NW side as well as at its SE side (see fig. 87). From the statistical analysis, however, it follows that this belt obliquely crosses the E-W striking *S*-planes. It also obliquely crosses the sedimentary stratification of the crystalline rocks which is parallel to the *S*-planes (e.g. photograph 9).

The Hercynian phase of folding about a N-S axis may cause two types of errors in the calculated means of the *S*-planes. Locally, the *S*-planes may have been dipping E or W prior to Alpine folding about an E-W axis. Such original dips may have influenced the present means of the *S*-planes which are assumed to be Alpine. Furthermore, some *S*-planes, measured in the outcrop, appeared to be S_2-planes under the microscope (Ch. 2). Although the deviation between the positions of S_2 and *S* cannot be a great one, as in that case separate maxima would appear in the pole diagram, a systematic error may have been introduced in this way. The S_2-planes are parallel to the axial planes of westward overturned folds.

Originally, they must have been dipping East, whereas the *S*-planes were subhorizontal.

Locally, the resultant angle may amount to 45° (Fig. 43 of appendix I, Cima d'Asta region, to which the same considerations may be applied).

These two types of errors in the Alpine position of the means of the *S*-planes, however, do not explain the difference in strike between the Gosaldo Crystalline and the adjacent Permotriassic.

They either have no influence at all, or they change the W strike into a strike that is more parallel to the Alpine strike, which is SW.

Fig. 85 shows a group of *S*-planes which have been folded symmetrically about the Hercynian N-S axis. This group has been rotated afterwards 40° about the Alpine E-W axis. It is evident that the mean strike of this last group is exactly E-W or parallel to the Alpine axis. When the Hercy-

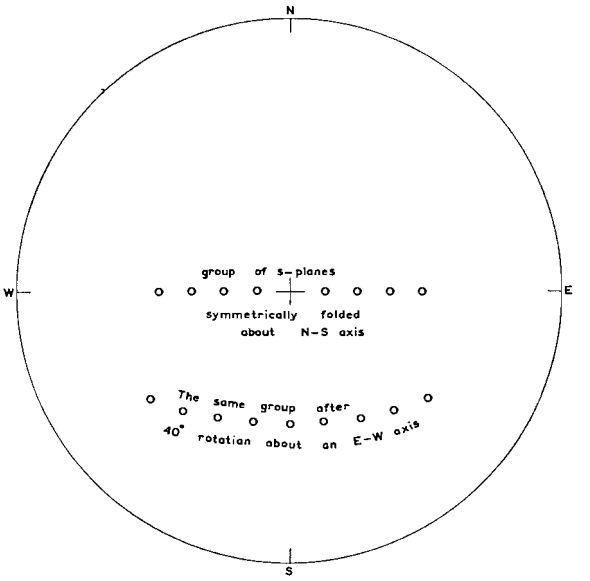

Fig. 85
(Schmidt net, lower hemisphere) For explanation see text.

nian folds are symmetrical, the Alpine mean strike of the *S*-planes is not influenced. When the Hercynian folds are overturned toward the West, the Alpine East strike must have changed into a NE strike. Also the originally East dipping S_2, possibly present in the group of *S*-planes, may have caused the E strike to become NE.

If present, the two described types of errors in the Alpine position of the mean *S*-plane are small. When they are of considerable size, they would be evident in the frequency distribution, as given by the pole diagram of the considered group of *S*-planes. Furthermore, they do not explain the different directions of strike of the crystalline rocks.

The mean azimuth lines of the m.f. are subparallel. This indicates that the North dip of the central crystalline rocks of the Gosaldo region originated by a rotation about an E-W axis, whereas the NW border has been rotated about a NE- and SW axis. The direction of the m.f. remains the same whether the *S*-planes are 40°rotated about an SW-NE axis or about an W-E axis. To prove this statement, the reader is referred to chapter 15 on the Cima d'Asta region.

The E-W strike of the central Crystalline has not been caused by a dextral rotation about a ver-

tical axis, as such a rotation would be indicated by bends of the mean azimuth lines of the m.f. It is explained by a thickening of the crystalline strata to the SE.

Fig. 86 is a schematical representation of Sheet VII. The *S*-planes are dipping approx. 40° in all places, whereas the direction of strike varies from SW on the northwestern side to W in the central part. The thickness has been estimated in two places (fig. 86).

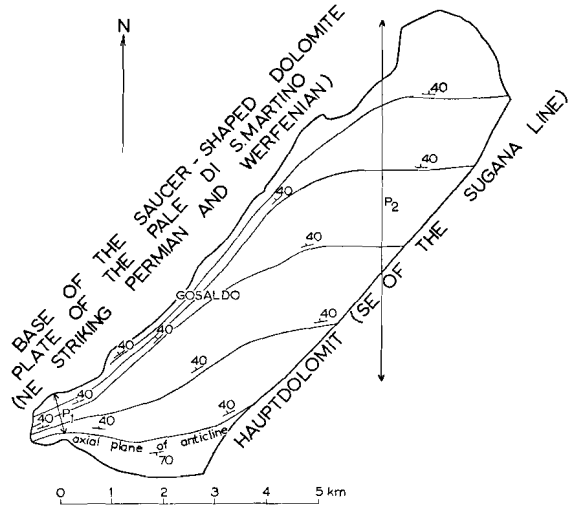

Fig. 86

Schematized structure map of the Gosaldo region. It is assumed that the mean dip is 40° in all the Crystalline North of the anticlinal axial plane.

In the SW corner, $d_1 = p_1 \sin 40° = ½$ km and at the Col Colazzo $d_2 = p_2 \sin 40° = 4½$ km.

The abrupt bends in the strike lines indicate a considerable thickening of the crystalline strata towards the central part. A thin series of about ½ km, which conformably dips under the overlying Permian, increases in thickness up to 4 km. This increase in thickness may be compared with the wedging out of the crystalline triangle in the Cima d'Asta region (fig. 78). Dealing with this crystalline triangle, proof was offered for the stereometric possibility of a gradual wedging out and a constant dip of about 35°. In the present region the stereometric feasibility of the schematic fig. is obvious, as wedging out is abrupt. The central and 40° N dipping crystalline rocks are passing into a thin and 40° NW dipping series towards the Northwest.

At their SE side the crystalline rocks are cut off by the Sugana Line and the variations in thickness cannot be followed into this direction.

It may be assumed that the wedging out is either partially due to a squeezing out of the thinner part or to thickening of the central part, which is also mechanical. As in the Cima d'Asta region, the crystalline rocks become thicker in a pressure shadow determined by the borders of rigid bodies (e.g. the reef dolomites of the Pale di San Martino).

On the other hand, crystallization as a result of mass supply partially may have caused the increase in thickness.

The central part of the Gosaldo Crystalline is formed by a gneiss, called "ortogneiss" by Castiglioni (1940). Fig. 87 shows the distribution of these gneisses in the Gosaldo region and in the Cima d'Asta region. Their borders unconformably intersect the *S*-planes of the crystalline rocks and the sedimentary stratification parallel to these *S*-planes. D'Amico (1957) concluded that the gneisses of the Cima d'Asta region originated by "granitization" developing new minerals in originally phyllitic rocks. This granitization was accompanied by Ca and Na supply, as indicated by chemical analyses (see chapter 20).

D'Amico also studied the petrography of the Gosaldo region. He also assumed mass supply to explain the gneisses (personal information).

Our structural analysis shows that the possible "granitized" rocks occur in the thicker parts of the Crystalline. A relation between a pressure shadow and crystallization of new minerals as a result of mass supply, seems to be reasonable.

The structures of the Permotriassic rocks in the Gosaldo region have an average strike of N 35° E. The folds and faults having this strike show mass displacements at right angles to this direction. These movements originated by regional compression. One might expect that the originally subhorizontal rocks would have moved also in planes at right angles to the regional direction of compression. For the greater part, their vertical N-S striking plane of movement, however, intersects the regional Alpine plane of movement with an angle of about 55°. The folding of the crystalline rocks about a subhorizontal E-W axis has probably not originated by regional Alpine compression only. The rotation into the 40° North dipping position probably partially originated by an

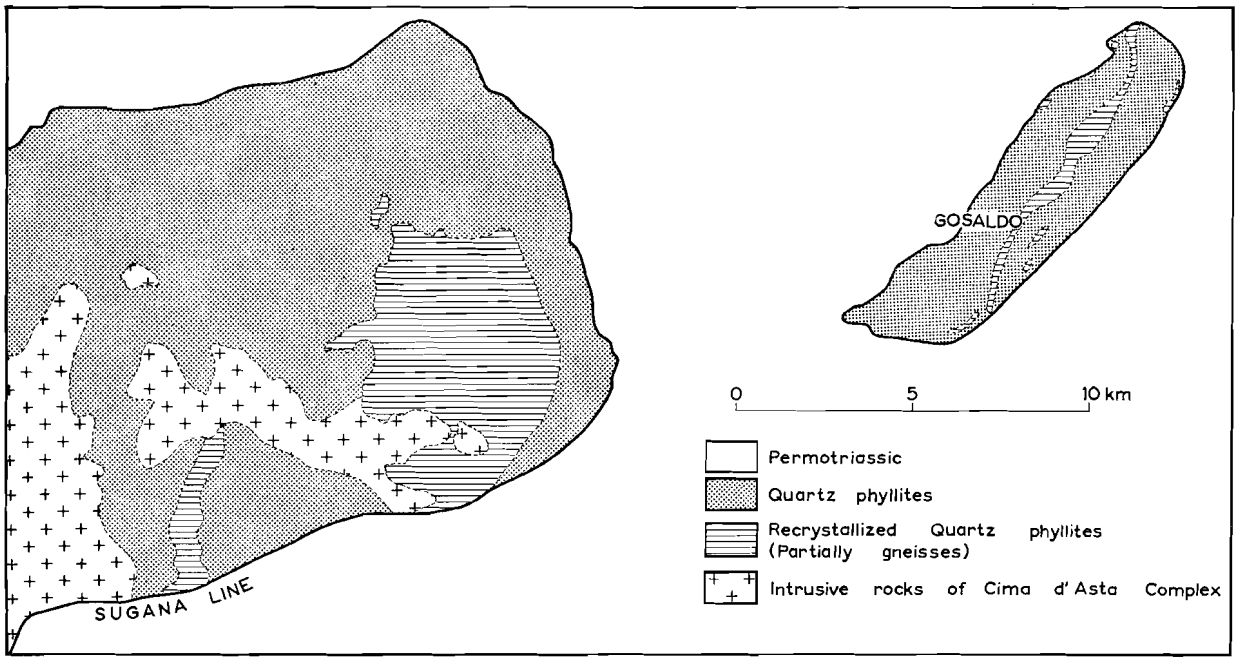

Fig. 87
Distribution of recrystallized quartz phyllites in the southern crystalline basement of the Dolomites, based on the Carta geologica, 22 and 23.

upward movement of the southern crystalline rocks with respect to the northern rocks. This upward movement was restricted to the present crystalline belt, as follows from its absence in the adjacent Permotriassic rocks. It is assumed that this upward movement is related to the intrusion of the Cima d'Asta granite. The crystalline material could escape vertically under the Gosaldo region, whereas in adjacent areas the upward movement was prevented by competent plates of reefdolomite.

The faults at the NW border of the crystalline rocks (Sheet VII) may be explained by this independent upward movement of the Gosaldo belt.

The anticlinal structure of the T. Mis at first may have been a doming structure which, thereafter, was compressed during the southward toppling over of the Sugana fault.

CHAPTER 18

GENERAL CONCLUSIONS ON THE HERCYNIAN TECTONICS SOUTH OF THE PUSTERIA LINE

The Hercynian structure of the crystalline rocks can be studied in the relatively small areas around the Dolomites where these rocks are exposed. The Hercynian folded crystalline basement has been deformed intensively during Alpine orogenesis, as indicated on Sheets II, III, V, VI, and VII (see Sheet I).

In the preceding chapters the influences of the Hercynian and Alpine orogenesis on the crystalline basement have been separately discussed.

This chapter deals with the Hercynian basement of which the Alpine deformations have been omitted.

The schistosity of the mesozonal micaschists is in all places parallel to the sedimentary stratification. This parallelism is found in the isoclinally folded series of the northern part of Sheet IV, Sheet III, Sheet II, the Carnian Alps, and the Thurntaler syncline North of the Pusteria line, as well as in the subhorizontal unfolded series of the southern part of Sheet IV, Sheet V, VI and VII.

Probably, the subhorizontal unfolded series

continues under the Dolomites and the plate of Permian quartz porphyries connecting the Bressanone region to the North and the regions South of them.

The isoclinally folded series probably originated from the subhorizontal unfolded series by major folding about an E-W axis. The size of the major folds is unknown but their shape is probably represented by fig. 59.

The steeply dipping schistosity of the isoclinally folded series passes gradually into the subhorizontal unfolded series. This transitional region is shown on Sheet IV. The enveloping contour of a certain bedding plane in the major anticlines is located some kilometers above the same bedding plane in the subhorizontal unfolded series. The average elevation of a bedding plane in the isoclinally folded series also lies above its counterpart in the unfolded series and the difference is about 10 kilometers. This amount has been estimated from the South dip in the transitional region (Sheet IV).

The folded series moved upward in relation to the unfolded series.

The isoclinally folded belt lies NNE of the unfolded belt. The lines indicating the intensity of folding make an acute angle with the strike lines.

The subhorizontal Bressanone region lies North of the isoclinally folded S. Stefano region. This implies an eastward steepening of the dips. Consequently, a convergence of strike lines appears to be present. This situation may be studied on Sheet IV. The isoclinally folded series apparently was moved towards the South in relation to the Western unfolded series (fig. 76). The Hercynian age of this phase of major folding follows from the Devonian and Carboniferous components in the Carnian Alps which obviously were compressed in the same way and at the same time as the other components of the isoclinally folded series. The phase of minor folding is younger than the phase of major folding as has been proved in chapter 12.

The compression from which the major folds originated had a N-S direction, whereas the minor folds originated by an E-W compression, as shown on Sheets IV, V, VI, and VII.

The interference of major folding and minor folding is depicted in the N-S cross section of fig. 88. The m.f. are subvertical in the isoclinally folded series at Chienes; they are dipping southward in the transitional region, and subhorizontal with a N-S azimuth in the unfolded region.

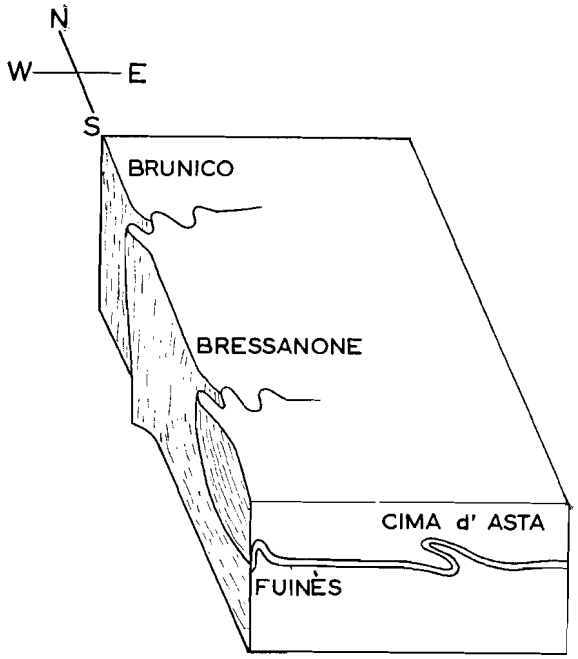

Fig. 88
Diagram of the South dip of the m.f. in the Bressanone region. The m.f. at Funès may be compared to the westward overturned m.f. of the Cima d'Asta region.

As evident from obvervations in Sheets V, VI and VII, westward overturned folds suggest a westward mass transport increasing in the higher levels (chapter 3).

The subvertical m.f. in the vicinity of Chienes also pass eastward into subhorizontal m.f. (see fig. 62). These observations are restricted to the isoclinally folded series. The Pusteria region forms the transitional region between the subvertical m.f. at Chienes and the subhorizontal m.f. in the Carnian Alps.

The mean m.f. changes gradually from a subhorizontal position in the Carnian Alps to a subvertical position in the northern part of the Bressanone region. From the latter region it changes into a subhorizontal position in the regions South of the Dolomites, and makes right angles with the subhorizontal axes of the Carnian Alps. This continuity indicates the existence of a single phase of minor folding in the Carnian Alps as well as in the Cima d'Asta region.

The facts that the Permian cuts off the m.f.

and that these m.f. have been observed in Verrucano pebbles, indicate their pre-Permian origin. This later phase of minor folding is also of Hercynian age.

In the Carnian Alps and the S. Stefano region, the axes of the m.f. are parallel to the axes of the major folds.

However, these m.f. may have originated later as they gradually pass into m.f. which are definitely younger than the major folds (Pusteria region).

At the end of this chapter, a theory will be carefully developed to explain the Hercynian kinematics summarized above.

A bed in the belt of isoclinally folded mica-schists has been eroded some kilometers deeper than the same bed in the unfolded series. This indicates that the isoclinally folded belt formed a Hercynian mountain range. The difference in height between the isoclinally folded series and the unfolded series probably originated during the phase of major folding, and was present prior to the phase of minor folding. This phase of minor folding may be considered as a gravitational levelling off of the Hercynian mountain range. Sideward spreading on a limited scale originated as a result of this gravitational process.

In the Carnian Alps and S. Stefano region the material could escape northward and southward. This may have caused a shortening along the vertical indicated by minor folds. In the western part of the mountain range, the material could escape westward, causing a horizontal E-W compression in the regions of Sheets IV, V, VI, and VII.

This explains two successive phases of Hercynian kinematics deduced above. It explains the gradual change of the mean m.f., and also the absolute direction of movement of the particles during minor folding.

On Sheets V, VI, and VII, the minor folds show overturn towards the West. They are accompanied by larger folds of 10 meters wide (Photographs 7 and 12) with gently East dipping axial planes.

This strong westward overturn probably not only indicates a westward transport of the upper layers with respect to the underlying layers, but also an absolute westward movement of the particles. It is not probable that the strong westward overturn was caused by an eastward underthrust.

As the particles moved westward South of the Dolomites, they probably also moved westward in the Bressanone region North of the Dolomites. The continuity of the movements requires that the particles moved into a 30° West dipping direction at Brunico-Monguelfo, and steeply downward at Villabassa, and vertically downward in the Carnian Alps and S. Stefano region (fig. 62).

This absolute direction of movement of the particles along regionally curved lines corresponds with the theory of sideward mass transport by gravitational spreading of a Hercynian mountain range, developed above.

CHAPTER 19

GENERAL CONCLUSIONS ON THE ALPINE TECTONICS SOUTH OF THE PUSTERIA LINE

The Alpine tectonics of the sedimentary rocks of the Dolomites are well known. The tectonics of the Permotriassic series have been discussed by many authors, whereas the tectonics of the crystalline basement were practically neglected.

As the Dolomites consist of only slightly folded saucer-shaped synclines, it may be stated that large-scale Alpine deformation has only taken place in the crystalline rocks.

The crystalline rocks have not formed a rigid basement of the more deformed sedimentary cover, but, on the contrary, the quartz porphyry plate and the reef-dolomites acted as rigid bodies overlying the more plastic crystalline basement.

It has been proved that

a. The S. Stefano Crystalline forms the core of an anticlinal structure which is about 6 km wide and has an amplitude of more than 3 km (fig. 49). The pre-Alpine isoclinally folded *S*-planes made the Alpine shearing movements possible.

b. The Pusteria Crystalline has been strongly compressed between the Austrian gneisses to

the North and the Dolomites to the South. The present width of 2½ km of the crystalline belt at S. Candido originated from another and also isoclinally folded belt, at least 7½ km wide, in which Alpine shearing movements took place.

c. The crystalline rocks of the Cima d'Asta region and the Gosaldo region show a thickening, respectively from 1 to 5 km and from ½ to 4½ km. These increases in thickness are probably due to a plastic deformation of the crystalline rocks, which were adjusted to the borders of the adjacent rigid sedimentary masses during the intrusion of the Cima d'Asta granite. The thickening probably was accompanied by crystallization with mass supply.

d. The crystalline rocks of the Strigno region overly Tertiary rocks; their position and their internal Alpine deformations indicate a southward overthrust along the subhorizontal *S*-planes.

The crystalline areas surrounding the Dolomites moved diapyrically upward with respect to the adjacent sedimentary masses.

a The S. Stefano and Pusteria crystalline rocks moved upward by squeezing out.

b. The Bressanone and Cima d'Asta crystalline masses were dragged upward by Alpine granite batholites.

Fig. 89 is a section across the western Dolomites. The saucer-shaped syncline of quartz porphyries and overlying Schlern dolomites is bordered by granite batholiths in the North and in the South.

c. The deviating Alpine strike of the Gosaldo Crystalline also indicates an upward movement independent of the surrounding rigid sedimentary masses.

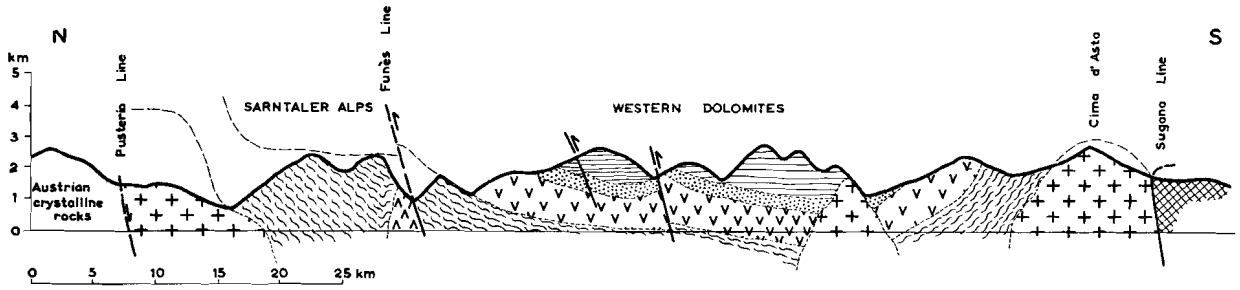

Fig. 89
Section across the western Dolomites, based on unpublished section by van Bemmelen. For legend see sheet I. Vertical exaggeration 2½x.

The quartz porphyry plate and the Dolomites together form a saucer-shaped syncline. This saucer probably originated by drag against the surrounding upward moving crystalline basement.

This quartz porphyry plate wedges out toward the East. The eastern Dolomites consist of reef dolomites surrounded by more plastic sedimentary strata. These strata have been folded to anticlinical structures which surround the saucer-shaped plates of reef dolomites (fig. 90). Due to their softness they have been eroded, and the cores of the dolomite saucers actually form the mountain summits.

On these summits "gliding nappes" occur, predominantly consisting of Hauptdolomit sheets on a base of the younger Cretaceous and Liassic strata. These gliding nappes have moved from the uplifted borders of the dolomite saucers toward their cores. This theory was proved by Accordi (1955, 1957).

The examples of overthrust folds and gliding nappes ("Gipfelfaltung" of the N. Italian Dolomites) are summarized on Sheet I. Different directions of movement are present. This demonstrates the local character of the deformations. The "Gipfelfaltung" was not caused by regional compression. The superficial nature of these deformations is indicated by the gradual continuation of the undisturbed underlying strata. Our Lefre and Civeron Nappes (chapter 16) may be compared to Accordi's gliding nappes.

Signorini (1951) was the first to emphasize the lack of regularity in the directions of the tectonical lines.

Fig. 90 represents his geologic map of the eastern Dolomites from which the faults have been omitted.

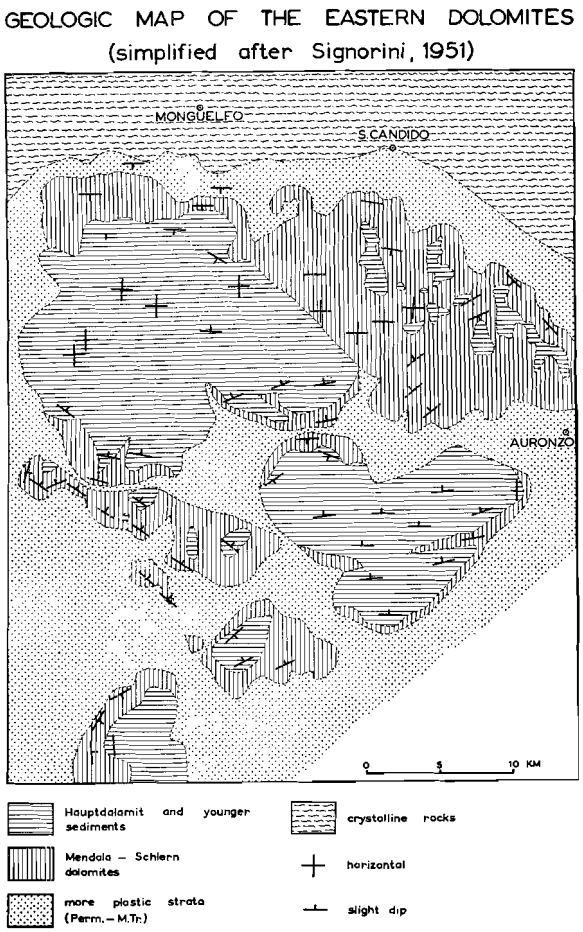

Fig. 90
Geologic map of the eastern Dolomites, based on Signorini's map (1951).

On this map the more plastic clastic sediments are indicated by dots, and show steeper dips than the enclosed dolomite saucers. Although not all these more plastic strata are Middle Triassic, as Permian and Werfenian strata are also present (Sheet I), which do not interfinger with the reef dolomites, it may be assumed that the present exposures of folded Permian and Werfenian strata have been overlain by more plastic and folded Middle Triassic strata. The Permian and Werfenian beds are also present below the reef dolomites, but probably they have not been folded in this protected position.

In consequence, the dotted areas in fig. 90 probably indicate the more plastic part of the Middle Triassic. They moved upward diapyrically by compression between the only slightly deformed dolomite saucers. These lower basins partially were filled up by gliding nappes ("Gipfelfaltung"). In the eastern Dolomites E-W strikes predominate but other directions of strike are frequently present.

With Signorini it is emphasized that these tectonics are local phenomena in contradistinction with Leonardi (1955), Fallot (1950), and other authors, who considered the Dolomites as compressed in a N-S direction, resulting in saucer-shaped synclines between sharper anticlines. However, also Leonardi (1955) mentioned the irregularities of his tectonic lines and the presence of cross folds.

In summary, it may be stated that the reef dolomites were deformed into saucer-shaped synclines surrounded by anticlines.

The region was shortened in all directions, predominantly in a N-S direction.

The faults of the Eastern Dolomites are southward overturned upthrusts. They suggest a mass transport toward the South (and toward the SW in the more western part). This southward movement which increases in higher strata is contrary to the "Gipfelfaltung" in the southern part of the Eastern Dolomites showing northward overturn. It also is opposite to the locally northward overturn found in the quartz porphyry plate of Bolzano (Trodena line South of Bolzano, see Sheet I; case 9 and 10 of table VII).

On account of this contrast, two phases of deformation may be distinguished.

1. The quartz porphyry plate and the Dolomites together were deformed into a saucer-shaped basin by diapyrical movements of the surrounding crystalline areas. North of the Cima d'Asta granite some overturn toward the North occurs. The case of the Trodena upthrust and case 10 of table VII are probably related to the Cima d'Asta intrusion. The larger distance of the northward overturn of case 9 makes such a relation doubtful. Perhaps other factors have been of influence. The eastern Dolomites together were formed as a saucer, consisting of smaller saucers with folds between them. The uplifted overlying strata moved toward the centre of the smaller saucers by gliding ("Gipfelfaltung").

2. The Eastern Dolomites were subjected to a southward overturn, which mainly resulted in upthrusts. These upthrusts together describe an arc between Bressanone and S. Stefano with a SSW directed convex side.

It is probable that phase 2 followed phase 1, but these two phases may have been synchronous.

The SSE border of the discussed region is formed by the Sugana fault. It is probably a normal fault, which afterwards toppled over towards the South (chapter 16).

The northern and northwestern border of the discussed region are formed respectively by the Pusteria Line and the Giudicaria Line. The Pusteria Line also is a normal fault which toppled over (chapter 13). This toppling over is indicated by the downward diminishing intensity of deformation of the Pusteria belt of quartz phyllites. The Pusteria Line passes into the Giudicaria Line which also has a faultplane dipping steeply below the crystalline rocks of its upper block, which belong to the Austrian nappes.

Furthermore, also along the Giudicaria Line, wedges of younger sediments are present, comparable with those of the western Drauzone (Dietzel 1960, van Hilten 1960), and practically everywhere intrusive rocks are also present. These analogous features indicate a similar origin. The tectonics of the Giudicaria Line seem to be more complicated. They will be discussed again in chapter 22, after a discussion of the tectonics of the adjacent crystalline rocks of the Austrian nappes.

PART IV

Position of the Dolomites and their basement in the Alpine framework

CHAPTER 20

PETROGRAPHY OF THE M. SPICO REGION

It was stated in the introduction that the crystalline rocks of the M. Spico region do not belong to the crystalline basement of the Dolomites, which is bordered to the North by the Pusteria Line.

It seems probable, however, that the Pusteria Line originated by an Alpine downthrow fault, causing the Dolomites and their basement to have subsided. At the northern side of this major fault rocks may be expected, which in the southern Alps are covered by the Dolomites and their basement.

This concept seems plausible as the Pusteria Line passes eastward into the gradually pinching out "Karnische Hauptüberschiebung". In this region, the Carnian quartz phyllites and the Thurntaler quartz phyllites, which may be correlated with the quartz phyllites of the crystalline basement of the Dolomites, indeed lie upon the older gneisses which are also present in the M. Spico region.

The crystalline rocks of the M. Spico region have been grouped geographically and the following units are distinguished from North to South (see the legend of Sheet VIII).

A. Tauern gneiss, containing augen-gneisses
B. saccharoidal limestones
C. ordinary gneisses
D. limestones
E. calcareous phyllites, containing green phyllites
F. serpentine and talc
G. quartz phyllites, containing green phyllites
H. ordinary gneisses of the M. Spico Nappe
I. M. Spico gneiss
JK. Rieserferner augen-gneisses, containing migmatites
L. Rieserferner tonalite.

§ 20A *Tauern gneiss, containing augen-gneisses*

North of the calcareous phyllites four types of rock have been mapped. Sander (1921) described a quartzite in the vicinity of point 2571 now classified as an ordinary gneiss which in some other places also appears to consist exclusively of quartz.

The term ordinary gneiss, also used by Palm (1960) covers the larger group of gneisses called "paragneisses" in literature. Some examples of these ordinary gneisses will be given presently. The somewhat genetic terms "para" and "ortho" are avoided because some "orthogneisses" among the Tauern gneisses are probably altered "paragneisses". Thus, confusion is caused in the terms paragneiss as used by Karl and orthogneiss as used by Bianchi.

The Tauern gneiss of the Zillertaler Alps is, in general, a tonalite gneiss (Karl, 1959). It was studied at first by Sander (1912, 1921, 1925) and later in greater detail by Christa (1931, Oberes Zemmgrund), and Bianchi (1934).

On the basis of Christa's and his own investigations in the Tauern, Karl gives the following synthesis of crystallization and deformation in the Zillertaler Alps (Karl, 1959, p. 101).

TABLE XXII

ORDER OF CRYSTALLIZATION AND DEFORMATION IN TONALITE GRANITES OF ZILLERTALER ALPS,
according to Karl (1959)

A First crystallization of:
  1 biotite + hornblende
  2 plagioclase
  3 (K. feldspar) + quartz
B Deformation

C Secondary Tauern crystallization of (now undeformed)

1 biotite + titanite + garnet + clinozoisite —epidote + hornblende
2 oligoclase + clinozoisite + zoisite + hornblende
3 quartz (+ K. feldspar)
4 carbonate.

This table is based on a detailed examination of slides by Karl (1959) and it can also be applied to our Tauern tonalite gneiss type I (see below).

According to Bianchi, all "orthogneisses" of the Zillertaler Alps originated by one and the same uniform process of differentiation.

On the basis of diagrams, giving the relation between the different geochemical parameters after Osann and Niggli, Bianchi stated that the "orthorocks" of the Aurina mountain chain in their different forms — as granulated non-orientated orthogneiss, schistose beds of different composition, "Schlieren", and aplite and lamprophyre dykes — compose a large geologic-petrographic unit. This belongs to a mixed magmatic province in the sense of Niggli, in the first place of an alkalic-calcic type with tendencies to an alkalic-sodic and particularly to a potassic type (Bianchi, 1934, p. 66).

This synthesis, based on many analyses, was critisized by Karl.

Karl (1960) stated that Bianchi made no distinction between his (Karl's) "tonalite granites" and "tonalitic gneisses". We will call both these rocks tonalite gneisses, type I and type II respectively. Table XXIII gives the mineral content of both types, determined from about 32 slides (fig. 91).

TABLE XXIII

MINERAL CONTENT OF TONALITE GNEISS

	Type I	Type II
generally > 5%	plagioclase	plagioclase
	quartz	quartz
	biotite	microcline
	epidote	biotite
		muscovite
		epidote
in some cases > 5%	K. feldspar	garnet
		K. feldspar (not microcline)
if present < 5%	garnet	clinozoisite
	apatite	chlorite
	muscovite	opaque minerals
	chlorite	zircon
	opaque minerals	apatite
	clinozoisite	titanite
	zircon	sillimanite
	titanite	calcite
	calcite	

According to Karl, type II is a tonalitized biotite-plagioclase gneiss (tonalitized ordinary gneiss) and the following arguments for the "para" character of type II were presented:

1. inverse zoning of the plagioclases (An_{10-30});
2. the presence of few microliths in the plagioclase crystals;
3. the growth of albite (An_{10-0});
4. the presence of muscovite;
5. the presence of more garnet;
6. the presence in the field of frequent distinct transitions into non-tonalitized biotite-plagioclase "para"gneisses and intercalations of metabasite lenses.

Most Tauern tonalite gneisses of the M. Spico region possess some of these properties and, therefore, Karl's distinction has been applied to them.

The following three arguments may be added:

7. sillimanite present in some cases;
8. the frequent presence of augen consisting of aggregates of microcline, plagioclase, and quartz;
9. the absence of basic "Schlieren" or other xenoliths.

On the basis of the mentioned microscopic differences, Karl divided Bianchi's tonalite gneisses into two types.

It appears that these types also can be distinguished petrochemically. Type II lies under type I in the FMC-S-AA triangle after Eskola (II contains less FMC than I), and mg > k is applicable to type I and k > mg to type II (Niggli parameters) (Karl, 1960).

Fig. 91 gives the position of 32 samples taken in the Tauern tonalite gneiss of the M. Spico region.

In practically all samples of type II, muscovite is present as a primary mineral.

The letter *a* means that the gneiss macroscopically is an augen-gneiss; *s* means microscopically sillimanite and *d* means that dioritic "Schlieren" occur.

The following types may be distinguished:
I, Ia, Id, Iad,
II, IIa, IIs, and IIas.
The ordinary gneiss has been indicated as III.
a is already given on sheet VIII with the symbol O (= augen-gneiss between Tauern gneisses).

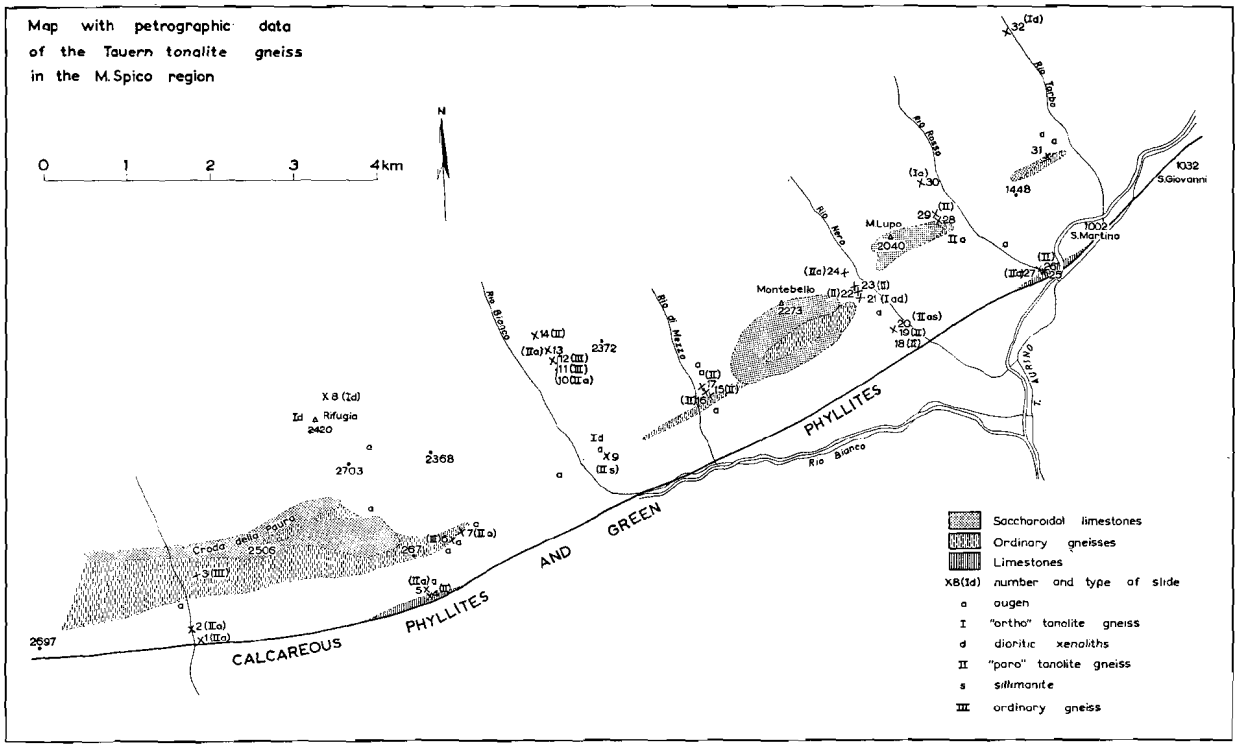

Fig. 91
Position of 32 slides and other data from the northern M. Spico region.

Both types may contain augen. The augen of type Ia consist of plagioclase-quartz, whereas those of type IIa may contain microline.

Sander and Bianchi mapped the Tauern gneiss as one unit with "ortho" character, which follows from the small differences between both types I and II. Karl (1960) distinguished two types, and added (p. 293) that the two types cannot be definitely distinguished macroscopically and in some cases even not microscopically.

It is concluded that the Tauern tonalite intrusion has tonalitized its mantle.

The mechanism of intrusion is comparable to that of the Pennine nappes. According to Karl and Schmidegg, the tonalite gneiss of the Zillertaler Alps is a large nappe (fig. 109). It is known that its core is a tonalite, in our region conformably surrounded by a tonalitized mantle of ordinary gneisses bordered by calcareous phyllites, the equivalent of the "schistes lustrés" of Ticino.

An abnormal position of the contact plane, as frequently observed by Karl (1959) in the front region of the nappe, has not been observed in the M. Spico region.

Dealing with the Pennine nappes of the Eastern Alps, Wenk (1956) is cited, who discussed the Pennine nappes as if it were the Zillertaler tonalite gneiss nappe.

„Am klarsten kann die Frage im tief durchfalten Gebiet der Tessiner Gneissdecken entschieden werden, und zwar bietet die Vall Verzasca besonders günstige Voraussetzungen für eine solche Untersuchung. Hier bilden die hellen quarzdioritischen (trondhjemitischen) Kerngesteine in formaler, architektonischer Hinsicht Musterbeispiele von Decken mit Stirn, Scheitel und Wurzel; diese quarzdioritischen Decken sind von einer sedimentogenen Gneisshülle umgeben, die

ihrerseits von metamorphem Mesozoikum lückenhaft umrahmt wird.

Die deckenartigen Kernkörper sind in der Stirnregion gneissig; gegen die Würzel hin werden sie oft massig-körnig. Auch volumenmässig nimmt das quarzdioritische Material zu gegen die Tiefe, die Wurzel. Typischerweise ändert von der Stirn gegen die Wurzel und vom hangenden gegen den liegenden Schenkel hin auch die Zusammensetzung der Hüllgneise. Sie werden feldspatreicher, glimmerärmer, zunehmend quarzdioritähnlich. Hauptsächlich Si und Na nehmen zu auf Kosten von Al, Fe, Mg, und K. Der Unterschied zwischen hellem Kerngneiss und dunklern sedimentogenem Hüllgneiss verschwindet in der Tiefe. Das soll uns veranlassen, die Grenzzone zwischen Hülle und Kern im Deckengebiet, wo sie am schärfsten hervortritt, genauer zu studieren", (Wenk, 1956, p. 86).

§ 20B *Saccharoidal limestones.*

In this connection the presence of saccharoidal limestones is important. These rocks exclusively consist of large parallel crystals causing a sort of schistosity.

On Sander's map (1921) which includes the western boundary of the Hohe Tauern, a limestone zone separates almost continuously the Tauern gneiss of the Zillertaler Alps from the ordinary gneisses of the "Untere Schieferhülle".

To the East, however, in the region covered by our map, the zone consists of a number of separate lenses. These resemble large "boudins" or mullion structures, wedging out parallel to the strike of the adjacent gneisses. A difference between the lenses and boudins is that the former in some cases show an alternation of gneiss and limestone, as can be seen on sheet VIII and in more detail in fig. 78 of appendix I.

According to Sander (1925, p. 28), a discontinuity is seen at the Tristenspitze (p. 257 North of Lappago) between the schistosity of the Tauern tonalite gneiss and the saccharoidal limestones and ordinary gneisses with quartzites. The author has not found such a structural discontinuity, but only a transition from ordinary gneiss to tonalite gneiss. This transition is due to tonalitization.

North of the Tristenspitze, both the limestone and the tonalite gneiss are striking ESE instead of ENE, as normal.

It seems reasonable to assume that the irregular lenses of saccharoidal limestones have been derived from a continuous layer of limestone within ordinary gneisses as found farther to the West.

It is assumed that the abnormal circumstances accompanying the tonalitization of the ordinary gneisses also caused a highly plastical behaviour of the limestones, as a result of which it is now present as lenses. During this process, the initially probably impure limestones recrystallized into pure saccharoidal limestones.

§ 20C *Ordinary gneisses.*

The term ordinary gneiss corresponds with the term "paragneiss" as used in literature.

According to Sander (1925, p. 18), the composition of this type of gneiss varies from a finegrained two-mica gneiss, rich in feldspar, to a phyllitic gneiss.

Bianchi (1934, p. 152) also described the most common type as a finegrained gneiss passing into a gneissic micaschist, containing above all quartz, and further biotite and muscovite, and less plagioclase. K. feldspar is rarely present as microcline.

The author found the mineral content of the ordinary gneisses in the Tauern gneisses to consist of (samples 3, 6, 10 and 11 of fig. 91):

in all cases > 5 %:	quartz
	biotite
	muscovite
in some cases > 5 %:	plagioclase
	garnet
	chlorite
if present < 5 %:	K. feldspar
	opaque minerals
	zircon
	epidote
	clinozoisite
	apatite

The sillimanite in some cases observed in the tonalite gneiss, type II, is probably a relict of the ordinary gneisses.

These gneisses must be partially similar to the "gneiss supérieurs" of Jung and Roques (1952) between the isogrades — chlorite + sillimanite, and + sillimanite — muscovite of Palm (1957).

The ordinary gneisses just as all other rocks in the M. Spico region have been subjected to the Tauern crystallization, and the micas e.g. are deformed as well as undeformed.

The ordinary gneisses in some cases pass into tonalite gneisses (type II). Samples 10 and 11 (fig. 91) belong to a small lense of ordinary gneiss, within tonalite gneisses (s. 12) (see fig. 77 of App.

I). These transitions can be studied in a single outcrop.

Transitions of the larger lenses which surround the saccharoidal limestones are more difficult to determine. It seems, however, that the boundary between ordinary gneiss and tonalite gneiss South of the Croda della Paura (Sheet VIII) intersects both the strike lines of schistosity and the formation boundaries.

The mean strikes of the samples of measurements 230 and 231 (App. II) are exactly parallel to the formation boundaries between calcareous phyllite and Tauern tonalite gneiss in the South, and between ordinary gneiss and saccharoidal limestone in the North.

The relation between saccharoidal limestone and ordinary gneiss is very interesting. It is stated as a rule that the saccharoidal limestone lenses are accompanied by ordinary gneisses except at their northern boundary, where they are directly in contact with the Tauern tonalite gneiss.

As it is probable that all gneisses around the saccharoidal limestones originally were ordinary gneisses and that part of them has been tonalitized, the process of tonalitization must have been obstructed by the presence of limestone. This is in correspondence with the fact the tonalitization stops at the northern boundary of the calcareous phyllites.

Sander (1925) mentioned that the limestones within the ordinary gneisses generally are accompanied by amphibolites.

In the case of the saccharoidal limestone lenses within the Tauern gneiss of the M. Spico region, only in a single sample amphibole (s. 21, fig. 91) has been encountered. This sample is from a massive rock in tonalite gneiss, type Iad, in the tonalite gneiss, type II, and probably belonging to a dyke. The rule that an amphibolitic contact zone accompanies limestones within gneisses is not valid in the present case.

§ 20D *Limestones.*

Some limestones occur at the boundary of the upper and lower mantle of the Tauern tonalite gneiss North of the Sasso Fondo (p. 2551). They are stratified and parallel to the contact planes between the upper and lower mantle and to the adjacent schistosity-planes. They are "Bänderkalke" and are different from the pure saccharoidal limestones. The limestones at S. Martino (s. 25 of fig. 91) resemble the saccharoidal limestones, but are less pure; they have enclosures of mica and quartz parallel to the stratification.

East of the M. Spico, limestones occur within the ordinary gneisses, and they are parallel to the schistosity-planes of these gneisses. In the gneisses of the M. Spico Nappe, generally the *S*-planes are also parallel to the stratification.

In some cases, the limestone content of the calcareous phyllites is so high that the name limestone must be used, but these limestones have not been distinguished on the map (Sheet VIII).

§ 20E *Calcareous phyllites, containing green phyllites.*

The calcareous phyllites are equivalent to the slightly metamorphic Mesozoic "Bündner Schiefer" ("schistes lustrés" or "calcescisti") of the Pennine nappes.

They consist of

generally > 5 %	calcite quartz muscovite plagioclase
in some cases > 5 %	epidote biotite
if present < 5 %	opaque minerals chlorite garnet zircon

The stratification is parallel to the *S*-planes. In some places, green phyllites are intercalated in the calcareous phyllites.

The green phyllites consist of:

generally > 5 %	quartz chlorite muscovite epidote calcite
in some cases > 5 %	green hornblende tremolite chinozoisite

if present < 5 %	tourmaline
	opaque minerals
	zircon
	garnet
	apatite

Photograph 26 represents a green phyllite collected North of Lappago. The macroscopic augen consist of albite. As this albite is accompanied by epidote, chinozoisite and calcite, it probably originated from a (more) Ca containing plagioclase. The high content of green hornblende renders Sander's (1925) name of amphibolite applicable. These green phyllites are probably metamorphic "ortho" rocks (e.g. tuffs) in all studied slides.

§ 20F. *Serpentine and talc.*

Lenses of serpentine and talc have been observed on the large overthrust plane along which the Austrian Nappe moved over the Mesozoic complex of calcareous phyllites (Sander, 1925). They are probably altered ophiolitic rocks. In the literature, these rocks are considered as the reduced equivalent of the Matrei Zone (chapter 22).

§ 20G. *Quartz phyllites, containing green phyllites.*

The gneisses of the M. Spico Nappe *) are underlain by westward wedging out quartz phyllites, in which green phyllites are present as intercalations.

The quartz phyllites consist of:

in all cases > 5 %	quartz
	muscovite
	chlorite
in some cases > 5 %	plagioclase
if present < 5 %	garnet
	opaque minerals
	tourmaline
	zircon

The chlorite partially is kelyphitic on garnet. The mineral content of quartz phyllites and green phyllites is approximately the same. A higher content of chlorite causes greener colour of the green phyllites, which are "para" rocks.

§ 20H. *Ordinary gneisses of the M. Spico Nappe.*

The mineral content of the ordinary gneisses of the M. Spico Nappe resembles that of the gneisses mentioned in § 20C.

In some places stratified limestones are present as intercalations (Sheet VIII). Their stratification is parallel to the *S*-planes of the gneisses. In consequence, the stratification of the gneisses is assumed to be indicated by the *S*-planes. Moreover, the contact planes with the underlying quartz phyllites and the overlying M. Spico and Anterselva gneisses, which possibly are the boundary planes of originally subhorizontal series, are also parallel to the *S*-planes.

§ 20I. *M. Spico gneiss.*

The M. Spico gneiss is of a light colour. The lack of any considerable content of dark minerals facilitates to distinguish these gneisses from the ordinary gneisses.

The M. Spico gneiss consists of quartz, plagioclase, and K. feldspar. Accessory minerals are clinozoisite, apatite, and opaque minerals. According to Sander and Bianchi, it is an "ortho" granite gneiss. This gneiss has also been found South of the M. Spico region (Section VIII) as the Anterselva gneiss.

In one of the slides of this Anterselva gneiss, riebeckite appeared to be present as a primary mineral.

In consequence of the conformity of the contact plane of this granite gneiss with the ordinary gneiss, it may be considered as an old laccolith (Sander, 1925).

§ 20J. *Riesenferner augen-gneisses, containing migmatites.*

The Riesenferner augen-gneiss in the M. Spico region is characterized by precipices. The distribution of the gneiss is shown on Sheet VIII, and as a whole on Sheet I.

The augen are generally a few cms large, but may exceed 10 cm. According to Bianchi (1934) the mineral content is microcline, albite, quartz, and muscovite.

*) The M. Spico Nappe consists of the gneiss complex overlying Mesozoic rocks in the M. Spico region and is part of the large Austrian Nappe. Its nappe structure is evident, whereas the nappe structure of the Austrian Nappe (chapter 23) is based on interpretation.

The mineral content of the Rieserferner augen-gneiss is:

Generally > 5 %	quartz plagioclase microcline
In some cases > 5 %	muscovite biotite chlorite hornblende epidote
If present < 5 %	opaque minerals zircon garnet apatite clinozoisite

The augen generally consist of perthitic microcline crystals. Bianchi (1934) mentioned this type of augen, but other augen have been found consisting of aggregates of microcline, albite, and quartz (photograph 27). Augen, consisting of albite and quartz only have been found too (photograph 28).

The augen may contain inclusions with a planation or lineation parallel to the schistosity, consisting of e.g. quartz, muscovite, biotite, apatite, and opaque minerals.

The poikiloblastic nature indicates that the augen were formed within an ordinary gneiss, the schistosity of which must have been present.

The distribution of the augen suggests that the genesis of the augen is related to the intrusion of the Rieserferner tonalite. For this reason, the name Rieserferner augen-gneiss is used. In the chapter on tectonics, a structural analysis of the M. Spico region will be given. It may be readily seen, that the Rieserferner augen-gneiss intersects the westward anticlinal continuation of the dome of the Rieserferner tonalite, and that it also intersects the syncline North of this anticline, both of which were formed in a later phase of Alpine orogenesis (Ch. 21). The outcrop of the Rieserferner augen-gneiss follows the northern border of the Rieserferner tonalite. Its western part lies above the probably westward and subsurface continuation of this tonalite, as follows from the presence of migmatites, generally containing leucocratic tonalites (see below).

The above concept differs from the opinion of Sander (1925), Bianchi (1934), and Dal Piaz (1933), who considered the Rieserferner augen-gneiss as a laccolith conformably intercalated in the ordinary gneisses. But the unconformable relationship is now well established, as the author has measured ± 200 planes of schistosity in the section Molini-Campo Tures. It could be concluded that the strike is E-W and, therefore, at right angles to the N-S running belt of augen-gneiss (see § 21A).

A supply of K may be expected from the relative abundance of K. feldspar. This is supported by comparing the petrochemical analyses of the Rieserferner augen-gneisses made by Becke and Semerano with those of the ordinary gneisses by Bianchi.

From the analyses given in table XXIV, the relative abundance of K_2O is obvious. The K_2O content of the Rieserferner tonalite is about the same as that of the ordinary gneiss. However, it is assumed that the intrusion of the tonalite caused migration of the potassium.

The possibility of a migration of K^+ions by means of a volatile-rich (predominantly H_2O) phase has been proved by Orville (1960). He described a mechanical process by which large amounts of K^+ and Na^+ ions can be transferred within a rock, if a thermal gradient is present. Potassium tends to migrate toward the low-temperature and sodium toward the high-temperature areas. An increase in pressure displaces the ion-exchange between the K and Na feldspar crystals and the K^+ and Na^+ ions in the same direction.

TABLE XXIV

RESULTS OF PETROCHEMICAL ANALYSES.

The values of d'Amico are means of (4) and (7) individual analyses.

Author of analysis	literature reference	analyzed rock	% K_2O	% Na_2O	% CaO	% Fe_2O_3 Fe O Mg O Mn O
Becke	Sander, 1925	Ries. aug. gn.	**4,26**	2,49	1,89	3,07
Semerano	Bianchi, 1934	„ „ „	**5,42**	2,86	1,58	3,16
Bianchi	Bianchi, 1934	ord. gn.	2,34	2,80	2,98	9,76
„	„ „	„ „	3,92	2,07	1,41	10,30
S. Morgante	Bianchi, 1934	Ries. tonalite	3,41	3,15	3,90	5,50
„	„ „	„ „	2,48	3,02	5,91	8,24
„	„ „	„ „	2,16	2,87	6,54	9,84
(4) d'Amico	d'Amico 1957	quartz phyllite	3,11	1,59	0,50	7,89
(7) „	„ „	ditto, "granitized"	3,60	2,78	2,17	6,02

The effect of an increase in pressure is the same as that of a decrease in temperature.

Experimental work supports Orville's mechanical explanation. Prior to Orville, the processes of ion-exchange, metasomatism, and granitization have been treated from a theoretical viewpoint only.

Actually, these processes are much more complicated. The K_2O-supply of the Rieserferner augen-gneiss is not accompanied by a decrease of the Na_2O content which remained the same during the ion-exchange. Calcium, iron, and other constituents are also involved in these processes. E.g. in d'Amico's (1957) "granitized" quartz phyllites, the K_2O content remained the same during granitization, whereas the Na_2O- and the CaO content increased and the FeO content decreased.

Next to ion-exchange also supply of matter may have taken place in certain areas.

The actual processes are complex because of the number of involved ions, crystals, and P,T conditions. The Rieserferner augen-gneiss does not entirely surround the Rieserferner tonalite. It is absent at its southside. The presence of a zone without K_2O supply between the two bodies must be explained by the complicated P,T conditions during metasomatism. The source of the K_2O is not known. The K_2O content of the tonalite as a whole is perhaps somewhat lower than that of the ordinary gneisses but the difference is too small to be determined from a few analyses.

The following observation should be mentioned.

East of Campo on the road to Riva, the contact zone of the tonalite is well-exposed. At two meters from the contact, an augen-gneiss occurs, resembling the common Rieserferner augen-gneiss, and with augen consisting of aggregates of microcline + plagioclase + quartz.

These augen also contain recrystallized biotite crystals. This has not been observed in the common Rieserferner-augen-gneiss. It is supposed that this type of augen-gneis is a contact-metamorphic rock. The biotite may have crystallized in the augen and the microcline may have been replaced by other minerals.

This hypothesis is supported by the augen texture in the borderzone of the tonalite. Some augen-shaped areas of a leucocratic tonalite occur in a matrix of the darker tonalite.

At about one meter from the contact, only the same darker homogenized tonalite may be observed. These observations support the opinion that at the contact some ordinary gneisses and augen-gneisses have been replaced metasomatically by tonalite possible under expulsion of potassium, which may have been a source of K_2O for the Rieserferner augen-gneiss.

Nevertheless, the ultimate *mise en place* has been a forceful intrusion as is shown by the dome structure (Ch. 21).

It is emphasized that our concepts based on a few observations should not be considered as proved. This would only be possible by detailed petrochemical analyses, which goes beyond the scope of this paper.

During the last years the augen of many East Alpine augen-gneisses have been the subject of petrographical examinations.

At first, Exner (1950) proved that the microcline augen in a granite gneiss at Badgastein belonged to the Tauern crystallization. These augen have a helical texture, indicating a rotation of about 90°, which must have originated during and after crystallization.

Rotations of augen have also been described by Collette (1959), who stated that rotation of some minerals as evident from helical textures may not have been caused by affine movements along schistosity-planes but by the behaviour of a more competent crystal of a special form within a less competent and compressed medium.

Such "snowball" textures have not been observed by us in the augen of the Rieserferner augen-gneiss, but the origin of the augen is ascribed also to a post-kinematic crystallization.

On the other hand, Frasl (1954 and 1957) proved that the microline augen of many East Alpine augen-gneisses had crystallized in a magma. One of his convincing arguments is the zoning, i.e. parallel arrangement, of the inclusions in some crystals.

The augen of the "filladi feldspatiche" of Trener (carta geologica, 22), later called "filladi granitizzate" by d'Amico (1957), resemble the augen of the Rieserferner augen-gneiss (our figures 42—47 of App. I), and occur in the Cima d'Asta region. Their distribution is shown in fig. 87.

These augen consist of microline and in places of orthoclase, and they are related to the intrusion of the Cima d'Asta intrusives (d'Amico 1957).

Fig. 47 of App. I shows that the locally folded schistosity may continue in the augen, and these must have crystallized later. As mentioned in chapter 17, the distribution of d'Amico's "granitized" rocks coincides with our areas of tectonical thickening. The observed thickening may be partially due to supply of material.

§ 20K. *Possibly metasomatic dykes of leucocratic tonalite.*

It has already been mentioned that the augen of the augen-gneiss do not in all places consist of microcline. In some cases they contain aggregates of microcline, albite and quartz, and in other cases they only contain albite with some quartz. In photograph 28 one of the latter is shown under the microscope. It appears to consist of albite as a new mineral, containing zoned inclusions of biotite and quartz, which are probably relicts of the partially replaced and partially included ordinary gneiss. The plagioclases are zoned in places.

In a number of places West of Molini (Sheet VIII), migmatites have been mapped.

A migmatite is a mixed rock in which a granitic component (in the broad sense of the phrase) is clearly recognizable (according to Turner and Verhoogen, 1951, p. 294). It can only be studied in the outcrop, as both components together are larger than the thin section area.

Palm (1957) stated the "granitic" component to be isotrope. We have also called those rocks migmatites, the "granitic" component of which shows parallel mica's. In consequence of the schistosity, this component of the migmatite will be called "dyke gneiss". The granitic component of the migmatite may be a dike gneiss or an isotropic rock. It traverses the Rieserferner augen-gneiss, which is the original rock as it is generally present in the M. Spico region, and only locally altered in migmatite.

The dyke gneiss in some places macroscopically and microscopically resembles the above described augen consisting of albite and quartz (photograph 29).

Next to the albite and quartz also mica crystals may be primary minerals. They are parallel to the schistosity in the adjacent augen-gneiss. The plagioclase consists of more or less euhedral coarse crystals, and many xenomorf grains of the matrix frequently showing zoning and gradually passing into each other.

The quartz also shows coarse and small grains. Accessory minerals are garnet, biotite (parallel to *S*), opaque minerals, epidote, clinozoisite, and apatite.

Next to the dyke gneisses, isotropic veins with the same mineral content may be observed. In

some cases, these contain coarse biotite, plagioclase, and quartz crystals, predominating over the matrix. Muscovite is present as a primary mineral.

As the original rock does not contain such coarse crystals without planation, it is supposed that these are new crystals. The dykes have the composition of a leucocratic tonalite.

The contacts between original rock and veins are always sharply defined (fig.'s 92 and 93).

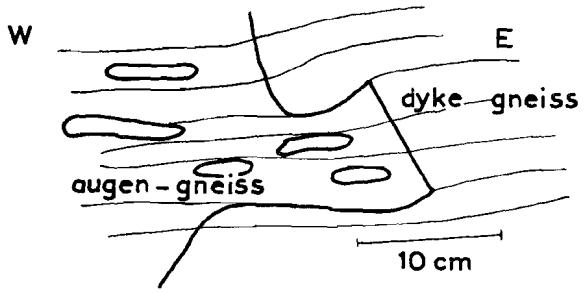

Fig. 92

Sketch of sharply defined contact between augen-gneiss (West) and dyke-gneiss (East) from migmatite West of Molini, M. Spico region. Grid co-ordinates 227—985. This S-planes are represented by lines, and actually have an orientation of 275°—17°.

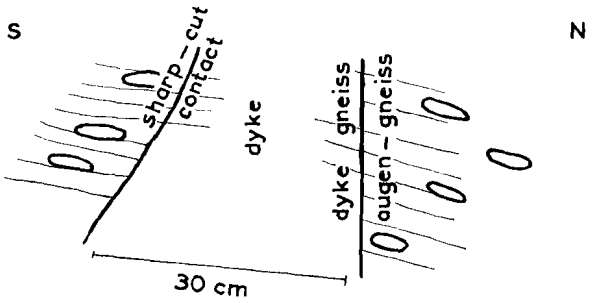

Fig. 93

Sketch of a leucocratic tonalite dyke and dyke-gneiss West of Molini, M. Spico region. Grid co-ordinates 227—985. The schistosity of the surrounding augen-gneiss in places may continue into the dyke. Position of *S*.: 310°—20°.

It is supposed that the parallel mica crystals are relicts of the transformed augen-gneiss, as crystal planation, if present, is parallel to the planation forming the schistosity of the adjacent augen-gneiss.

Muscovite, which probably is a relict, was also an important relict mineral in the tonalitized gneisses (tonalite gneiss, type II, § 20A).

Other explanations are less acceptable. Mica crystals in an intruding dyke cannot be expected to be orientated parallel to the schistosity of the intruded rock.

The explanation that muscovite crystals have grown simultaneously in original rock and dyke after the intrusion, is rejected for the following reason. The schistosity of the ordinary gneisses and Rieserferner augen-gneisses has been subjected to doming and folding by the rising Rieserferner tonalite, which caused different attitudes of *S* in the migmatite areas (Sections VII-IX). Consequently, the schistosity can hardly be ascribed to a later stress field which could create a uniform subparallel schistosity in the entire M. Spico region. The dykes definitely belong to the intrusion of the Rieserferner tonalite, in view of their mineral content and their geographic position. The intrusion is definitely younger than the schistosity in the M. Spico region.

Interesting are the local open anticlines formed by dyke gneiss schistosity (figure 94).

The genesis of these folds follows from the lower part of figure 94. When the dyke gneiss with its subhorizontal schistosity was compressed from the sides, it was bent into anticlines. The dips on the limbs of these anticlines became steeper up to a certain degree. Then the anticlinal crest was broken and the upward movement took place along the schistosity-planes which became steeper by this process.

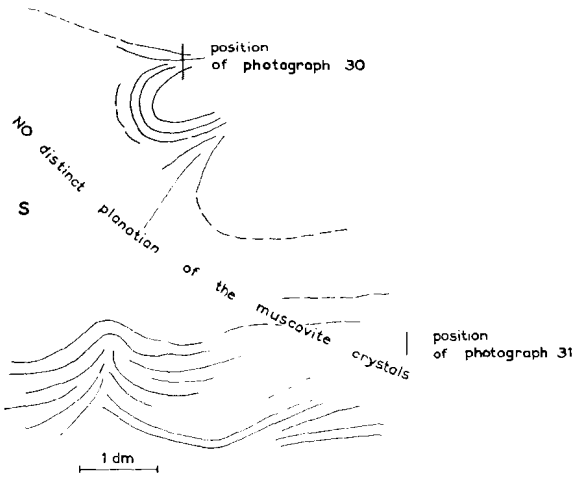

Fig. 94

Sketch of the schistosity of a dyke-gneiss with indication of thin sections (photographs 30 and 31) at approximately right angles to the subvertical drawing plane. The schistosity is caused by parallel muscovite crystals in an albite-quartz rock West of Molini, M. Spico region. Grid co-ordinates 227—985.

Corresponding synclines have not been found. This may be attributed to a possible upward es-

cape. The plastic dyke material moved upward and it is assumed that such plastic movements could reach such a degree that the original schistosity disappears and that the dyke of metasomatic origin could be isotropically injected into the adjacent rock. This might be the origin of the observed isotropic dykes. On the other hand, fig. 94 shows that between areas with orientated muscovite (photograph 30) areas are present without such orientation (photograph 31). Possibly, the muscovite has been replaced for the greater part.

In conclusion, it is stated that the Rieserferner tonalite intruded into a series of ordinary gneisses. This was locally preceded by the formation of a zone of augen-gneisses with locally some migmatites. The Rieserferner tonalite partially seems to be a anatexite (§ 20 J). This tonalite has an intermediate position between a real anatexite and a real intrusive rock with only some contact metamorphism.

The term anatexite is used as by the French petrologists. Jung and Roques (1952) supposed that in the subsurface of France a "front des migmatites" moved across the regional metamorphic series. In this case an anatexitic granite was preceded firstly by augen-gneisses and secondly by migmatites.

§ 20L *Rieserferner tonalite.*

The Rieserferner tonalite belongs to the periadriatic intrusives, intruded during Miocene time (Karl, 1959). The coarse crystals generally show no orientation. If some biotite crystals show planation, they parallel the dome-shaped contact plane of the intrusive body.

CHAPTER 21

TECTONICS OF THE M. SPICO REGION

Fig.'s 32 - 75 of appendix I show the type of deformation generally found in the M. Spico region. The minor folds as depicted in these figures are present in 1) the Tauern tonalite gneiss of the Zillertaler Alps, 2) the inner and outer mantle ("untere" and "obere Schieferhülle" respectively); the first consists of partially tonalitized ordinary gneisses and saccharoidal limestones, the second of Mesozoic calcareous phyllites and green phyllites, 3) the overlying partially granitized ordinary gneisses of the M. Spico Nappe.

These minor folds indicate a general northward overturn, which originated by a northward mass transport, the intensity of which increased towards higher strata. The northward overturn of the minor structures is in correspondence with the regional tectonics. The gneisses of the M. Spico belong to the Austrian Nappe, which has been thrusted over the Mesozoic of the outer mantle of the Tauern Inlier. The participation of Mesozoic strata demonstrates the Alpine age of these kinematics. The Alpine deformation types of the M. Spico region are in contradistinction with the Hercynian deformation types of the crystalline basement of the Dolomites. Most crystals (e.g. the biotite crystal of fig. 76 in App. I) are post-kinematic, and belong to the so-called Alpine "Tauern Kristallisation". This is also in contrast to the pre-kinematic crystallization of the Hercynian folded crystalline basement of the Dolomites, South of the Pusteria Line.

This basement rests upon gneisses which may be different from the gneisses of the M. Spico region. The gneisses South of the Pusteria Line are overlain by rocks without an Alpine northward overturn. Their deformation during this Alpine phase, if present, must be smaller than of the corresponding M. Spico gneisses, the overlying rocks of which have largely been affected by Alpine kinematics.

"Tauern Kristallisation" may be present in the not-exposed gneisses South of the Pusteria Line. The absence of post-kinematic crystals in the greater part of the exposed crystalline basement of the Dolomites does not necessarily imply the absence of these crystals in lower levels.

In conclusion, it is stated that somewhere between the Pusteria Line and the M. Spico region a belt of strongly Alpine deformed rocks is separated from a belt of not, or slightly, Alpine deformed rocks.

From a petrographical point of view, the Tau-

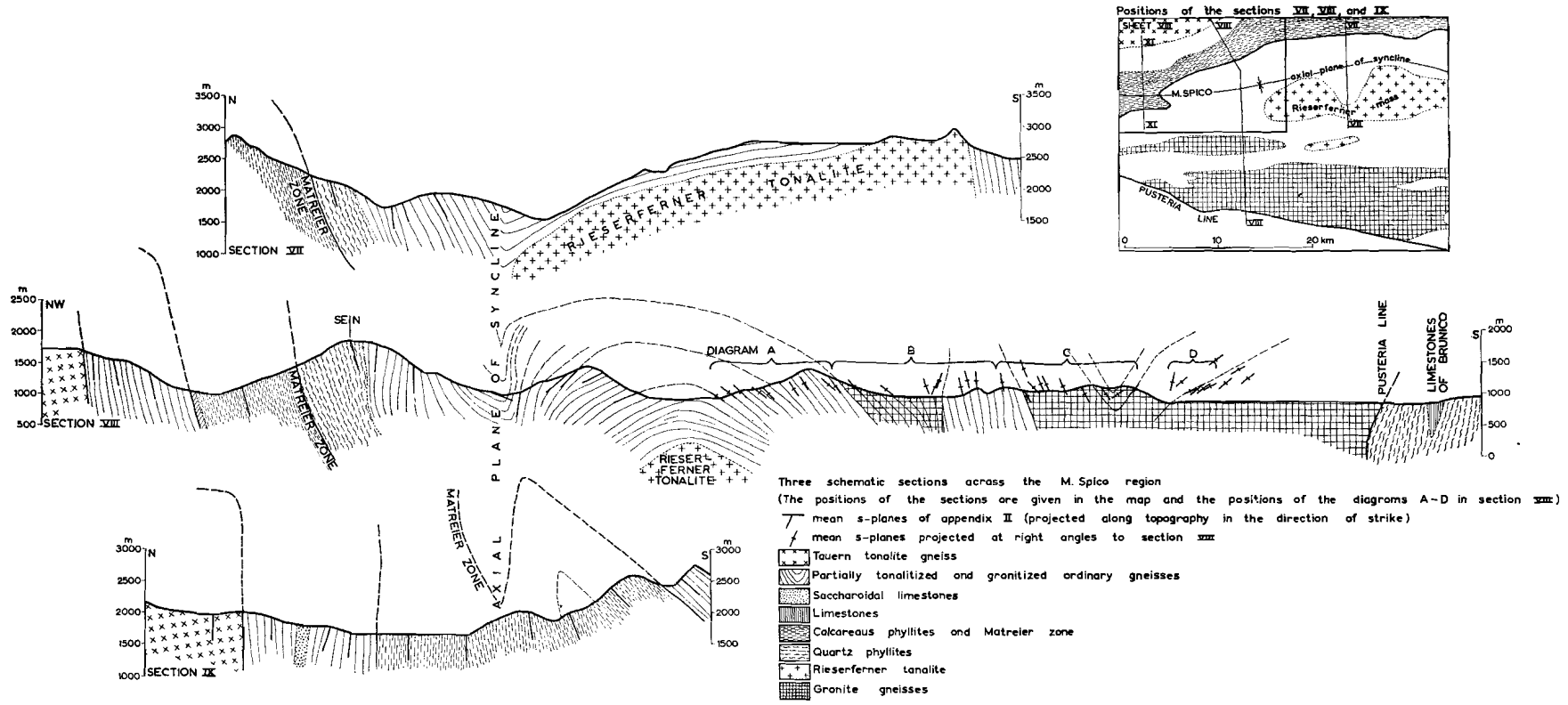

Fig. 95

Three sections across the M. Spico region. The diagrams A, B, C, and D are given in fig. 98.

ern tonalite gneisses of the Zillertaler Alps may be compared to the Pennine nappes of Ticino (Chapter 22).

This analogy also exists with respect to the structure. Fig. 109 represents a section across the Hohe Tauern by Karl and Schmidegg (Karl, 1959). The Zillertaler tonalite gneiss forms a northward overturned nappe with a mantle of ordinary gneiss and "Bündner Schiefer" just as the Pennine nappes of Switzerland represented by fig. 108 (according to Argand).

In sections VIII and IX (fig. 95), only the steep so-called "root zone" of the large Zillertaler Nappe (Sheet I) is shown.

It is assumed that a tonalitic rock was injected subhorizontally into its mantle of gneisses and "Bündner Schiefer" during Early and Middle Alpine orogenesis.

The steepness of the root zone may have originated by a Late Alpine doming up of the Tauern Inlier. This assumption follows from the following arguments. 1) The parallelism between the steep root zone of the Zillertaler Nappe and the major thrust plane over which the gneisses of the M. Spico Nappe moved over the "Bündner Schiefer". This major zone of overthrust probably was flat and not folded locally. At present, it is folded as shown in the Sections VIII and IX. When the present syncline and anticline are unfolded, the original subhorizontal position of the root zone of the Zillertaler Nappe is demonstrated.

2) The axial planes of the minor folds of the M. Spico region are subparallel to the *S*-planes, whether the latter are subvertical or subhorizontal. During their formation they probably were parallel to each other. The above unfolding reestablishes the parallelism, and the axial planes of the minor folds assume a subhorizontal position which might be expected of minor folds during large-scale mass transport.

The first phase of Alpine orogenesis in the M. Spico region consists of injection of a Pennine type nappe and overthrusting movements of the M. Spico Nappe over this Pennine unit. The M. Spico Nappe has been described by Sander (1925). It belongs to the upper Austrian Nappe. In the following chapter it will be suggested that the overthrust movements of the M. Spico Nappe occurred in two Alpine phases.

For the present, the Late Alpine kinematics of the M. Spico region will be analyzed. The starting point for the discussion of these movements is a series of subhorizontal rocks consisting of the Zillertaler "ortho" tonalite gneiss, its partially tonalitized lower mantle of ordinary gneisses and limestones, and its upper mantle of calcareous phyllites with green phyllites ("Bünder Schiefer"). The subhorizontal rocks include furthermore the gneisses of the M. Spico Nappe. During Late Alpine orogenesis two E-W striking doming structures originated: a) The Tauern dome North of the M. Spico region and b) the Rieserferner dome in the M. Spico region.

A syncline originated between these two domes. The primary vertical movements of the domes caused secondary sideward movements which may be deduced from the isoclinal character of the intermediate syncline and of the anticlinal structure West of the Rieserferner dome (Section IX). The latter cannot be explained by doming only.

These tectonics are represented in three sections across the M. Spico region (fig. 95).

The eastern section (VII) is across the Rieserferner tonalite which is covered by gently North dipping gneisses. The anticlinal structure of the gneiss mantle evidently originated by doming above the intrusion. The central section (VIII) is West of the Rieserferner tonalite. The tonalite core is not exposed but the anticlinal structure of the mantle also originated by doming.

The western section IX shows an isoclinally folded series. The Rieserferner intrusion must have determined the position of an anticline and of a syncline. Afterwards, these originally gentle folds became isoclinal by sideward compression.

Our theory on the genesis of the isoclinal series of the crystalline basement of the Dolomites represented in fig. 59 is confirmed by the gradual transition of an isoclinally folded series into a gentler folded series.

The westward increasing folding-intensity with increasing dips caused the convergence of the axial planes in this direction (fig. 95).

The axial plane of the syncline and the contact plane between the upper and lower mantle of the Tauern tonalite also converge westward.

A comparison of the sections VIII and IX demonstrates that the latter convergence is not due

to westward increasing dips, as most strata are subvertical in the compared parts of these sections.

In consequence (see chapter 15), this convergence may be explained by a wedging out caused by the following features.

1) The dislodged slices of marmor, talc, and serpentine, together forming the Matrei shear zone at the base of the M. Spico Nappe, are overlain by a series of quartz phyllites wedging out westward. This wedging out probably originated during the earlier Alpine orogenesis preceding the late Alpine orogenesis now under discussion. 2) The mean axis of m.f. dips eastward in the calcareous phyllites between Lappago and Lutago. The maximum mean dip is 37° E, and the individual m.f. may dip 70° E. This East dip decreases southward and northward to the subhorizontal m.f. of the Tauern tonalite gneisses.

As shown in the Chapters 10 and 12, an upward rotation of the m.f. and a convergence of the subvertical *S*-planes in the same direction indicate an increasing squeezing out in this direction caused by increasing compression between rigid masses.

A westward increasing compression follows from a comparison of the sections VIII and IX. It is possible that the compression continued in the surroundings of Lappago (section IX), also after the series became isoclinally folded. This later compression was made possible by squeezing out of the material along the subvertical *S*-planes. This vertical movement is the latest Alpine movement in the M. Spico region. The mentioned East dip of the m.f. is in contrast to the gentle West dip in the western border area of the Tauern Inlier.

East of sheet VIII the gneisses locally show westward dipping m.f. Measurements sample 262 (App. II) has a mean m.f. of 247° - 40°. This deviating mean m.f. is accompanied by a mean *S* of 77° - 69°, and disappears to the South (meas. sample 260 with mean S : 73° - 63° and mean m.f.: 253° - 15°) as well as to the North (meas. sample 264 with mean *S*: 92° - 81° and mean m.f.: 270° - 15°).

The mean strikes of the *S*-planes suggest an eastward convergence.

Although this area has not been examined in detail, the available data suggest an eastward convergence of the *S*-planes, accompanied by an upward rotation of the m.f. in this direction. This situation probably originated by a local eastward increasing compression of the gneisses. The rotation of the m.f. is opposite to the rotation of the m.f. between Lappago and Lutago.

The variation of the mean dip of the m.f. is rather abrupt at the boundary of the calcareous phyllites and the Tauern gneisses. Whereas the latter maintained their original subhorizontal m.f., the block of calcareous phyllites as a whole rotated about 25° along this boundary plane. Such a difference of dip between the m.f. of adjacent rocks does not indicate a difference of age of the m.f. A similar shape of the m.f. in the lower and upper mantle of the Zillertaler "ortho" tonalite indicates their formation during one and the same phase of compression. Later internal rotation along the *S*-planes frequently occurred in the crystalline basement of the Dolomites (e.g. fig. 43).

For this reason, Karl's statement (1939) that the 30°—35° difference between the dips of his augen granite gneisses and the Zillertaler tonalite gneisses (in the eastern part of the NW boundary) point to a different time of origin, is questionable. Moreover, this difference disappears gradually to the West.

§ 21A *The Rieserferner dome.*

In Chapter 20 it has been explained that the intrusion of the Rieserferner tonalite may be explained firstly by stoping and secondly by anatexis.

The contact plane is subparallel to the *S*-planes and the stratification of the overlying gneisses.

The gneisses above the contact plane are altered by contact metamorphism (Dal Piaz, 1934).

The meas. samples 263 and 267 (App. II) have been collected in the contact metamorphic gneisses North of the Rieserferner tonalite. They are disturbed by faults as indicated by the fig.'s 85 and 86 of appendix I. These faults may be interpreted as gently dipping normal faults, formed by tension in the roof gneisses. The uniformity of the rocks affected by faulting does not permit to determine the net slip.

In some cases, the dip of the *S*-planes changes abruptly at the fault planes, from which considerable rotational movements may be concluded. The stretching must have been large, as also in-

dicated by abrupt changes in thickness (see fig. 82 of appendix I).

The contact-metamorphism is restricted to a zone of some hundreds of meters. In those places where the contact plane is subvertical, a small zone of intensive drag of the mantle gneisses, resulting in a subvertical position, may occur. This feature has been observed most clearly along the Rio di Riva (meas. sample 259 of App. II, Sheet VIII).

As indicated before, the influence of the intrusion is not limited to such a small border area. The intrusion caused large-scale doming in the overlying gneisses, and also metasomatism in the Rieserferner augen-gneisses. These augen-gneisses hitherto have been considered as a conformably intercalated "ortho" (granite) gneiss, but the unconformable character of this augen-gneisses belt around the Rieserferner tonalite will be proved by the following detailed analysis (see also § 20J).

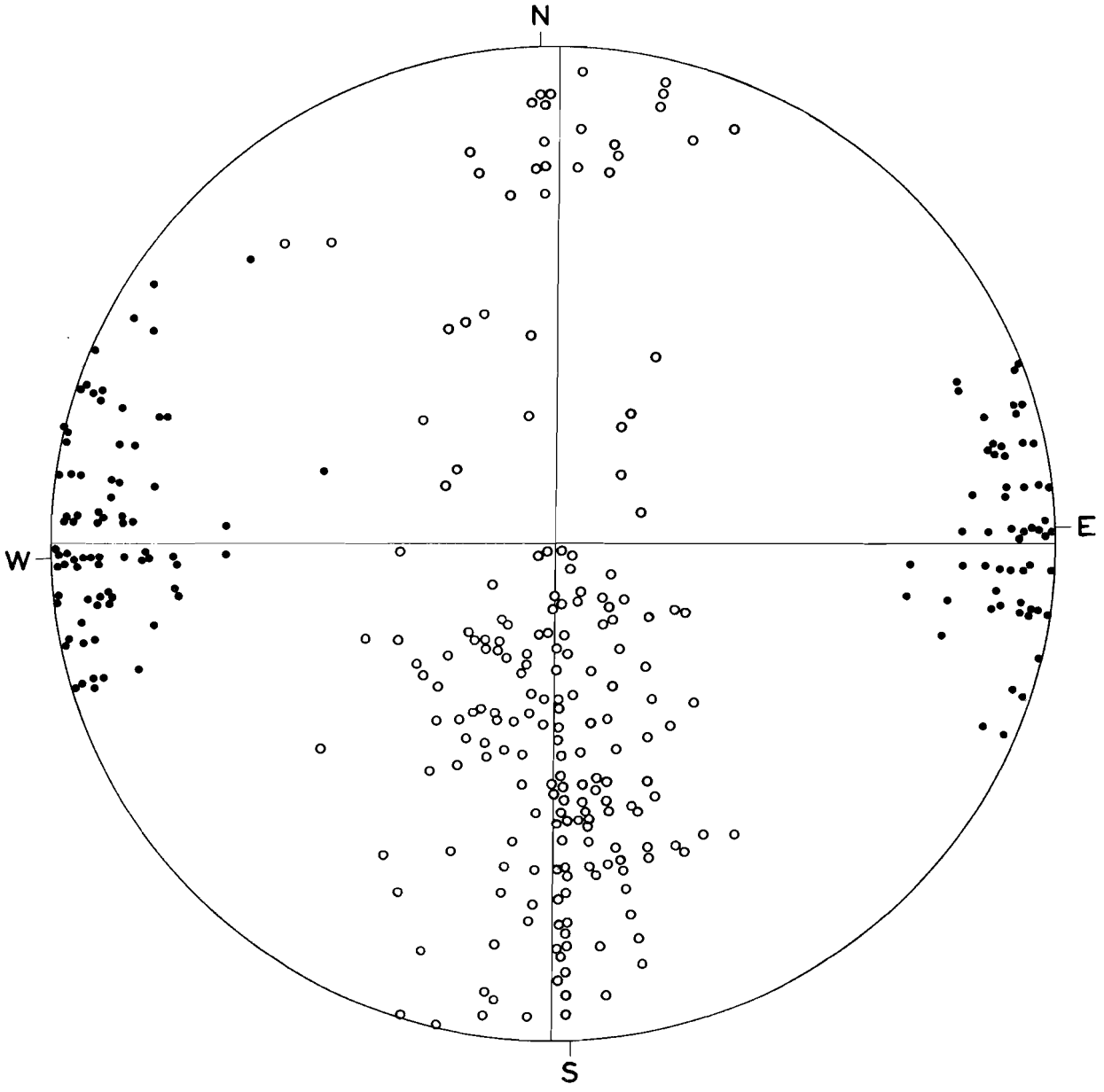

Fig. 96

Diagram (Schmidt net, lower hemisphere) of 196 *S*-poles and 113 m.f. from the Campo di Tures-Molini section across the Rieserferner augen-gneiss. The *S*-poles lie in the depicted 2°—90° plane. The m.f. scatter around the 92°—0° axis.

Fig. 96 is a pole diagram with the measurements of a N-S section between Campo Tures and Molini. The 194 *S* and 132 m.f. of the measurements samples 219, 225, 226, and 227 mainly form the 196 *S* and 133 m.f. of fig. 96.

This N-S section is parallel to the N-S striking belt of Rieserferner augen-gneisses, which westward and eastward passes into ordinary gneisses.

The 196 *S*, which are measured at about 10 m interval, are dispersed around the plane 2°—90°. Their dispersion indicates folding around a subhorizontal E-W axis. The 133 m.f. are scattered around this mean value of 92°—0°. In consequence, the axes of the m.f. are parallel to the axis of the anticlinal structure.

This parallelism does not imply a synchronous genesis, because the origin of the minor structures preceded the origin of the dome.

Fig. 97 is a histogram of the observed dips of the *S*-planes of fig. 96. The individual *S* have been projected in the mean 2°—90° plane by rotating their pole in a plane determined by this pole and the mean fold axis 92°—0°. The mean dip in this part of the northern limb of the dome is 43°.

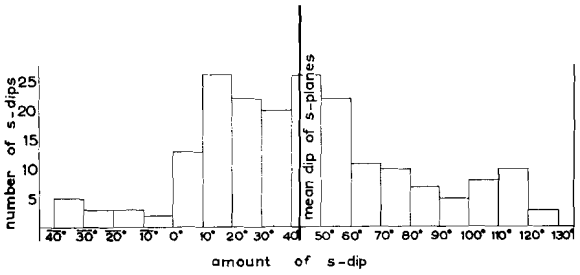

Fig. 97
Histogram of the 196 *S*-dips of fig. 96.
For further explanation see text.

This analysis is in agreement with the situation as shown in section VIII. The difference between the shape of the dome and a true anticline is that in the dome the central subhorizontal part is larger and passes abruptly into the subvertical limbs.

The particular coffin-shape of the dome is explained by the position of the contact-plane between the gneisses and the underlying intrusive body. The belt of Rieserferner augen-gneiss is at right angles to the well-established strike direction of the *S*-planes. The other disconformities between the *S*-planes and the contact planes of the Rieserferner augen-gneiss have been summarized in the preceding chapter.

CHAPTER 22

TECTONICS OF THE CRYSTALLINE ROOT ZONE OF THE EASTERN ALPS

Most authors accept the following geometric structure of the Eastern Alps (Sheet I).

The autochthonous Flysch belt in the North and the Mesozoic "Bündner Schiefer" of the Prätigau region, and the Engadin and Tauern Inliers, are overlain by large overthrust nappes, the so-called "Austrian Nappes".

These nappes consist of Mesozoic rocks in the Northern Limestone Alps, and of crystalline rocks in the Central Alps. The direction of movement of the nappes was North, and their southside with steeply dipping strata is called the "root zone" of the Eastern Alps.

This root zone lies North of the Insubric Line, NW of the Giudicaria Line, and North of the Pusteria Line.

In the Peio region, in the SE part of the Ötz Mass, and in the Defereggen Mountains, the root zone is characterized by folds with subvertical axes. This style of folding was called "Schlingenbau" by Schmidegg, who mapped the above regions (Schmidegg, 1933).

His observations on the structure of the individually considered areas have been summarized in Sheet I. It will be attempted to integrate the particular cases of "Schlingenbau" into a single geometric pattern which originated during a phase of Alpine orogenesis. This phase is considered as intermediate between the earlier overthrusting movements of the Austrian nappes and the Late Alpine kinematics. The latter consist of (a) doming of the Tauern and the Rieserferner tonalite (Chapter 21), and (b) the Late Alpine kinematics of the areas, South of the Pusteria Line (Chapter 19).

The M. Spico region is located North of the

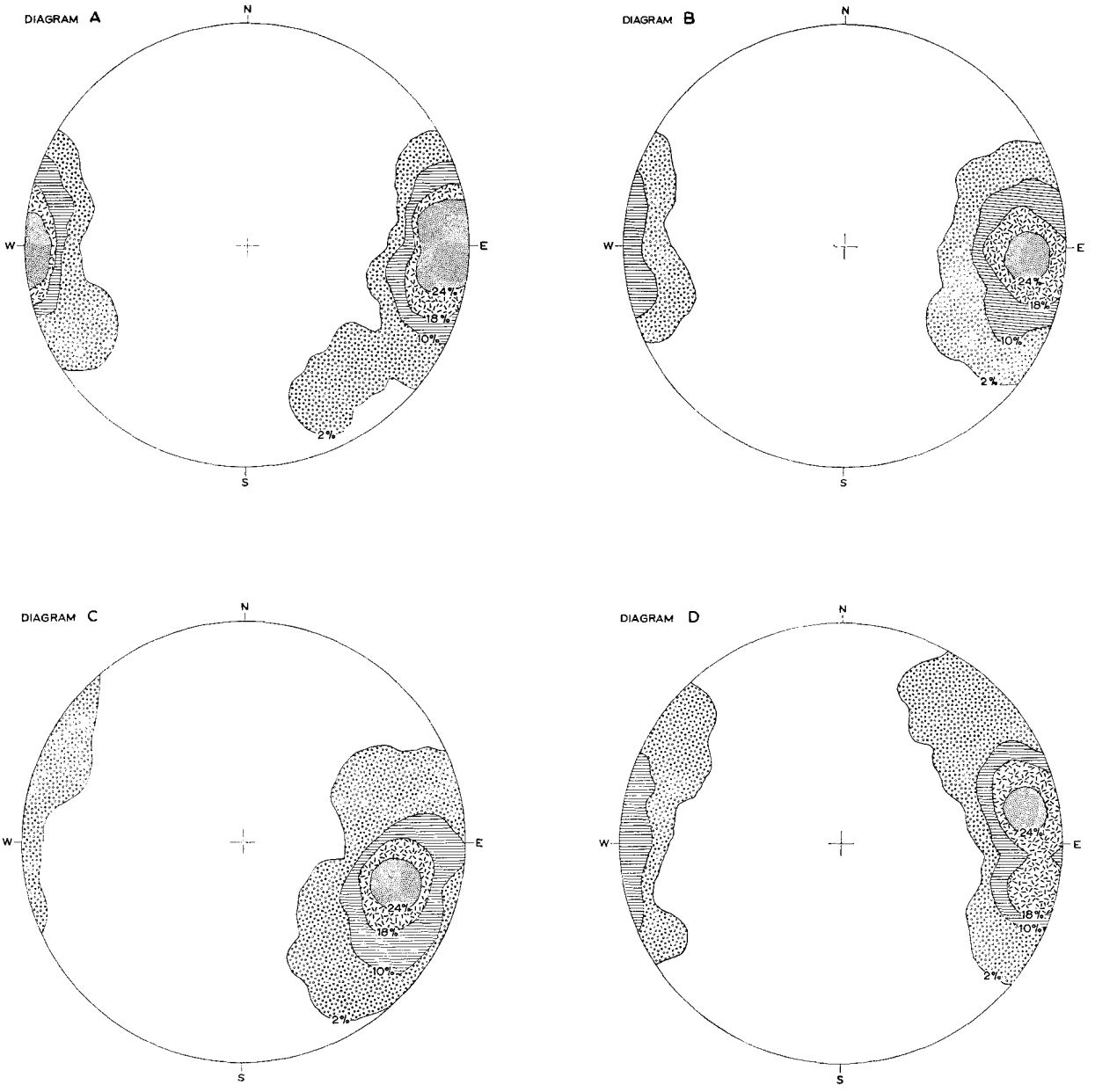

Fig. 98

Four diagrams, A, B, C, and D, (Schmidt net, lower hemisphere) with contoured groups of respectively 82, 83, 83, and 82 m.f. The positions of the diagrams are given in fig. 95.

root zone. It has been stated that the steep dips of this region have a Late Alpine origin, synchronous with the intrusion of the Rieserferner tonalite which belongs to the Miocenian periadriatic plutonic bodies.

Section VIII shows a cross section through the root zone North of Brunico. This part, investigated by Groenewold, will be discussed in the following paragraph. It is followed by a discussion of the tectonics of the Upper Gail Valley gneisses, examined by Felix. The data are from unpublished Utrecht-survey reports by H. Groenewold (1960) and R. Felix (1959).

§ 22A. *A cross section North of Brunico* (see Section VIII of fig. 95)

The mean *S*-planes projected in that part of section VIII which is located between the axial plane of the Rieserferner dome and the Pusteria

Line have been computed from groups of about 15 individual *S*-planes each. The mean co-ordinates and the mean elevation of each group have been determined and all means have been projected at right angles to the cross section.

This part of Section VIII may be divided into three parts.

1. The southern limb of the Rieserferner dome.

2. The steeply dipping root zone.

3. A gentle syncline of the Anterselva granite gneiss which is cut-off by the Pusteria Line to the South.

The borders of these three parts are not definitely known. The northern part of the Anterselva granite gneiss for the greater part belongs to 1, as gentle South dips are present and as this rock is found again in the core of the M. Spico syncline.

The width of the root zone is probably 2 km approximately, as the southern part of the Anterselva gneiss consists of a gentle syncline. This syncline continues eastward and abuts against the Defereggen "Schlinge" (see Sheet I).

In interpreting the structures of section VIII, the presence of a root zone in this section may be doubted. The Rieserferner anticline might gradually pass into the syncline to the South.

The entire section VIII might be explained by doming and folding of a subhorizontal series of gneisses, as assumed for the M. Spico region in the preceding chapter. The structure of the adjacent areas, however, does not confirm such an assumption.

The Defereggen "Schlinge" with its subvertical axis, which originated by E-W compression, cannot be explained by simple doming accompanied by compression. The "Schlinge" must have been present during the intrusion of the Rieserferner tonalite. This implies the existence of a zone of subvertical *S*-planes or a root zone of the Austrian Nappe prior to the Late Alpine phase of doming.

This zone wedged out from the Defereggen "Schlinge" into the small root zone of section VIII. This will be discussed more comprehensively at the end of this chapter.

Four diagrams A, B, C and D (fig. 98) show the positions of the mean axes of the minor folds along the discussed part of section VIII. The widths of the sample areas are indicated by braces in the section. The groups have means of 90°—6°, 93°—18°, 106°—30°, and 80°—16° respectively. These East dips may have a structural meaning, as will be discussed presently.

§ 22B. *Gneisses of the Upper Gail Valley.*

The distribution of the Upper Gail Valley gneisses is shown on Sheet I. They are bordered in the South by the "Carnian major upthrust", and in the North by the Thurntaler Syncline which consists of quartz phyllites, and the Drauzone.

The "Carnian major upthrust" is the eastward continuation of the Pusteria Line. As mentioned before, it disappears to the East. The gneisses of the Upper Gail Valley represent the strata underlying the quartz phyllites of the Carnian Alps and the Thurntaler syncline. The situation indicates the similarity of the rocks at both sides of the Pusteria Line and its eastward prolongation.

A distinction between Austrian and Dinarian crystalline rocks cannot be made.

The Thurntaler quartz phyllites overly ordinary gneisses, as well in the North as in the South. The gneisses in the North show "Schlingenbau". The subvertical axis of this Defereggen "Schlinge" and the subvertical axes of the minor folds gradually disappear upward in the overlying quartz phyllites (Schmidegg, 1937).

We may distinguish a) an infrastructure consisting of ordinary gneisses with Schlingenbau and gently folded Anterselva granite gneiss, and b) a suprastructure consisting of meso- and epizonal micaschists (quartz phyllites of the Thurntaler syncline, the crystalline basement of the Dolomites, and the "Carnian" rocks). The latter do not show subvertical axes of the m.f. The Thurntaler quartz phyllites have subhorizontal axes in the major and minor folds. The azimuth generally is ENE. The pattern of the quartz phyllites South of the Pusteria Line has been discussed in part III. The m.f. of the rocks in the western Carnian Alps are subhorizontal with an ESE azimuth (unpublished survey report of R. Felix, 1959).

The Upper Gail Valley gneisses belong to the infrastructure. Fig. 99 shows that the position of the axes of the m.f. of the biotite gneisses and am-

phibolites of the westernmost 5 km of this zone (between Sillian and St. Oswald) differs from the subhorizontal position of the m.f. in the adjacent suprastructure.

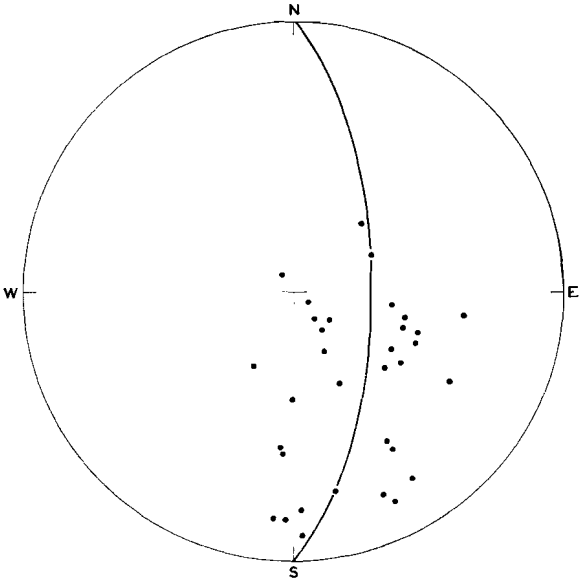

Fig. 99
Diagram (Schmidt net, lower hemisphere) with 33 m.f. of the westernmost 5 km of the Upper Gail Valley gneisses.

The discussed gneisses are only locally exposed and it was not possible to obtain a clear structural picture. The *S*-planes are strongly folded and have different positions.

The 33 plotted foldaxes vary in position between steeply dipping East and subhorizontal N-S. The distribution may be interpreted as being in accordance with the infrastructure of the Defereggen Mountains. The shape of the southern part of the Defereggen "Schlinge" indicates E-W compression.

It is assumed that the Upper Gail Valley gneisses originally possessed *S*-planes with a subvertical to gently South dipping position. These *S*-planes were subjected to E-W compression, thus causing subvertical m.f. in the subvertical *S*-planes and slightly South dipping m.f. in the slightly South dipping *S*-planes.

In chapter 11 it was shown that the m.f. are distributed in a plane at right angles to the direction of compression. If it is assumed that this plane has a N-S strike, its dip can be computed. In fig. 99 the plane has been constructed in such a way that one half of the m.f. lies above and one half below the plane. It is a median plane (see Chapter 7) and its position is 0°—67°. This result corresponds with the infrastructure of the Defereggen "Schlinge", the m.f. of which in some places also dip steeply eastward. The line along which compression took place dips 23° westward.

This agrees with Paulitsch's (1960) investigations on the Upper Gail Valley gneisses between S. Oswald and Obertilliach (the westernmost 25 km). He gives a diagram with 38 m.f. in this region, and concludes that two families of respectively E-W and N-S striking m.f. occur. The N-S striking m.f., which predominate in our diagram, appear to be younger than the E-W striking m.f. This is in support of our view that the N-S striking m.f. belong to an Alpine phase, whereas the E-W striking m.f. might have a Hercynian age, just as the m.f. of the adjacent suprastructure.

In conclusion, it may be stated that a distinction in suprastructure and infrastructure is allowed. As the steep folding of the infrastructure must have an Alpine age, it follows that the infrastructure was deformed below the suprastructure, during Alpine orogenesis, in which an E-W shortening has not been observed.

§ 22C. *"Schlingenbau" of the Infrastructure.*

In the preceding chapter it has been demonstrated that gneisses which underly the mesozonal micaschists in the Defereggen Mountains have steep axes of the major "Schlinge" and the accompanying m.f.

The same difference between infrastructure and suprastructure is found in the surroundings of the Schneeberger Zone and the Peio region (Sheet I).

The Schneeberger zone is probably separated by a fault from the northern gneisses of the southeastern Ötz Mass. The infrastructure North of this fault is characterized by "Schlingenbau" with subvertical m.f. The suprastructure of the Schneeberger micaschists only shows subhorizontal m.f., except at its southwestern border zone which belongs to the Ötz "Schlinge". The Schneeberger micaschists belong to a synclinal structure in the gneisses of the Austrian Ötz Nappe. The E-W striking overturned m.f. (e.g. App. I, figs. 59, 60, and 61) are probably Alpine and may be compared to the m.f. of the M. Spico region. This possibly Alpine age is in contradistinction with the Hercynian age of the m.f. of the micaschists of the

Thurntaler syncline and the crystalline basement of the Dolomites.

The third example of adjacent infrastructure and suprastructure is found in the Peio region. The Peio Line separates katazonal gneisses with "Schlingenbau" from meso- and epizonal micaschists located to the NW (Andreatta, 1948). The latter belong to a syncline with possibly an upward disappearing "Schlinge"-like structure (Sheet I).

The three mentioned cases permit the following generalization. The crystalline root zone shows "Stockwerk" tectonics. Below a suprastructure of mesozonal micaschists with subhorizontal (probably Hercynian and Alpine) foldaxes, an infrastructure of katazonal gneisses occurs with subvertical foldaxes.

§ 22D. *Shape of the "Schlinge".*

The above conclusion was already drawn by Andreatta (1948) with respect to the Ortler region. He interpreted the "Schlinge" as "vortex" structures (see fig. 100).

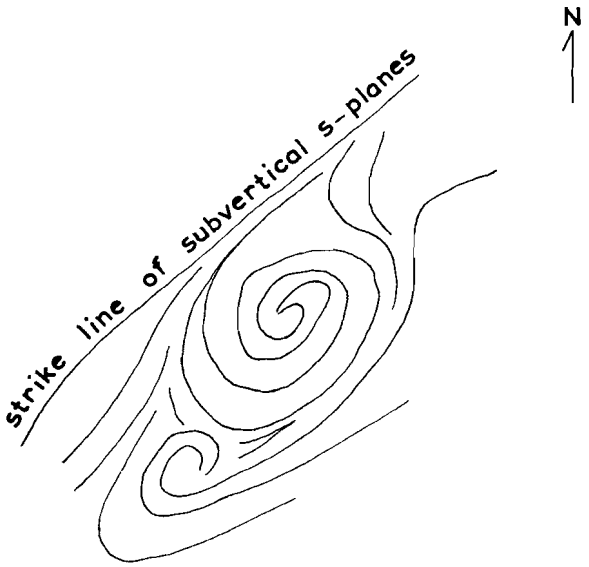

Fig. 100
Ortler ordinary gneisses with "vortex" structure according to Andreatta. (Part of Gortani's fig. 2, 1956; without indication of scale).

It is based on the assumption that a certain *S*-plane was rolled up. This proces is mechanically not possible, and the resulting "vortex" structures actually do not occur. We concur with Schmidegg's structural concept (1932, 1936). He introduced the term "Schlinge" (= sinuosity). According to Schmidegg, a "Schlinge" is formed by bending of subvertical *S*-planes in consequence of a subhorizontal compression. This idea is supported by Wenk (1934) who described a "Schlinge" in the southern Silvretta Mass. Fig. 101 shows two small "Schlinge" of the Peio region, the Mt. Pin "Schlinge", and the Le Mandrie "Schlinge". It appears that the subvertical Northeast striking *S*-planes NW of the Giudicaria Line have been compressed in NE—SW direction.

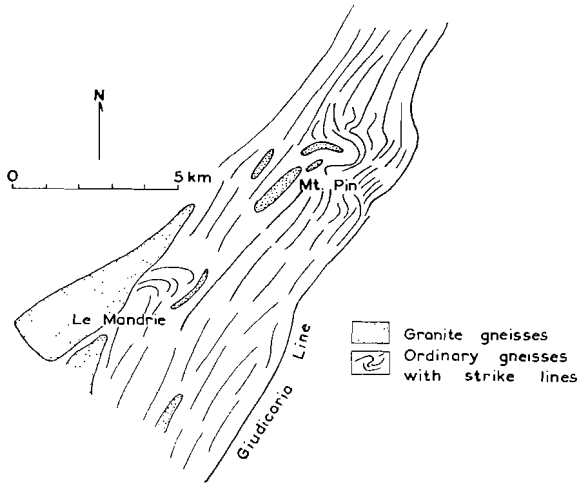

Fig. 101
Mt. Pin and Le Mandrie "Schlinge" according to Schmidegg's map (1936).

Two types of "Schlinge" originated.

1. The Mt. Pin "Schlinge" consists of folds with well-developed bends.

2. The Le Mandrie "Schlinge" is a fold with only one visual bend. After passing the visual part of the "Schlinge", the *S*-planes seem to continue in the opposite direction.

The "Schlinge" are local phenomena, the strike of which deviates from the regional strike which is parallel to the Giudicara Line.

For this reason, the Le Mandrie "Schlinge" must have another limb, as the *S*-planes must continue, not in the opposite direction but in the same direction and parallel to the Giudicaria Line. This other limb cannot be observed, as a visual bend is absent. This absence may due to new movements along the old *S*-planes during the formation of the "Schlinge". This process is analogous to the folding represented by fig. 59 and fig. 94.

In conclusion, it is stated that all "Schlinge" must have two limbs. Generally the bend of the one limb is well developed, whereas the bend of the other limb is absent. This result has been applied on the larger Ötz- and Defereggen "Schlinge". The position of the other limb is indicated by convergence of the *S*-plane (Sheet I). From Schmidegg's maps it seems that the *S*-planes turn 180° after passing the bend of a "Schlinge"; he left the existence of the other limb out of consideration.

§ 22E. *"Schlingenbau" considered as a result of Alpine compression.*

The Alpine phase of "Schlingenbau" is intermediate between the formation of the Pennine and Austrian nappes, and the gravitational tectonics caused by the Late Alpine uplift along the Tauern-Engadin axis.

Harland and Bayly (1958) have developed a theory for explaining folds with subvertical axes in some orogenes. When a subhorizontal series of strata is compressed laterally, the strata may obtain a subvertical position. If this subvertical series afterwards is subjected to unequal compression, as shown in fig. 45, the plastic material may continue to be squeezed upward, but sideward movements may occur also. In that case the latter take place from the more compressed central area towards the less compressed sides of the belt. These sideward movements cause folding with a subvertical axis.

It appears to be possible to explain the observed East Alpine "Schlinge" accordingly.

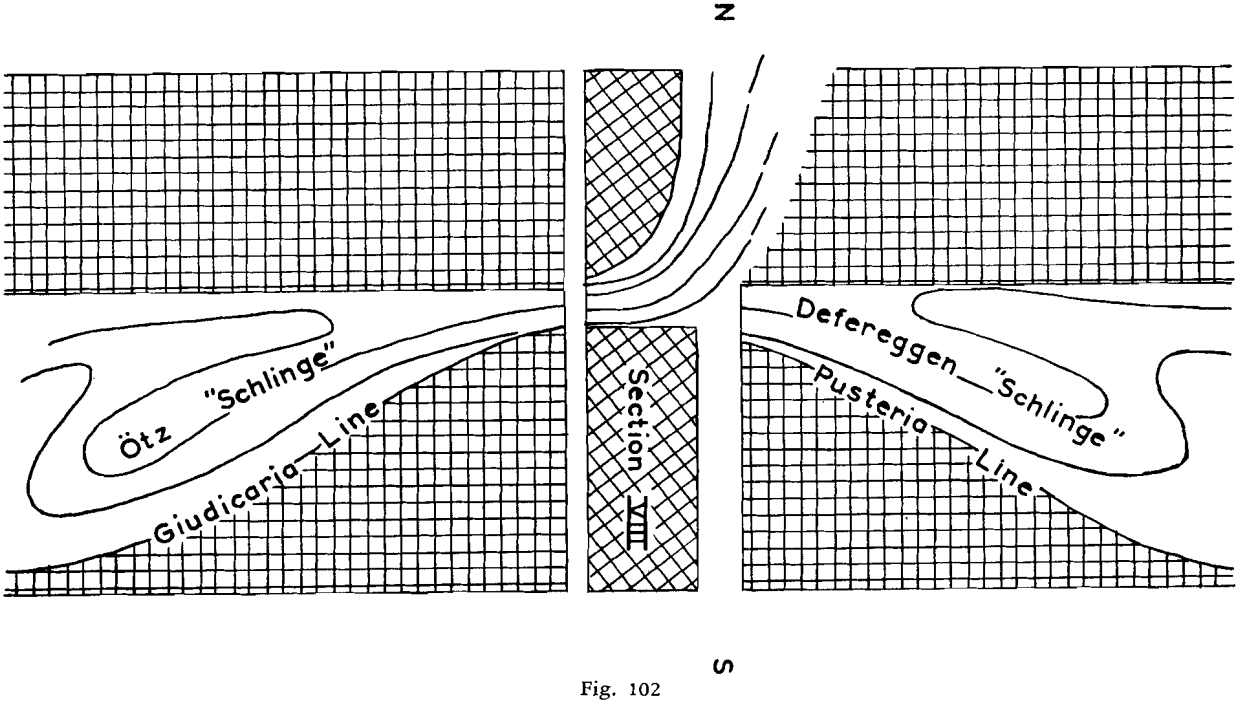

Fig. 102

Harland and Bayly's concept (1958) of "Schlingenbau" applied to the East Alpine root zone. For further explanation see text.

Fig. 102 represents a plastic zone which was squeezed out between rigid masses. Most material was replaced in the central area, through which a cross section is drawn. It is assumed that the southern block unequally moved northward, causing folds overturned to the North in the central section, and respectively westward and eastward mass transport in the adjacent areas. An analysis of Sheet I shows that fig. 102 may schematically represent the East Alpine root zone.

The central section corresponds with our section VIII with its small root zone. The northern rigid mass is formed by the Tauern Inlier and the northern Ötz Mass, and the southern rigid mass is bordered by the Giudicaria Line and the Pusteria Line (or more precisely by the northern boundary

of the Anterselva granite gneiss).

The western and eastern "Schlinge" correspond with the actual Ötz- and Defereggen "Schlinge". Actually, the structure is not as symmetrical as suggested by fig. 102.

The present theory is supported by the following considerations.

1. The strike lines of the Austrian Nappe strongly converge from the ± 80 km wide section between the Engadin and Peio regions to the ± 10 km wide section at the western boundary of the Tauern Inlier. This width of ± 10 km originated from a width of ± 80 km by (a) a steepening of the dips and (b) upward and lateral squeezing out. The eastern part of the structure (Defereggen "Schlinge") shows less convergence.

2. The E-W strike of the Silvretta Mass, the northern Ötz Mass, and the surroundings of the Tauern Inlier may be considered as the regional Alpine direction of strike.

The rigid crystalline basement of the Dolomites was moved towards the North, thus causing the large wrench flexure of the Crystalline NW of the Giudicaria line. The Northeast direction of the Giudicaria Line may be considered as a local deviation of the above mentioned Alpine E-W strike.

The structure of the Crystalline indicates that the Giudicaria Line originated by a sinistral wrench movement. The crystalline rocks of the Peio region were plastically deformed in the zone of flowage. The overlying rocks probably were deformed in the zone of fracture, and this resulted in wrench faults.

The Dolomites moved northward with respect to the Bergamasc Alps. In consequence, wrench faults might be expected in the Brenta region, South of the Peio region, as the Permotriassic rocks of the Brenta region were deformed in the zone of fracture.

Trevisan (1930) developed a mechanical theory of sinistral wrench faulting in the Brenta region. This is represented in fig. 103 (according to De Sitter, 1956 b), and corresponds with the expected wrench movement.

The downward increasing intensity of deformation is analogous to our interpretation that the lower infrastructure is more deformed than the upper suprastructure (see § 22B and C).

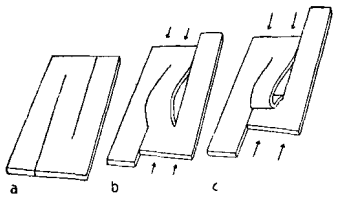

Fig. 103

Diagram for explaining the origin of the Brenta faults according to Trevisan (de Sitter's fig. 115, 1956 b).

3. It is assumed that the southern rigid mass moved northward. In consequence, the plastic material of the compressed belt with a position closer to the southern border has moved earlier and further than the material at the northern border. The material of the southern part indeed moved sidewards with respect to the material of the northern part (Sheet I and fig. 102). This "Vergenz" of the "Schlinge" may be compared to the overturn of the folds of table VII. In the preceding paragraph it was assumed that the material of the central area moved upward and that not all material East of the central area moved eastward.

An upward movement implies subhorizontal axes of the accompanying folds. As the material close to the southern border moved further, these folds will show an overturn toward the North.

The M. Spico region actually shows folds overturned to the North, and they may be considered to belong to the present tectonic pattern. In Chapter 21, in the discussion of the m.f., it was assumed that they belong to the overthrusting phase of the Austrian Nappe. Both assumptions can be justified. For the present, it is not possible to determine the phase of folding of the individual m.f.

Probably, they partially belong to the "Schlinge" phase, as may be explained as follows. The actual m.f. in the root zone of section VIII are dipping 18° East. The steeply South dipping *S*-planes of the northern limb of the Anterselva granite gneiss syncline have 30° East dipping m.f.

During an excursion to the Staller Sattel, the author found the following dips of a number of individual m.f.: 65°, 60°, 72° 62°, 65°, 60°, 70°, 70°, 65°, and 65° E.

In consequence, the m.f. in this most northwestern part of the Defereggen "Schlinge" have an average dip of ± 65° East, which corresponds

with the dip of the m.f. of the subvertical *S*-planes of the Upper Gail Valley gneisses.

At a point between the Staller Sattel and Section VIII (at the eastern border of the Lago di Anterselva), 5°, 10°, 20°, 34°, 30°, 40°, 40°, 50°, and 42° East dipping m.f. have been measured.

Although the results are too scarse for determining the regional structure, a gradual transition may be considered to exist between the gently East dipping m.f. of section VIII into the subvertical m.f. of the Defereggen "Schlinge" proper.

This transition is represented in fig. 104.

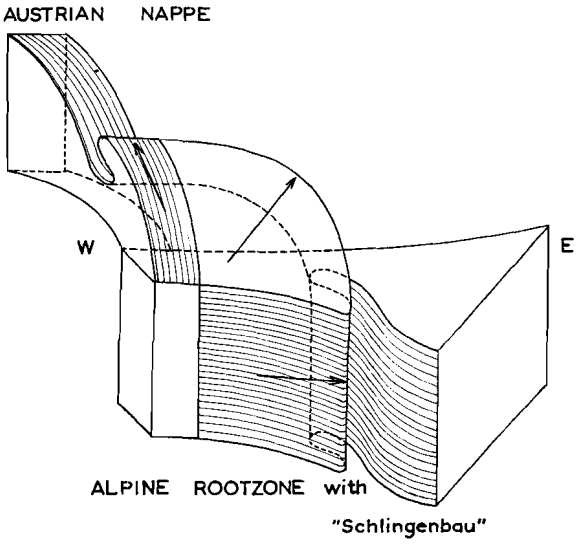

Fig. 104

Diagram with the transition of the northward overturned folds in the vicinity of section VIII (fig. 95) into the Defereggen "Schlinge" with sinistral "Vergenz". For further explanation see text.

Gradually transisting minor folds have originated synchronously. It is concluded that the greater part of the subhorizontal m.f. in the central area of fig. 104 were formed during the intermediate phase of orogenesis.

§ 22F *The Giudicaria Line.*

From the preceding paragraphs it does not follow that the Giudicaria Line corresponds with a wrench fault. The Giudicaria fault probably is a toppled over normal fault, as suggested by van Bemmelen (1957). This is further indicated by the fieldwork of Dietzel (1960) and van Hilten (1960) (see also Chapter 19).

The following three theories have been developed concerning the steeply Northwest dipping Giudicaria fault.

1. It is a sinistral wrench fault.
2. It is an upthrust fault, due to NW underthrusting of the South-Alpine block.
3. It is a normal fault with a fault plane secondary toppled over in Southeast direction.

ad 1) According to Trevisan (1939), Staub (1949), de Sitter (1956a and b), and others, the Insubric Line and the Pusteria Line originally formed a single straight line.

In that case the Giudicaria fault would have displaced the Insubric Line in NE direction. As discussed earlier in this chapter, the present author partially concurs with this concept.

The Dolomites block was probably displaced by a wrench flexure in the underlying crystalline rocks, and by a zone of wrench faults in the overlying Permotriassic. This zone actually is present in the Brenta region.

The Insubric, Giudicaria, and Pusteria Lines have not corresponded with faults during this earlier Alpine phase, as they do at present. They only indicated the strike of the crystalline root zone. During later Alpine orogenesis, when the Tauern-Engadin axis was raised with respect to the Po Plain and the Venetian Plain, a large normal fault developed. The strike of this fault became parallel to the strike of the underlying crystalline rocks. This normal fault then toppled over toward its downthrown block as was suggested by van Bemmelen (1957).

During this same phase, other step faults developed, e.g. the Sugana fault and the Valtrompia fault. The first also toppled over toward the South (see chapter 19).

De Sitter (1956b) assumed that the relatively less compressed Dolomites block was pushed northward with respect to the more compressed Bergamasc Alps. During the deformation at the Giudicaria wrench fault, the Sugana Line continuously remained in a direct line with the Valtrompia Line (Sheet I).

These faults, however, are of later origin, and no conclusions can be drawn from them concerning earlier Alpine movements.

It seems more reasonable to assume that wrench movements extended southward. According to

Fallot the northward overturned deformations of the Bergamasc Alps — which according to de Sitter would indicate an internal shortening of this block with respect to the Dolomites block — only exist in a 15 km wide zone (Fallot, 1950). Consequently, these northward overturned deformations are to small to explain the assumed relative compression which would amount to 40 km at the most.

ad 2) Dal Piaz (1942) and Vecchia (1957) advocated that the discussed lines correspond to upthrust faults. According to Dal Piaz, the Giudicaria upthrust developed during the late Insubric phase (chapter 23) of the Upper Oligocene and continued to exist until Upper Miocene by underthrusting of the southern block. Approximately at the transition of Oligocene and Miocene, the Periadriatic bodies intruded during a decrease in orogenetic compression.

Such underthrust movements explain the present dip of the faultplane. The intensity of the deformation, however, decreases downward, and a southern overthrust is more probable than a northern underthrust (chapter 19).

ad 3) In chapter 19 and at the beginning of this paragraph, it has been discussed that the Giudicaria Line probably is a toppled over normal fault. Its course, however, was determined by the infrastructure of the adjacent katazonal gneisses, which originated during an earlier phase of Alpine folding.

CHAPTER 23

GENERAL CONCLUSIONS ON THE ALPINE TECTONICS OF THE EASTERN ALPS

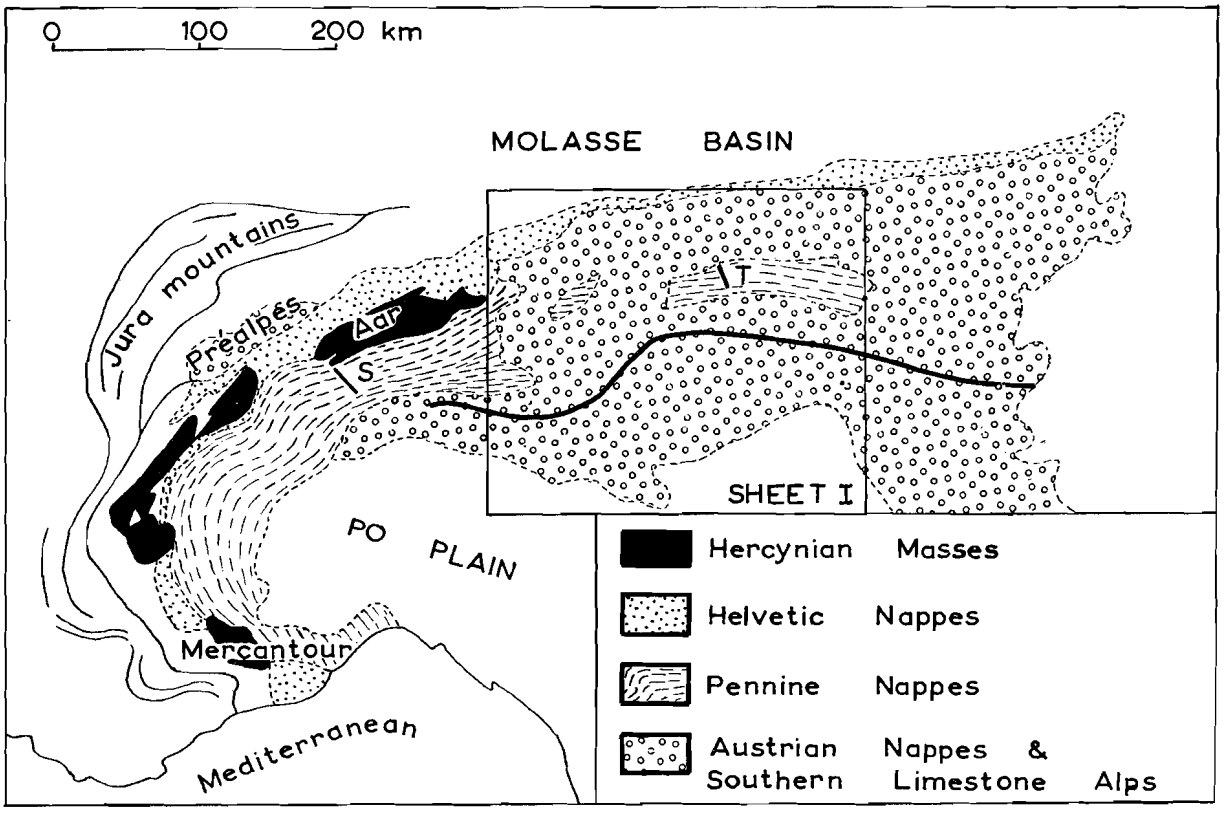

Fig. 105

Staub's tectonic map of the Alps (based on Escher's fig. 471, 1954). Sheet I, the Tauern section (T) = fig. 109, and the Simplon section (S) = fig. 108 are depicted.

Fig. 105 is a tectonic sketch map of the Alps, based on Staub's map (1923), showing the position of sheet I.

The three principally different types of nappes, Helvetides, Austrides, and Pennides, have been indicated.

For the explanation of the relations between these nappes in the western Alps, van Bemmelen (1960a) gives a structural scheme of the Lower Middle Tertiary situation before the the Insubric uplift (fig. 106). He assumed that as a result of physico-chemical processes an asthenolith with a relative low density ($\varrho = 2{,}5$) developed in the present Po Plain, and moved upward. This vertical movement caused a sideward escape of material. The overlying sedimentary cover was subjected to epidermal gravity tectonics (Helvetides).

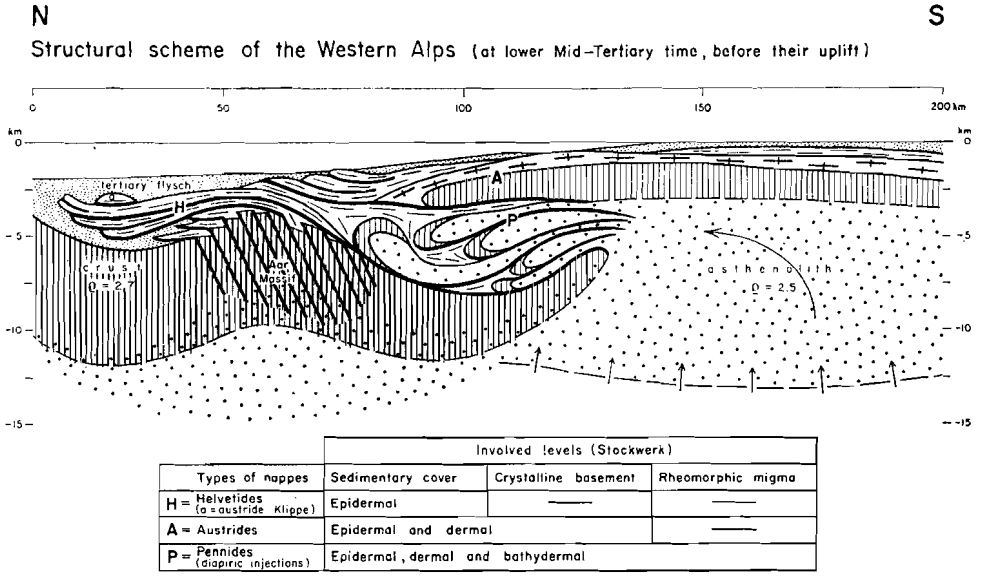

Fig. 106

Structural scheme of the western Alps before their Insubric uplift according to van Bemmelen (1960 a, fig. 4).

The underlying crystalline rocks participated in these gravitational movements by forming the Austrides. Still deeper, in the bathydermal "Stockwerk", the Pennides were injected, and a lower and upper mantle of crystalline rocks and "schistes lustrés" were formed around the Alpine intrusive bodies.

The presence of the Helvetides is mainly restricted to the western Alps. They form an arc surrounding the present Hercynian masses uplifted during Late Alpine orogenesis. The Helvetide sedimentation area was situated at the inner side of the arc of Hercynian masses (fig. 105). Its limestone facies differs from the monotonous "schistes lustrés" facies of the more southern basin which was to be injected by the Pennides. The subsidence and sedimentation of the Helvetide and Pennide basins occurred mainly during the Jurassic and Cretaceous. The Austride sediments developed mainly during the Permotriassic in the more southern basin. Part of these sediments was discussed in Chapter 5.

After this short summary of Alpine tectonics, particular attention will be paid to the Austrian nappes (§ 23A) and the Pennine nappes (§ 23B).

§ 23A *Austrian Nappes.*

The Helvetide basin became narrower in eastern direction. The Pennide basin continued from the western Alps into the eastern Alps, where the width amounted to more than 100 km. The "schistes lustrés" actually occur in the Engadin and Tauern Inliers. The entire Pennide zone is overlain by the Austrian overthrust sheets consisting of a) mainly gneisses in the Silvretta and Ötz Mass and in the regions South and East of the Tauern Inlier; b) quartz phyllites and graywackes, North of the Tauern Inlier, and c) Mesozoic sediments with Austride facies in the Northern Limestone Alps.

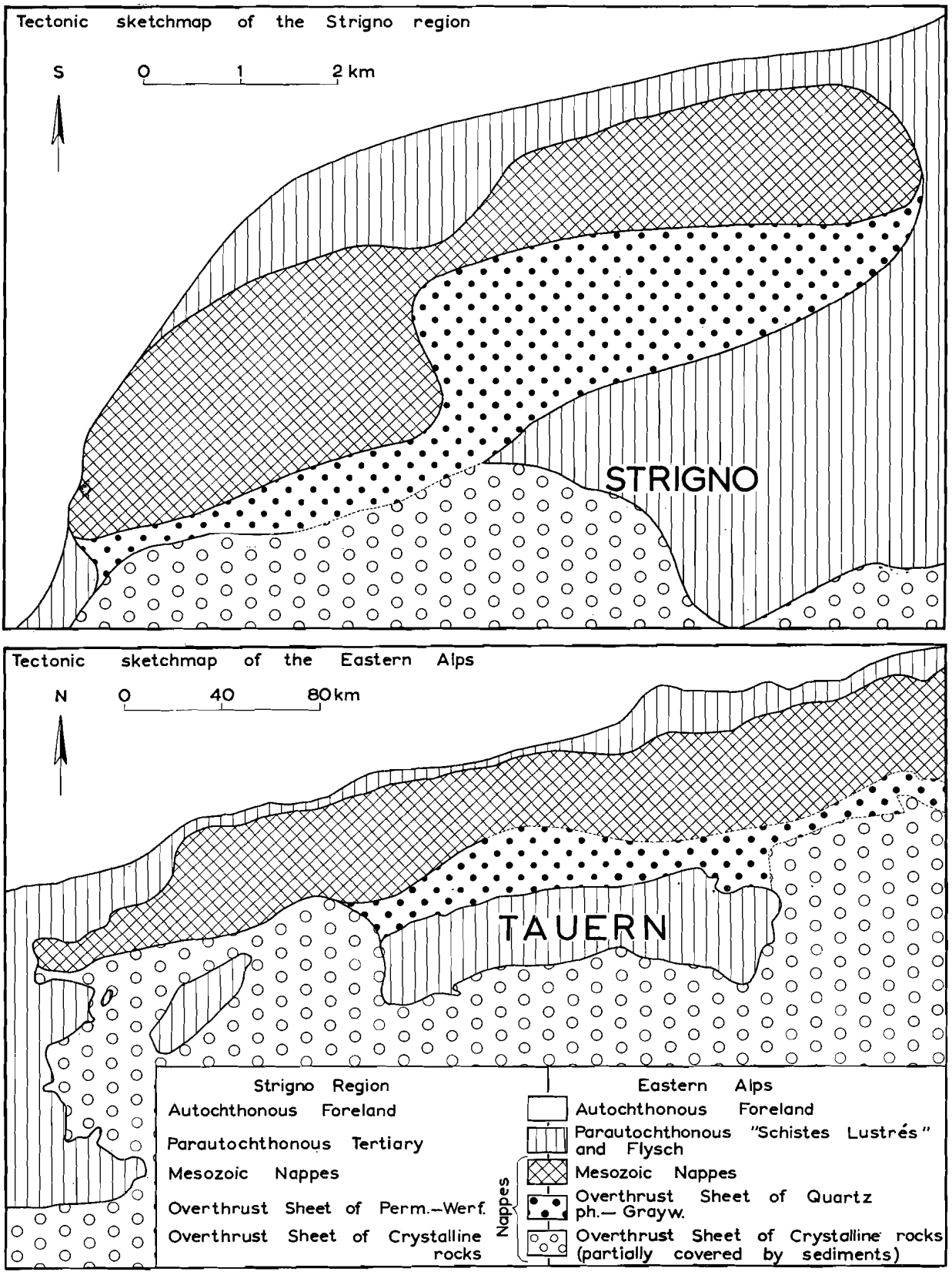

Fig. 107
A comparison between the Eastern Alps (lower side) and the Strigno region (upper side). For explanation see text.

This large Upper Austrian Nappe overthrusted the Pennide basin for more than 100 km. Actually, the situation is more complicated than discussed because below the Upper Austrian Nappe, Lower and Middle Austrian nappes are present, for instance, the "Matrei Zone" of the Tauern Inlier which was overridden by the large Upper Austrian Nappe. Furthermore, the Mesozoic of the eastern side of the Ötz Mass is overlain by the Steinach Nappe consisting of quartz phyllites and Carboniferous (sheet I).

If these complications are left out of consideration, the situation is simplified to fig. 107 (lower side) which may be compared to a tectonic sketch-map of the Strigno region (fig. 107 upper side).

The following five analogous units have been indicated by similar symbols in this figure.

1) The autochthonous foreland.

As illustrated by section V and VI (fig. 83), this foreland in the Strigno region consists of undisturbed subhorizontal Permotriassic sediments. In the eastern Alps, it is formed by crystalline rocks covered by the Bavarian Molasse.

2) Parautochthonous rocks.

In the Strigno region these rocks are Tertiary. In the western area they are subhorizontal and they have been overridden by the nappes (Sections V and VI). The Tortonian sediments were deposited during the formation of the nappes, as presumably Tortonian conglomerates occur between the units 3 and 4. The analogous "schistes lustrés" of the East Alps partially were injected by Pennine nappes.

The M. Lefre and Civeron Nappes at their South side are bordered by a strongly folded belt of Tortonian rocks which may be compared to the Helvetic belt and the Flysch belt in front of the Allgäu Nappe of the eastern Alps.

3) Mesozoic nappes.

The M. Lefre and Civeron nappes are formed by sliding of the sedimentary cover of the Cima d'Asta quartz phyllites. The uppermost strata moved furthest foreward and as a result the parautochthonous mantle of Tertiary in the South is covered by Upper Triassic strata, whereas older rocks are absent.

The Austrian Limestone Nappe (= Northern Limestone Alps) is more complicated. According to older concepts it is formed by accumulation of secondary nappes. In the western area the Allgäu Nappe was assumed to be covered by the Lechtal Nappe, and the latter by the Inntal Nappe. The modern German schools (Kockel, Richter, Schmidt-Thomé) consider the upper nappes as mushroom folds squeezed out from the lower nappes (Sheet I).

The sliding of the Mesozoic nappes over the underlying crystalline rocks probably was not large, as the Ötz Crystalline SW of Innsbruck is covered by Mesozoic rocks which might have been deposited South of the Mesozoic of the Northern Limestone Alps. Furthermore, the contact between the Mesozoic of the Staufen Nappe and the underlying graywackes is normal.

In consequence, the large overthrust plane of the Austrian nappes was probably located between the units 2 and 3 - 5 combined.

4) The subhorizontal Permian and Werfenian strata of the Strigno region may be compared with the subhorizontal quartz phyllites and graywackes North of the Tauern Inlier of the eastern Alps. Both have an intermediate position between the over- and underlying units 3 and 5.

5) Overthrust sheet of crystalline rocks.

The quartz phyllites of the Strigno region at Carzano lie on Tertiary. These rock units are compared with the Austrian gneisses of e.g. the Silvretta and Ötz Masses which form a sheet, several kilometers thick, and are partially covered by sedimentary rocks.

Because of the structural resemblance, the kinematics of the Strigno region may serve as a model for the kinematics of the eastern Alps.

It has been discussed in chapter 16, that during the Tortonian a tectonic graben originated South of the Sugana Line. This graben formed a morphologic depression which was filled up by nappes sliding down from the North.

The Strigno area is about 40 times smaller than the analogous area of the eastern Alps, and can be easier surveyed. On the other hand, its dimensions and the time range of its kinematics can be compared with the dimensions and time range of the Austride tectonics.

Our conclusion is that the Austrian Nappe probably originated by a sideward (i.e. northward) spreading out of a column consisting of the units 5, 4 and 3 over unit 2. This gravitational concept was developed by van Bemmelen (1933, 1960a and b). He assumed that the above mentioned Po Plain asthenolith continued eastward into the Adriatic Tumor, which was largely submarine and did not cause an uplift of strata above sea-level, was simultaneously counteracted by downsliding and spreading of the rocks toward the Tauern Foredeep, located to the North.

The tectonics of the eastern Alps are more complicated than the Strigno tectonics, as the former were subsequently uplifted along the Tauern-Engadin axis in Oligocene-Miocene time. This later Alpine uplift caused 1) Northward movements with further compression in the Northern Limestone Alps, North of the axis of uplift; e.g. the northern borderfault of the Ötz Mass at that time was possibly formed as a toppled over normal fault.

2) Southward movements with compression in the still undisturbed Southern Limestone Alps, South of the axis of uplift.

All tectonics described in part III belong to this Late Alpine phase.

The occurrence of the Austrides is restricted to the eastern Alps. According to earlier concepts they must have covered the western Alps where they should be absent at present due to erosion.

De Sitter (1956) a.o. assumed that the Austrides have developed only in the eastern Alps. The Préalpes formerly were considered as Austrides, (e.g. Staub's concept in our fig. 105). Their sediments are now considered as deposited between the Helvetide and Pennide basin (de Sitter, 1956) or in the Pennide basin (Trümpy, 1958). For this reason, they cannot be considered anymore as being an argument for the presence of a large Austrian Nappe in the western Alps.

The following argumentation supports this view. As shown in fig. 105, the Alps are arc-shaped at their western side. The material moved outward at right angles to the arc. In the hitherto discussed areas it moved northward. West of the Po Plain, however, it moved Westward and SW of the Po Plain (Mercantour region) southwestward and southward. The arc-shape is explained by assuming that the Cretaceous Tumor disappeared in the western Po Plain. If this tumor caused the gravitational downsliding of the Austrian Nappe, a more than 100 km northward movement in the western Alps cannot have taken place next to a more than 100 km southward movement in the Mercantour region. Although the Austrian nappes might have been lengthened during their formation, the available space is insufficient for more than 100 km of large nappes to move north-, west-, and southward, unless large crustal shortening is accepted.

It is possible to explain Alpine tectonics as secondary reactions to the formation of an asthenolith as proposed by van Bemmelen. For the Alps these secondary reactions principally are the formation of sliding nappes in the upper strata and the injection of magmatic material in lower strata.

It is interesting to compare the region under discussion with the Caledonides of East Greenland, where the upper strata are hardly deformed whereas the lower "Stockwerk" is characterized by a nappe structure analogous to the Pennine nappes of the Alps (e.g. Wenk, 1956, Haller's fig. 7, 1956).

The relatively undeformed shape of the upper strata demonstrates the absence of crustal shortening. For this reason, crustal shortening in the Alps may be considered as absent too, although the strong deformation of the upper "Stockwerk" prevents a direct conclusion to be drawn. Gravimetric calculations are not in contradiction with the no-crustal shortening concept of van Bemmelen (van Bemmelen, 1953 and Hospers, 1957).

§ 23B *Pennine Nappes.*

Hitherto the tectonics of the upper "Stockwerk" have been considered to be gravitational (epidermal and dermal tectonics of van Bemmelen, fig. 106). They are characterized by an upward increasing degree of deformation.

In the lower "Stockwerk" also movements occurred (bathydermal tectonics of van Bemmelen); rheomorphic migma was horizontally injected. These tectonics also may affect the upper "Stockwerk" causing a downward degree of deformation as a result of drag.

The Pennides are present in the western Alps as well as in the eastern Alps. The figures 108 and 109 represent the Simplon section and a Tauern

section; the positions of both sections are indicated in fig. 105.

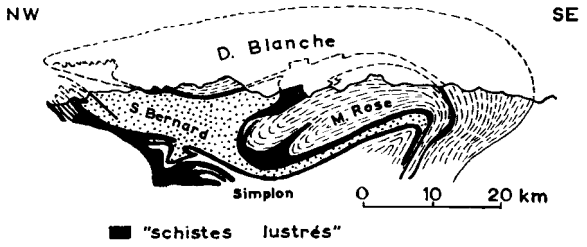

Fig. 108
Classical section across the Pennine nappes at the Simplon Pass according to Argand (see e.g. Heim, 1922, Profil 2 of Tafel XXIII). Position depicted in fig. 105.

According to Argand, the order of injection in the Simplon nappes was: 1° S. Bernard Nappe, 2° D. Blanche Nappe, and 3° M. Rose Nappe (fig. 108).

Karl and Schmidegg assumed that the Zillertaler Nappe is the only Pennide of the western Tauern Inlier. The northern augen-granite gneiss is considered as a pre-Alpine mass, which may be compared with the Hercynian masses of the Western Alps.

Some structural questions are unsolved; the M. Rose and S. Bernard nappe have elsewhere been assumed to form a single unit (Goguel, 1952), and

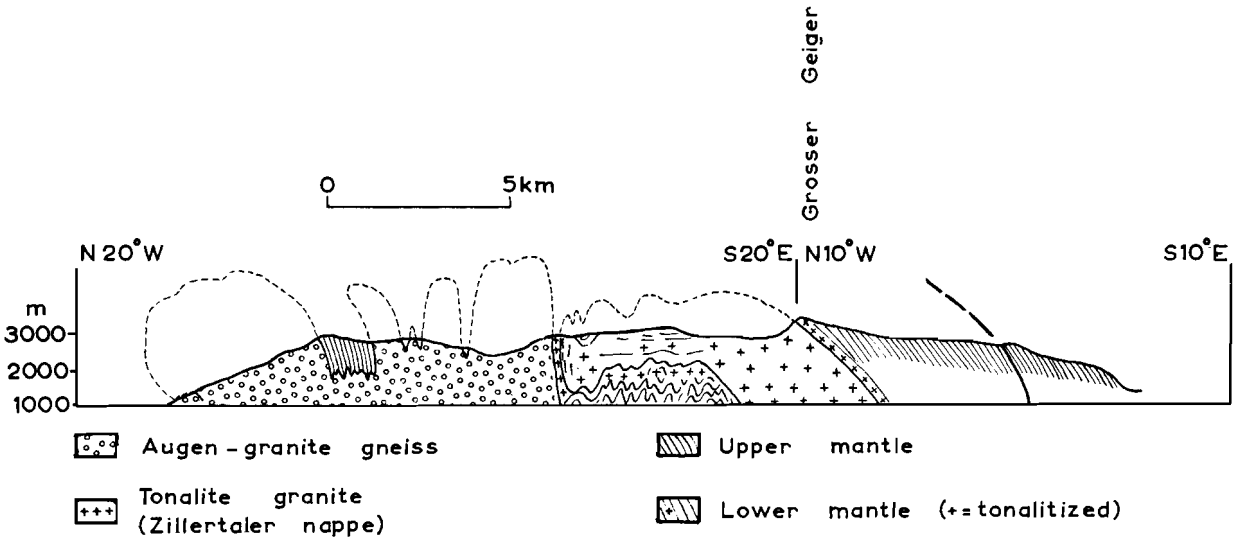

Fig. 109
Section across the western Tauern Inlier according to Karl and Schmidegg (Karl, 1959, Tafel III). Position depicted in fig. 105.

Karl's augen-granite gneisses perhaps belong to another Pennide.

Pennides with a core of an Alpine "ortho" rock and a mantle of partially crystalline rocks and partially "schistes lustrés" are present in the lower "Stockwerk" of the Alps. Wenk (1953) assumed an Alpine age of the "ortho" cores for the western Alps and Karl (1959) considered the tonalite cores of the eastern Alps to be of the same age.

Staub and Argand assumed the steep root zone of the Pennides of the Western Alps to have formed during the Insubric phase when the originally flat Pennides became steeper at their backside. As discussed in chapter 21 this concept is supported by the tectonics of the M. Spico region. At the other hand, Wenk (1953) considered the vertical position of the root zone in the western Alps as a primary structure caused by vertical intrusion of the syntectonic "ortho" cores.

The structure of the Pennides suggests large-scale subhorizontal mass transport in the lower "Stockwerk". Our Alpine intermediate phase (§ 22E) might have originated by a mass transport in lower levels which cannot be studied directly. It caused the relative northward movements of the Dolomites block.

The "Schlingenbau" of the East Alpine root zone generally was considered as pre-Alpine. We have argued that they are of Alpine age and this feature may be compared with the "Schlingenbau" in the northern and southern zone of the Pennides of Ticino, investigated by Wenk (1955).

It may be stated that the Alps are an example of an orogene which originated in two main phases as was suggested by van Bemmelen (1960a and b). During the first phase, the material moved outward from the Po- and Venetian Plain centre. During the second phase, considerable smaller movements occurred from the Tauern-Engadin axis outward. Crustal shortening during these two phases of Alpine orogenesis is not probable.

The accumulation of different types of nappes, and the formation of isoclinal series of strata with subvertical positions suggesting local shortening, probably were accompanied by equivalent stretching of the compressed strata and their extensions in adjacent areas.

Accumulation of nappes without shortening of the framework is evident for smaller more surveyable areas as the Strigno region.

The M. Spico region (section VIII) indicates that an isoclinal subvertical series of strata can be formed by doming. The resulting structures do not prove shortening of the framework, as their limbs were simultaneously elongated by stretching.

APPENDIX I

94 sketches of minor structures from the crystalline basement of the Dolomites, and the M. Spico region.

These drawings are more or less schematic as topographic irregularities have been eliminated. They all represent cross sections which are about at right angles to the axis of the minor structure; they belong to the chapter on folds of the crystalline rocks (Ch. 3) and are also illustrations of the minor folds compiled in appendix II. The folded rock is a quartz phyllite, unless another rock is indicated. Grid co-ordinates are given in parentheses.

Hercynian minor structures of the Pusteria Crystalline.

1 (813-827)
2 (813-827)
3 (813-828)
4 (814-831) - boulder
5 (809-827)
6 (817-826) - tendency to parallel folding
7 (814-811)
8 (903-812) - some S_2 formation
9 (723-863) - green phyllite with accordion folding
10 (922-803)
11 (813-802)
12 (726-812)
13 (983-818) - mushroom-shaped fold
14 (854-831)
15 (851-828) - mushroom-shaped fold
16 (833-813) - the eastermost syncline shows no crestal bend; this has been broken by shearing movements along the old *S*-planes
17 (839-813) - plastical folding indicated by (dotted) quartz veins
18 (813-826) - sharply defined (dotted) quartz lenses
19 (802-821) - ditto
20 (792-825) - irregular quartz veins
21 (823-825) - quartz lens exercising protection against crumpling
22 (807-819) - bending of the competent quartz veins, and S_2 formation in the phyllitic material
23 (710-797) - conglomeratic quartzite with reddish quartz pebbles elongated in the direction of the axes of minor folds

Hercynian minor structures of the Bressanone Crystalline

24 (044-773)
25 (048-781) - ribs and minor folds; the ribs are restricted to places with coarse albite crystals
26 (113-804) - S_2 intersecting S_1
27 (209-757) - parallel folded quartz vein

Hercynian minor structures of the S. Stefano Crystalline

28 (104-624) - *S*-plane with readily steepening of the axes of minor folds
29 (102-631) - quartzite
30 (103-641)
31 (106-645) - ribs and younger minor folds with slightly different axes
32 (103-641) - quartzitic phyllite
33 (102-649) - quartzite

Hercynian minor structures of the Cima d'Asta Crystalline

34 (101-146)
35 (051-200) - disharmonic folding with westward overturn
36 (066-131) - quartzite with mushroom-shaped fold indicating that conclusions on regional mass transport cannot be based on single overturned minor folds
37 (971-154) - disharmonic folding with westward overturn
38 (081-145) - quartzite
39 (015-205) - quartzite (left side of sketch = eastern side)

40 (086-137) - subhorizontal S_2 in the phyllitic material; the competent quartz veins have been bent
41 (971-074) - folded quartz veins
42 (136-182) - folded S_2-planes (different scales parallel and at right angles to S_2) secondary mineralogic banding parallel to S_2 being an alternation of (indicated) feldspar-mica and quartz rock
43 (136-182) - ditto; the angle between S_1 and S_2 amounts to about 45°
44 (080-130) - feldspar augen
45 (136-175) - ditto
46 (136-175) - ditto, originally conformably intercalated (?) and later intersecting the S-planes as euhedral poikiloblasts
47 (136-175) - ditto, intersecting the minor folds

Alpine minor structures of the crystalline basement of the Dolomites

48 (982-801) - Southward overturned overthrust flexure and fault in the Upper Silurian (?) limestone of Prato alla Drava, Pusteria region
49 (910-800) - flexure zone from eastern Pusteria region
50 (947-797) - Alpine minor fold with eastward overturn intersecting the Hercynian minor folds at right angles; eastern Pusteria region
51a(954-802) - Alpine bends of Hercynian minor folds, Pusteria region
51b(126-603) - ditto, S. Stefano region
51c(128-603) - ditto
52 (043-701) - minor graben structure at M. Croce Pass, North of S. Stefano region, indicating SW-NE extension
53 (205-766) - two intersecting systems of flexure zones, maximum shortening along the vertical, Bressanone region
54 (089-136) - fold with minor folds in cataclastic rock, parallel to the Alpine Sugana Line and at right angles to the Hercynian minor folds, Cima d'Asta region
55 (061-155) - flexure zones (left side of sketch = southeastern side), Cima d'Asta region
56 (971-075) - see 53, Cima d'Asta region
57 (953-058) - disharmonic folding with axes parallel to the Sugana Line and at right angles to the Hercynian minor folds, indicating Alpine shearing movements; this minor structure has been taken from the steep limb of an Alpine major fold South of Samone, Strigno region
58 (953-058) - boudins of quartz vein, indicating Alpine stretching in N-S direction, Strigno region

Alpine minor structures of the M. Spico Crystalline

59 (775-058) - ordinary gneiss
60 - ordinary gneiss at Moos (Schneeberger Zone)
61 - amphibolite with anticline without crestal bend; point 1280 along the Moos-Timmels section across the Schneeberger Zone
62 (139-968) - Rieserferner augen-gneiss
63 (246-000) - ditto
64 (150-973) - ditto
65 (244-999) - ditto
66 (217-044) - calcareous phyllite, the folded layer is more calcareous
67 (147-975) - calcareous phyllite
68 (245-999) - Rieserferner augen-gneiss
69 (246-009) - ditto
70 (123-986) - calcareous phyllite
71 (254-987) - ordinary gneiss
72 (153-021) - map of minor folds with subvertical axes in stratified limestone
73 (756-029) - contact-metamorphic gneiss
74 (186-045) - tonalite gneiss, type IIa; in the crestal bends some S_2 formation (not indicated)
75 (205-063) - tonalite gneiss, type II
76 (167-036) - ditto
77 (166-050) - transition between ordinary gneiss and tonalite gneiss, type II
78 (206-062) - tonalite gneiss, type II, intercalated between saccharoidal limestones

79 (191-032) - calcareous phyllite; map of boudinlike structure with quartz lens
80 (247-002) - Rieserferner augen-gneiss, wedging out
81 (245-011) - ditto
82 (255-991) - contact-metamorphic gneiss, wedging out
83 - Anterselva granite gneiss with southward overturned overthrust flexures, East of S. Maddalena in Casies (Defereggen Mountains)
84 (140-046) - southward overturned overthrust flexure in tonalite gneiss, type I (position of figure to the left of fig. 80)
85 (747-021) - low angle normal faults in contact-metamorphic roof gneisses of the Rieserferner tonalite, indicating stretching
86 (753-026) - ditto

Some Alpine minor structures of the Permotriassic of the Dolomites

87 (162-591) - map of flexure with subvertical axis in Bellerophon limestones, S. Stefano region (case 6 of table VII)
88 (162-591) - ditto
89 (069-562) - southward overturned minor fold in Werfenian beds, S. Stefano region (case 4 of table VII)
90 (059-558) - steeply East dipping minor fold from the southern limb of the Ansiei Werfenian syncline, S. Stefano region (case 5 of table VII)
91 (950-013) - southward overturned minor overthrust faults in Tortonian beds of Strigno region
92 (085-117) - cleavage in Biancone limestones of Cima d'Asta region; the distance between the cleavage-planes amounts to about 1 cm
93 (285-793) - minor normal fault in Permotriassic of Pusteria region
94 (278-786) - minor wrench fault in Permotriassic of Pusteria region

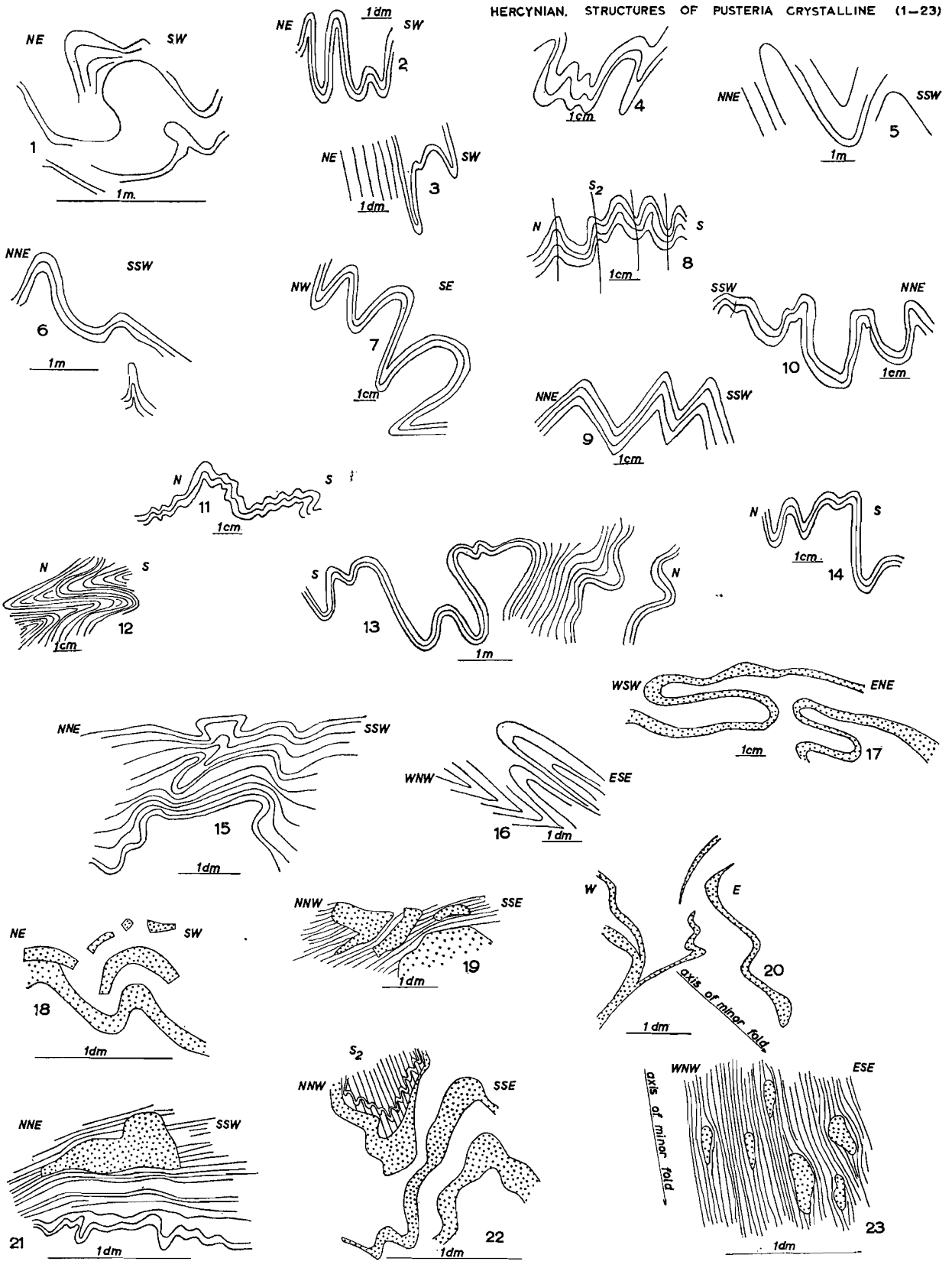
HERCYNIAN. STRUCTURES OF PUSTERIA CRYSTALLINE (1–23)
NE
SW
1
1m.
NE
1dm
SW
2
NE
SW
3
1dm
1cm
4
NNE
SSW
5
1m
NNE
SSW
6
1m
NW
SE
7
1cm
S2
N
S
8
1cm
SSW
NNE
10
1cm
NNE
SSW
9
1cm
N
S
11
1cm
N
S
12
1cm
S
N
13
1m
N
S
1cm.
14
WSW
ENE
1cm
17
NNE
SSW
15
1dm
WNW
ESE
16
1dm
NE
SW
18
1dm
NNW
SSE
19
1dm
W
E
axis of minor fold
20
1 dm
S2
NNW
SSE
22
1dm
NNE
SSW
21
1dm
WNW
ESE
axis of minor fold
23
1dm

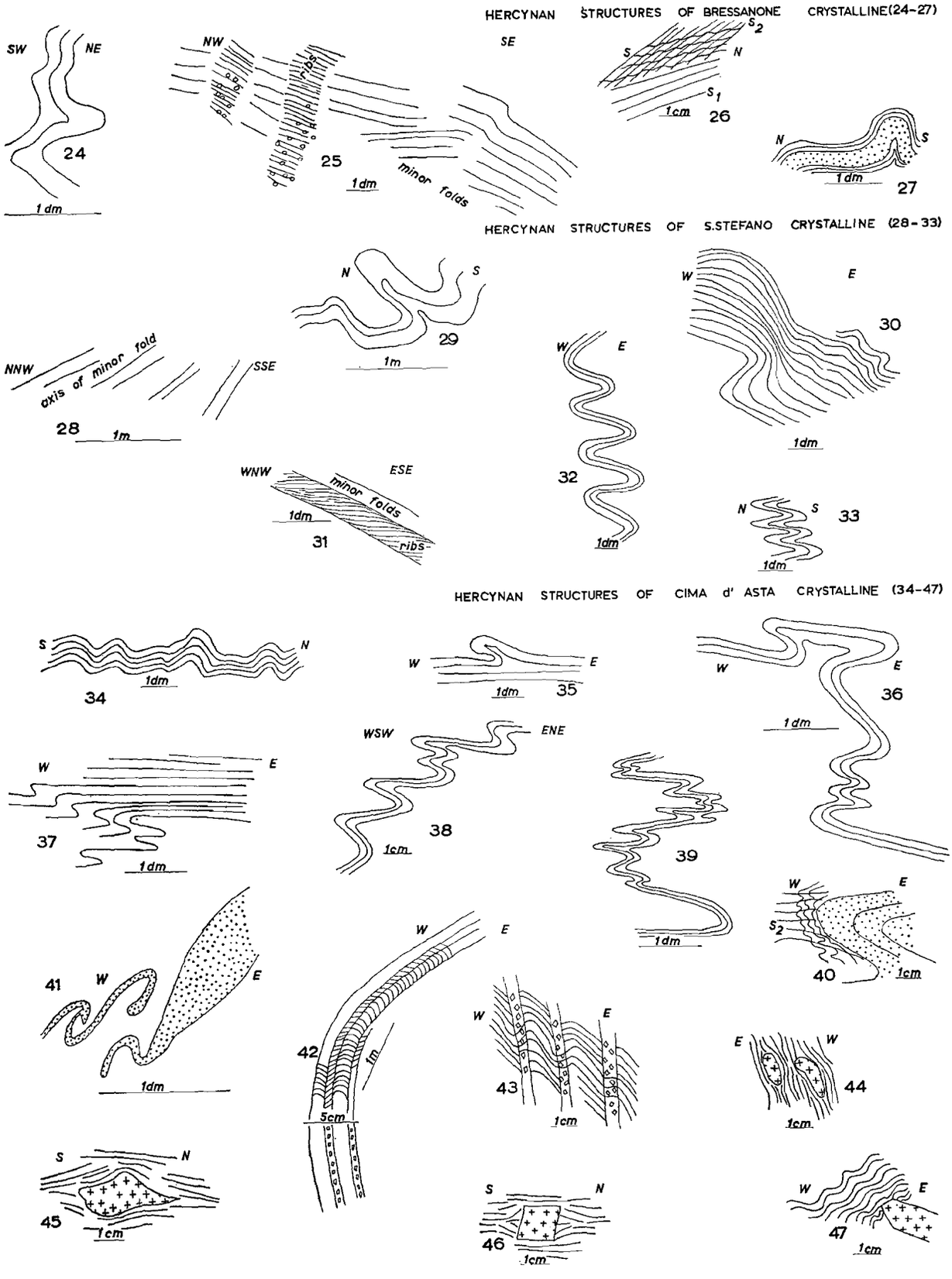
HERCYNAN STRUCTURES OF BRESSANONE CRYSTALLINE(24-27)
SW
NE
24
1 dm
NW
SE
ribs
25
1 dm
minor folds
S2
S
N
S1
1 cm
26
N
S
1 dm
27
HERCYNAN STRUCTURES OF S.STEFANO CRYSTALLINE (28-33)
N
S
29
1m
NNW
axis of minor fold
SSE
28
1m
W
E
30
1 dm
W
E
32
1dm
WNW
ESE
minor folds
1dm
31
ribs
N
S
33
1dm
HERCYNAN STRUCTURES OF CIMA d' ASTA CRYSTALLINE (34-47)
S
N
1dm
34
W
E
1dm
35
W
E
36
1 dm
W
E
37
1 dm
WSW
ENE
38
1cm
39
1 dm
W
E
S2
40
1cm
41
W
E
1dm
W
E
42
1m
5cm
W
E
43
1cm
E
W
44
1cm
S
N
45
1 cm
S
N
46
1cm
W
E
47
1cm

ALPINE STRUCTURES OF CRYSTALLINE BASEMENT OF DOLOMITES (48-58)

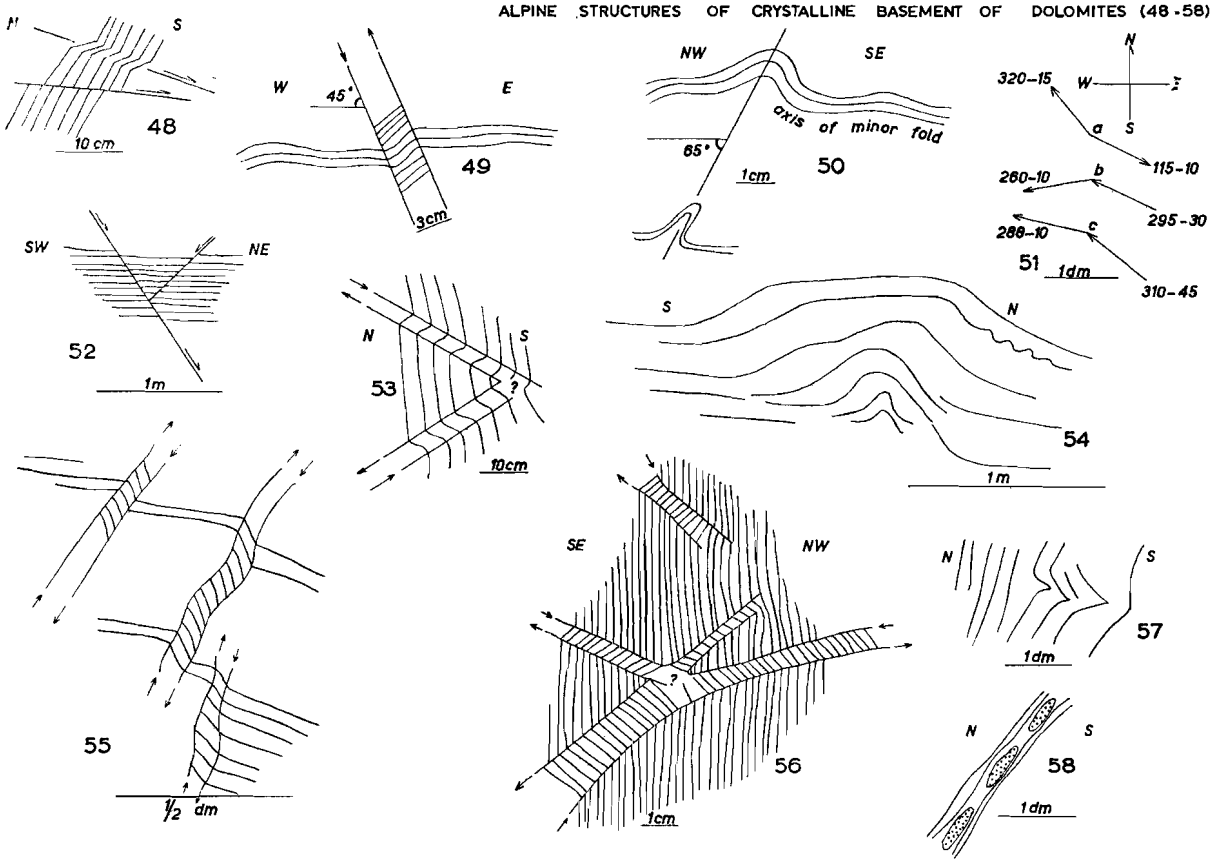

ALPINE STRUCTURES OF M.SPICO CRYSTALLINE (59-69)

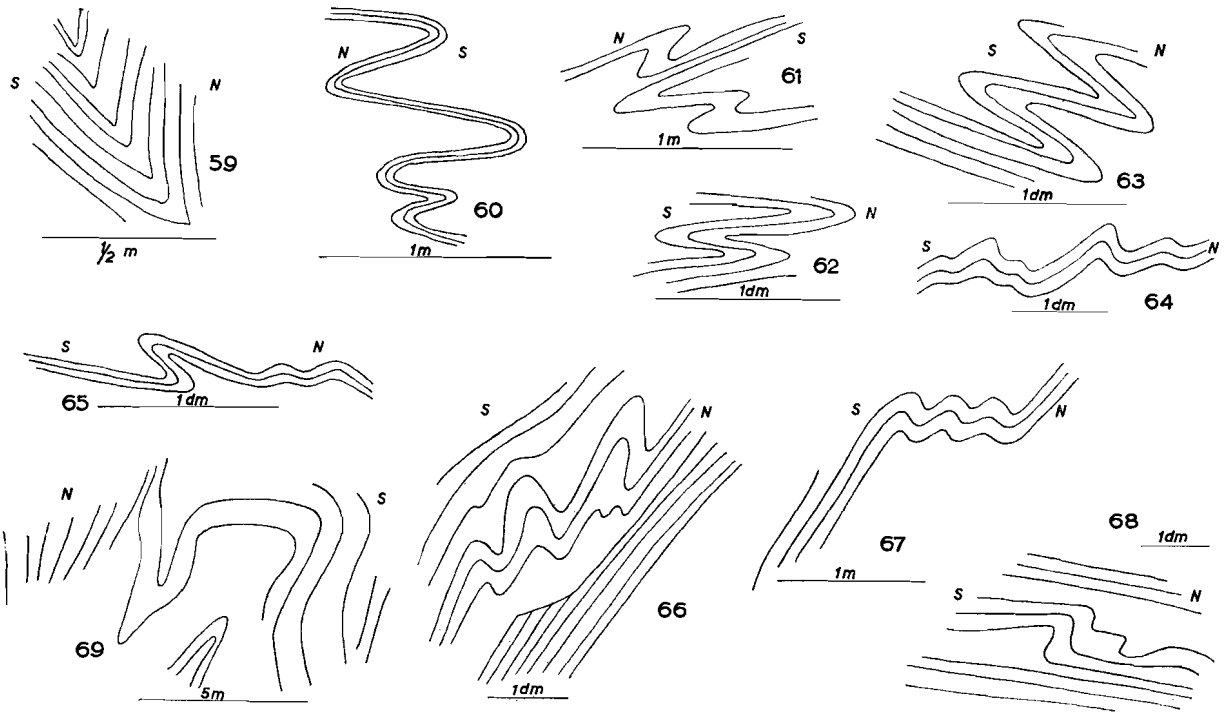

ALPINE STRUCTURES OF M.SPICO CRYSTALLINE (70–86)

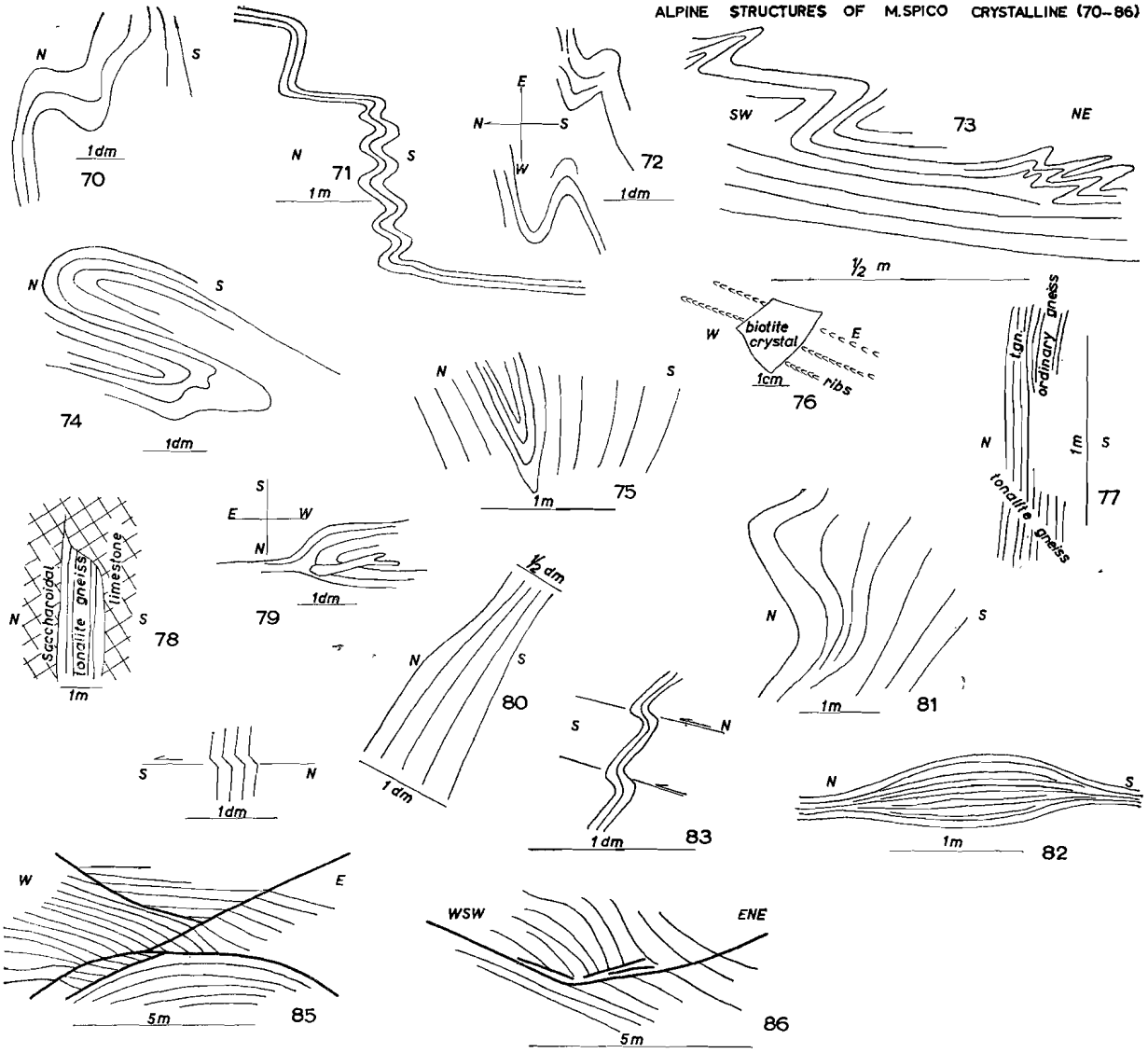

SOME ALPINE STRUCTURES OF PERMOTRIASSIC OF DOLOMITES (87–94)

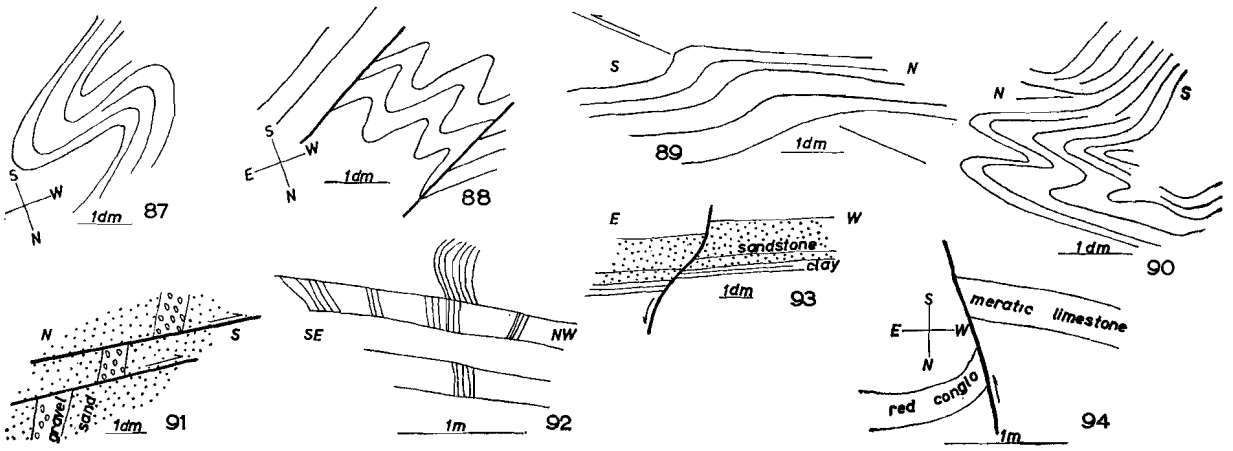

APPENDIX II

Tables of the positions of the *S*-planes and the minor folds

The positions of the individual *S*-planes and the minor folds are given with their grid co-ordinates. The grid is shown on the map sheets. The grid co-ordinates are accurate up to 50 m.

The position of the *S*-planes is given by strike and dip. The strike is defined as direction of dip minus 90° (according to Trooster and van Landewijk, 1958).

The position of the minor folds is given by azimuth and dip. The azimuth is the direction of dip.

E.g., in meas. sample 1:
co-ordinates of the grid: 101-633 with
position of *S*-plane : 235°-37° and
position of m.f. : 360°-45°, and so on.

The grid co-ordinates of the measurements of the samples 90, 91, and 138-141 are missing.

Groups of measurements have been collected in measurements samples (= meas. samples), consisting of a number of *S*-planes and minor folds.

E.g., meas. sample 1 (38 s. and 52 m.f.).

The *S*-planes of a meas. sample have a mean *S*., and the minor folds have a mean m.f. Both these means thave their own grid co-ordinates.

E.g. the mean *S*. of meas. sample 1 is 289° - 65° with grid co-ordinates 102-631 and the mean m.f. is 305° - 7° with 102 - 632.

These means have been calculated by approximation and are represented by the mean strike and the mean dip of the *S*-planes, and the mean azimuth and the mean dip of the minor folds respectively.

The meas. samples have been collected by:

S. Stefano region (1- 16)
by F. P. Agterberg (1958)
Pusteria region (17- 91)
by F. P. Agterberg (1957)
Bressanone region (92-114)
by F. P. Agterberg (1957-'58)
Bressanone region (115-141)
by G. H. W. Nijenhuis (1958)
Bressanone region (142)
by B. G. Engelen (1959)
Cima d'Asta region (143-173)
by F. P. Agterberg (1959)
Cima d'Asta region (174-192)
by T. L. R. Findhammer (1959)
Gosaldo region (193-215)
by M. Freudenthal (1959)
M. Spico region (216-270)
by F. P. Agterberg (1960)

Apart from the measurements by Findhammer and Freudenthal (174-215) the strikes of the *S*-planes and the azimuths of the minor folds are given without the magnetic correction of —2°.

REMARKS:

1. Measurements in slumped blocks may have caused occasional errors.

2. If the dispersion is strong, some measurements of other populations of m.f. may occur amongst the measured m.f., e.g., younger Alpine m.f. or Hercynian m.f. formed simultaneously but at right angles to the general m.f. (crossfolds as shown by photograph 4).

3. In the Cima d'Asta and Gosaldo regions some *S* actually are S_2. However, the position of S_2 approximates the position of the original undeformed S_1.

The above mentioned errors may influence the calculated means. The influence, if present, is small, as larger numbers of deviating measurements do not occur (see the pole diagrams of appendix III).

Tables of the positions of the schistosity - planes and the axes of the minor folds in the S. Stefano region (Sheet II).

(The strikes of the s-planes and the azimuths of the m.f. are given without the magnetic correction of — 2°.)

Meas. sample 1 (38 s. and 52 m.f.)

	mean s.	mean m.f.
102—631	289°— 65°	
102—632		305°— 7°

co-ordinates of the grid	position of s-plane	position of m.f.
101—633	235°— 37°	360°— 45°
	265°— 47°	365°— 35°
	315°— 70°	265°—-30°
	315°— 90°	315°— 15°
	300°— 65°	285°—-52°
	245°— 45°	295°— -2°
	275°— 95°	290°— 30°
		315°—-17°
103—640	280°— 70°	272°—-29°
	280°— 75°	300°— -5°
	310°—102°	280°— 40°
	290°— 83°	310°—-43°
		302°—-48°
		265°—-45°
		330°— 20°
		295°— 50°
		295°— 5°
101—625	280°— 60°	
103—622	225°— 43°	320°— 25°
	235°— 33°	275°— 33°
	240°— 42°	360°—-30°
	225°— 55°	280°— 40°
	235°— 55°	
	210°— 35°	
104—623	340°— 85°	295°— 10°
	335°—125°	345°— 32°
	340°— 80°	330°— 60°
100—631	315°— 25°	310°— 0°
104—626	360°— 85°	330°—-20°
102—629	295°— 50°	300°— 40°
	290°— 65°	300°— 5°
	295°— 55°	290°— 30°
		285°— 20°
		320°— 35°
		305°— 0°
		325°— 15°
102—630	280°— 65°	340°— 40°
	290°— 60°	285°— 10°
	310°— 65°	
102—631	285°—105°	290°— 10°
	295°— 45°	265°—-12°
		295°— 5°
		310°— 15°
		300°—-30°
103—633		285°—-30°
		320°— -5°
103—634	295°—123°	290°—-10°
103—635	335°— 52°	285°—-20°
		320°— 15°
		320°— 10°
		300°— 10°
103—636	315°— 60°	300°— 20°
	320°— 40°	310°— 12°
	310°— 58°	270°— -5°
103—637	315°— 70°	295°— 0°
104—640	290°— 43°	335°— 30°

Meas. sample 2 (14 s. and 33 m.f.)

	mean s.	mean m.f.
104—646	308°— 52°	
104—646		114°— 15°

co-ordinates of the grid	position of s-plane	position of m.f.
106—645	290°— 60°	115°— 10°
	290°— 58°	70°— 20°
	315°— 60°	95°— 12°
		110°— 18°
		100°— 15°
		120°— 0°
		120°— 10°
		130°— 22°
		82°— 28°
		110°— 25°
		115°— 25°
105—646	305°— 40°	130°— 0°
	325°— 55°	130°— 10°
	298°— 38°	128°— 5°
		110°— 3°
		87°— 15°
104—646	315°— 52°	120°— 10°
	305°— 48°	115°— 20°
	330°— 32°	130°— 20°
	310°— 57°	125°— 34°
		115°— 30°
		110°— 20°
103—647		112°— 28°
		140°— 12°
		125°— 23°
		140°— 5°
102—647	295°— 60°	90°— 20°
		100°— 10°
102—648	290°— 65°	105°— 10°
	315°— 42°	120°— 18°
	330°— 53°	125°— 17°
		150°— 0°
102—649		80°— 5°

Meas. sample 3 (17 s. and 26 m.f.)

	mean s.	mean m.f.
096—655	298°— 48°	
097—654		291°— 8°

co-ordinates of the grid	position of s-plane	position of m.f.
098—652	270°— 50°	295°— 20°
	320°— 57°	310°— 17°
	270°— 50°	310°— 30°
		280°— 8°
		350°— 38°
		265°—-17°
		305°— 10°
		290°— 13°
		300°— 2°
		330°— 12°
		285°— 25°
097—653	320°— 57°	330°— 20°
		315°— 5°
		250°—-10°
		250°—-15°
096—657	310°— 17°	285°— -3°
	300°— 32°	295°— 3°
	295°— 60°	270°—-15°
	— 0°	275°—-22°
	310°— 30°	260°—-30°
	300°— 55°	260°— -3°
096—658	310°— 75°	300°— 10°
095—657	270°— 40°	330°— 25°
		280°— 28°
094—656	290°— 65°	300°— 55°
	270°— 70°	250°— 0°
	325°— 60°	
094—655	300°— 60°	
092—651	310°— 30°	

Meas. sample 4 (8 s. and 26 m.f.)

	mean s.	mean m.f.
081—642	311°— 30°	
081—642		315°— 18°

co-ordinates of the grid	position of s-plane	position of m.f.
082—643	300°— 55°	320°— 10°
	305°— 35°	320°— 18°
		315°— 15°
		300°— 30°
		305°— 3°
		325°— 15°
081—643	335°— 40°	275°— -5°
	315°— 20°	320°— 28°

		335°— 15°
		350°— 20°
		315°— 2°
		300°— 23°
		245°—−15°
		310°— 18°
081—642	315°— 25°	325°— 18°
		335°— 30°
		360°— 30°
		330°— 35°
		315°— 35°
		280°— 22°
		335°— 8°
		300°— 10°
080—641	275°— 45°	300°— 43°
	315°— 25°	335°— 33°
		330°— 7°
081—641	330°— −5°	305°— 25°

Meas. sample 5 (13 s. and 14 m.f.)

	mean s.	mean m.f.
109—648	296°— 48°	
108—648		112°— 14°

co-ordinates of the grid	position of s-plane	position of m.f.
107—647	315°— 50°	130°— 5°
	305°— 65°	135°— 10°
108—648	325°— 43°	85°— 25°
	290°— 33°	145°— 20°
	305°— 40°	120°— 0°
	275°— 45°	105°— 2°
		105°— 27°
		110°— 13°
109—649	315°— 30°	95°— 3°
	293°— 50°	95°— 27°
	290°— 42°	110°— 25°
		125°— 18°
109—650	265°— 65°	100°— 18°
	290°— 57°	
109—648	295°— 50°	
110—648	290°— 55°	105°— 0°

Meas. sample 6 (16 s. and 22 m.f.)

	mean s.	mean m.f.
098—610	268°— 58°	
100—610		295°— 14°

co-ordinates of the grid	position of s-plane	position of m.f.
106—613	280°— 70°	275°—−38°
		265°— 20°
105—613	260°— 55°	285°— 25°
	250°— 65°	260°— −5°
107—610		305°— 27°
105—612		300°— 30°
103—612	335°— 90°	335°— 20°
	265°— 43°	320°— 30°
		330°— 15°
		360°— 15°
103—607		260°— 30°
		300°— 25°
103—606		280°— −3°
		290°— 10°
101—607	275°— 65°	300°— 10°
102—603	315°— 75°	
	260°— 48°	
098—607	285°— 60°	320°— 27°
	230°— 60°	
093—610	260°— 67°	270°— 20°
		295°— 5°
092—611	240°— 40°	275°— 22°
	230°— 43°	315°— 10°
	308°— 50°	290°— 10°
091—612	240°— 38°	270°— 12°
089—613	255°— 65°	

Meas. sample 7 (7 s. and 23 m.f.)

	mean s.	mean m.f.
113—621	295°— 58°	
112—620		329°— 33°

co-ordinates of the grid	position of s-plane	position of m.f.
109—617	255°— 50°	350°— 30°
		315°— 40°
110—618		310°— 42°
		340°— 50°
111—619	255°— 68°	345°— 15°
		330°— 33°
		315°— 35°
		360°— 25°
		265°— 50°
		325°— 40°
		370°— 50°
		395°— 40°
		345°— 40°
		340°— 70°
112—619		315°— 55°
		345°— 40°
112—620	260°— 45°	360°— 48°
115—622	315°— 60°	340°— 30°
	345°— 50°	320°— 27°
	345°— 45°	340°— 3°
		225°—−15°
115—623	290°— 90°	290°— 0°
		320°— 20°

Meas. sample 8 (10 s. and 26 m.f.)

	mean s.	mean m.f.
116—628	287°— 54°	
116—627		107°— 16°

co-ordinates of the grid	position of s-plane	position of m.f.
116—625	275°— 70°	160°—−10°
116—626	260°— 95°	135°— 40°
	280°— 60°	95°— 40°
	275°— 65°	80°— 25°
		110°— 25°
		75°— 20°
		105°— 18°
		100°— 10°
		110°— 23°
116—627	320°— 45°	95°— 40°
		120°— 40°
		95°— 25°
		95°— 25°
		100°— 5°
		85°— 25°
		110°— 15°
117—628	270°— 40°	
117—629	320°— 40°	120°—−18°
		115°— 0°
		100°— 10°
116—628	285°— 45°	105°— 12°
	265°— 7°	105°— 10°
		110°— 10°
113—627		100°— 0°
118—633	320°— 75°	140°—−15°
		110°— 15°
		105°— 25°

Meas. sample 9 (14 s. and 13 m.f.)

	mean s.	mean m.f.
129—646	299°— 68°	
129—646		112°— 15°

co-ordinates of the grid	position of s-plane	position of m.f.
133—642	320°— 80°	130°— 10°
128—646	300°— 90°	115°— 0°
	285°— 67°	115°— 30°
	320°— 70°	120°— 0°
	260°— 75°	106°— 11°
	295°— 90°	100°— 40°
	305°— 60°	90°— 12°
	300°— 45°	117°— 25°
	295°— 50°	110°— 23°
	280°— 68°	
	310°— 60°	
130—647	330°— 80°	150°— 10°
130—648	300°— 63°	70°— 25°
		100°— 30°
128—647	285°— 55°	135°—−20°

Meas. sample 10 (14 m.f.)

	mean m.f.
075—653	342°— 21°

co-ordinates of the grid	position of s-plane	position of m.f.
074—652		330°— 0°
		340°— 15°
		335°— 5°
		330°— 57°

075—653		325°— 25°
		355°— 15°
		330°— 5°
		335°— 23°
		320°— 10°
		377°— 30°
		345°— 15°
		345°— 45°
		350°— 35°
		350°— 20°

Meas. sample 11 (19 s. and 29 m.f.)

	mean s.	mean m.f.
106—591	264°— 90°	
110—589		275°— 41°

co-ordinates of the grid	position of s-plane	position of m.f.
112—586	253°— 80°	240°— 40°
		255°— 40°
		245°— 43°
		240°— 65°
		270°— 80°
108—584		285°— 23°
119—588	235°— 70°	320°— 70°
		305°— 58°
118—588	255°— 60°	290°— 60°
		340°— 50°
		335°— 40°
110—588	240°— 83°	255°— 12°
		240°— 15°
		265°— 22°
		275°— 35°
		275°— 35°
		255°— 32°
109—589	255°— 70°	
107—591	270°— 75°	270°— 35°
	265°— 85°	280°— 12°
	285°—110°	
106—592	275°—130°	
105—592	280°—120°	
104—592	250°—115°	
104—592	270°—120°	
102—593	275°— 97°	290°— 20°
	285°— 75°	270°— 40°
		285°— 43°
	270°— 90°	275°— 35°
	265°— 60°	265°— 73°
	275°— 75°	265°— 30°
	250°— 100°	250°— 48°
	255°— 95°	240°— 50°
117—584		310°— 30°
116—584		280°— 60°

Meas. sample 12 (17 s. and 30 m.f.)

	mean s.	mean m.f.
161—614	289°— 56°	
159—613		89°— 16°

co-ordinates of the grid	position of s-plane	position of m.f.
165—612	265°— 60°	30°— 40°
		35°— 50°
		105°— 30°
		95°— 20°
165—613	275°— 80°	110°—-23°
	290°— 60°	
165—614	270°— 35°	95°— 15°
	260°— 65°	
	290°— 43°	
164—615	325°— 55°	
164—616	295°—120°	
163—617	320°— 30°	20°— 35°
		120°— 13°
		95°— 3°
162—617		95°—-18°
161—621	280°— 45°	120°— 0°
	285°— 45°	95°— 0°
161—623	275°— 45°	135°— -5°
		55°—-15°
		80°— 20°
158—613	305°— 40°	105°— 30°
		105°—-28°
157—613	345°— 42°	80°— 30°
		95°— 28°
		80°— 40°
155—610	315°— 55°	125°— 50°
		130°— 25°
		107°— 45°
		85°— 55°
149—606		55°— 35°
150—605		90°—-20°
		15°—-22°
151—604		150°—-20°
151—603	270°— 65°	
	250°— 75°	105°—-45°
		52°—106°

Meas. sample 13 (9 m.f.)

	mean m.f.
154—586	109°— 60°

co-ordinates of the grid	position of s-plane	position of m.f.
154—586		110°— 60°
		140°— 40°
		90°— 80°
		175°— 80°
		25°— 50°
		130°— 65°
		95°— 47°
		85°— 50°
		130°— 65°

Meas. sample 14 (24 m.f.)

	mean m.f.
138—599	294°— 21°

co-ordinates of the grid	position of s-plane	position of m.f.
138—598		310°— 30°
		300°— 35°
		285°— 20°
		295°— 55°
		275°— 40°
		290°— 50°
		280°— 35°
138—599		280°— 40°
		295°— 25°
		285°— 5°
		280°— 5°
		285°— 0°
		300°— 5°
		285°— 20°
		270°—-40°
		315°— 15°
		315°— 55°
138—600		290°— 40°
		290°— 25°
		280°— 30°
137—600		310°— 10°
		305°—-10°
137—602		330°— 10°
		300°— 5°

Meas. sample 15 (25 m.f.)

	mean m.f.
127—603	311°— 17°

co-ordinates of the grid	position of s-plane	position of m.f.
130—601		290°— 10°
		330°— 15°
		335°— 25°
129—601		290°— 20°
		285°— 25°
126—603		325°— 25°
127—603		330°— 45°
		295°— 30°
		260°— 10°
128—603		320°— 10°
		280°— 20°
		310°— 45°
		310°— 10°
		307°— 10°
		295°— 5°
		310°— 30°
		300°— 7°
127—604		305°— 20°
		340°— 10°
		290°— 10°
		340°— 10°
123—606		325°— 25°

122—605	315°— 15°
	360°— 0°
	330°— −5°

Meas. sample 16 (13 m.f.)	
	mean m.f.
120—601	308°— 19°

co-ordinates of the grid	position of s-plane	position of m.f.
121—602		270°— 0°
		320°— 0°
		350°— 30°
120—601		305°— 40°
		310°— 20°
		315°— 10°
		305°— 30°
		310°— 22°
118—600		290°— 15°
		300°— 25°
119—599		320°— 0°
		295°— 15°
		310°— 35°

Tables of the positions of the axes of the minorf olds in the Pusteria region (Sheet III).

(The azimuths of the m.f. are given without the magnetic correction of — 2°.)

Meas. sample 18: 10 m.f.	
	mean m.f.
785—829	81°— 51°

co-ordinates of the grid	position of m.f.
784—829	90°— 30°
	70°— 50°
	50°— 68°
	50°— 67°
	90°— 55°
	100°— 40°
	67°— 35°
785—829	86°— 53°
	110°— 55°
	98°— 55°

Meas. sample 19: 17 m.f.	
	mean m.f.
801—820	94°— 33°

co-ordinates of the grid	position of m.f.
799—819	108°— 32°
800—819	120°— 55°
	110°— 40°
	96°— 41°
	95°— 39°
	105°— 40°
	90°— 45°
803—821	78°— 22°
802—821	75°— 40°
	95°— 25°
	85°— 25°
	95°— 30°
802—821	95°— 25°
	90°— 20°
802—820	90°— 25°
	90°— 25°
	75°— 30°

Meas. sample 20: 13 m.f.	
	mean m.f.
812—827	142°— 25°

co-ordinates of the grid	position of m.f.
813—826	110°— 30°
813—827	135°— 30°
	150°— 20°
	155°— 40°
	150°— 20°
813—828	141°— 23°
814—830	150°— 15°
809—827	130°— 35°
810—828	130°— 40°
812—827	135°— 20°
	150°— 15°
	155°— 10°
812—826	150°— 22°

Meas. sample 21: 20 m.f.	
	mean m.f.
820—824	108°— 13°

co-ordinates of the grid	position of m.f.
817—826	157°— 19°
	120°— 20°
	125°— 10°
	140°— 10°
	140°— 10°
819—826	145°— 5°
818—827	155°— 5°
	160°— 10°
819—828	165°— 10°
823—825	130°— 30°
	115°— 20°
	115°— 15°
822—822	95°— 0°
818—820	60°— 25°
	60°— 15°
	60°— 20°
	55°— 15°
	68°— 18°
819—819	45°— 10°
820—819	45°— 0°

Meas. sample 22: 24 m.f.	
	mean m.f,
801—823	94°— 37°

co-ordinates of the grid	position of m.f.
800—824	90°— 40°
	95°— 30°
	110°— 50°
	100°— 38°
	100°— 0°
	77°— 40°
	85°— 45°
	65°— 60°
	92°— 39°
	90°— 35°
	110°— 38°
800—824	95°— 30°
800—823	105°— 40°
801—823	110°— 40°
	105°— 50°
	81°— 41°
	85°— 35°
	115°— 35°
	105°— 35°
801—822	90°— 40°
802—821	75°— 40°
	95°— 25°
	85°— 25°
	95°— 30°

Meas. sample 23: 28 m.f.	
	mean m.f.
806—818	69°— 21°

co-ordinates of the grid	position of m.f.
806—818	70°— 20°
	60°— 20°
	70°— 20°
	60°— 20°
	60°— 25°
	50°— 15°
	60°— 20°
	80°— 20°
805—817	75°— 15°
	80°— 40°
	75°— 15°
804—816	100°— 25°
	75°— 20°
	60°— 40°
	75°— 25°
	100°— 40°
	85°— 20°
803—816	95°— 45°
807—818	45°— 5°
	40°— 15°
807—819	70°— 15°
	65°— 25°
	70°— 30°
	75°— 25°
	65°— 10°
809—819	60°— 20°
809—820	40°— −5°
809—821	60°— 0°

Meas. sample 24: 16 m.f.	
	mean m.f.
814—819	229°— 8°

co-ordinates of the grid	position of m.f.
814—819	210°— 15°
	220°— 10°

	235°	5°
	225°	5°
	210°	−5°
	220°	0°
	240°	−5°
	230°	0°
813—818	240°	20°
	205°	5°
	230°	15°
815—818	270°	35°
815—819	230°	15°
	220°	5°
	245°	10°
816—818	230°	0°

Meas. sample 25: 19 m.f.

	mean m.f.	
813—812	56°	15°

co-ordinates of the grid	position of m.f.	
818—815	45°	10°
816—815	60°	5°
815—816	35°	−18°
814—813	50°	20°
809—813	60°	30°
807—811	60°	20°
	75°	30°
	70°	45°
	100°	50°
	50°	30°
815—811	45°	5°
	50°	10°
	50°	10°
	60°	10°
	40°	5°
	60°	20°
814—814	60°	5°
	55°	0°
	40°	5°

Meas. sample 26: 26 m.f.

	mean m.f.	
837—828	139°	6°

co-ordinates of the grid	position of m.f.	
836—829	150°	−10°
	135°	10°
836—828	130°	0°
	160°	−10°
	130°	0°
	115°	−5°
	155°	25°
	140°	0°
	135°	0°
	155°	0°
	110°	15°
837—828	110°	5°
	135°	10°
	135°	25°
	150°	15°
	155°	10°
	155°	5°
	120°	10°
	125°	20°
	150°	10°
	150°	0°
838—828	130°	30°
	150°	0°
	155°	−10°
	140°	0°
839—828	135°	0°

Meas. sample 27: 14 m.f.

	mean m.f.	
847—829	110°	8°

co-ordinates of the grid	position of m.f.	
845—828	100°	0°
	105°	20°
	130°	0°
845—829	100°	15°
	98°	9°
	110°	15°
845—830	92°	15°
844—830	100°	10°
850—831	140°	0°
	125°	10°
851—829	120°	5°
851—828	105°	0°
	105°	10°
	110°	0°

Meas. sample 28: 16 m.f.

	mean m.f.	
826—813	51°	24°

co-ordinates of the grid	position of m.f.	
825—816	60°	15°
	35°	35°
	60°	25°
	40°	0°
	30°	15°
826—816	70°	15°
826—815	45°	25°
826—812	75°	30°
827—812	70°	35°
	35°	25°
	60°	20°
	60°	20°
829—811	45°	35°
	45°	35°
824—808	60°	25°
	20°	35°

Meas. sample 29: 11 m.f.

	mean m.f.	
854—830	104°	11°

co-ordinates of the grid	position of m.f.	
852—827	105°	10°
853—827	90°	0°
	115°	30°
855—831	110°	10°
	120°	5°
	115°	7°
	95°	0°
854—832	90°	15°
	105°	5°
	95°	20°
	105°	20°

Meas. sample 30: 11 m.f.

	mean m.f.	
855—824	105°	21°

co-ordinates of the grid	position of m.f.	
853—824	110°	20°
	110°	20°
854—823	100°	30°
	105°	10°
	105°	20°
	90°	30°
	90°	40°
	95°	30°
858—825	120°	20°
858—824	120°	10°
	110°	5°

Meas. sample 31: 39 m.f.

	mean m.f.	
831—811	41°	24°

co-ordinates of the grid	position of m.f.	
831—808	45°	30°
	50°	35°
	20°	55°
	76°	38°
	122°	−8°
	40°	25°
	15°	60°
	25°	25°
831—809	40°	30°
	60°	50°
	75°	30°
	50°	40°
831—810	35°	30°
	60°	30°
	45°	20°
	55°	20°
	35°	25°
831—811	45°	20°
	35°	20°
	45°	40°
	35°	15°
	45°	30°
	50°	25°
831—812	30°	25°
	30°	15°
	40°	20°
	20°	20°
831—813	20°	10°
	35°	25°
	20°	13°
	30°	10°
	25°	20°
	30°	10°
	40°	20°
833—812	40°	0°
	30°	15°
	40°	20°
833—813	30°	15°
834—812	45°	20°

Meas. sample 32: 27 m.f.

	mean m.f.	
839—813	49°	38°

co-ordinates of the grid	position of m.f.	
839—812	30°	25°
	35°	35°
	30°	35°
	70°	45°
	75°	40°
	30°	30°
	55°	35°
839—813	70°	40°
	40°	50°
	0°	60°
	70°	35°
	50°	30°
	50°	25°
	35°	35°
	40°	35°
	25°	45°
	45°	35°
	25°	40°
839—814	65°	30°
	60°	50°
	85°	40°
	45°	40°
	75°	40°
839—815	45°	30°
	50°	60°
	60°	40°
	70°	25°

Meas. sample 33: 14 m.f.	
	mean m.f.
841—817	73°— 30°

co-ordinates of the grid	position of m.f.
840—816	95°— 25°
	75°— 25°
841—816	75°— 30°
	85°— 30°
	80°— 35°
	75°— 25°
	80°— 40°
	50°— 25°
	45°— 40°
841—817	85°— 25°
	80°— 40°
	45°— 40°
841—818	60°— 45°
842—818	90°— 0°

Meas. sample 34: 16 m.f.	
	mean m.f.
854—814	49°— 34°

co-ordinates of the grid	position of m.f.
854—817	65°— 45°
854—816	35°— 50°
	25°— 40°
	30°— 65°
854—815	30°— 45°
854—814	60°— 40°
	90°— 30°
	40°— 40°
	30°— 25°
	65°— 25°
854—813	30°— 45°
	50°— 30°
	60°— 35°
854—812	60°— 30°
	65°— 25°
	45°— 35°

Meas. sample 35: 25 m.f.	
	mean m.f.
864—811	49°— 25°

co-ordinates of the grid	position of m.f.
866—809	40°— 25°
866—810	40°— 50°
	45°— 45°
	40°— 25°
	85°— 20°
	80°— 30°
865—810	50°— 30°
	80°— 15°
863—811	50°— 30°
	0°— 10°
	85°— 50°
	45°— 35°
863—812	40°— 25°
	25°— 15°
	65°— 30°
	55°— 40°
	70°— 35°
	65°— 30°
	45°— 25°
	75°— 25°
863—813	55°— 15°
	20°— 10°
	40°— 5°
	20°— 0°
	5°— 0°

Meas. sample 36: 19 m.f.	
	mean m.f.
864—814	43°— 19°

co-ordinates of the grid	position of m.f.
863—813	40°— 10°
863—814	40°— 15°
	35°— 12°
	60°— 20°
	60°— 20°
	30°— 0°
863—815	75°— 10°
	45°— 15°
	50°— 15°
863—816	30°— 35°
863—817	55°— 15°
	30°— 30°
867—814	70°— 10°
	30°— 5°
	45°— 35°
	20°— 20°
	0°— 10°
867—813	45°— 40°
867—812	60°— 45°

Meas. sample 37: 16 m.f.	
	mean m.f.
969—795	109— 16°

co-ordinates of the grid	position of m.f.
974—795	110°— 15°
	115°— 20°
	105°— 25°
	115°— 15°
	120°— 15°
967—795	115°— 15°
	110°— 15°
	105°— 12°
	100°— 15°
	100°— 25°
	110°— 20°
	110°— 20°
968—795	105°— 20°
	100°— 10°
	120°— 0°
	105°— 15°

Meas. sample 38: 13 m.f.	
	mean m.f.
860—831	103°— 6°

co-ordinates of the grid	position of m.f.
855—833	90°— 15°
	75°— 10°
856—831	110°— 15°
	95°— 0°
	95°— 15°
861—829	110°— 10°
863—830	120°— 10°
	120°— 0°
	90°— 5°
864—831	110°— 0°
	90°— 0°
	120°— 0°
864—832	120°— 0°

Meas. sample 39: 36 m.f.	
	mean m.f.
751—831	69°— 26°

co-ordinates of the grid	position of m.f.
749—831	95°— 40°
	35°— 40°
	45°— 30°
	90°— 40°
	90°— 35°
	30°— 40°
748—832	90°— 25°
	95°— 30°
	80°— 20°
747—831	65°— 20°
	60°— 25°
	65°— 35°
	65°— 20°
	80°— 20°
754—830	90°— 30°
	90°— 25°
	65°— 20°
	60°— 15°
	60°— 15°
	65°— 20°
753—831	60°— 10°
	65°— 40°
	60°— 30°
	50°— 25°
	60°— 30°
	60°— 15°
	60°— 15°
	60°— 5°
752—830	75°— 25°
	65°— 17°
	60°— 30°
751—831	85°— 35°
	80°— 25°
	65°— 30°
	80°— 35°
	90°— 20°

Meas. sample 40: 12 m.f.	
	mean m.f.
750—833	110°— 49°

co-ordinates of the grid	position of m.f.
749—833	95°— 40°
	105°— 40°
750—833	120°— 60°
	120°— 65°
	115°— 45°
751—833	120°— 50°
	100°— 50°
	115°— 38°
	100°— 55°
	115°— 60°
	105°— 50°
	110°— 40°

Meas. sample 41: 25 m.f.	
	mean m.f.
758—831	97°— 37°

co-ordinates of the grid	position of m.f.
756—833	70°— 20°
758—833	75°— 30°
758—832	90°— 45°
759—831	90°— 40°
	105°— 40°
	100°— 20°
	115°— 40°
	105°— 30°
759—830	100°— 45°
758—830	90°— 50°
	115°— 30°
	100°— 65°
	105°— 65°
757—830	95°— 33°
	100°— 40°
	110°— 20°
	105°— 42°
	95°— 25°
	70°— 30°
	80°— 5°
759—834	105°— 50°
	100°— 45°
	95°— 40°
	120°— 45°
	90°— 40°

Meas. sample 42: 20 m.f.	mean m.f.
778—840	102°— 58°

co-ordinates of the grid	position of m.f.
779—840	100°— 65°
	90°— 60°
	115°— 80°
	95°— 50°
	105°— 52°
	120°— 65°
778—840	100°— 43°
	105°— 50°
	95°— 60°
778—841	105°— 40°
	105°— 80°
777—840	90°— 42°
	115°— 55°
776—839	95°— 55°
	85°— 42°
	115°— 60°
777—840	110°— 55°
	110°— 75°
777—842	95°— 65°
	85°— 70°

Meas. sample 43: 12 m.f.	mean m.f.
752—844	105°— 55°

co-ordinates of the grid	position of m.f.
753—843	110°— 60°
	125°— 60°
	110°— 50°
	105°— 55°
752—843	95°— 40°
	95°— 55°
751—843	90°— 45°
	95°— 70°
750—843	130°— 80°
	90°— 30°
752—848	120°— 45°
	90°— 75°

Meas. sample 44: 28 m.f.	mean m.f.
877—808	52°— 19°

co-ordinates of the grid	position of m.f.
874—806	75°— 10°
873—806	65°— 10°
877—807	45°— 20°
	85°— 15°
878—808	40°— 30°
	30°— 40°
	20°— 0°
	45°— 10°
	35°— 0°
	95°—−10°
	100°— 50°
	20°— 30°
	— 90°
	30°— 25°
	40°— 10°
	45°— 5°
	40°— 20°
	35°— 40°
	5°— −5°
	50°— 15°
	30°— 5°
	100°—−15°
	45°— 0°
	30°— 15°
	20°— 20°
	105°— 45°
	75°— 45°
	95°— 25°

Meas. sample 45: 14 m.f.	mean m.f.
882—814	82°— 49°

co-ordinates of the grid	position of m.f.
881—811	90°— 50°
	60°— 60°
882—813	80°— 50°
	40°— 30°
882—815	80°— 55°
	80°— 40°
	110°— 50°
	90°— 45°
	90°— 60°
	75°— 50°
883—814	100°— 35°
	90°— 60°
	90°— 35°
886—814	70°— 70°

Meas. sample 46: 22 m.f.	mean m.f.
892—816	94°— 6°

co-ordinates of the grid	position of m.f.
889—815	110°— 5°
	100°— 30°
892—818	90°— 45°
	90°—−10°
893—818	85°— 0°
	85°— 0°
893—817	100°—−10°
	90°—−10°
	90°— 0°
	85°— 20°
	75°— 0°
	90°— 10°
892—816	130°—−15°
	90°— 25°
	80°— 0°
	95°— 17°
892—815	95°— 30°
	70°— 10°
	100°— 0°
	110°— 0°
	95°— 0°
	110°—−10°

Meas. sample 47: 34 m.f.	mean m.f.
895—821	85°— 11°

co-ordinates of the grid	position of m.f.
894—820	105°— 15°
	90°— 20°
	95°— 30°
896—821	80°— 10°
898—822	90°— 0°
	57°—−13°
891—821	60°— 20°
	81°— 28°
894—824	90°— 0°
893—823	95°— 25°
893—822	75°— 0°
	85°— 0°
	80°— 0°
	70°— 15°
	75°— 15°
893—821	75°— 3°
	90°— 25°
	95°— 15°
	80°— 5°
	80°— 10°
895—818	85°— 20°
895—819	100°— 10°
896—819	90°— 10°
	90°— 12°
	43°— 40°
897—820	95°— 7°
	100°— 5°
	90°— 5°
	90°— 5°
898—821	85°— 12°
	95°— 15°
899—822	90°— 0°
900—822	100°— 0°
	85°— 0°

Meas. sample 48: 28 m.f.	mean m.f.
901—813	93°— 7°

co-ordinates of the grid	position of m.f.
903—812	105°— 0°
	90°— 0°
	75°— 5°
	70°— −3°
	90°— 0°
	90°— −5°
902—812	95°— 0°
	120°— 20°
	90°— 15°
	100°— 15°
901—813	95°— 0°
	100°— 10°
	95°— 20°
	80°— 15°
900—813	85°— 5°
	100°— 0°
	100°— 0°
	105°— 10°
	85°— 0°
899—813	80°— 10°
	85°— 5°
	95°— 15°
898—814	100°— 0°
	80°— 43°
	100°— 5°
	90°— 0°
897—814	110°— 0°
	90°— 20°

Meas. sample 49: 16 m.f.	mean m.f.
895—808	117°— 23°

co-ordinates of the grid	position of m.f.
892—808	110°— 20°
893—808	105°— 20°
894—808	90°— 20°
	90°— 50°
	110°— 15°
	105°— 20°
895—808	110°— 25°
	115°— 15°
	125°— 20°
896—808	155°— 50°
	95°— 45°
	130°— 20°
	140°— 30°
896—807	135°— 0°
895—807	120°— 0°
	135°— 10°

Meas. sample 50: 9 m.f.	mean m.f.
901—801	286°— 14°

co-ordinates of the grid	position of m.f.
901—801	290°— 10°
	290°— 15°

	270°— 25°
	285°— 15°
	300°— 20°
	285°— 10°
	295°— 15°
	275°— 10°
	285°— 10°

Meas. sample 51: 28 m.f.

	mean	m.f.
910—799	271°—	6°

co-ordinates of the grid	position of m.f.
912—797	285°— 20°
	285°— 50°
	270°— 10°
	270°—−10°
	235°—−30°
911—798	265°— 0°
	250°— 10°
	260°— 12°
	270°—−10°
911—799	270°—−10°
	240°—−20°
	280°—−15°
910—800	270°—−20°
	265°—−25°
	290°— 5°
	270°— 40°
	270°— 20°
	270°— 35°
	270°— 20°
909—801	270°— 10°
	290°— 30°
	290°— 30°
	240°— 10°
	325°—−15°
	250°— 17°
	255°— 25°
909—802	270°— 0°
	315°—−20°

Meas. sample 52: 17 m.f.

	mean	m.f.
914—807	284°—	17°

co-ordinates of the grid	position of m.f.
913—808	310°— 15°
	285°— 25°
	300°— 0°
	280°— 15°
	275°— 20°
	300°— 15°
913—809	290°— 15°
	285°— 10°
	285°— 30°
914—809	305°— 0°
	280°— 0°
915—808	290°— 30°
916—806	240°— 0°
916—805	270°— 30°
	270°— 40°
	275°— 25°
	295°— 20°

Meas. sample 53: 6 m.f.

	mean	m.f.
917—803	282°—	18°

co-ordinates of the grid	position of m.f.
917—804	280°— 20°
	270°— 35°
917—803	310°— 30°
917—802	280°— 10°
918—801	290°— 15°
	260°— −3°

Meas. sample 54: 22 m.f.

	mean	m.f.
922—803	300°—	15°

co-ordinates of the grid	position of m.f.
923—801	285°—−25°
922—802	300°—−10°
	330°—−25°
922—803	320°— 10°
	290°— 25°
	280°— 5°
	315°— 20°
	270°— 10°
	310°— 45°
	330°— 45°
	345°— 20°
	270°— 35°
	300°— 30°
	300°— 25°
	310°— 30°
	325°— 30°
	260°— 25°
	285°— 0°
	275°— 25°
923—804	290°— −5°
923—805	305°— 20°
923—806	295°— 0°

Meas. sample 55: 19 m.f.

	mean	m.f.
930—803	323°—	6°

co-ordinates of the grid	position of m.f.
931—804	310°— 10°
	320°— 5°
	300°— 5°
930—803	320°— 10°
	315°— 0°
	320°— 10°
	320°— 10°
	325°— 0°
	315°— 5°
930—802	325°— 5°
	350°— 5°
929—802	330°— 0°
	315°— 5°
	320°— 5°
	305°— 3°
	320°— 0°
	320°— 10°
	360°— 10°
928—801	340°— 10°

Meas. sample 56: 29 m.f.

	mean	m.f.
886—795	62°—	12°

co-ordinates of the grid	position of m.f.
884—796	90°— 10°
	60°— 0°
	90°— 30°
	30°— 10°
	40°— 0°
885—796	55°— 0°
	60°— 25°
	65°— 0°
	75°— 25°
	30°— 0°
	60°— 5°
	65°— 15°
886—795	60°— 30°
	75°— 30°
	60°— 10°
	60°— 15°
	55°— 10°
	50°— 20°
887—795	75°— 5°
	65°— 0°
	60°— 10°
	70°— 0°
	75°— 10°
	50°— 15°
	50°— 5°
888—795	55°— 17°
	65°— 15°
	80°— 20°
889—797	70°— 15°

Meas. sample 57: 20 m.f.

	mean	m.f.
910—810	114°—	1°

co-ordinates of the grid	position of m.f.
903—808	110°— 15°
	105°— 3°
	100°— 5°
	100°— −5°
	100°— −5°
906—809	120°— −5°
909—810	112°— 20°
	115°— 18°
912—811	115°— 12°
	110°— 0°
	125°— 0°
	125°— 0°
	105°— 0°
	115°—−10°
	125°—−30°
	130°—−20°
	125°— 0°
915—813	125°— 0°
	110°— 7°
	110°— 5°

Meas. sample 58: 25 m.f.

	mean	m.f.
942—796	117°—	6°

co-ordinates of the grid	position of m.f.
942—793	90°— 5°
	105°— 0°
	115°— 15°
942—794	140°— 0°
	135°— 0°
	130°— 0°
942—795	100°— 20°
	120°— 30°
942—796	105°— 20°
	100°— 10°
	110°— 20°
	125°— 0°
942—799	165°—−40°
941—797	115°—−10°
	150°— 0°
937—797	120°— 10°
	120°— 15°
936—795	115°— 25°
946—794	125°—−10°
946—795	105°— 0°
947—796	105°— 2°
947—797	110°— 20°
	135°— 15°
946—797	90°— 5°
945—797	105°—−10°

Meas. sample 59: 12 m.f.

	mean	m.f.
943—810	318°—	13°

co-ordinates of the grid	position of m.f.
942—809	325°— 10°
943—810	285°— −7°
	295°— 25°

	335°	35°
	320°	25°
	325°	25°
	320°	15°
	325°	0°
	330°	10°
	320°	5°
	295°	15°
944—809	335°	3°

Meas. sample 60: 19 m.f.	mean	m.f.
953—805	293°	12°

co-ordinates of the grid	position of m.f.	
953—806	290°	0°
953—805	300°	40°
	310°	30°
	330°	48°
953—802	285°	15°
	275°	−5°
	285°	0°
	295°	0°
	320°	15°
954—801	285°	10°
	300°	15°
952—806	285°	0°
	285°	0°
953—808	275°	0°
	280°	0°
	265°	0°
	290°	0°
	330°	30°
	280°	25°

Meas. sample 61: 19 m.f.	mean	m.f.
955—794	101°	4°

co-ordinates of the grid	position of m.f.	
954—797	100°	5°
	120°	10°
	125°	−20°
	130°	0°
954—795	105°	−15°
	105°	7°
955—794	110°	10°
	100°	10°
	90°	25°
	90°	0°
955—793	95°	0°
	105°	5°
	105°	0°
	70°	0°
	90°	5°
	90°	10°
	100°	0°
956—793	90°	20°
956—792	90°	10°

Meas. sample 62: 8 m.f.	mean	m.f.
973—799	109°	12°

co-ordinates of the grid	position of m.f.	
973—799	107°	5°
	120°	20°
	110°	5°
	110°	15°
	107°	5°
	100°	15°
	105°	12°
974—799	110°	15°

Meas. sample 63: 16 m.f.	mean	m.f.
813—801	93°	23°

co-ordinates of the grid	position of m.f.	
813—802	70°	15°
813—801	60°	15°
	90°	40°
	85°	25°
	105°	15°
	110°	20°
	95°	10°
	119°	20°
	105°	0°
	75°	45°
	105°	40°
	107°	30°
	95°	20°
	80°	25°
	95°	22°
	90°	25°

Meas. sample 64: 30 m.f.	mean	m.f.
782—815	129°	35°

co-ordinates of the grid	position of m.f.	
783—819	140°	20°
	140°	15°
	160°	15°
783—818	135°	35°
	105°	30°
	130°	30°
	125°	40°
783—815	130°	35°
	135°	20°
	140°	45°
783—814	130°	55°
	125°	50°
	125°	50°
	135°	70°
	140°	60°
	155°	45°
782—813	160°	55°
	165°	30°
	125°	40°
	125°	35°
	105°	15°
	80°	35°
	125°	30°
	140°	17°
	125°	30°
781—813	105°	35°
	112°	30°
	115°	30°
	125°	30°
	105°	25°

Meas. sample 65: 28 m.f.	mean	m.f.
774—801	123°	10°

co-ordinates of the grid	position of m.f.	
774—803	135°	0°
	110°	5°
	130°	30°
	125°	5°
	115°	−10°
	140°	0°
	120°	15°
	110°	5°
774—802	140°	5°
	130°	0°
	130°	10°
774—800	120°	15°
	135°	0°
	117°	20°
	110°	5°
774—799	110°	0°
	120°	30°
	112°	17°
	135°	15°
775—798	105°	10°
	110°	20°
774—801	125°	0°
	125°	10°
	125°	0°
	135°	25°
	125°	10°
	120°	5°
	130°	20°

Meas. sample 66: 21 m.f.	mean	m.f.
788—798	124°	11°

co-ordinates of the grid	position of m.f.	
788—796	135°	0°
	135°	12°
787—797	125°	10°
	120°	25°
	122°	0°
	120°	−8°
786—797	130°	−5°
	132°	5°
787—797	125°	15°
	132°	5°
	105°	15°
788—798	125°	12°
	115°	20°
	120°	25°
	115°	35°
789—799	120°	5°
790—800	105°	5°
	130°	15°
790—801	100°	0°
791—801	140°	25°
	145°	10°

Meas. sample 67: 14 m.f.	mean	m.f.
793—804	107°	19°

co-ordinates of the grid	position of m.f.	
791—801	107°	0°
	105°	35°
	120°	10°
792—802	85°	25°
	125°	30°
792—803	110°	10°
793—804	105°	10°
	125°	10°
793—805	110°	15°
	115°	15°
	105°	20°
793—806	100°	30°
794—807	100°	20°
	90°	35°

Meas. sample 68: 23 m.f.	mean	m.f.
802—801	110°	20°

co-ordinates of the grid	position of m.f.	
803—803	100°	0°
	110°	10°
	105°	12°
	105°	17°
802—802	110°	20°
	130°	20°
	110°	20°
	95°	20°
	105°	25°
	95°	25°
	100°	25°
	105°	30°
	110°	15°

	95°— 25°
801—801	105°— 25°
	90°— 30°
801—800	95°— 35°
	105°— 15°
	90°— 15°
	145°— 20°
	130°— 15°
	135°— 20°
801—799	150°— 15°

Meas. sample 69: 19 m.f.

	mean m.f.
799—798	96°— 13°

co-ordinates of the grid	position of m.f.
801—799	105°— 35°
	90°— 25°
800—799	105°— 15°
	90°— 20°
	100°— 0°
800—798	110°— 5°
	90°— 0°
	105°— 17°
	110°— 12°
799—798	90°— 15°
	90°— 40°
799—797	80°— 10°
	90°— 20°
978—797	95°— 15°
	90°— 15°
	107°— 0°
	90°— 5°
	100°— 0°
	95°— 0°

Meas. sample 70: 9 m.f.

	mean m.f.
812—792	89°— 19°

co-ordinates of the grid	position of m.f.
812—792	80°— 20°
	100°— 10°
	95°— 25°
	85°— 25°
	90°— 20°
	90°— 15°
813—791	85°— 10°
	90°— 20°
	85°— 25°

Meas. sample 71: 25 m.f.

	mean m.f.
835—793	91°— 25°

co-ordinates of the grid	position of m.f.
835—798	85°— 25°
	80°— 25°
834—796	90°— 30°
	100°— 25°
	90°— 15°
835—795	107°— 5°
	90°— 15°
	90°— 15°
835—794	115°— 25°
	90°— 30°
	100°— 30°
835—793	90°— 25°
	95°— 35°
	105°— 35°
835—792	92°— 35°
	90°— 35°
	95°— 15°
835—791	85°— 15°
	90°— 40°
835—790	85°— 45°
	80°— 25°
	90°— 25°
	95°— −1°
	55°— 9°
	84°— 40°

Meas. sample 72: 22 m.f.

	mean m.f.
237—854	106°— 58°

co-ordinates of the grid	position of m.f.
236—854	90°— 60°
	60°— 60°
	80°— 40°
	90°— 60°
237—854	105°— 70°
	100°— 65°
	105°— 40°
	115°— 55°
	110°— 53°
	80°— 47°
	140°— 65°
	100°— 75°
	120°— 55°
	105°— 57°
	115°— 62°
	105°— 45°
238—853	85°— 50°
	90°— 55°
	120°— 62°
	125°— 75°
240—854	125°— 60°
242—855	165°— 70°

Meas. sample 73: 11 m.f.

	mean m.f.
759—829	103°— 53°

co-ordinates of the grid	position of m.f.
759—829	105°— 45°
	95°— 55°
	100°— 57°
	102°— 40°
	120°— 50°
	100°— 45°
	95°— 50°
	105°— 65°
	104°— 55°
	110°— 65°
	95°— 55°

Meas. sample 74: 14 m.f.

	mean m.f.
758—810	96°— 26°

co-ordinates of the grid	position of m.f.
758—810	105°— 10°
	90°— 25°
	110°— 10°
	105°— 30°
	107°— 32°
	100°— 30°
	103°— 15°
	95°— 30°
	80°— 30°
	105°— 25°
	60°— 20°
	85°— 30°
	95°— 33°
	97°— 40°

Meas. sample 75: 11 m.f.

	mean m.f.
757—806	80°— 14°

co-ordinates of the grid	position of m.f.
758—805	85°— 23°
	78°— 5°
	83°— 5°
757—806	90°— 25°
	70°— 12°
	85°— 10°
	70°— 12°
756—806	75°— 10°
	85°— 20°
	75°— 20°
	80°— 10°

Meas. sample 76: 17 m.f.

	mean m.f.
750—808	85°— 20°

co-ordinates of the grid	position of m.f.
752—807	65°— 8°
	80°— 30°
	75°— 30°
	85°— 15°
	85°— 40°
	80°— 25°
	80°— 15°
751—807	90°— 15°
	70°— 28°
750—808	90°— 25°
	70°— 10°
	95°— 15°
748—810	100°— 0°
	80°— 22°
	105°— 30°
	97°— 20°
	95°— 15°

Meas. sample 77: 20 m.f.

	mean m.f.
744—814	106°— 38°

co-ordinates of the grid	position of m.f.
747—815	90°— 15°
742—815	120°— 35°
	95°— 45°
	100°— 45°
	105°— 20°
	100°— 30°
743—814	130°— 35°
	125°— 55°
	105°— 40°
744—813	105°— 55°
	95°— 45°
	105°— 35°
	90°— 45°
	90°— 40°
	90°— 30°
	125°— 40°
	125°— 40°
745—813	100°— 30°
	120°— 35°
	103°— 40°

Meas. sample 78: 17 m.f.

	mean m.f.
746—806	98°— 39°

co-ordinates of the grid	position of m.f.
746—808	95°— 25°
	110°— 30°
	90°— 25°
746—807	110°— 50°
	105°— 40°
	90°— 30°
	105°— 57°
	105°— 15°
	105°— 50°
	90°— 25°
746—806	90°— 20°
	90°— 35°
	100°— 50°
746—805	105°— 50°
	80°— 55°

746—804	90°— 55°
	105°— 45°

Meas. sample 79: 17 m.f.
mean m.f.

747—800	91°— 43°

co-ordinates of the grid	position of m.f.
746—802	115°— 40°
	80°— 45°
	135°— 40°
747—802	75°— 40°
	85°— 55°
	90°— 40°
	95°— 45°
747—801	90°— 35°
747—798	80°— 30°
748—798	60°— 50°
748—797	60°— 55°
	95°— 45°
	40°— 70°
744—799	105°— 50°
745—800	140°— 32°
746—802	110°— 20°
	85°— 40°

Meas. sample 80: 19 m.f.
mean m.f.

740—796	86°— 41°

co-ordinates of the grid	position of m.f.
739—795	90°— 50°
739—796	55°— 35°
	75°— 30°
	70°— 35°
	85°— 40°
	60°— 50°
740—796	90°— 45°
	60°— 30°
	60°— 45°
	90°— 20°
	70°— 50°
	105°— 25°
741—796	105°— 40°
	120°— 50°
	90°— 45°
	85°— 35°
	105°— 35°
741—797	145°— 70°
742—797	80°— 50°

Meas. sample 81: 17 m.f.
mean m.f.

721—862	102°— 40°

co-ordinates of the grid	position of m.f.
719—862	102°— 48°
	97°— 38°
	105°— 35°
	95°— 50°
	100°— 45°
	90°— 53°
720—862	115°— 45°
	105°— 35°
	100°— 30°
721—862	115°— 30°
	100°— 25°
	110°— 25°
	105°— 25°
722—863	105°— 50°
723—863	110°— 30°
	100°— 50°
	75°— 60°

Meas. sample 82: 26 m.f.
mean m.f.

709—798	101°— 47°

co-ordinates of the grid	position of m.f.
710—799	115°— 45°
	100°— 50°
	60°— 45°
	90°— 60°
	85°— 43°
	80°— 60°
	95°— 45°
710—798	70°— 45°
	90°— 50°
	100°— 35°
710—797	105°— 30°
	115°— 35°
	95°— 45°
	140°— 33°
	110°— 30°
708—798	70°— 40°
	85°— 60°
	120°— 60°
	90°— 60°
707—797	100°— 53°
	105°— 57°
	115°— 57°
	140°— 50°
	90°— 25°
	135°— 45°
	125°— 60°

Meas. sample 83: 50 m.f.
mean m.f.

287—795	116°— 26°

co-ordinates of the grid	position ofm.f.
291—797	120°— 55°
	90°— 70°
	145°— 40°
290—796	135°— 40°
	115°— 30°
	95°— 50°
289—795	105°— 45°
	110°— 30°
	130°— 45°
	110°— 40°
288—795	105°— 38°
	125°— 20°
	110°— 15°
	130°— 25°
	120°— 10°
	120°— 30°
287—795	85°— 20°
	145°— 5°
	160°— 10°
	150°— 15°
	110°— 35°
	115°— 7°
	125°— 10°
	140°— 27°
	135°— 40°
	155°— 10°
286—794	135°— −5°
	130°— 0°
286—795	80°— 5°
	90°— 15°
	85°— 15°
	105°— 10°
	110°— 15°
285—795	90°— −5°
	115°— 15°
	120°— −5°
286—794	135°— 15°
	115°— 25°
285—793	135°— 15°
284—793	140°— 20°
	100°— 20°
	125°— 35°
	120°— 40°
	125°— 35°
	120°— 35°
	105°— 65°
	125°— 35°
283—792	100°— 45°
	115°— 38°
	115°— 35°

Meas. sample 84: 23 m.f.
mean m.f.

283—797	108°— 39°

co-ordinates of the grid	position of m.f.
277—795	105°— 40°
	90°— 35°
278—795	105°— 50°
	95°— 35°
	115°— 50°
282—797	135°— 30°
	115°— 35°
	115°— 45°
	105°— 40°
	110°— 20°
	90°— 30°
285—797	115°— 38°
	105°— 35°
	130°— 50°
	95°— 35°
	100°— 43°
	120°— 40°
	115°— 50°
	105°— 40°
	100°— 35°
	105°— 45°
	110°— 40°
	95°— 40°

Meas. sample 85: 39 m.f.
mean m.f.

727—812	96°— 24°

co-ordinates of the grid	position of m.f.
726—811	60°— 25°
	60°— 20°
	120°— 25°
	90°— 30°
	110°— 25°
	100°— 25°
	80°— 30°
	75°— 20°
	90°— 15°
	80°— 23°
	100°— 30°
	90°— 25°
	105°— 30°
	105°— 25°
	95°— 28°
727—812	95°— 22°
	75°— 20°
	80°— 25°
	110°— 17°
	105°— 12°
	80°— 30°
	80°— 15°
	120°— 25°
	115°— 20°
	90°— 45°
	85°— 45°
727—813	75°— 18°
	85°— 18°
	125°— 35°
	110°— 25°
	103°— 22°
	75°— 20°
	100°— 15°
728—814	125°— 30°
	110°— 15°
	110°— 20°
728—815	100°— 30°

	120°— 30°
	115°— 22°

Meas. sample 86: 18 m.f.	mean m.f.
728—817	99°— 34°

co-ordinates of the grid	position of m.f.
728—815	105°— 40°
	105°— 37°
	95°— 22°
728—816	90°— 35°
	110°— 40°
	100°— 30°
	90°— 12°
728—817	95°— 40°
	95°— 37°
	80°— 27°
729—817	115°— 37°
	90°— 25°
	110°— 30°
	120°— 55°
	105°— 35°
729—818	105°— 15°
	90°— 45°
	85°— 50°

Meas. sample 87: 18 m.f.	mean m.f.
716—798	84°— 47°

co-ordinates of the grid	position of m.f.
713—801	95°— 35°
	100°— 55°
	95°— 35°
	90°— 50°
	85°— 57°
	70°— 30°
713—800	105°— 55°
	75°— 57°
714—798	85°— 60°
715—797	80°— 40°
716—795	65°— 55°
	60°— 52°
723—794	85°— 40°
722—794	75°— 35°
721—794	75°— 45°
	100°— 50°
720—795	60°— 60°
	105°— 40°

Meas. sample 88: 32 m.f.	mean m.f.
267—837	106°— 38°

co-ordinates of the grid	position of m.f.
262—838	95°— 45°
263—838	105°— 40°
263—837	155°— 45°
	100°— 55°
	110°— 35°
	115°— 25°
264—837	100°— 45°
	90°— 40°
264—836	90°— 45°
	105°— 43°
	115°— 46°
265—836	105°— 40°
	110°— 40°
	110°— 40°
266—836	100°— 35°
266—835	100°— 35°
	90°— 35°
267—835	110°— 40°
	115°— 37°
	100°— 30°
267—836	125°— 40°
	115°— 37°
	115°— 40°
271—837	120°— 30°
272—838	105°— 30°
	95°— 35°
	90°— 30°
	100°— 35°
	85°— 37°
	110°— 30°
	110°— 25°
	90°— 45°

Meas. sample 89: 18 m.f.	mean m.f.
278—845	111°— 50°

co-ordinates of the grid	position of m.f.
280—843	120°— 30°
	115°— 48°
	115°— 35°
	110°— 37°
279—844	100°— 42°
	60°— 60°
	140°— 55°
277—846	110°— 55°
276—846	120°— 25°
	115°— 55°
	95°— 52°
	105°— 58°
	110°— 60°
	90°— 60°
	115°— 65°
	120°— 55°
275—847	140°— 53°
	110°— 55°

Meas. sample 90: 22 m.f.	mean m.f.
714—805	111°— 24°

	75°— 30°
	85°— 0°
	85°— 5°
	90°— 10°
	90°— 35°
	95°— 25°
	105°— 0°
	100°— 35°
	105°— 0°
	105°— 30°
	105°— 35°
	115°— 30°
	115°— 30°
	120°— 24°
	120°— 25°
	120°— 29°
	125°— 25°
	130°— 33°
	130°— 33°
	135°— 20°
	140°— 44°
	150°— 30°

Meas. sample 91: 40 m.f.	mean m.f.
716—813	110°— 19°

	584°—587°
	85°— 4°
	90°— 10°
	90°— 10°
	90°— 35°
	95°— 10°
	100°— 10°
	100°— 25°
	100°— 25°
	100°— 30°
	100°— 35°
	100°— 50°
	105°— 0°
	105°— 10°
	105°— 20°
	105°— 20°
	105°— 20°
	105°— 25°
	105°— 40°
	110°— 20°
	110°— 22°
	110°— 25°
	110°— 40°
	115°— 0°
	115°— 10°
	115°— 12°
	115°— 14°
	115°— 15°
	115°— 20°
	115°— 30°
	117°— 10°
	120°— 10°
	120°— 10°
	120°— 15°
	120°— 25°
	125°— 10°
	125°— 12°
	130°— 50°
	135°— 10°
	135°— 15°
	110°— 6°

Tables of the positions of the schistosity-planes and the axes of the minor folds in the Bressanone region (Sheet IV).

(The strikes of the s-planes and the azimuths of the m.f. are given without the magnetic correction of — 2°.)

Meas. sample 92: 37 m.f.	mean m.f.
207—851	219°— 77°

co-ordinates of the grid	position of m.f.
204—849	260°— 65°
	190°— 80°
	— 90°
	300°— 60°
	— 90°
	260°— 65°
	220°— 80°
	260°— 80°
	230°— 85°
	230°— 85°
205—849	230°— 55°
	245°— 55°
	235°— 77°
	180°— 70°
	265°— 55°
	265°— 60°
206—850	250°—135°
	235°—100°
	240°— 60°
	220°—110°
206—851	210°— 70°
203—849	210°— 55°
204—849	210°— 85°
	250°—100°
206—852	240°—110°

211—855	210°— 70°
	160°— 58°
	150°— 65°
	195°— 77°
210—855	215°— 75°
	190°— 75°
	180°— 70°
	165°— 70°
	180°— 80°
	200°— 60°
	180°— 80°
	190°— 80°

Meas. sample 93: 17 m.f.	mean m.f.
184—862	196°— 73°

co-ordinates of the grid	position of m.f.
182—864	230°— 60°
	200°— 80°
	210°— 65°
	205°— 55°
	190°— 70°
	250°—115°
	— 90°
	220°— 70°
186—861	130°— 60°
	210°— 75°
	270°— 70°
	150°— 50°
	200°—100°
	130°— 70°
	205°— 65°
	190°— 70°
	150°— 80°

Meas. sample 94: 26 m.f.	mean m.f.
233—833	105°— 54°

co-ordinates of the grid	position of m.f.
232—834	80°— 50°
	115°— 62°
	110°— 45°
232—833	110°— 60°
	100°— 35°
	110°— 55°
	100°— 60°
	105°— 50°
	120°— 60°
233—833	100°— 50°
	80°— 55°
	100°— 57°
	110°— 57°
	112°— 53°
	85°— 55°
235—832	110°— 45°
	105°— 80°
	115°— 45°
	120°— 50°
232—834	115°— 45°
	105°— 45°
	90°— 60°
	95°— 65°
	110°— 35°
233—834	105°— 65°
	125°— 55°

Meas. sample 95: 32 m.f.	mean m.f.
187—831	106°— 58°

co-ordinates of the grid	position of m.f.
187—834	110°— 75°
	65°— 70°
	105°— 65°
	105°— 75°
187—833	105°— 65°
187—832	110°— 70°
	150°—110°
	115°— 50°
	95°— 70°
	105°— 70°
	110°— 55°
	90°— 65°
	100°— 40°
	90°— 60°
187—831	90°— 30°
	125°— 50°
	120°— 60°
	105°— 50°
	115°— 40°
	120°— 45°
	117°— 60°
	95°— 55°
	90°— 50°
188—830	115°— 50°
	100°— 60°
	115°— 55°
	100°— 45°
	85°— 50°
	107°— 60°
	105°— 50°
	125°— 45°
	110°— 50°

Meas. sample 96: 23 m.f.	mean m.f.
208—788	88°— 39°

co-ordinates of the grid	position of m.f.
	115°— 60°
210—785	100°— 55°
	130°— 50°
	140°— 40°
	100°— 30°
211—786	80°— 20°
	65°— 35°
210—787	65°— 15°
	70°— 20°
	55°— 15°
	90°— 45°
	85°— 40°
	75°— 25°
	80°— 30°
	80°— 25°
207—790	95°— 35°
	60°— 40°
	35°— 65°
	85°— 40°
	95°— 45°
	90°— 40°
	100°— 40°
	85°— 40°
206—790	105°— 40°
	60°— 65°
	110°— 45°
	70°— 40°
206—791	90°— 50°
	90°— 30°
	95°— 53°
	110°— 53°
	95°— 35°

Meas. sample 97 (30 s. and 34 m.f.)	mean s.	mean m.f.
778—046	118°— 47°	
775—045		142°— 25°

co-ordinates of the grid	position of s-plane	position of m.f.
773—042	130°— 50°	145°— 30°
	105°— 40°	130°— 20°
		135°— 45°
773—041	115°— 45°	110°— −5°
	115°— 60°	170°— 55°
	110°— 57°	155°— 35°
773—044	50°— 45°	135°— 25°
	70°— 50°	175°— 45°
	115°— 45°	155°— 35°
	125°— 33°	165°— 15°
	115°— 45°	170°— 30°
	150°— 55°	150°— 20°
774—044		145°— 25°
		110°— 60°
776—045	145°— 45°	145°— 10°
	100°— 85°	100°— 25°
	100°— 45°	165°— 20°
	80°— 50°	170°— 25°
		145°— 42°
		145°— 45°
780—047	125°— 35°	135°— 30°
	125°— 40°	150°— 18°
	115°— 38°	
781—047	125°— 45°	90°—−30°
781—048	150°— 35°	
782—048	95°— 35°	155°— 15°
	145°— 65°	140°— 25°
782—048	120°— 33°	125°— 15°
	110°— 55°	130°— 15°
	95°— 45°	150°— 20°
	140°— 40°	160°— 35°
		135°— 20°
		155°— 30°
		155°— 13°
		65°— 35°
783—048	115°— 42°	170°— 23°
	135°— 45°	
	150°— 62°	
	175°— 35°	

Meas. sample 98 (20 s. and 22 m.f.)	mean s.	mean m.f.
	132°— 50°	
086—813		
086—812		160°— 36°

co-ordinates of the grid	position of s-plane	position of m.f.
088—811	150°— 40°	120°— 42°
	135°— 50°	150°— 5°
	130°— 60°	150°— 25°
	150°— 72°	202°— 57°

		148°— 15°
		145°— 45°
		145°— 60°
		155°— 55°
088—811	130°— 68°	150°— 50°
	125°— 60°	135°— 50°
	140°— 65°	135°— 65°
	135°— 83°	
	130°— 68°	
087—813	135°— 43°	170°— 40°
	145°— 45°	135°— 35°
		180°— 27°
		170°— 23°
086—814	120°— 28°	190°— 25°
	135°— 35°	170°— 25°
	130°— 35°	
086—815	130°— 37°	195°— 30°
	135°— 33°	
082—814	135°— 55°	160°— 25°
	140°— 50°	200°— 40°
083—814	110°— 45°	
078—811	95°— 33°	160°— 32°
		155°— 30°

Meas. sample 99 (17 s. and 14 m.f.)

	mean s.	mean m.f.
065—807	117°— 41°	
066—809		145°— 23°

co-ordinates of the grid	position of s-plane	position of m.f.
061—802	110°— 15°	150°— 25°
	90°— 40°	152°— 12°
	45°— 25°	130°— 15°
	130°— 40°	145°— 35°
	115°— 42°	
	130°— 50°	
	130°— 30°	
	120°— 25°	
068—811	105°— 55°	135°— 40°
	60°— 50°	145°— 35°
	125°— 50°	125°— 40°
	125°— 40°	175°— 50°
	140°— 60°	130°— 10°
		145°— 20°
		155°— 27°
068—812	130°— 42°	150°— 0°
	160°— 44°	150°— 12°
	135°— 45°	145°— 5°
	140°— 50°	

Meas. sample 100 (23 s. and 15 m.f.)

	mean s.	mean m.f.
112—805	127°— 40°	
112—805		163°— 35°

co-ordinates of the grid	position of s-plane	position of m.f.
113—804	147°— 68°	150°— 60°
	140°— 50°	130°— 55°
	130°— 50°	175°— 22°
	125°— 60°	185°— 40°
	140°— 45°	125°— 30°
	155°— 20°	
	105°— 32°	
113—805	117°— 48°	160°— 42°
	125°— 25°	200°— 22°
	115°— 55°	195°— 50°
	120°— 28°	190°— 30°
	115°— 42°	165°— 42°
	110°— 50°	180°— 45°
	130°— 30°	
112—805	120°— 35°	
	150°— 35°	
	140°— 15°	
	125°— 40°	
110—806	117°— 50°	135°— 10°
	125°— 35°	185°— 28°
	125°— 33°	120°— 25°
	135°— 35°	145°— 30°
	105°— 45°	

Meas. sample 101 (15 s. and 11 m.f.)

	mean s.	mean m.f.
002—723	124°— 34°	
002—723		155°— 19°

co-ordinates of the grid	position of s-plane	position of m.f.
002—722	100°— 38°	160°— 27°
002—723	135°— 40°	155°— 15°
	115°— 27°	150°— 12°
	125°— 35°	155°— 30°
	115°— 54°	145°— 30°
	115°— 30°	150°— 32°
	145°— 55°	160°— 23°
	130°— 40°	155°— 22°
	120°— 17°	
	115°— 42°	
	120°— 27°	
	100°— 24°	
003—724	155°— 40°	160°— 10°
	145°— 48°	165°— 20°
	— 0°	145°— −8°

Meas. sample 102 (20 s. and 24 m.f.)

	mean s.	mean m.f.
004—797	84°— 48°	
004—797		161°— 38°

co-ordinates of the grid	position of s-plane	position of m.f.
007—798	135°— 58°	155°— 40°
	75°— 50°	150°— 45°
	90°— 37°	155°— 35°
	100°— 53°	225°— 35°
		145°— 42°
		125°— 50°
006—798	85°— 50°	160°— 35°
	65°— 50°	130°— 42°
	60°— 52°	185°— 50°
	65°— 50°	150°— 30°
005—798	90°— 35°	195°— 45°
004—797	83°— 60°	165°— 42°
	75°— 55°	
003—797	100°— 78°	90°— 45°
002—796	105°— 40°	155°— 48°
001—794	75°— 20°	190°— 30°
000—794	90°— 40°	160°— 35°
	65°— 35°	170°— 23°
	95°— 50°	180°— 25°
	60°— 42°	195°— 30°
		185°— 40°
		125°— 42°
004—798		165°— 30°
		155°— 43°
006—798	80°— 57°	160°— 25°
	85°— 40°	

Meas. sample 103 (21 s. and 21 m.f.)

	mean s.	mean m.f.
971—793	95°— 46°	
972—793		177°— 36°

co-ordinates of the grid	position of s-plane	position of m.f.
982—795	93°— 54°	185°— 55°
973—793	140°— 55°	160°— 50°
	110°— 50°	180°— 40°
	133°— 45°	192°— 60°
	115°— 42°	195°— 47°
		165°— 40°
		187°— 45°
		165°— 48°
972—794	123°— 35°	155°— 33°
	130°— 40°	195°— 30°
	90°— 35°	185°— 35°
971—794	130°— 42°	205°— 40°
	90°— 40°	183°— 17°
		195°— 42°
		130°— 15°
970—793	55°— 45°	180°— 13°
	80°— 35°	165°— 35°
	90°— 45°	
968—793	55°— 45°	190°— 30°
	50°— 60°	170°— 25°
	75°— 70°	170°— 22°
	90°— 62°	
	100°— 30°	
	80°— 30°	
967—793	65°— 45°	165°— 38°
	105°— 65°	

Meas. sample 104 (21 s. and 21 m.f.)

	mean s.	mean m.f.
022—829	20°— 41°	
023—829		143°— 36°

co-ordinates of the grid	position of s-plane	position of m.f.
022—830	30°— 30°	140°— 25°

	−10°— 55°	130°— 25°
	25°— 35°	140°— 35°
	−5°— 40°	145°— 27°
	10°— 30°	140°— 34°
	25°— 35°	145°— 32°
	35°— 28°	
	20°— 40°	
	30°— 40°	
022—829	20°— 43°	145°— 25°
	25°— 50°	174°— 38°
	20°— 60°	155°— 40°
	20°— 40°	
023—829	0°— 50°	140°— 42°
	20°— 42°	138°— 40°
	20°— 43°	125°— 35°
	30°— 35°	138°— 40°
	5°— 48°	
023—828	0°— 35°	133°— 33°
	33°— 45°	155°— 47°
	60°— 37°	145°— 45°
		145°— 40°
		153°— 47°
		140°— 35°
		140°— 42°
		145°— 37°

Meas. sample 105 (15 s. and 14 m.f.)

	mean s.	mean m.f.
042—843	111°— 62°	
041—843		128°— 43°

co-ordinates of the grid	position of s-plane	position of m.f.
042—844	120°— 60°	115°— 57°
	120°— 75°	115°— 30°
	125°— 62°	110°— 50°
	130°— 65°	100°— 35°
	120°— 65°	120°— 52°
	115°— 57°	110°— 65°
	105°— 60°	
043—843	113°— 80°	113°— 40°
	120°— 60°	135°— 45°
	133°— 45°	130°— 15°
	100°— 60°	120°— 45°
	112°— 52°	
	125°— 65°	
039—839	75°— 85°	
038—840	45°— 45°	150°— 45°
		150°— 45°
		150°— 42°
		170°— 35°

Meas. sample 106 (28 s. and 22 m.f.)

	mean s.	mean m.f.
009—766	159°— 15°	
009—766		175°— 4°

co-ordinates of the grid	position of s-plane	position of m.f.
012—766	— 0°	185°— −5°
	107°—−12°	175°—−10°
011—767	120°— 5°	170°— 0°
	150°— 40°	165°— 25°
	125°— 16°	
010—767	135°— 27°	
009—768	165°— 34°	170°— 15°
	140°— 20°	
009—767	140°— 32°	150°—−10°
	180°— 20°	200°— 12°
	200°— 40°	185°— 10°
	155°— 5°	175°— 22°
010—765	130°— 20°	165°— 3°
	140°— 15°	170°— 3°
	155°— 2°	
009—765	170°— 7°	165°— 3°
	200°— 10°	160°— −7°
	195°— 20°	190°— 0°
009—764	160°— 5°	190°— 10°
	180°— 10°	170°— 3°
	210°—−25°	175°— 12°
	220°— 2°	175°— 0°
	170°— −4°	195°—−10°
		190°— 10°
009—763	125°— 35°	
	160°— −3°	
011—764	150°— 30°	155°— 0°
	185°— 35°	170°— −5°
	130°— 35°	

Meas. sample 107 (20 s. and 16 m.f.)

	mean s.	mean m.f.
021—756	142°— 17°	
021—756		168°— 13°

co-ordinates of the grid	position of s-plane	position of m.f.
021—756	145°— 35°	170°— 22°
	150°— 30°	165°— 15°
	155°— 15°	165°— 10°
		175°— 9°
		195°— 25°
020—756	120°— 14°	200°— 22°
	145°— 27°	155°— 15°
	165°— 15°	150°— 8°
	160°—−20°	
	120°— 25°	
	130°— 15°	
	110°— 28°	
020—755	122°— 22°	130°— 4°
	170°— 18°	190°— 7°
	90°— 15°	157°— 0°
		135°— 23°
		190°— 0°
021—755	150°— 15°	155°— 15°
	170°— 19°	
	140°— 13°	
	130°— 3°	
	180°— 25°	
021—756	150°— 22°	165°— 15°
	140°— 10°	185°— 20°

Meas. sample 108 (18 s. and 11 m.f.)

	mean s.	mean m.f.
025—806	120°— 55°	
025—806		156°— 37°

co-ordinates of the grid	position of s-plane	position of m.f.
025—806	120°— 47°	155°— 30°
	135°— 52°	160°— 27°
	123°— 50°	155°— 34°
	107°— 60°	145°— 40°
	122°— 60°	145°— 40°
	115°— 54°	165°— 48°
	95°— 60	175°— 45°
	110°— 58°	
	123°— 45°	
	100°— 50°	
024—807	110°— 77°	150°— 35°
	130°— 62°	150°— 33°
	135°— 60°	160°— 35°
	100°— 56°	155°— 35°
	140°— 55°	
	130°— 50°	
	140°— 45°	
	130°— 50°	

Meas. sample 109 (25 s. and 19 m.f.)

	mean s.	mean m.f.
086—875	95°— 56°	
086—875		142°— 44°

co-ordinates of the grid	position of s-plane	position of m.f.
086—876	60°— 35°	150°— 42°
	80°— 55°	190°— 47°
	120°— 43°	160°— 52°
	105°— 40°	
086—875	120°— 52°	130°— 50°
	65°— 45°	155°— 32°
	85°— 35°	125°— 45°
	120°— 55°	110°— 50°
	75°—110°	120°— 20°
	60°— 65°	135°— 50°
	60°— 72°	145°— 37°
	170°— 32°	145°— 35°
	80°— 55°	155°— 25°
	135°— 90°	
	150°— 70°	
	145°— 90°	
	130°— 47°	
086—847	60°— 50°	140°— 50°
	60°— 35°	160°— 25°
	80°— 72°	90°— 60°
	85°— 35°	145°— 50°
	110°— 60°	155°— 58°
	95°— 40°	145°— 50°
	45°— 60°	135°— 65°
	67°— 47°	

Meas. sample 110 (20 s. and 21 m.f.)

	mean s.	mean m.f.
209—756	85°— 69°	
209—756		106°— 43°

co-ordinates of the grid	position of s-plane	position of m.f.
209—755	75°— 65°	90°— 30°
	95°— 80°	95°— 42°
	80°— 65°	115°— 58°
	85°— 80°	100°— 35°
	95°— 83°	100°— 48°
	80°— 75°	90°— 50°
	90°— 75°	115°— 40°
	90°— 70°	125°— 48°
		100°— 45°
209—756	95°— 62°	160°— 60°
	80°— 72°	95°— 35°
		110°— 45
208—756	30°— 50°	115°— 45°
	80°— 70°	105°— 58°
	105°— 75°	110°— 35°
	87°— 65°	105°— 32°
	90°— 48°	90°— 38°
208—757	100°— 80°	110°— 35°
	75°— 60°	95°— 42°
	102°— 70°	
208—758	80°— 75°	105°— 37°
	85°— 65°	100°— 55°

Meas. sample 111 (26 s. and 17 m.f.)

	mean s.	mean m.f.
206—769	101°— 82°	
206—769		115°— 52°

co-ordinates of the grid	position of s-plane	position of m.f.
206—766	105°—100°	130°— 60°
	105°— 65°	140°— 40°
	85°— 65°	105°— 55°
	107°— 87°	
206—767	100°— 67°	120°— 57°
	95°— 83°	135°— 63°
	115°— 75°	105°— 45°
	110°— 68°	105°— 62°
		100°— 67°
206—768	95°— 100°	130°— 55°
	95°— 130°	
	135°— 150°	
	120°— 115°	
	105°— 82°	
206—769	90°— 70°	100°— 35°
	105°— 68°	
206—770	90°— 80°	125°— 55°
	90°— 65°	115°— 57°
	100°— 75°	
206—771	105°— 78°	135°— 45°
	80°— 65°	
	95°— 70°	
207—772	85°— 83°	115°— 52°
	100°— 80°	95°— 40°
	100°— 73°	95°— 65°
	110°— 65°	105°— 38°
206—769	105°— 70°	

Meas. sample 112 (24s. and 29 m.f.)

	mean s.	mean m.f.
195—804	107°— 85°	
196—804		103°— 51°

co-ordinates of the grid	position of s-plane	position of m.f.
195—805		100°— 50°
		90°— 35°
		115°— 55°
		105°— 40°
195—804		90°— 45°
		120°— 65°
		110°— 40°
		105°— 55°
		90°— 60°
		100°— 50°
		110°— 40°
		105°— 70°
		95°— 45°
		100°— 55°
196—803		110°— 55°
		80°— 60°
		120°— 40°
197—803		120°— 45°
		125°— 70°
		95°— 50°
		120°— 65°
		100°— 50°
		110°— 30°
		80°— 50°
		105°— 45°
		100°— 40°
198—802		95°— 55°
		95°— 53°
		85°— 65°
195—804	100°— 60°	
	95°— 70°	
	80°— 68°	
	90°— 87°	
	80°— 78°	
	135°— 90°	
	160°—120°	
	145°— 72°	
	90°— 75°	
	85°— 87°	
	125°— 85°	
	85°— 62°	
	90°— 80°	
195—803	120°— 90°	
	85°— 83°	
	65°— 80°	
	80°— 75°	
	125°—100°	
	110°— 90°	
	105°— 87°	
	125°—105°	
	160°—115°	
	125°—100°	
	100°— 72°	

Meas. sample 113 (20 s. and 24 m.f.)

	mean s.	mean m.f.
163—877	107°— 75°	
163—876		203°— 74°

co-ordinates of the grid	position of s-plane	position of m.f.
161—877	65°— 95°	210°—120°
	90°— 90°	270°—100°
	115°— 85°	134°— 75°
	87°— 90°	— 90°
	100°— 70°	
	80°— 75°	
161—876	100°— 75°	— 90°
		120°— 60°
		170°— 58°
		155°— 75°
162—877	85°— 45°	160°— 32°
	130°— 40°	220°— 60°
	130°— 57°	210°— 55°
163—877	100°— 55°	165°— 48°
	125°— 65°	185°— 73°
164—876	125°— 67°	165°— 75°
	105°— 60°	
	130°— 100°	
	135°— 85°	220°— 85°
	125°—105°	— 90°
	90°— 85°	255°— 55°
	115°— 83°	225°— 75°
	105°— 75°	— 90°
		275°— 60°
		240°— 75°
		260°— 60°
		225°— 85°
		190°—100°

Meas. sample 114 (8 s. and 24 m.f.)

	mean s.	mean m.f.
133—877	93°— 67°	
133—877		192°— 73°

co-ordinates of the grid	position of s-plane	position of m.f.
136—877	110°— 95°	160°— 83°
		130°—116°
		— 90°
135—877	105°— 80°	110°—125°
	120°— 35°	230°— 52°
133—877	90°— 37°	210°— 65°
	45°— 90°	195°— 45°
	95°— 52°	245°—120°
		145°—125°
		225°— 75°

		190°— 35°
		195°— 50°
		— 90°
		210°— 70°
		270°— 75°
		195°— 62°
		200°— 60°
		170°— 57°
134—877	90°— 70°	215°— 65°
		215°— 50°
		230°— 50°
		180°— 58°
		190°— 70°
		170°— 68°
	85°— 80°	

Meas. sample 115 (39 m.f.)

	mean m.f.
991—700	17°— 0°

co-ordinates of the grid	position of s-plane	position of m.f.
988—702		30°— 5°
		30°—−15°
		10°—−30°
		−25°—−10°
		20°— 3°
		60°—−30°
		30°— 35°
991—701		−10°— −3°
		−5°— 5°
		3°— 3°
		5° — −8°
		40°— −7°
		−20°— 3°
		−20°— 5°
		−15°— 5°
		−20°— 5°
		17°— 2°
		15°— 5°
		15°— −1°
		−2°— 5°
		0°— 2°
		50°— −8°
992—700		20°—−10°
		25°—−10°
		25°—−10°
		30°— −3°
		5°— 3°
		10°— 15°
993—698		45°— 30°
		20°— 30°
		10°— 20°
		35°— 30°
994—697		45°— −5°
		50°—−10°
		55°—−10°
		30°— −5°
		35°— −5°
		−20°— −7°
		20°— −8°

Meas. sample 116 (30 m.f.)

	mean m.f.
001—694	204°— 16°

co-ordinates of the grid	position of s-plane	position of m.f.
998—695		175°— 10°
		170°— 8°
		220°— 5°
001—694		215°— 5°
		230°— 5°
		215°— 7°
		220°— 10°
		205°— 30°
		190°— 30°
		195°— 35°
		212°— 18°
		190°— 22°
		195°— 20°
		180°— 27°
		213°— 14°
		255°— −6°
		250°— 5°
		256°— 15°
		200°— 28°
		235°— 25°
		190°— 30°
		217°— 18°
		220°— 13°
		196°— 24°
		155°— 6°
		165°— 20°
		175°— 4°
003—695		190°— 20°
		212°— 18°
		172°— 8°

Meas. sample 117 (14 s. and 27 m.f.)

	mean s.	mean m.f.
058—685	90°— 34°	
058—685		189°— 23°

co-ordinates of the grid	position of s-plane	position of m.f.
058—685	95°— 30°	200°— 7°
	70°— 35°	230°— 6°
	85°— 47°	160°— 25°
	115°— 43°	215°— 17°
	104°— 50°	235°— 32°
	65°— 25°	205°— 50°
	80°— 25°	253°— 15°
	100°— 20°	150°— 25°
	90°— 25°	215°— 45°
	90°— 35°	210°— 42°
	123°— 48°	135°— 8°
	85°— 30°	145°— 10°
	65°— 20°	163°— 25°
	90°— 40°	146°— 15°
		245°— 10°
		230°— 25°
		255°— 25°
		210°— 30°
		230°— 28°
		165°— 15°
		175°— 28°
		130°— 30°
		125°— 20°
		140°— 20°
		135°— 27°
		190°— 47°
		220°— 15°

Meas. sample 118 (16 s. and 45 m.f.)

	mean s.	mean m.f.
075—679	87°— 38°	
074—679		158°— 23°

co-ordinates of the grid	position of s-plane	position of m.f.
084—682	105°— 34°	135°— 8°
	110°— 33°	233°— 20°
	80°— 35°	120°— 40°
	80°— 34°	210°— 35°
	60°— 40°	135°— 20°
		150°— 24°
		135°— 23°
		140°— 24°
		240°— 4°
		150°— 5°
		155°— 8°
071—678	90°— 50°	183°— 6°
	65°— 35°	100°—−10°
	85°— 32°	225°— 20°
	95°— 30°	215°— 10°
	85°— 48°	218°— 10°
	93°— 70°	100°— 3°
	65°— 25°	130°— 23°
	90°— 30°	200°— 20°
	120°— 36°	200°— 34°
	80°— 37°	140°— 30°
	90°— 35°	150°— 28°
		170°— 20°
		140°— 34°
		140°— 34°
		140°— 39°
		135°— 27°
		100°—−10°
		103°—−17°
		153°— 20°
		180°— 40°
		195°— 40°
		216°— 30°
		200°— 35°
		143°— 40°
		155°— 30°
		153°— 20°
		150°— 26°

		153°— 34°
		166°— 33°
		150°— 35°
		145°— 30°
		130°— 30°
		130°— 46°
		110°— 35°

Meas. sample 119 (65 s. and 119 m.f.)

	mean s.	mean m.f.
020—686	131°— 40°	
020—686		156°— 14°

co-ordinates of the grid	position of s-plane	position of m.f.
018—688	170°— 47°	175°— 6°
	165°— 53°	175°— 12°
	152°— 46°	178°— 10°
	148°— 52°	180°— 15°
	140°— 37°	175°— 25°
	148°— 37°	176°— 27°
	132°— 40°	170°— 20°
	127°— 36°	180°— 18°
	145°— 43°	175°— 2°
	125°— 44°	162°— 11°
	143°— 40°	172°— 30°
	145°— 55°	173°— 28°
	120°— 37°	160°— 28°
	125°— 34°	180°— 16°
		180°— 20°
		165°— 28°
		165°— 31°
		200°— 35°
		196°— 38°
		160°— 27°
022—685	130°— 45°	160°— 20°
		168°— 14°
		165°— 16°
016—677	140°— 55°	140°— 23°
	130°— 40°	130°— 23°
	70°— 25°	140°— 17°
		140°— 20°
		145°— 18°
023—687	93°— 37°	200°— 18°
	130°— 25°	175°— 12°
	110°— 42°	197°— 38°
	135°— 30°	170°— 26°
	100°— 42°	163°— 13°
		165°— 11°
		180°— 12°
		192°— 5°
		200°— −2°
		200°— −2°
		202°—−10°
018—687	165°— 49°	93°—−36°
	182°— 34°	126°—−28°
	162°— 34°	124°—−40°
		117°— 32°
	158°— 36°	220°— 31°
	155°— 34°	220°— 32°
	165°— 32°	245°— 32°
	112°— 38°	237°— 35°
	123°— 27°	102°—−31°
	133°— 28°	80°—−28°
	122°— 60°	95°—−16°
	125°— 50°	185°— 4°
	140°— 47°	190°— 20°
	135°— 40°	105°—−35°
	103°— 60°	146°— 14°
		83°—−34°
		125°— 40°
019—688	112°— 47°	108°— 2°
	60°— 26°	114°— 0°
	93°— 29°	93°— 13°
	110°— 32°	110°— 22°
	113°— 43°	93°— 1°
		146°—18°
		150°— 19°
		80°—−18°
		123°— 11°
		120°— −2°
		152°— 1°
		137°— −3°
		135°— −5°
		125°— 37°
		81°—−37°
		150°— 31°
		240°— 48°
		175°— 28°
		135°— 16°
022—685	116°—35°	99°— −2°
	120°— 37°	110°— 4°
	137°— 28°	120°— −6°
	135°— 27°	152°— 20°
	136°— 44°	180°— 24°
	137°— 58°	150°— 16°
	145°— 40°	100°— 5°
	125°— 43°	115°— 1
	128°— 46°	115°— 4°
	90°— 42°	110°—−11°
	123°— 33°	165°— 12°
	133°— 46°	95°— −4°
	141°— 45°	115°— −2°
	153°— 29°	182°— 40°
	148°— 38°	195°— 38°
	138°— 37°	183°— 41°
	126°— 40°	175°— 32°
	142°— 31°	115°—−28°
		122°— −9°
		115°— 5°
		173°—−20°
		170°— 18°
		162°— 21°
		135°— 1°
		141°— 1°
		140°— 5°
		171°— 18°
		180°— 36°
		170°— 35°
		165°— 40°
		196°— 44°
		205°— 16°
		226°— 44°
		205°— 22°
		187°— 42°
		184°— 33°
		232°— 36°
	145°— 55°	165°— 28°
	120°— 37°	165°— 31°
	95°— 47°	165°— 34°
	125°— 55°	200°— 35°
		196°— 38°
		160°— 27°
		138°— 5°

Meas. sample 120 (4 s. and 9 m.f.)

	mean s.	mean m.f.
983—693	114°— 32°	
983—693		201°— 23°

co-ordinates of the grid	position of s-plane	position of m.f.
983—693	90°— 28°	180°— 38°
	90°— 39°	178°— 40°
	110°— 24°	225°— 2°
	165°— 36°	210°— 9°
		220°— 19°
		220°— 18°
		202°— 28°
		195°— 23°
		180°— 16°

Meas. sample 121 (26 s. and 30 m.f.)

	mean s.	mean m.f.
043—706	104°— 35°	
044—706		154°— 27°

co-ordinates of the grid	position of s-plane	position of m.f.
035—707	95°— 23°	155°— 20°
	110°— 42°	120°— 16°
	125°— 55°	150°— 22°
	105°— 43°	165°— 30°
	108°— 33°	175°— 38°
	95°— 37°	145°— 9°
	135°— 40°	145°— 22°
	115°— 25°	
040—707	95°— 15°	185°— 35°
	123°— 35°	187°— 35°
	90°— 40°	183°— 34°
	85°— 45°	135°— 50°
	115°— 48°	160°— 38°
	140°— 34°	150°— 48°
		135°— 6°
046—706	80°— 40°	165°— 44°
	95°— 34°	185°— 44°

		155°— 8°
049—705	95°— 19°	165°— 20°
	120°— 20°	155°— 17°
	90°— 25°	170°— 12°
	78°— 32°	138°— 48°
	87°— 42°	135°— 45°
	103°— 30°	80°— −5°
	100°— 45°	145°— 35°
		160°— 40°
		150°— 15°
		145°— 35°
057—702	105°— 22°	200°— 28°
	120°— 50°	160°— 23°
	100°— 28°	115°— 5°

Meas. sample 122 (27 s. and 29 m.f.)

	mean s.	mean m.f.
018—726	86°— 41°	
018—727		158°— 39°

co-ordinates of the grid	position of s-plane	position of m.f.
017—727	87°— 33°	190°— 36°
		185°— 35°
017—726	65°— 30°	155°— 35°
	98°— 34°	240°— 34°
	65°— 35°	155°— 48°
019—727	95°— 35°	167°— 40°
	85°— 45°	100°— 20°
	65°— 40°	150°— 32°
	90°— 54°	160°— 44°
	70°— 32°	170°— 40°
	66°— 43°	150°— 35°
	76°— 42°	150°— 52°
	65°— 40°	150°— 40°
	60°— 52°	170°— 60°
	60°— 45°	168°— 60°
	87°— 70°	178°— 36°
	60°— 68°	135°— 25°
	90°— 30°	168°— 46°
	55°— 40°	182°— 44°
	93°— 45°	160°— 40°
	115°— 30°	78°— 45°
	100°— 38°	95°— 50°
	110°— 43°	97°— 48°
	100°— 50°	125°— 20°
	130°— 40°	160°— 30°
	110°— 23°	200°— 43°
	105°— 32°	155°— 43°
	118°— 35°	185°— 28°
		190°— 22°

Meas. sample 123 (26 s. and 4 m.f.)

	mean s.	mean m.f.
013—715	104°— 30°	
013—715		171°— 14°

co-ordinates of the grid	position of s-plane	position of m.f.
009—711	60°— 30°	190°— 12°
	30°— 35°	145°— 15°
	62°— 20°	
	50°— 30°	
	100°— 25°	
	115°— 30°	
	130°— 40°	
013—711	95°— 40°	
	120°— 25°	
	95°— 30°	
	−80°— 35°	
	165°— 30°	
009—716	165°— 30°	
	90°— 30°	
	105°— 23°	
	115°— 30°	
	145°— 30°	
017—718	115°— 37°	165°— 2°
	155°— 15°	
018—719	95°— 30°	185°— 25°
	87°— 30°	
	87°— 40°	
020—719	100°— 25°	
	85°— 35°	
019—717	105°— 35°	
	140°— 20°	

Meas. sample 124 (44 s. and 37 m.f.)

	mean s.	mean m.f.
964—679	114°— 25°	
964—679		189°— 15°

co-ordinates of the grid	position of s-plane	position of m.f.
965—683	120°— 22°	190°— 18°
	100°— 22°	240°— 10°
	120°— 30°	210°— 20°
	185°— 60°	235°— 5°
	150°— 43°	180°— 20°
	90°— 30°	210°— 8°
	90°— 17°	170°— 15°
	95°— 40°	175°— 37°
	70°— 38°	205°— 25°
	130°— 20°	195°— 22°
	50°— 37°	180°— 25°
	153°— 25°	170°— 8°
	150°— 30°	180°— 27°
	140°— 40°	150°— 25°
	135°— 22°	155°— 27°
	100°— 25°	195°— 10°
	160°— 17°	195°— 20°
	110°— 37°	180°— 3°
	150°— 35°	205°— −3°
	90°— 40°	200°— 20°
	90°— 37°	205°— 22°
	85°— 27°	
	70°— 35°	
	95°— 15°	
	150°— 36°	
962—671	70°— 25°	190°— 20°
	85°— 10°	170°— 20°
	100°— 20°	195°— 7°
	105°— 20°	210°— 10°
	145°— 25°	185°— 10°
	150°— 28°	195°— 3°
	153°— 30°	190°— 20°
	160°— 25°	205°— 8°
	150°— 25°	210°— 2°
	105°— 10°	210°— 7°
	65°— 18°	155°— 10°
	160°— 32°	175°— 7°
	75°— 10°	
	140°— 30°	
	140°— 15°	
961—678	195°—−40°	175°— 15°
		165°— 15°
		175°— 3°
		170°— 24°
963—681	45°— 20°	
	50°— 22°	
966—683	65°— 25°	

Meas. sample 125 (23s. and 24 m.f.)

	mean s.	mean m.f.
953—675	218°— 29°	
953—675		358°— 8°

co-ordinates of the grid	position of s-plane	position of m.f.
953—675	295°—−31°	345°— 10°
	223°— 34°	358°— 16°
	227°— 20°	351°— 11°
	210°— 26°	372°— 7°
	213°— 33°	340°— 10°
	207°— 36°	342°— 9°
	215°— 43°	350°— −2°
	227°— 35	325°— 12°
	229°— 37°	362°— 22°
	220°— 30°	354°— 14°
	225°— 23°	381°— −1°
	218°— 31°	372°— 13°
	197°— 37°	346°— 6°
	208°— 30°	367°— 9°
	213°— 25°	366°— 10°
	214°— 27°	344°— 8°
	220°— 38°	358°— −3°
	210°— 33°	360°— 17°
	192°— 38°	357°— 12°
	211°— 27°	343°— 14°
	218°— 32°	382°— 8°
	200°— 34°	390°—−20°
	215°— 34°	

957—674		358°— 7°
		357°— 7°

Meas. sample 126 (34s. and 20 m.f.)

	mean s.	mean m.f.
997—711	155°— 23°	
997—710		187°— 9°

co-ordinates of the grid	position of s-plane	position of m.f.
998—711	65°— 25°	180°— 18°
	130°— 20°	165°— −1°
	90°— 23°	155°— −3°
		180°— 15°
		165°— 5°
997—709	105°— 20°	195°— 22°
	165°— 35°	222°— 20°
	167°— 35°	197°— 22°
	90°— 20°	195°— 20°
	120°— 15°	180°— 18°
	190°— 25°	190°— 7°
	185°— 10°	198°— 5°
	175°— 30°	183°— 2°
	180°— 25°	180°— −3°
	185°— 15°	185°— 1°
	200°— 30°	190°— 2°
	185°— 22°	180°—−25°
	180°— 25°	185°— 1°
	195°— 16°	185°— 25°
	145°— 20°	
	155°— 25°	
	60°— 12°	
999—712	157°— 20°	
	182°— 32°	
000—709	158°— 35°	
	210°— 33°	
000—714	165°— 22°	230°— 20°
	168°— 20°	
	180°— 20°	
	155°— 12°	
	150°— 30°	
	185°— 15°	
	150°— 22°	
	122°— 22°	
	135°— 25°	
	170°— 30°	

Meas. sample 127 (15 s. and 27 m.f.)

	mean s.	mean m.f.
946—663	171°—−5°	
946—663		171°— 5°

co-ordinates of the grid	position of s-plane	position of m.f.
949—665	155°—−17°	190°—−13°
	165°—−30°	130°— 15°
	170°—−20°	170°— −2°
		140°— 15°
		120°— 20°
		115°— 25°
		175°— 10°
		160°— 15°
945—662	152°— 5°	172°—−12°
		198°— 9°
	90°— 3°	218°— 1°
	200°— 18°	193°— 6°
	210°—−11°	192°— 9°
	156°— 14°	204°— 14°
	192°— −9°	211°— 2°
	150°— 18°	208°— 1°
	165°— 4°	207°— −8°
	230°—−17°	135°—−25°
	210°—−27°	157°— 13°
	203°—−19°	164°— 9°
	120°— 11°	196°— 7°
		193°— −2°
		204°— 2°
		170°— 17°
		135°— 6°
		168°— 13°
		93°— 1°

Meas. sample 128 (11 s. and 9 m.f.)

	mean s.	mean m.f.
941—649	101°— 36°	
943—648		188°— 31°

co-ordinates of the grid	position of s-plane	position of m.f.
940—650	153°— 13°	178°— 12°
	108°— 25°	218°— 10°
	160°— 35°	225°— 12°
	165°— 25°	
	48°— 21°	
	65°— 29°	
	66°— 25°	
943—646	96°— 73°	158°— 62°
	93°— 56°	130°— 66°
	96°— 71°	160°— 58°
947—648	60°— 25°	210°— 25°
		210°— 20°
		205°— 18°

Meas. sample 129 (24 s. and 50 m.f.)

	mean s.	mean m.f.
036—750	104°— 29°	
036—749		172°— 18°

co-ordinates of the grid	position of s-plane	position of m.f.
035—754	100°— 32°	175°— 35°
	90°— 30°	200°— 45°
	55°— 40°	175°— 33°
	83°— 35°	230°— 15°
	100°— 28°	175°— 25°
		173°— 30°
034—752	100°— 40°	240°— 24°
	93°— 30°	238°— 24°
	120°— 25°	220°— 15°
	140°— 35°	240°— 5°
	120°— 42°	165°— 34°
		170°— 15°
		165°— 15°
		140°— −2°
		245°—−15°
		185°— 40°
		240°— 50°
		195°— 40°
		190°— 42°
037—748	115°— 28°	100°— −7°
	102°— 30°	120°— 2°
	98°— 31°	130°— 2°
	100°— 40°	150°— 17°
	80°— 28°	140°— 15°
	122°— 40°	135°— 27°
	80°— 17°	132°— 27°
	80°— 13°	150°— 8°
	142°— 13°	156°— 20°
	110°— 15°	127°— 28°
		130°— 20°
		135°— 27°
		155°— 33°
		155°— 25°
		133°— 22°
		150°— 28°
		150°—−13°
		135°— 5°
		150°— 2°
		97°—−23°
038—746	130°— 35°	190°— 28°
	93°— 18°	177°— 27°
	125°— 25°	162°— 10°
	123°— 20°	248°— −5°
		248°—−10°
		190°— 22°
		180°— 30°
		173°— 27°
		170°— 12°
		190°— 25°
		180°— 17°

Meas. sample 130 (10 s. and 22 m.f.)

	mean s.	mean m.f.
045—754	116°— 23°	
045—754		168°— 20°

co-ordinates of the grid	position of s-plane	position of m.f.
045—754	128°— 20°	156°— 10°
	70°— 15°	210°— 25°
	107°— 22°	235°— 35°
	105°— 35°	162°— 10°
	85°— 20°	150°— 5°
	123°— 28°	140°— 10°
	120°— 27°	140°— 5°
	143°— 10°	150°— 10°
	134°— 40°	147°— 16°

		210°— 25°
		170°— 23°
		150°— 8°
		140°— 9°
		196°— 40°
		170°— 42°
		178°— 30°
		148°— 15°
		162°— 23°
		175°— 31°
		162°— 28°
		160°— 36°
		190°— 5°
053—748	140°— 17°	

Meas. sample 131 (24 s. and 41 m.f.)

	mean s.	mean m.f.
041—725	114°— 37°	
041—725		179°— 27°

co-ordinates of the grid	position of s-plane	position of m.f.
040—727	133°— 22°	240°—-25°
	107°— 33°	155°— 24°
	105°— 30°	163°— 25°
	130°— 40°	150°— 26°
	134°— 30°	205°— 41°
	126°— 32°	173°— 35°
	135°— 40°	200°— 33°
	118°— 37°	200°— 25°
	122°— 34°	118°— 5°
	108°— 32°	100°— -5°
	132°— 34°	177°— 20°
		190°— 25°
		165°— 17°
		152°— 15°
		195°— 33°
		160°— 18°
		175°— 30°
		150°— 7°
041—724	106°— 41°	195°— 37°
	100°— 41°	180°— 34°
	113°— 38°	165°— 37°
	107°— 36°	160°— 30°
	100°— 45°	180°— 23°
	102°— 48°	182°— 24°
	97°— 46°	221°— 35°
	113°— 39°	205°— 40°
	127°— 37°	203°— 43°
	125°— 42°	210°— 33°
	102°— 42°	180°— 42°
	86°— 39°	120°— 15°
	97°— 38°	136°— 24°
		172°— 30°
		180°— 34°
		212°— 40°
		200°— 42°
		165°— 32°
		160°— 35°
		196°— 38°
		160°— 33°
		170°— 37°
		215°— 37°

Meas. sample 132 (15 s. and 48 m.f.)

	mean s.	mean m.f.
052—718	129°— 39°	
051—719		192°— 25°

co-ordinates of the grid	position of s-plane	position of m.f.
048—723		215°— 25°
		203°— 25°
		255°— 42°
		258°— 45°
		205°— 30°
		205°— 22°
		245°— 45°
		250°—-47°
		248°—-45°
052—718	145°— 30°	165°— 8°
	132°— 38°	160°— 13°
	130°— 43°	165°— 16°
	125°— 35°	210°— 43°
	112°— 30°	165°— 23°
	140°— 38°	168°— 13°
	100°— 34°	148°— 44°
	132°— 38°	105°—-10°
	133°— 35°	105°— -9°
	147°— 40°	247°— 38°
	140°— 53°	175°— 32°
	128°— 36°	165°— 16°
	135°— 43°	162°— 22°
	132°— 40°	230°— 25°
	106°— 45°	170°— 26°
		178°— 28°
		150°— 15°
		190°— 37°
		196°— 34°
		170°— 18°
		280°— 25°
		180°— 35°
		182°— 40°
		172°— 28°
		250°— 43°
		185°— 37°
		255°— 26°
		246°— 42°
		176°— 28°
		183°— 31°
		185°— 28°
		217°— 13°
		160°— 30°
		185°— 38°
		188°— 36°
		155°— 28°
		150°— 30°
		178°— 35°
		160°— 34°

Meas. sample 133 (21 s. and 58 m.f.)

	mean s.	mean m.f.
153—779	112°— 91°	
151—781		112°— 36°

co-ordinates of the grid	position of s-plane	position of m.f.
147—782	130°— 77°	140°— 57°
	140°— 84°	132°— 62°
	122°— 80°	136°— 40°
	130°— 83°	120°— 40°
	120°— 90°	142°— 56°
	123°— 80°	150°— 32°
	138°— 88°	140°— 60°
		135°— 42°
		148°— 50°
		148°— 58°
155—778	93°— 98°	93°— 35°
	98°—102°	100°— 10°
	80°— 88°	100°— 40°
	95°— 88°	103°— 45°
	90°— 95°	90°— 83°
	77°—136°	95°— 25°
	105°— 92°	105°— 44°
		105°— 5°
		95°— 7°
		93°— 3°
		95°— 3°
		130°— 48°
		128°— 42°
		108°— 18°
		120°— 57°
		114°— 12°
		108°— 0°
		98°— 28°
161—774	120°— 80°	90°— 45°
	122°— 83°	110°— 55°
	110°— 82°	120°— 53°
	110°— 78°	122°— 47°
	122°— 82°	120°— 30°
		150°— 65°
		75°— 17°
		110°— 30°
		125°— 53°
		115°— 63°
		140°— 63°
		130°— 60°
		155°— 68°
155—783	95°—135°	80°— 33°
		87°— 30°
		105°— 8°
		82°— 35°
		60°— 5°
		60°— 27°
143—787		80°— 5°
		75°— 11°
		85°— -8°
		90°—-10°
140—788		80°— -3°

		88°— −2°
127—793	130°— 83°	157°— 58°
		150°— 64°
		115°— 48°
		156°— 62°
		108°— 50°

Meas. sample 134 (43 s. and 17 m.f.)

	mean s.	mean m.f.
136—766	97°— 55°	
135—767		153°— 40°

co-ordinates of the grid	position of s-plane	position of m.f.
134—771	100°— 65°	130°— 32°
	115°— 61°	130°— 25°
	118°— 68°	130°— 35°
	128°— 76°	125°— 28°
	110°— 55°	145°— 38°
	85°— 37°	165°— 37°
	60°— 34°	150°— 40°
	100°— 45°	170°— 47°
	80°— 45°	137°— 43°
	120°— 65°	180°— 46°
	105°— 65°	135°— 43°
	105°— 57°	165°— 46°
	135°— 63°	
	120°— 60°	
	104°— 49°	
	110°— 62°	
	87°— 52°	
	123°— 66°	
	97°— 64°	
	87°— 46°	
	135°— 75°	
	118°— 62°	
	130°— 62°	
136—765	100°— 42°	160°— 45°
	88°— 52°	
	84°— 55°	
	80°— 48°	
	88°— 64°	
	85°— 47°	
	86°— 46°	
	107°— 56°	
	110°— 55°	
	87°— 58°	
138—762	100°— 46°	175°— 38°
	100°— 50°	
	75°— 50°	
141—754	65°— 48°	160°— 49°
	87°— 53°	165°— 51°
	67°— 50°	
	72°— 50°	
142—751	90°— 55°	185°— 45°
	60°— 49°	
	70°— 47°	

Meas. sample 135 (50 s. and 41 m.f.)

	mean s.	mean m.f.
081—703	89°— 50°	
080—703		142°— 38°

co-ordinates of the grid	position of s-plane	position of m.f.
081—702	105°— 41°	161°— 33°
	95°— 30°	165°— 31°
	83°— 36°	153°— 36°
	90°— 41°	200°— 33°
	85°— 36°	180°— 40°
	78°— 34°	152°— 33°
	72°— 48°	148°— 32°
	82°— 43°	173°— 38°
	67°— 52°	162°— 33°
	68°— 48°	185°— 45°
	87°— 46°	155°— 32°
	100°— 40°	135°— 36°
	78°— 39°	184°— 37°
	93°— 52°	120°— 36°
	91°— 65°	170°— 36°
	96°— 60°	150°— 32°
	86°— 57°	170°— 50°
	100°— 68°	167°— 61°
	86°— 58°	110°— 38°
	112°— 70°	108°— 37°
	92°— 77°	120°— 38°
	87°— 67°	188°— 60°
	83°— 70°	115°— 56°
	90°— 82°	115°— 41°
	103°— 87°	85°— 13°
	97°— 87°	82°— 15°
		106°— 55°
		107°— 43°
		97°— 10°
		105°— 42°
		102°— 45°
085—704	100°— 45°	140°— 33°
	85°— 43°	
	76°— 24°	
	64°— 33°	
	72°— 31°	
	87°— 33°	
	87°— 28°	
	82°— 32°	
	90°— 25°	
073—704	96°— 73°	158°— 62°
	93°— 56°	130°— 66°
	96°— 71°	160°— 58°
		85°— 20°
077—701	110°— 90°	
078—703	65°— 34°	155°— 34°
	54°— 40°	150°— 36°
	75°— 41°	
	62°— 40°	
081—705	107°— 43°	170°— 28°
	101°— 39°	135°— 25°
	100°— 46°	167°— 46°
	93°— 35°	
	100°— 45°	
083—707	125°— 45°	
	112°— 58°	

Meas. sample 136 (12 s. and 17 m.f.)

	mean s.	mean m.f.
990—643	124°— 43°	
990—643		144°— 17°

co-ordinates of the grid	position of s-plane	position of m.f.
984—641	154°— 42°	110°— −7°
	117°— 26°	153°— 12°
	138°— 36°	150°— 18°
	127°— 29°	102°— −20°
		90°— −25°
993—644	110°— 28°	140°— 8°
	84°— 39°	173°— 27°
	123°— 48°	143°— 28°
	129°— 64°	135°— 15°
	116°— 55°	185°— 4°
	137°— 48°	147°— 25°
	121°— 50°	132°— 55°
	132°— 50°	148°— 32°
		162°— 38°
		165°— 33°
		147°— 20°
		166°— 34°

Meas. sample 137 (24 s. and 29 m.f.)

	mean s.	mean m.f.
000—642	305°— 55°	
000—642		81°— 38°

co-ordinates of the grid	position of s-plane	position of m.f.
999—642	305°— 73°	120°— 52°
	314°— 72°	122°— 33°
	323°— 62°	115°— 52°
	318°— 58°	153°— −26°
	331°— 60°	42°— 65°
	274°— 27°	30°— 33°
	305°— 27°	85°— −2°
	282°— 31°	10°— 45°
	295°— 32°	79°— 57°
	297°— 64°	66°— 47°
	302°— 52°	85°— 45°
	306°— 58°	95°— 41°
	305°— 62°	87°— 31°
	298°— 67°	96°— 52°
	315°— 67°	105°— 37°
	320°— 58°	112°— 32°
	322°— 60°	109°— 27°
	322°— 50°	47°— 53°
	312°— 63°	65°— 48°
	290°— 53°	40°— 50°
		70°— 47°
003—643	305°— 54°	53°— 55°
	287°— 55°	

	312°— 52°	80°— 33°
	275°— 63°	75°— 48°
		85°— 33°
		70°— 34°
		75°— 27°
		90°— 20°
		87°— 28°

Meas. sample 138 (46 s. and 31 m.f.)

	mean s.	mean m.f.
963—688	103°— 24°	
963—688		178°— 7°

co-ordinates of the grid	position of s-plane	position of m.f.
	145°— 34°	178°— 18°
	181°— 74°	186°— 23°
	160°— 36°	180°— 12°
	166°— 26°	125°—−20°
	102°— 54°	192°— 1°
	135°— 27°	200°— 19°
	110°— 41°	120°— 17°
	87°— 37°	212°— 9°
	22°— 52°	185°— 19°
	37°— 40°	180°— 13°
	116°— 30°	174°— 10°
	103°— 36°	181°— 1°
	127°— 16°	178°— 26°
	180°— 30°	225°— 13°
	150°— 7°	220°— 16°
	175°— 37°	233°— 14°
	61°— 21°	120°—−11°
	55°— 29°	123°— −2°
	61°— 17°	98°—−30°
	123°— 25°	228°— 7°
	15°— 11°	155°— 12°
	166°— 12°	208°— 8°
	62°— 7°	212°— −3°
	182°— 7°	100°— 12°
	158°— 24°	222°— −5°
	170°— 22°	215°— 12°
	93°— 22°	125°— 20°
	120°— 12°	266°—−10°
	72°— 23°	137°— 5°
	187°— 21°	110°— 6°
	74°— 55°	240°— −8°
	65°— 29°	
	78°— 30°	
	22°— 38°	
	35°— 22°	
	40°— 25°	
	56°— 38°	
	70°— 22°	
	95°— 45°	
	60°— 29°	
	155°— 4°	
	86°— 22°	
	80°— 19°	
	120°— 30°	
	15°— 23°	
	180°— 35°	

Meas. sample 139 (68 s. and 34 m.f.)

	mean s.	mean m.f.
965—692	140°— 40°	
965—692		154°— 13°

co-ordinates of the grid	position of s-plane	position of m.f.
	140°— 45°	180°— 46°
	128°— 33°	185°— 32°
	145°— 50°	186°— 33°
	143°— 50°	200°— 53°
	122°— 80°	120°—−38°
	145°— 52°	136°—−32°
	135°— 55°	136°—−13°
	140°— 61°	118°—−25°
	142°— 50°	205°— 45°
	165°— 57°	128°— 7°
	140°— 56°	166°—−10°
	135°— 60°	125°— 6°
	158°— 46°	215°— 57°
	145°— 49°	116°— −5°
	159°— 53°	108°—−17°
	143°— 52°	175°— 28°
	142°— 52°	122°— 18°
	145°— 51°	125°— 25°
	170°— 47°	118°— 13°
	148°— 56°	150°— 12°
	132°— 56°	175°— 50°
	140°— 60°	188°— 42°
	142°— 54°	177°— 58°
	130°— 70°	145°— 30°
	151°— 52°	135°— 20°
	142°— 55°	188°— 17°
	128°— 72°	190°— 16°
	97°— 70°	130°— −6°
	123°— 75°	135°— 0°
	120°— 74°	130°— −8°
	122°— 71°	124°— 14°
	150°— 56°	132°— 6°
	140°— 50°	192°— −6°
	137°— 58°	190°— 6°
	103°— 60°	
	96°— 28°	
	78°— 47°	
	116°— 38°	
	126°— 64°	
	140°— 74°	
	155°— 83°	
	131°— 60°	
	116°— 42°	
	133°— 49°	
	130°— 56°	
	160°— 30°	
	110°— 12°	
	100°— 14°	
	215°— 7°	
	183°— 26°	
	205°— 12°	
	200°— 15°	
	160°— 7°	
	70°—−18°	
	204°— 14°	
	214°— 7°	
	68°—−12°	
	183°— 22°	
	110°— 13°	
	220°— 32°	
	60°—−18°	
	55°—−20°	
	195°— 27°	
	140°— 25°	
	181°— 14°	
	80°— 15°	
	110°— 15°	
	220°— 36°	

Meas. sample 140 (27 s. and 23 m.f.)

	mean s.	mean m.f.
961—699	307°— 25°	
961—699		45°— 11°

co-ordinates of the grid	position of s-plane	position of m.f.
	275°— 15°	−28°— 25°
	280°— 25°	98°—−10°
	295°— 28°	−40°— −5°
	283°— 31°	40°— 29°
	290°— 24°	−35°— 25°
	288°— 18°	52°— 14°
	280°— 18°	0°— 4°
	300°— 37°	−20°— 10°
	240°— 24°	−10°— 17°
	275°— 34°	10°—−25°
	260°— 29°	10°— −1°
	340°— 25°	60°— 13°
	315°— 24°	85°— 20°
	320°— 35°	88°— 15°
	315°— 26°	105°— 13°
	330°— 35°	85°— 7°
	295°— 30°	80°— 16°
	350°— 38°	81°— 4°
	320°— 36°	32°— −2°
	350°— 20°	102°— 3°
	315°— 8°	32°— 2°
	335°— 22°	105°— −2°
	325°— 25°	100°— 15°
	375°— 17°	
	320°— 19°	
	305°— 35°	
	325°— 10°	

Meas. sample 141 (39 s. and 32 m.f.)

	mean s.	mean m.f.
958—705	90°— 29°	
958—705		183°— 21°

co-ordinates of the grid	position of s-plane	position of m.f.
	75°— 20°	220°— −5°
	125°— 22°	215°—−17°

100°— 15°	217°—⁻15°	
136°— 15°	255°— 17°	
60°— 17°	190°— 10°	
80°— 6°	240°— 15°	
57°— 7°	163°— 6°	
90°— 10°	140°— 10°	
23°—⁻20°	150°— 7°	
161°— 16°	135°— 13°	
120°— 26°	140°—⁻10°	
132°— 16°	120°— 3°	
127°— 43°	125°— 21°	
90°— 18°	140°— 17°	
97°— 19°	140°— 4°	
110°— 18°	140°— 16°	
137°— 22°	150°— 23°	
80°— 23°	225°— 7°	
95°— 24°	215°— 30°	
50°— 24°	217°— 23°	
52°— 30°	200°— 46°	
56°— 29°	187°— 43°	
82°— 27°	178°— 45°	
115°— 45°	210°— 48°	
68°— 27°	110°— 34°	
85°— 60°	227°— 30°	
45°— 40°	137°— 35°	
40°— 36°	223°— 54°	
40°— 30°	226°— 23°	
100°— 38°	200°— 34°	

98°— 37°	202°— 48°	
100°— 51°	205°— 50°	
112°— 52°		
115°— 36°		
108°— 42°		
110°— 39°		
85°— 55°		
90°— 60°		
70°— 60°		

Meas. sample 142 (33 s. and 32 m.f.)

	mean s.	mean m.f.
222—778	82°— 78°	
222—779		84°— 47°

co-ordinates of the grid	position of s-plane	position of m.f.
218—782	95°— 40°	75°— 50°
	60°— 28°	85°— 40°
	75°— 48°	68°— 48°
	80°— 90°	65°— 60°
		55°— 42°
		65°— 58°
219—781	95°— 88°	95°— 42°
	95°— 90°	85°— 50°
		100°— 65°
		110°— 58°

222—779	95°— 68°	85°— 35°
	50°— 62°	85°— 48°
223—778	75°— 68°	95°— 60°
	65°— 62°	90°— 38°
	60°— 85°	85°— 35°
		75°— 40°
223—777	70°— 55°	110°— 40°
	95°— 80°	105°— 35°
	90°— 87°	80°— 55°
	93°— 88°	
	93°— 90°	
	105°— 90°	
	95°— 90°	
	88°— 85°	
	95°— 90°	
224—777	80°— 80°	90°— 48°
	95°— 90°	95°— 58°
	90°— 88°	100°— 52°
	80°— 88°	75°— 53°
	80°— 88°	80°— 50°
	88°— 78°	85°— 50°
	80°— 80°	88°— 75°
	85°— 85°	90°— 20°
	75°— 82°	70°— 35°
	65°— 77°	110°— 35°
	80°— 90°	70°— 35°
	60°— 72°	65°— 40°
	75°— 88°	50°— 60°

Tables of the positions of the schistosity-planes and the axes of the minor folds in the Cima d'Asta region (Sheet V).

(The strikes of the s-planes and the azimuths of the m.f. of the meas. samples 143-173 are given without the magnetic correction of — 2°.)

Meas. sample 143 (28 s. and 18 m.f.)

	mean s.	mean m.f.
098—149	275°— 25°	
099—149		298°— 12°

co-ordinates of the grid	position of s-plane	position of m.f.
103—144	270°— 20°	290°— 0°
	250°— 20°	285°— 5°
	210°— 20°	275°— 12°
		290°— 10°
	240°—⁻10°	280°— ⁻10°
102—145	220°— 27°	240°— 0°
	255°— 35°	
	260°— 50°	
	335°— 35°	
102—147	275°— 15°	335°— 10°
101—146	320°— 40°	260°—⁻40°
	350°— 40°	265°—⁻30°
	360°— 35°	250°—⁻20°
	290°—⁻35°	320°— 30°
	280°—⁻20°	
092—158	285°— 45°	300°— 30°
		300°— 20°
092—157	245°— 32°	
092—156	270°— 53°	310°— 57°
	250°— 60°	310°— 57°
	240°— 65°	
	265°— 50°	
092—155	270°—⁻40°	
098—150	255°— 38°	
	240°—⁻45°	
097—150	290°— 35°	350°— 25°
	320°— 30°	350°— 12°
	300°— 40°	360°— 40°
	275°— 30°	
095—147	290°— 40°	

Meas. sample 144 (31 s. and 21 m.f.)

	mean s.	mean m.f.
098—139	264°— 33°	
097—138		331°— 23°

co-ordinates of the grid	position of s-plane	position of m.f.
101—143	310°— 45°	320°— 0°
101—139	255°— 50°	275°—⁻10°

	285°— 35°	
	275°— 45°	
100—138	270°— 35°	285°— 20°
	270°— 40°	
	285°— 40°	
	255°— 35°	
096—137	250°— 35°	335°— 35°
	270°— 32°	330°— 30°
	280°— 35°	330°— 25°
	270°— 30°	320°— 20°
		330°— 30°
095—137	240°— 40°	315°— 30°
	285°— 50°	335°— 35°
	270°— 20°	375°— 30°
	270°— 40°	330°— 33°
	300°— 35°	335°— 25°
098—137	290°— 30°	330°— 20°
	240°— 50°	340°— 40°
	260°— 30°	340°— 30°
		340°— 35°
099—138	260°— 20°	335°— 35°
	240°— 20°	310°— 12°
	250°— 25°	
	260°— 27°	

099—141	285°— 40°	
098—142	185°— 10°	
	210°— 40°	
099—143	245°— 33°	360°— 10°
	275°— 15°	390°— 5°
	280°— 20°	
	250°— 30°	

Meas. sample 145 (17 s. and 14 m.f.)

	mean s.	mean m.f.
093—140	292°— 29°	
093—140		348°— 19°

co-ordinates of the grid	position of s-plane	position of m.f.
096—140	320°— 20°	370°—−15°
		315°— 5°
095—139	345°— 30°	
095—140	295°— 25°	350°— 20°
		320°— 25°
		365°— 30°
094—141	250°— 30°	330°— 32°
	305°— 27°	
093—141	285°— 40°	350°— 35°
	290°— 30°	375°— 20°
	285°— 20°	
092—141	275°— 28°	335°— 0°
	310°— 35°	345°— 0°
090—140		355°— 10°
090—139	300°— 10°	
	275°— 20°	
091—139	290°— 43°	360°— 22°
092—138	255°— 50°	340°— 48°
093—138	315°— 40°	
	300°— 25°	
094—138	280°— 27°	355°— 30°

Meas. sample 146 (25 s. and 21 m.f.)

	mean s.	mean m.f.
083—134	250°— 24°	
083—135		350°— 17°

co-ordinates of the grid	position of s-plane	position of m.f.
081—129		325°—−10°
		350°— −3°
080—129	210°— 20°	350°— −5°
	180°— 25°	
080—129	185°— 50°	
079—133	160°— 25°	
081—135	245°— 13°	300°— 10°
	275°— 20°	325°— 30°
	275°— 35°	330°— 25°
	275°— 15°	330°— 25°
	245°— 20°	
082—135	240°— 10°	350°— 12°
	240°— 28°	345°— 18°
	260°— 20°	
083—135	235°— 30°	350°— 27°
	225°— 20°	345°— 15°
	260°— 30°	315°— 33°
	280°— 20°	365°— 30°
	285°— 20°	
	270°— 42°	
084—136	285°— 15°	350°— 25°
	230°— 20°	
084—137		350°— 12°
085—137		400°— 20°
		370°— 25°
086—136	295°— 5°	395°— 20°
		395°— 25°
		375°— 15°
087—136	275°— 20°	
	315°— 35°	
	285°— 35°	
088—136	220°— 20°	335°— 10°

Meas. sample 147 (16 s. and 20 m.f.)

	mean s.	mean m.f.
069—129	137°— 16°	
068—130		161°— 4°

co-ordinates of the grid	position of s-plane	position of m.f.
070—130	160°— 40°	155°— −5°
	165°— 33°	165°— 5°
	210°—−21°	115°— 13°
069—129	155°— 47°	175°— 10°
	60°— 20°	145°— 15°
	85°— 25°	160°— 5°
	180°—−43°	155°— 15°
	105°— 15°	165°— 15°
	70°— 12°	170°— 12°
	55°— 10°	170°— 15°
	130°— 20°	
	185°— 30°	
	145°— 15°	
068—130	170°— 30°	160°— 0°
	— 0°	170°— −3°
	180°— 15°	175°— 0°
		160°— 10°
066—131		160°— −5°
		200°— 0°
		150°— −5°
		180°— 7°
		165°— 0°
065—132		125°—−20°

Meas. sample 148 (27 m.f.)

	mean m.f.
061—127	158°— 2°
061—128	

co-ordinates of the grid	position of s-plane	position of m.f.
061—133		135°— 15°
		185°— 10°
		165°— 3°
		145°— 3°
		160°—−10°
061—132		165°— −5°
062—131		145°— 3°
		135°—−15°
		160°— 0°
162—130		150°— 0°
		165°—−12°
162—129		150°—−10°
061—129		125°— 12°
		150°— 0°
		145°— 0°
		120°— 25°
061—128		160°— 8°
		170°— 0°
		160°— 12°
060—127		170°— 0°
		138°— 0°
059—125		140°— 10°
059—122		210°— 0°
060—122		190°— 0°
061—121		210°— 15°
062—121		155°— −7°
		150°— 10°

Meas. sample 149 (17 s. and 21 m.f.)

	mean s.	mean m.f.
025—220	289°— 33°	
025—221		336°— 24°

co-ordinates of the grid	position of s-plane	position of m.f.
024—219	290°— 55°	330°— 35°
	285°— 32°	320°— 35°
	295°— 30°	355°— 30°
	310°— 40°	315°— 35°
	260°— 33°	330°— 50°
	275°— 35°	
025—220	285°— 40°	310°— 32°
	285°— 33°	315°— 25°
	305°— 35°	345°— 40°
	290°— 43°	340°— 20°
	335°— 25°	320°— 10°
	240°— 35°	335°— 52°
	280°— 37°	300°— 10°
025—221	260°— 22°	330°— 23°
	305°— 27°	340°— 30°
		330°— 20°
026—221	295°— 15°	355°— 25°
026—223	315°— 30°	335°— 10°
		340°— 10°
026—225		365°— 20°
		385°— 0°
026—226		360°— 0°

Meas. sample 150 (24 s. and 18 m.f.)

	mean s.	mean m.f.
060—155	270°— 36°	
059—154		9°— 24°

co-ordinates of the grid	position of s-plane	position of m.f.
063—158	255°— 40°	−30°— 30°
	265°— 40°	
	265°— 25°	
	255°— 45°	
062—159	280°— 47°	60°— 20°
	270°— 42°	60°— 0°
	305°— 60°	0°— 33°
	245°— 45°	−10°— 10°
	255°— 35°	
	245°— 20°	
060—155	350°— 40°	
	270°— 22°	
060—156	330°— 55°	25°— 33°
	265°— 37°	25°— 15°
	260°— 27°	35°— 12°
	260°— 45°	35°— 20°
	255°— 30°	15°— 25°
	270°— 25°	−15°— 30°
	285°— 35°	
055—148	225°— 25°	−5°— 25°
		−30°— 27°
		−5°— 30°
054—148	270°— 45°	
055—148	270°— 35°	15°— 60°
	250°— 20°	45°— 20°
	270°— 33°	−30°— 20°
		−20°— 28°

Meas. sample 151 (8 s. and 12 m.f.)

	mean s.	mean m.f.
072—161	241°— 11°	
072—160		350°— 3°

co-ordinates of the grid	position of s-plane	position of m.f.
071—160	320°— 8°	350°— 0°
		350°— 0°
072—160	190°— 7°	325°— 3°
	190°— 5°	335°— 5°
		330°— 15°
		345°— 0°
		345°— 5°
		365°— 0°
		400°—−15°
072—161	225°—− 5°	315°— 7°
	170°— 7°	365°— 10°
	205°— 25°	370°— 10°
073—162	330°— 15°	
	300°— 28°	

Meas. sample 152 (22 s. and 18 m.f.)

	mean s.	mean m.f.
068—198	288°— 38°	
068—199		336°— 21°

co-ordinates of the grid	position of s-plane	position of m.f.
069—197	270°— 45°	350°— 10°
		335°— 12°
067—198	255°— 32°	380°— 32°
	285°— 25°	305°— 27°
	245°— 25°	
067—201	300°— 35°	345°— 20°
	285°— 35°	335°— 15°
		320°— 8°
		345°— 28°
		335°— 5°
067—200	255°— 35°	300°— 12°
	255°— 38°	325°— 25°
	280°— 38°	345°— 35°
	300°— 35°	325°— 23°
	280°— 35°	360°— 25°
	275°— 28°	300°— 20°
066—200	300°— 35°	340°— 20°
069—197	330°— 55°	
	290°— 40°	
070—197	300°— 47°	
	340°— 50°	
	325°— 50°	
	315°— 45°	
	285°— 33°	
	285°— 40°	
071—196	285°— 40°	375°— 27°
		335°— 40°

Meas. sample 153 (8 s. and 21 m.f.)

	mean s.	mean m.f.
013—206	209°— 25°	
014—205		344°— 7°

co-ordinates of the grid	position of s-plane	position of m.f.
012—206	185°— 50°	365°— 12°
	190°— 50°	335°— −3°
	195°— 40°	315°— 22°
013—206	180°— 57°	365°— 0°
	285°— 30°	360°— 23°
014—206	125°—−38°	345°— 18°
		330°— 0°
015—205	220°— 22°	320°—−15°
	290°—−12°	330°— 35°
		320°—−15°
		345°— 30°
		345°— 20°
		355°— 18°
		338°— 17°
		365°— −7°
		340°— −7°
		375°— 12°
		325°—−12°
		345°—−12°
		370°— 0°
018—206		330°— 10°

Meas. sample 154 (14 s. and 18 m.f.)

	mean s.	mean m.f.
061—204	274°— 28°	
061—204		346°— 21°

co-ordinates of the grid	position of s-plane	position of m.f.
061—202	305°— 27°	335°— 15°
	295°— 35°	340°— 15°
	288°— 32°	355°— 20°
		380°— 18°
062—203	345°—−30°	350°— 28°
062—204	290°— 35°	355°— 15°
	225°— 35°	330°— 35°
	280°— 28°	350°— 32°
	240°— 45°	355°— 35°
	255°— 33°	335°— 8°
		325°— 0°
		315°— 10°
062—205	250°— 35°	340°— 18°
	300°— 30°	350°— 30°
	240°— 33°	345°— 30°
		360°— 35°
057—206	255°— 33°	325°— 28°
	270°— 15°	375°— 12°

Meas. sample 155 (19s. and 6 m.f.)

	mean s.	mean m.f.
972—075	273°— 74°	
971—075		268°— 87°

co-ordinates of the grid	position of s-plane	position of m.f.
971—075	270°— 80°	270°— 85°
	275°— 80°	270°— 80°
	270°— 90°	275°— 70°
	280°— 75°	270°— 80°
	260°— 75°	— 90°
	265°— 78°	
	255°— 80°	
	275°— 90°	
	265°— 80°	
	285°— 65°	
	270°— 75°	
	285°— 80°	
	260°— 90°	
	270°— 90°	
	270°— 65°	
	275°— 73°	
	300°— 55°	
972—077		255°—115°
976—076	270°— 40°	
	290°— 50°	

Meas. sample 156 (20 s. and 13 m.f.)		
	mean s.	mean m.f.
044—215	249°— 30°	
044—215		345°— 21°

co-ordinates of the grid	position of s-plane	position of m.f.
045—215	255°— 27°	335°— 13°
	240°— 17°	365°— 17°
	270°— 17°	345°— 30°
	235°— 35°	330°— 25°
	305°— 25°	
	265°— 28°	
	230°— 35°	
	265°— 37°	
044—214	235°— 25°	
044—215	235°— 22°	355°— 5°
	195°— 37°	345°— 13°
	205°— 30°	360°— 15°
	195°— 40°	350°— 27°
	205°— 35°	365°— 8°
	270°— 23°	360°— 22°
	190°— 37°	
043—216	305°— 25°	325°— 28°
	255°— 25°	
043—214	290°— 35°	340°— 37°
	335°— 50°	310°— 27°

Meas. sample 157 (22 s. and 27 m.f.)		
	mean s.	mean m.f.
043—219	273°— 39°	
043—219		341°— 32°

co-ordinates of the grid	position of s-plane	position of m.f.
043—218	270°— 37°	340°— 33°
	275°— 40°	355°— 30°
	310°— 35°	375°— 30°
	260°— 60°	360°— 33°
		320°— 55°
043—219	315°— 50°	335°— 48°
	305°— 20°	325°— 35°
	265°— 43°	355°— 37°
	275°— 33°	350°— 25°
	250°— 42°	340°— 35°
	215°— 35°	335°— 40°
	305°— 45°	340°— 32°
	295°— 60°	320°— 37°
	250°— 43°	345°— 33°
	300°— 23°	350°— 30°
	315°— 32°	335°— 27°
	230°— 35°	325°— 37°
	275°— 35°	320°— 40°
043—220	285°— 60°	315°— 35°
042—219	225°— 30°	320°— 12°
	270°— 37°	345°— 20°
	215°— 37°	340°— 12°
		340°— 35°
		350°— 38°
		335°— 30°
043—218	295°— 30°	380°— 28°
		360°— 25°

Meas. sample 158 (8 s. and 32 m.f.)		
	mean s.	mean m.f.
076—227	289°— 39°	
075—226		348°— 37°

co-ordinates of the grid	position of s-plane	position of m.f.
076—227	265°— 40°	355°— 45°
	300°— 58°	360°— 40°
	270°— 47°	350°— 43°
	300°— 57°	345°— 45°
	285°— 43°	355°— 45°
		355°— 37°
		350°— 37°
		345°— 20°
075—227		340°— 37°
		340°— 40°
074—220		350°— 35°
		345°— 50°
		325°— 40°
		350°— 47°
		330°— 30°
		345°— 17°
		365°— 7°
074—221	320°— 58°	370°— 28°
074—227		360°— 32°
		375°— 37°
074—228		370°— 32°
074—229		360°— 27°
		330°— 40°
		340°— 42°
		340°— 32°
		335°— 43°
076—228	270°— 35°	360°— 50°
	305°— 50°	330°— 50°
		340°— 38°
		340°— 50°
		335°— 37°
077—227		330°— 42°

Meas. sample 159 (11 s. and 30 m.f.)		
	mean s.	mean m.f.
054—231	314°— 31°	
053—232		354°— 19°

co-ordinates of the grid	position of s-plane	position of m.f.
057—231	325°—350°	350°— 10°
056—231	265°— 50°	375°— 60°
		400°— 35°
055—231	330°— 50°	315°— 20°
	240°— 22°	345°— 20°
	375°— 52°	325°— 12°
		375°— 17°
054—232	310°— 32°	340°— 10°
	320°— 45°	350°— 15°
	355°— 50°	340°— 15°
		360°— 20°
		380°— 7°
		350°— 10°
		360°— 3°
		380°— 20°
		335°— 12°
		350°— 15°
		360°— 12°
		360°— 10°
054—233	320°— 32°	370°— 20°
		365°— 20°
		345°— 15°
		345°— 35°
		345°— 20°
048—232	375°— 45°	345°— 17°
	235°— 45°	340°— 25°
047—231		325°— 28°
046—231		365°— 17°
		355°— 30°
044—230		370°— 12°

Meas. sample 160 (29 s. and 37 m.f.)		
	mean s.	mean m.f.
989—195	204°— 32°	
989—194		10°— 7°

co-ordinates of the grid	position of s-plane	position of m.f.
990—196	230°— 25°	20°— 0°
	195°— 50°	0°— 18°
		30°— 3°
		25°— 5°
		−15°— 15°
990—195	220°— 40°	20°— 10°
	210°— 30°	10°— 10°
	190°— 22°	5°— 8°
	240°— 27°	15°— 7°
	185°— 50°	25°— 0°
	225°— 30°	15°— 2°
	200°— 30°	20°— 0°
	210°— 35°	10°— 5°
	195°— 32°	40°— −5°
	190°— 25°	−15°— 0°
		25°— 5°
		45°— 10°
		−15°— 20°
		15°— 0°
989—195	245°— 5°	5°— 0°
	210°— 33°	10°— 3°
	225°— 42°	25°— 5°
	220°— 35°	20°— 0°
	170°— 30°	20°— −3°
	175°— 35°	10°— 8°
	200°— 25°	
	205°— 25°	

988—194	215°— 25°	25°— 5°
	245°— 30°	−10°— 22°
	185°— 40°	−20°— 25°
	200°— 48°	5°—−15°
	180°— 35°	−35°— 0°
		20°— 10°
987—193	170°— 12°	15°— −7°
987—192	240°— 50°	5°— 3°
	140°— 33°	0°— 20°
		25°— 20°
		−5°— 23°
986—192	215°— 32°	
986—191		−5°— 13°

Meas. sample 161 (44 s. and 43 m.f.)

	mean s.	mean m.f.
980—181	238°—28°	
980—181		339°— 19°

co-ordinates of the grid	position of s-plane	position of m.f.
983—187	215°— 20°	320°— 20°
	175°— 30°	290°— 30°
983—186	190°— 30°	320°— 12°
983—184	315°— 45°	345°— 15°
	210°— 60°	305°— 40°
983—183	240°— 10°	340°— 10°
982—183	240°— 30°	350°— 30°
	240°— 35°	
982—182	215°— 10°	320°— 18°
	230°— 20°	325°— 20°
	230°— 35°	310°— 25°
	210°— 45°	315°— 15°
		320°— 30°
982—180	225°— 20°	325°— 30°
	265°— 30°	315°— 20°
	270°— 30°	335°— 27°
	260°— 40°	315°— 25°
	285°— 27°	330°— 28°
	225°— 20°	335°— 25°
	240°— 50°	325°— 40°
	235°— 50°	360°— 40°
	305°— 38°	335°— 35°
980—182	185°— 20°	385°— 2°
	290°— 28°	330°— 15°
	225°— 20°	
980—181	180°— 7°	350°— 2°
979—181	200°— 30°	345°— 7°
	210°— 13°	365°— 5°
	230°— 5°	355°— 50°
	240°— 23°	305°— 15°
	220°— 10°	345°— 5°
	270°— 25°	370°— 5°
	260°— 25°	
976—178	240°— 20°	375°— 12°
	200°— 10°	365°— 3°
	310°— 22°	340°— 10°
	220°— 30°	385°— 0°
		355°— 15°
		370°—−12°
975—178	260°— 23°	365°— 7°
	225°— 22°	360°— 17°
	275°— 48°	365°— 30°
	250°— 43°	
	245°— 30°	
980—179	240°— 35°	335°— 38°
	280°— 40°	340°— 30°
		340°— 20°
981—179	190°— 20°	280°— 10°

Meas. sample 162 (30 m.f.)

	mean m.f.
081—214	350°— 30°

co-ordinates of the grid	position of s-plane	position of m.f.
082—213		375°— 30°
		345°— 25°
		365°— 30°
		355°— 28°
		345°— 25°
		355°— 40°
081—214		330°— 15°
		340°— 30°
		355°— 25°
		345°— 7°
		330°— 10°
		310°— 12°
		365°— 27°
		360°— 40°
		365°— 33°
		365°— 28°
		330°— 5°
		285°— 40°
		355°— 50°
		380°— 62°
		365°— 38°
		365°— 35°
		335°— 40°
080—214		345°— 33°
		365°— 30°
		345°— 40°
		345°— 32°
080—213		335°— 30°
079—213		345°— 28°
		395°— 45°

Meas. sample 163 (22 s. and 32 m.f.)

	mean s.	mean m.f.
052—200	256°— 32°	
052—200		341°— 22°

co-ordinates of the grid	position of s-plane	position of m.f.
054—200	210°— 10°	345°— 10°
	190°— 30°	340°— 5°
		330°— −3°
		290°— 15°
		390°— 0°
		320°— 10°
		350°— 20°
		320°— 0°
052—201	290°— 37°	380°— 25°
	300°— 52°	315°— 17°
	300°— 40°	325°— 17°
052—200	240°— 30°	335°— 20°
	260°— 35°	350°— 20°
	220°— 50°	310°— 35°
	290°— 40°	320°— 10°
	265°— 37°	335°— 25°
	285°— 30°	340°— 20°
	225°— 25°	335°— 25°
		335°— 25°
		340°— 20°
		345°— 20°
051—200	265°— 32°	335°— 32°
051—199	185°— 50°	355°— 15°
		330°— 28°
		345°— 33°
	240°— 15°	340°— 10°
	235°— 15°	330°— 10°
	220°— 15°	335°— 25°
		330°— 30°
051—198	255°— 20°	350°— 7°
		360°— 3°
	290°— 80°	360°— 67°
	250°— 45°	340°— 45°
		380°— 75°

Meas. sample 164 (25 s. and 34 m.f.)

	mean s.	mean m.f.
066—136	252°— 18°	
066—136		330°— 9°

co-ordinates of the grid	position of s-plane	position of m.f.
065—132	290°— 18°	335°— 3°
	290°— 25°	330°— 5°
	220°— 15°	320°— 10°
		360°— 30°
066—133	295°— 40°	340°— 25°
	300°— 28°	345°— −8°
	165°— 5°	320°— −8°
	280°— 10°	325°— 2°
		320°— 5°
066—134	270°— 13°	330°— 22°
066—135	165°— 30°	325°— 0°
	245°— 20°	345°— 15°
	290°— 22°	315°— 5°
064—136	260°— 20°	315°— 30°
	300°— 18°	330°— 15°
	240°— 10°	350°— 3°
		325°— 0°
		335°— 5°
065—137	285°— 22°	330°— 7°
	265°— 10°	335°— 5°
	255°— 20°	320°— 12°

066—138	320°—	20°	340°—	3°
	295°—	12°	315°—	0°
	240°—	5°	330°—	5°
	260°—	20°	305°—	−10°
	160°—	15°	340°—	5°
	160°—	15°	310°—	2°
	170°—	10°	340°—	10°
067—140			335°—	20°
067—142	280°—	18°	350°—	35°
			340°—	20°
			335°—	12°
068—142			300°—	20°
069—143			340°—	0°

Meas. sample 165 (16s. and 29 m.f.)

	mean s.	mean m.f.
955—075	316°— 32°	
955—075		8°— 18°

co-ordinates of the grid	position of s-plane	position of m.f.
955—073	340°— −8°	15°— 0°
955—074	360°— 25°	10°— 0°
	340°— 25°	10°— 15°
	285°— 33°	15°— 30°
	340°— 35°	0°— 3°
	330°— 45°	−10°— 2°
	320°— 42°	10°— 15°
		−5°— 3°
955—075	310°— 27°	15°— 27°
	355°— 38°	25°— 22°
	345°— 50°	5°— 18°
	325°— 25°	−5°— 10°
	330°— 33°	30°— 28°
955—076	330°— 45°	40°— 35°
	415°—−40°	0°— 27°
956—077	410°—−20°	10°— 22°
	295°— 30°	30°— 35°
		−5°— 25°
		0°— 35°
		0°— 30°
		0°— 30°
		20°— 20°
		5°— 30°
955—074		−5°— 15°
		−15°— 15°
		−15°— 10°
		−15°— 10°
954—074		15°— −5°
954—072		50°— 12°

Meas. sample 166 (44 s. and 27 m.f.)

	mean s.	mean m.f.
963—121	196°— 31°	
963—121		355°— 15°

co-ordinates of the grid	position of s-plane	position of m.f.
963—128	195°— 25°	330°— 12°
	190°— 25°	395°— 5°
965—124	215°— 35°	350°— 23°
	190°— 55°	
966—123	140°— 35°	350°— 8°
	185°— 25°	350°— −3°
965—123	155°— 10°	365°— 8°
	175°— 15°	340°— 10°
	180°— 25°	340°— 10°
	165°— 40°	
	180°— 38°	
	165°— 25°	
	170°— 50°	
965—122	160°— 20°	350°— 5°
968—121	170°— 40°	
	155°— 50°	
	135°— 22°	
	185°— 30°	
964—121	180°— 35°	360°— 25°
964—120	200°— 22°	345°— 18°
963—120	175°— 40°	
963—119	215°— 27°	360°— 12°
	215°— 30°	380°— 30°
	265°— 34°	345°— 12°
	235°— 34°	
	185°— 20°	
963—120	230°— 60°	355°— 8°
	230°— 37°	350°— 30°
	260°— 35°	360°— 35°
	240°— 40°	375°— 18°
	200°— 62°	
	210°— 50°	
963—119	230°— 50°	410°— 25°
962—119	150°— 20°	365°— −3°
961—120	185°— 32°	355°— 10°
	225°— 23°	325°— 5°
	220°— 23°	350°— 17°
	240°— 15°	360°— 20°
	185°— 20°	355°— 10°
	220°— 20°	330°— 18°
	230°— 25°	340°— 35°
960—120	240°— 25°	
955—122	180°— 12°	
954—123	170°— 23°	

Meas. sample 167 (29 s. and 31 m.f.)

	mean s.	mean m.f.
972—153	267°— 27°	
972—153		346°— 20°

co-ordinates of the grid	position of s-plane	position of m.f.
969—154	290°— 15°	400°— 0°
971—153	255°— 40°	380°— 25°
	295°— 15°	390°— 20°
	205°— 48°	325°— 12°
		345°— 30°
972—153	305°— 30°	345°— 22°
	260°— 25°	350°— 22°
	310°— 30°	355°— 10°
	345°— 15°	360°— 10°
	245°— 28°	360°— 22°
	250°— 28°	355°— 15°
	240°— 15°	330°— 20°
	245°— 30°	350°— 20°
	255°— 37°	338°— 15°
	280°— 27°	342°— 25°
	295°— 22°	340°— 15°
	280°— 35°	330°— 17°
	303°— 35°	
	280°— 15°	
973—153	230°— 30°	340°— 25°
	235°— 10°	340° 28°
	200°— 40°	340°— 28°
	205°— 22°	335°— 18°
	240°— 30°	340°— 25°
	290°— 20°	345°— 15°
	330°— 33°	345°— 18°
		350°— 12°
		340°— 30°
		355°— 10°
974—150	250°— 30°	330°— 18°
	265°— 30°	325°— 27°
	295°— 35°	325°— 27°
	275°— 25°	335°— 28°

Meas. sample 168 (40 s. and 36 m.f.)

	mean s.	mean m.f.
979—140	236°— 30°	
979—140		340°— 18°

co-ordinates of the grid	position of s-plane	position of m.f.
976—146	220°— 20°	345°— 20°
	265°— 40°	310°— 45°
		345°— 20°
976—145	275°— 28°	330°— 10°
	210°— 23°	340°— 22°
	230°— 15°	340°— 18°
		335°— 10°
976—144	220°— 23°	330°— 23°
	190°— 25°	325°— 5°
977—143	240°— 45°	355°— 25°
978—139	200°— 20°	320°— 15°
	200°— 35°	325°— 12°
	200°— 22°	340°— 8°
	295°— 45°	360°— 15°
977—139	190°— 15°	335°— 30°
	280°— 60°	370°— 33°
	260°— 40°	345°— 45°
	210°— 57°	345°— 20°
	270°— 25°	355°— 20°
977—138	265°— 23°	335°— 38°
978—138	220°— 25°	340°— 33°
979—138	285°— 25°	355°— 5°
	320°— 20°	325°— 3°
	210°— 35°	330°— 3°
	180°— 30°	
980—137	270°— 40°	
	215°— 55°	

	205°— 58°	
	305°— 55°	
	255°— 50°	
980—139	200°— 15°	335°— 12°
	220°— 15°	332°— 10°
981—140	210°— 18°	352°— 25°
	196°— 15°	355°— 10°
	196°— 15°	355°— 12°
982—139	207°— 25°	350°— 12°
	205°— 15°	345°— 10°
982—138	260°— 30°	332°— 10°
	275°— 20°	335°— 10°
	295°— 20°	340°— 15°
	275°— 35°	342°— 15°
	210°— 15°	335°— 12°

Meas. sample 169 (19s. and 25 m.f.)

	mean s.	mean m.f.
971—138	227°— 18°	
972—138		342°— 10°

co-ordinates of the grid	position of s-plane	position of m.f.
973—138	300°— 20°	325°— 10°
	230°— 27°	330°— 27°
	170°— 25°	350°— 0°
		320°— 12°
		355°— 10°
		345°— 15°
973—137	240°— 15°	340°— 10°
	270°— 20°	380°— 7°
		335°— 12°
972—137	265°— 5°	338°— 15°
	240°— 32°	360°— 7°
	245°— 30°	350°— 7°
	265°— 15°	342°— 15°
	310°— 30°	335°— −5°
971—137	255°— 30°	340°— 12°
	175°— 15°	345°— 10°
		355°— 10°
971—139	190°— 33°	340°— 12°
		340°— 7°
		360°— 10°
970—139	150°—−20°	330°— 10°
	165°— 25°	340°— 10°
	165°— −8°	325°— 5°
	145°— 20°	335°— 10°
	315°— 20°	
970—140	215°— 15°	325°— 12°

Meas. sample 170 (31 s. and 29 m.f.)

	mean s.	mean m.f.
935—151	226°— 25°	
935—151		353°— 12°

co-ordinates of the grid	position of s-plane	position of m.f.
936—150	215°— 20°	335°— 10°
	200°— 3°	355°— 0°
	165°— 15°	370°— 12°
	215°— 15°	370°— 10°
	215°— 45°	360°— 13°
	190°— 37°	345°— 18°
	255°— 33°	
935—150	245°— 27°	345°— 7°
	170°— 8°	375°— 15°
	250°— 35°	350°— 18°
	230°— 33°	380°— 28°
	280°— 50°	340°— 0°
	200°— 33°	380°— 15°
	285°— 38°	350°— 30°
	225°— 43°	350°— 12°
	275°— 35°	
935—151	140°— 8°	335°— 15°
	195°— 30°	325°— 27°
	240°— 22°	365°— 25°
	250°— 15°	372°— 4°
	240°— 22°	355°— 5°
	180°— 23°	345°— 10°
		340°— 12°
934—151	218°— 20°	325°— 5°
	235°— 12°	335°— 8°
	235°— 15°	355°— 12°
934—152	225°— 12°	355°— 8°
	230°— 13°	348°— 10°
933—152	285°— 37°	355°— 17°
	220°— 35°	
932—153	195°— 13°	345°— 5°
	225°— 25°	370°—−15°

Meas. sample 171 (35 s. and 41 m.f.)

	mean s.	mean m.f.
974—164	176°— 2°	
974—164		347°— 5°

co-ordinates of the grid	position of s-plane	position of m.f.
970—168	85°— 3°	325°—−20°
	135°— 23°	330°— 12°
	240°—−15°	330°—−15°
	95°— 18°	315°— −5°
	240°— 27°	330°— 10°
	220°— 15°	
970—167	95°— 18°	295°— 8°
971—166	90°— 12°	295°—−10°
	245°— 12°	330°—−15°
		330°—−10°
		345°— −8°
		330°— −7°
972—166	155°—−30°	360°— 12°
973—165	150°—−30°	370°— 10°
	210°— 20°	340°— 12°
	90°—−25°	390°— 8°
	245°— 20°	380°— 8°
		360°— 13°
974—164	185°— −5°	335°— 8°
	225°—−22°	385°— 15°
	150°—−12°	345°— 3°
	155°—−18°	360°— 0°
		365°— 2°
		335°— 7°
974—163	210°— 8°	360°— 7°
	85°—−15°	345°— 15°
	135°—−30°	345°— 15°
975—163	220°— −2°	360°— 0°
975—162	135°—−45°	360°— 22°
976—162	125°—−20°	380°— 15°
	210°— 35°	355°— 25°
	245°— 30°	350°— 10°
977—162	235°— 25°	352°— 5°
	215°— 15°	350°— 12°
	185°— 20°	345°— 5°
	200°— 12°	345°— 3°
	130°— 18°	350°— 12°
	190°— 15°	320°— 0°
978—162	195°— 20°	350°— 3°
	200°— 25°	345°— 5°
		340°— 25°
978—161	225°— 12°	375°— 7°

Meas. sample 172 (33 s. and 39 m.f.)

	mean s.	mean m.f.
984—165	262°— 19°	
984—165		353°— 9°

co-ordinates of the grid	position of s-plane	position of m.f.
983—165	195°— 23°	370°— 8°
	275°— 25°	360°— 22°
	230°— 32°	325°— 0°
	195°—−37°	345°— 3°
	360°— 25°	
983—166	355°— 45°	360°— 10°
		360°— 3°
		355°—−10°
984—166	360°— 30°	330°—−12°
	200°—−18°	380°— 12°
	355°—−20°	355°— 15°
	210°— 27°	365°— 12°
	345°— 20°	360°— 20°
		360°— 23°
		365°— 3°
984—167		350°— 10°
984—168	200°— 18°	380°— 10°
		375°— 3°
		335°— 13°
984—169	250°— 15°	365°— 12°
983—164	355°— 25°	370°— 10°
	350°— 20°	365°— 15°
	315°— 20°	362°— 15°
	340°— 40°	350°— 5°
984—164	308°— 25°	350°— 10°
	285°— 30°	346°— 15°
	300°— 15°	350°— 12°
	260°— 22°	345°— 12°
	320°— 20°	355°— 5°
	240°— 20°	352°— 10°
	280°— 12°	360°— 10°
	260°— 16°	346°— 7°
	220°— 12°	337°— 5°

	230°— 25°	335°— 10°
	220°— 40°	320°— 8°
	195°— 28°	350°— 5°
	220°— 18°	355°— 12°
	195°— 15°	352°— 5°
984—165	190°— 20°	335°— 5°
	200°— 20°	338°— 5°

Meas. sample 173 (30 s. and 29 m.f.)

	mean s.	mean m.f.
912—124	268°— 32°	
912—124		358°— 22°

co-ordinates of the grid	position of s-plane	position of m.f.
914—122	255°— 40°	385°— 17°
	270°— 37°	375°— 15°
	290°— 48°	335°— 30°
913—122	245°— 18°	370°— 15°
	255°— 25°	358°— 15°
	275°— 30°	375°— 23°
	270°— 20°	365°— 15°
	275°— 25°	370°— 20°
	275°— 30°	375°— 35°
	245°— 37°	330°— 25°
	250°— 20°	370°— 15°
	290°— 30°	
913—123	230°— 20°	335°— 15°
	290°— 30°	335°— 10°
	300°— 50°	355°— 40°
	270°— 30°	360°— 15°
	265°— 25°	375°— 20°
	265°— 30°	365°— 15°
912—125	295°— 30°	350°— 27°
	275°— 30°	350°— 10°
	295°— 55°	345°— 47°
	265°— 30°	355°— 20°
911—125	275°— 35°	360°— 35°
	255°— 30°	350°— 12°
	265°— 33°	365°— 35°
911—126	250°— 30°	360°— 15°
	275°— 30°	355°— 5°
	265°— 35°	355°— 32°
910—126	260°— 35°	360°— 30°
910—127	255°— 45°	345°— 30°

Meas. sample 174 (15 s. and 47 m.f.)

	mean s.	mean m.f.
167—252	327°— 48°	
168—251		16°— 30°

co-ordinates of the grid	position of s-plane	position of m.f.
167—255	268°—750°	58°— 55°
	289°— 37°	23°— 42°
		43°— 47°
		38°— 35°
		43°— 42°
		38°— 48°
		28°— 50°
		33°— 45°
		28°— 38°
167—254		26°— 35°
		18°— 40°
		23°— 25°
		13°— 20°
168—252		13°— 30°
		3°— 35°
		13°— 25°
		8°— 35°
		18°— 25°
169—251		8°— 25°
		13°— 27°
		23°— 45°
		13°— 20°
		3°— 27°
		13°— 35°
170—252	348°— 50°	25°— 40°
	373°— 62°	−2°— 24°
	313°— 42°	
	336°— 43°	
168—250	313°— 30°	28°— 20°
	298°— 30°	
168—249		33°— 30°
		23°— 25°
168—248	338°— 65°	18°— 45°
	336°— 54°	13°— 35°
169—246		23°— 0°
		8°— 15°
		23°— 20°
		8°— 20°
		13°— 20°
		13°— 5°
168—245		3°— 25°
		13°— 20°
		8°— 30°
		8°— 25°
166—253	350°— 42°	−15°— 18°
		−9°—−26°
165—253	336°— 53°	−5°— 44°
	338°— 53°	0°— 34°
	323°— 57°	−4°— 27°
	331°— 54°	−2°— 27°

Meas. sample 175 (17 s. and 39 m.f.)

	mean s.	mean m.f.
156—226	322°— 25°	
157—226		354°— 15°

co-ordinates of the grid	position of s-plane	position of m.f.
151—231		348°— 12°
		353°— 10°
152—230	323°— 45°	363°— 20°
	333°— 35°	343°— 20°
	336°— 55°	373°— 30°
		348°— 15°
157—231	348°— 27°	353°— 15°
		348°— 12°
164—225	402°—−25°	385°— 16°
		367°— 7°
160—227	318°— 30°	356°— 14°
	312°— 38°	348°— 15°
	308°— 27°	364°— 25°
		396°— 23°
161—221	305°— 19°	352°— 12°
	330°— 28°	348°— 14°
		356°— 9°
		384°— 25°
		358°— 10°
		353°— 10°
		358°— 12°
161—220		358°— 14°
157—225	324°— 20°	346°— 10°
		348°— 4°
		353°— 15°
156—225		346°— 15°
		353°— 17°
		352°— 11°
155—224	298°— 24°	345°— 19°
	311°— 21°	364°— 7°
		375°— 24°
153—225	320°— 12°	336°— 8°
		338°— 18°
		344°— 17°
152—227		348°— 21°
		340°— 22°
153—227	326°— 24°	344°— 13°
	263°— 15°	326°— 26°
155—227	318°— 27°	342°— 9°

Meas. sample 176 (13 s. and 27 m.f.)

	mean s.	mean m.f.
128—271	264°— 30°	
132—269		10°— 30°

co-ordinates of the grid	position of s-plane	position of m.f.
138—267		−17°— 20°
		−27°— 17°
133—268		28°— 45°
		38°— 47°
		23°— 45°
		43°— 40°
132—268	343°— 32°	23°— 30°
	248°— 30°	40°— 35°
		48°— 30°
		−12°— 12°
		−17°— 18°
		13°— 30°
		13°— 33°
136—268		−17°— 10°
		−32°— 8°
135—268	313°—−20°	−27°— 20°
134—269		33°— 35°
		3°— 35°
132—270		18°— 40°
		18°— 30°
		13°— 40°

128—273	250°— 45°	
	273°— 42°	
	253°— 38°	
127—272	275°— 35°	
	238°— 30°	
126—271	283°— 30°	18°— 25°
	263°— 25°	38°— 40°
		8°— 20°
125—270	253°— 38°	8°— 25°
	253°— 35°	3°— 30°
	343°— 25°	1°— 45°

Meas. sample 177 (32 s. and 58 m.f.)

	mean s.	mean m.f.
137—179	303°— 28°	
137—179		35°— 16°

co-ordinates of the grid	position of s-plane	position of m.f.
138—174	313°— 40°	366°— 35°
	295°— 25°	343°— 19°
137—175	248°— 21°	343°— 20°
	253°— 20°	343°— 20°
	238°— 18°	333°— 20°
	266°— 21°	333°— 22°
	253°— 24°	373°— 17°
	258°— 15°	
137—177		353°— 25°
		373°— 5°
		343°— 10°
137—178	328°— 20°	348°— 10°
	308°— 15°	378°— 20°
	313°— 30°	363°— 12°
	343°— 32°	353°— 12°
		358°— 10°
		343°— 5°
136—180	293°— 22°	328°— 12°
	238°— 18°	353°— 15°
		353°— 15°
		338°— 15°
137—182	343°— 32°	358°— 20°
	323°— 40°	358°— 22°
	323°— 40°	368°— 20°
	338°— 65°	343°— 10°
	313°— 35°	348°— 10°
	338°— 30°	363°— 15°
	343°— 30°	333°— 15°
	303°— 35°	348°— 12°
		368°— 20°
		338°— 10°
138—180	278°— 20°	348°— 5°
	338°— 55°	348°— 12°
		358°— 20°
		353°— 5°
		348°— 10°
		358°— 10°
		348°— 17°
		348°— 15°
		338°— 25°
		353°— 13°
		368°— 20°
		358°— 25°
		358°— 10°
		358°— 15°
137—180	318°— 32°	318°— 0°
	313°— 20°	343°— 15°
	293°— 20°	348°— 15°
	288°— 15°	368°— 13°
	308°— 25°	353°— 13°
		343°— 20°
		343°— 23°
		338°— 28°
		363°— 20°
		358°— 15°
137—179	333°— 35°	358°— 25°
	318°— 32°	343°— 8°
	333°— 22°	353°— 18°
		358°— 15°

Meas. sample 178 (33 s. and 37 m.f.)

	mean s.	mean m.f.
125—275	258°— 31°	
126—275		5°— 28°

co-ordinates of the grid	position of s-plane	position of m.f.
125—274	313°— 45°	13°— 43°
	278°— 28°	8°— 30°
	283°— 26°	3°— 25°
	253°— 48°	8°— 30°
	273°— 30°	−17°— 30°
	273°— 35°	−17°— 27°
124—275	283°— 34°	28°— 34°
	278°— 37°	3°— 40°
	263°— 29°	13°— 35°
		33°— 40°
123—275	298°— 39°	26°— 48°
	253°— 23°	18°— 27°
	248°— 35°	18°— 30°
	248°— 38°	18°— 25°
		18°— 35°
		3°— 35°
		33°— 25°
122—274	243°— 36°	13°— 35°
	278°— 30°	8°— 25°
	233°— 53°	−7°— 35°
	238°— 25°	−22°— 27°
	248°— 28°	
	243°— 37°	
	238°— 35°	
130—276	218°— 23°	28°— 18°
	243°— 12°	−7°— 20°
129—276	283°— 20°	18°— 17°
	248°— 22°	−7°— 21°
	243°— 19°	−2°— 16°
	246°— 24°	−2°— 18°
	273°— 25°	−22°— 15°
	248°— 33°	−7°— 35°
128—276	223°— 46°	−2°— 30°
	248°— 28°	8°— 17°
	293°— 23°	−17°— 23°
		13°— 15°
		−27°— 23°
		−22°— 25°
		18°— 22°
127—276	253°— 20°	3°— 26°
	231°— 33°	

Meas. sample 179 (16 s. and 43 m.f.)

	mean s.	mean m.f.
179—218	355°— 50°	
179—218		357°— 13°

co-ordinates of the grid	position of s-plane	position of m.f.
178—215	355°— 40°	358°— 10°
		373°— 15°
		358°— 10°
		348°— 5°
179—216	358°— 40°	353°— 3°
		363°— 7°
		370°— 15°
		378°— 8°
		343°— 7°
		363°— 7°
		353°— 10°
		348°— 15°
		353°— 20°
180—216	338°— 45°	348°— 20°
	343°— 55°	353°— 20°
	343°— 50°	368°— 25°
		343°— 15°
		333°— 15°
		343°— 13°
		343°— 9°
		358°— 23°
181—217	358°— 60°	353°— 12°
	348°— 50°	358°— 10°
	348°— 65°	358°— 15°
		358°— 18°
182—217	340°— 63°	348°— 25°
		358°— 24°
		358°— 10°
182—219		348°— 4°
		348°— 12°
		358°— 20°
		353°— 17°
		348°— 22°
177—221	358°— 48°	353°— 2°
	343°— 45°	358°— 0°
	363°— 35°	370°— 0°
	373°— 53°	378°— 6°
	378°— 42°	368°— 9°
	383°— 44°	395°— 6°
	343°— 78°	363°— 23°
		378°— 14°
		358°— 15°
		353°— 11°

Meas. sample 180 (24 s. and 41 m.f.)

	mean s.	mean m.f.
120—268	244°— 33°	
120—268		7°— 27°

co-ordinates of the grid	position of s-plane	position of m.f.
121—270	235°— 43°	30°— 32°
	253°— 17°	13°— 22°
	303°— 30°	28°— 35°
	293°— 36°	−12°— 28°
	265°— 33°	18°— 21°
		26°— 28°
		−22°— 29°
120—269	233°— 37°	3°— 32°
	245°— 27°	23°— 27°
	250°— 27°	−2°— 43°
		16°— 24°
		8°— 35°
	246°— 38°	18°— 26°
		28°— 45°
118—269	266°— 36°	18°— 22°
	223°— 23°	−22°— 30°
		8°— 24°
122—268	216°— 46°	3°— 21°
	193°— 40°	3°— 15°
	243°— 45°	16°— 26°
	261°— 33°	−19°— 41°
	248°— 33°	−2°— 42°
	243°— 29°	21°— 39°
	218°— 30°	13°— 27°
		5°— 28°
		0°— 24°
		8°— 31°
		−5°— 20°
		−2°— 27°
		1°— 20°
		−12°— 35°
		5°— 30°
115—266	233°— 32°	13°— 24°
	218°— 31°	−10°— 17°
	228°— 28°	3°— 34°
		18°— 15°
118—262	248°— 27°	8°— 20°
	248°— 24°	6°— 26°
	235°— 42°	8°— 17°
		18°— 18°
		13°— 26°

Meas. sample 181 (14 s. and 54 m.f.)

	mean s.	mean m.f.
121—255	243°— 36°	
121—255		5°— 26°

co-ordinates of the grid	position of s-plane	position of m.f.
121—258	263°— 32°	8°— 28°
		11°— 31°
122—259		13°— 29°
		−2°— 29°
		−10°— 30°
		−14°— 11°
		16°— 20°
		13°— 19°
		13°— 29°
123—259	235°— 51°	10°— 24°
		18°— 31°
		13°— 23°
		11°— 27°
		−12°— 15°
		6°— 12°
		33°— 24°
124—259	258°— 40°	−9°— 23°
	273°— 35°	18°— 26°
		23°— 25°
124—258		6°— 19°
122—254	256°— 30°	−7°— 28°
		−12°— 26°
		−17°— 24°
		3°— 29°
		−12°— 30°
121—254	228°— 20°	3°— 14°
	233°— 26°	3°— 20°
	205°— 41°	−17°— 26°
		18°— 24°
		−2°— 28°
117—252	248°— 36°	−15°— 25°
	263°— 36°	6°— 35°
		−12°— 26°
		8°— 17°
		−27°— 10°
		13°— 29°
		−2°— 29°
		26°— 22°
	261°— 27°	−9°— 36°
		−17°— 28°
		21°— 24°
		28°— 22°
		−14°— 19°
		−22°— 31°
		23°— 24°
120—254	198°— 34°	
123—254	218°— 58°	18°— 38°
	258°— 34°	13°— 31°
		15°— 40°
		16°— 36°
		21°— 36°
		5°— 34°
		23°— 28°
124—253		6°— 15°
		8°— 23°

Meas. sample 182 (22 s. and 46 m.f.)

	mean s.	mean m.f.
135—198	314°— 13°	
136—197		355°— 13°

co-ordinates of the grid	position of s-plane	position of m.f.
139—196	253°— 12°	366°— 11°
	366°— 17°	338°— 7°
		343°— 16°
		348°— 4°
		358°— 10°
138—196	348°— 28°	366°— 15°
	322°— 26°	368°— 23°
		343°— 8°
		363°— 14°
		348°— 11°
		353°— 12°
		358°— 11°
		361°— 20°
		370°— 23°
138—197	328°— 29°	350°— 17°
		353°— 16°
		363°— 20°
		358°— 26°
135—197	318°— 33°	
132—197	325°— 32°	365°— 18°
	318°— 46°	341°— 4°
	223°— 15°	370°— 20°
	273°— 14°	361°— 14°
	235°— 10°	348°— 6°
		353°— 20°
		353°— 11°
		358°— 20°
133—198	373°— 26°	348°— 6°
		361°— 13°
		358°— 13°
134—198	328°— 19°	313°— 7°
	308°— 11°	383°— 15°
	308°— 9°	358°— 6°
	268°— 24°	365°— 18°
		358°— 14°
135—198	323°— 29°	338°— 8°
	388°—−12°	343°— 14°
		351°— 8°
135—199	363°—−25°	358°— 13°
	288°— 17°	353°— 5°
		353°— 13°
		358°— 15°
136—200	371°—−26°	338°— 24°
	283°— 10°	363°— 7°
		346°— 8°
		358°— 10°
137—201		365°— 7°

Meas. sample 183 (30 s. and 38 m.f.)

	mean s.	mean m.f.
084—253	232°— 37°	
084—253		2°— 27°

co-ordinates of the grid	position of s-plane	position of m.f.
084—250	223°— 30°	−2°— 28°
	228°— 47°	6°— 32°
	238°— 46°	5°— 23°
	216°— 48°	10°— 27°
	238°— 51°	−12°— 40°
	256°— 42°	24°— 32°
	218°— 49°	−2°— 30°
	208°— 37°	15°— 26°

			21°— 30°
			14°— 34°
			−5°— 18°
			6°— 34°
084—251	238°— 33°		−2°— 24°
	250°— 34°		1°— 27°
	240°— 41°		25°— 24°
	228°— 43°		−10°— 25°
	210°— 35°		−14°— 34°
			−11°— 22°
			13°— 28°
			13°— 33°
			6°— 26°
084—252	213°— 48°		8°— 34°
	244°— 36°		−9°— 32°
	206°— 33°		−7°— 17°
085—253	248°— 30°		
084—257	218°— 42°		30°— 24°
	226°— 32°		−2°— 33°
	252°— 42°		−12°— 32°
	231°— 31°		3°— 32°
	215°— 28°		−14°— 21°
	218°— 42°		
083—258	235°— 29°		−17°— 19°
	250°— 36°		3°— 26°
	233°— 21°		33°— 17°
	268°— 28°		−10°— 24°
082—258	233°— 35°		−2°— 27°
	258°— 42°		13°— 22°
	213°— 21°		8°— 18°
			−12°— 12°
081—259			−24°— 23°

Meas. sample 184 (27 s. and 30 m.f.)

	mean s.	mean m.f.
074—257	237°— 32°	
076—254		1°— 29°

co-ordinates of the grid	position of s-plane	position of m.f.
081—249	253°— 42°	23°— 33°
	243°— 40°	28°— 32°
	258°— 35°	−7°— 40°
		10°— 25°
		18°— 46°
		3°— 30°
		18°— 21°
		8°— 27°
		20°— 27°
		3°— 30°
		18°— 34°
076—254	248°— 25°	20°— 20°
	216°— 29°	−2°— 30°
	203°— 33°	1°— 20°
	233°— 33°	13°— 23°
	261°— 30°	−2°— 30°
	210°— 38°	−7°— 31°
	248°— 19°	8°— 28°
		5°— 22°
071—259	241°— 34°	−12°— 30°
	208°— 35°	−14°— 30°
	240°— 30°	−17°— 28°
	248°— 30°	
	245°— 38°	
	213°— 15°	
	240°— 37°	
071—260	223°— 27°	−12°— 38°
	236°— 22°	13°— 39°
	238°— 36°	−22°— 29°
	256°— 27°	−27°— 14°
	228°— 30°	−17°— 20°
	248°— 33°	
070—261	233°— 50°	−20°— 32°
	248°— 25°	−10°— 24°
	241°— 26°	−17°— 31°
	238°— 38°	

Meas. sample 185 (27 s. and 33 m.f.)

	mean s.	mean m.f.
116—187	294°— 27°	
117—187		348°— 12°

co-ordinates of the grid	position of s-plane	position of m.f.
116—180	308°— 25°	358°— 11°
		368°— 10°
115—182	278°— 14°	348°— 12°
116—182	303°— 27°	348°— 6°
	333°— 40°	343°— 3°
	328°— 31°	343°— 10°
	343°— 34°	350°— 9°
		363°— 14°
		358°— 9°
		343°— 10°
		350°— 3°
115—183	280°— 24°	338°— 25°
		353°— 22°
117—186	238°— 24°	338°— 16°
118—188	258°— 14°	340°— 10°
		345°— 11°
		338°— 14°
		316°— 12°
119—189	293°— 26°	346°— 13°
	278°— 25°	358°— 22°
	288°— 26°	346°— 20°
	243°— 25°	343°— 15°
	273°— 20°	348°— 11°
	260°— 36°	350°— 14°
	268°— 38°	340°— 8°
		353°— 10°
		341°— 9°
118—196	303°— 30°	363°— 20°
	293°— 32°	345°— 20°
	318°— 28°	346°— 14°
	306°— 32°	366°— 13°
	338°— 28°	
118—195	305°— 15°	351°— 8°
118—193		343°— 7°
111—183	305°— 36°	
	291°— 22°	
	298°— 32°	
	321°— 18°	
	295°— 24°	

Meas. sample 186 (32 s. and 32 m.f.)

	mean s.	mean m.f.
130—229	319°— 39°	
129—225		354°— 18°

co-ordinates of the grid	position of s-plane	position of m.f.
123—221		318°— 14°
		341°— 5°
128—221	348°— 56°	358°— 14°
	332°— 68°	348°— 25°
	338°— 68°	344°— 18°
	333°— 57°	346°— 17°
		358°— 23°
		372°— 12°
		366°— 15°
		370°— 25°
		340°— 18°
		353°— 16°
		350°— 14°
		343°— 12°
129—222	358°— 66°	353°— 11°
	333°— 60°	348°— 10°
	366°— 55°	370°— 20°
	348°— 48°	353°— 20°
	333°— 33°	368°— 28°
		358°— 20°
		348°— 26°
		353°— 14°
128—231	328°— 30°	355°— 15°
	360°— 52°	366°— 23°
	328°— 25°	
128—233	268°— 25°	358°— 28°
	310°— 31°	378°— 16°
	320°— 20°	
	266°— 27°	
	276°— 23°	
	303°— 33°	
	313°— 22°	
130—234	300°— 47°	
	296°— 45°	
	263°— 44°	
132—233	315°— 22°	346°— 24°
	323°— 34°	336°— 26°
	308°— 28°	353°— 16°
	331°— 38°	343°— 22°
	318°— 34°	
	315°— 49°	
133—226	288°— 26°	365°— 17°
	273°— 28°	363°— 19°
	298°— 28°	
	330°— 27°	

Meas. sample 187 (17 s. and 19 m.f.)

	mean s.	mean m.f.
190—194	17°— 54°	
190—194		18°— 11°

co-ordinates of the grid	position of s-plane	position of m.f.
189—192		3°— 8°
		−10°— 5°
		24°— 3°
		−14°— 14°
190—194	25°— 38°	38°— 10°
	41°— 45°	53°— 5°
	26°— 48°	−22°— 8°
	21°— 54°	23°— 11°
	15°— 48°	28°— 16°
	22°— 56°	18°— 10°
	12°— 57°	15°— 10°
	15°— 53°	18°— 8°
	8°— 61°	
	13°— 52°	
190—195	4°— 50°	26°— 16°
	22°— 61°	15°— 13°
	13°— 57°	38° — 12°
	9°— 49°	24°— 12°
	8°— 60°	38°— 22°
	21°— 53°	12°— 10°
	21°— 60°	20°— 16°

Meas. sample 188 (17 s. and 19 m.f.)

	mean s.	mean m.f.
182—207	342°— 31°	
182—207		353°— 9°

co-ordinates of the grid	position of s-plane	position of m.f.
187—198	341°— 42°	348°— 20°
	347°— 60°	350°— 12°
182—213	343°— 25°	361°— 16°
	343°— 23°	356°— 4°
	345°— 28°	348°— 6°
	331°— 28°	358°— 10°
182—212	346°— 36°	363°— 8°
	358°— 32°	343°— 5°
180—207	333°— 35°	328°— 10°
	345°— 27°	353°— 8°
	343°— 20°	348°— 12°
	333°— 19°	356°— 3°
181—204	344°— 27°	363°— 7°
	341°— 43°	353°— 7°
	348°— 35°	360°— 10°
	338°— 26°	358°— 11°
	335°— 26°	348°— 7°
		358°— 3°
		353°— 7°

Meas. sample 189 (28 s. and 33 m.f.)

	mean s.	mean m.f.
100—224	312°— 46°	
102—225		348°— 30°

co-ordinates of the grid	position of s-plane	position of m.f.
101—224	303°— 40°	373°— 35°
	314°— 50°	343°— 36°
		338°— 28°
102—225	333°— 64°	346°— 32°
	317°— 46°	335°— 32°
103—225	308°— 54°	350°— 36°
	320°— 46°	343°— 26°
	318°— 52°	
103—226	328°— 50°	348°— 28°
	328°— 74°	333°— 24°
	333°— 42°	346°— 24°
		340°— 24°
108—227	338°— 57°	351°— 24°
	305°— 40°	348°— 26°
	343°— 40°	355°— 28°
		358°— 31°
		365°— 27°
		356°— 29°
		363°— 28°
		353°— 30°
		358°— 27°
099—224	313°— 40°	333°— 33°
	311°— 44°	353°— 27°
	328°— 54°	340°— 40°
	326°— 38°	333°— 36°
	275°— 41°	333°— 35°
	280°— 44°	330°— 38°
	281°— 47°	
097—223	318°— 41°	361°— 23°
	291°— 38°	363°— 27°
	298°— 45°	363°— 36°
	326°— 45°	363°— 38°
	330°— 34°	
096—223	320°— 34°	355°— 34°
	278°— 40°	341°— 32°
	273°— 40°	326°— 20°

Meas. sample 190 (37 s. and 36 m.f.)

	mean s.	mean m.f.
153—256	322°— 46°	
153—256		352°— 33°

co-ordinates of the grid	position of s-plane	position of m.f.
156—260	248°— 33°	373°— 28°
	248°— 40°	333°— 35°
	348°— 45°	351°— 40°
	258°— 38°	341°— 43°
	365°— 48°	356°— 33°
	328°— 38°	352°— 43°
	266°— 50°	332°— 52°
	348°— 47°	338°— 48°
	341°— 42°	346°— 36°
	343°— 39°	348°— 37°
	337°— 30°	
157—259	336°— 47°	346°— 33°
	335°— 47°	353°— 42°
	278°— 38°	340°— 32°
	328°— 57°	344°— 32°
	342°— 58°	
158—258	316°— 43°	340°— 37°
	348°— 58°	334°— 34°
	334°— 58°	365°— 38°
	325°— 52°	352°— 27°
158—257	341°— 51°	350°— 26°
148—248	331°— 37°	342°— 33°
147—249	308°— 37°	358°— 37°
148—250	308°— 45°	351°— 32°
149—252	343°— 34°	363°— 33°
	341°— 50°	370°— 30°
	350°— 52°	368°— 30°
	323°— 50°	378°— 34°
	326°— 44°	
149—253	338°— 55°	358°— 30°
	288°— 35°	353°— 28°
	345°— 57°	358°— 28°
		353°— 26°
		350°— 24°
148—255	326°— 47°	351°— 20°
	313°— 36°	358°— 25°
148—256	340°— 45°	346°— 22°
147—257	338°— 45°	358°— 20°
147—258	291°— 32°	370°— 28°

Meas. sample 191 (23 s. and 23 m.f.)

	mean s.	mean m.f.
161—205	336°— 38°	
161—205		353°— 12°

co-ordinates of the grid	position of s-plane	position of m.f.
162—209	328°— 38°	346°— 30°
	343°— 40°	351°— 23°
	341°— 30°	358°— 16°
	353°— 38°	370°— 12°
160—209	355°— 38°	348°— 10°
	346°— 33°	
160—208	318°— 34°	338°— 10°
	318°— 39°	340°— 7°
	336°— 36°	343°— 9°
	328°— 52°	346°— 8°
	345°— 48°	368°— 7°
	346°— 44°	356°— 8°
160—204	328°— 34°	358°— 14°
160—203	336°— 43°	341°— 11°
	328°— 32°	363°— 14°
	340°— 48°	361°— 10°
		351°— 12°
161—200	343°— 34°	360°— 18°
	343°— 35°	350°— 8°
	340°— 30°	338°— 9°
	298°— 36°	368°— 22°
	342°— 25°	356°— 7°

	338°— 30°	353°— 5°	
	340°— 50°	358°— 5°	

Meas. sample 192 (20 s. and 20 m.f.)		
	mean s.	mean m.f.
073—196	267°— 38°	
073—196		351°— 19°

co-ordinates of the grid	position of s-plane	position of m.f.
072—196	273°— 37°	358°— 23°
	273°— 40°	335°— 14°
	293°— 42°	350°— 18°
	248°— 38°	348°— 28°
	253°— 40°	373°— 18°
072—197	268°— 38°	341°— 16°
	301°— 39°	355°— 17°
	273°— 32°	361°— 15°
	268°— 40°	338°— 27°
	288°— 34°	348°— 22°
	303°— 36°	346°— 33°
	283°— 41°	343°— 20°
	268°— 35°	363°— 20°
	278°— 37°	338°— 19°
	293°— 43°	358°— 28°
	233°— 30°	350°— 8°
078—195	198°— 44°	368°— 17°
	258°— 27°	361°— 10°
	228°— 45°	348°— 12°
077—193	258°— 46°	345°— 22°

Tables of the positions of the schistosity-planes and the axes of the minor folds in the Gosaldo region (Sheet VII).

Meas. sample 193 (39 s. and 22 m.f.)		
	mean s.	mean m.f.
702—286	227°— 47°	
703—286		356°— 23°

co-ordinates of the grid	position of s-plane	position of m.f.
701—281	200°— 44°	360°— 45°
	195°— 65°	355°— 50°
	210°— 48°	365°— 50°
	220°— 55°	
703—281	225°— 50°	
	215°— 50°	
703—280	230°— 43°	370°— 31°
	210°— 50°	382°— 37°
699—287	285°— 54°	
	250°— 59°	
700—288	230°— 36°	
702—288	240°— 42°	
	250°— 60°	
701—288	170°— 44°	345°— −4°
	235°— 57°	330°—−11°
	170°— 30°	
702—288	255°— 56°	
	245°— 47°	
	245°— 51°	
703—289	235°— 61°	380°— 40°
	230°— 75°	385°— 30°
	235°— 57°	390°— 32°
	150°— 41°	410°— 10°
	280°— 50°	385°— 25°
	227°— 21°	322°— 26°
	210°— 55°	355°— 3°
	165°— 70°	
	255°— 45°	
	310°— 15°	
703—288	205°— 35°	300°— 40°
	235°— 50°	400°— 10°
	225°— 34°	315°— 15°
	270°— 85°	315°— 25°
	210°— 48°	345°— 30°
	255°— 30°	390°—−16°
	165°— 2°	
704—286	285°— 35°	315°— 19°
		315°— 22°
700—282	205°— 50°	
	230°— 43°	

Meas. sample 194 (35 s. and 21 m.f.)		
	mean s.	mean m.f.
708—284	265°— 44°	
707—283		8°— 36°

co-ordinates of the grid	position of s-plane	position of m.f.
707—280	300°— 45°	345°— 43°
	260°— 48°	340°— 48°
		345°— 38°
		370°— 28°
704—279	270°— 42°	350°— 44°
	240°— 42°	380°— 19°
	220°— 52°	360°— 48°
	230°— 55°	370°— 42°
705—279	260°— 66°	
	245°— 60°	
706—280	275°— 70°	
	290°— 40°	
	260°— 40°	
	295°— 48°	
708—279	260°— 33°	360°— 32°
	295°— 40°	360°— 31°
	242°— 40°	
707—283	250°— 41°	335°— 41°
	252°— 38°	
709—283	300°— 49°	375°— 47°
711—286	255°— 42°	352°— 38°
	246°— 39°	
711—288	230°— 42°	
	240°— 39°	
	250°— 35°	
709—288	255°— 37°	370°— 30°
	245°— 43°	400°— 16°
	255°— 61°	370°— 36°
	280°— 51°	395°— 44°
	254 — 30	412 — 41
	245 — 30	
	265 — 15	
707—287	310 — 50	345 — 40°
	315°— 38°	
706—287	280°— 42°	340°— 20°
	293°— 45°	310°— 20°
	302°— 45°	

Meas. sample 195 (42 s. and 13 m.f.)		
	mean s.	mean m.f.
715—282	249°— 43°	
715—282		357°— 34°

co-ordinates of the grid	position of s-plane	position of m.f.
716—283	275°— 45°	345°— 36°
	250°— 46°	350°— 46°
	285°— 37°	365°— 45°
	250°— 46°	370°— 51°
	225°— 60°	
716—282	285°— 47°	
	260°— 51°	
717—281	265°— 20°	
717—279	235°— 60°	
	210°— 55°	
	205°— 60°	
	215°— 51°	
	210°— 36°	
716—280	250°— 24°	
716—281	265°— 25°	380°— 24°
	235°— 38°	
	264°— 41°	
713—283	245°— 50°	365°— 48°
	245°— 40°	350°— 20°
	210°— 22°	
	220°— 50°	
	280°— 25°	
715—280	210°— 55°	355°— 16°
	230°— 20°	340°— 14°
	220°— 40°	
	215°— 47°	
	250°— 22°	
715—277	220°— 50°	

	215°— 39°	350°— 36°
712—286	286°— 49°	355°— 35°
	235°— 61°	
	255°— 40°	
713—285	220°— 55°	
	255°— 42°	
	248°— 47°	
715—283	300°— 52°	362°— 38°
	300°— 42°	355°— 38°
	305°— 46°	
	290°— 45°	
	310°— 50°	
712—287	255°— 45°	
	255°— 48°	

Meas. sample 196 (39 s. and 33 m.f.)

	mean s.	mean m.f.
699—275	290°— 38°	
699—276		4°— 19°

co-ordinates of the grid	position of s-plane	position of m.f.
699—278	262°— 55°	330°— 52°
		335°— 42°
698—278	235°— 60°	395°— 18°
	245°— 90°	405°— 20°
	215°— 60°	402°— 35°
699—277	— 0°	370°— 3°
	360°—−26°	380°— 8°
	360°—−20°	355°— −6°
		380°— 5°
		375°— 8°
		360°— 0°
		355°— 0°
698—276	360°— 48°	365°— 8°
	345°— 30°	385°—−26°
	370°— 25°	385°— 35°
	225°— 36°	360°— 41°
	250°— 41°	335°— 20°
	260°— 8°	365°— 19°
	265°— 20°	335°— 22°
	245°— 24°	
	235°— 25°	
698—275	260°— 90°	— 90°
	255°— 78°	335°— 78°
	250°— 50°	375°— 22°
	340°— 24°	360°— 6°
699—275	305°— 45°	341°— 18°
	310°— 30°	335°— 10°
	300°— 20°	370°—−22°
	300°— 37°	
	310°— 22°	
703—277	315°— 26°	340°— 20°
	295°— 36°	360°—−23°
	280°— 36°	
702—274	305°— 24°	365°— 21°
698—273	338°— 52°	390°— 40°
	320°— 36°	
	313°— 50°	
697—273	295°— 47°	370°— 40°
	297°— 53°	
697—275	265°— 40°	352°— 23°
697—274	270°— 34°	375°— 30°
	253°— 42°	
	290°— 60°	
	310°— 55°	

Meas. sample 197 (41 s. and 38 m.f.)

	mean s.	mean m.f.
706—275	269°— 44°	
706—275		350°— 29°

co-ordinates of the grid	position of s-plane	position of m.f.
704—278	285°— 35°	350°— 35°
	270°— 35°	355°— 27°
	284°— 49°	320°— 24°
		335°—−15°
704—277	280°— 54°	332°— 46°
	295°— 60°	
703—277	250°— 47°	326°— 42°
	305°— 59°	315°— 7°
703—272	192°— 36°	345°— 39°
	208°— 42°	335°— 37°
	210°— 39°	
704—271	310°— 26°	335°— 21°
	280°— 34°	335°— 17°
704—270	285°— 18°	335°— 12°
704—269	295°— 33°	380°— 28°
	270°— 35°	355°— 22°
	275°— 35°	375°— 20°
	262°— 20°	
	270°— 37°	
	285°— 58°	
707—273	283°— 45°	
707—275	300°— 45°	365°— 32°
	265°— 34°	377°— 42°
	290°— 41°	400°— 33°
	260°— 53°	390°— 48°
	265°— 42°	320°— 26°
	280°— 48°	330°— 55°
	270°— 46°	360°— 46°
		365°— 40°
708—278	250°— 95°	365°— 62°
	245°— 93°	
	275°— 57°	
	272°— 64°	
709—278	255°— 36°	360°— 32°
	265°— 37°	335°— 30°
	270°— 32°	380°— 33°
	280°— 36°	345°— 19°
		382°— 10°
709—276	283°— 46°	355°— 33°
706—277	255°— 40°	355°— 32°
		360°— 36°
		320°— 22°
		335°— 27°
705—277	240°— 55°	340°— 44°
	245°— 34°	335°— 26°
	255°— 30°	340°—−35°
702—272	300°— 46°	360°— 40°

Meas. sample 198 (19 s. and 13 m.f.)

	mean s.	mean m.f.
716—270	260°— 49°	
716—271		328°— 29°

co-ordinates of the grid	position of s-plane	position of m.f.
712—274	265°— 30°	320°— 26°
	210°— 36°	340°— 24°
	265°— 29°	
713—271		335°— 0°
715—274	180°— 37°	330°— 32°
		335°— 8°
		310°— 32°
715—272	230°— 45°	280°— 30°
		345°— 15°
718—269	305°— 56°	
	280°— 41°	
	280°— 86°	
	265°— 63°	350°— 65°
718—268	255°— 45°	
	265°— 84°	
717—268	275°— 51°	320°— 30°
	286°— 42°	360°— 26°
	245°— 41°	360°— 27°
	240°— 25°	
	235°— 30°	
717—267	275°— 90°	275°— 58°
	285°— 47°	
	295°— 60°	

Meas. sample 199 (26 s. and 11 m.f.)

	mean s.	mean m.f.
311—266	239°— 51°	
310—267		10°— 37°

co-ordinates of the grid	position of s-plane	position of m.f.
309—268	241°— 52°	
	210°— 63°	
314—265	303°— 65°	
	304°— 65°	
309—268	225°— 47°	
310—267	220°— 48°	0°— 27°
	235°— 23°	30°— 22°
	224°— 56°	−10°— 30°
	240°— 48°	15°— 35°
	250°— 48°	25°— 40°
	245°— 48°	5°— 40°
	250°— 46°	5°— 40°
	236°— 50°	
311—266	230°— 40°	25°— 25°
	235°— 47°	10°— 31°
	240°— 45°	
	240°— 50°	
	255°— 45°	

	245°— 48°	
	240°— 51°	
	220°— 25°	
	220°— 57°	
311—265	240°— 69°	2°— 60°
	210°— 70°	4°— 54°
	215°— 55°	
308—264	245°— 60°	

Meas. sample 200 (47 s. and 58 m.f.)

	mean s.	mean m.f.
301—255	233°— 48°	
298—253		4°— 33°

co-ordinates of the grid	position of s-plane	position of m.f.
301—258	222°— 52°	380°— 25°
	210°— 40°	380°— 50°
	240°— 62°	345°— 35°
	245°— 41°	340°— 33°
	210°— 42°	325°— 36°
		342°— 30°
301—257	210°— 62°	350°— 50°
	220°— 56°	305°— 55°
	230°— 62°	
	205°— 64°	
	208°— 60°	
	240°— 59°	
	235°— 49°	
	255°— 60°	
	260°— 35°	
	240°— 50°	
	215°— 40°	
	235°— 26°	
	245°— 60°	
299—253	313°— 45°	355°— 15°
	260°— 34°	365°— 30°
	240°— 20°	380°— 25°
		380°— 20°
298—250	255°— 47°	368°— 44°
301—256	230°— 54°	360°— 38°
	240°— 47°	370°— 33°
	225°— 48°	360°— 25°
	250°— 36°	365°— 32°
	220°— 35°	385°— 27°
	210°— 58°	350°— 42°
	215°— 44°	
	265°— 50°	
	245°— 44°	
	250°— 40°	
300—255	225°— 61°	365°— 35°
	225°— 60°	
	235°— 37°	
	240°— 50°	
301—257	195°— 38°	380°— 35°
	215°— 43°	
	190°— 60°	
302—256	205°— 70°	
	210°— 60°	
302—251	240°— 50°	345°— 40°
	260°— 38°	340°— 34°
	230°— 48°	
302—250		335°— 37°
		375°— 32°
296—247	240°— 34°	375°— 20°
	265°— 31°	
298—251		385°— 42°
		385°— 44°
		390°— 23°
298—254		390°— 34°
		376°— 38°
		385°— 34°
		371°— 31°
		372°— 32°
		376°— 32°
297—251		380°— 28°
		377°— 24°
		367°— 22°
296—254		377°— 51°
		368°— 49°
		367°— 46°
		385°— 56°
		376°— 46°
		367°— 41°
		381°— 40°
		360°— 36°
296—253		326°— 25°
		340°— 27°
		355°— 30°
		360°— 32°
296—252		345°— 34°
		347°— 30°
		345°— 14°
		331°— 25°
		368°— −6°
296—249	210°— 35°	375°— 20°
		383°— 16°
		360°— 21°

Meas. sample 201 (31 s. and 10 m.f.)

	mean s.	mean m.f.
695—260	286°— 39°	
693—262		354°— 24°

co-ordinates of the grid	position of s-plane	position of m.f.
695—268	335°— 54°	345°— 10°
	332°— 47°	
	185°— 64°	
703—268	290°— 37°	330°— 30°
	275°— 37°	
	260°— 50°	
701—267	340°— 26°	350°— 27°
	305°— 42°	360°— 12°
	304°— 20°	
698—258	340°— 40°	330°— 0°
	340°— 36°	340°— 0°
694—257	260°— 34°	360°— 32°
	308°— 29°	
693—257	300°— 33°	
692—257	225°— 45°	
693—258	283°— 54°	
	286°— 40°	
694—260	265°— 50°	365°— 45°
	255°— 50°	380°— 47°
	280°— 48°	
695—262	270°— 40°	380°— 35°
698—266	295°— 42°	
	298°— 48°	
693—255	295°— 39°	
	240°— 18°	
689—252	303°— 45°	
	290°— 32°	
	300°— 26°	
	270°— 29°	
	275°— 32°	
	270°— 25°	

Meas. sample 202 (9 s. and 8 m.f.)

	mean s.	mean m.f.
310—253	269°— 39°	
310—251		2°— 28°

co-ordinates of the grid	position of s-plane	position of m.f.
314—254	265°— 50°	400°— 14°
312—249	280°— 31°	
309—248		325°— 16°
		325°— 34°
		360°— 20°
		340°— 14°
307—248	264°— 40°	
307—249	280°— 41°	335°— 44°
308—254	330°— 13°	
311—258	230°— 60°	405°— 45°
	240°— 59°	405°— 35°
	260°— 44°	
310—251	275°— 16°	

Meas. sample 203 (19 s. and 27 m.f.)

	mean s.	mean m.f.
297—244	247°— 39°	
297—242		0°— 36°

co-ordinates of the grid	position of s-plane	position of m.f.
297—246	240°— 36°	330°— 40°
	246°— 36°	370°— 28°
	230°— 36°	360°— 30°
	230°— 41°	
	245°— 32°	
299—246	235°— 65°	350°— 45°
	225°— 42°	365°— 41°
	235°— 44°	
	243°— 38°	
298—244	210°— 40°	355°— 40°
	245°— 39°	350°— 40°
	280°— 49°	
	280°— 46°	
290—2[illegible]6	245°— 28°	375°— 25°

	245°— 25°	360°— 25°
294—241	290°— 40°	372°— 45°
		375°— 42°
291—238		370°— 28°
		370°— 32°
		355°— 40°
		345°— 40°
295—242	240°— 45°	350°— 40°
		350°— 40°
		352°— 36°
296—242		355°— 43°
		330°— 30°
		400°— 35°
		375°— 35°
297—243	265°— 30°	345°— 34°
	255°— 30°	350°— 35°
295—240		350°— 35°
		370°— 34°
		380°— 38°

Meas. sample 204 (25 s.)

	mean s.
707—259	256°— 32°

co-ordinates of the grid	position of s-plane	position of m.f.
712—261	190°— −7°	
	310°—−39°	
	315°—−28°	
	220°— 66°	
	250°— 34°	
	235°— 37°	
711—262	235°— 32°	
	300°— 92°	
	285°— 53°	
	280°— 70°	
711—264	215°— 22°	
	240°— 17°	
714—265	325°— 52°	
714—264		
703—256	285°— 36°	
	280°— 20°	
	290°— 21°	
	265°— 35°	
	260°— 45°	
	235°— 27°	
703—254	245°— 25°	
	220°— 10°	
	240°— 30°	
701—252	225°— 46°	
	215°— 60°	
701—257	235°— 33°	

Meas. sample 205 (39 s. and 15 m.f.)

	mean s.	mean m.f.
302—240	237°— 41°	
302—242		335°— 32°

co-ordinates of the grid	position of s-plane	position of m.f.
300—246	230°— 40°	335°— 54°
	230°— 55°	
301—245	202°— 58°	380°— 9°
	205°— 50°	
302— 245	215°— 57°	325°— 53°
	220°— 51°	335°— 50°
	215°— 62°	
304—245	235°— 46°	310°— 40°
	250°— 45°	325°— 40°
		330°— 20°
301—243	245°— 65°	
	240°— 60°	
304—242	285°— 56°	340°— 25°
	250°— 32°	
	248°— 30°	
	240°— 32°	
300—237	232°— 30°	366°— 27°
	250°— 28°	
	255°— 30°	
300—238	235°— 25°	
	225°— 25°	
	225°— 28°	
301—239	225°— 42°	330°— 30°
	270°— 34°	345°— 37°
	245°— 35°	330°— 35°
	246°— 48°	
303—239	230°— 26°	340°— 24°
	265°— 31°	315°— 15°
	232°— 34°	318°— 14°
	236°— 36°	
302—238	235°— 27°	
	246°— 41°	
	210°— 43°	
	223°— 37°	
301—237	260°— 47°	
303—238	250°— 36°	
	255°— 34°	
	255°— 37°	
303—236	220°— 51°	
	225°— 38°	

Meas. sample 206 (19 s. and 22 m.f.)

	mean s.	mean m.f.
306—243	242°— 36°	
306—242		348°— 16°

co-ordinates of the grid	position of s-plane	position of m.f.
309—246	165°— 40°	390°— 10°
	270°— 37°	
308—246	240°— 21°	330°— 15°
		320°— 20°
305—245	260°— 42°	345°—−34°
		335°— 25°
306—245	200°— 30°	385°— 20°
	210°— 36°	340°— 19°
	230°— 36°	335°— 37°
	240°— 30°	330°— 35°
	230°— 26°	
	245°— 37°	
308—245		325°— 10°
		330°—−11°
		340°— 2°
306—242	260°— 30°	
	280°— 30°	
	290°— 40°	
	255°— 66°	
	250°— 34°	
	240°— 60°	
304—240		340°— 28°
		350°— 21°
		345°— 30°
		340°— 34°
		355°— 25°
		370°— 25°
		372°— 34°
306—236		340°— −8°
		338°—−10°
305—238	245°— 23°	
	250°— 28°	
	246°— 30°	
307—239		402°— 15°

Meas. sample 207 (9 s. and 29 m.f.)

	mean s.	mean m.f.
310—239	192°— 5°	
311—240		334°— 11°

co-ordinates of the grid	position of s-plane	position of m.f.
311—245	210°— −6°	
	198°—−22°	
315—246		350°—−25°
		350°— 36°
		370°— −3°
		368°— 32°
310—240		350°— 0°
		330°— 9°
		353°— 23°
		340°— 6°
		360°— 0°
312—237		320°— −6°
		336°— −3°
311—235	224°— 22°	255°— 50°
	220°— 16°	
	192°— 23°	
311—234		260°— 37°
		405°— 22°
		330°— 10°
311—236		330°— 4°
		302°— 13°
309—238	221°— 34°	

	215°— 28°	
310—241		343°— 5°
		322°— 12°
		303°— −5°
		334°— 5°
		336°— 10°
		347°— 13°
		335°— 14°
		335°— 16°
310—242	129°—−33°	327°— 16°
	123°—−14°	336°— 9°
		338°— 9°
		332°— 16°

Meas. sample 208 (14 s. and 20 m.f.)

	mean s.	mean m.f.
286—231	232°— 40°	
286—230		351°— 35°

co-ordinates of the grid	position of s-plane	position of m.f.
284—234	240°— 45°	345°— 47°
	245°— 38°	355°— 33°
	230°— 50°	360°— 57°
	225°— 57°	365°— 30°
285—235	240°— 50°	380°— 52°
	210°— 79°	363°— 30°
		365°— 48°
		377°— 55°
284—232	248°— 39°	360°— 41°
		365°— 42°
		360°— 30°
289—231	230°— 34°	366°— 27°
	225°— 35°	365°— 20°
287—224	240°— 16°	330°— 28°
	270°— 19°	333°— 20°
287—223	223°— 52°	345°— 46°
		319°— 15°
		316°— 19°
289—228	208°— 22°	322°— 35°
	215°— 24°	329°— 31°

Meas. sample 209 (29 s. and 36 m.f.)

	mean s.	mean m.f.
297—227	254°— 30°	
297—228		340°— 15°

co-ordinates of the grid	position of s-plane	position of m.f.
294—227	240°— 23°	330°— 25°
	230°— 31°	350°— 35°
	240°— 26°	330°— 30°
296—227	235°— 34°	355°— 16°
	240°— 51°	346°— 15°
	220°— 62°	360°— 12°
297—229	190°— 35°	345°—−15°
	245°— 15°	340°—−23°
298—231	235°— 32°	375°— 20°
	250°— 35°	368°— 40°
		365°— 29°
		365°— 20°
299—233	280°— 25°	365°— −5°
		330°— 15°
300—235	305°— 20°	345°— 28°
	310°— 28°	342°— 24°
	310°— 20°	
294—224	200°— 56°	322°— 36°
	209°— 50°	302°— 34°
	214°— 24°	
	207°— 28°	
295—226	290°— 28°	320°— 25°
		315°— 10°
		330°— 4°
		325°— 11°
		315°— −4°
		325°— 2°
296—226	290°— 16°	340°— 16°
	315°— 22°	345°— 25°
	295°— 25°	335°— 1°
	295°— 36°	340°— 15°
	290°— 25°	330°— 18°
		325°— 11°
		330°— 7°
297—227	285°— 19°	355°— 20°
	190°— 45°	350°— 17°
	190°— 31°	
299—227	280°— 16°	338°— 6°
	290°— 18°	350°— 12°
		342°— 22°

Meas. sample 210 (29 s. and 10 m.f.)

	mean s.	mean m.f.
303—229	211°— 33°	
303—228		329°— 22°

co-ordinates of the grid	position of s-plane	position of m.f.
306—236	169°— 50°	
	184°— 45°	
	189°— 47°	
	192°— 22°	
303—235	185°— 42°	
	195°— 41°	
303—234	205°— 27°	365°— 25°
	185°— 32°	
303—233	285°— 40°	
	280°— 65°	
303—225	271°— 44°	
301—228	195°— 18°	305°— 21°
	200°— 22°	
	175°— 26°	
	250°— 14°	
302—228	200°— 28°	340°— 20°
	220°— 22°	347°— 20°
305—229	220°— 11°	325°— 18°
	210°— 26°	305°— 25°
	210°— 17°	310°— 22°
	216°— 24°	315°— 24°
303—222	192°— 44°	
	193°— 48°	
	235°— 35°	360°— 6°
	235°— 21°	320°— 42°
	210°— 58°	
	210°— 35°	
	210°— 36°	
	205°— 26°	

Meas. sample 211 (13 s. and 27 m.f.)

	mean s.	mean m.f.
270—218	226°— 31°	
271—218		350°— 14°

co-ordinates of the grid	position of s-plane	position of m.f.
269—216	212°— 26°	335°— 27°
	204°— 26°	336°— 14°
	200°— 15°	
269—217	193°— 37°	355°— 26°
	205°— 39°	360°— 17°
	202°— 35°	342°— 26°
		344°— 13°
269—218	226°— 69°	356°— 33°
		346°— 62°
		330°— 56°
		365°—−31°
		373°—−28°
		379°—−26°
272—221	280°— 15°	361°— 7°
	250°— 12°	350°— 1°
		340°— 13°
		349°— 8°
271—217		370°— 1°
		358°— 8°
272—218	270°— 22°	340°— 39°
	286°— 16°	351°— 24°
	202°— 52°	346°— 25°
	214°— 44°	365°— 12°
270—219		356°— 18°
		365°— 12°
273—221		358°— 3°
278—223		310°— 12°
		310°— 10°

Meas. sample 212 (22 m.f.)

	mean m.f.
281—218	343°— 13°

co-ordinates of the grid	position of s-plane	position of m.f.
271—213		347°— 25°
		352°— 25°
		354°— 29°
274—216		345°— 7°
		345°— 13°
271—214		320°— 75°
		340°— 65°
280—217		346°— 38°
		351°— 36°
287—223		320°— 11°

		324°— 4°
		339°— 15°
		369°— 3°
		358°— −6°
		329°— 7°
		318°— 8°
285—215		315°— −2°
		365°—−19°
		355°—−30°
		330°—−24°
283—221		360°— 9°
		370°— −4°

Meas. sample 213 (27 s. and 16 m.f.)

	mean s.	mean m.f.
293—216	211°— 40°	
293—214		351°— 30°

co-ordinates of the grid	position of s-plane	position of m.f.
293—213	205°— 67°	390°— 67°
	300°— 67°	345°— 63°
	230°— 70°	
	300°— 50°	
	290°— 65°	
	140°—−62°	
291—218	162°— 30°	330°— −8°
	187°— 12°	358°— −4°
	160°— 18°	347°— 0°
	178°— 15°	355°— −4°
	185°— −5°	320°— 11°
	160°— 15°	
294—217		335°— −8°
		340°— 4°
		340°— 14°
292—221	175°— 30°	
	160°— 52°	
	178°— 80°	
	180°— 42°	
292—222	175°— 24°	
299—220	215°— 13°	
	240°— 32°	
	240°— 40°	
292—214		342°— 30°
291—216	180°— 37°	
	180°— 19°	
293—211	252°— 67°	365°— 64°
	275°— 76°	362°— 66°
	235°— 64°	328°— 64°
	275°— 70°	358°— 66°
	230°— 82°	405°— 62°

Meas. sample 214 (14 s. and 43 m.f.)

	mean s.	mean m.f.
263—210	245°— 40°	
261—211		3°— 28°

co-ordinates of the grid	position of s-plane	position of m.f.
256—211	280°— 28°	355°— 25°
		356°— 27°
		358°— 22°
		365°— 19°
257—211		385°— 14°
		369°— 13°
259—210	286°— 51°	360°— 36°
	285°— 36°	357°— 44°
	270°— 31°	355°— 53°
		359°— 45°
		357°— 48°
		353°— 39°
		349°— 22°
		358°— 31°
		353°— 32°
		366°— 24°
		371°— 16°
		365°— 19°
		376°— 24°
259—209	220°— 52°	376°— 41°
	210°— 43°	354°— 35°
		369°— 33°
		367°— 33°
		367°— 27°
		335°— 2°
269—211	223°— 52°	
	210°— 56°	
266—211		360°— 36°
		361°— 26°
		370°— 12°
		371°— 23°
		346°— 29°
		355°— 28°
264—210	220°— 34°	380°— 14°
	231°— 26°	372°— 10°
	210°— 63°	
265—209	260°— 35°	380°— 40°
	265°— 24°	373°— 45°
	256°— 30°	375°— 42°
		354°— 25°
		363°— 28°
266—217		353°— 21°
		366°— 30°
		355°— 28°
		363°— 18°
		364°— 32°

Meas. sample 215 (17 s. and 40 m.f.)

	mean s.	mean m.f.
279—206	78°— 70°	
273—205		146°— 44°

co-ordinates of the grid	position of s-plane	position of m.f.
286—205	70°— 80°	
	60°— 75°	
286—206	60°— 51°	80°— 64°
	90°— 75°	65°— 64°
	80°— 60°	80°— 50°
	70°—105°	
	70°— 80°	
	80°— 90°	
267—207	91°— 23°	180°— 19°
	100°— 21°	170°— 25°
	82°— 22°	185°— 19°
		161°— 15°
268—207		173°— 22°
		172°— 17°
		167°— 20°
		175°— 20°
		173°— 21°
269—206		145°— 60°
		140°— 51°
		175°— 46°
		180°— 50°
		156°— 63°
		162°— 69°
		164°— 58°
		174°— 68°
275—203		120°— 32°
		172°— 31°
		200°— 60°
		111°— 41°
		160°— 29°
		133°— 36°
		135°— 51°
		160°— 51°
		150°— 47°
		165°— 51°
		153°— 61°
		147°— 65°
		90°— 50°
		124°— 48°
		155°— 46°
		119°— 49°
276—205	60°— 86°	126°— 63°
	70°— 90°	122°— 46°
	80°— 90°	121°— 45°
	80°— 80°	103°— 36°
	82°— 71°	
	95°— 88°	

Tables of the positions of the schistosity-planes and the minor folds in the M. Spico region (Sheet VIII).

(The strikes of the s-planes and the azimuths of the m.f. are given without the magnetic correction of — 2°.)

Meas. sample 216 (40 s. and 53 m.f.)

	mean s.	mean m.f.
128—002	90°— 89°	
128—002		91°— 37°

co-ordinates of the grid	position of s-plane	position of m.f.
132—003	85°— 85°	85°— 30°
	95°— 93°	90°— 17°
	105°— 97°	105°— 30°
	115°—105°	115°— 30°
	100°—100°	
131—003	95°— 95°	95°— 27°
	80°— 87°	80°— 25°
	90°— 90°	80°— 40°
	95°—100°	80°— 50°
	85°— 80°	90°— 40°
	80°— 83°	90°— 30°
	75°— 87°	90°— 65°
	98°— 90°	95°— 55°
		90°— 50°
		90°— 10°
		85°— 40°
		85°— 35°
		80°— 32°
		95°— 30°
130—002	95°— 87°	75°— 25°
	90°— 70°	90°— 25°
	85°— 82°	100°— 30°
		90°— 35°
129—002	90°—110°	85°— 17°
	95°— 75°	100°— 17°
	100°— 90°	100°— 60°
	90°— 82°	90°— 40°
	85°— 78°	100°— 32°
	85°— 95°	100°— 70°
		95°— 50°
		85°— 48°
128—003	80°—110°	70°— 65°
126—003	90°— 82°	80°— 20°
124—002	90°— 87°	95°— 45°
	90°—100°	90°— 30°
	95°— 80°	90°— 48°
	95°— 78°	105°— 28°
	70°— 93°	120°— 45°
		110°— 35°
		100°— 38°
		90°— 15°
		90°— 35°
123—002	85°— 90°	90°— 27°
	90°— 83°	100°— 30°
	105°— 40°	105°— 25°
	75°— 90°	80°— 32°
	90°— 83°	90°— 35°
122—002	95°— 97°	75°— 33°
	85°— 95°	80°— 42°
	90°— 98°	85°— 38°
	95°— 92°	80°— 40°
	90°— 95°	90°— 48°
		80°— 57°
121—002	90°—102°	85°— 55°

Meas. sample 217 (32 s. and 29 m.f.)

	mean s.	mean m.f.
139—992	93°— 84°	
141—991		92°— 11°

co-ordinates of the grid	position of s-plane	position of m.f.
144—988	95°— 85°	95°— 0°
145—988	90°— 73°	90°— 0°
	95°— 75°	95°— 5°
	115°— 63°	105°— 7°
	100°— 68°	90°—-20°
145—989	90°— 83°	90°— 0°
	80°— 80°	90°— -7°
	100°— 78°	80°— 0°
	100°— 90°	85°— 15°
	95°— 85°	105°— -8°
		100°— 10°
146—990		90°— 15°
		90°— -5°
		100°— 0°
137—995	95°— 75°	100°— 28°
	100°— 80°	105°— 38°
	120°— 95°	115°— 25°
	145°— 95°	90°— 35°
	90°—118°	100°— 30°
	80°— 80°	95°— 10°
	115°—100°	
138—992	80°— 90°	85°—-10°
	80°— 75°	85°— 15°
	75°— 95°	75°— 0°
	80°— 85°	80°— 5°
	85°— 85°	
	75°— 80°	
137—992	90°— 80°	75°— 20°
	75°— 90°	85°— 40°
	85°— 80°	
136—992	95°— 90°	95°— 25°
	90°— 85°	90°— 20°
	85°— 80°	90°— 20°
	90°— 85°	
	90°— 80°	
	90°— 95°	

Meas. sample 218 (35 s. and 33 m.f.)

	mean s.	mean m.f.
192—978	106°— 44°	
192—978		96°— 6°

co-ordinates of the grid	position of s-plane	position of m.f.
192—977	60°— 75°	60°— -7°
	60°— 83°	60°— 5°
	80°— 90°	75°— 18°
	55°—105°	75°— 10°
	115°— 70°	65°— 0°
	60°— 72°	90°— 10°
	75°— 55°	80°— 15°
192—978	75°— 40°	75°— 10°
	85°— 50°	85°— 7°
	90°— 50°	85°— -3°
	80°— 55°	75°— 15°
	85°— 65°	80°— 5°
	95°— 47°	95°— 0°
	95°— 55°	100°— 5°
	110°— 15°	115°— 10°
	105°— 53°	90°—-15°
	120°— 65°	115°— 8°
	97°— 77°	95°— 0°
	95°— 65°	100°— 2°
	110°— 60°	100°— -5°
192—978	150°—-25°	120°— 10°
192—980	125°—-25°	120°— 0°
	70°— 17°	115°— 15°
	105°— 30°	125°— 12°
	70°— 30°	115°— 20°
	75°— 42°	130°— 35°
191—980	90°— 32°	120°—-30°
	50°— 30°	
191—979	80°— 20°	120°— 7°
	95°— 30°	130°— 3°
	125°— 28°	
	150°—-17°	115°— 7°
	125°—-10°	130°— 10°
192—973	60°— 62°	55°— 25°
	70°— 58°	70°— 5°

Meas. sample 219 (65 s. and 45 m.f.)

	mean s.	mean m.f.
246—001	273°— 45°	
247—001		90°— -9°

co-ordinates of the grid	position of s-plane	position of m.f.
247—001	260°— 40°	90°— -5°
	265°— 45°	85°— -5°

	275°— 65°	75°— −2°
	255°— 55°	95°—−35°
	275°— 62°	90°—−20°
	270°— 60°	80°—−20°
	270°— 65°	90°—−25°
	270°— 65°	90°—−20°
	270°— 65°	90°—−35°
	270°— 60°	90°— −8°
247—002	275°— 85°	85°—−25°
	260°— 55°	90°—−25°
	270°— 80°	85°—−25°
	267°— 70°	85°— 10°
	265°— 40°	95°— −5°
	280°— 40°	75°—−15°
	280°— 55°	100°—−20°
	300°— 60°	90°— −5°
	260°— 55°	75°— 0°
	270°— 70°	80°— −5°
	265°— 45°	
	265°— 55°	
	285°— 90°	
248—002	270°— 70°	100°—−12°
	270°— 75°	95°—−10°
	270°— 75°	85°—−12°
		95°—−15°
		90°—−10°
248—003	280°— 50°	100°—−13°
247—001	260°— 55°	110°—−50°
	270°— 40°	85°— 0°
246—001	280°— 60°	75°— 3°
	290°— 75°	110°— −5°
	295°— 65°	
	270°— 40°	
	270°— 50°	
	270°— 55°	
246—000	265°— 48°	75°— −5°
	265°— 35°	90°— −2°
	265°— 45°	100°—−10°
	240°— 15°	95°— −5°
	230°— 35°	95°—−10°
	260°— 43°	75°— −7°
	255°— 45°	
	265°— 25°	
	— 0°	
	255°— 22°	
245—000	270°— 32°	95°— −3°
	265°— 15°	95°— −3°
	250°— 10°	90°— 2°
	275°— 15°	85°— 6°
	285°— 22°	105°— 0°
	220°— 20°	100°— 0°
	270°— 30°	
	315°— 30°	
	285°— 35°	
	295°— 35°	
	260°— 40°	
	285°— 30°	
	270°— 38°	
	270°— 25°	
245—999	305°— 15°	85°— 17°
	335°— 35°	95°— 20°
	315°— 20°	80°— 10°
	300°— 15°	
	300°— 18°	
	260°— 10°	

Meas. sample 220 (31 s. and 23 m.f.)

	mean s.	mean m.f.
217—048	68°— 76°	
216—048		72°— 24°

co-ordinates of the grid	position of s-plane	position of m.f.
217—044	70°— 85°	65°— 15°
	80°— 87°	80°— 20°
	65°— 90°	70°— 30°
	65°— 90°	70°— 15°
	75°— 55°	
	70°— 65°	
	60°— 65°	
	65°— 80°	
218—049	70°— 65°	
	75°— 75°	80°— 25°
	70°— 85°	70°— 22°
	65°— 83°	60°— 23°
217—049	70°— 85°	70°— 15°
	60°— 85°	65°— 30°
	70°— 73°	75°— 30°
	60°— 73°	65°— 22°
	65°— 50°	65°— 30°
	60°— 70°	80°— 25°
	60°— 70°	
	70°— 60°	
	50°— 65°	60°— 25°
218—050	80°— 85°	80°— 10°
	65°— 70°	85°— 25°
215—050	85°— 63°	80°— 25°
	65°— 87°	55°— 40°
214—050	70°— 70°	70°— 15°
	65°—80°	
214—049	70°— 80°	75°— 40°
	75°— 90°	75°— 20°
217—046	70°—100°	80°— 35°
213—050	75°— 78°	70°— 13°

Meas. sample 221 (33 s. and 30 m.f.)

	mean s.	mean m.f.
177—971	87°— 83°	
177—971		87°— 4°

co-ordinates of the grid	position of s-plane	position of m.f.
177—971	90°— 90°	85°— 13°
	95°— 55°	80°— −5°
	80°— 78°	50°—−10°
	75°— 85°	50°—−30°
	60°— 85°	80°— 0°
	80°— 90°	75°—−12°
	73°— 82°	95°— 10°
	85°— 85°	80°—−18°
	75°— 80°	90°— −5°
	75°— 83°	80°—−20°
	75°— 80°	85°— 12°
	90°— 83°	95°— −3°
	80°— 78°	100°— 15°
	95°— 85°	90°— 5°
	95°— 67°	90°— −3°
	100°— 78°	
	110°— 85°	
	90°— 78°	
	90°— 85°	
176—971	85°— 82°	85°— 15°
	90°— 90°	85°— 20°
	100°— 75°	100°— 25°
	100°— 90°	100°— 20°
	90°— 80°	90°— 23°
	90°— 87°	100°— 12°
	85°— 90°	95°— 7°
	90°— 95°	85°— 12°
	95°— 87°	90°— 10°
	90°— 85°	95°— 5°
	100°— 75°	92°— 3°
		110°— 0°
176—972	80°— 90°	80°— 15°
	80°— 80°	80°— 0°
	80°— 85°	85°— 10°

Meas. sample 222 (17 s. and 18 m.f.)

	mean s.	mean m.f.
149—973	82°— 53°	
149—973		89°— 20°

co-ordinates of the grid	position of s-plane	position of m.f.
150—974	75°— 45°	95°— 20°
	70°— 20°	100°— 15°
	85°— 35°	90°— 25°
	75°— 43°	
149—973	80°— 65°	80°— 23°
	85°— 50°	90°— 25°
	90°— 70°	90°— 23°
	90°— 55°	90°— 20°
	70°— 60°	85°— 23°
	80°— 70°	80°— 22°
		90°— 20°
	75°— 63°	80°— 30°
148—973	100°— 55°	105°— 20°
	80°— 58°	75°— 15°
	65°— 50°	90°— 10°
	95°— 65°	75°— 10°
	90°— 55°	85°— 27°
	90°— 50°	100°— 22°
		100°— 18°

Meas. sample 223 (42 s. and 43 m.f.)		
	mean s.	mean m.f.
146—973	82°— 64°	
146—973		88°— 14°

co-ordinates of the grid	position of s-plane	position of m.f.
148—973	80°— 75°	85°— 20°
147—974	110°— 22°	120°— 12°
147—975	85°— 65°	100°— 17°
	95°— 65°	90°— 12°
	85°— 80°	100°— 22°
	75°— 90°	
147—974	65°— 95°	78°— 8°
	80°— 85°	80°— 7°
	95°—105°	100°— 0°
	100°— 90°	
146—974	80°— 75°	90°— 10°
	75°— 70°	75°— 10°
	70°—100°	75°— 10°
	75°— 40°	70°— 5°
	75°—122°	75°— 22°
	75°— 62°	95°— 20°
	80°— 33°	75°— 15°
	75°— 55°	90°— 15°
	65°— 65°	95°— 15°
		90°— 20°
		90°— 18°
		85°— 25°
		90°— 25°
		100°— 25°
		85°— 25°
146—973	70°— 40°	100°— 20°
	80°— 80°	90°— 10°
	75°— 80°	80°— 28°
	70°— 65°	80°— 25°
	75°— 60°	70°— 28°
	80°— 60°	90°— 20°
	80°— 63°	70°— 20°
	80°— 32°	75°— 5°
145—973	90°— 70°	100°— 15°
	85°— 50°	90°— 15°
	85°— 60°	95°— 10°
	105°— 55°	
145—972	75°— 45°	80°— 10°
	75°— 55°	70°— −3°
	80°— 40°	95°— 5°
	85°— 58°	
	90°— 70°	
	110°— 50°	90°— 3°
144—972	90°— 50°	95°— 0°
	80°— 58°	90°— 15°
	80°— 55°	85°— 12°
	70°— 70°	90°— 12°
	75°— 40°	95°— 15°

Meas. sample 224 (26 s. and 20 m.f.)		
	mean s.	mean m.f.
138—968	80°— 41°	
138—968		84°— 10°

co-ordinates of the grid	position of s-plane	position of m.f.
140—968	65°— 40°	80°— 25°
	80°— 50°	90°— 28°
		100°— 28°
		95°— 22°
139—968	75°— 45°	75°— 25°
	65°— 60°	70°— 5°
	85°— 50°	
	65°— 22°	
138—968	75°— 40°	90°— 3°
	80°— 40°	75°— 2°
	65°— 30°	80°— 10°
	70°— 40°	75°— 15°
	75°— 20°	80°— 2°
	80°— 42°	95°— 0°
	85°— 30°	90°— 5°
	90°— 65°	95°— 20°
	75°— 50°	
	90°— 42°	
138—169	85°— 32°	75°— 6°
	70°— 40°	75°— 3°
	70°— 45°	80°— 0°
	80°— 43°	55°— −3°
	70°— 68°	90°— −5°
	72°— 60°	
	75°— 50°	
	115°— 32°	
139—169	100°— 20°	110°— 10°
	115°— 22°	

Meas. sample 225 (57 s. and 42 m.f.)		
	mean s.	mean m.f.
243—997	282°— 25°	
243—997		99°— 5°

co-ordinates of the grid	position of s-plane	position of m.f.
245—999	270°— 17°	80°— 3°
	285°— 18°	105°—−12°
	235°— 15°	95°—−15°
	— 0°	
	300°— 43°	
	270°— 25°	
	270°— 45°	
244—999	295°— 20°	80°— 0°
	275°— 25°	
244—998	230°— 12°	115°— 3°
	265°— 18°	100°—−12°
	295°— 30°	110°— −5°
	315°— 25°	75°— 12°
	255°— 5°	110°— 0°
	260°— 40°	105°— 0°
	270°— 20°	115°— 8°
	270°— 8°	85°— 3°
	280°— 15°	
	310°— 20°	135°—−18°
	315°— 2°	105°— 0°
243—998	360°— 25°	100°— 22°
	270°— 10°	100°— 3°
	310°— 20°	98°— 13°
	305°— 20°	85°— 10°
	270°— 43°	
	330°— 12°	
243—997	300°— 18°	100°— 5°
	310°— 30°	110°— 5°
	300°—−22°	110°— −5°
	250°— 10°	
	280°— 25°	
242—997	290°— 35°	100°— 30°
	260°— 30°	90°— 20°
	305°— 35°	95°— 7°
	255°— 30°	100°— 0°
	285°— 20°	95°— 10°
	290°— 30°	125°— −5°
242—996	290°— 35°	125°— 0°
	295°— 30°	120°— −5°
	320°— 52°	80°— 10°
	270°— 35°	95°— 12°
	265°— 50°	80°— 0°
242—995	210°—−20°	105°— 0°
	250°— 55°	105°— 22°
	290°— 55°	90°— 15°
	300°— 33°	70°— 15°
	320°— 30°	95°— 30°
	220°—−20°	
	290°— 2°	
	260°— 45°	
	330°— 30°	
242—994	250°— 25°	80°— 10°
	275°— 30°	90°— 10°
	280°— 28°	90°— 0°
	280°— 80°	110°— 0°
	290°— 30°	110°— 2°
	280°— 35°	

Meas. sample 226 (32 s. and 21 m.f.)		
	mean s.	mean m.f.
245—011	270°— 81°	
244—011		90°— 2°

co-ordinates of the grid	position of s-plane	position of m.f.
244—012	285°—100°	100°— 13°
	285°— 97°	95°— 15°
	270°—115°	95°— 6°
	270°—110°	85°— 10°
	265°—120°	90°— 0°
244—011	260°— 52°	90°— −7°
	270°— 55°	85°—−10°
	270°— 45°	100°— 7°
	275°— 55°	75°— 5°
	265°— 43°	100°— −5°
	255°— 35°	80°— −7°

	270°— 55°	75°— 5°
	255°— 45°	70°— 0°
	260°— 65°	100°— −3°
	260°— 60°	
	240°— 20°	
	280°— 70°	
245—010	290°— 90°	90°— 0°
	265°— 80°	90°— 3°
	260°— 70°	90°— 5°
	280°— 80°	95°— 0°
	270°—100°	90°— 0°
	270°—120°	
	275°—115°	
	270°—100°	
	280°— 85°	
246—010	280°—110°	90°— 0°
	270°—100°	100°— 12°
	275°—107°	
	270°—100°	
	285°— 95°	
	270°— 85°	

Meas. sample 227 (40 s. and 24 m.f.)

	mean s.	mean m.f.
247—005	260°— 49°	
247—005		91°— −5°

co-ordinates of the grid	position of s-plane	position of m.f.
246—009	235°— 25°	80°— −5°
	280°—−22°	120°—−10°
248—003	295°— 40°	90°— 0°
	260°— 75°	100°— 5°
	250°— 70°	80°— 12°
	245°— 55°	90°—−10°
	230°— 13°	90°— 7°
	245°— 35°	85°—−12°
	275°— 45°	
	250°— 42°	
	240°— 5°	
247—003	220°— 15°	110°—−20°
	210°— 23°	
	315°—−15°	
247—004	225°—−30°	70°— 15°
	240°— 30°	80°— 5°
	210°— 10°	85°—−10°
	245°—−40°	90°— 8°
	300°—−25°	70°— 0°
	270°— 40°	
	235°—115°	
247—005	260°—115°	
247—006	290°—105°	110°—−18°
	295°—100°	105°—−15°
	280°—110°	85°—−12°
	270°—115°	90°—−20°
	280°—115°	85°— 0°
	300°—−35°	
247—007	340°—−15°	90°—−15°
	275°— 95°	80°— 10°
	260°—110°	
	250°—130°	
	255°—130°	
	250°— 55°	85°— 0°
247—008	270°— 45°	110°—−10°
	255°— 53°	95°—−17°
	250°— 45°	
	240°— 58°	
	270°— 70°	
	240°— 35°	

Meas. sample 228 (40 s. and 30 m.f.)

	mean s.	mean m.f.
169—999	270°— 33°	
168—999		74°— 10°

co-ordinates of the grid	position of s-plane	position of m.f.
172—995	300°— 45°	75°— 25°
	330°— 30°	
	345°— 12°	
171—997	255°— 52°	70°— 5°
	235°— 35°	65°— 3°
	250°— 40°	60°— 3°
	250°— 50°	50°— 0°
	245°— 30°	65°— 5°
	260°— 63°	
	235°— 28°	
	240°— 50°	
	255°— 35°	
	235°— 45°	
171—998	290°— 35°	70°— 0°
	240°— 45°	
	245°— 45°	
	245°— 45°	
170—999	250°— 30°	70°— −5°
	245°— 55°	75°— 0°
	290°— 40°	100°— 3°
	275°— 50°	80°— 3°
	260°— 52°	70°— 12°
	255°— 35°	
169—999	240°— 35°	65°— −3°
	230°— 50°	60°—−20°
166—999	320°— 20°	85°— 20°
	290°— 60°	70°— 17°
	330°— 20°	85°— 20°
	355°— 22°	80°— 18°
	290°— 50°	90°— 17°
	285°— 30°	65°— 28°
	320°— 25°	80°— 30°
	330°— 23°	80°— 15°
	295°— 28°	90°— 20°
	195°—−20°	75°— 20°
	295°— 25°	80°— 22°
		85°— 12°
165—999	330°— 12°	75°— 10°
	285°— 15°	75°— 10°
	190°—−20°	65°— 5°
	200°—−17°	75°— 15°

Meas. sample 229 (52 s. and 37 m.f.)

	mean s.	mean m.f.
125—011	89°— 91°	
124—012		87°— 32°

co-ordinates of the grid	position of s-plane	position of m.f.
130—007	75°—100°	
	110°—107°	
	100°—102°	
	90°— 95°	
129—006	85°— 90°	
	90°—110°	
	80°— 95°	
128—006	100°— 95°	
	85°—100°	
	85°— 90°	
126—007	95°—105°	
	85°—100°	
	90°— 97°	
125—010	70°—112°	
	90°— 90°	
125—011	85°—102°	95°— 37°
	85°— 85°	105°— 33°
	80°— 85°	80°— 30°
	80°— 85°	85°— 37°
	85°— 85°	80°— 35°
	90°— 90°	75°— 30°
	75°— 95°	80°— 42°
	90°— 90°	75°— 35°
	85°— 80°	85°— 40°
	90°— 83°	90°— 30°
	90°— 90°	85°— 32°
	90°— 95°	85°— 25°
	90°— 90°	90°— 27°
		90°— 35°
		90°— 30°
124—012	70°— 85°	90°— 20°
	85°— 85°	70°— 30°
	90°— 90°	85°— 30°
	90°— 90°	90°— 27°
	90°— 87°	90°— 30°
		90°— 30°
123—012	90°— 80°	100°—30°
	90°— 80°	80°— 40°
	85°— 85°	70°— 25°
	70°— 90°	80°— 20°
	90°— 83°	95°— 20°
	90°— 95°	
123—014	95°— 85°	90°— 40°
123—015	90°—100°	60°— 60°
	80°— 85°	95°— 30°
	95°— 90°	90°— 33°
	90°— 95°	80°— 40°
	105°— 92°	90°— 27°
	70°— 75°	60°— 27°
	90°—105°	100°— 35°
	90°— 87°	115°— 35°
	120°— 82°	

124—015°	85°— 65°	95°— 22°
	105°— 80°	110°— 33°
	105°— 80°	

Meas. sample 230 (22 s. and 17 m.f.)		
	mean s.	mean m.f.
123—020	268°— 85°	
123—019		267°— −1°

co-ordinates of the grid	position of s-plane	position of m.f.
124—017	260°— 85°	260°—−20°
	280°— 83°	270°—−15°
	265°— 85°	
	265°— 90°	
123—018	275°— 90°	275°— −5°
	270°— 95°	275°—−10°
	275°— 85°	
123—019	265°— 85°	275°—−12°
	265°— 75°	265°—−15°
	265°— 90°	270°— −5°
123—020	260°— 85°	270°— −2°
	255°— 90°	260°— −5°
	270°— 90°	265°— 5°
	250°— 83°	270°— 15°
	275°— 85°	260°— 22°
	265°— 95°	260°—−10°
	260°— 85°	270°— 12°
	280°— 75°	
122—021	280°— 97°	260°— 25°
	275°— 85°	275°— 5°
	270°— 80°	260°— 7°
	260°— 60°	

Meas. sample 231 (16 s. and 12 m.f.)		
	mean s.	mean m.f.
125—023	274°— 73°	
125—023		274°— 6°

co-ordinates of the grid	position of s-plane	position of m.f.
123—025	275°— 60°	270°— 20°
	255°— 63°	275°— 15°
	270°— 87°	270°— 5°
124—024	275°— 67°	270°— 3°
	265°— 70°	
	275°— 75°	
	280°— 65°	
125—023	280°— 75°	285°—−15°
	280°— 78°	270°— −5°
	270°— 70°	270°— 3°
	270°— 87°	275°— 0°
	275°— 50°	270°— 0°
	270°— 83°	
126—022	285°— 80°	285°— 15°
	285°— 68°	270°— 2°
	280°— 85°	280°— 25°

Meas. sample 232 (33 s. and 36 m.f.)		
	mean s.	mean m.f.
124—985	92°— 69°	
124—985		94°— 8°

co-ordinates of the grid	position of s-plane	position of m.f.
131—990	85°— 80°	85°— 10°
	100°— 80°	85°— 15°
		90°— 8°
130—989	85°— 83°	95°— 15°
128—989	95°— 90°	90°— 10°
127—988	95°—100°	90°— 0°
	90°— 85°	90°— −2°
	95°— 98°	85°— 5°
126—988	95°— 93°	95°— 0°
	115°— 75°	105°— 10°
123—986	100°—102°	95°— 3°
	110°— 55°	100°— 15°
	95°— 80°	100°— 10°
	70°— 60°	90°— 0°
123—985	105°— 53°	90°— 7°
	105°— 60°	100°— 5°
	110°— 90°	110°— 3°
	95°— 50°	100°— 7°
	80°— 33°	95°— 15°
	80°— 65°	110°— 20°
	65°— 35°	100°— 15°
	95°— 70°	100°— 7°
123—984	105°— 80°	100°— 5°
122—983	100°— 55°	100°— 2°
122—982	105°— 65°	95°— 3°
		105°— 10°
122—981	80°— 60°	85°— 10°
	90°— 30°	80°— 7°
	80°— 85°	85°— 3°
	90°— 62°	75°— 8°
	85°— 75°	95°— 12°
	90°— 72°	95°— 5°
	85°— 63°	90°— 13°
	85°— 42°	85°— 10°
		90°— 10°
122—980	70°— 45°	90°— 5°

Meas. sample 233 (25 s. and 25 m.f.)		
	mean s.	mean m.f.
126—979	89°— 46°	
126—979		98°— 9°

co-ordinates of the grid	position of s-plane	position of m.f.
123—980	95°—102°	90°— 5°
	90°— 90°	90°— 7°
124—980	100°— 90°	95°— 12°
	85°— 60°	90°— 12°
	95°— 45°	100°— 13°
		90°— 13°
125—980	85°— 50°	95°— 15°
	90°— 60°	95°— 0°
	95°— 30°	100°— 0°
	95°— 50°	90°— 0°
	87°— 48°	100°— 10°
	105°— 28°	117°— 5°
126—979	90°— 35°	110°— 7°
	95°— 25°	100°— 2°
127—979	110°— 40°	105°— 2°
	90°— 50°	100°— 5°
	80°— 40°	80°— 7°
	60°— 30°	95°— 15°
	75°— 32°	120°— 7°
	105°— 43°	
128—978	80°— 35°	90°— 25°
	70°— 25°	100°— 10°
	85°— 43°	100°— 13°
	75°— 45°	95°— 12°
129—978	95°— 20°	105°— 20°
	85°— 30°	100°— 0°

Meas. sample 234 (23 s. and 24 m.f.)		
	mean s.	mean m.f.
099—001	88°— 93°	
099—001		88°— 23°

co-ordinates of the grid	position of s-plane	position of m.f.
098—999	90°— 87°	90°— 15°
099—000	85°— 90°	85°— 15°
	85°—107°	90°— 17°
	85°— 93°	75°— 20°
	85°— 90°	90°— 25°
	90°— 90°	90°— 17°
	80°— 78°	90°— 25°
	100°—100°	85°— 20°
	85°—115°	100°— 30°
		80°— 25°
		90°— 45°
099—001	90°— 95°	75°— 38°
	85°— 90°	85°— 15°
	95°— 75°	90°— 20°
	90°— 90°	100°— 30°
	85°—100°	75°— 15°
	85°— 83°	80°— 28°
	80°—104°	90°— 23°
	110°—110°	80°— 22°
	85°—100°	100°— 30°
	95°— 82°	100°— 20°
099—002	90°— 90°	80°— 10°
	75°— 80°	100°— 28°
	95°— 85°	100°— 15°
100—002	80°— 95°	

Meas. sample 235 (39 s. and 35 m.f.)		
	mean s.	mean m.f.
213—981	283°— 8°	
213—981		100°— 8°

co-ordinates of the grid	position of s-plane	position of m.f.
214—980	290°— 50°	110°— 0°
	290°— −5°	100°— 0°
	— 0°	95°— 0°

	260°— 15°	100°— 5°
	255°— 13°	85°— 10°
	265°— 17°	110°— 8°
	270°— 22°	95°— 10°
	330°— 5°	75°— 5°
	210°— 12°	105°— −3°
	295°— 35°	100°— 20°
213—980	270°— 17°	100°— 15°
	255°— −7°	55°— −7°
	310°— 25°	110°— 13°
	255°—−40°	115°— 5°
	320°— 20°	110°—−10°
	250°—−10°	
	255°— 10°	
213—981	290°— 25°	110°— 13°
	275°— 30°	100°— 12°
	305°— 40°	110°— 7°
	290°— 33°	115°— 15°
	330°— 17°	110°— 20°
	250°—−20°	100°— 3°
	345°— 10°	110°— 12°
	310°—−15°	
213—982	265°—−15°	105°— 5°
	240°—−15°	
212—982	335°— 40°	95°— 35°
	230°— 37°	85°— 0°
	295°— 8°	100°— 10°
	315°—−40°	115°— 12°
	260°— 20°	90°— 10°
213—982	330°— 15°	90°— 12°
	260°—−48°	90°— 12°
	315°— 20°	85°— 15°
	195°— 10°	105°— −3°
	285°—−60°	105°— 5°
	340°— 20°	95°— 10°
	330°— 20°	110°— 18°

Meas. sample 236 (17 s. and 16 m.f.)

	mean s.	mean m.f.
141—003	278°— 69°	
141—003		88°— 21°

co-ordinates of the grid	position of s-plane	position of m.f.
140—002	280°— 60°	80°— 20°
	280°— 73°	100°— 25°
	295°— 85°	115°— 20°
	285°— 55°	95°— 25°
	285°— 60°	75°— 30°
	285°— 60°	80°— 27°
141—002	275°— 60°	85°— 23°
	275°— 85°	95°— 25°
	280°— 80°	95°— 25°
141—003	280°— 60°	95°— 17°
142—003	270°— 50°	75°— 10°
	275°— 70°	80°— 25°
	275°— 75°	85°— 13°
	275°— 55°	90°— 12°
143—004	265°— 75°	90°— 25°
	255°— 85°	75°— 15°
143—005	295°— 87°	

Meas. sample 237 (30 s. and 32 m.f.)

	mean s.	mean m.f.
255—986	266°—−13°	
255—986		90°— 1°

co-ordinates of the grid	position of s-plane	position of m.f.
255—990	280°— 22°	105°— 0°
	300°— 10°	75°—−10°
	300°— 23°	75°— 0°
	275°—−28°	90°— −5°
	260°— 50°	70°— 3°
		75°— 5°
255—989	285°— 23°	105°— −8°
	225°—−22°	80°— 13°
	210°—−12°	75°— 18°
254—989	330°— 25°	80°— 15°
254—987	210°— −7°	90°— 0°
	— 0°	80°— 10°
	220°—−35°	100°—−10°
	295°—−55°	105°— −5°
254—983	235°—−30°	105°— 20°
	260°— −8°	90°— 5°
	345°— 23°	85°— 23°
254—982	285°— 43°	80°— 0°
	290°—−45°	105°— −7°
	260°—−30°	110°— −5°
	255°—−32°	90°— 3°
	225°—−40°	95°— 5°
	290°—−50°	70°— 25°
		80°— 10°
		115°—−15°
254—981	275°—−30°	75°— −3°
	285°—−35°	80°—−20°
258—986	215°— 20°	110°—−20°
	295°—−40°	80°—−30°
256—987	265°—−48°	95°— 13°
	245°—−32	90°— 0°
	265°—−30°	
255—987	230°—−15°	110°— 12°

Meas. sample 238 (22 s. and 22 m.f.)

	mean s.	mean m.f.
258—977	96°— 51°	
258—977		98°— 0°

co-ordinates of the grid	position of s-plane	position of m.f.
257—977	105°— 40°	120°— −5°
	100°— 45°	105°— 5°
257—976	105°— 53°	107°— 2°
	100°— 60°	105°— 7°
	110°— 50°	115°—−12°
	100°— 40°	90°— −3°
	95°— 60°	90°— 0°
	103°— 50°	100°— 3°
257—977	95°— 55°	100°— 7°
	105°— 40°	100°— 13°
	100°— 43°	100°— 0°
	105°— 40°	
258—977	80°— 43°	90°— 8°
	85°— 50°	95°— 12°
	75°— 47°	80°—−27°
	75°— 45°	100°— 8°
	95°— 43°	100°— 15°
	85°— 65°	115°— 10°
		75°—−15°
259—978		90°— 5°
258—980	95°— 53°	90°—−10°
	105°— 65°	110°— −5°
	100°— 70°	85°— −8°
258—981	90°— 55°	

Meas. sample 239 (27 s. and 16 m.f.)

	mean s.	mean m.f.
241—980	94°— 43°	
241—981		105°— 12°

co-ordinates of the grid	position of s-plane	position of m.f.
240—982	90°— 50°	95°— 13°
	70°— 47°	80°— 10°
240—981	70°—−30°	90°— −8°
	70°— 38°	
241—981	115°— 40°	95°— −3°
	105°— 42°	100°— 20°
	95°— 50°	115°— 25°
	95°— 35°	110°— 10°
	90°— 38°	105°— 25°
	105°— 60°	120°— 28°
	110°— 60°	110°— 0°
	90°— 30°	
	55°— 32°	
	115°— 50°	
241—980	125°— 80°	118°— 0°
242—980	70°— 60°	80°— 10°
	100°— 55°	125°— 20°
	110°— 28°	125°— 30°
	130°— 45°	
242—979	90°— 43°	90°— −2°
	85°— 45°	120°— 10°
	60°— 45°	
	90°— 47°	
	95°— 40°	
	100°— 35°	
	100°— 45°	
	120°— 50°	

Meas. sample 240 (28 s. and 26 m.f.)

	mean s.	mean m.f.
245—965	106°— 64°	
245—965		268°— 7°

co-ordinates of the grid	position of s-plane	position of m.f.
245—966	135°— 90°	315°—−35°
	112°— 80°	280°— 17°
	120°— 55°	265°— 10°
	115°— 50°	250°— 20°
	140°— 55°	280°— 35°

	135°— 50°	265°— 13°
	145°— 25°	280°— 18°
	100°— 67°	
246—966	85°— 60°	265°— 7°
	78°— 53°	250°— 30°
		220°— 30°
246—965	115°— 60°	285°— 5°
	110°— 25°	270°— −5°
	165°— 20°	260°— 18°
	105°— 55°	285°— 7°
	65°— 87°	260°— 15°
	120°— 90°	250°— 20°
245—965	75°— 80°	250°— −5°
	80°— 80°	255°— 15°
	80°— 70°	250°— 2°
	85°—100°	275°—−12°
	110°— 40°	255°— 0°
	103°— 65°	270°—−12°
	97°— 62°	280°— 0°
	95°— 73°	295°—−17°
	105°— 70°	290°— 5°
	100°— 60°	
	110°— 82°	
244—965	75°— 80°	260°— 0°

Meas. sample 241 (36 s. and 26 m.f.)

	mean s.	mean m.f.
237—016	94°— 20°	
237—016		284°— 3°

co-ordinates of the grid	position of s-plane	position of m.f.
238—015	90°— 55°	270°— 0°
	90°— 70°	295°— 0°
	95°— 50°	280°— 10°
	95°— 50°	290°— 3°
	105°— 33°	280°— −3°
	95°— 33°	280°— 0°
	100°— 25°	285°— −5°
	105°— 40°	
	110°— 45°	
	120°— 50°	
	80°— 43°	
237—016	95°—−40°	290°— 3°
	105°—−60°	295°— 10°
	85°—−30°	285°— 10°
	110°—−45°	290°— 2°
	50°—−13°	295°— 10°
	85°—−30°	280°— 10°
	95°—−32°	300°— 10°
	90°—−15°	295°— 3°
	170°— 10°	290°— 10°
	10°—−10°	270°— 3°
	20°—−10°	270°— 20°
	20°— −5°	250°—−10°
	170°— 10°	270°—−15°
	— 0°	
	55°—−35°	
	80°— 50°	
237—017	115°— 45°	285°— 10°
	120°— 60°	300°— 30°
	100°— 90°	280°—−10°
	115°— 57°	290°— −3°
	115°— 50°	295°— −5°
	115°— 63°	280°—−13°
	105°— 30°	
	95°— 55°	
	80°— 38°	

Meas. sample 242 (44 s. and 46 m.f.)

	mean s.	mean m.f.
239—028	75°— 91°	
239—028		254°— 10°

co-ordinates of the grid	position of s-plane	position of m.f.
241—025	75°— 87°	258°— 0°
	80°— 85°	255°— 15°
	70°—110°	260°— 10°
	90°— 80°	260°— 7°
	80°— 65°	250°— 10°
	80°— 65°	255°— 10°
	65°— 90°	260°— 3°
	75°—100°	250°— 10°
	65°—100°	255°— 0°
	85°— 78°	260°—−10°
		250°—−10°
		265°— 10°
240—026	90°— 70°	265°— 15°
	95°—100°	280°—−15°
	75°—117°	265°— 0°
241—027	65°— 85°	255°— 22°
241—028	85°—115°	255°— 0°
	85°—120°	265°— 12°
	90°— 98°	275°— 5°
	100°— 30°	275°— 20°
239—029	70°—105°	260°— 15°
	80°—118°	240°— 18°
	65°— 95°	255°— 25°
	65°—115°	245°— 45°
	80°— 95°	255°— 35°
	80°—107°	245°— 20°
	65°—117°	265°— 12°
	85°—145°	240°— 3°
	75°— 85°	255°— 0°
238—029	75°— 70°	250°— 3°
	75°— 90°	255°— 10°
	75°—100°	255°— 0°
	60°— 85°	240°— 23°
	65°—100°	245°— 15°
	65°— 78°	250°— −2°
	60°— 85°	245°— −2°
	70°—100°	240°— 45°
		250°—−12°
238—030	75°— 87°	250°— 10°
	70°— 95°	240°— 40°
	60°— 85°	275°— 10°
	85°— 40°	245°— 12°
	65°— 78°	240°— 33°
	70°— 95°	
237—030	75°— 85°	255°— 0°
	75°— 90°	255°— 10°
	70°— 80°	240°—−10°

Meas. sample 243 (36 s. and 32 m.f.)

	mean s.	mean m.f.
235—033	78°— 96°	
235—033		260°— 8°

co-ordinates of the grid	position of s-plane	position of m.f.
236—031	75°— 70°	265°— 3°
	85°— 97°	265°— −2°
	75°— 78°	253°— −7°
	85°— 80°	265°—−10°
	80°— 90°	260°— 0°
	80°— 90°	260°— 5°
	85°—100°	280°—−10°
235—031	75°—102°	250°— 28°
	60°—110°	250°— 35°
	70°—105°	270°— 32°
	65°— 95°	245°— 30°
	75°—105°	240°— 22°
	60°—100°	240°— 25°
	70°— 90°	250°— 10°
234—032	75°— 78°	260°— −5°
	85°— 90°	265°—−15°
	90°—100°	280°—−15°
233—033	75°— 85°	260°— −5°
	85°— 80°	265°—−10°
	90°— 90°	270°— −3°
	85°—100°	265°— 10°
	65°— 80°	255°— 3°
	60°—115°	255°— 25°
234—033	80°—130°	260°— −5°
	100°—135°	280°— 3°
	80°—122°	265°— −2°
235—033	70°—127°	265°— 40°
	85°— 90°	
	70°—120°	
235—034	75°—130°	
235—035	95°—100°	280°— 10°
	90°—110°	
235—037	85°—100°	265°— 0°
234—038	60°— 65°	240°—−10°
	80°— 60°	245°— 30°
	95°— 40°	245°— 30°

Meas. sample 244 (42 s. and 35 m.f.)

	mean s.	mean m.f.
170—028	79°— 81°	
170—028		78°— 31°

co-ordinates of the grid	position of s-plane	position of m.f.
173—031	75°— 75°	70°— 15°
	70°— 80°	
171—028	73°— 80°	75°— 37°
	70°— 90°	75°— 40°
	75°— 90°	75°— 30°

171—027	75°— 80°	75°— 30°
	75°— 90°	75°— 27°
	75°— 87°	75°— 38°
	70°— 78°	70°— 25°
	75°— 90°	75°— 30°
	70°— 80°	70°— 25°
	75°— 83°	75°— 38°
070—027	70°— 93°	70°— 28°
	65°— 73°	60°— 38°
070—026	95°— 70°	
	75°— 85°	
	80°— 80°	
070—025	75°— 90°	75°— 28°
168—026	85°— 75°	85°— 32°
	80°— 80°	70°— 40°
	90°— 80°	90°— 22°
167—026	85°— 75°	85°— 25°
	80°— 75°	80°— 20°
	95°— 65°	95°— 20°
	95°— 65°	100°— 30°
	95°— 65°	95°— 15°
	90°— 75°	90°— 15°
	90°— 60°	
166—026	85°— 80°	105°— 15°
	90°— 55°	
	90°— 80°	
173—031	80°— 85°	80°— 30°
	80°— 80°	80°— 30°
	82°— 75°	80°— 35°
171—030	80°— 90°	80°— 17°
	70°— 92°	60°— 45°
	75°— 90°	75°— 43°
170—029	65°—108°	50°— 40°
	60°— 70°	70°— 40°
	80°—105°	85°— 60°
	70°— 95°	60°— 35°
168—026	75°— 70°	90°— 30°

Meas. sample 245 (24 s. and 20 m.f.)

	mean s.	mean m.f.
158—021	68°— 80°	
158—021		74°— 18°

co-ordinates of the grid	position of s-plane	position of m.f.
159—022	65°— 87°	65°— 10°
	85°— 90°	85°— 5°
	70°— 83°	70°— 10°
	80°— 90°	85°— 5°
	70°— 70°	75°— 20°
	85°— 90°	85°— 3°
	55°— 70°	
158—021	55°— 80°	55°— 5°
	50°— 70°	75°— 30°
	75°— 70°	75°— 15°
	75°— 85°	65°— 5°
	65°— 70°	105°— 20°
	90°— 60°	70°— 30°
	50°— 65°	40°— 10°
	50°— 75°	60°— 25°
	60°— 90°	60°— 28°
	60°— 80°	80°— 13°
	55°— 78°	
	75°— 85°	
	75°— 90°	75°— 25°
	85°— 85°	85°— 35°
	75°— 90°	80°— 27°
	70°— 85°	
156—021	65°— 85°	80°— 35°

Meas. sample 246 (42 s. and 37 m.f.)

	mean s.	mean m.f.
154—027	79°— 82°	
154—027		80°— 4°

co-ordinates of the grid	position of s-plane	position of m.f.
152—022	90°— 90°	90°— 12°
	75°— 90°	75°— 5°
151—022	85°— 90°	85°— 10°
	80°— 85°	80°— 5°
	85°— 90°	95°— −5°
	75°— 80°	78°— 12°
	80°— 85°	75°— 30°
152—023	70°—100°	85°— 25°
	75°— 80°	90°— 7°
	85°— 90°	70°— 15°
	85°— 95°	
	85°— 75°	
	75°— 80°	
	90°— 80°	
	70°— 85°	
	75°— 75°	
154—028	75°— 77°	75°— 8°
	75°— 70°	75°— 12°
155—028	75°— 78°	75°— 17°
	80°— 75°	80°— 0°
	75°— 80°	80°— 10°
	80°— 77°	80°— −7°
	80°— 65°	90°— 10°
	90°— 75°	90°—−10°
155—029	80°— 78°	80°— −5°
	75°— 70°	75°— 10°
	85°— 80°	85°— −5°
	70°— 80°	80°— 15°
	80°— 75°	70°—−15°
	75°— 80°	80°—−22°
	85°— 78°	75°— 0°
	70°— 90°	85°— 5°
	75°— 90°	70°—−10°
		75°— 10°
155—030	85°— 70°	85°— 10°
	85°— 85°	85°— −5°
156—030	85°— 78°	85°— 10°
	85°— 78°	85°— 3°
157—030	60°— 90°	60°— 5°
	85°— 85°	85°—−15°
	80°— 85°	95°— 20°
	75°— 90°	75°— −7°
152—028	65°— 90°	65°— 7°

Meas. sample 247 (48 s. and 39 m.f.)

	mean s.	mean m.f.
229—985	283°— 24°	
229—985		90°— 4°

co-ordinates of the grid	position of s-plane	position of m.f.
227—984	305°— 5°	75°— 7°
	300°— 20°	95°— 10°
	335°— 3°	70°— 2°
	360°— 5°	80°— 0°
	— 0°	85°— 5°
	260°—−35°	90°—−10°
	260°— 30°	95°— −5°
	280°— 40°	85°— −5°
	325°— 65°	90°— 3°
	245°— 38°	95°— 15°
	305°— 10°	90°— 0°
	280°— 20°	
	290°— 20°	
	270°— 43°	
	275°— 17°	
228—985	280°— 17°	90°— 4°
	250°— 17°	95°— −2°
	270°— 30°	65°— 0°
	275°— 58°	85°—−10°
	255°— 15°	90°— −3°
	280°— 20°	100°— −2°
	310°— 20°	95°— 10°
	310°— 12°	95°— 10°
	260°— 30°	100°— 3°
	260°— 15°	85°— 3°
	— 0°	105°— 0°
229—986	280°— 20°	95°— 3°
	280°— 25°	90°— 5°
	290°— 33°	100°— 0°
	250°— 25°	85°— 3°
	295°— 20°	100°— 8°
	280°— 28°	100°— −3°
	285°— 32°	95°— 0°
230—986	300°— 35°	100°— 5°
	290°— 25°	
	270°— 30°	
231—987	260°— 30°	80°— 0°
	240°— 12°	75°— −5°
	270°— 40°	90°— 5°
	285°— 33°	85°— 15°
	285°— 35°	95°— 15°
	265°— 40°	
	270°— 30°	
232—987	325°— 30°	95°— 23°
	340°— 10°	100°— 0°
	255°— 20°	
235—988	260°— 40°	90°— 15°
	285°— 22°	80°— 13°

Meas. sample 248 (27 s. and 15 m.f.)

	mean s.	mean m.f.
217—064	67°— 77°	
219—064		69°— 7°

co-ordinates of the grid	position of s-plane	position of m.f.
226—061	85°—100°	70°— 38°
	70°— 95°	70°— 25°
	75°—110°	70°— 30°
	70°— 93°	
	70°— 90°	
225—061	80°— 88°	80°— 30°
	75°— 90°	75°— 2°
	55°— 90°	55°— 20°
214—065	70°— 75°	75°— 10°
	75°— 70°	65°— 12°
	60°— 60°	60°—-10°
	55°— 80°	65°— -5°
	70°— 73°	70°—-15°
	65°— 70°	
214—066	60°— 63°	65°— 0°
	65°— 70°	70°— 7°
	60°— 60°	70°—-20°
	65°— 75°	75°—-20°
	70°— 63°	
	75°— 80°	
	70°— 70°	
	70°— 80°	
	65°— 65°	
213—067	60°— 60°	
	55°— 60°	
	60°— 70°	
	60°— 73°	

Meas. sample 249 (40 s. and 36 m.f.)

	mean s.	mean m.f.
211—071	68°— 88°	
211—071		69°— -5°

co-ordinates of the grid	position of s-plane	position of m.f.
213—067	75°— 65°	70°— 2°
	75°— 80°	70°— 0°
212—068	60°—115°	70°— 12°
	60°— 83°	
	55°—110°	
212—069	60°— 83°	73°— 3°
	65°—103°	60°—-10°
	75°— 85°	60°— 5°
	70°—102°	
	60°— 40°	
212—070	75°— 80°	85°— -5°
	75°— 70°	80°— -5°
	80°— 95°	70°— -8°
211—071	70°— 70°	70°—-12°
	65°— 83°	70°— 0°
	65°—110°	65°— -5°
211—072	65°— 80°	60°— -5°
	75°— 85°	75°— 0°
	75°— 90°	75°— -8°
	70°—110°	70°— 0°
	65°— 85°	65°—-15°
	70°— 78°	70°— 0°
	63°— 85°	63°— -3°
	70°— 80°	70°— 0 °
	70°— 70°	70°— 5°
	75°— 80°	75°— 8°
	55°— 90°	65°— -5°
	80°— 95°	80°— -5°
	80°—100°	80°—-15°
	70°—100°	70°— -7°
	60°— 63°	60°— 0°
	70°— 93°	70°— 0°
	65°— 95°	75°—-23°
	60°— 90°	60°—-45°
211—073	60°— 85°	60°—-15°
	65°—115°	75°— 15°
	60°— 90°	60°— 0°
	70°— 95°	75°—-20°
	70°—105°	70°— 5°
	60°— 90°	60°— -7°

Meas. sample 250 (31 s. and 21 m.f.)

	mean s.	mean m.f.
205—057	63°— 78°	
205—057		65°— 15°

co-ordinates of the grid	position of s-plane	position of m.f.
208—054	60°— 75°	60°— 25°
	70°— 70°	70°— 27°
	60°— 80°	60°— 17°
	60°— 75°	60°— 30°
205—056	60°— 70°	60°— 15°
	65°— 80°	65°— 20°
	55°— 55°	60°— -5°
	75°— 70°	95°— 15°
	70°— 70°	57°— 10°
	57°— 85°	
	60°— 70°	
	45°— 83°	
	60°— 70°	
	60°— 80°	
	70°— 72°	
	70°— 80°	
205—057	70°— 78°	75°— 25°
	50°— 75°	55°— 7°
	60°— 90°	60°— 10°
	50°— 70°	
204—058	60°— 65°	60°— 10°
	70°— 80°	70°— 15°
	55°— 70°	70°— 20°
	60°— 85°	60°— 0°
	60°— 75°	65°— 15°
	65°— 95°	60°— 10°
	60°— 90°	
203—059	80°— 90°	70°— 7°
	70°— 70°	70°— 7°
	70°—105°	70°— 25°
	65°—105°	

Meas. sample 251 (34 s. and 29 m.f.)

	mean s.	mean m.f.
204—061	66°— 81°	
204—061		67°— 9°

co-ordinates of the grid	position of s-plane	position of m.f.
203—059	60°—105°	60°— 10°
	60°— 85°	60°— 15°
203—060	80°— 80°	80°— 3°
	65°—105°	65°— 2°
	95°— 80°	65°— 5°
	60°— 70°	65°— 3°
202—060	70°— 85°	60°— 7°
	45°— 70°	70°— 8°
	65°— 85°	65°— 10°
	60°— 83°	60°— 18°
202—061	60°— 40°	60°— 0°
	60°—110°	60°— 5°
	65°— 90°	65°— 15°
202—062	65°— 70°	65°— 5°
205—062	65°— 85°	70°— 20°
	70°— 67°	
205—063	65°— 83°	65°— 10°
	65°— 78°	65°— 13°
	70°—105°	70°— 12°
	75°— 90°	90°— 15°
	75°— 55°	85°— 15°
	85°— 97°	
205—062	80°— 70°	75°— 8°
	70°— 73°	70°— 7°
	60°— 80°	60°— 13°
	60°— 70°	
206—062	65°— 80°	65°— 0°
206—063	70°— 55°	
206—062	60°— 85°	
	60°— 90°	60°— 12°
207—061	60°— 80°	60°— 15°
	50°— 65°	60°— 22°
	70°— 80°	70°— 5°
	70°— 98°	70°— 0°

Meas. sample 252 (24 s. and 22 m.f.)

	mean s.	mean m.f.
139—046	82°— 90°	
137—045		88°— 2°

co-ordinates of the grid	position of s-plane	position of m.f.
135—045		100°— 0°
		95°—-10°
		90°—-10°
136—045		100°— 0°
		90°— -7°
		85°— -3°
		75°— 2°
		80°— 8°
		80°— 0°
		80°— 0°
		80°— 5°

		100°—−10°
		100°— 7°
137—045		105°— 0°
138—045	80°— 90°	
	80°— 78°	
	85°— 80°	
	75°— 70°	
	85°— 80°	
139—046	85°— 80°	85°— 5°
	80°— 80°	90°— 0°
	90°— 95°	85°— 12°
	85°—100°	80°— 20°
	75°—100°	80°— 10°
	80°— 95°	
	75°— 90°	
	75°—100°	
	80°—115°	
	80°—110°	
	90°—105°	
	80°— 93°	
140—046	80°— 75°	80°— 0°
	80°— 90°	80°— 2°
	85°— 85°	
	80°—100°	
	90°—105°	
141—046	90°— 80°	90°— 8°
141—047	85°— 80°	

Meas. sample 253 (27 s. and 23 m.f.)

	mean s.	mean m.f.
146—037	84°— 89°	
146—038		80°— −2°

co-ordinates of the grid	position of s-plane	position of m.f.
145—040	80°— 80°	80°— 0°
	80°— 85°	60°—−10°
	85°— 80°	80°—−10°
	80°— 80°	80°—−10°
	105°— 70°	110°—−10°
	85°— 75°	85°— −5°
	85°— 90°	85°— −3°
	75°— 90°	75°—−10°
	80°— 97°	80°— −5°
	80°— 90°	
145—039	85°— 93°	85°— 0°
	80°—102°	80°— 5°
	80°— 80°	80°— 7°
146—040	70°—106°	85°— 3°
	105°—105°	80°— 5°
	75°—105°	75°— 5°
147—039	75°— 87°	75°— −2°
	80°— 95°	80°— 0°
147—033	85°— 90°	85°— 3°
	80°—105°	80°— −7°
	75°—102°	75°— 0°
147—032	80°— 72°	80°— 0°
	70°— 75°	70°— −7°
148—031	85°— 95°	85°— 0°
	105°— 95°	
	120°— 75°	
148—030	85°— 85°	

Meas. sample 254 (26 s. and 23 m.f.)

	mean s.	mean m.f.
154—014	91°— 89°	
154—014		91°— 22°

co-ordinates of the grid	position of s-plane	position of m.f.
155—017	80°— 90°	80°— 28°
155—016	70°—100°	70°— 30°
	105°— 90°	105°— 27°
	105°— 90°	105°— 23°
154—016	95°— 85°	95°— 30°
	95°— 85°	95°— 15°
	100°— 90°	100°— 25°
154—015	110°— 85°	110°— 23°
	100°— 80°	100°— 27°
	90°— 75°	90°— 27°
	90°— 85°	90°— 28°
	100°— 90°	100°— 15°
153—015	90°— 80°	90°— 20°
154—013	90°— 95°	90°— 18°
	100°— 95°	100°— 10°
	95°— 93°	95°— 25°
	90°— 90°	90°— 40°
		80°— 25°
155—012	80°— 80°	80°— 23°
	70°— 80°	75°— 20°
	75°— 90°	90°— 20°
	90°—100°	
153—013	95°— 95°	95°— −3°
154—013	95°— 97°	95°— 15°
	85°— 90°	85°— 30°
	93°— 90°	93°— 17°
	80°— 98°	80°— 25°

Meas. sample 255 (16 s. and 14 m.f.)

	mean s.	mean m.f.
166—052	256°— 78°	
166—052		75°— −2°

co-ordinates of the grid	position of s-plane	position of m.f.
166—050	260°— 75°	75°— 0°
166—051	260°— 82°	80°—−15°
	265°— 85°	85°— −5°
	260°— 97°	
166—052	260°— 65°	75°— 10°
	255°— 90°	75°— 5°
	260°— 60°	80°— 0°
	250°— 70°	70°— −3°
	255°— 65°	65°— −5°
	250°— 75°	70°— 0°
	250°— 85°	70°—−17°
	245°— 87°	
165—052	255°— 90°	75°— −3°
	260°— 65°	80°— 10°
	255°— 85°	75°— 0°
165—053	260°— 75°	80°— 0°

Meas. sample 256 (29 s. and 28 m.f.)

	mean s.	mean m.f.
185—046	68°— 85°	
185—046		69°— 11°

co-ordinates of the grid	position of s-plane	position of m.f.
186—044	60°— 75°	60°— 20°
	65°— 75°	65°— 5°
	65°— 83°	65°— 13°
186—045	70°— 80°	70°— 7°
	55°— 60°	55°— 0°
185—045	75°— 80°	75°— 5°
	65°— 90°	
	60°— 80°	
185—046	70°— 95°	70°— 20°
	60°— 78°	60°— 8°
	55°— 68°	60°— 15°
	65°— 80°	65°— 25°
	60°— 70°	65°— 30°
	75°— 87°	60°— 25°
	70°— 85°	75°— 20°
	65°— 80°	70°— 35°
	65°— 70°	65°— 12°
	70°—100°	65°— 15°
	65°— 80°	70°— 5°
		65°— 0°
185—047	70°—110°	75°— 13°
	70°— 90°	70°— 20°
	75°— 98°	75°— 5°
	60°— 95°	60°— 2°
185—048	70°— 90°	70°— 12°
	90°—105°	90°— 18°
	75°— 70°	75°— −7°
	85°—102°	85°— 5°
184—049	65°—100°	65°— −8°
184—050	80°— 95°	80°— −3°

Meas. sample 257 (17s. and 18 m.f.)

	mean s.	mean m.f.
191—033	81°— 66°	
191—033		86°— 29°

co-ordinates of the grid	position of s-plane	position of m.f.
191—034	90°— 65°	90°— 20°
	80°— 65°	80°— 33°
	85°— 65°	100°— 30°
	75°— 60°	80°— 35°
191—033	80°— 70°	80°— 23°
	75°— 67°	90°— 25°
	90°— 60°	90°— 15°
	80°— 80°	80°— 25°
191—032	70°— 50°	75°— 45°
	85°— 60°	75°— 25°
	75°— 80°	85°— 35°
	85°— 70°	80°— 27°
	90°— 70°	85°— 30°
	80°— 70°	100°— 35°
	80°— 67°	85°— 30°

			95°—	35°
191—031	85°—	60°	100°—	25°
	75°—	62°	80°—	20°

Meas. sample 258 (25 s. and 14 m.f.)

	mean s.	mean m.f.
256—991	279°— 22°	
256—991		291°— 8°

co-ordinates of the grid	position of s-plane	position of m.f.
255—990	290°— 20°	300°— 10°
255—991	330°— −7°	280°— 5°
	325°— 15°	310°— 25°
	295°— 32°	300°— 3°
	255°— 23°	295°— 10°
	240°— 22°	295°— 5°
	290°— 23°	275°— 2°
	290°— 25°	
	295°— 57°	
	295°— 35°	
	270°— 30°	
256—991	295°— 37°	295°— 12°
	225°— 10°	280°— −5°
	225°— 25°	260°— 5°
	260°— 30°	300°— 8°
	270°— 27°	285°—−15°
	310°— 25°	
256—992	220°— 28°	300°— 25°
	260°— 25°	295°— 18°
	360°—−20°	
	255°— 40°	
	285°— 20°	
	275°— 18°	
	270°—−12°	
257—992	295°— 33°	

Meas. sample 259 (12 s.)

	mean s.
269—005	233°— 93°

co-ordinates of the grid	position of s-plane	position of m.f.
269—004	225°—100°	
	245°— 93°	
	230°— 80°	
	240°— 87°	
269—005	240°— 70°	
	250°— 75°	
	210°—110°	
	225°—110°	
	240°—105°	
	230°—103°	
	240°—110°	
270—003	220°— 70°	

Meas. sample 260 (30 s. and 29 m.f.)

	mean s.	mean m.f.
768—047	75°— 63°	
768—047		255°— 13°

co-ordinates of the grid	position of s-plane	position of m.f.
769—047	70°— 60°	260°— 10°
	85°— 70°	270°— 12°
	85°— 55°	255°— 15°
768—047	85°— 40°	260°— 7°
	80°— 65°	270°— 8°
		255°— 0°
768—046	85°— 45°	255°— 20°
	85°— 55°	265°— 10°
	85°— 78°	255°— 10°
	80°— 75°	250°— 35°
	80°— 75°	260°— 10°
	80°— 55°	
	85°— 75°	
767—046	85°— 45°	285°— 3°
	90°— 65°	260°— 20°
	80°— 60°	260°— 10°
767—045	85°— 60°	260°— 23°
	85°— 62°	250°— 13°
	80°— 75°	260°— 22°
767—044	65°— 75°	240°— 15°
	75°— 68°	260°— 12°
	70°— 80°	255°— 10°
	75°— 68°	265°— 25°
766—044	80°— 75°	245°— 25°
769—052	65°— 50°	240°— 10°
	50°— 58°	230°— 8°
	50°— 52°	245°— 2°
768—052	70°— 65°	240°— 20°
	50°— 60°	235°— 0°
	35°— 60°	260°— 5°
769—050	70°— 75°	255°— 25°

Meas. sample 261 (28 s. and 29 m.f.)

	mean s.	mean m.f.
209—006	80°— 82°	
209—006		82°— 22°

co-ordinates of the grid	position of s-plane	position of m.f.
207—007	55°— 80°	55°— 20°
	70°— 90°	70°— 15°
	70°— 80°	70°— 25°
	70°— 75°	68°— 23°
	70°— 90°	70°— 8°
208—006	75°— 75°	75°— 10°
	75°— 90°	75°— 20°
209—007	70°— 75°	70°— 25°
	70°— 73°	75°— 30°
	80°— 90°	80°— 30°
210—007	80°— 87°	80°— 30°
	75°— 90°	75°— 30°
	75°— 75°	75°— 20°
	75°— 80°	75°— 20°
	75°— 80°	75°— 20°
	75°— 80°	75°— 20°
	70°— 65°	80°— 30°
212—007	65°— 58°	90°— 30°
	75°— 90°	75°— 35°
	85°— 90°	85°— 35°
214—009	65°— 70°	65°— 33°
	90°— 65°	95°— 30°
210—000	120°— 97°	110°— 20°
	105°— 85°	110°— 35°
		105°— 27°
209—000	100°—102°	100°— 10°
	100°— 90°	100°— −7°
207—000	105°— 80°	105°— 12°
203—001	90°— 87°	95°— 12°

Meas. sample 262 (26 s. and 30 m.f.)

	mean s.	mean m.f.
771—054	79°— 69°	
771—054		249°— 40°

co-ordinates of the grid	position of s-plane	position of m.f.
772—053	105°— 73°	270°— 60°
	110°— 70°	260°— 55°
	130°— 60°	265°— 55°
	75°— 60°	250°— 45°
		260°— 55°
		250°— 40°
		260°— 42°
771—053	70°— 78°	255°— 40°
	60°— 63°	240°— 30°
	75°— 75°	255°— 28°
	100°— 58°	250°— 32°
	90°— 70°	240°— 33°
		255°— 28°
770—053	90°— 60°	230°— 22°
	80°— 65°	240°— 37°
	65°— 65°	250°— 45°
	75°— 80°	270°— 48°
	90°— 70°	250°— 35°
069—053	70°— 63°	250°— 40°
	90°— 50°	240°— 43°
	70°— 63°	235°— 30°
	60°— 47°	235°— 35°
772—055	30°—110°	270°— 62°
		255°— 57°
773—055	75°— 90°	240°— 30°
	80°— 58°	255°— 33°
	65°— 70°	255°— 52°
	70°— 90°	
773—056	75°—102°	265°— 7°
	65°— 45°	210°— 25°
	85°— 58°	215°— 48°

Meas. sample 263 (34 s. and 22 m.f.)

	mean s.	mean m.f.
733—027	274—° 24°	
754—027		277°— 9°

co-ordinates of the grid	position of s-plane	position of m.f.
753—026	330°— 50°	300°—−10°

	280°— 20°	
	320°— 32°	
	330°— 13°	
	260°— 30°	
753—027	265°— 15°	
	260°— 20°	
	260°— 28°	
754—027	285°— 25°	275°—−12°
	260°— 33°	280°— 12°
	270°— 23°	260°— −5°
	295°— 28°	
753—026	310°— 30°	
	280°— 20°	
752—026	280°— 15°	280°— 0°
	300°— 30°	295°— 3°
	270°— 30°	280°— 3°
	270°— 35°	283°— 10°
	270°— 10°	280°— 0°
	370°—−15°	295°— 20°
751—026	240°— 27°	270°— 2°
	280°— 20°	300°— 20°
	270°— 15°	
	210°— 12°	
755—027	315°—−40°	280°— 10°
	300°— 30°	270°— 10°
755—028	230°— 20°	265°— 20°
	245°— 40°	260°— 25°
	260°— 30°	270°— 10°
	255°— 60°	255°— 15°
	250°— 50°	255°— 10°
756—029	250°— 35°	265°— 6°
	225°— 20°	270°— 12°
	215°— 20°	295°— 30°

Meas. sample 264 (19 s. and 20 m.f.)

	mean s.	mean m.f.
774—057	94°— 81°	
774—057		273°— 15°

co-ordinates of the grid	position of s-plane	position of m.f.
773—057	65°— 87°	245°— 13°
	70°— 78°	250°— 5°
	85°— 70°	270°— 35°
	100°— 68°	265°— 30°
	95°— 82°	270°— 30°
	90°— 83°	275°— 10°
	90°— 78°	270°— 0°
	75°— 58°	270°— 5°
		255°— 10°
774—057	140°— 95°	320°— 30°
	75°— 65°	255°— 25°
	120°— 90°	295°— 15°
	95°— 80°	270°— 0°
		275°— 10°
775—058	70°— 75°	270°— 15°
	105°— 70°	290°—−10°
776—058	95°— 90°	270°— 15°
	90°— 90°	270°— 18°
	100°— 60°	280°— 32°
	105°— 90°	285°— 8°
	120°—122°	

Meas. sample 265 (17 s. and 17 m.f.)

	mean s.	mean m.f.
788—069	72°— 74°	
788—069		71°— −4°

co-ordinates of the grid	position of s-plane	position of m.f.
788—067	75°— 50°	70°—−12°
	55°— 83°	50°— 20°
	70°— 60°	70°— 0°
	60°— 63°	60°— 10°
	85°— 95°	85°— 7°
788—069	60°— 85°	60°— 5°
	80°— 90°	80°— 7°
	80°— 60°	80°— −5°
	90°— 60°	75°—−10°
	70°— 58°	70°—−12°
	75°— 60°	75°—−10°
	60°— 75°	60°—−18°
	90°— 70°	90°— −2°
789—070	65°— 90°	65°—−15°
	70°— 97°	70°—−10°
	70°— 90°	70°— −2°
790—074	70°— 80°	70°—−22°

Meas. sample 266 (15 s. and 13 m.f.)

	mean s.	mean m.f.
794—074	76°— 72°	
794—074		252°— 10°

co-ordinates of the grid	position of s-plane	position of m.f.
795—074	90°— 80°	270°— −5°
	90°— 65°	250°— 15°
	75°— 78°	250°— 5°
	70°— 70°	230°— 3°
	75°— 75°	
	50°— 70°	
794—074	90°— 80°	270°— 5°
	55°— 60°	220°— 38°
	75°— 75°	255°— 7°
	70°— 55°	250°— 0°
	60°— 62°	230°— 33°
	80°— 90°	260°— 0°
	90°— 65°	270°— 0°
	90°— 78°	270°— 20°
	75°— 75°	255°— 10°

Meas. sample 267 (28 s. and 28 m.f.)

	mean s.	mean m.f.
757—031	246°— 20°	
757—031		263°— 2°

co-ordinates of the grid	position of s-plane	position of m.f.
756—029	240°— 25°	245°— 20°
	210°— 10°	240°— 6°
	230°— 25°	270°— 10°
	250°— 30°	270°— 9°
	250°— 25°	260°— 10°
	190°— 10°	240°— 5°
	240°— 20°	240°— −5°
757—030	245°— 15°	270°— 10°
	270°— 25°	270°— −5°
	240°— 20°	275°— 8°
	190°— 15°	260°— 8°
	240°— 15°	270°— 10°
	240°— 20°	270°— 10°
	240°— 30°	270°— 15°
757—031	270°— 20°	255°— −5°
	260°— 30°	265°— −6°
	270°— 30°	270°— 0°
	270°— 35°	255°— 2°
	270°— 15°	270°— −5°
	250°— 20°	270°— −5°
	300°— 15°	265°—−12°
757—032	250°— 15°	270°— −5°
	220°— 10°	265°— −3°
	235°— 25°	270°— 5°
	225°— 5°	270°— 2°
758—033	300°— 30°	270°—−15°
	245°— 15°	265°— −5°
	235°— 15°	245°— 0°

Meas. sample 268 (22 s. and 17 m.f.)

	mean s.	mean m.f.
223—033	75°— 76°	
223—033		74°— −8°

co-ordinates of the grid	position of s-plane	position of m.f.
223—033	75°— 68°	75°— 0°
	85°— 80°	70°—−25°
	75°— 87°	75°—−25°
	70°— 70°	70°— 13°
	80°— 82°	80°—−25°
	75°— 75°	75°— −7°
	75°— 73°	75°—−10°
	75°— 75°	75°—−20°
	80°— 82°	90°— 0°
	90°— 90°	90°— −3°
	90°— 65°	75°—−13°
	75°— 70°	80°— −5°
	60°— 73°	60°—−12°
	80°— 65°	
	60°— 90°	
	70°— 80°	
222—032	90°— 60°	
221—032	70°— 70°	70°—−15°
	80°— 70°	50°— 12°
	50°— 82°	80°— 22°
	80°— 63°	70°—−17°
	70°— 95°	

Meas. sample 269 (19 s. and 18 m.f.)

	mean s.	mean m.f.
171—041	77°— 90°	
172—040		78°— 6°

co-ordinates of the grid	position of s-plane	position of m.f.
172—039	75°— 90°	75°— −2°
172—040	78°— 80°	78°— 5°
	75°— 87°	75°— 5°
	75°— 97°	75°— 8°
	90°—105°	90°— 0°
	75°— 90°	75°— 5°
	80°—105°	80°— 12°
	85°— 82°	85°— 15°
	70°— 75°	70°— 18°
	100°— 80°	100°— −2°
	65°— 80°	65°— 10°
171— 041	75°— 92°	70°— 10°
	70°—110°	70°— 5°
	80°—107°	80°— 10°
	85°— 80°	85°—−10°
	80°— 90°	80°— 0°
170—042	60°— 75°	60°— 17°
	85°— 85°	85°— 10°
	60°—100°	

Meas. sample 270 (18 s. and 18 m.f.)

	mean s.	mean m.f.
227—076	65°— 79°	
227—076		66°— 3°

co-ordinates of the grid	position of s-plane	position of m.f.
227—076	65°— 82°	65°— 15°
227—075	60°— 73°	60°— −5°
	60°— 80°	60°— 0°
	60°— 70°	60°— −7°
	60°— 75°	75°— 7°
227—076	60°— 72°	60°— 3°
	65°— 75°	65°— 2°
	70°—102°	70°— 3°
	60°— 72°	60°— 5°
227—077	65°— 75°	65°— 3°
	70°— 82°	75°— 10°
	70°— 72°	70°— −3°
	60°— 82°	60°— 0°
	60°— 95°	60°— 10°
	70°— 80°	60°— −5°
	65°— 80°	65°— 2°
226—078	65°— 80°	90°— 10°
	78°— 80°	70°— −2°

APPENDIX III

Pole diagrams (Schmidt net, lower hemisphere) of the meas. samples 1-270 of appendix II.

The *S*-poles are indicated by circles, the axes of the m.f. by points. Coinciding measurements are indicated by cross strokes.

The approximate mean *S*. and mean m.f. of appendix II are represented by a rectangle and a triangle respectively.

All pole diagrams have been corrected with the magnetic correction.

The numbers of *S*-planes and minor folds of a meas. sample are given in parentheses. E.g., meas. sample 1 (38 *S* and 52 m.f.).

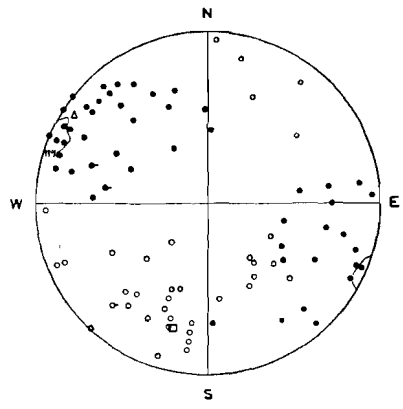

Meas. sample 1
(38 s. and 52 m.f.)

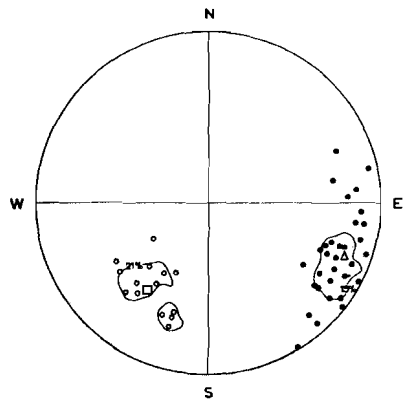

Meas. sample 2
(14 s. and 33 m.f.)

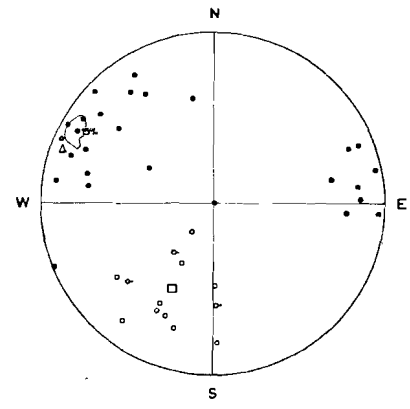

Meas. sample 3
(17 s. and 26 m.f.)

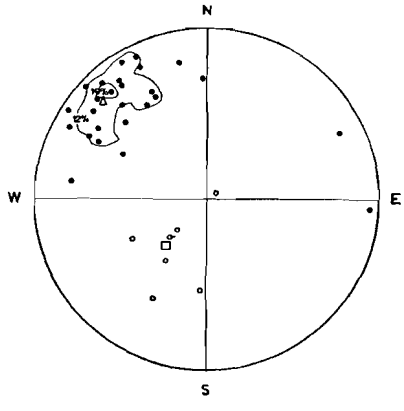

Meas. sample 4
(8 s. and 26 m.f.)

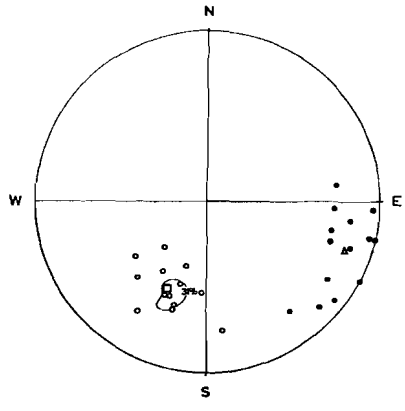

Meas. sample 5
(13 s. and 14 m.f.)

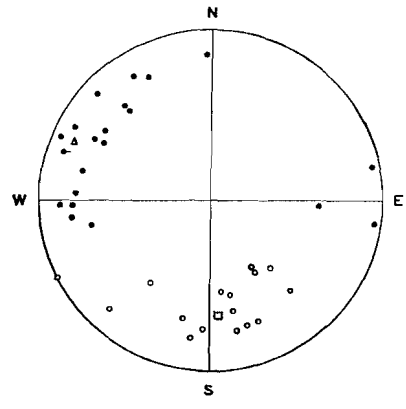

Meas. sample 6
(16 s. and 22 m.f.)

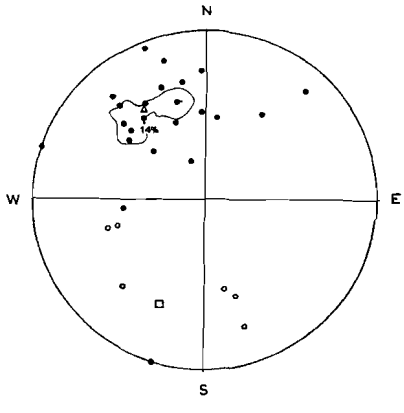

Meas. sample 7
(7 s. and 23 m.f.)

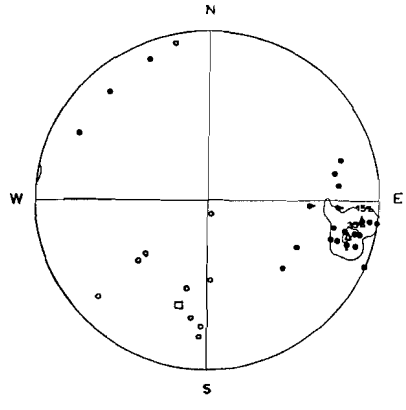

Meas. sample 8
(10 s. and 26 m.f.)

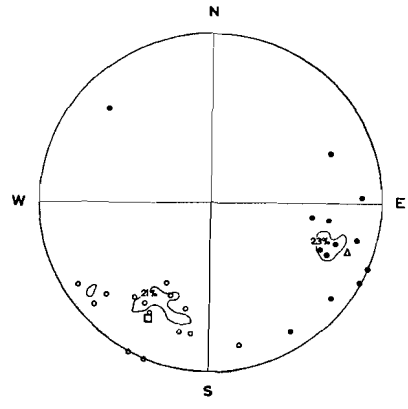

Meas. sample 9
(14 s. and 13 m.f.)

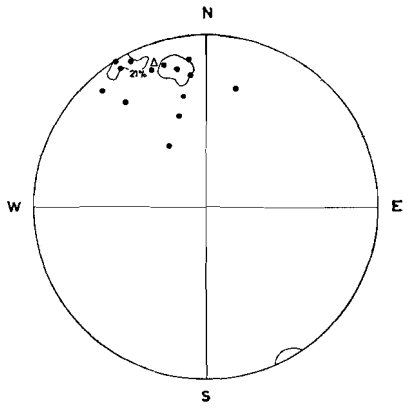

Meas. sample 10
(14 m.f.)

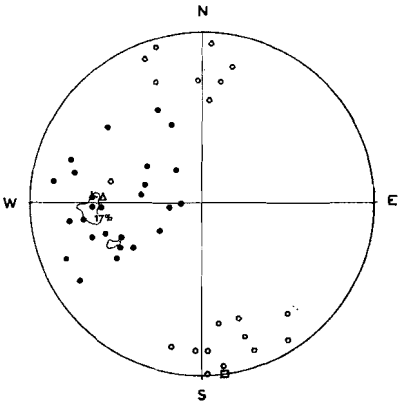

Meas. sample 11
(19 s. and 29 m.f.)

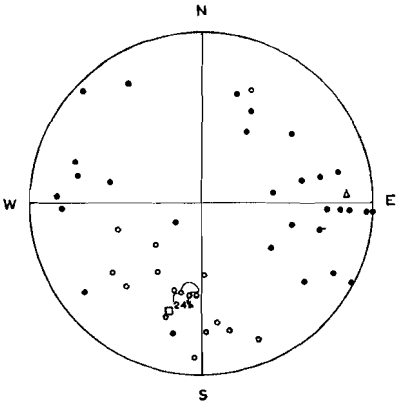

Meas. sample 12
(17 s. and 30 m.f.)

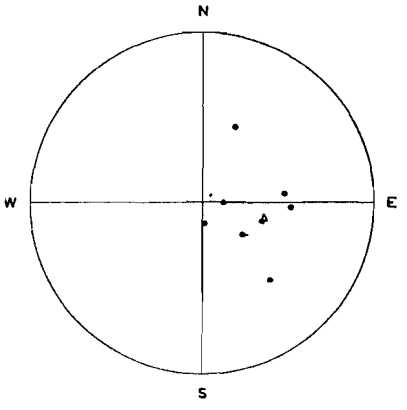

Meas. sample 13
(9 m.f.)

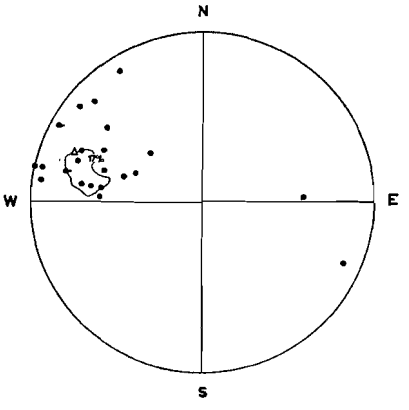

Meas. sample 14
(24 m.f.)

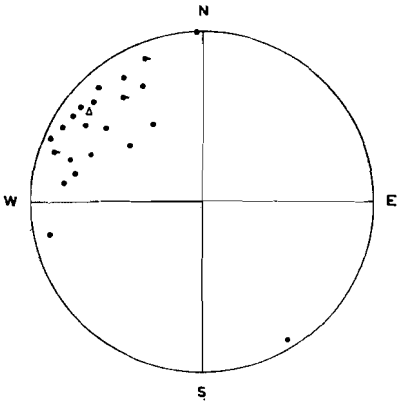

Meas. sample 15
(25 m.f.)

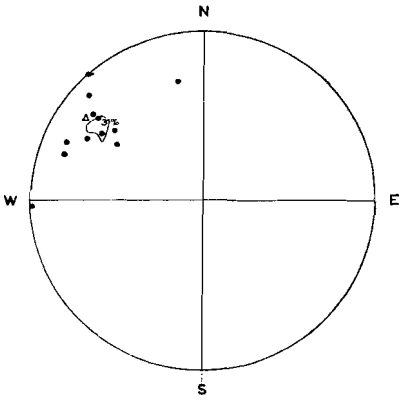

Meas. sample 16
(13 m.f.)

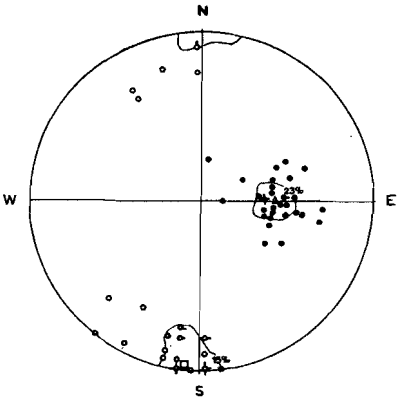

Meas. sample 17
(33 s. and 35 m.f.)

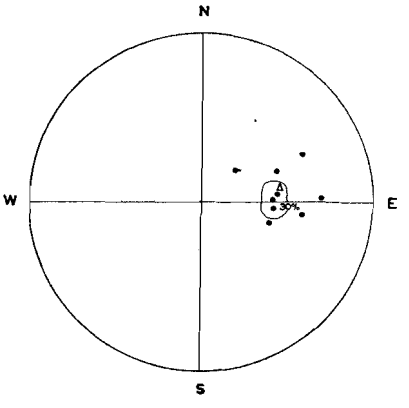

Meas. sample 18
(10 m.f.)

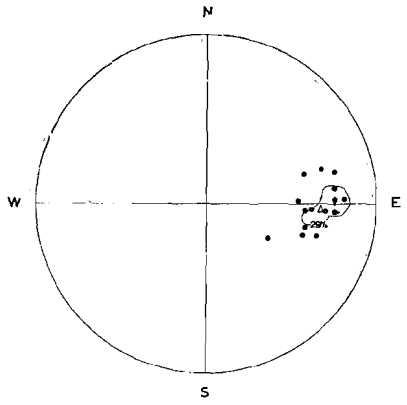

Meas. sample 19
(17 m.f.)

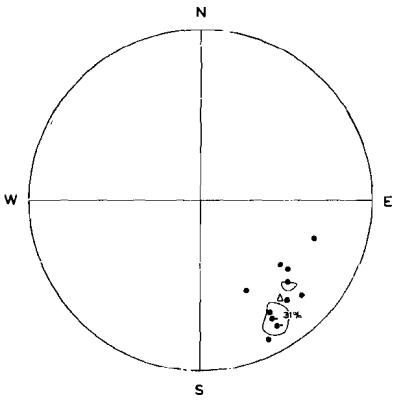

Meas. sample 20
(13 m.f.)

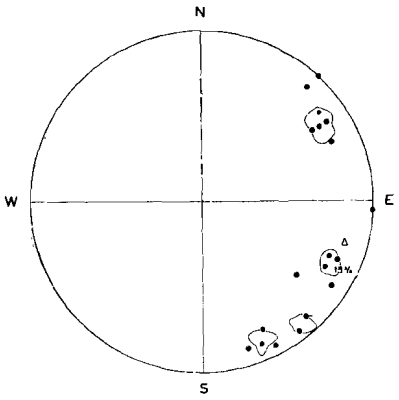

Meas. sample 21
(20 m.f.)

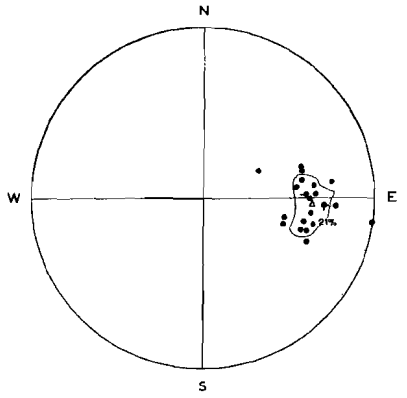

Meas. sample 22
(24 m.f.)

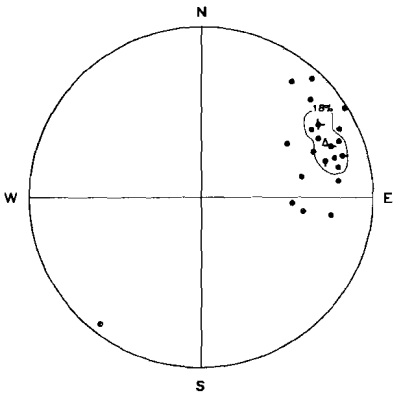

Meas. sample 23
(28 m.f.)

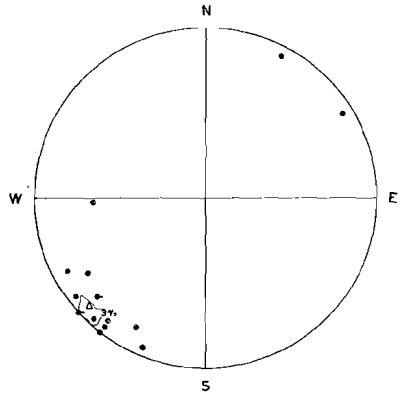

Meas. sample 24
(16 m.f.)

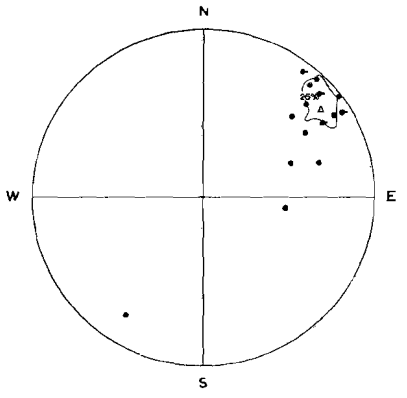

Meas. sample 25
(19 m.f.)

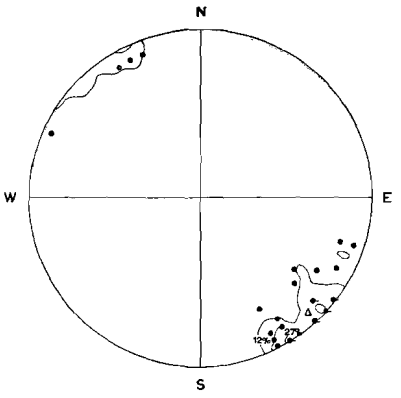

Meas. sample 26
(26 m.f.)

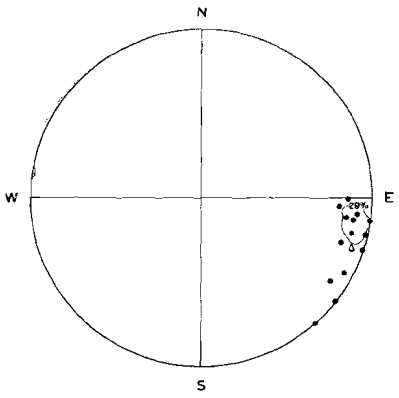

Meas. sample 27
(14 m.f.)

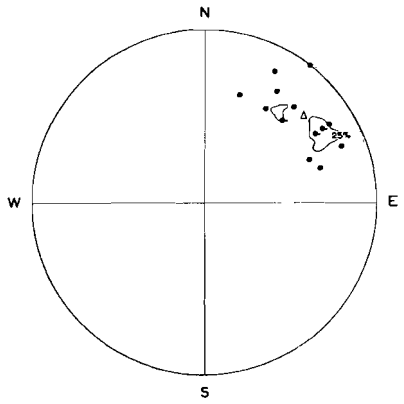

Meas. sample 28
(16 m.f.)

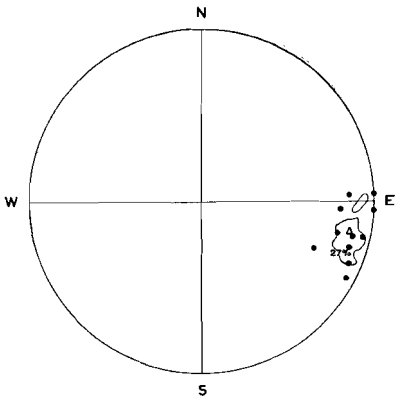

Meas. sample 29
(11 m.f.)

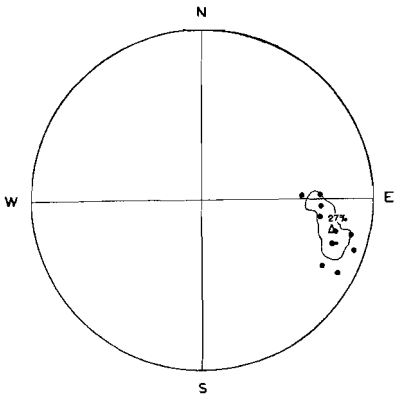

Meas. sample 30
(11 m.f.)

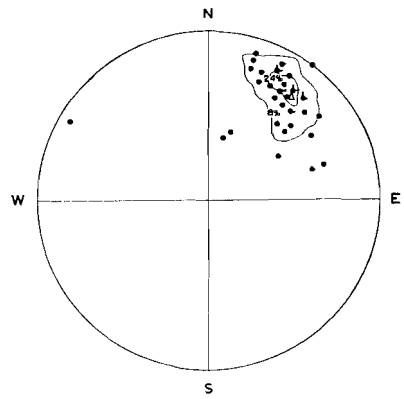

Meas. sample 31
(39 m.f.)

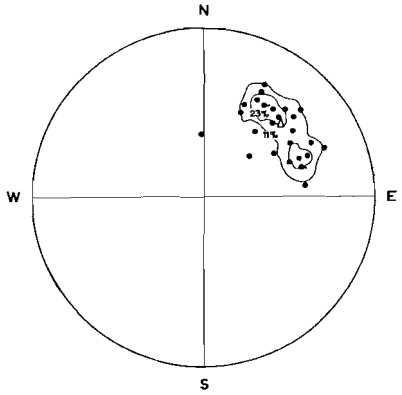

Meas. sample 32
(27 m.f.)

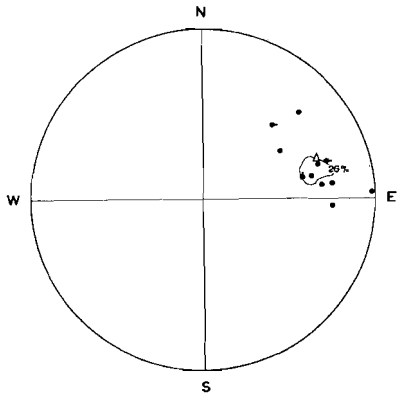

Meas. sample 33
(14 m.f.)

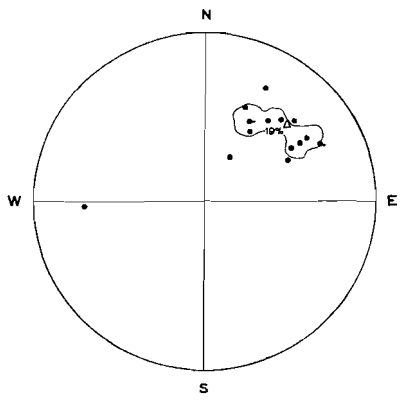

Meas. sample 34
(16 m.f.)

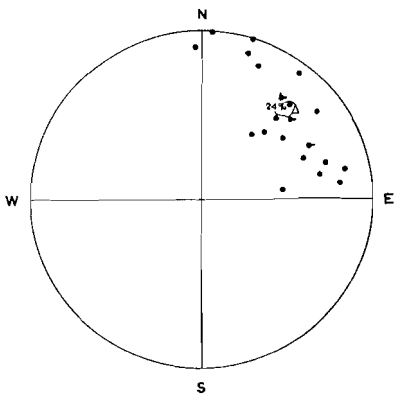

Meas. sample 35
(25 m.f.)

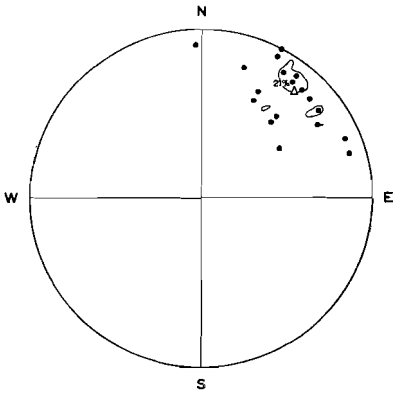

Meas. sample 36
(19 m.f.)

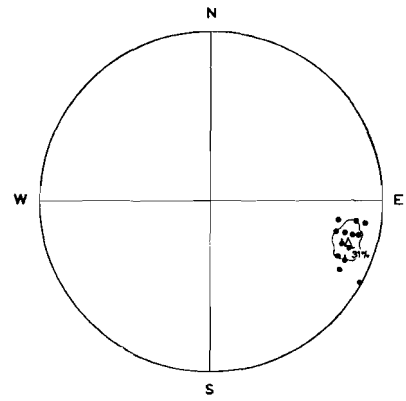

Meas. sample 37
(16 m.f.)

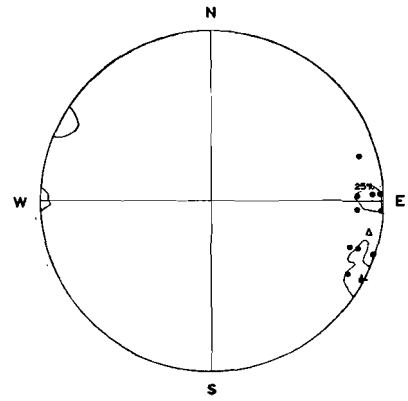

Meas. sample 38
(13 m.f.)

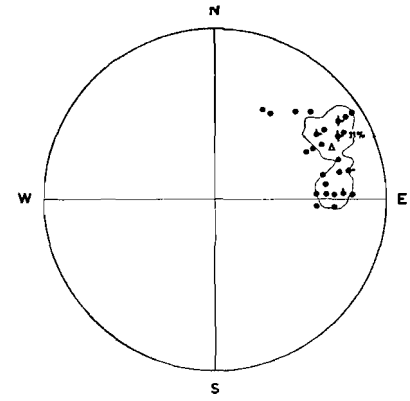

Meas. sample 39
(36 m.f.)

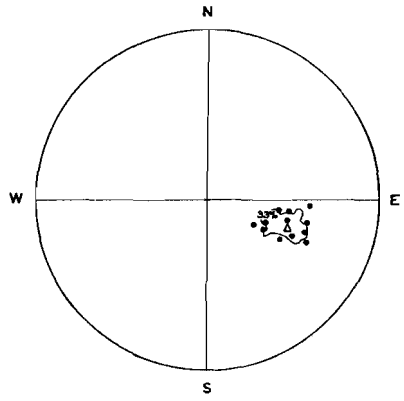

Meas. sample 40
(12 m.f.)

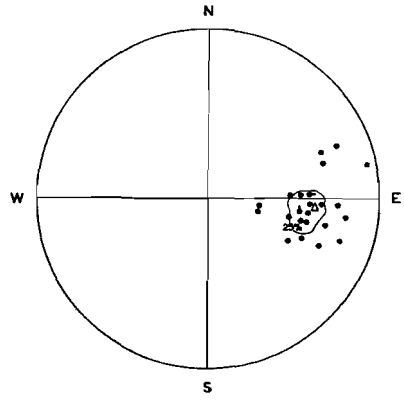

Meas. sample 41
(25 m.f.)

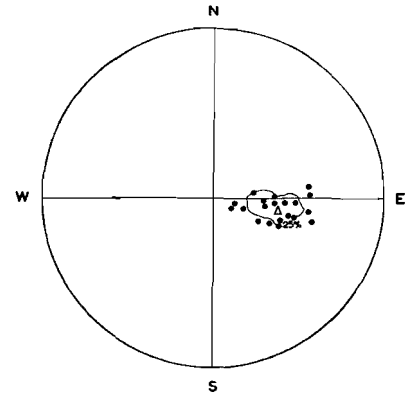

Meas. sample 42
(20 m.f.)

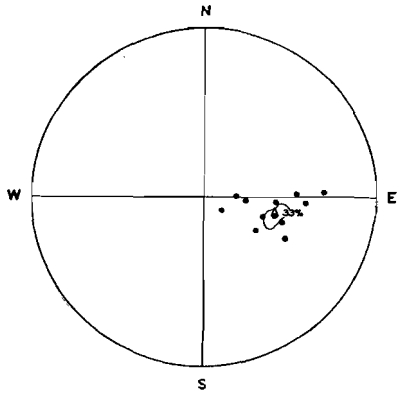

Meas. sample 43
(12 m.f.)

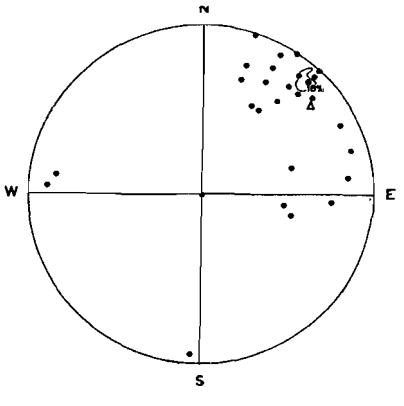

Meas. sample 44
(28 m.f.)

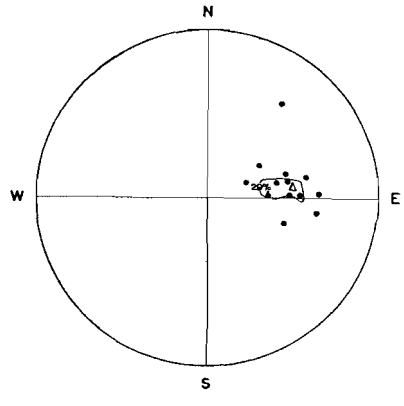

Meas. sample 45
(14 m.f.)

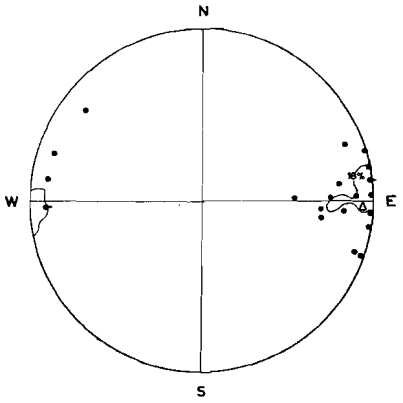

Meas. sample 46
(22 m.f.)

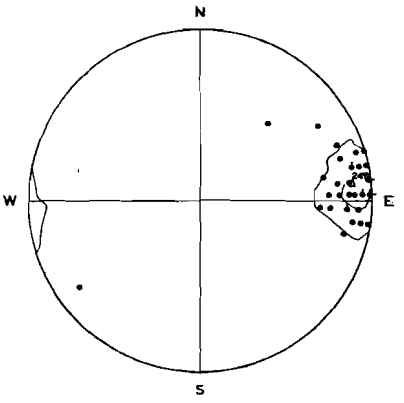

Meas. sample 47
(34 m.f.)

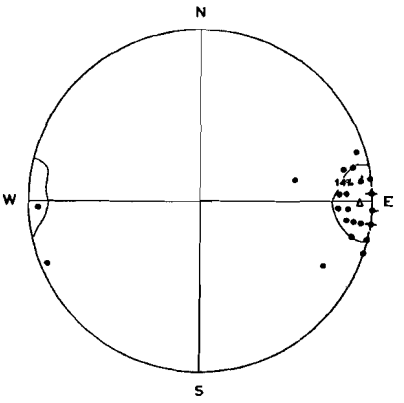

Meas. sample 48
(28 m.f.)

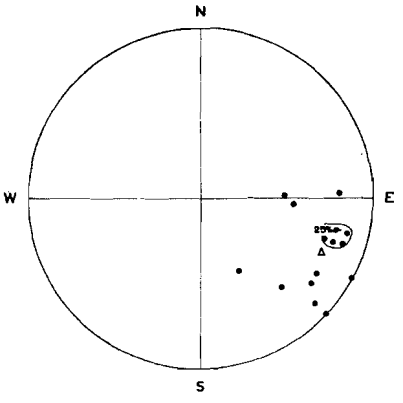

Meas. sample 49
(16 m.f.)

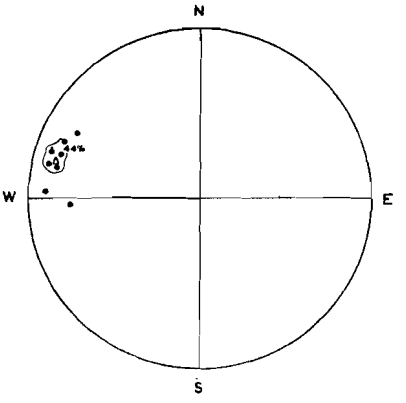

Meas. sample 50
(9 m.f.)

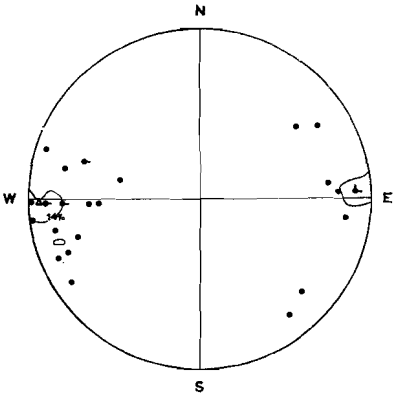

Meas. sample 51
(28 m.f.)

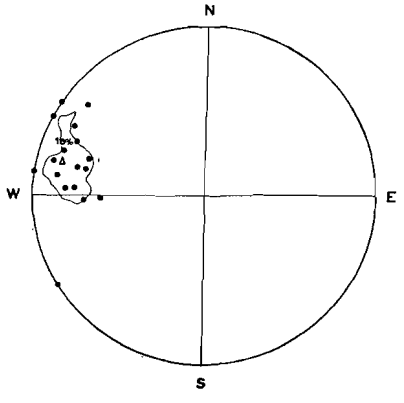

Meas. sample 52
(17 m.f.)

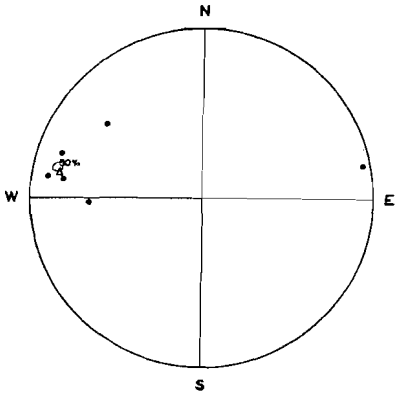

Meas. sample 53
(6 m.f.)

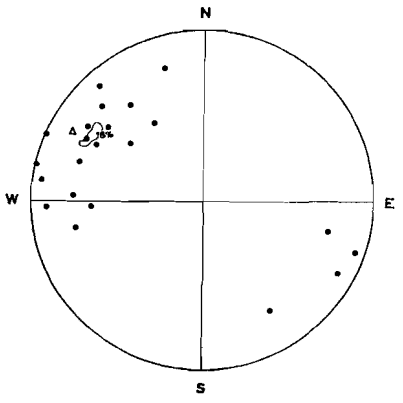

Meas. sample 54
(22 m.f.)

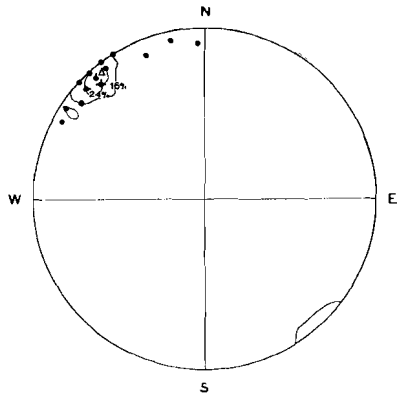

Meas. sample 55
(19 m.f.)

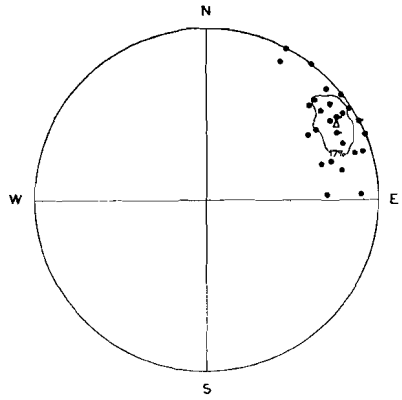

Meas. sample 56
(29 m.f.)

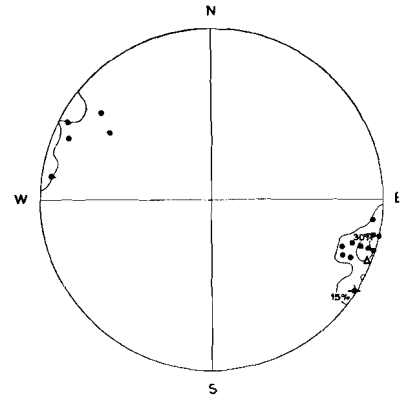

Meas. sample 57
(20 m.f.)

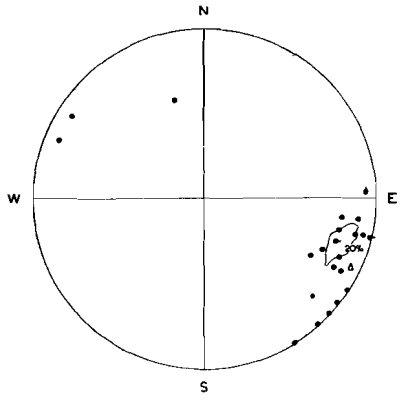

Meas. sample 58
(25 m.f.)

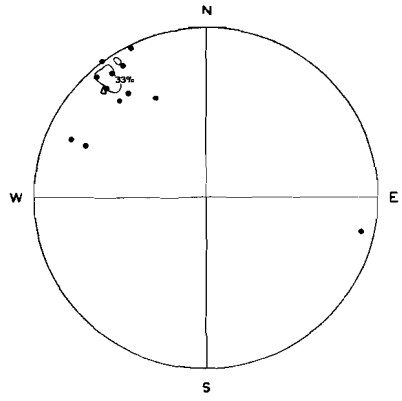

Meas. sample 59
(12 m.f.)

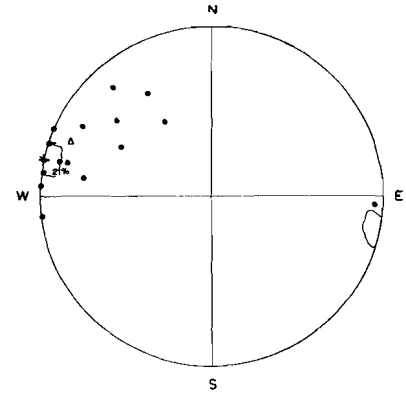

Meas. sample 60
(19 m.f.)

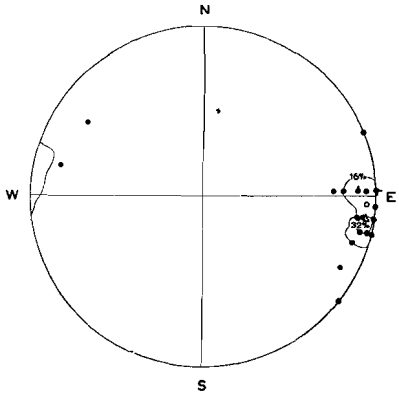

Meas. sample 61
(19 m.f.)

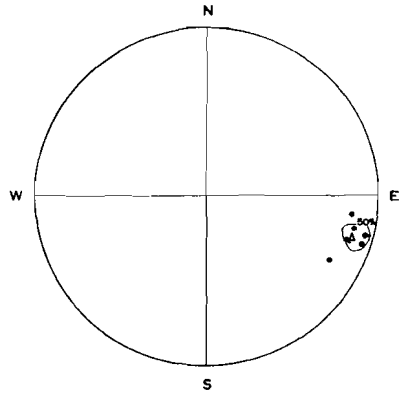

Meas. sample 62
(8 m.f.)

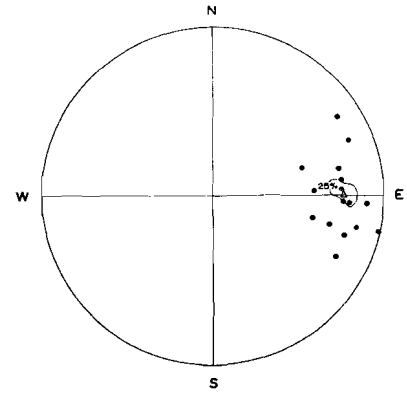

Meas. sample 63
(16 m.f.)

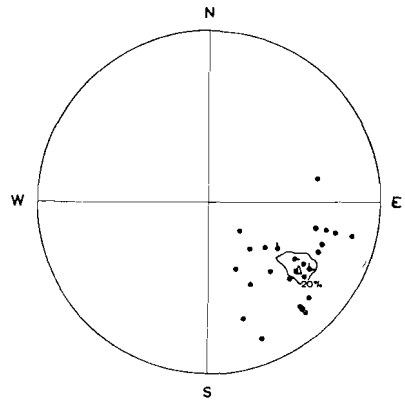

Meas. sample 64
(30 m.f.)

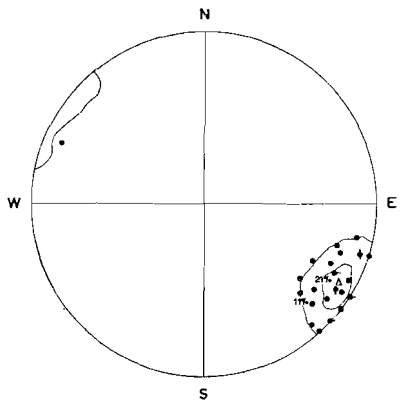

Meas. sample 65
(28 m.f.)

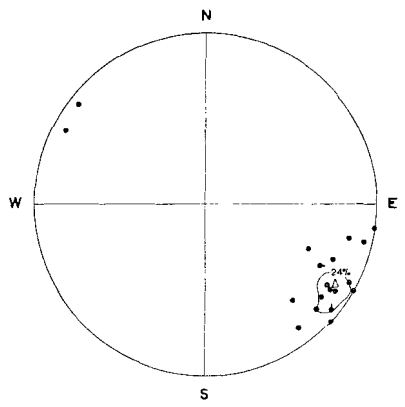

Meas. sample 66
(21 m.f.)

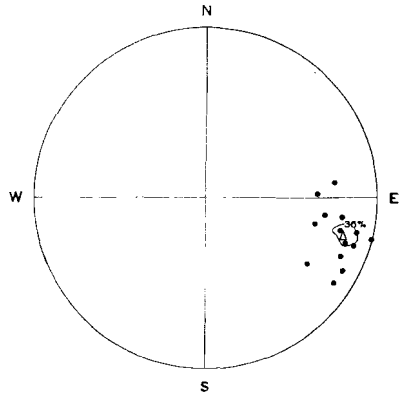

Meas. sample 67
(14 m.f.)

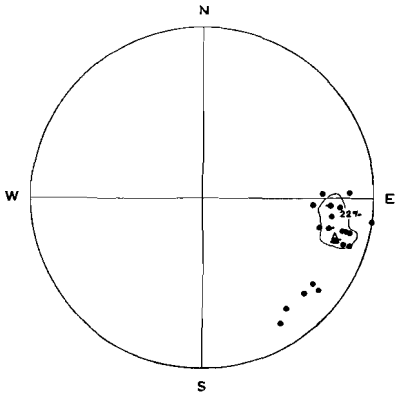

Meas. sample 68
(23 m.f.)

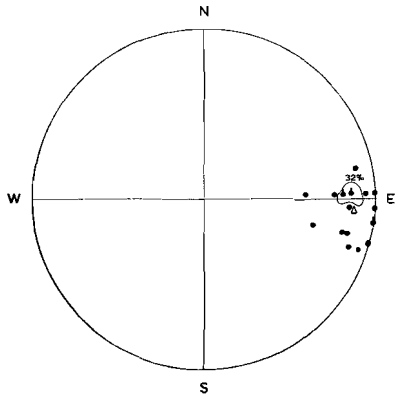

Meas. sample 69
(19 m.f.)

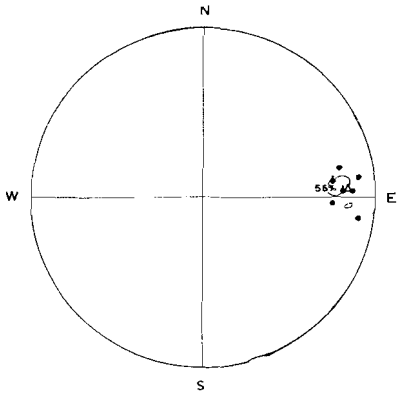

Meas. sample 70
(9 m.f.)

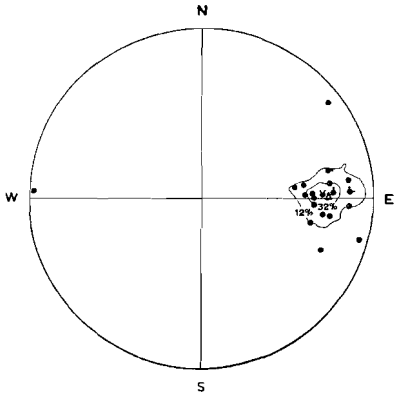

Meas. sample 71
(25 m.f.)

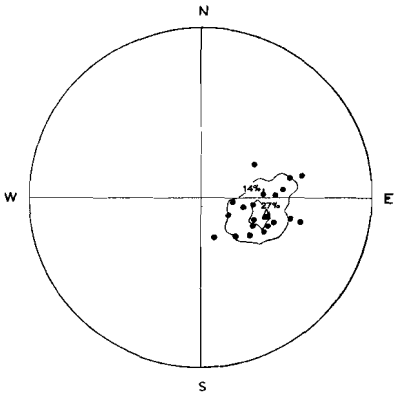

Meas. sample 72
(22 m.f.)

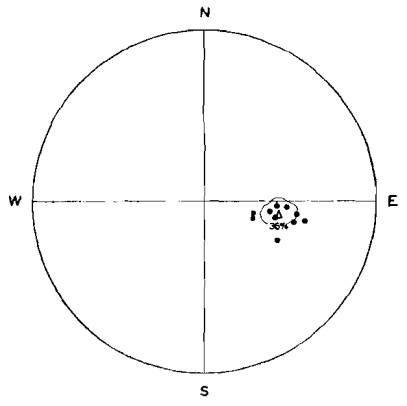

Meas. sample 73
(11 m.f.)

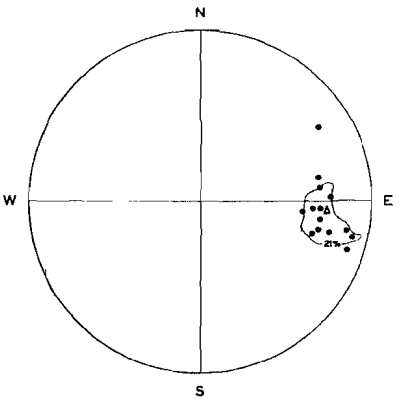

Meas. sample 74
(14 m.f.)

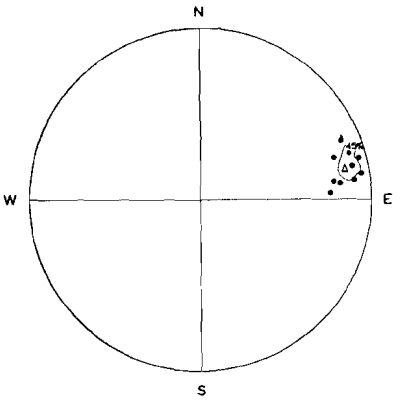

Meas. sample 75
(11 m.f.)

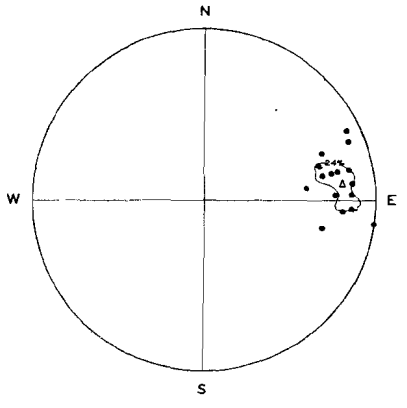

Meas. sample 76
(17 m.f.)

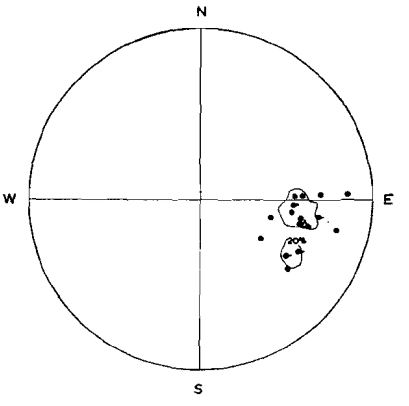

Meas. sample 77
(20 m.f.)

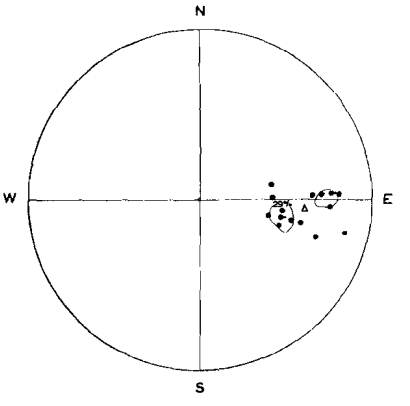

Meas. sample 78
(17 m.f.)

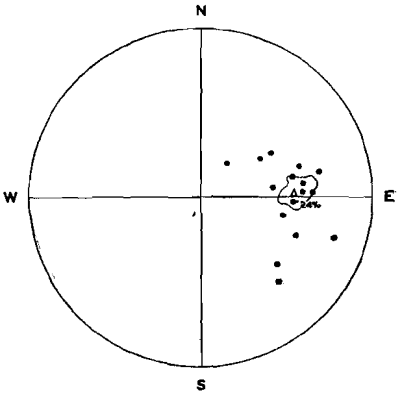

Meas. sample 79
(17 m.f.)

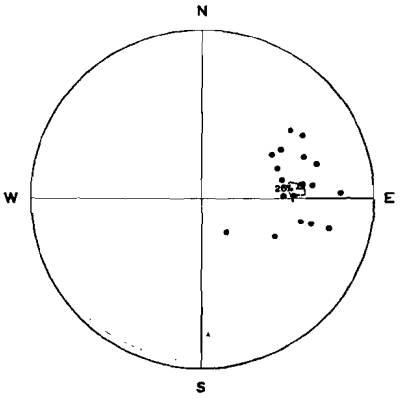

Meas. sample 80
(19 m.f.)

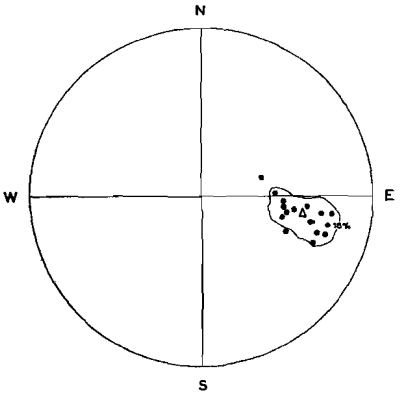

Meas. sample 81
(17 m.f.)

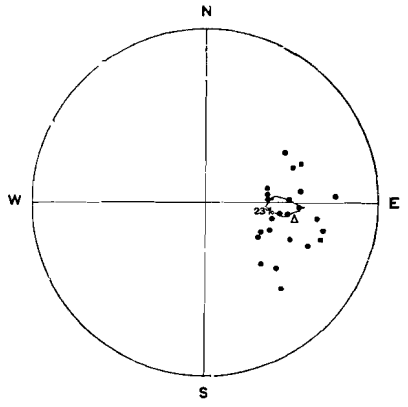

Meas. sample 82
(26 m.f.)

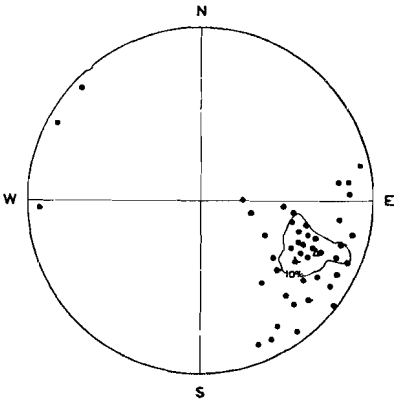

Meas. sample 83
(50 m.f.)

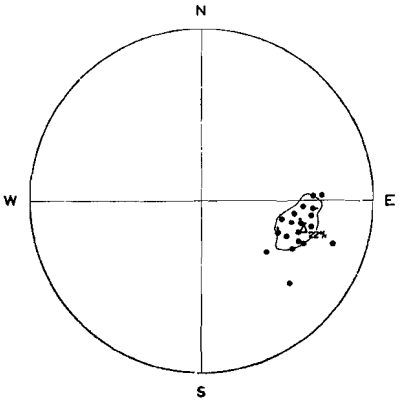

Meas. sample 84
(23 m.f.)

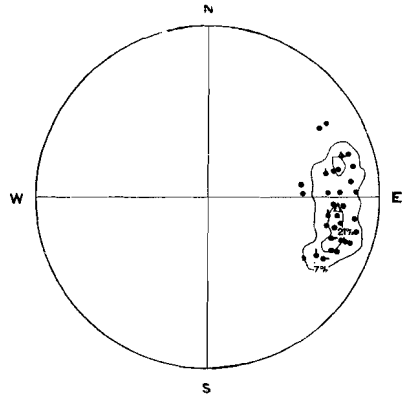

Meas. sample 85
(39 m.f.)

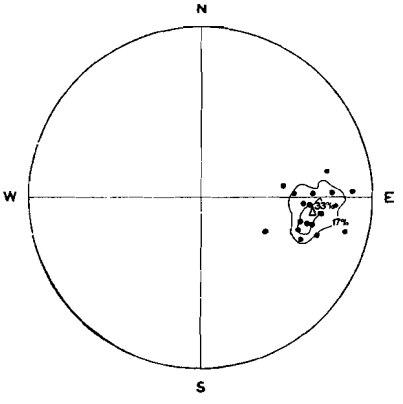

Meas. sample 86
(18 m.f.)

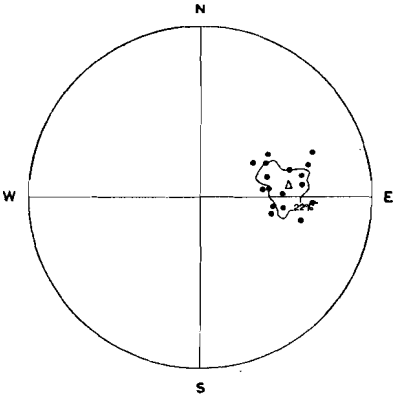

Meas. sample 87
(18 m.f.)

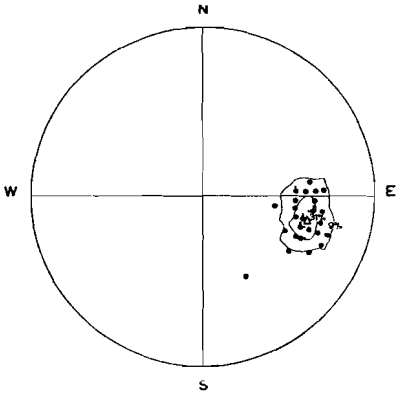

Meas. sample 88
(32 m.f.)

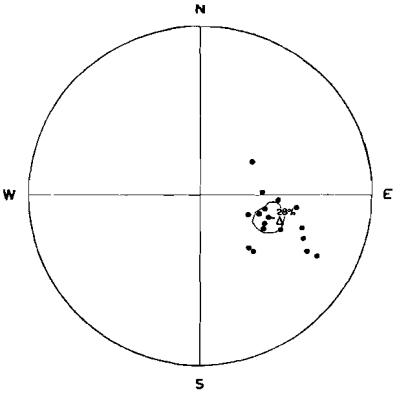

Meas. sample 89
(18 m.f.)

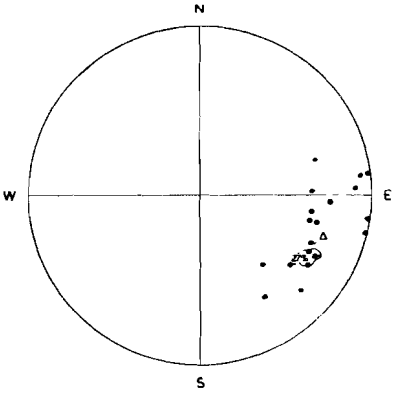

Meas. sample 90
(22 m.f.)

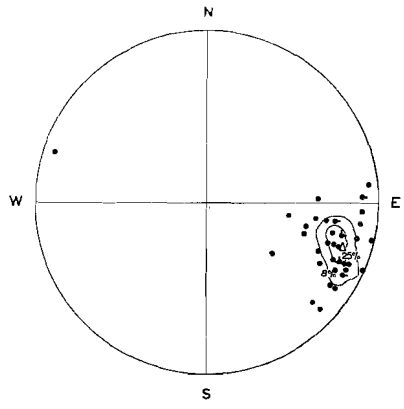

Meas. sample 91
(40 m.f.)

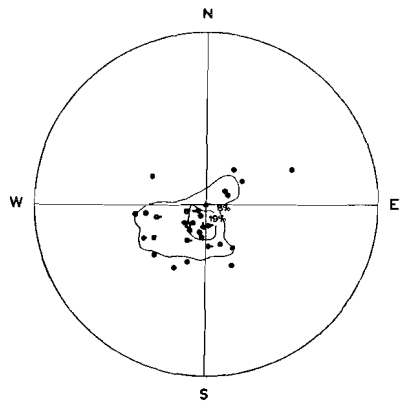

Meas. sample 92
(37 m.f.)

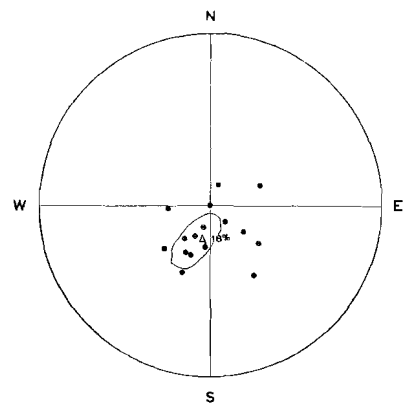

Meas. sample 93
(17 m.f.)

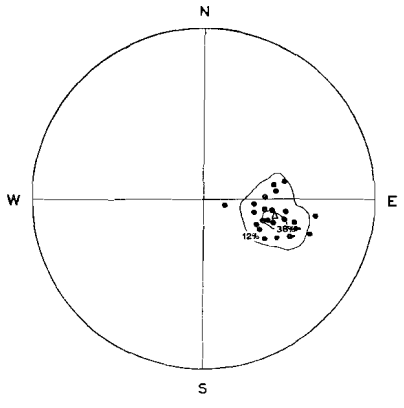

Meas. sample 94
(26 m.f.)

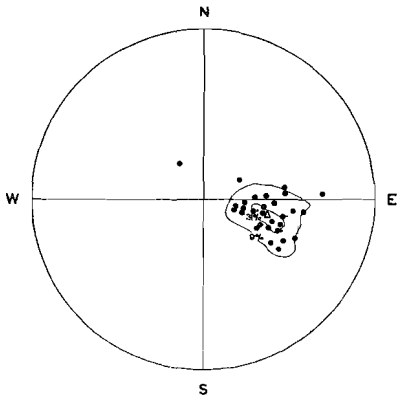

Meas. sample 95
(32 m.f.)

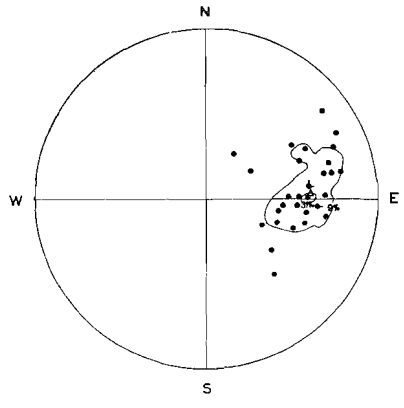

Meas. sample 96
(32 m.f.)

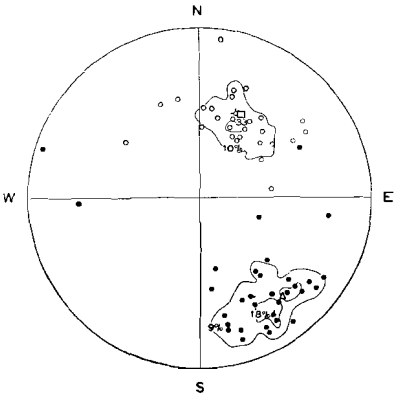

Meas. sample 97
(30 s. and 34 m.f.)

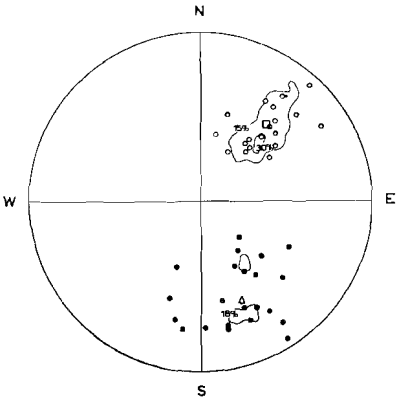

Meas. sample 98
(20 s. and 22 m.f.)

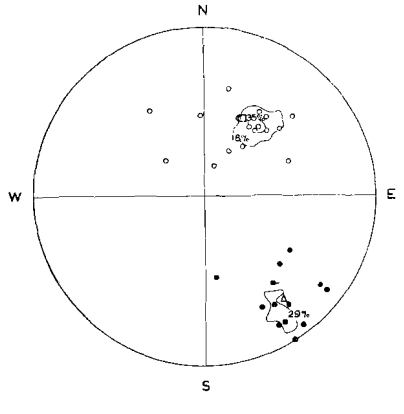

Meas. sample 99
(17 s. and 14 m.f.)

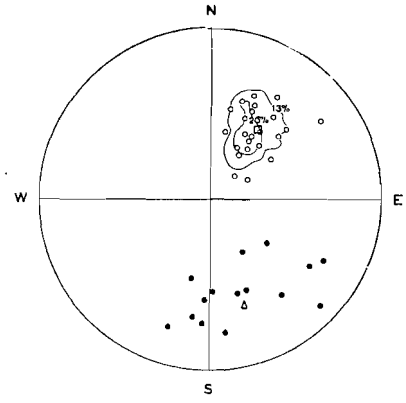

Meas. sample 100
(23 s. and 15 m.f.)

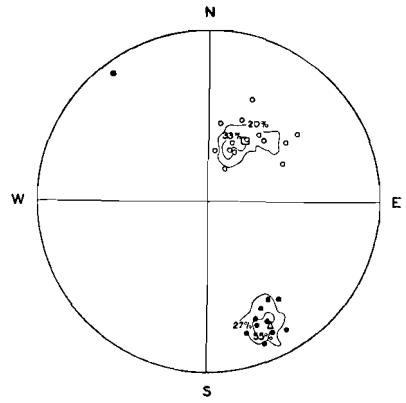

Meas. sample 101
(15 s. and 11 m.f.)

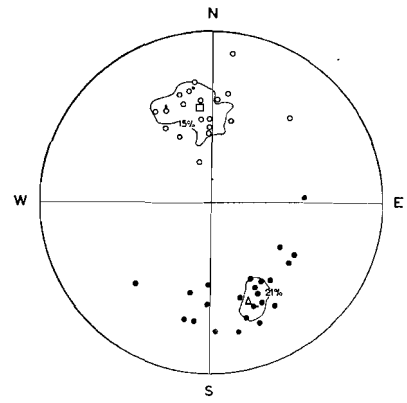

Meas. sample 102
(20 s. and 24 m.f.)

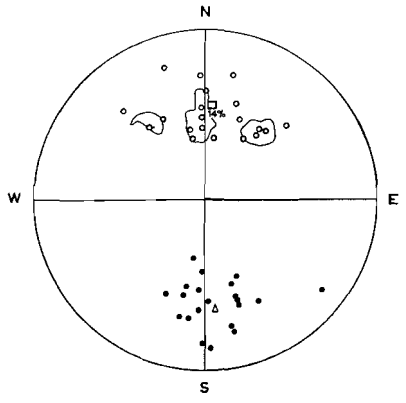

Meas. sample 103
(21 s. and 21 m.f.)

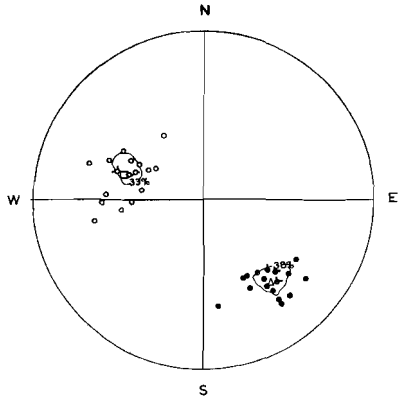

Meas. sample 104
(21 s. and 21 m.f.)

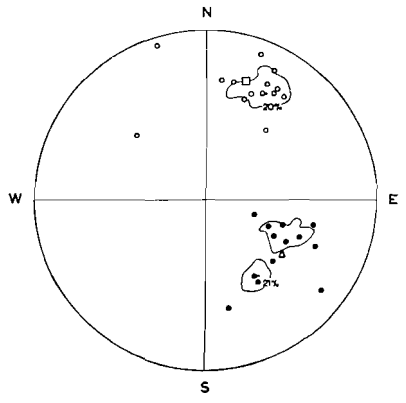

Meas. sample 105
(15 s. and 14 m.f.)

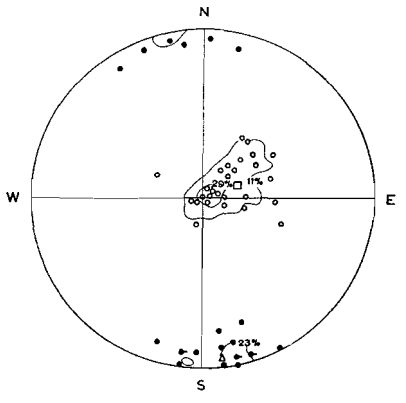

Meas. sample 106
(28 s. and 22 m.f.)

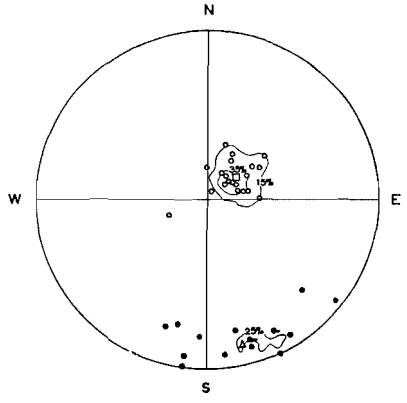

Meas. sample 107
(20 s. and 16 m.f.)

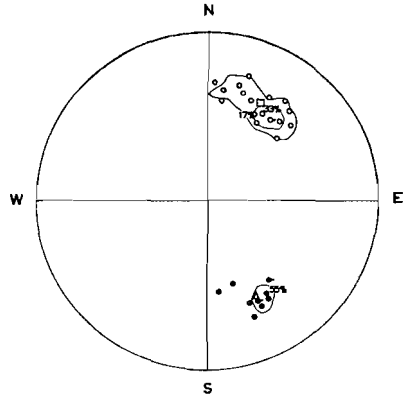

Meas. sample 108
(18 s. and 11 m.f.)

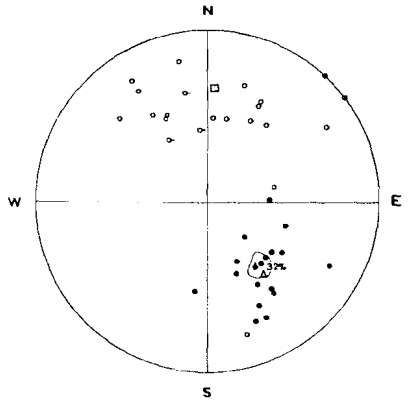

Meas. sample 109
(25 s. and 19 m.f.)

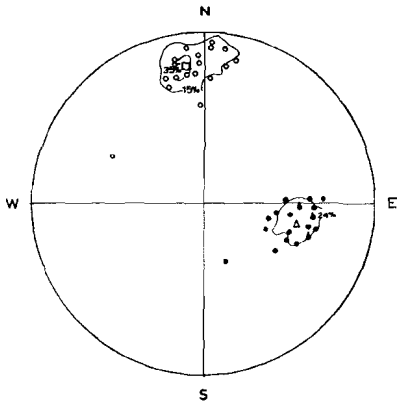

Meas. sample 110
(20 s. and 21 m.f.)

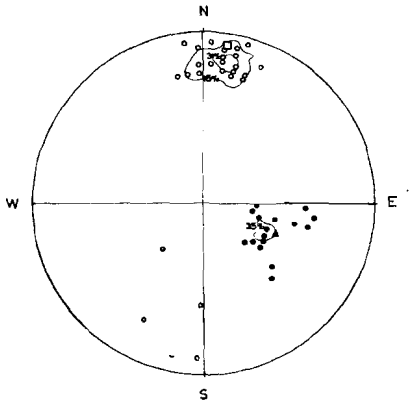

Meas. sample 111
(26 s. and 17 m.f.)

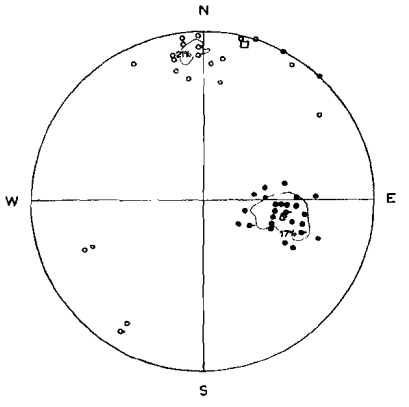

Meas. sample 112
(24 s. and 29 m.f.)

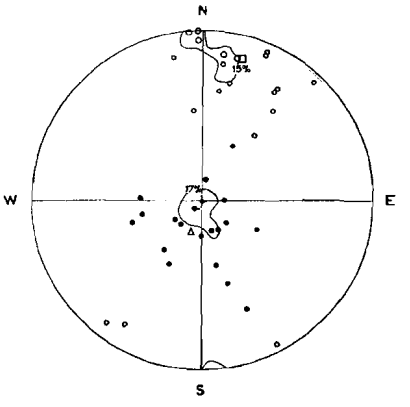

Meas. sample 113
(20 s. and 24 m.f.)

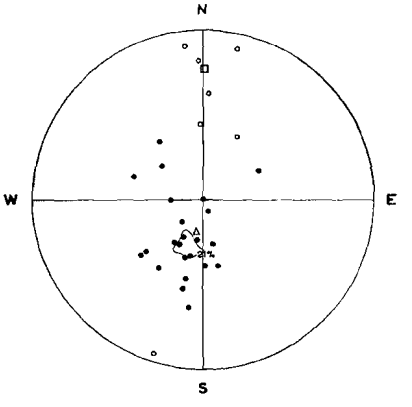

Meas. sample 114
(8 s. and 24 m.f.)

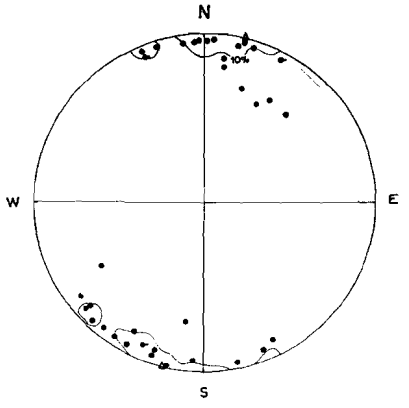

Meas. sample 115
(39 m.f.)

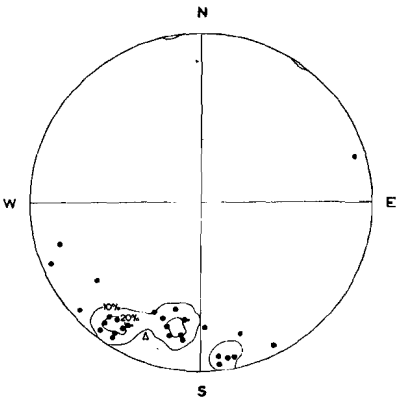

Meas. sample 116
(30 m.f.)

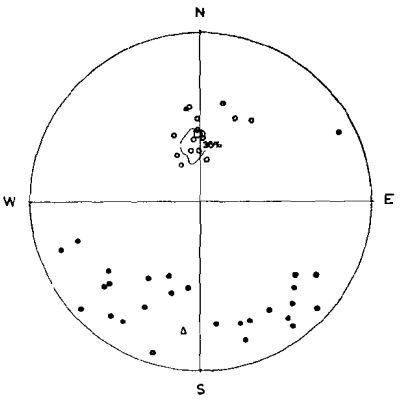

Meas. sample 117
(14 s. and 27 m.f.)

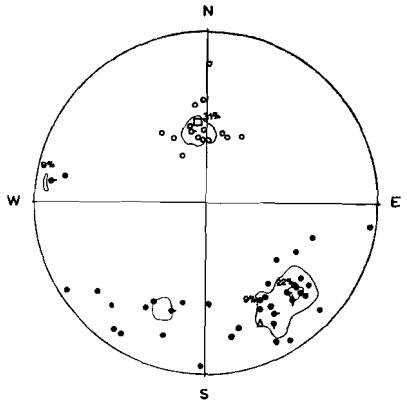

Meas. sample 118
(16 s. and 45 m.f.)

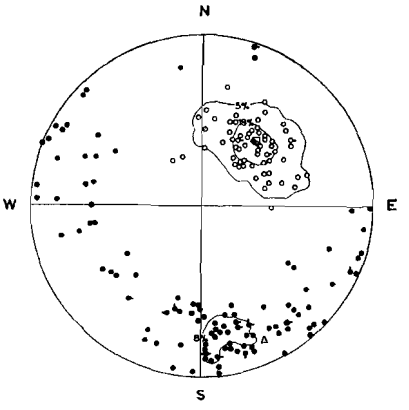

Meas. sample 119
(65 s. and 119 m.f.)

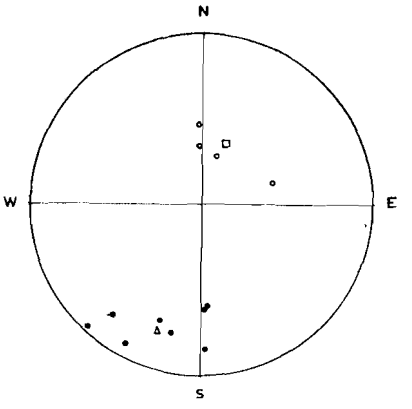

Meas. sample 120
(4 s. and 9 m.f.)

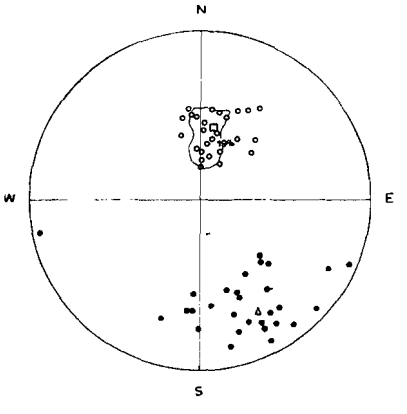

Meas. sample 121
(26 s. and 30 m.f.)

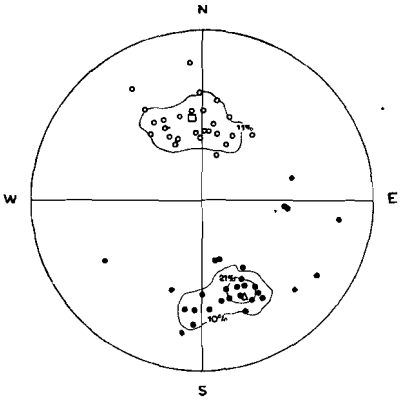

Meas. sample 122
(27 s. and 29 m.f.)

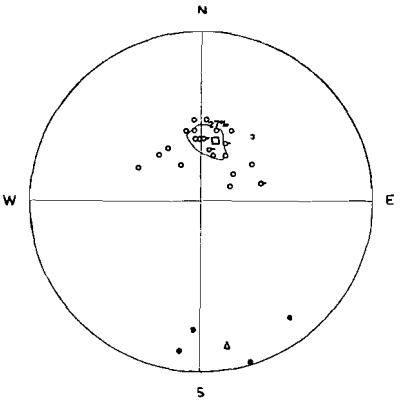

Meas. sample 123
(26 s. and 4 m.f.)

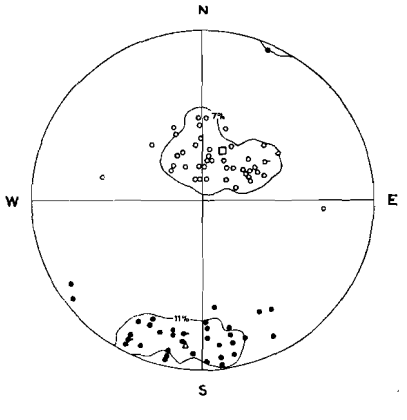

Meas. sample 124
(44 s. and 37 m.f.)

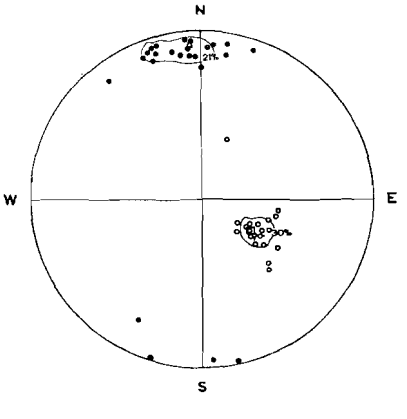

Meas. sample 125
(23 s. and 24 m.f.)

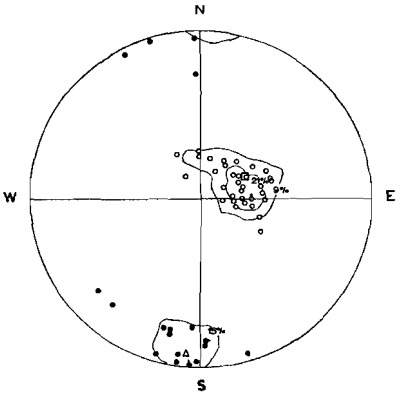

Meas. sample 126
(34 s. and 20 m.f.)

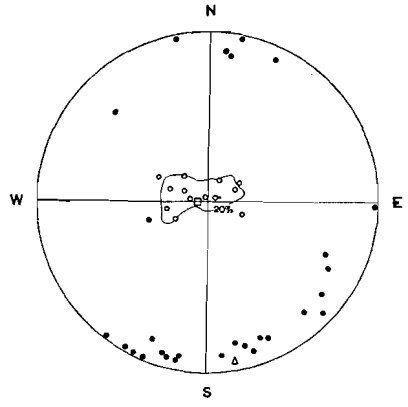

Meas. sample 127
(15 s. and 27 m.f.)

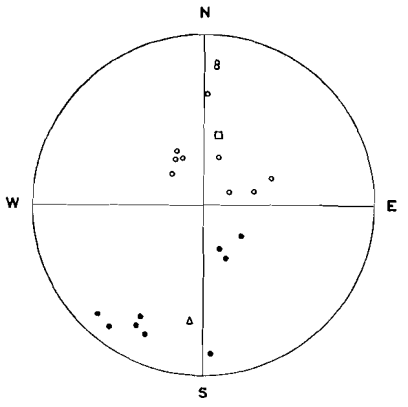

Meas. sample 128
(11 s. and 9 m.f.)

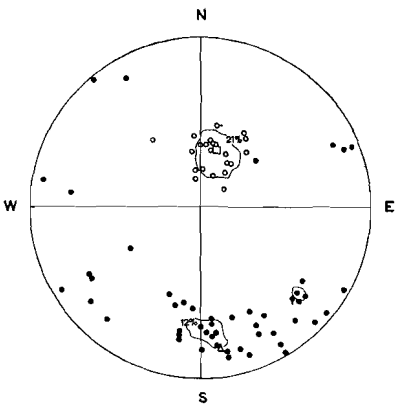

Meas. sample 129
(24 s. and 50 m.f.)

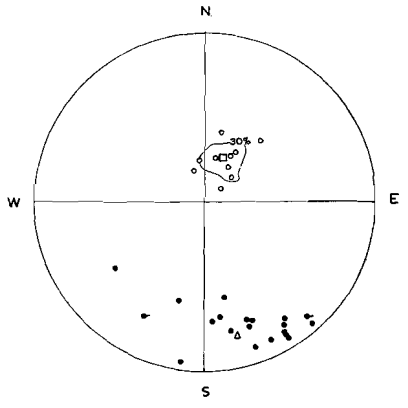

Meas. sample 130
(10 s. and 32 m.f.)

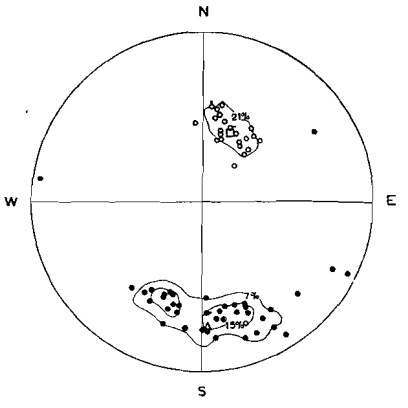

Meas. sample 131
(24 s. and 41 m.f.)

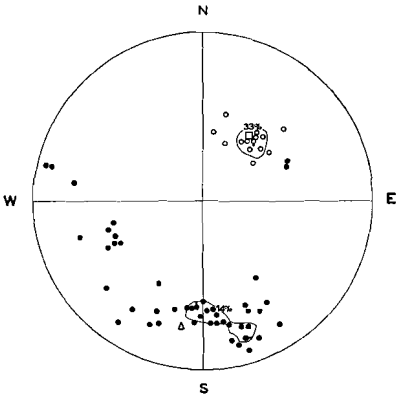

Meas. sample 132
(15 s. and 48 m.f.)

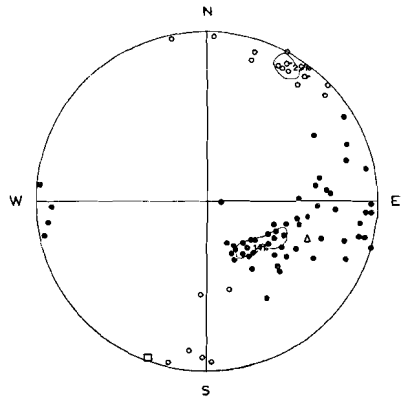

Meas. sample 133
(21 s. and 58 m.f.)

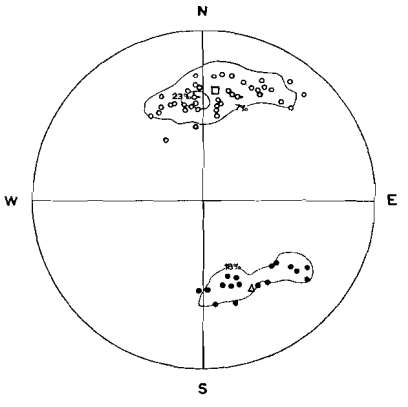

Meas. sample 134
(43 s. and 17 m.f.)

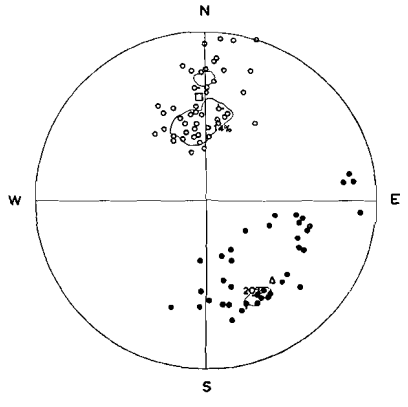

Meas. sample 135
(50 s. and 41 m.f.)

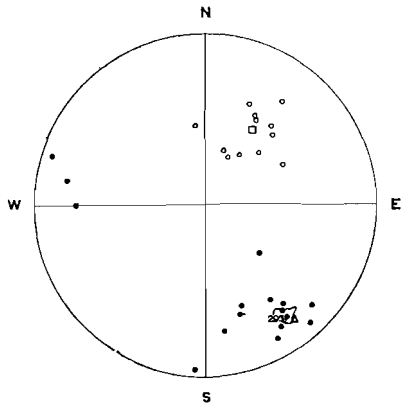

Meas. sample 136
(12 s. and 17 m.f.)

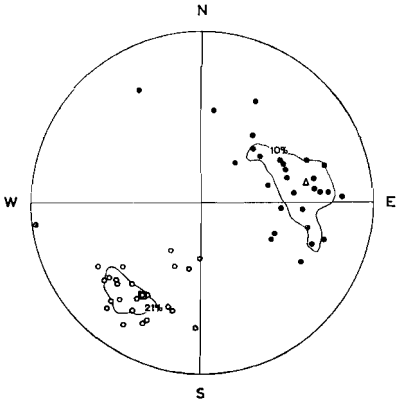

Meas. sample 137
(24 s. and 29 m.f.)

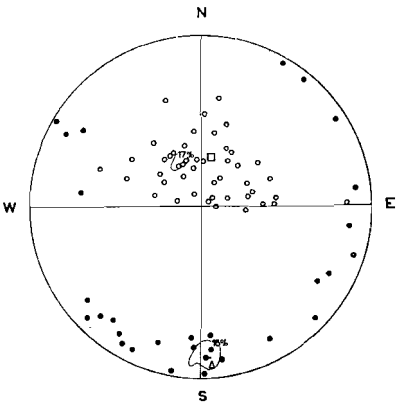

Meas. sample 138
(46 s. and 31 m.f.)

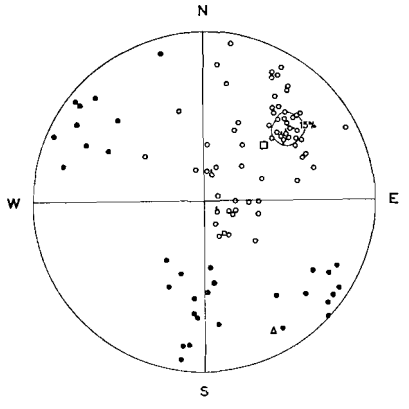

Meas. sample 139
(68 s. and 34 m.f.)

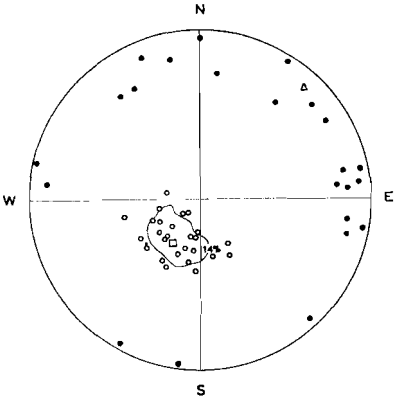

Meas. sample 140
(27 s. and 23 m.f.)

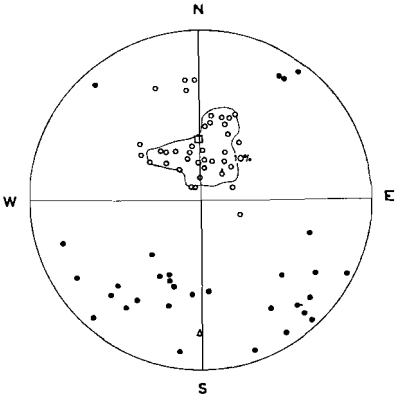

Meas. sample 141
(39 s. and 32 m.f.)

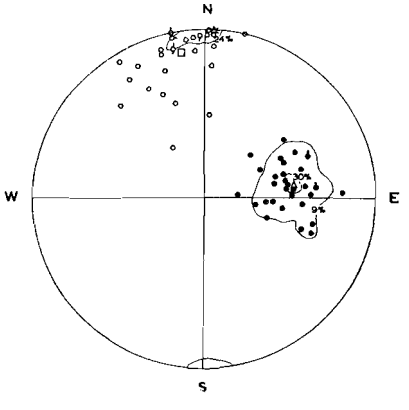

Meas. sample 142
(33 s. and 32 m.f.)

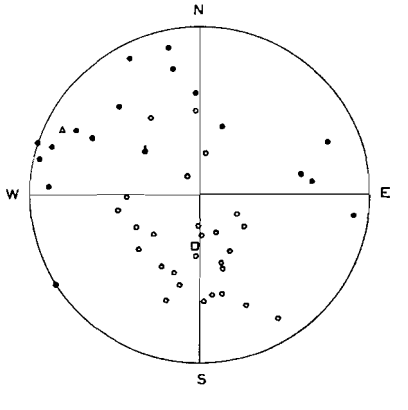

Meas. sample 143
(28 s. and 18 m.f.)

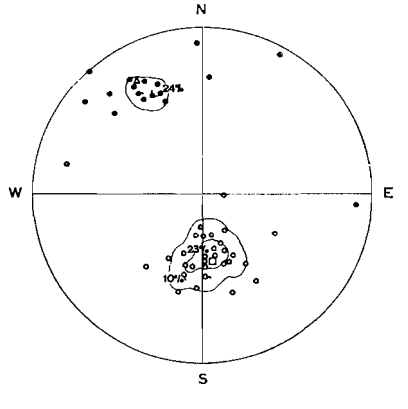

Meas. sample 144
(31 s. and 21 m.f.)

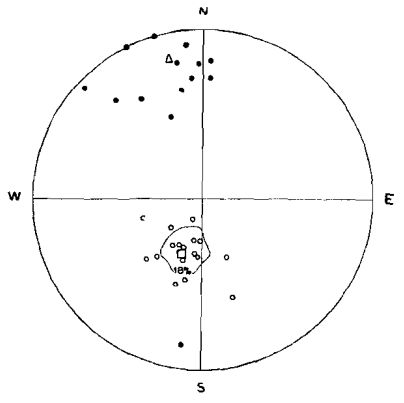

Meas. sample 145
(17 s. and 14 m.f.)

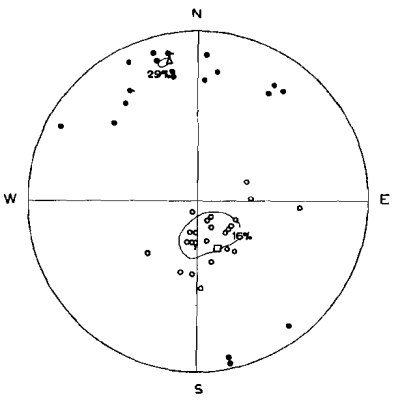

Meas. sample 146
(25 s. and 21 m.f.)

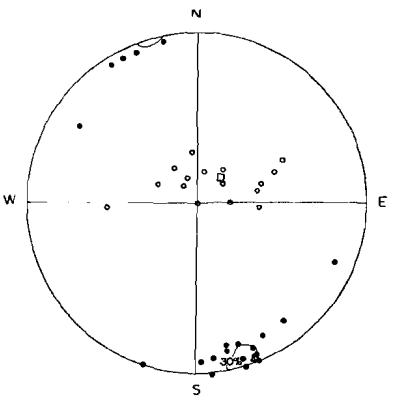

Meas. sample 147
(16 s. and 20 m.f.)

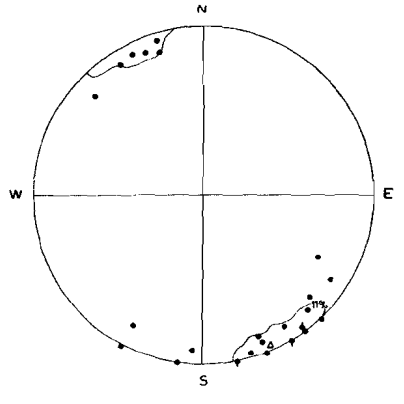

Meas. sample 148
(27 m.f.)

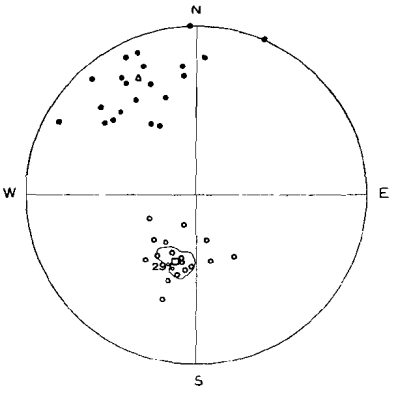

Meas. sample 149
(17 s. and 21 m.f.)

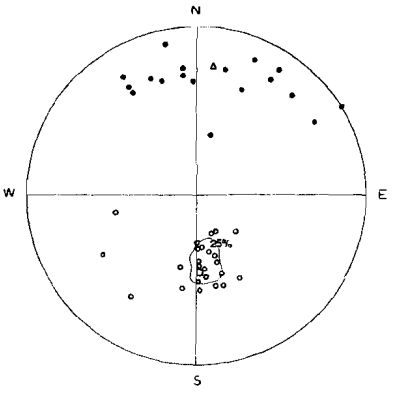

Meas. sample 150
(24 s. and 18 m.f.)

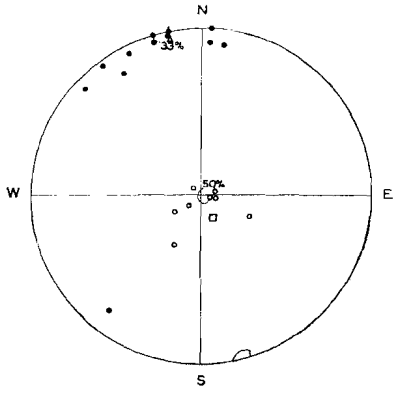

Meas. sample 151
(8 s. and 12 m.f.)

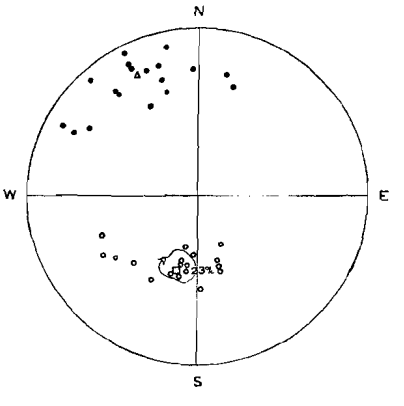

Meas. sample 152
(22 s. and 18 m.f.)

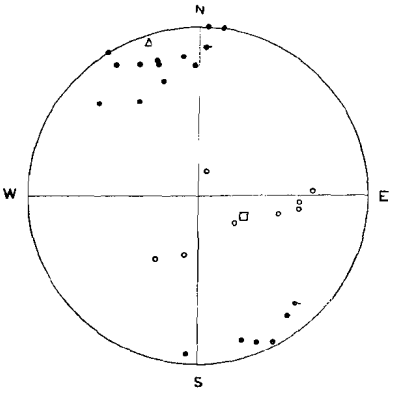

Meas. sample 153
(8 s. and 21 m.f.)

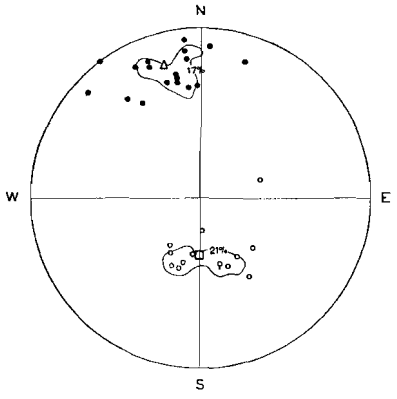

Meas. sample 154
(14 s. and 18 m.f.)

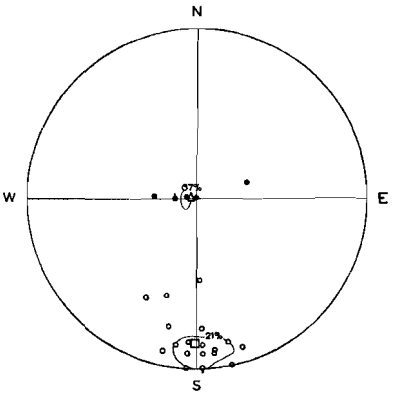

Meas. sample 155
(19 s. and 6 m.f.)

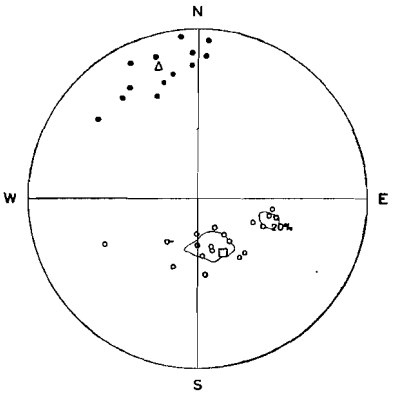

Meas. sample 156
(20 s. and 13 m.f.)

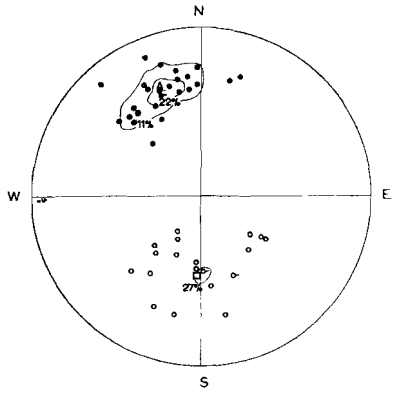

Meas. sample 157
(22 s. and 27 m.f.)

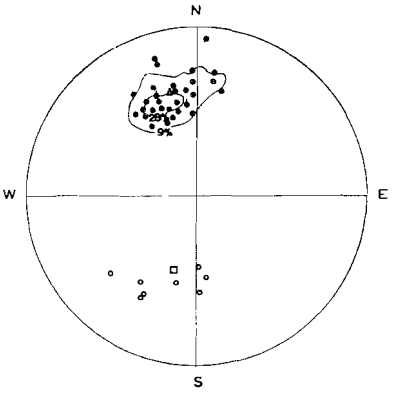

Meas. sample 158
(8 s. and 32 m.f.)

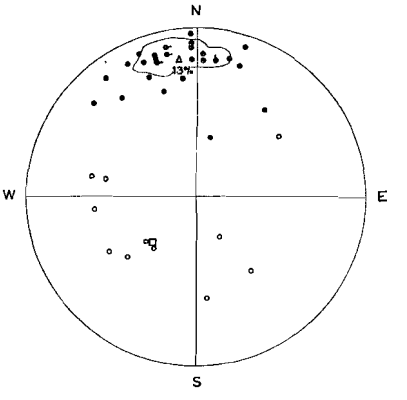

Meas. sample 159
(11 s. and 30 m.f.)

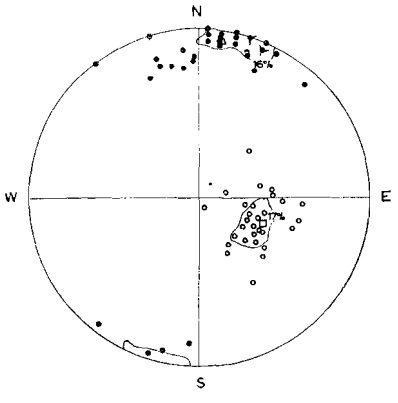

Meas. sample 160
(29 s. and 37 m.f.)

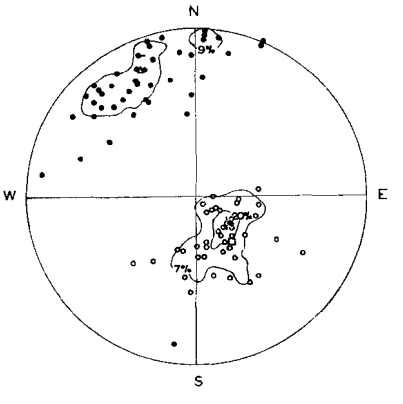

Meas. sample 161
(44 s. and 43 m.f.)

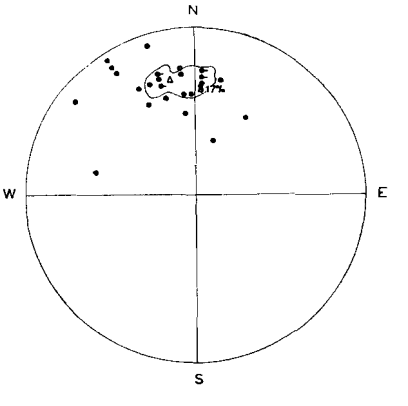

Meas. sample 162
(30 m.f.)

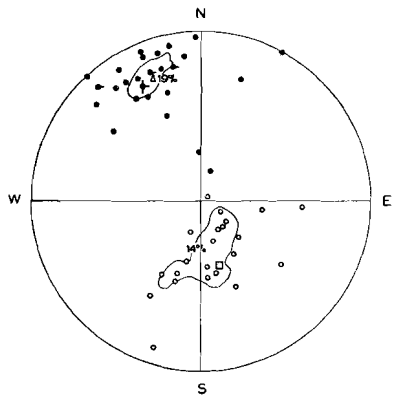

Meas. sample 163
(22 s. and 32 m.f.)

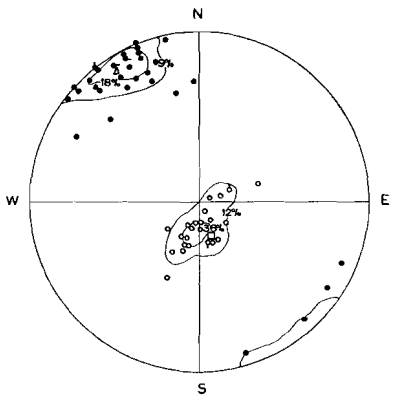

Meas. sample 164
(25 s. and 34 m.f.)

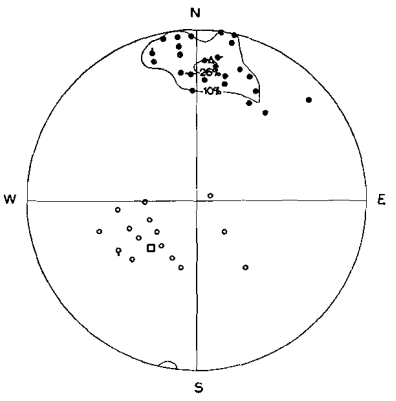

Meas. sample 165
(16 s. and 29 m.f.)

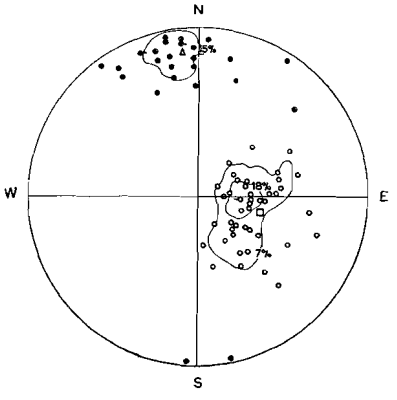

Meas. sample 166
(44 s. and 27 m.f.)

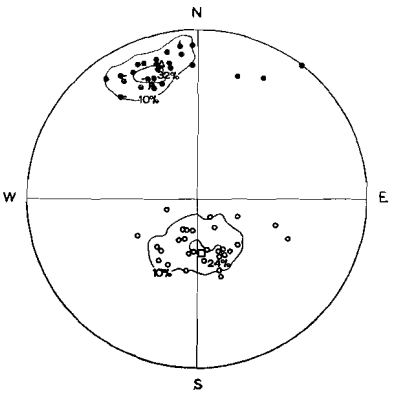

Meas. sample 167
(29 s. and 31 m.f.)

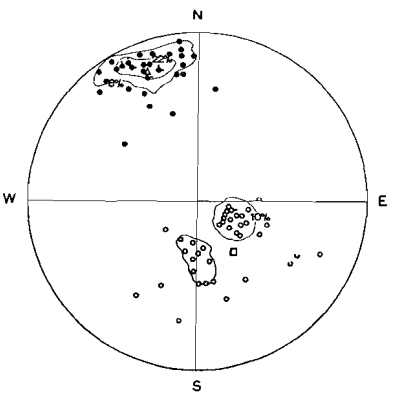

Meas. sample 168
(40 s. and 36 m.f.)

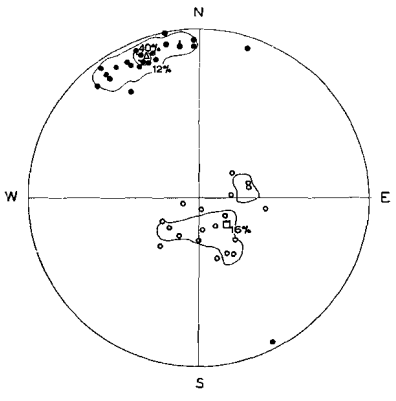

Meas. sample 169
(19 s. and 25 m.f.)

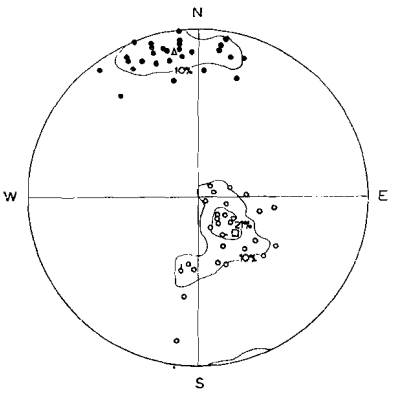

Meas. sample 170
(31 s. and 29 m.f.)

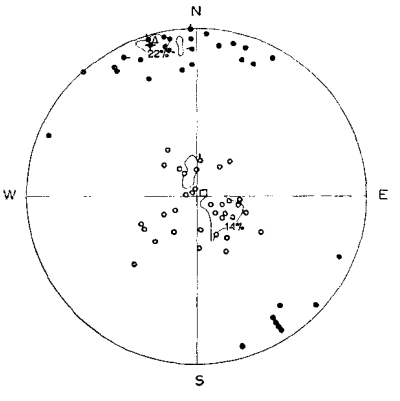

Meas. sample 171
(35 s. and 41 m.f.)

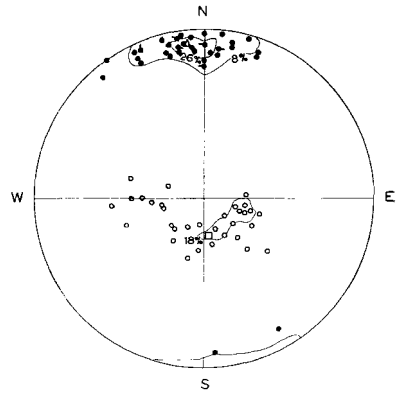

Meas. sample 172
(33 s. and 39 m.f.)

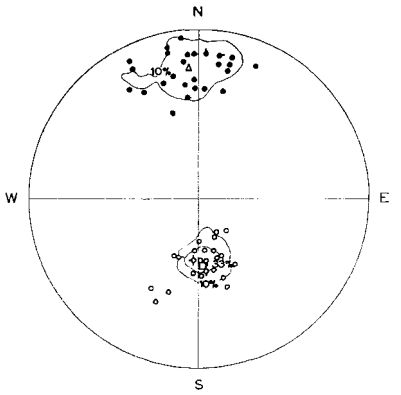

Meas. sample 173
(30 s. and 29 m.f.)

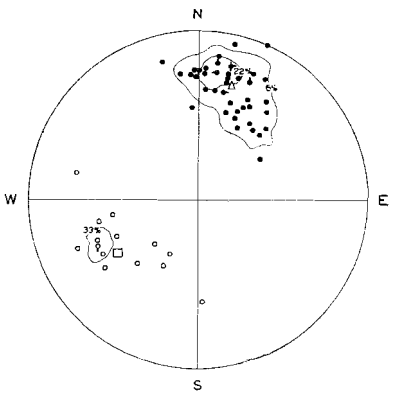

Meas. sample 174
(15 s. and 47 m.f.)

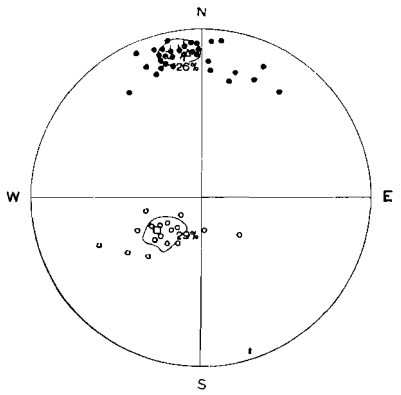

Meas. sample 175
(17 s. and 39 m.f.)

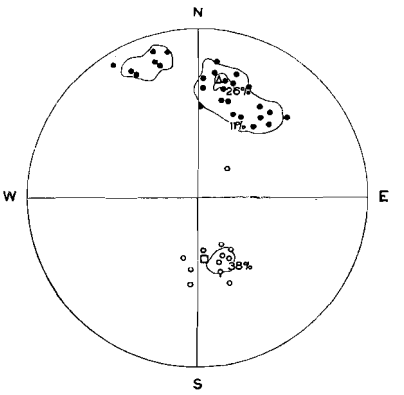

Meas. sample 176
(13 s. and 27 m.f.)

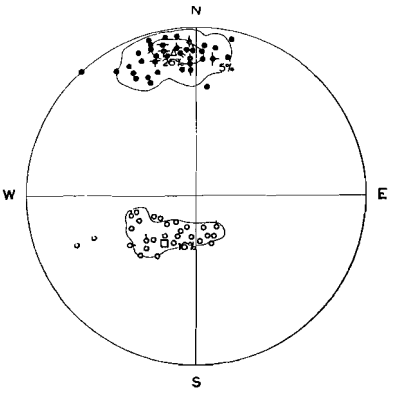

Meas. sample 177
(32 s. and 58 m.f.)

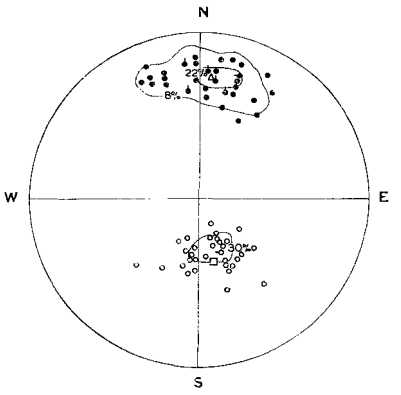

Meas. sample 178
(33 s. and 37 m.f.)

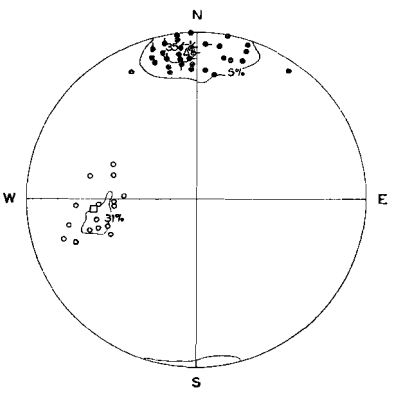

Meas. sample 179
(16 s. and 43 m.f.)

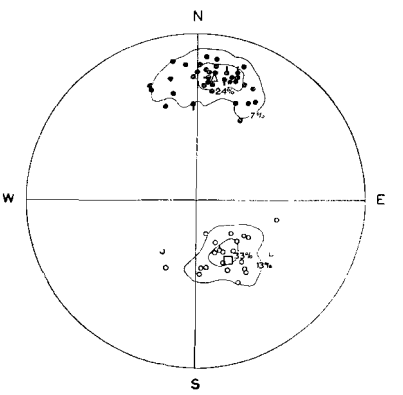

Meas. sample 180
(24 s. and 41 m.f.)

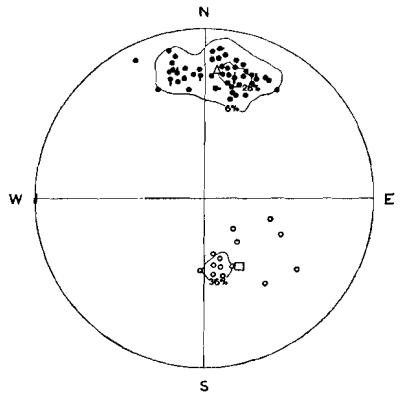

Meas. sample 181
(14 s. and 54 m.f.)

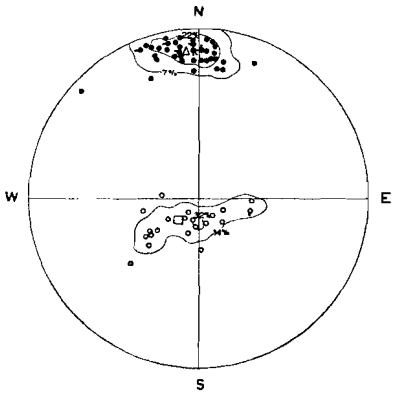

Meas. sample 182
(22 s. and 46 m.f.)

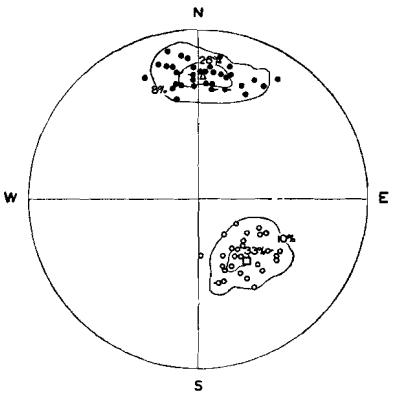

Meas. sample 183
(30 s. and 38 m.f.)

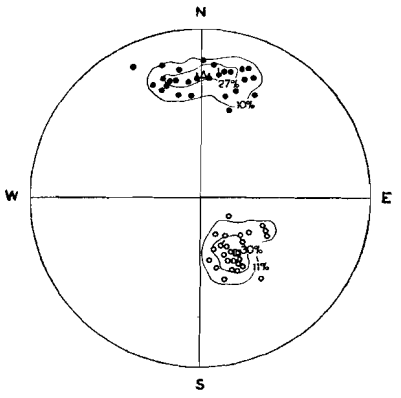

Meas. sample 184
(27 s. and 30 m.f.)

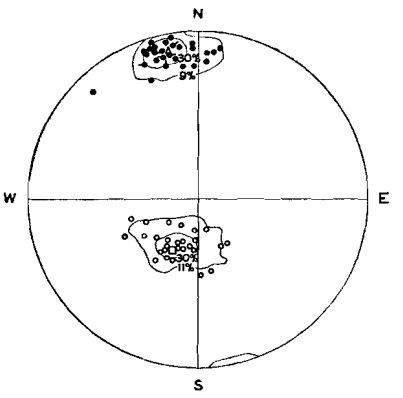

Meas. sample 185
(27 s. and 33 m.f.)

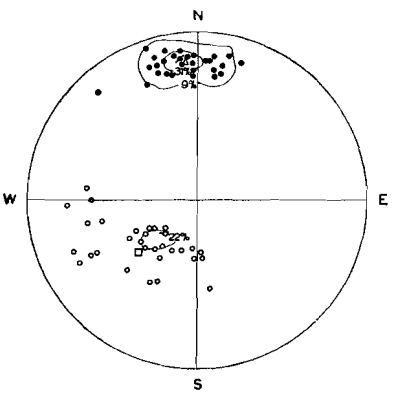

Meas. sample 186
(32 s. and 32 m.f.)

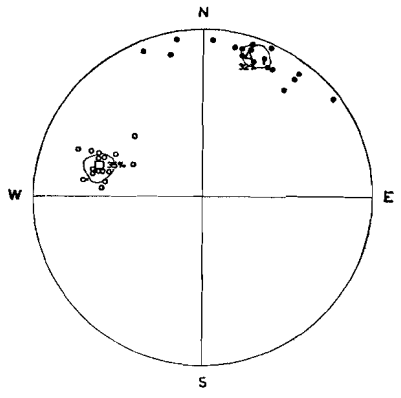

Meas. sample 187
(17 s. and 19 m.f.)

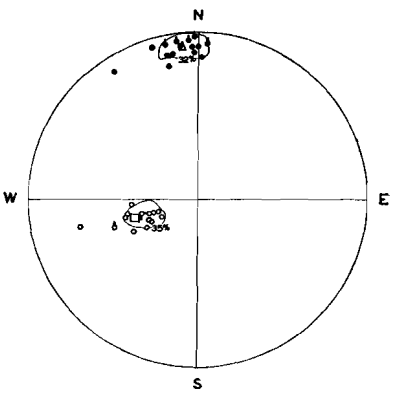

Meas. sample 188
(17 s. and 19 m.f.)

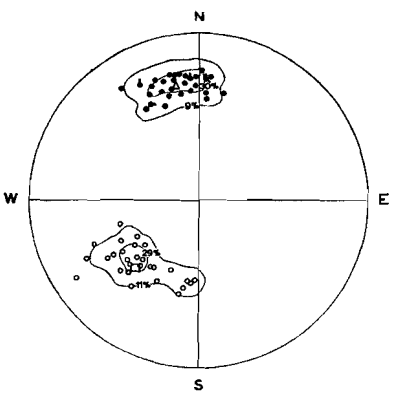

Meas. sample 189
(28 s. and 33 m.f.)

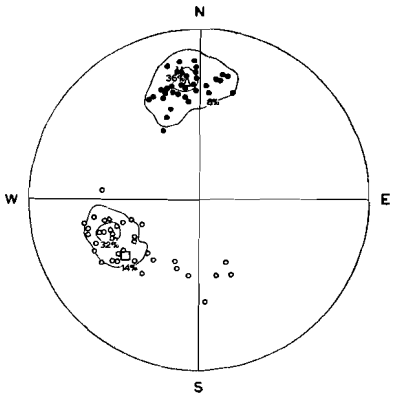

Meas. sample 190
(37 s. and 36 m.f.)

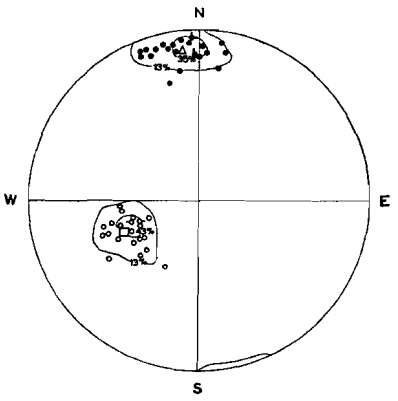

Meas. sample 191
(23 s. and 23 m.f.)

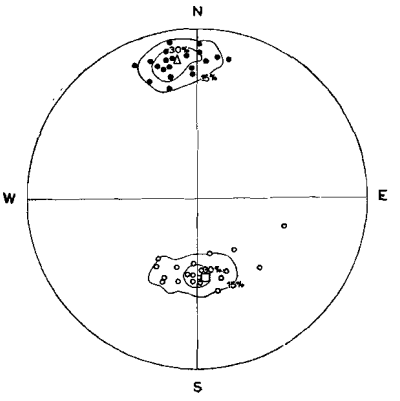

Meas. sample 192
(20 s. and 20 m.f.)

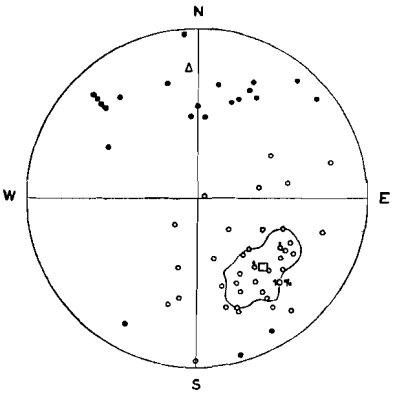

Meas. sample 193
(39 s. and 22 m.f.)

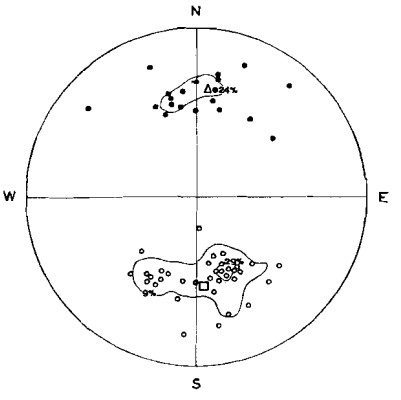

Meas. sample 194
(35 s. and 21 m.f.)

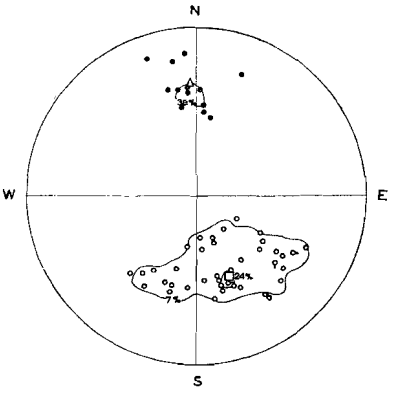

Meas. sample 195
(42 s. and 13 m.f.)

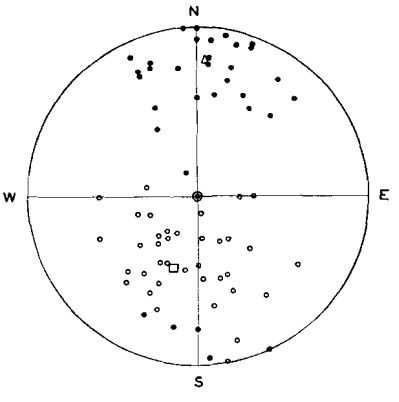

Meas. sample 196
(39 s. and 33 m.f.)

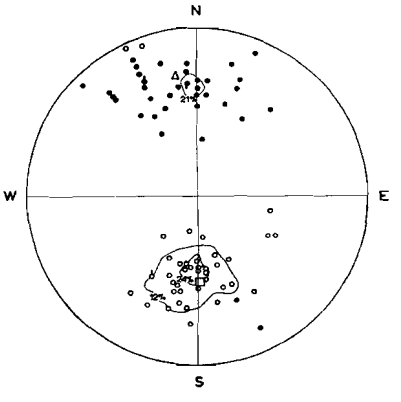

Meas. sample 197
(41 s. and 38 m.f.)

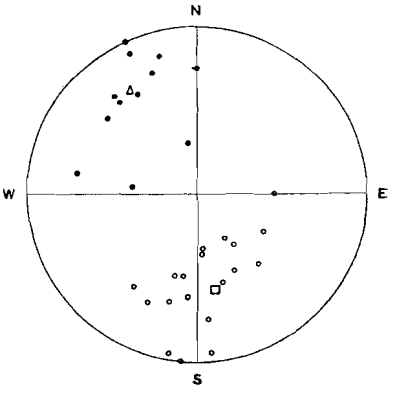

Meas. sample 198
(19 s. and 13 m.f.)

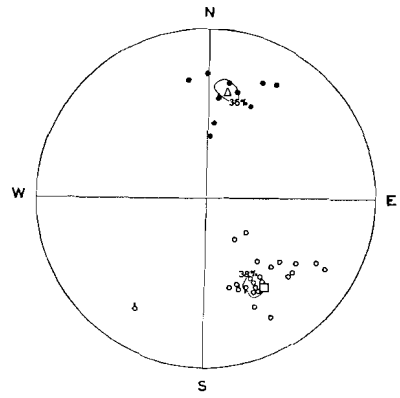

Meas. sample 199
(26 s. and 11 m.f.)

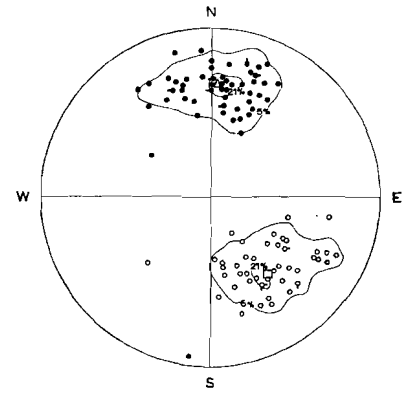

Meas. sample 200
(47 s. and 58 m.f.)

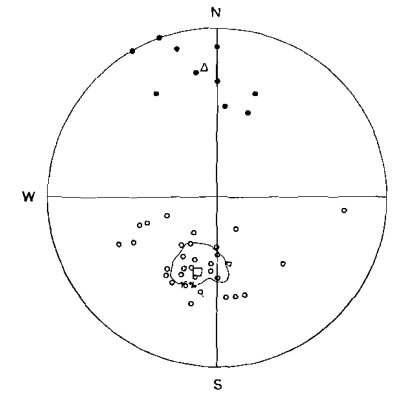

Meas. sample 201
(31 s. and 10 m.f.)

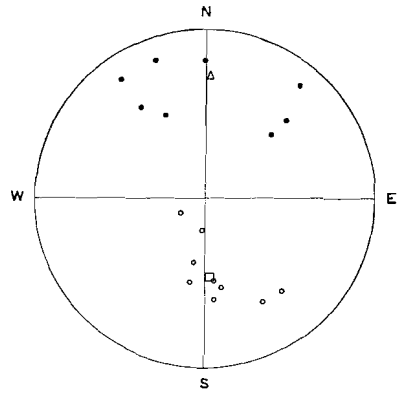

Meas. sample 202
(9 s. and 8 m.f.)

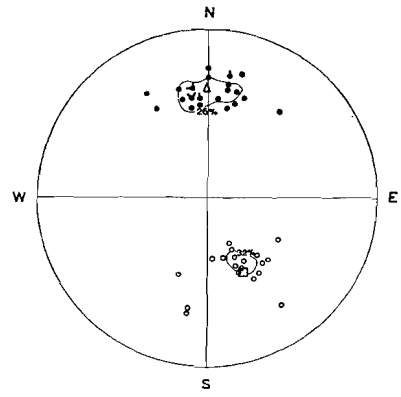

Meas. sample 203
(19 s. and 27 m.f.)

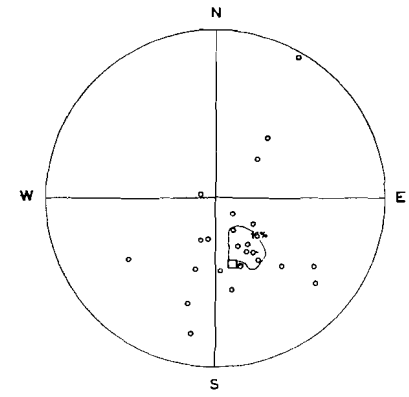

Meas. sample 204
(25 s.)

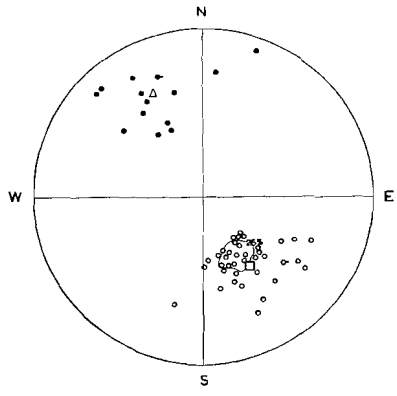

Meas. sample 205
(39 s. and 15 m.f.)

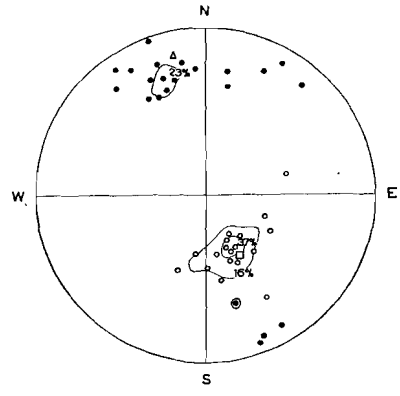

Meas. sample 206
(19 s. and 22 m.f.)

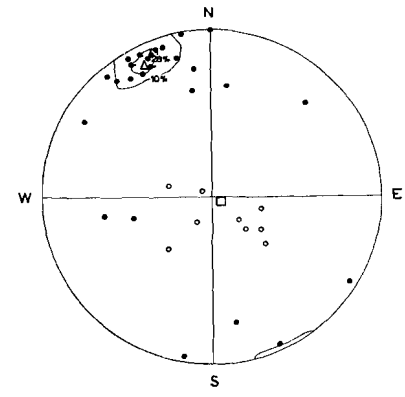

Meas. sample 207
(9 s. and 29 m.f.)

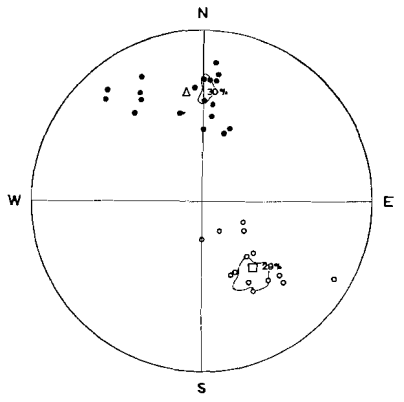

Meas. sample 208
(14 s. and 20 m.f.)

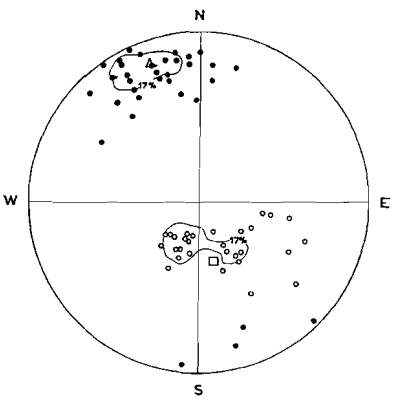

Meas. sample 209
(29 s. and 36 m.f.)

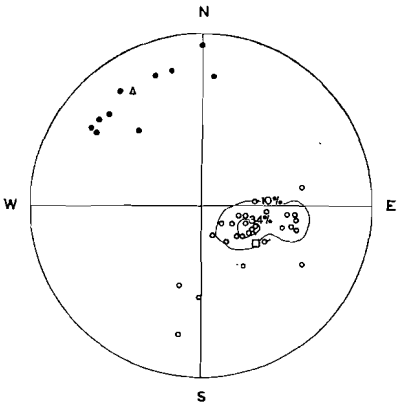

Meas. sample 210
(29 s. and 10 m.f.)

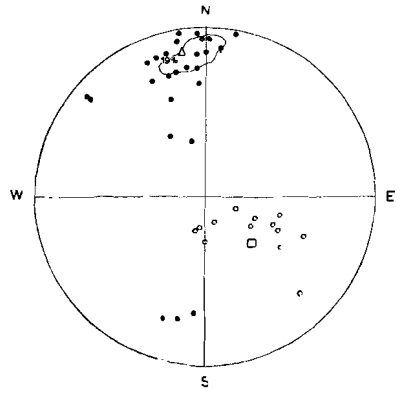

Meas. sample 211
(13 s. and 27 m.f.)

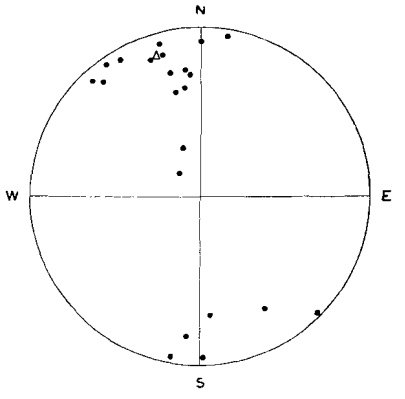

Meas. sample 212
(22 m.f.)

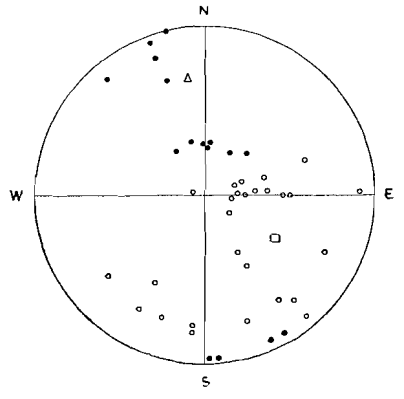

Meas. sample 213
(27 s. and 16 m.f.)

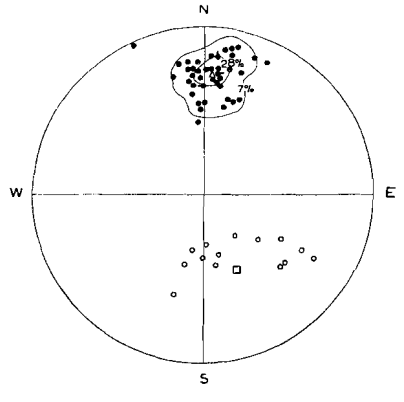

Meas. sample 214
(14 s. and 43 m.f.)

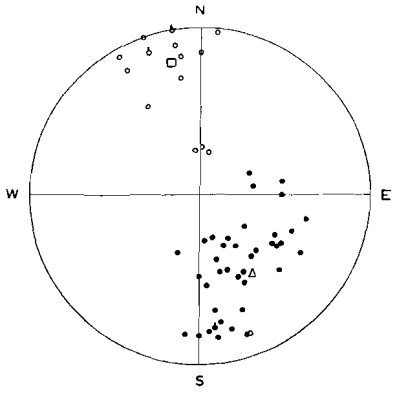

Meas. sample 215
(17 s. and 40 m.f.)

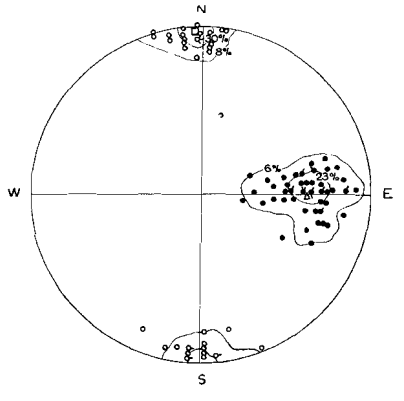

Meas. sample 216
(40 s. and 53 m.f.)

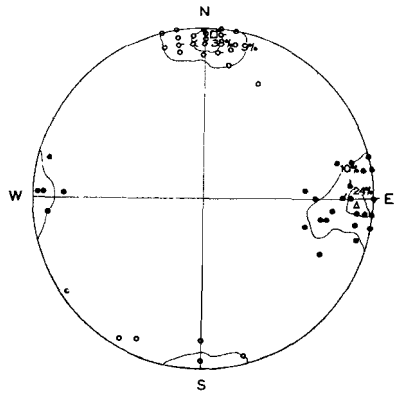

Meas. sample 217
(32 s. and 29 m.f.)

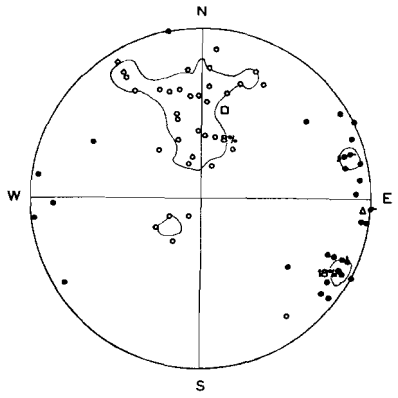

Meas. sample 218
(35 s. and 33 m.f.)

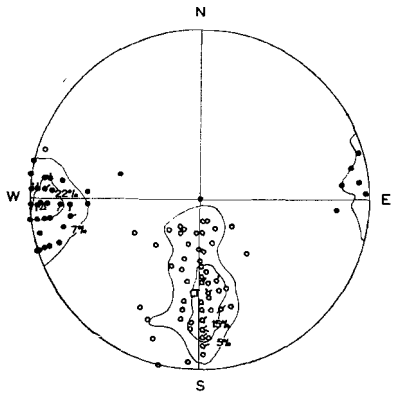

Meas. sample 219
(65 s. and 45 m.f.)

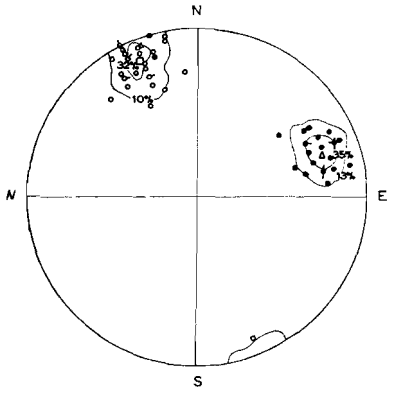

Meas. sample 220
(31 s. and 23 m.f.)

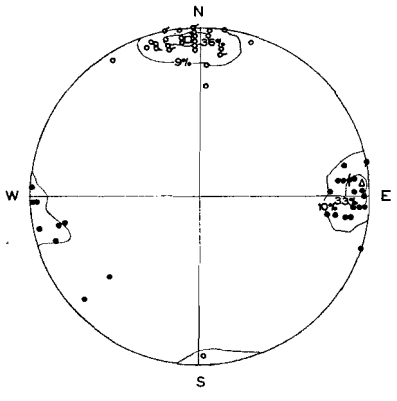

Meas. sample 221
(33 s. and 30 m.f.)

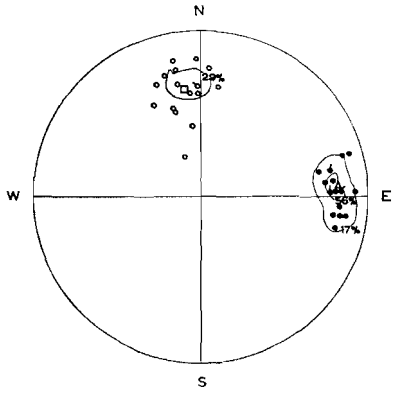

Meas. sample 222
(17 s. and 18 m.f.)

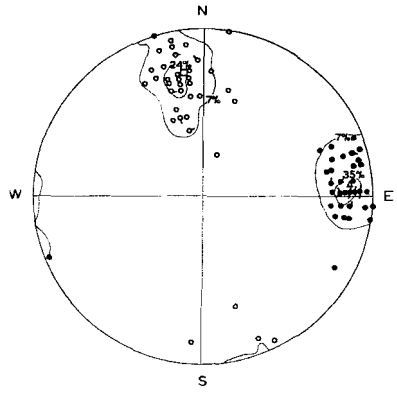

Meas. sample 223
(42 s. and 43 m.f.)

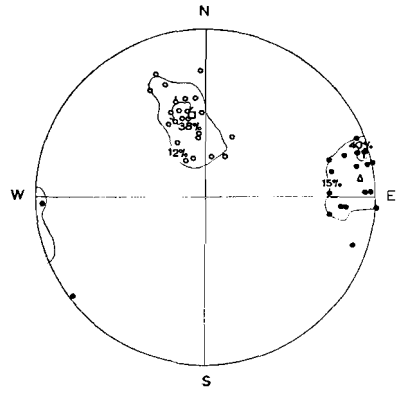

Meas. sample 224
(26 s. and 20 m.f.)

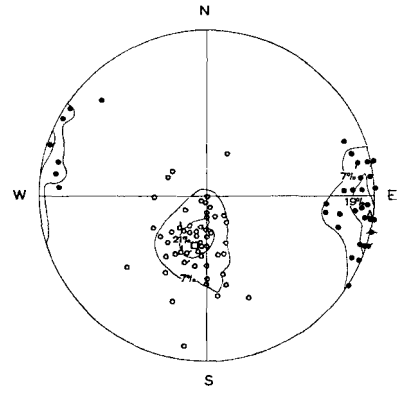

Meas. sample 225
(57 s. and 42 m.f.)

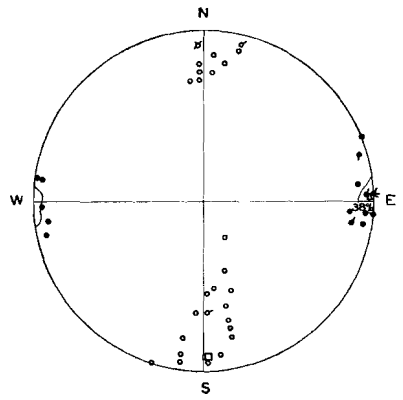

Meas. sample 226
(32 s. and 21 m.f.)

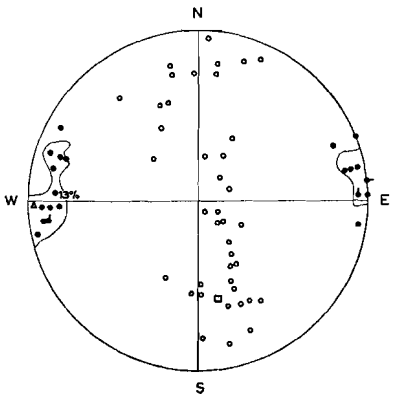

Meas. sample 227
(40 s. and 24 m.f.)

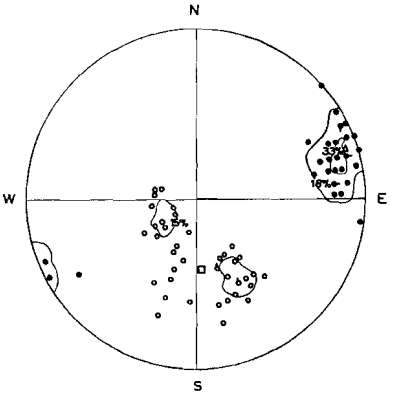

Meas. sample 228
(40 s. and 30 m.f.)

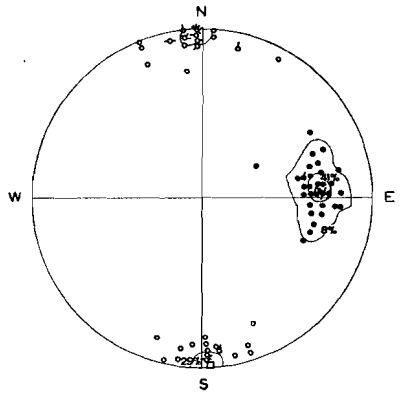

Meas. sample 229
(52 s. and 37 m.f.)

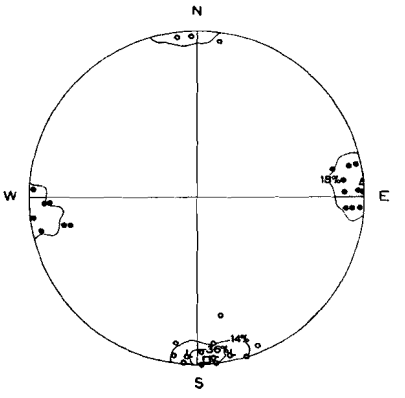

Meas. sample 230
(22 s. and 17 m.f.)

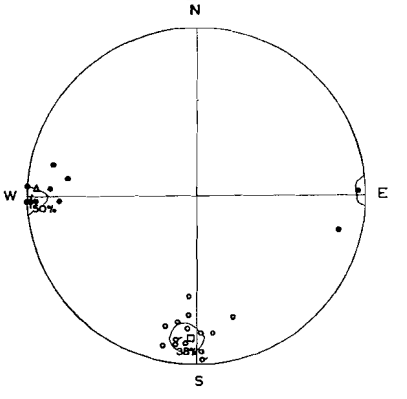

Meas. sample 231
(16 s. and 12 m.f.)

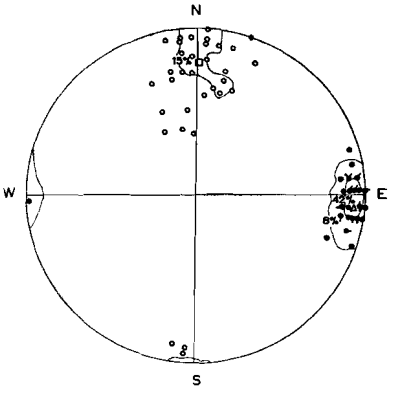

Meas. sample 232
(33 s. and 36 m.f.)

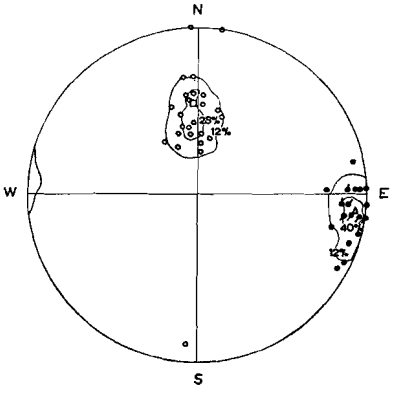

Meas. sample 233
(25 s. and 25 m.f.)

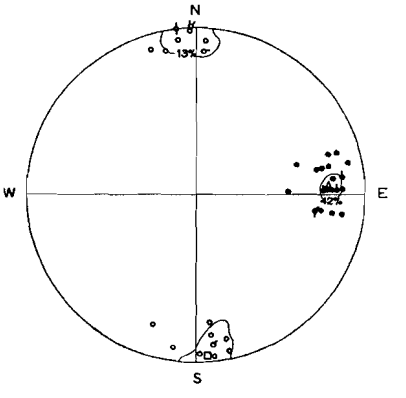

Meas. sample 234
(23 s. and 24 m.f.)

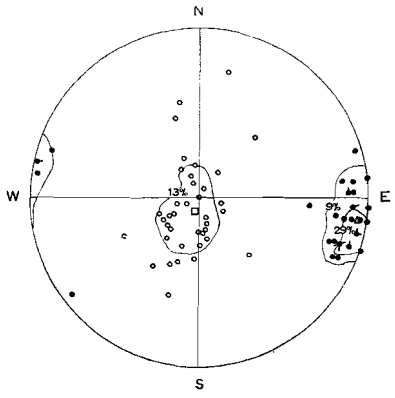

Meas. sample 235
(39 s. and 35 m.f.)

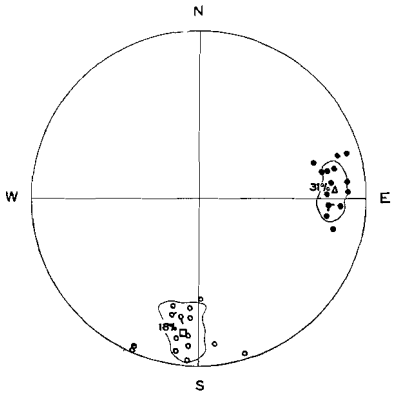

Meas. sample 236
(17 s. and 16 m.f.)

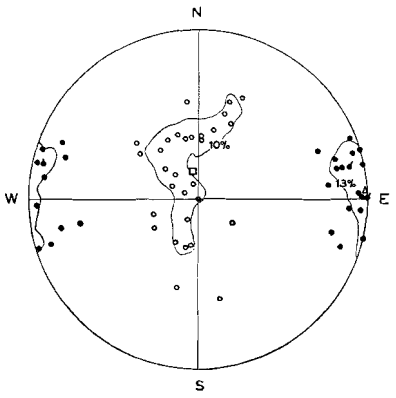

Meas. sample 237
(30 s. and 32 m.f.)

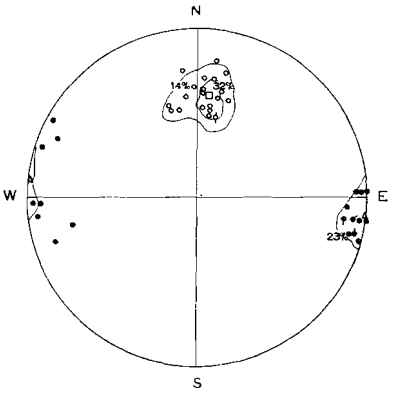

Meas. sample 238
(22 s. and 22 m.f.)

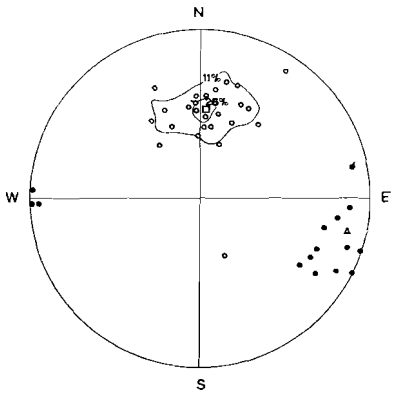

Meas. sample 239
(27 s. and 16 m.f.)

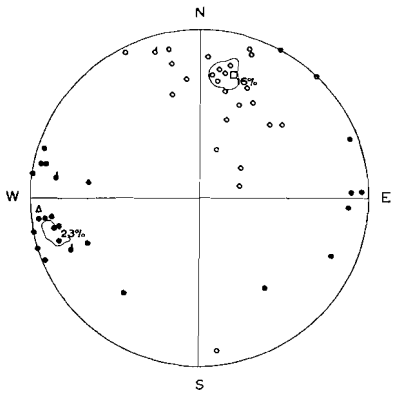

Meas. sample 240
(28 s. and 26 m.f.)

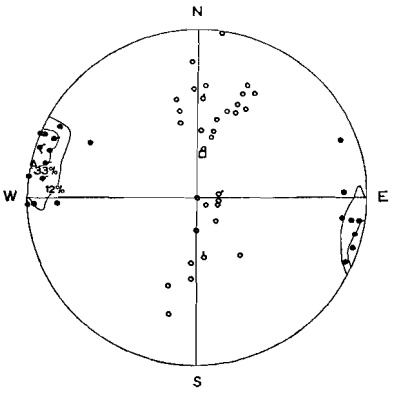

Meas. sample 241
(36 s. and 26 m.f.)

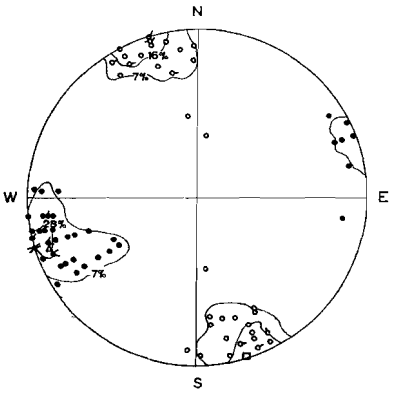

Meas. sample 242
(44 s. and 46 m.f.)

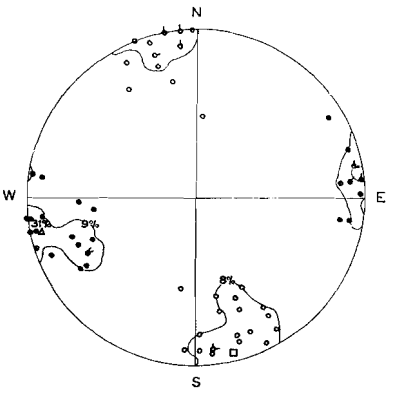

Meas. sample 243
(36 s. and 32 m.f.)

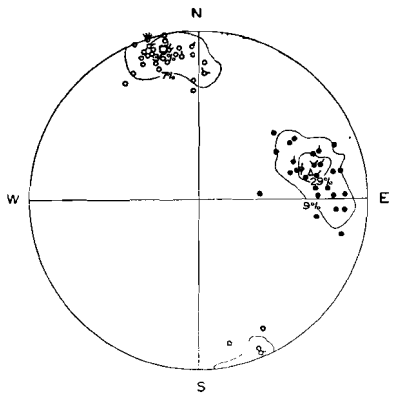

Meas. sample 244
(42 s. and 35 m.f.)

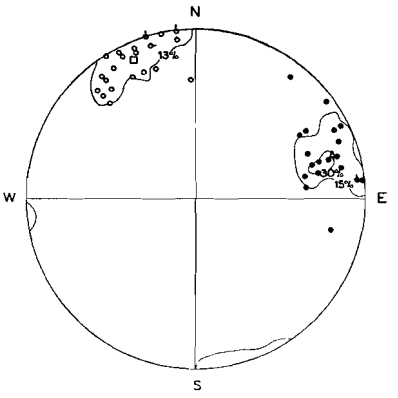

Meas. sample 245
(24 s. and 20 m.f.)

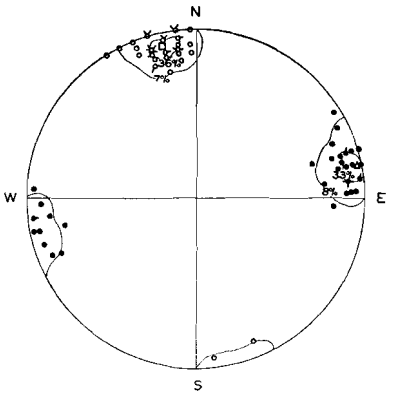

Meas. sample 246
(42 s. and 37 m.f.)

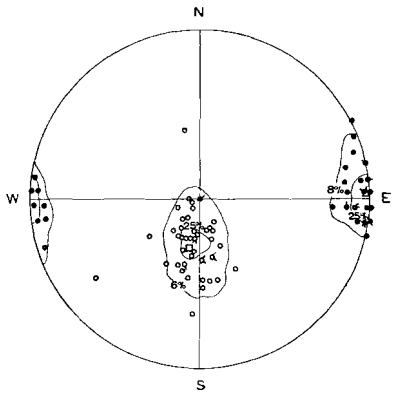

Meas. sample 247
(48 s. and 39 m.f.)

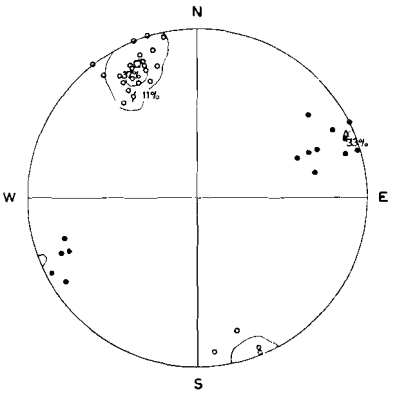

Meas. sample 248
(27 s. and 15 m.f.)

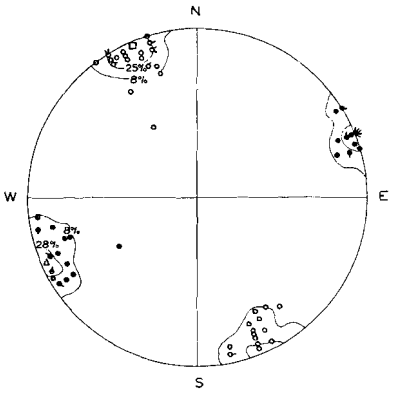

Meas. sample 249
(40 s. and 36 m.f.)

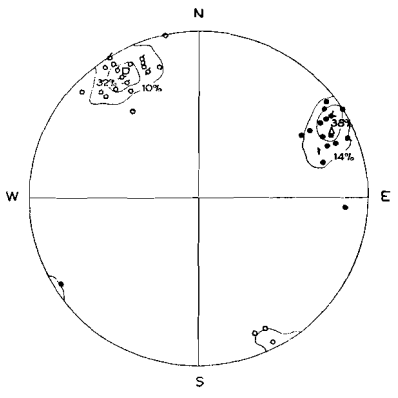

Meas. sample 250
(31 s. and 21 m.f.)

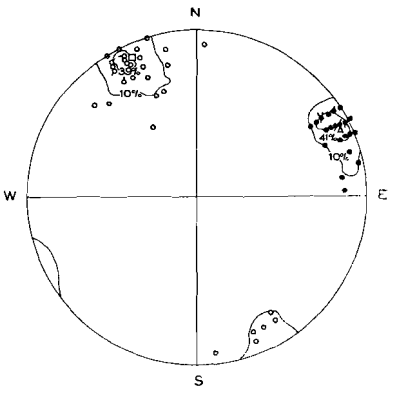

Meas. sample 251
(31 s. and 29 m.f.)

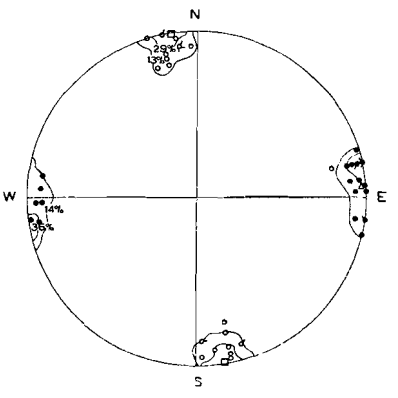

Meas. sample 252
(24 s. and 22 m.f.)

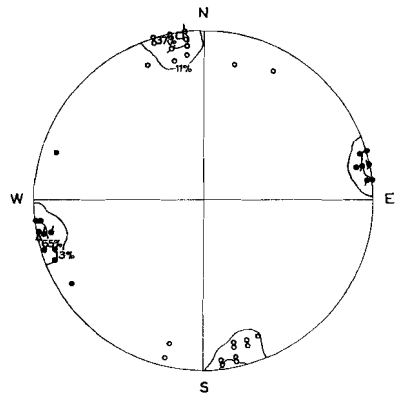

Meas. sample 253
(27 s. and 23 m.f.)

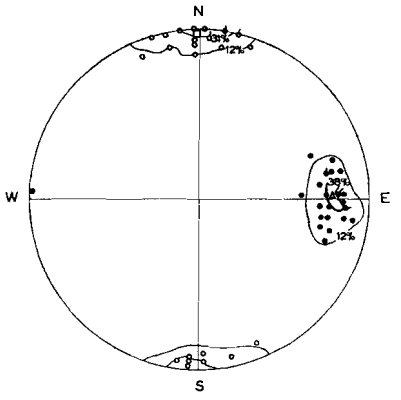

Meas. sample 254
(26 s. and 26 m.f.)

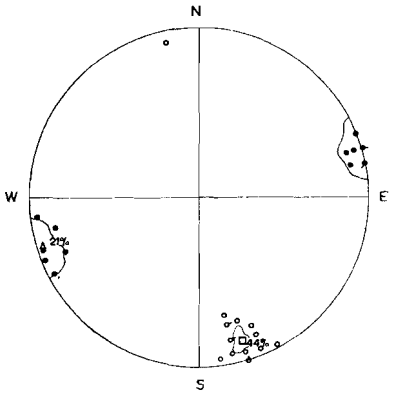

Meas. sample 255
(16 s. and 14 m.f.)

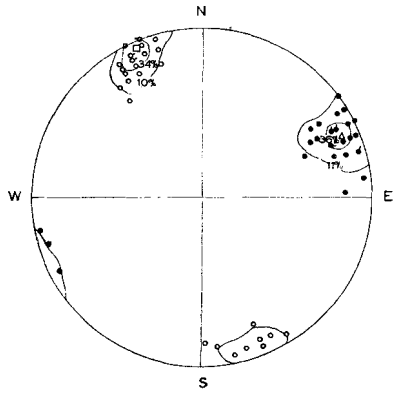

Meas. sample 256
(29 s. and 28 m.f.)

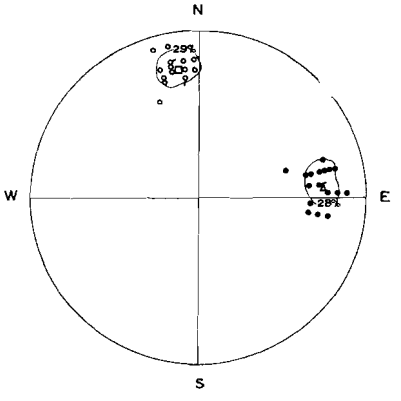

Meas. sample 257
(17 s. and 18 m.f.)

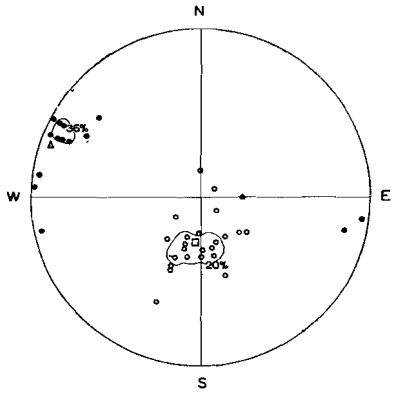

Meas. sample 258
(25 s. and 14 m.f.)

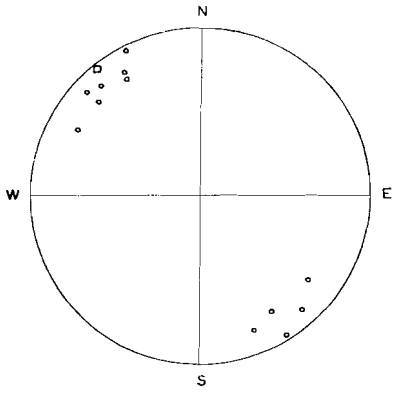

Meas. sample 259
(12 s.)

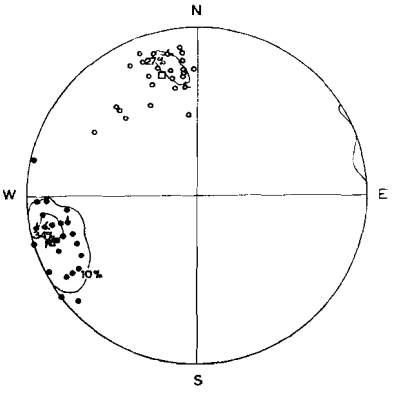

Meas. sample 260
(30 s. and 29 m.f.)

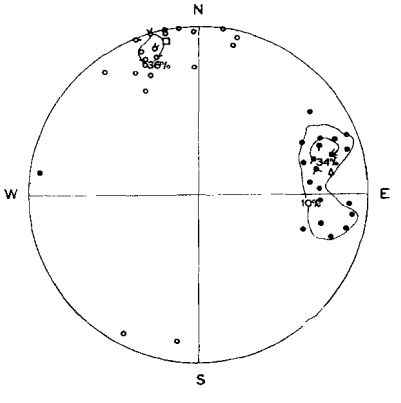

Meas. sample 261
(28 s. and 29 m.f.)

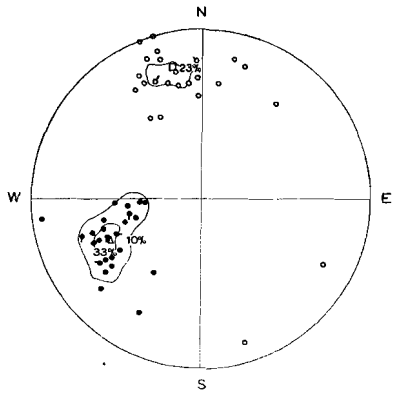

Meas. sample 262
(26 s. and 30 m.f.)

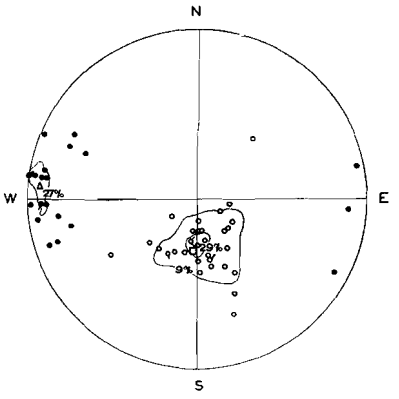

Meas. sample 263
(34 s. and 22 m.f.)

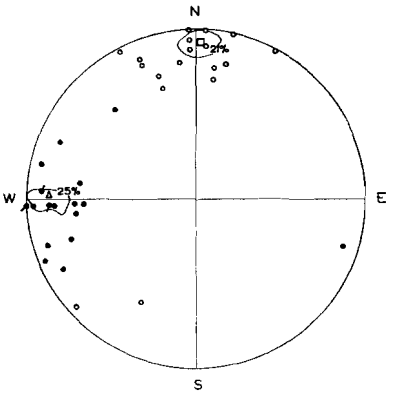

Meas. sample 264
(19 s. and 20 m.f.)

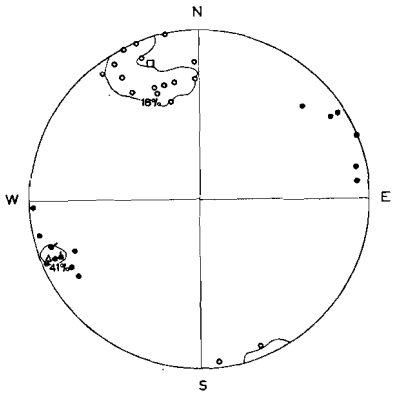

Meas. sample 265
(17 s. and 17 m.f.)

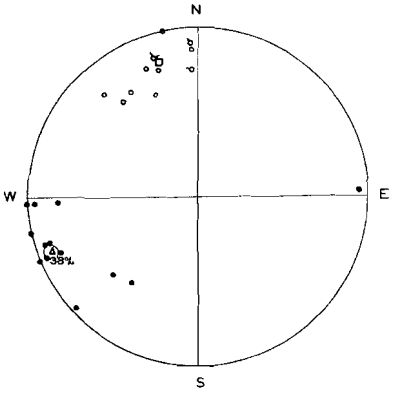

Meas. sample 266
(15 s. and 13 m.f.)

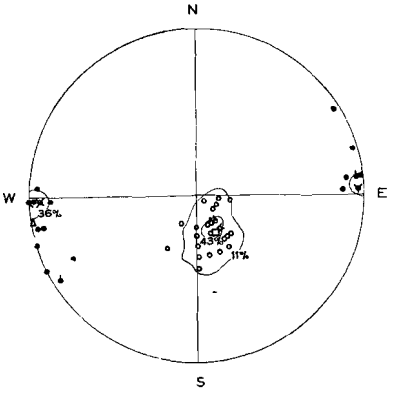

Meas. sample 267
(28 s. and 28 m.f.)

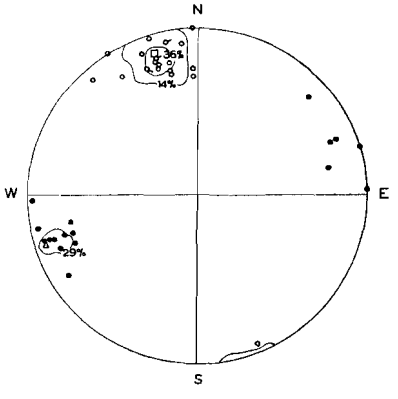

Meas. sample 268
(22 s. and 17 m.f.)

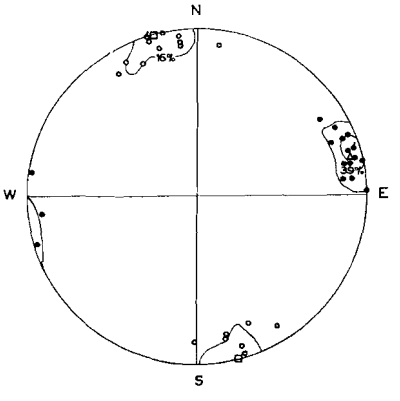

Meas. sample 269
(19 s. and 18 m.f.)

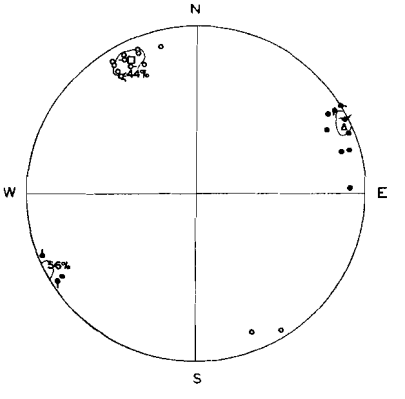

Meas. sample 270
(18 s. and 18 m.f.)

LITERATURE REFERENCES:

ACCORDI, B. (1955) — Le dislocazioni delle Cime (Gipfelfaltungen) delle Dolomiti. Ann. Univ. Ferrara, *2*, 2, pp. 65-188.

ACCORDI, B. (1957) — Nuove ricerche sui corrugamenti di vetta (Gipfelfaltungen) delle Dolomiti Occidentali. Boll. Soc. Geol. Ital., *56*, pp. 1-23.

AGTERBERG, F. P. (1959) — On the measuring of strongly dispersed minor folds. Geol. en Mijnb., Nw. S., *21*, 5, 133-137.

AGTERBERG, F. P. (1961) — The skew frequency-curve of some ore minerals. Geol. en Mijnb., Nw. S., *23*, 4, pp. 149-162.

ANDERSON, E. M. (1951) — The dynamics of faulting. Oliver and Boyd, Edinburgh.

ANDREATTA, C. (1932) — Ricerche petrografiche sulla regione di Cima d'Asta I. Mem. Ist. Geol. Univ. Padova, *10*.

ANDREATTA, C. (1934) — La disposizione di microliti micacei in plagioclasi di rocce intrusive (Analisi strutturale di rocce, IV). Per Min., *5*, pp. 217-235.

ANDREATTA, C. (1948) — La "Linea di Peio" nel massiccio dell' Ortler e le sue miloniti. Acta Geol. Alp., *1*, pp. 1-63.

ANDREATTA, C. (1952) — Polymetamorphose und Tektonik in der Ortlergruppe. N. Jb. Min., 1952, pp. 13-28.

ANDREATTA, C. (1959) — Nuove osservazioni sulla serie basale della zona meridionale del sistema vulcanico atesino. Acc. Naz. Lincei, Ser. 8, *24*, 2, pp. 172-178.

ANGEL, F. (1954) — Petrochemie der Hochalm-Ankogel-Gesteine. Jb. Geol. B. Anst., *97*, 1, pp. 1-16.

ARGAND, E. (1916) — Sur l'arc des Alpes occidentales. Ecl. Geol. Helv., *14*, pp. 145-191.

BELOUSSOV, V. V. (1956) — Grundlagen der allgemeinen Geotektonik. Geol. Rundschau, *45*, 2, pp. 353-369.

BELOUSSOV, V. V. (1958) — Some factors governing the development of the earth's crust. Endeavour, *17*, 68, pp. 173-180.

BEMMELEN, R. W. VAN (1933) — Die Anwendung der Undationstheorie auf das Alpine System in Europa. Proc. K.N. Akad. W., *36*, pp. 686-694.

BEMMELEN, R. W. VAN (1949) — The geology of Indonesia. Government Printing Office, The Hague.

BEMMELEN, R. W. VAN (1953) — Problemen van Alpiene gebergtevorming. Geol. en Mijnb., Nw. S., *15*, 4, pp. 99-102.

BEMMELEN, R. W. VAN (1954) — Mountain building. Nijhoff, The Hague.

BEMMELEN, R. W. VAN (1955) — Tectogenèse par gravité. Bull. Soc. Belge Géol., *64*, 1, pp. 95-123.

BEMMELEN, R. W. VAN (1956) — The geochemical control of tectonic activity. Geol. en Mijnb., Nw. S., *18*, 4, pp. 131-144.

BEMMELEN, R. W. VAN (1957) — Beitrag zur Geologie der westlichen Gailtaler Alpen (Kärnten, Österreich). Jb. Geol. B. Anst., *100*, 2, pp. 179-212.

BEMMELEN, R. W. VAN (1958) — Stromingsstelsels in de silikaatmantel. Geol. en Mijnb., Nw. S., *20*, 1, pp. 1-17.

BEMMELEN, R. W. VAN (1960a) — New views on East-Alpine orogenesis. Report of the Int. Geol. Congress, XXI Session, Norden, Part XVIII.

BEMMELEN, R. W. VAN (1960b) — Zur Mechanik der Ostalpine Deckenbildung. Geol. Rundschau (in press).

BEMMELEN, R. W. VAN (1960c) — Die Methoden in der Geologie. Mitt. Geol. Ges. Wien, *53*, pp. 35-52.

BEMMELEN, R. W. VAN (1961) — Scientific character of geology. Journ. Geol. (in press).

BIANCHI, A. (1934) — Studi petrografici sull' Alto Adige orientale e regioni limitrofe. Mem. Ist. Geol. Univ. Padova, *10*.

BIANCHI, A. and Gb. DAL PIAZ (1939) — La monografia geologica-petrografica sull' Alto Adige orientale e regioni limitrofe. Relazione sui risultati e aggiornamento critico dei problemi. Per. Min., *10*.

BUSK, H. G. (1929) — Earth Flexures. Cambridge University Press.

CADISCH, J. (1953) — Geologie der Schweizer Alpen. Wepf & Co., Basel.

CAREY, S. W. (1958) — A tectonic approach to continental drift. Continental drift symposium, Hobart, Tasmania.

Carta geologica delle tre Venezie (Foglio 4a, 4b, 11, 12, 13, 21, 22, and 23). Giardi, Firenze.

CASTIGLIONI, B. (1939) — Il gruppo delle Pale di San Martino e le valli limitrofe. Mem. Ist. Geol. Univ. Padova, *13*.

CHRISTA, E. (1931) — Das Gebiet des oberen Zemmgrundes in den Zillertaleralpen. Jb. Geol. B. Anst., *81*, pp. 533-634.

CLOOS, E. (1947) — Oolite deformation in the South Mountain-fold, Maryland. Bull. Geol. Soc. Am., *58*, pp. 843-918.

CLOOS, H. (1936) — Einführung in die Geologie. Borntraeger, Berlin.

COLLETTE, B. J. (1958) — On the origin of schistosity, I and II. Proc. K. N. Akad. W., Ser. B, *61*, 2, pp. 121-139.

COLLETTE, B. J. (1959) — On helicitic structures and the occurrence of elongate crystals in the direction of the axis of a fold. Proc. K. N. Akad. W., Ser. B, *62*, 3, pp. 161-171.

CORNELIUS, H. P. and M. CORNELIUS-FURLANI (1922) — Über gangförmige Eruptivbreccien aus dem Villnösstal (Südtirol). Centralbl. Min. Geol. Pal., 1922, pp. 110-114.

CORNELIUS, H. P. and M. CORNELIUS-FURLANI (1931) — Die Insubrische Linie vom Tessin bis zum Tonalepass. Denkschr. Akad. Wiss. Wien, *102*, pp. 207-301.

CORNELIUS-FURLANI, M. (1924) — Zur Kenntnis der Villnösser Linie. Verh. Geol. B. Anst., 1924, 7, pp. 125-131.

CRAMER, H. (1946) — Mathematical methods of statistics. Princeton Math. Ser. 9, Princeton University Press.

DAL PIAZ, Gb. (1931) — Sull' andamento delle linee di dislocazione che accompagnano i massicci intrusivi di Monte Croce, Ivigna, Bressanone nell' Alto Adige. Rend. Acc. Naz. Lincei, Cl. Sc. Fis., *14*, p. 310.

DAL PIAZ, Gb. (1934) — Studi geologici sull' Alto Adige orientale e regioni limitrofe. Mem. Ist. Geol. Univ. Padova, *10*.

DAL PIAZ, Gb. (1937) — La struttura geologica delle Austridi. Nota V. Ancora sul sistema austroalpino delle Alpi Orientali. Rend. Acc. Naz. Lincei, *25*, Ser. 6a, 8, pp. 392-398.

DAL PIAZ, Gb. (1942) — Geologia della bassa valle d'Ultimo e del massiccio granitico di Monte Croce. Mem. Mus. Stor. Nat. Venezia Trident., *5*, 2.

DALY, R. A. (1933) — Igneous rocks and the depths of the earth. McGraw-Hill, New York.

D'AMICO, C. (1956) — Le rocce intrusive della dorsale Arinàs-Redàsega (cristallino di Cima d'Asta). Acta Geol. Alpina, *6*, p. 5-78.

D'AMICO, C. (1957) — Studio delle filladi e delle rocce granitizzate derivate dall' alta Val Cismon (cristallino di Cima 'dAsta). Rend. Soc. Min. Ital., *13*, pp. 1-49.

D'AMICO, C. (1958) — I filoni lamprofirici di Alpe Tognola (cristallino di Cima d'Asta). Rend. Soc. Min. Ital., *14*, pp. 1-8.

DIETZEL, G. F. L. (1960) — Geology and permian paleomagnetism of the Merano region (Province of Bolzano, N. Italy). Doct. thesis Utrecht, Geologica Utraiectina, *4*.

ESCHER, B. G. (1954) — Grondslagen der Algemene Geologie. Wereldbibl. N.V., Amsterdam.

EXNER, C. (1951) — Mikroklinporphyroblasten mit helizitischen Einschlusszügen bei Badgastein. Tschermaks Min. Petr. Mitt., *2*, 3, pp. 355-374.

EXNER, C. (1954) — Die Südost-Ecke des Tauernfensters bei Spittal an der Drau. Jb. Geol. B. Anst., *97*, 1, pp. 17-37.

FALLOT, P. (1950) — Remarques sur la tectonique de couverture dans les Alpes Bergamasques et les Dolomites. Bull. Soc. Géol. France, 5e Ser., *20*, pp. 183-195.

FALLOT, P. (1955) — Les dilemmes tectoniques des Alpes Orientales. Ann. Soc. Géol. Belg., *78*, pp. 147-170.

FISHER, R. (1953) — Dispersion on a sphere. Proc. R. Soc. London, *217*, pp. 295-305.

FOURMARIER, P. (1951) — Schlistosité, foliation et microplissement. Arch. Sciences Geneva, *156*, pp. 5-23.

FOURMARIER, P. (1959) — Le granite et les déformations mineurs des roches. K. Akad. Belg., Wetensch., 8e Verh., *31*, 3.

FRASL, G. (1954) — Anreichen schmelzflüssigen und hochtemperierten Wachstums an den grossen Kalifeldspaten einiger Porphyrgranite, Porphyrgranitgneise und Augengneise Österreichs. Jb. Geol. B. Anst., *97*, 1, pp. 71-134.

FRASL, G. (1957) — Der heutige Stand der Zentralgneisforschung in den Ostalpen. Joanneum Min. Mitt., *2*, pp. 41-63.

FRASL, G. (1958) — Zur Gliederung der Schieferhülle in den mittleren Hohen Tauern. Jb. Geol. B. Anst., *101*, 3, pp. 323-472.

FREUDENTHAL, H. (1957) — Waarschijnlijkheid en Statistiek. F. Bohn N.V., Haarlem.

FURLANI, M. (1912) — Der Drauzug in Hochpustertal. Mitt. Geol. Ges. Wien, *5*, pp. 252-271.

FURLANI, M. (1921) — Der Triaszonen im Hochpustertal, Eisack und Pensertal in Tirol. Denkschr. Akad. Wiss. Wien, *97*, pp. 33-54.

FURLANI, M. (1922) — Considerazioni orogenetiche sul limite alpino-dinarico in Pusteria. Acc. Ven. Trent. Istr., *12-13*.

GEYER, G. (1899) — Uggowitzer Breccie und Verrucano. Verh. K. K. Geol. R. Anst., 1899, p. 418.

GEYER, G. (1902) — Geologische Specialkarte, 1 : 75.000, SW-Gruppe, Nr. 70. K. K. Geol. R. Anst., Wien.

GEYER, G. (1902) — Erlaüterungen zur Geologischen Karte, SW-Gruppe, Nr. 70, Sillian und St. Stefano del Comelico. K. K. Geol. R. Anst., Wien.

GOGUEL, J. (1952) — Traité de Tectonique. Masson & Cie., Paris.

GORTANI, M. (1956) — Recenti progressi nella conoscenza strutturale dell' Italia. Geotektonisches Symposium zu Ehren von H. Stille, pp. 143-176. Enke, Stuttgart.

GRUBERMANN, U. and P. NIGGLI (1924) — Die Gesteinsmetamorphose. Borntraeger, Berlin.

HAARMANN, E. (1930) — Die Oszillations-Theorie. Enke, Stuttgart.

HALD, A. (1957) — Statistical theory with engineering applications. Wiley & S., New York.

HALD, A. (1960) — Statistical tables and formulas. Wiley & S., New York.

HALLER, J. (1956) — Probleme der Tiefentektonik. Bauformen im Migmatit. Stockwerk der Ostgrönländischen Kaledoniden. Geol. Rundschau, *45*, 2, pp. 159-167.

HARLAND, W. B. and M. B. BAYLY (1958) — Tectonic Regimes. Geol. Mag., *95*, 2, pp. 89-104.

HEIM, A. (1922) — Geologie der Schweiz, Band II. Tauchnitz, Leipzig.

HEINRICH, E. W. (1956) — Microscopic Petrography. McGraw-Hill, New York.

HEISSEL, W. and J. LADURNER (1936) — Geologie des Gebietes von Villnöss-Gröden-Schlern-Rosengarten. Jb. Geol. B. Anst., *86*, pp. 1-63.

HERITSCH, F. (1923) — Die Grundlagen der alpinen Tektonik. Borntraeger, Berlin.

HILTEN, D. VAN (1960) — Geology and permian paleomagnetism of the Val-di-Non area, W. Dolomites, N. Italy. Doct. thesis Utrecht, Geologica Ultraiectina, *5*.

HOEPPENER, R. (1956) — Zum Problem der Bruchbildung. Schieferung und Faltung. Geol. Rundschau, *45*, 2, pp. 247-283.

HOSPERS, J. (1957) — Gravity and crustal shortening in the Alps. Geol. en Mijnb., Nw. S., *19*, 1, pp. 1-18.

HUCKRIEDE, R. and V. JACOBSHAGEN (1958) — Ein Querschnitt durch die Nördlichen Kalkalpen (Oberstdorf-Pettneu). Zeitschr. D.G.G., *109*, pp. 373-388.

JEFFREYS, H. (1929) — The Earth. Cambridge University Press.

JUNG, J. and M. ROCQUES (1952) — Introduction à l'étude zonéographique des formations cristallophylliennes. Bull. Serv. Carte Géol. France, *50*, Nr. 235.

KARL, F. (1954) — Der derzeitige Stand B-achsialer Gefügeanalysen in den Ostalpen. Jb. Geol. B. Anst., *97*, 1, pp. 135-154.

KARL, F. (1959) — Vergleichende petrographische Studien an den Tonalitgraniten der Hohen Tauern und den Tonalit-Graniten einiger periadriatischer Intrusivmassive. Jb. Geol. B. Anst., *102*, 1, pp. 1-192.

KARL, F. and G. MORTEANI (1960) — Ein Vergleich der Ergebnisse von A. Bianchi und F. Karl über die granitischen Gesteine des Zillertales und des Grossvenedigers (Hohe Tauern). Tschermaks Min. Petr. Mitt., *7*, 3, pp. 290-316.

KAYSER, E. and R. BRINKMANN (1954) — Abriss der Geologie, II. Enke, Stuttgart.

KING HUBBERT, M. and W. W. RUBEY (1959) — Rôle of Fluid-Filled Porous Solids ands Its Application to Overthrust Faulting. Bull. Geol. Soc. Am., *70*, pp. 115-166.

KLEBELSBERG, R. VON (1935) — Geologie von Tirol. Borntraeger, Berlin.

KRAUS, E. (1951) — Die Baugeschichte der Alpen. Akademie-Verlag, Berlin.

KÜNDIG, E. (1956) — The position in time and space of the ophiolites with relation to orogenic metamorphism. Geol. en Mijnb., Nw. S., *18*, 4, pp. 106-114.

KÜPPER, H. (1960) — Erlaüterungen zu einer tektonischen Übersichtsskizze des weiteren Wiener Raumes. Mitt.

Geol. Ges. Wien, *53*, pp. 1-33.

LEONARDI, P. (1955) — Breve sintesi geologica delle Dolomiti occidentali. Boll. Soc. Geol. Ital., *54*, 1, pp. 1-140.

LOVERING, J. P. (1958) — The nature of the Mohorovičic Discontinuity. Trans. Am. Geoph. Un., *39*, pp. 947-955.

MITTEMPERGHER, M. (1958) — La serie effusiva paleozoica del Trentino-Alto Adige. Studi Ric. Div. Geom. G.N.R.M. Roma, *1*, pp. 61-145.

MOLENGRAAFF, G. J. H. (1941) — Geologische Constructiemethoden. Waltman, Delft.

MUTSCHLECHNER, G. (1932) — Geologie der St. Vigiler Dolomiten. Jb. Geol. B. Anst., *82*, pp. 163-274.

MUTSCHLECHNER, G. (1933) — Geologie des Gebietes zwischen St. Cassian und Buchenstein (Südtiroler Dolomiten). Jb. Geol. B. Anst., *83*, pp. 199-232.

NABHOLZ, W. K. (1953) — Das mechanische Verhalten der granitischen Kernkörper der tiefen penninischen Decken bei der Alpinen Orogenese. C. R. Congr. Int. Géol. Alg., *3*, pp. 9-23.

OGILVIE-GORDON, M. M. (1929) — Geologie des Gebietes von Pieve (Buchenstein, St. Cassian) und Cortina d'Ampezzo. Jb. Geol. B. Anst., *79*, pp. 357-424.

OGILVIE-GORDON, M. M. (1934) — Geologie von Cortina d'Ampezzo und Cadore. Jb. Geol. B. Anst., *84*, pp. 59-215.

ORVILLE, P. M. (1960) — Alkali feldspar-alkali chloride hydrothermal ion-exchange. Ann. Rep. Geoph. Lab. Carnegie Inst. Washington, 1959—'60, pp. 104-107.

PALM, Q. A. (1957) — Les roches cristallines des Cevennes Medianes à hauteur de Largentière. Doct. thesis Utrecht, Geologica Utraiectina, *3*.

PALM, Q. A. (1960) — Wet and dry regional metamorphism. Geol. en Mijnb., Nw. S., *22*, 6, pp. 244-252.

PAULITSCH, P. (1960) — Das Kristallin zwischen Tassenbach und Obertilliach, Osttirol, und seine Metamorphose. Verh. Geol. B. Anst., 1, pp. 103-118.

PHILLIPS, F. C. (1955) — The Use of Stereographic Projection in Structural Geology. Arnold, London.

PINCUS, H. J. (1951) — Statistical methods applied to the study of rock fractures. Bull. Geol. Soc. Am., *62*, pp. 81-130.

RAMBERG, H. (1952) — The origin of metamorphic and metasomatic rocks. University Chicago Press.

REINHARD, M. (1953) — Über das Grundgebirge des Sottoceneri im südlichen Tessin. Ecl. Geol. Helv., *46*, 2, pp. 214-222.

REITHOFER, O. (1928) — Geologie der Puezgruppe (Südtiroler Dolomiten). Jb. Geol. B. Anst., *78*, pp. 257-326.

RICHTER, M. (1956) — Über den Bau der Vorarlberger Alpen zwischen Oberem Lech, Flexenpass und Ill Geotektonisches Symposium zu Ehren von H. Stille, pp. 190-204. Enke, Stuttgart.

RICHTER, M. (1958) — Über Dehnung und Längung der Gebirge während der Faltung. Geol., 7, pp. 312-318.

RIECKE, E. (1912) — Zur Erniedrigung des Schmelzpunktes durch einseitigen Druck oder Zug. Zentralbl. Min., 1912, pp. 95-104.

RUBEY, W. W and M. KING HUBBERT (1959) — Overthrust Belt in Geosynclinal Area of Western Wyoming in light of Fluid-Pressure Hypothesis. Bull. Geol. Soc. Am., *70*, pp. 167-206.

RUTTEN, M. G. (1955) — Schistosity in the Rhenic Massif and the Ardennes. Geol. en Mijnb., Nw. S., *17*, pp. 47-56.

SANDER, B. (1906) — Geologische Beschreibung des Brixner Granits. Jb. K. K. Geol. R. Anst., *56*, pp. 707-744.

SANDER, B. (1912) — Über einige Gesteinsgruppen des Tauernwestendes. Jb. K. K. Geol. R. Anst., *62*, 2, pp. 219-288.

SANDER, B. (1921) — Geologische Studien am Westende der Hohen Tauern, II Bericht. Jb. Geol. St. Anst., *70*, 3-4, pp. 273-296.

SANDER, B. (1925) — Note illustrative della carta geologica delle Tre Venezie, Foglio Bressanone. Soc. Coop. Tipogr., Padova.

SANDER, B. (1950) — Einführung in die Gefügekunde der geologischen Körper, I and II. Springer, Wien.

SCHAFFER, F. X. (1951) — Geologie von Österreich. Deuticke, Wien.

SCHEIDEGGER, A. E. (1958) — Principles of geodynamics. Springer, Berlin.

SCHIEFERDECKER, A. A. G. (1959) — Geological Nomenclature. Noorduyn & Zn. N.V., Gorinchem.

SCHMIDEGG, O. (1933) — Neue Ergebnisse in den südlichen Ötztaler Alpen. Verh. Geol. B. Anst., 5-6, pp. 83-95.

SCHMIDEGG, O. (1936) — Steilachsige Tektonik und Schlingenbau auf der Südseite der Tiroler Zentralalpen. Jb. Geol. B. Anst., *86*, 2, pp. 115-149.

SCHMIDEGG, O. (1937) — Der Triaszug von Kalkstein im Schlingengebiet der Villgrater Berge (Osttirol). Jb. Geol. B. Anst., *87*, 1-2, pp. 111-132.

SCHMIDEGG, O. (1954) — Achsen- und Flächengefüge beiderseits des Silltalbruches zwischen Innsbruck und Matrei. Tschermaks Min. Petr. Mitt., 4, 1-4, pp. 125-137.

SEMENZA, E. (1959) — Osservazioni sulla tettonica del fianco sinistro della Valle del Piave nel tratto tra Lozzo e Pieve di Cadore. Accad. Naz. Lincei, Ser. 8, *27*, 6, pp. 397-404.

SEMENZA, E. (1960) — Nuovi studi tettonici nella Valle del Vaiont e zone limitrofe. Accad. Naz. Lincei, Ser. 8, *28*, 2, pp. 223-229.

SIGNORINI, R. (1951) — Osservazioni sulla struttura e la morfologia delle Dolomiti orientali. Boll. Soc. Geol. Ital., *70*, 3, pp. 545-564.

SIGNORINI, R. (1955) — Discutendo sulle interpretazioni tettoniche delle Dolomiti. Boll. Soc. Geol. Ital., *54*, 1, pp. 150-157.

SIMAIKA, J. B. and E. W. DEEG (1957) — Zur statistischen Analyse geologischer Diagramme. Geol. Rundschau, *46*, 2, pp. 545-557.

SIMBOLI, G. (1959) — Sopra una tormalinite di Alpe Valliselle (Gruppo di Cima d'Asta). Acta Geol. Alpina, 7, pp. 177-189.

SITTER, L. U. DE (1941) — De Tektonik van eenvoudige Structuren. Brill, Leiden.

SITTER, L. U. DE and C. M. DE SITTER-KOOMANS (1949) — The geology of the Bergamasc Alps, Lombardia, Italy. Leidse Geol. Med., *14*B, pp. 1-257.

SITTER, L. U. DE (1956a) — A comparison between the Lombardy Alps and the Dolomites. Geol. en Mijnb., Nw. S., *18*, 3, pp. 70-77.

SITTER, L. U. DE (1956b) — Structural geology. McGraw-Hill, London.

SITTER, L. U. DE (1958) — Boudins and parasitic folds in relation to cleavage and folding. Geol. en Mijnb., Nw. S., *20*, 8, pp. 277-286.

SITTER, L. U. DE (1960) — Conclusion and conjectures on successive tectonic phases. Geol. en Mijnb., Nw. S., *22*, 5, pp. 195-197.

SKALL, H. (1959) — Petrographisch-tektonische Studien an den Gesteinen der Östlischen Sarntaler Alpen. Inaugural-Diss., Innsbruck, 1959; Verh. Geol. B. Anst. (in press).

STAUB, R. (1924) — Der Bau der Alpen. Versuch einer Synthese. Beitr. Geol. Karte Schweiz N. F., *52*, Bern.

SUTTON, J. (1960) — Some crossfolds and related structures in Northern Scotland. Geol. en Mijnb., Nw. S., *22*, 5, pp. 149-162.

Tectonic outline maps of G.V.-meeting at Bad Tölz (1960) by H. BÖGEL, G. LENSCH ,and W. ZACHER (introduction), by H. PICHLER (exc. CI), and by W. ZACHER (exc. CIII). Unpublished excursion guides.

TELLER, F. (1883) — Neue Vorkommnisse diploporenführender Dolomite und dolomitischer Kalke im Bereiche der altkristallinen Schichtreihe Mitteltirols. Verh. Geol. R. Anst., 1883, p. 193.

TELLER, F. and C. VON JOHN (1882) — Geologische-petrographische Beiträge zur Kenntnis der dioritischen Gesteine von Klausen in Südtirol. Jb. K. K. Geol. R. Anst., *32*, 4, pp. 589-685.

TERRY, R. D. and G. V. CHILINGAR (1955) — Comparison charts for visual estimation of percentage composition. Journ. Sed. Petrol., *25*, 3, pp. 229-234.

TOLLMANN, A. (1958) — Geologie der Mosermannlgruppe (Radstädter Tauern). Jb. Geol. B. Anst., *101*, 1, pp. 79-115.

TOLLMANN, A. (1959) — Der Deckenbau der Ostalpen auf Grund der Neuuntersuchung des Zentralalpinen Mesozoikums. Mitt. Ges. Geol. Bergb. Stud. Wien, *10*, pp. 1-62.

TRENER, G. B. (1957a) — Bericht aus der Gegend von Borgo; Reisebericht aus der Cima d'Asta Gruppe; Reisebericht aus der Gegend der Cima d'Asta; Vorlage der geologischen Karte des Lagorai und Cima d'Asta-Gebirges. Studi Trentini Sc. Nat., *1*, A. 34, pp. 81-103.

TRENER, G. B. (1957b) — Geologia delle regioni circonstanti al massiccio granitico di Cima d'Asta. Studi Trentini Sc. Nat., *2*, A. 34, pp. 419-594.

TREVISAN, L. (1939) — Il gruppo di Brenta (Trentino occidentale). Mem. Ist. Geol. Univ. Padova, *13*.

TROOSTER, S. G. and J. E. J. M. VAN LANDEWIJK (1958) — Inleiding in de geologische metingen en constructies. Publicatie van het Min. Geologisch Instituut te Utrecht.

TRUMPY, R. (1958) — Remarks on the pre-orogenic history of the Alps. Geol. en Mijnb., Nw. S., *20*, 10, pp. 340-352.

TURNER, F. J. (1957) — Lineation, symmetry, and internal movement in monoclinic tectonite fabrics. Bull. Geol. Soc. Am., *68*, 1, pp. 1-18.

TURNER, F. J. and J. VERHOOGEN (1951) — Igneous and metamorphic petrology. McGraw-Hill, New York.

VECCHIA, O. (1952) — Sui principali caratteri strutturali dell'Italia settentrionale dedotti dalle misure gravimetriche. Riv. Geof. Appl. *13*, 1, pp. 3-37.

VECCHIA, O. (1957a) — Significato del fascio tettonico Guidicario-Atesino. Boll. Soc. Geol. Ital., *76*, pp. 1-57.

VECCHIA, O. (1957b) — Aspects Géologiques et Géophysiques des Failles Lithosphériques. Geol. Rundschau, *46*, 1, pp. 50-69.

VENING MEINESZ, F. A. (1950) — Kort overzicht der Kartografie. Noordhoff, Groningen.

VENZO, S. (1940) — Studio geotettonico del Trentino meridionale-orientale tra Borgo Valsugana e M. Coppolo. Mem. Ist. Geol. Univ. Padova, *14*.

VETTERS, H. (1947) — Erläuterungen zur Geologischen Karte von Österreich und seinen Nachbargebieten. Geol. B. Anst., Wien.

VISTELIUS, A. B. (1960) — The skew frequency distributions and the fundamental law of the geochemical processes. Journ. Geol., *68*, 1, pp. 1-22.

WAARD, D. DE (1952) — Linear structures in the phyllite area of the Cevennes, France. Indon. Journ. Nat. Sc., *3-4*, pp. 61-70.

WAARD, D. DE (1955) — The inventory of minor structures in a simple fold. Geol. en Mijnb., Nw. S., *17*, 1, pp. 1-11.

WAHLSTROM, E. E. (1950) — Introduction to igneous petrology. Wiley & S., New York.

WENK, E. (1934) — Beiträge zur Petrografie und Geologie des Silvretta-kristallins. Schweiz. Min. Petr. Mitt., *14*, pp. 196-278.

WENK, E. (1948) — Ostalpines und penninisches Kristallin. Schweiz. Min. Petr. Mitt., *28*, pp. 761-771.

WENK, E. (1953) — Principelles zur geologisch-tektonischen Gliederung des Penninikums im zentralen Tessin. Ecl. Geol. Helv., *46*, pp. 9-22.

WENK, E. (1955) — Eine Strukturkarte der Tessineralpen. Schweiz. Min. Petr. Mitt., *35*, 2, pp. 311-319.

WENK, E. (1956) — Alpines und ostgrönländisch-kaledonisches Kristallin, ein tektonisch-petrogenetischer Vergleich. Verh. Naturf. Ges. Basel, *67*, 2, pp. 75-102.

WENK, E. and J. HALLER (1953) — Geological explorations in the Petermann region, western part of Fraenkels land, East Greenland. Medd. om Grønland, *111*, 3, pp. 1-48.

WIEBOLS, J. (1938) — Geologie der Brentagruppe. Jb. Geol. B. Anst., *88*, pp. 261-350.

WILLIAMS, A. (1958) — Oblique-Slip Faults and Rotated Stress Systems. Geol. Mag., *95*, 3, pp. 207-218.

ZWART, H. J. (1960) — Relations between folding and metamorphism in the Central Pyrenees, and their chronological succession. Geol. en Mijnb., Nw. S., *22*, 5, pp. 163-180.

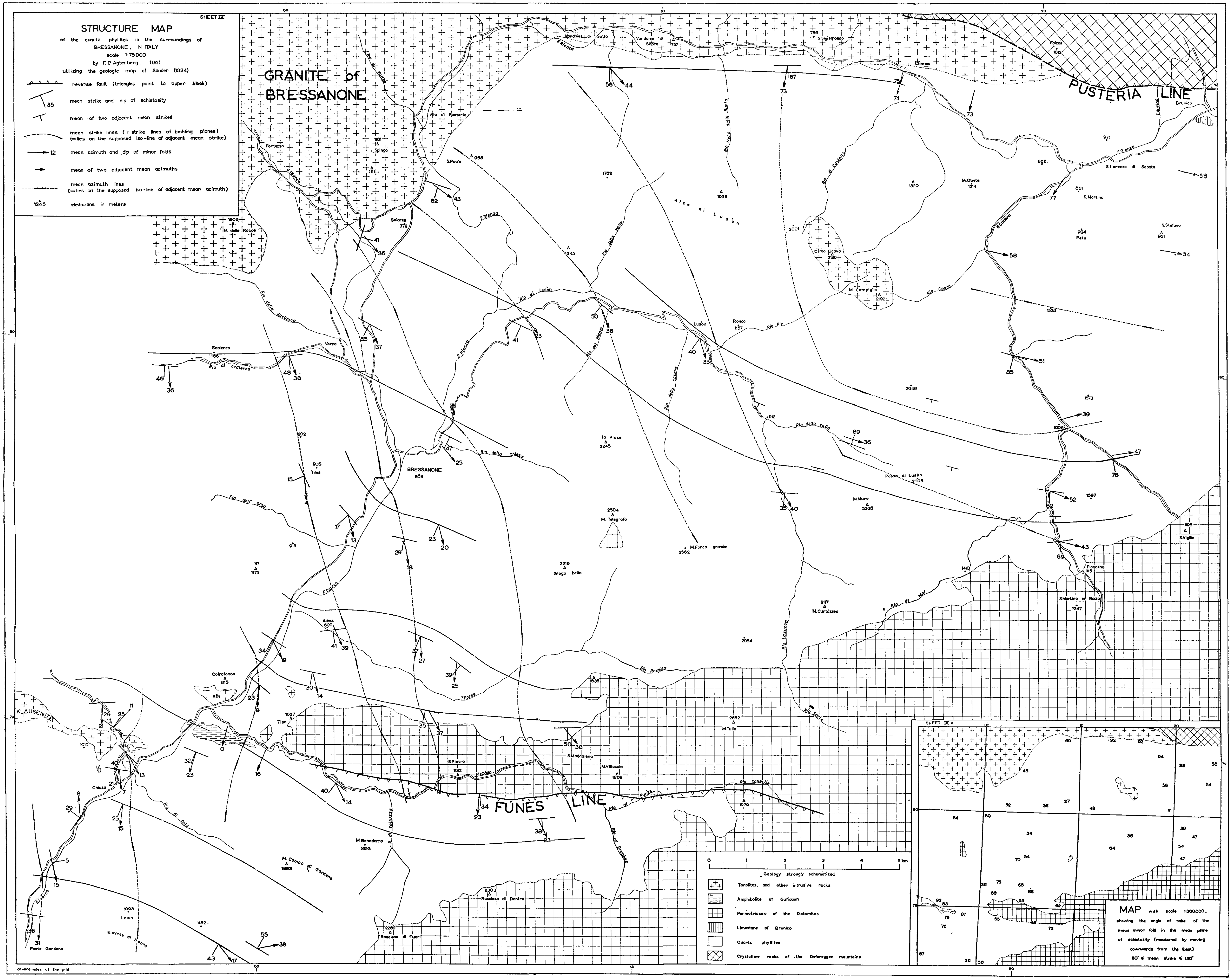
SHEET IV
STRUCTURE MAP
of the quartz phyllites in the surroundings of
BRESSANONE, N. ITALY
scale 1:75.000
by F.P. Agterberg, 1961
utilizing the geologic map of Sander (1924)
reverse fault (triangles point to upper block)
35
mean strike and dip of schistosity
mean of two adjacent mean strikes
mean strike lines (= strike lines of bedding planes)
(— lies on the supposed iso-line of adjacent mean strike)
12
mean azimuth and dip of minor folds
mean of two adjacent mean azimuths
mean azimuth lines
(— lies on the supposed iso-line of adjacent mean azimuth)
1245
elevations in meters
GRANITE of BRESSANONE
PUSTERIA LINE
FUNES LINE
KLAUSENITE
BRESSANONE
Brunico
Fortezza
Sciaves
Scaleres
Chiusa
Ponte Gardena
Alpe di Lusòn
Plose
M. Telegrafo
Rio di Lusòn
Rio della Chiesa
Rio di Funes
0 1 2 3 4 5 km
Geology strongly schematized
Tonalites, and other intrusive rocks
Amphibolite of Gufidaun
Permotriassic of the Dolomites
Limestone of Brunico
Quartz phyllites
Crystalline rocks of the Defereggen mountains
SHEET IV a
MAP with scale 1:300.000, showing the angle of rake of the mean minor fold in the mean plane of schistosity (measured by moving downwards from the East)
80° ≤ mean strike ≤ 130°
co-ordinates of the grid

SHEET III

SCHEMATIC GEOLOGIC MAP

of the quartz phyllites to the south of the Pusteria line between Brunico and Prato alla Drava, N.ITALY
scale 1:50000
by F.P.Agterberg 1961 utilizing the geologic maps of Cornelius Furlani (1912), Dal Piaz (1930), and Merla (1930)

5 mean azimuth and dip of minor folds
mean azimuth lines ⋈ mean strike lines of subvertical schistosity
(⋈ strike lines of bedding planes)
(lies on the supposed iso-line of adjacent mean azimuth)

0 1 2 km

reverse fault (triangles point to upper block) — I = 10–29°, V = 30–49°, II = 50–69°, III = 70–89°, ⊣ = vert.

sinistral wrench fault

1234 elevations in meters

PUSTERIA LINE

CRYSTALLINE ROCKS OF THE DEFEREGGEN MOUNTAINS

Brunico
Rasùn – Valdaora
1013
Sorafurcia 1360
Plan de Corones
2273
Monguelfo
EGGERBERG
Villabassa
1158
Dobbiaco
1206
Planca di Sotto
1239
Prato alla Drava
1128
S. Candido
Braies
1350
Rio di Casies
R. Pienza
Rio Furcia
Rio di S. Silvestro
R. di Braies
R. Drava

Quaternary
Tonalites
Basic dyke
Mesozoic of the western Drauzone
Anisian
Werfenian
Bellerophon limestones and Upper Permian dolomites
Grödener sandstones and conglomerates
Upper Silurian (?) limestones
Quartz phyllites
Green phyllites
Conglomeratic quartzite

co-ordinates of the grid

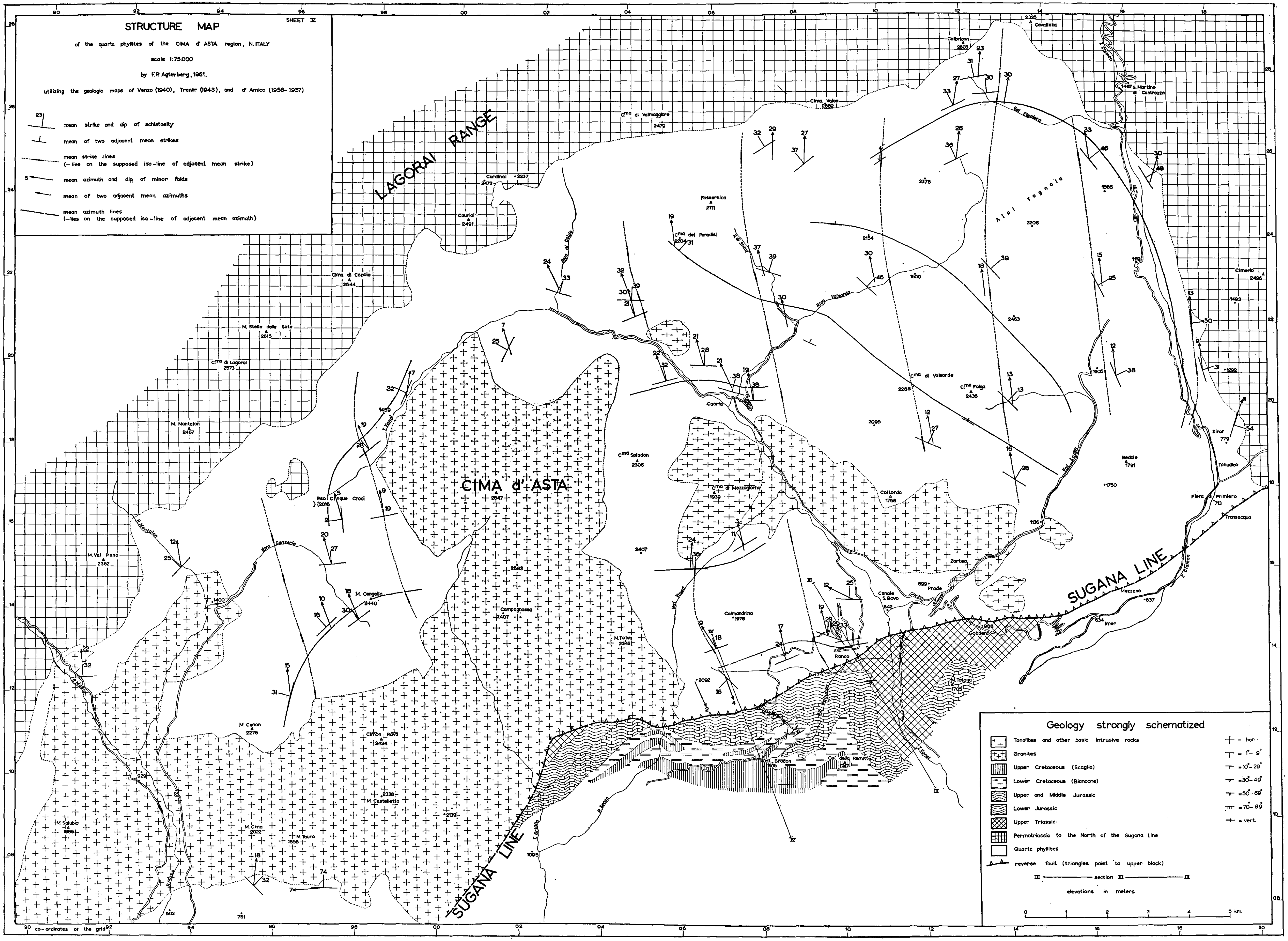
STRUCTURE MAP
SHEET V
of the quartz phyllites of the CIMA d' ASTA region, N. ITALY
scale 1:75.000
by F.P. Agterberg, 1961,
utilizing the geologic maps of Venzo (1940), Trener (1943), and d' Amico (1956-1957)
mean strike and dip of schistosity
mean of two adjacent mean strikes
mean strike lines
(—lies on the supposed iso-line of adjacent mean strike)
mean azimuth and dip of minor folds
mean of two adjacent mean azimuths
mean azimuth lines
(—lies on the supposed iso-line of adjacent mean azimuth)
LAGORAI RANGE
CIMA d' ASTA
SUGANA LINE
SUGANA LINE
Geology strongly schematized
Tonalites and other basic intrusive rocks
Granites
Upper Cretaceous (Scaglia)
Lower Cretaceous (Biancone)
Upper and Middle Jurassic
Lower Jurassic
Upper Triassic
Permotriassic to the North of the Sugana Line
Quartz phyllites
reverse fault (triangles point to upper block)
section III
elevations in meters
= hor.
= 1°– 9°
= 10°– 29°
= 30°– 49°
= 50°– 69°
= 70°– 89°
= vert.
0 1 2 3 4 5 km.
co-ordinates of the grid
Colbricon
Cavallazza
S. Martino di Castrozza
Cima Valon
Cma di Valmaggiore
Cardinal
Cauriol
Cima di Copola
Fossernica
Cma del Paradisi
Alpi Tognola
M. Stelle delle Sute
Cma di Lagorai
M. Montalon
Cma Spiadon
Cma di Mezzogiorno
Cma di Valsorda
Cma Folga
Coltorda
Bedole
Siror
Tonadico
Fiera di Primiero
Transacqua
Mezzano
Imer
Zortea
Prade
Canale S. Bovo
Caoria
Passo Cinque Croci
M. Cengello
M. Val Piano
Campagnassa
M. Tolva
Calmandrino
Ronco
Gobbera
M. Totoga
Cost. Brocon
Col della Remitta
M. Cenon
Cimon Rava
M. Castelletto
M. Salubio
M. Cima
M. Tauro
Cimerlo
Val Cigolera
Riva Valsorda
Val Lozen
Riva Conseria
Val Vanoi
T. Cismon
T. Maso

SHEET VII

STRUCTURE MAP

of the surroundings of GOSALDO, N. ITALY

scale 1:50.000 by F.P.Agterberg, 1961

utilizing the geologic map of Castiglioni (1939)

Permotriassic

Quartz phyllites, and other crystalline rocks

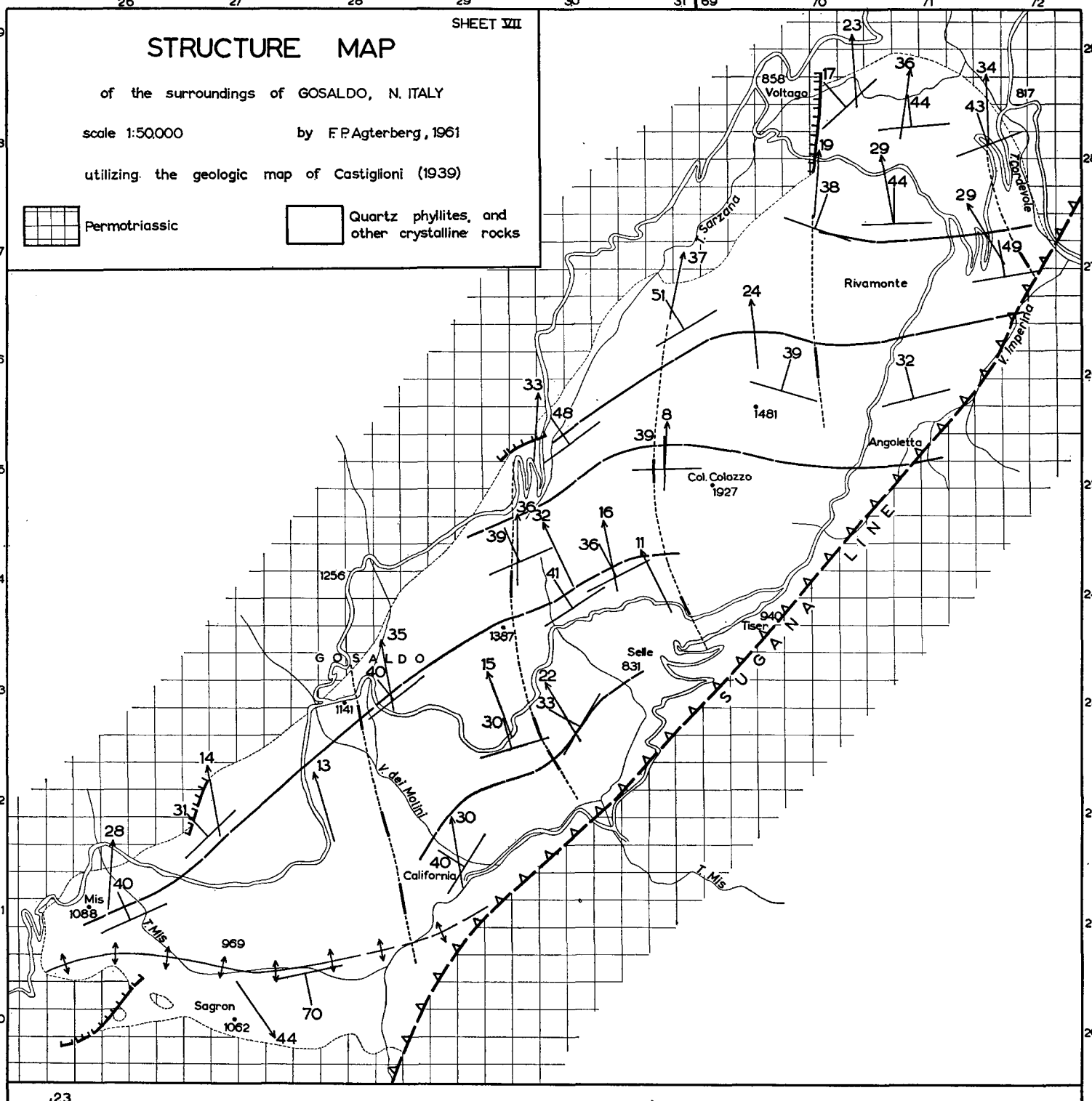

23 mean strike and dip of schistosity – planes

mean strike lines (– lies on the supposed iso-line of adjacent mean strike)

45 mean azimuth and dip of minor folds

mean azimuth lines (– lies on the supposed iso-line of adjacent mean azimuth)

axial plane of anticline

reverse fault

normal fault

triangles and barbs point to upper block

1246 elevation in meters

0 1 2 3 km

co-ordinates of the grid

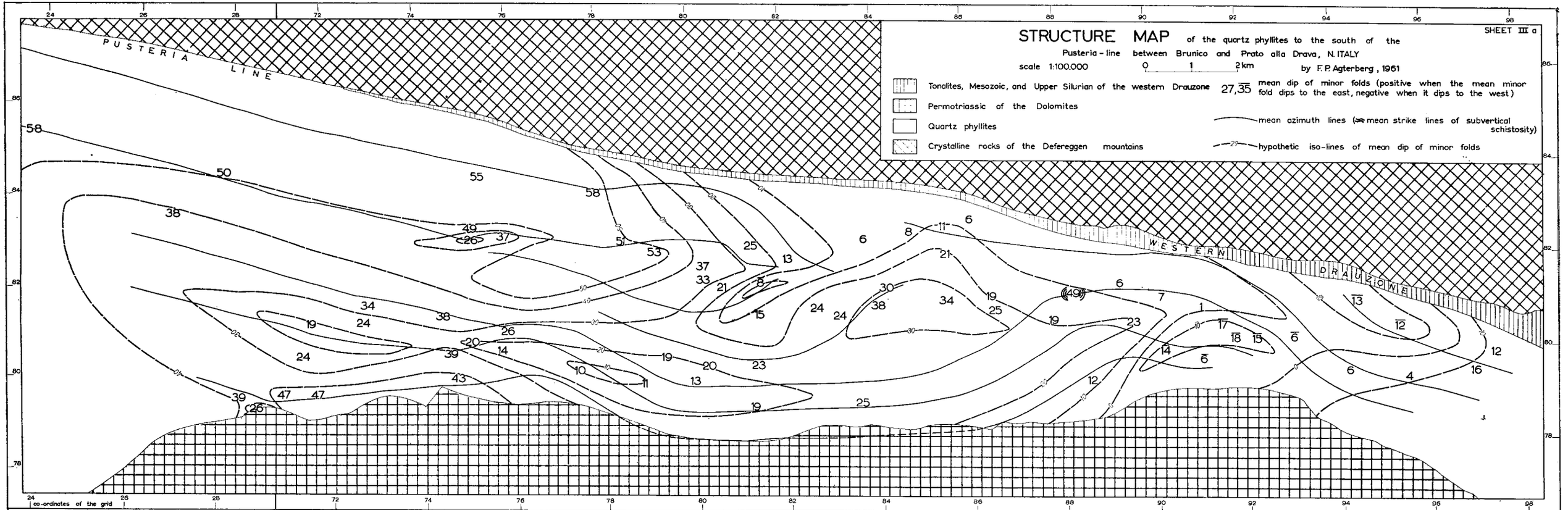
SHEET III a
STRUCTURE MAP of the quartz phyllites to the south of the Pusteria - line between Brunico and Prato alla Drava, N. ITALY
scale 1:100.000
0 1 2 km
by F. P. Agterberg, 1961
Tonalites, Mesozoic, and Upper Silurian of the western Drauzone
Permotriassic of the Dolomites
Quartz phyllites
Crystalline rocks of the Defereggen mountains
27,35 mean dip of minor folds (positive when the mean minor fold dips to the east, negative when it dips to the west)
mean azimuth lines (= mean strike lines of subvertical schistosity)
hypothetic iso-lines of mean dip of minor folds
PUSTERIA LINE
WESTERN DRAUZONE
co-ordinates of the grid

SCHEMATIC GEOLOGIC MAP

of the M.SPICO REGION, N. ITALY

scale 1:50.000

by F.P. Agterberg, 1961

utilizing the geologic map of B.Sander (1924)

0 1 2 3 4km.

SHEET VIII

- Tauern – gneiss
- containing augen – gneisses
- Saccharoidal limestones
- Ordinary gneisses
- Limestones
- Calcareous phyllites
- Green phyllites
- Serpentine and talc
- Quartz phyllites
- Gneiss of M.Spico
- Riesenferner augen–gneiss
- containing migmatites
- Riesenferner tonalite
- mean strike and dip of schistosity
- mean azimuth and dip of minor folds
- axial plane of syncline
- axial plane of anticline
- elevation in meters

Rio Rosso, Rio Torbo, S. Giovanni, 1032, M. Lupo, 2040, 1448, S. Martino, 1002, T. AURINO, Montebello, 2273, Rio di Mezzo, Rio Bianco, Rio Nero, Rifugio, 2420, 2372, 2368, 2703, Croda della Paura, 2505, 2571, 1330, Rio Bianco, Lutago, 971, 2069, Rio di Poia, R. Michele, Col del Lago, 2697, Sasso Tondo, 2551, Val dei Coroni, Rio di Lappago, Lappago, 1436, 2280, 2355, M. Cesa, 2187, Valle del Passo, Passennock, 2668, Giogo Gallina, 2473, 2348, M. SPICO, 2523, 2103, Campo Tures, 885, Rio di Riva, Rio Luppaleto, Molini, 856, Caminata in Tures, Dosso della Cascata, 2314, Selva dei Molini, 1179, 1081, Rio Selva dei Molini, Rio Valburga

co-ordinates of the grid

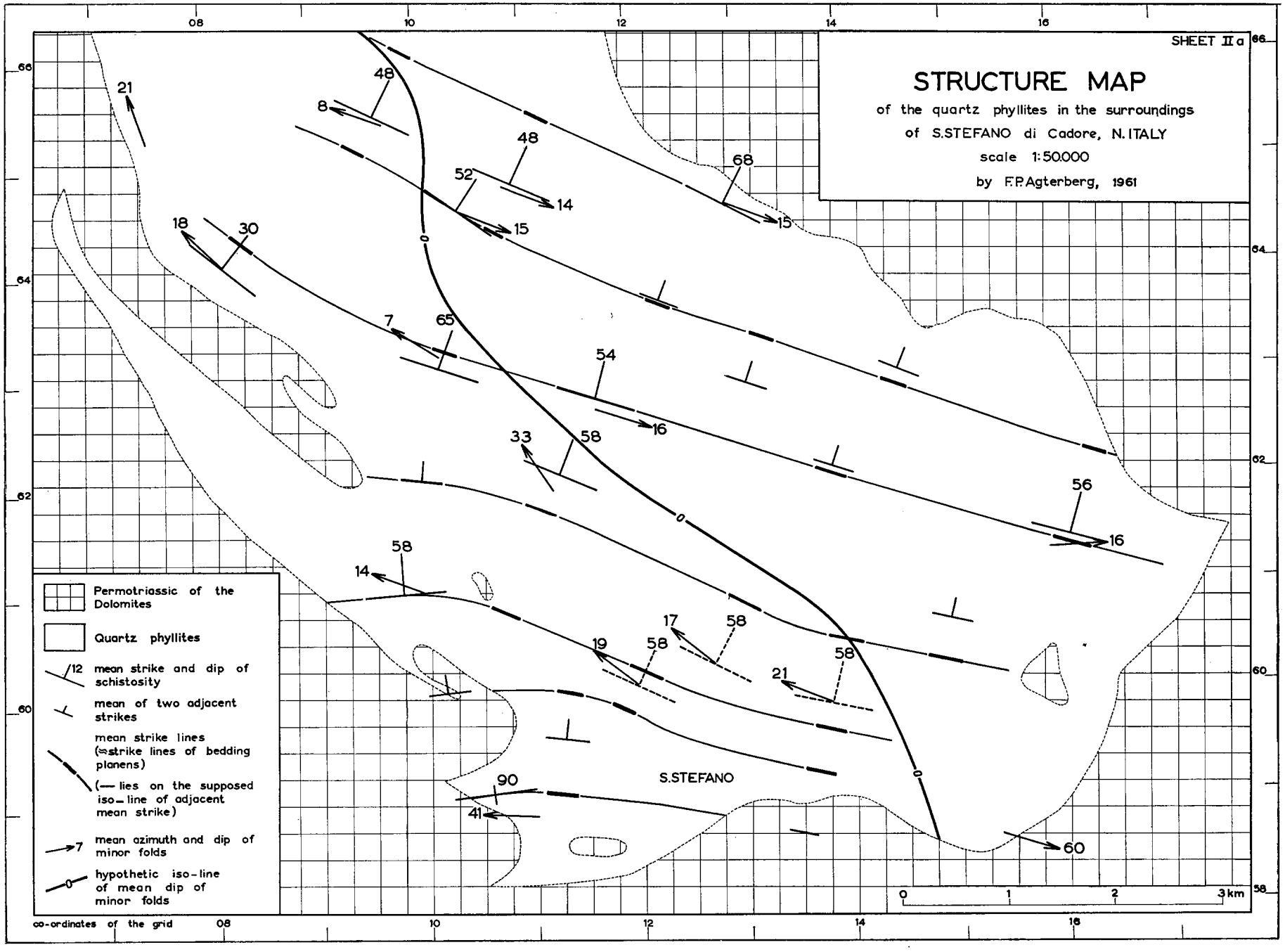
SHEET II a
STRUCTURE MAP
of the quartz phyllites in the surroundings
of S.STEFANO di Cadore, N. ITALY
scale 1:50.000
by F.P.Agterberg, 1961
Permotriassic of the Dolomites
Quartz phyllites
/12 mean strike and dip of schistosity
mean of two adjacent strikes
mean strike lines (≈strike lines of bedding planens)
(— lies on the supposed iso-line of adjacent mean strike)
→7 mean azimuth and dip of minor folds
hypothetic iso-line of mean dip of minor folds
S.STEFANO
0 1 2 3 km
co-ordinates of the grid
08
10
12
14
16
66
64
62
60
58

SHEET II

SCHEMATIC GEOLOGIC MAP

of the surroundings of

S. STEFANO di Cadore N. ITALY

scale: 1 : 50 000

by F.P.Agterberg, 1961

utilizing the geologic maps of Geyer (1902)
Ogilvie–Gordon (1927) and Gortani (1933)

- Jurassic siliceous limestones
- Red Liassic limestones
- Rhätic limestones and marls
- Hauptdolomit (Norian)
- Raibler strata of S. Stefano
- Wengen and S. Cassiano strata
- Buchensteinstrata with Pietraverde
- Anisian–Ladinian (Dolomites of Mendola–Schlern with limestone base and locally a marly intercalation)
- Werfenian
- Upper Permian dolomites and Bellerophon limestones
- Permian gipsiferous marls and gypsum
- Quartz porphyries
- Grödener sandstones and conglomerates
- Quartz phyllites of the crystalline basement (symbols give mean strike of schistosity)
- Green phyllites
- Quartzitic phyllites and quartzites
- Conglomeratic quartzites

M. Aiarnola 2456Δ · M. Spina Δ1986 · M. S. Daniele 2235 · M. Curie Δ2034 · M. Zovo Δ1944 · M. Aquda 1585 · M. Piedo Δ1661 · M. Col Δ2078 · M. Tudaio 2114Δ · M. Tezza piccolo 2353

Bosco della Ferrera · Rio della Madonna · Costa Secca · Rio Somera · Padola · Rio Dosoledo · Sopalù · Candide · Costa · Costa Fronta · R. Larice · R. Ciamara · R. Rin · R. Fondaccia · Ostº alle Alpi · Costalta · Campitello · Costalissoio · S. Pietro · L. di Selva · Col Caradies · Costone di Dantoz · L. Cestella · Danta · F. PADOLA · Col dei Morti · Campolango · F. PIAVE · S. STEFANO di Cadore · Transaqua · Pra Becchei · Rio Maurita · Rio Giaf · Rio Pinie · Villapiccola · Lago di S. Caterina · Valle Secossa · Valle Ostera · Via S. Rocco · Via di Pale · F. ANSIEI · VOLTAGO · AURONZO · Col della Cite · Rio Frisone

1597 · 1752 · 1903 · 1353 · 1303 · 1637 · 1373 · 1561 · 1514Δ · 1406 · 1415 · 1419 · 908 · 1751 · 2017 · 1700 · 2037 · 1448 · 1432 · 886 · 830

- = hor
- = 1–9°
- = 10–29°
- = 30–49°
- = 50–69°
- = 70–89°
- vert.

reverse fault · normal fault · dextral wrench fault — triangles and barbs point to upper block

Section I — I

Elevations in meters

0 1 2 3 4 km

98 Co-ordinates of the grid 00 02 04 06 08 10 12 14 16 18

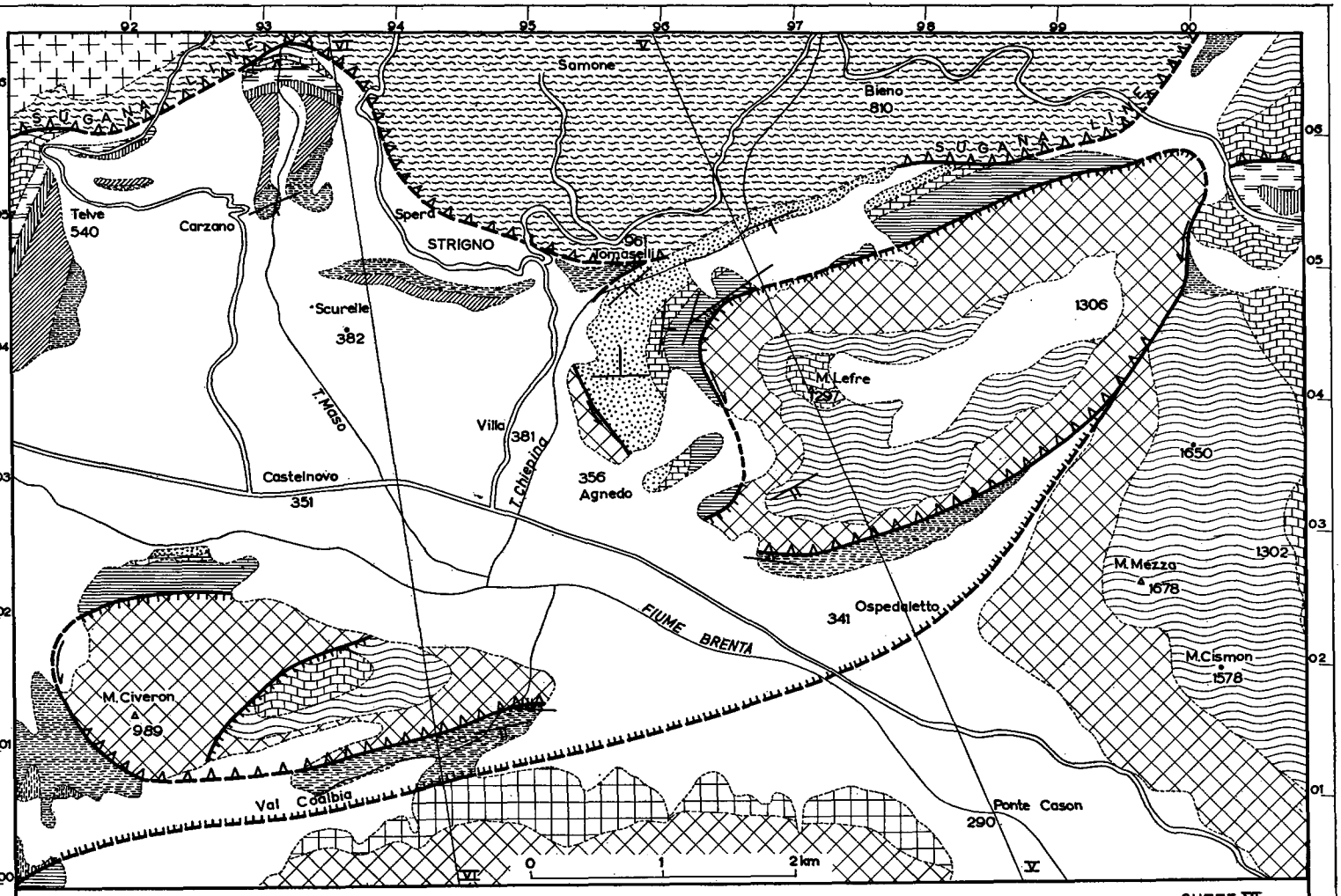

SHEET VI

SCHEMATIC GEOLOGIC MAP

OF THE SURROUNDINGS OF STRIGNO, N. ITALY scale 1:50.000

after S. Venzo (1940) with some additions by F. P. Agterberg, 1961

- Quaternary
- Upper Miocene
- Middle and Lower Miocene
- Oligocene and Eocene
- Upper Cretaceous (Scaglia)
- Lower Cretaceous (Biancone)
- Upper and Middle Jurassic
- Lower Jurassic
- Upper Triassic
- Ladinian
- Werfenian
- Bellerophon limestones
- Grödener sandstones and conglomerates, Tuffs
- Quartz phyllites (quaternary omitted)
- Granite

2467 elevation in meters

reverse fault } triangles and barbs point to upper block

normal fault

wrench fault

= 1 – 9°

= 10 – 29°

= 30 – 49°

= 50 – 69°

= 70 – 89°

V —— SECTION —— V

co-ordinates of the grid 93 94 95 96 97 98 99 00 01

SHEET I

SCHEMATIC TECTONIC MAP OF WESTERN PART OF EASTERN ALPS

by F.P.Agterberg 1961

scale 500.000

based on H.Vetters's geologic map (1923), utilizing some data of B.Accordi (1955,1957), R.W. van Bemmelen (1957, and unpublished tectonic sketchmap of the Alps), Carta geologica delle tre Venezie (Foglio 4a, 4b, 11, 12, 13, 21, 22, and 23), G.F.L.Dietzel (1960), C.Exner (1954), P.Fallot (1950, 1955), G.Frasl (1958), D.van Hilten (1960), F.Karl (1953, 1959), H.Küpper (1959), P.Leonardi (1955), M.Richter (1956), F.X.Schaffer's volume (1951), O.Schmidegg (1933, 1936, 1937, 1954), R.Signorini (1951), L.U.de Sitter and C.M.de Sitter-Koomans (1949), R.Staub (1923), Tectonic outline maps of G.V.-meeting at Bad Tölz (1960) (by H.Bögel, G.Lensch, and W.Zacher (introduction) by H.Pichler (exc C1), and by W.Zacher (exc C III)), A.Tollmann (1959), and L.Trevisan (1939).

CENTRAL ALPS (locally not shaded)

Upper Austrian Nappes
- Rieserferner augen-gneiss
- Periadriatic granites and tonalites
- Steinach Nappe (quartz phyllites & Carboniferous)
- Triassic
- Graywacke Zone
- Granite gneisses between ordinary gneisses
- Ordinary gneisses with strike lines, containing eclogites in Silvretta and Ötz Nappes
- Quartz phyllite of Schneeberger Zone and Upper Inn Valley
- Quartz phyllites of Thurntaler Syncline

Lower and Middle Austrian Nappes
- Permotriassic

Pennine Inliers
- Schistes lustrés ("obere Schieferhülle" in Tauern)
- Micaschists ("untere Schieferhülle" of Tauern)
- Tauern granite gneisses
- Tauern tonalite gneisses

- All types of faults

NORTHERN LIMESTONE ALPS
- BAVARIAN MOLASSE
- Flysch Zone
- Helvetic Zone
- Upper Austrian Nappes
- Gosau strata & Lower Tertiary
- Mesozoic

SOUTHERN LIMESTONE ALPS
- Jurassic-Lower Tertiary
- Carnian and Norian
- Anisian and Ladinian
- Permian and Werfenian
- Quartz porphyries of Bolzano
- Crystalline Basement
- Gneisses of Upper Gail Valley
- Periadriatic granites and tonalites
- Lower Tertiary Basalts
- Tonalite of Chiusa (Klausenite)
- Mesozoic and Cenozoic in Bergamasc Alps, Brenta Region, and Adriatic Outer Belt.
- G / Overthrust-folds with direction of movement, "Gipfelfaltung" in the N.Italian Dolomites
- CENOZOIC OF PO PLAIN AND VENETIAN PLAIN

0 10 20 30 40 50 km.